frontiers | Research Topics

Community series in identification, function and mechanisms of interferon induced genes associated with viruses, volume II

Edited by
Chang Li, Linzhu Ren, Penghua Wang and Jieying Bai

Published in
Frontiers in Immunology

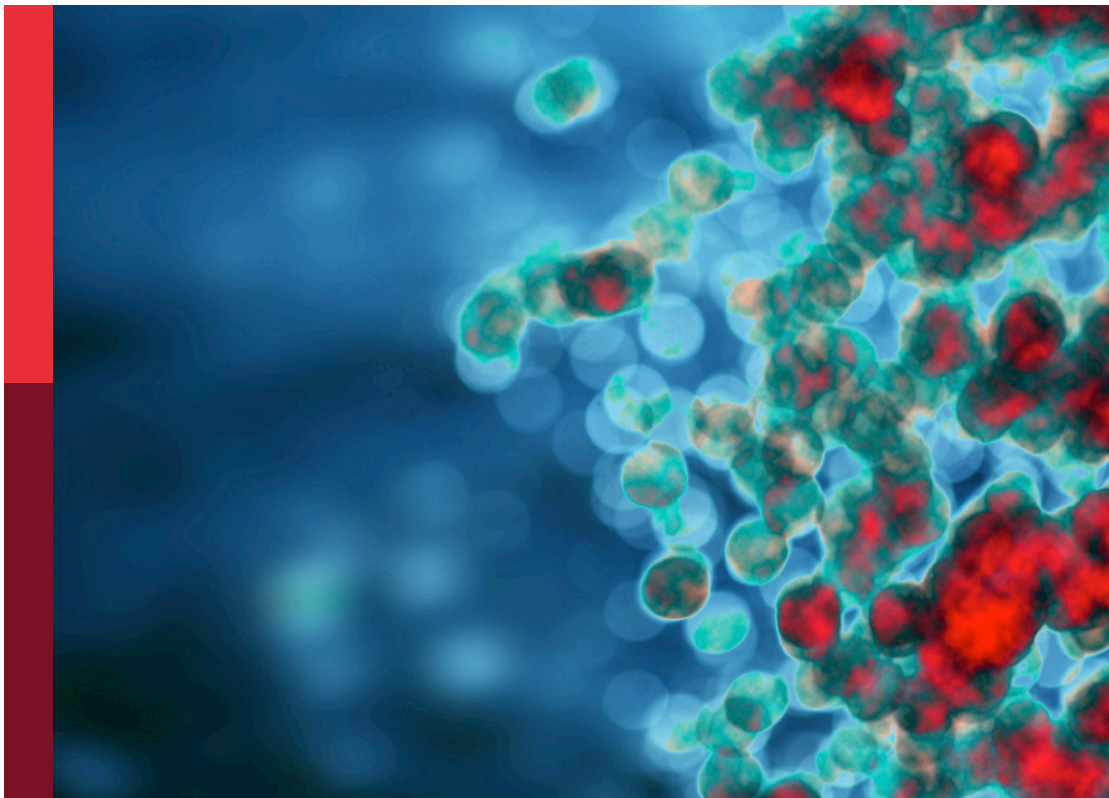

ISSN 1664-8714
ISBN 978-2-8325-3388-8
DOI 10.3389/978-2-8325-3388-8

About Frontiers

Frontiers is more than just an open access publisher of scholarly articles: it is a pioneering approach to the world of academia, radically improving the way scholarly research is managed. The grand vision of Frontiers is a world where all people have an equal opportunity to seek, share and generate knowledge. Frontiers provides immediate and permanent online open access to all its publications, but this alone is not enough to realize our grand goals.

Frontiers journal series

The Frontiers journal series is a multi-tier and interdisciplinary set of open-access, online journals, promising a paradigm shift from the current review, selection and dissemination processes in academic publishing. All Frontiers journals are driven by researchers for researchers; therefore, they constitute a service to the scholarly community. At the same time, the *Frontiers journal series* operates on a revolutionary invention, the tiered publishing system, initially addressing specific communities of scholars, and gradually climbing up to broader public understanding, thus serving the interests of the lay society, too.

Dedication to quality

Each Frontiers article is a landmark of the highest quality, thanks to genuinely collaborative interactions between authors and review editors, who include some of the world's best academicians. Research must be certified by peers before entering a stream of knowledge that may eventually reach the public - and shape society; therefore, Frontiers only applies the most rigorous and unbiased reviews. Frontiers revolutionizes research publishing by freely delivering the most outstanding research, evaluated with no bias from both the academic and social point of view. By applying the most advanced information technologies, Frontiers is catapulting scholarly publishing into a new generation.

What are Frontiers Research Topics?

Frontiers Research Topics are very popular trademarks of the *Frontiers journals series*: they are collections of at least ten articles, all centered on a particular subject. With their unique mix of varied contributions from Original Research to Review Articles, Frontiers Research Topics unify the most influential researchers, the latest key findings and historical advances in a hot research area.

Find out more on how to host your own Frontiers Research Topic or contribute to one as an author by contacting the Frontiers editorial office: frontiersin.org/about/contact

Community series in identification, function and mechanisms of interferon induced genes associated with viruses, volume II

Topic editors

Chang Li — Chinese Academy of Agricultural Sciences (CAAS), China
Linzhu Ren — Jilin University, China
Penghua Wang — UCONN Health, United States
Jieying Bai — Academy of Military Medical Sciences (AMMS), China

Citation

Li, C., Ren, L., Wang, P., Bai, J., eds. (2023). *Community series in identification, function and mechanisms of interferon induced genes associated with viruses, volume II*. Lausanne: Frontiers Media SA. doi: 10.3389/978-2-8325-3388-8

Table of contents

frontiers | Frontiers in Immunology

TYPE Editorial
PUBLISHED 16 August 2023
DOI 10.3389/fimmu.2023.1269413

OPEN ACCESS

EDITED AND REVIEWED BY
Francesca Granucci,
University of Milano-Bicocca, Italy

*CORRESPONDENCE
Chang Li
lichang78@163.com
Linzhu Ren
linzhu@jlu.edu.cn

RECEIVED 30 July 2023
ACCEPTED 31 July 2023
PUBLISHED 16 August 2023

CITATION
Bai J, Ren L and Li C (2023) Editorial: Community series in identification, function, and mechanisms of interferon induced genes associated with viruses, volume II.
Front. Immunol. 14:1269413.
doi: 10.3389/fimmu.2023.1269413

Editorial: Community series in identification, function, and mechanisms of interferon induced genes associated with viruses, volume II

Jieying Bai[1], Linzhu Ren[2]* and Chang Li[3]*

[1]Non-Human Primate Research Center, Institute of Molecular Medicine, Peking University, Beijing, China, [2]College of Animal Sciences, Key Lab for Zoonoses Research, Ministry of Education, Jilin University, Changchun, China, [3]Research Unit of Key Technologies for Prevention and Control of Virus Zoonoses, Chinese Academy of Medical Sciences, Changchun Veterinary Research Institute, Chinese Academy of Agricultural Sciences, Changchun, China

KEYWORDS

interferons, interferon stimulated genes, innate immunity, infection, interaction

Editorial on the Research Topic
Community series in identification, function, and mechanisms of interferon induced genes associated with viruses, volume II

Research on the antiviral mechanisms mediated by interferon (IFN) and IFN-stimulated genes (ISGs) is a longstanding topic (1) within the field. The continuous discovery of new IFN or its subtype and ISG is of great significance to clarify the new antiviral mechanisms and the interaction between host and pathogen (1, 2). However, we have a long way to go before we fully understand these IFNs and ISGs. Based on a previous collection of articles (1), this Research Topic continues this work related to IFNs and ISGs.

To explore the stimulation of IFNs during porcine alphaherpesvirus pseudorabies virus (PRV), Yin et al. evaluated the expression of type I and III IFNs and their antiviral activities against PRV in different porcine epithelial cells: porcine kidney epithelial cells (PK-15), primary respiratory epithelial cells (PoREC) and intestinal porcine epithelial cells (IPEC-J2). The results showed that PRV induced a variety of infection-dependent type I IFN responses and a prominent III IFN response in PK-15 cells, whereas a rapid and temporal expression of type I and type III IFNs were triggered in IPEC-J2 cells, and no detectable type I or type III IFN responses were observed in PoREC. Surprisingly, both type I and type III IFNs in the pretreatment group exhibited antiviral activities against PRV, but only IFN-α in PK-15 cells and type III IFN in IPEC-J2 cells could effectively inhibit PRV infection. Moreover, Daza-Cajigal et al. reported that partial JAK1 deficiency impairs STAT1 phosphorylation and IFN-γ-inducible gene expression in THP-1 cells, and IFN-γ-induced phagosome acidification and apoptosis in myeloid cells. Partial JAK1 deficiency also weakened the antiviral response in EBV-B cells but enhances the survival of mycobacterial and salmonella in myeloid cells. These results indicate that the IFN responses induced by viral infection depend on the virus-infected cell types.

Furthermore, the stimulation of IFN response also depends on the virus and its replication ability and adaptability in cells. For example, Laine et al. found that the replication of sublineages Omicron BA.1, BA.2, and recombinant sublineage XJ in human lung epithelial Calu-3 cells was weakened compared to Alpha and Delta. The activation of the primary innate immune signaling pathway by SARS-CoV-2 variants is relatively weak, however, all variants stimulate enough interferon to induce the activation of STAT2 and the production of ISGs.

Another contribution in this Research Topic also describes the induction and activation of IFNs on immune cells and ISGs. Li et al. found that the STING-IKKβ-Relish-AMPs axis acts a critical role in shrimp against Vibrio parahaemolyticus infection. After being induced, type I IFNs can stimulate B cells and classical dendritic cells (cDCs) through Th1 and Tfh cell-dependent pathways, thus driving the formation of the germinal center (GC) and the distribution of the IgG subclass against the pathogens (Dahlgren et al.). The interferon response networks induced by lipopolysaccharide (LPS) can also be used to predict the level of severe lower respiratory infections in infancy (Read et al.). Among the networks, IRF1 is identified as a master regulator of the IFN response. In addition, type I IFNs, especially IFNα14 and IFNβ, exhibit super activation on Natural killer (NK) cells, which can enhance the anti-leukemic function of NK cells and prolong the survival of leukemia mice models (Barnes et al.). The unmodified mRNA vaccine can induce type I IFNs or its downstream signaling cascades, which play crucial roles in inducing robust anti-tumor T-cell response to control tumor growth and metastasis (Sittplangkoon et al.). These results further confirm that IFNs and ISGs not only have antiviral and antibacterial effects but also play important roles in anticancer.

Notably, IFN-based therapy may also increase the risk of autoimmune thyroid diseases in patients with HCV infection (Chou et al.). The upregulated type I IFNs and ISGs can enhance myeloid DC $CD1C^{+}$ subpopulation in patients with mutations in three prime repair DNA exonuclease 1 (TREX1), which may associate with the perpetuation of TREX1-induced chilblain lupus and other type I interferonopathies (Eugster et al.). The question of how to effectively activate IFN responses, what makes it play an effective anti-pathogen and anti-cancer role, and how to reduce or control its side effects are among the problems that need to be solved urgently.

In summary, IFN responses and induced-ISGs are double-edged swords, and how to make effective use of them will be an important research hotspot in the future. This community series further provides strong theoretical support for the application and research of IFNs and ISGs. With further applications of multi-omics and high-throughput technology, research on and applications of IFNs and ISGs will also be vigorously promoted in this field in the future.

Author contributions

CL: Conceptualization, Writing – original draft, Writing – review & editing. JB: Conceptualization, Writing – original draft, Writing – review & editing. LR: Conceptualization, Writing – original draft, Writing – review & editing.

Funding

This work was supported by the National Key Research and Development Program of China [No. 2021YFD1801103], Jilin Province Science and Technology Development Projects [No.: 20230508088RC], and the CAMS Innovation Fund for Medical Sciences [2020-12M-5-001].

Conflict of interest

The authors declare that the research was conducted in the absence of any commercial or financial relationships that could be construed as a potential conflict of interest.

Publisher's note

References

1. Ren L, Bai J, Li C. Editorial: Identification, function and mechanisms of interferon induced genes associated with viruses. *Front Immunol* (2022) 13:1126639. doi: 10.3389/fimmu.2022.1126639

2. Chen J, Li P, Zou W, Jiang Y, Li L, Hao P, et al. Identification of a novel interferon lambda splice variant in chickens. *J Virol* (2023) 97:e0174322. doi: 10.1128/jvi.01743-22

frontiers | Frontiers in Immunology

ORIGINAL RESEARCH
published: 13 July 2022
doi: 10.3389/fimmu.2022.932388

Type I Interferons Promote Germinal Centers Through B Cell Intrinsic Signaling and Dendritic Cell Dependent Th1 and Tfh Cell Lineages

Madelene W. Dahlgren[1†], Adam W. Plumb[2†], Kristoffer Niss[3], Katharina Lahl[1,2], Søren Brunak[2,3] and Bengt Johansson-Lindbom[1,2]*

[1] Immunology Section, Lund University, Lund, Sweden, [2] Department of Health Technology, Technical University of Denmark, Lyngby, Denmark, [3] Novo Nordisk Foundation Center for Protein Research, University of Copenhagen, Copenhagen, Denmark

OPEN ACCESS

Edited by:
Aaron James Marshall, University of Manitoba, Canada

Reviewed by:
Irah L King, McGill University, Canada
Steven M Kerfoot, Western Universit, Canada

***Correspondence:**
Bengt Johansson-Lindbom
bengt.johansson_lindbom@med.lu.se

[†]These authors have contributed equally to this work

Specialty section:
This article was submitted to B Cell Biology, a section of the journal Frontiers in Immunology

Received: *29 April 2022*
Accepted: *21 June 2022*
Published: *13 July 2022*

Citation:
Dahlgren MW, Plumb AW, Niss K, Lahl K, Brunak S and Johansson-Lindbom B (2022) Type I Interferons Promote Germinal Centers Through B Cell Intrinsic Signaling and Dendritic Cell Dependent Th1 and Tfh Cell Lineages. Front. Immunol. 13:932388. doi: 10.3389/fimmu.2022.932388

Type I interferons (IFNs) are essential for antiviral immunity, appear to represent a key component of mRNA vaccine-adjuvanticity, and correlate with severity of systemic autoimmune disease. Relevant to all, type I IFNs can enhance germinal center (GC) B cell responses but underlying signaling pathways are incompletely understood. Here, we demonstrate that a succinct type I IFN response promotes GC formation and associated IgG subclass distribution primarily through signaling in cDCs and B cells. Type I IFN signaling in cDCs, distinct from cDC1, stimulates development of separable Tfh and Th1 cell subsets. However, Th cell-derived IFN-γ induces T-bet expression and IgG2c isotype switching in B cells prior to this bifurcation and has no evident effects once GCs and *bona fide* Tfh cells developed. This pathway acts in synergy with early B cell-intrinsic type I IFN signaling, which reinforces T-bet expression in B cells and leads to a selective amplification of the IgG2c$^+$ GC B cell response. Despite the strong Th1 polarizing effect of type I IFNs, the Tfh cell subset develops into IL-4 producing cells that control the overall magnitude of the GCs and promote generation of IgG1$^+$ GC B cells. Thus, type I IFNs act on B cells and cDCs to drive GC formation and to coordinate IgG subclass distribution through divergent Th1 and Tfh cell-dependent pathways.

Keywords: Type I Interferons, germinal center (GC) B cells, IgG subclass antibodies, Tfh cells, Th1 cells, antibody responses

INTRODUCTION

Neutralizing antibody responses develop within germinal centers (GCs); histological structures that arise within lymphoid tissues due to antigen-driven clonal B cell expansion. GCs are also thought to represent key sites for breach of tolerance in development of autoimmune disease (1). GC B cell responses rely on T follicular helper (Tfh) cells, which support B cell expansion, facilitate antibody affinity maturation and eventually select GC B cells into the compartments of long-lived plasma cells or memory B cells (2).

Type I interferons (IFNs), including a single IFN-β and several IFN-α proteins, are rapidly produced in response to viral and bacterial infections and signal through the common and ubiquitously expressed heterodimeric IFN-α receptor (IFNAR) (3). Initially discovered for their ability to induce the "antiviral state" in host cells, type I IFNs are also associated with a plethora of immune-regulatory functions essential for antiviral immunity (4). The importance of type I IFNs in controlling SARS-CoV-2 is also evident from the presence of neutralizing autoantibodies against these cytokines, or mutations in type I IFN signaling pathways, in a significant proportion of patients developing severe COVID-19 disease (5–7). Furthermore, elevated type I IFN production is a hallmark of systemic autoimmune diseases, with a strong correlation between the IFN gene expression signature and clinical manifestations in SLE (8–11). When co-injected with a protein antigen, IFN-α has sufficient adjuvant activity to induce GC formation (12) and GC B cell responses have been shown to depend on type I IFNs both during viral infections (13) and in autoimmune models (14, 15). While we and others have shown that type I IFN signaling in cDCs augments generation of Tfh cells (16, 17), direct signaling in B- and T- cells has also been implicated in type I IFN-dependent enhancement of humoral immunity and autoimmunity (12, 13, 15, 18, 19). The relative contribution of these pathways, and how they interact with the type I IFN – cDC – Tfh cell axis to enhance and modulate the GC response, is however unclear.

Different IgG subclasses are associated with distinct effector mechanisms. In C57BL/6 mice, complement-fixing IgG2c (IgG2a in the BALB/c strain) is more efficient than other subclasses in neutralizing viruses (20) and is also associated with more severe pathology in lupus models (21). The transcription factor T-bet induces class switch recombination (CSR) to IgG2a/c (22). T-bet expression in B cells appears to have effects beyond CSR (23) and was recently shown to be required for generation of protective anti-influenza stalk region-specific antibodies (24). Mouse IgG2a/c may hence represent a useful surrogate marker for antibody responses driven by T-bet expressing B cells, with relevance for the human setting. Purified IFN-β can enhance production of all IgG subclasses in mice and a similarly broad and type I IFN-dependent isotype distribution is induced through the adjuvant effects of the synthetic dsRNA analogue polyinosinic-polycytidylic acid (poly I:C) (25). Other studies suggest that type I IFNs preferentially promote IgG2a/c (26, 27), and B cell-intrinsic type I IFN signaling mediates IgG2a/c CSR in the T cell-independent response to NP-Ficoll (28). The importance of this pathway in GC B cell responses is however less clear and the IgG2a/c subclass has more frequently been associated with strong Th1 immunity and IFN-γ production (29, 30).

Type I IFNs can both inhibit and promote generation of IFN-γ producing Th1 cells, with a general trend that sustained type I IFN responses during chronic infections suppress Th1 immunity (4). Through binding to endosomal TLR3 and the cytoplasmic RNA helicase MDA5, poly I:C instead triggers a transient systemic type I IFN response that peaks 3-6 hours after injection (31, 32), and an almost identical pattern in type I IFN production is observed for novel mRNA vaccination regimens (33). In contrast to the chronic infection models, this short-lived type I IFN response leads to Th1-biased immunity with abundant IFN-γ production from CD4 and CD8 T cells and in particular from NK cells (31). How this IFN-γ response develops, and what impact it has on GC B cell differentiation remains to be determined.

MATERIALS AND METHODS

Study Design

This study sought to determine pleiotropic effects and identify the cellular targets of acute type I IFN signaling on the germinal center B cell response. By selectively blocking receptor signaling in defined target populations, or permitting signaling to occur only during defined time windows, we unravel how GCs with broad IgG subclass distribution develop in mice immunized with OVA plus poly I:C. All experiments were performed according to protocols approved by the Lund/Malmo animal ethical committee (Sweden).

Mice

C57Bl/6 mice (wild type [wt]) were purchased from Taconic (Ejby, Denmark), *Ifngr1*$^{-/-}$ (B6.129S7-*Ifngr1*^{tm1agt}/J) and *Ifng*$^{-/-}$ (B6.129S7-*Ifng*^{tm1Ts}/J) mice purchased from The Jackson Laboratory (Bar Harbor, ME, USA). *Il27ra*$^{-/-}$ (B6N.129P2-Il27ra^{tm1Mak}/J), *Ifnar1*$^{-/-}$ (on a C57Bl/6 background), B6.SJL (B6.SJL-Ptprca Pepcb/BoyJ) and OT-II (B6.Cg-Tg(TcraTcrb) 425Cbn/J), KN2 (Il4$^{tm1(CD2)Mmrs}$) (34), *CD11c-cre* (B6.Cg-Tg (Itgax-cre)1-1Reiz/J), *XCR1-cre* (Xcr1$^{Cre-mTFP1}$) (35) and *Ifnar1*$^{fl/fl}$ (Ifnar1^{tm1Uka}) (36) mice were bred and maintained at the Biomedical Center animal facility, Lund University. *Ifnar1*$^{fl/fl}$ (Ifnar1^{tm1Uka}). CD45.1^{+}CD45.2^{+} OT-II and C57Bl/6 mice were generated by breeding B6.SJL (CD45.1^{+}) mice with OT-II or C57Bl/6 (CD45.2^{+}) mice, respectively. *Ifng*$^{-/-}$ and *Ifnar1*$^{-/-}$ mice were crossed to OT-II B6xB6.SJL mice to generate *Ifng*$^{-/-}$ and *Ifnar1*$^{-/-}$ OT-II mice. KN2-OT-II mice were generated by crossing KN2 and OTII mice. *CD11c-Cre.Ifnar1*$^{fl/fl}$ and *XCR1-cre.Ifnar1*$^{fl/fl}$ mice were generated by crossing *Ifnar1*$^{fl/fl}$ to *CD11c-cre* and *XCR1-cre*, respectively. Mice were included in experiments at 8-12 weeks of age.

Adoptive Transfers, Immunizations and mAb Treatment

CD4^{+} OT-II cells were isolated from spleen and LNs from OT-II*B6SJL mice with the EasySep mouse CD4^{+} T cell isolation kit (Stemcell Technologies, Vancouver, BC, Canada), according to manufacturer's protocol. Enriched CD4^{+} cells (>90% purity) were labelled with 5μM CellTrace Violet (Life Technologies, Carlsbad, CA, USA) and 5000 - 5 x 10^{5} cells/recipient were transferred intravenously (i.v.) as indicated. 16-20 hours after transfer, recipients were immunized with 100 μg poly I:C (*In vivo*Gen) together with 300μg OVA or NP-OVA (Biosearch Technologies, Novato, CA, USA), as indicated, by intraperitoneal (i.p.) injection. Type I IFN and IFN-γ signaling

was blocked by injection of 1 mg of anti-mIFNAR1 (MAR1-5A3) or anti-mIFN–γ (XMG1.2) respectively, at indicated time-points and control mice were treated with equal amounts of mIgG1 (MOPC-21) or rIgG1 (HRPN), all from BioXcell (West Lebanon, NH, USA).

Bone Marrow Chimeras

To generate mixed BM chimeras, BM cells from age matched (8-12 weeks) wt, *Ifnar1*$^{-/-}$, *Il27r*$^{-/-}$ or *Ifngr1*$^{-/-}$ donor mice were isolated and re-suspended in sterile PBS. A 1:1 mixture of wt and *Ifnar1*$^{-/-}$, *Il27r*$^{-/-}$ or *Ifngr1*$^{-/-}$ BM cells (2-3x10^6 total cells) were transferred into lethally irradiated (900 cGy) recipients (CD45.1$^+$CD45.2$^+$ B6.SJL x C57Bl/6 or CD45.1$^+$B6.SJL). Recipient mice were thereafter kept on Ciprofloxacin for 2 weeks. At 8 weeks after transfer, mice were bled to assess reconstitution by flow cytometry. Whole BM chimeric mice were generated by reconstituting irradiated wt (C57Bl/6) and *Ifnar1*$^{-/-}$ mice with wt or *Ifnar1*$^{-/-}$ BM, otherwise as described above.

Abs and Reagents

Flow-cytometry analyses were performed with Abs conjugated to FITC, PE, PerCP-Cy5.5, allophycocyanin, eFluor 450, Alexa Fluor 700, PE-Cy7, allophycocyanin-Cy7, Brilliant Violet 605, or biotin. The following Abs were used: anti-B220 (RA3-6B2), anti-CD4 (L3T4), anti-IFN-γ (XMG1.2), anti-GL-7 (GL-7), anti-CD38 (90), anti-T-bet (eBio4B10) (eBioscience, San Diego, CA, USA); anti-CXCR5 (2G8), anti-CD62L (MEL-14), anti-CD44, anti-CD95 (Jo2), anti-Bcl6 (K112-91), anti-TCR Vβ 5.1/5.2 (MR9-4), anti-TCR Vα2 (B20.1) (BD Biosciences, San Jose, CA, USA); anti-IgD (11-26c.2a), anti-CD138 (281–2), anti-CD45.1 (A20), anti-CD45.2 (104), anti-IgM (RMM-1), anti-IgG1 (RMG1-1), anti-IgG2b (RMG2b-1) (BioLegend, San Diego, CA, USA); anti-IgG2c (polyclonal) (Southern Biotech, Birmingham, AL, USA); and donkey anti-rat F(ab')2 fragment (polyclonal) (Jackson Immunoresearch, West Grove, PA, USA). Streptavidin conjugated to eFluor450 (eBioscience), allophycocyanin (Biolegend), and PE (Southern Biotech) were used as secondary reagents in combination with biotinylated Abs. For detection of NP- or OVA-binding cells, PE-conjugated NP (Biosearch Technologies) or Alexa 647-conjugated OVA (Molecular Probes, Eugene, OR, USA) was used, respectively. Dead cells were excluded using propidium iodide or Live/Dead Fixable Aqua Dead Cell Stain Kit (Molecular Probes).

Flow Cytometry

Single cell suspensions were prepared by mechanical disruption and filtered through 70μm cell strainers. RBCs were lysed with ACK buffer. For IgG analysis, cells were blocked with anti-FcR mAb (2.4G2) in 10% rat serum and thereafter incubated with isotype specific anti-IgG antibodies (see Abs and reagents). Remaining anti-mouse IgG reactivity were subsequently blocked with 10% mouse serum before incubation with fluorophore-conjugated mAbs. CXCR5 was detected as previously described (16) and followed by intracellular staining of Bcl6 and T-bet. Intracellular IFN-γ was detected after re-stimulation in complete medium with PMA (50 ng/ml) ionomycin (500 ng/ml; both Sigma-Aldrich, St. Louis, MN, USA), and Brefeldin A (eBioscience) for 3 hours. All intracellular staining was done using the FoxP3 Fixation/Permeabilization kit (eBioscience). Data was acquired on a LSRII or FACS AriaII and analyzed with FlowJo software (BD Bioscience).

NP-Specific ELISA

NP-specific serum antibodies were measured by ELISA. 96-well EIA/RIA plates (Sigma Aldrich) were coated overnight with 0.5ug/ml NP$_{23}$-BSA in PBS at room temperature and thereafter washed once in wash buffer (PBS+ 0.1% Tween20) and blocked with sample buffer (1% BSA in PBS) for 1 h and thereafter washed twice. Samples were diluted in sample buffer at 1:100 and 1:5000 and subsequently added in duplicates and incubated for 2 hours. Plates were washed four times before biotinylated anti-mouse IgG, anti-mouse IgG2c (polyclonal; both Southern Biotech), or anti-mouse IgG1 (RMG1-1) (BioLegend) was added in sample buffer, incubated for 1 h, and subsequently washed four times. Thereafter, Horseradish peroxidase (HRP) conjugated streptavidin was added and incubated for 45 minutes. After four washes, plates were developed with 3,3′,5,5′-Tetramethylbenzidine (TMB) and absorbance values were read at 450 nm on a SPECTROstar Nano (BMG Labtech, Ortenberg. Germany). NP-specific standard was prepared by pooling day 14 sera from NP-OVA immunized WT mice and used for all ELISAs to calculate serum titers (determined as 4x background OD value).

Cell Sort and cDNA Preparation and Quantitative Real-Time PCR

F Total OT-II cells (Live, singlet, CD4$^+$ CD45.1$^+$ B220$^-$) or GC B cells (Live, singlet, B220$^+$Fas$^+$CD38$^-$ CD45.1$^+$ or CD45.1$^-$) were sorted from immunized recipients directly into RLT buffer supplemented with 1% β-ME (Qiagen, Hilden, Germany). mRNA was extracted with an RNeasy Micro Kit (Qiagen) and either used for sequencing or converted into cDNA using a SuperScript III First-Strand cDNA kit according to manufacturer's protocol (Thermo Fisher, Waltham, MA, USA). Quantitative RT-PCRs were performed using SYBR GreenER qPCR SuperMix (mo Fisher) with 0.5 μM forward and reverse primers in a final volume of 20 μl. Reactions were run and recorded on an iCycler (Bio-Rad, Hercules, CA, USA).

Primer Sequences

Actb: forward; 5′-CCACAGCTGAGAGGGAAATC-3′, reverse; 5′-CTTCTCCAGGGAGGAAGAGG-3′, *Bcl6*: forward; 5′-GT ACCTGCAGATGGAGCATGT-3′; reverse; 5′-CTCTTCA CGGGGAGGTTTAAGT-3′, *Tbx21*: forward; 5′-CAACA ACCCCTTTGCCAAAG-3′; reverse; 5′-TCCCCCAAGCA GTTGACAGT-3′, *Ighg2c*: forward; 5′-CAGACCATCA CCTGCAATGT-3′; reverse; 5′- CATGGGGGACACTCT TTGAG-3′, *Ctse*: forward; 5′-ATTCTGGAGGTCTCAT AACTTGGAC-3′; reverse; 5′- TGCCAAAGTATTCCATA TCCAGGTA-3′.

Bulk mRNA Sequencing and Analysis

Paired-end RNA sequences were processed with AdapterRemoval (v. 2.1.3) (Lindgreen, 2012), setting the minimum quality to 20, minimum length to 25, collapsing reads when possible and removing Nextera adapters. The first seven base pairs were removed them using seqtk (v. 1.0). For each sample, files with collapsed and singleton reads were aligned to the mouse genome (Ensembl GRCm38.84) using HISAT2 (v. 2.0.1) (Kim et al., 2019). Gene expression profiles were generated using HTSeq (v. 0.11.1) (Anders et al., 2015) with default settings. For each group, genes that had >50 raw counts in >2 samples in either the wildtype- or the knockout condition were included in the analysis. Differential expression analyses were performed in R (R Core Team, 2018) using the edgeR package (McCarthy et al., 2012). Normalization factors were calculated using the trimmed mean of M-values (TMM) method. The edgeR general linear model was used for the differential expression analysis. Differentially expressed genes with a false discovery rate of <5% were considered statistically significant.

Statistical Analysis

Data were analyzed with Prism version 6.0 (GraphPad Software). Analysis of statistical significance was done using one-way ANOVA with Kruskal-Wallis multiple comparison test for tree or more groups, or Mann-Whitney U test for two unpaired groups. Differences were considered significant when $p \leq 0.05$ (*p≤0.05, **p<0.01and ***p<0.001).

RESULTS

Reduced GC B Cell Response in Ifnar1$^{-/-}$ Mice Involves Loss of Both IgG1^{+} and IgG2c^{+} GC B Cells

To determine how type I IFNs affect GC B cell differentiation at the level of individual IgG subclasses, *Ifnar1*$^{-/-}$ mice were immunized i.p. with OVA and poly I:C. To visualize concurrent CD4 T cell responses (see below), mice received 5000 CD45 congenic OT-II cells. Thus, all cells are unable to respond to type I IFNs in these recipients except for a small and physiologically relevant number of antigen-specific CD4 T cells. The percentage and number of GC B cells were similar between unimmunized wt and *Ifnar1*$^{-/-}$ mice (**Figures 1A, B** and **Suppelementary Figure S1**), in line with reports of an important role for B cell IFN-γ receptor signaling, and not type I IFNs, in driving spontaneous GC formation in wt C57BL/6 mice (37, 38). When analyzed 3 days after immunization, neither wt nor *Ifnar1*$^{-/-}$ mice had mounted a GC B cell response exceeding the pre-existing GC B cell numbers (**Figure S1**). Eight days after immunization, a strong splenic GC B cell response had developed in wt mice (**Figures 1A, B**). Such response was however not evident in immunized *Ifnar1*$^{-/-}$ mice (**Figures 1A, B**). Furthermore, the absence of increased GC B cell numbers eight days after immunization in these mice was not merely due to delayed kinetics in the absence of type I IFN signaling, as numbers of GC B cells remained unchanged relative to unimmunized *Ifnar1*$^{-/-}$ controls 14 days after immunization (**Suppelementary Figure 1**).

The response induced by immunization of wt mice involved similar numbers of IgG1^{+} and IgG2c^{+} GC B cells (**Figures 1C–E** and **Suppelementary Figure S1**). Due to the robust magnitude of this response, pre-existing GCs made a very small and negligible contribution to the isotypes expressed by GC B cells in immunized wt mice. In *Ifnar1*$^{-/-}$ mice, we observed a significantly increased percentage of IgG1^{+} GC B cells after immunization (**Figure 1C, D** and **Suppelementary Figure S1**), indicating that an IgG1^{+} GC B cell response to some extent had developed also in the absence of type I IFN signaling. However, in this set of experiments we could not detect a corresponding increase in the number of IgG1^{+} GC B cells (**Figure 1D** and **Suppelementary Figure S1**). In contrast to IgG1, there was no significant increase in either percentage or number of IgG2c^{+} GC B cells in immunized as compared to non-immunized *Ifnar1*$^{-/-}$ mice (**Figures 1C, E** and **Suppelementary Figure S1**). Finally, the impairment of the antigen-specific GC B cell response in *Ifnar1*$^{-/-}$ mice was confirmed by OVA staining of GC B cells at day 14 (**Figures 1F, G**).

The majority of antigen-specific plasma cells (PCs) present in spleen around eight days after immunization are thought to be derived from GCs (39). The total number of splenic OVA-binding CD138^{+} PCs was approximately 10-fold lower in *Ifnar1*$^{-/-}$ compared to wt mice (**Figures 1H, I**), and both IgG1- and in particular IgG2c-producing cells were affected (**Figure 1J**). In addition, the few IgG1^{+} PCs present in *Ifnar1*$^{-/-}$ mice appeared to produce antibodies of lower affinity than their counterparts in wt animals, as indicated by a reduced percentage of OVA-binding IgG1 PC binding high levels of OVA in these mice (**Suppelementary Figure S1**). These results were further corroborated by serological studies where *Ifnar1*$^{-/-}$ mice essentially failed to mount an NP-specific IgG2c response after administration of NP-conjugated OVA plus poly I:C whereas their NP-specific IgG1 titers were reduced only 6.9- and 4.2-fold at two and four weeks after immunization, respectively (**Figure 1K, L**). Antigen-specific IgG1 titers however then declined more rapidly in the *Ifnar1*$^{-/-}$ mice and after one year they had an almost 80-fold lower NP-specific IgG1 titer than wt controls, indicating that the longevity of the specific IgG1 response was affected in the absence of type I IFN signaling (**Figure 1K**). Collectively these results demonstrate that type I IFNs are essential for GC formation induced by poly I:C, affecting both the quantity and quality of the response and, moreover, demonstrate that type I IFN signaling promotes the generation of both IgG1^{+} and, in particular, IgG2c^{+} GC B cells.

Tfh Cells and IFN-γ Producing Th1 Cells Develop Concurrently in Response to Poly I:C and Are Both Reduced in *Ifnar1*$^{-/-}$ Mice

We have previously shown that early Tfh cell fate commitment is reduced in *Ifnar1*$^{-/-}$ mice (as assessed three days after immunization) (16). To assess the relationship between Tfh and Th1 cell development, and to determine how type I IFN impacts on the accumulation of these subsets at the peak of the GC reaction eight days after immunization, we analyzed transferred OT-II cells in the same cohorts of mice as

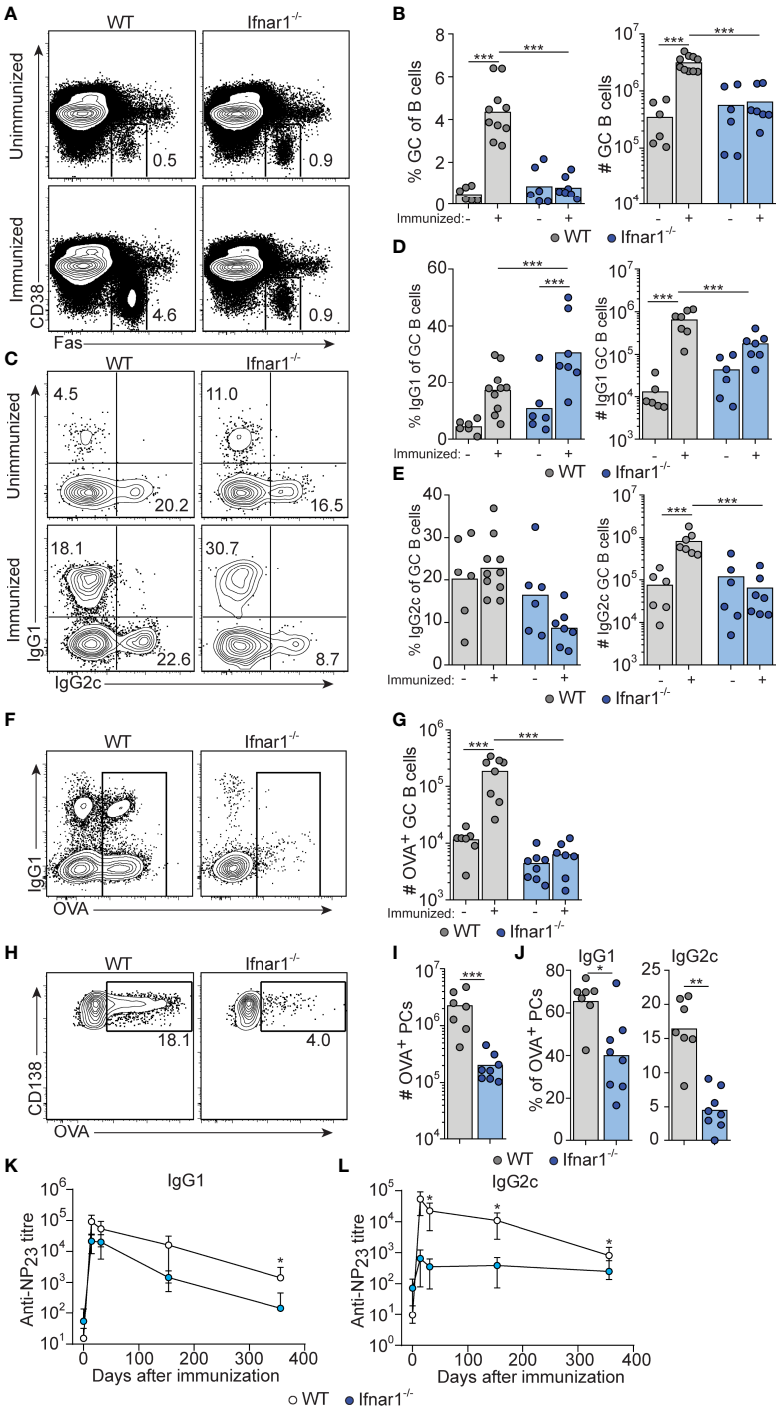

FIGURE 1 | Attenuated GC B cell responses in *Ifnar1*$^{-/-}$ mice. WT or *Ifnar1*$^{-/-}$ mice were transferred with 5000 OTII cells and immunized with OVA/poly I:C **(A–J)** or NP-OVA/poly I:C **(K, L)**. **(A–J)** Flow cytometry analysis of splenocytes 8 days **(A–E** and **H–J)** or 14 days **(F, G)** after immunization. **(A, B)** Analysis of GC B cells after gating on total B cells (CD4$^-$ B220$^+$). Representative plots **(A)** and pooled results of percentages and numbers of GC B cells **(B)** are shown. **(C–E)** IgG subclass distribution among GC B cells. Representative contour plots of IgG1 versus IgG2c expression **(C)** and pooled results of percentages and numbers of IgG1$^+$ **(D)** and IgG2c$^+$ **(E)** GC B cells are shown. **(F, G)** OVA-binding GC B cells. Representative contour plots of binding of OVA-Alexa647 versus IgG1 expression after gating on GC B cells **(F)** and pooled results of numbers of OVA-binding GC B cells **(G)** are shown. **(H–J)** OVA-binding PCs. Representative contour plots showing intracellular binding of OVA-Alexa647 after gating on B220^{low} CD138$^+$ PCs **(H)**, and pooled results of total number **(I)** and percentage of IgG1$^+$ or IgG2c$^+$ **(J)** OVA-binding PCs. Results are pooled from three **(A–E, H–J)** or two **(F, G)** individual experiments and symbols represents individual mice. **(K, L)** Serum titers of NP_{23}-specific IgG1 **(K)** and IgG2c **(L)**, before and indicated time points after immunization. Results obtained from one experiment where mice (n=6 per group) were monitored over one year period of time. *p≤0.05, **p<0.01 and ***p<0.001.

described above. *Ifnar1*$^{-/-}$ mice had fewer total OT-II cells in their spleens as compared to wt controls, confirming that type I IFNs enhance expansion and survival of activated CD4^{+} T cells (40, 41) (**Figure 2A**). Furthermore, Tfh cells were additionally affected in the *Ifnar1*$^{-/-}$ mice, as evident from a significantly reduced percentage of CXCR5^{high} Bcl6^{+} OT-II cells (**Figures 2B, C**). T-bet drives Th1 cell differentiation and is required for IFN-γ expression by CD4^{+} T cells (42). OT-II cells with detectable T-bet expression were confined to the Bcl6^{-} subset in the wt animals and in agreement with previously published results (31) IFN-γ expression was essentially lost in the *Ifnar1*$^{-/-}$ recipients, as was expression of T-bet (**Figures 2D–G**). Collectively, these results show that Tfh cells and IFN-γ producing Th1 cells exist as mutually exclusive subsets at the peak of the GC reaction and that both subsets depend on type I IFNs for their development.

Early IFN-γ Derived From Cognate CD4+ T Cells Acts Directly on B Cells to Drive IgG2c CSR Without Enhancing the Overall Magnitude of the GC B Cell Response

IFN-γ represents a well-established *in vitro* switch factor for the IgG2a/c subclass (43). B cell intrinsic IFN-γ signaling can also underlie GC formation in murine autoimmune models (37, 38). To

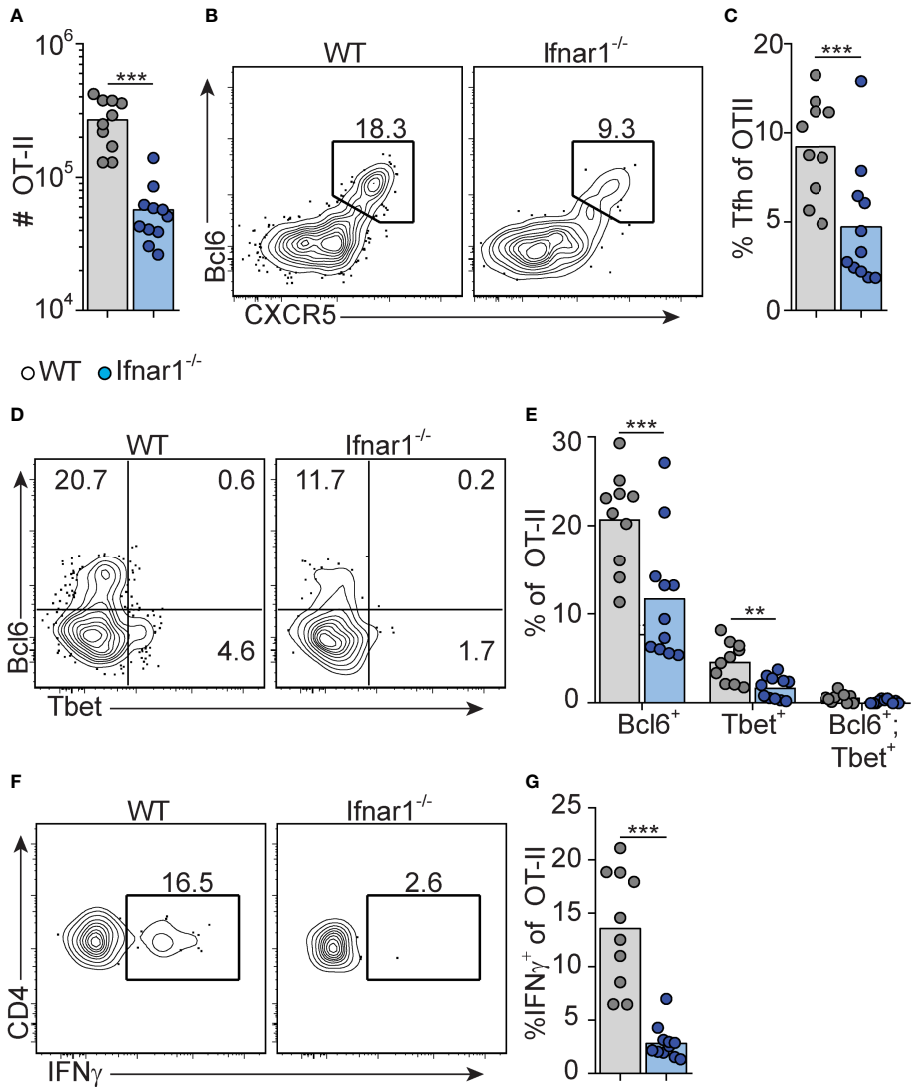

FIGURE 2 | Type I IFN signaling augments Tfh and is required for Th1 cell differentiation. WT and *Ifnar1*$^{-/-}$ mice were transferred with 5000 OT-II cells and immunized with OVA/pI:C. Donor B220^{-} CD4^{+} CD45.2^{+} OT-II cells in spleens were analyzed by flow cytometry 8 dpi. **(A)** Number of OT-II cells. **(B, C)** Quantification of CXCR5^{+}Bcl6^{+} Tfh cells. Representative contour plots **(B)** and pooled results of percentages of Tfh cells **(C)**. **(D, E)** Analysis of Bcl6 versus T-bet expression. Representative contour plots **(D)** and pooled results of percentages of OT-II cells displaying single- or co-expression of Bcl6 and T-bet, respectively. **(F, G)** IFN-γ expression. Representative contour plots **(F)** and pooled results of percentage of OT-II cells expressing IFN-γ **(G)**. Results are pooled from three individual experiments and each symbol represents one mouse. **p<0.01 and ***p<0.001.

determine the role of B cell intrinsic IFN-γ signaling in the GC B cell response driven by OVA/poly I:C, we made mixed bone marrow (BM) chimeric mice. Irradiated wt mice were grafted with wt BM (CD45.1$^+$, CD45.2$^+$) mixed with *Ifngr1*$^{-/-}$ or wt control BM (both CD45.2 single positive) at a 1:1 ratio. Analysis of splenocytes eight days after immunization showed that GC B cells developed equally well from *Ifngr1*$^{-/-}$ and wt B cells (**Figures 3A, B**), demonstrating that IFN-γ signaling in B cells is not involved in the type I IFN dependent GC B cell expansion. In contrast, CSR to IgG2c was strongly reduced in the *Ifngr1*$^{-/-}$ as compared to wt GC B cells present in the same mouse (**Figures 3A, B**). In agreement with the ability of IFN-γ to inhibit CSR to IgG1 and IgE (29, 43), the impaired IgG2c CSR in *Ifngr1*$^{-/-}$ B cells was compensated by an increased percentage of IgG1$^+$ GC B cells (**Figures 3A, B**). Given that IL-27 represents an additional IgG2a/c switch factor (44) and can be produced by myeloid cells in response to type I IFNs (45, 46), we performed analogous experiments with mixed wt/*Il27ra*$^{-/-}$ BM chimeras. These experiments did not reveal any significant differences between wt and *Il27ra*$^{-/-}$ B cells (**Suppelementary Figures S2A, B**).

To determine if IFN-γ from cognate CD4$^+$ T cells is sufficient for driving IgG2c CSR in B cells, we transferred IFN-γ sufficient or deficient OT-II cells into *Ifng*$^{-/-}$ mice and again evaluated the splenic response eight days after immunization. IFN-γ-deficient OT-II cells supported a GC B cell response of a comparable magnitude as their wt counterparts (**Figure 3C**). However, compared to mice receiving wt OT-II cells, recipients of *Ifng*$^{-/-}$ OT-II cells developed GCs with a strong and selective reduction in IgG2c, again compensated by an increase in IgG1 (**Figure 3D, E**). These experiments thus demonstrate an important role for IFN-γ derived from cognate CD4$^+$ T cells in stimulating IgG2c CSR, but not for enhancing the overall magnitude of the GCs.

IFN-γ producing Tfh cells have been suggested to underpin IgG2a/c CSR within GCs (47). Given that Tfh cells largely lacked expression of T-bet at the peak of the poly I:C driven GC response (see **Figures 2D, E**), we considered the possibility that IFN-γ stimulates IgG2c CSR at an earlier stage and before evident GC formation. To assess this, we injected an IFN-γ neutralizing antibody either before or 72 hours after immunization. Regardless of the timing, this treatment had no impact on the percentage of total GC B cells detected eight days after immunization and staining with fluorescently labeled OVA confirmed an equal percentage of OVA-specific GC B cells in both experimental groups and in mice receiving an isotype control mAb (**Figures 3F–H**). However, treatment with anti-IFN-γ before immunization resulted in significantly fewer OVA-specific GC B cells expressing IgG2c as compared to isotype control treated mice (**Figure 3I, J**). This reduction was again reciprocated by an increased percentage of cells expressing IgG1 (**Figures 3I, J**). No such effects on the IgG subclass distribution were observed when treatment with anti-IFN-γ instead was started 72 hours after immunization (**Figures 3I, J**). Accordingly, IFN-γ acts on B cells within the first 72 hours after immunization and prior to GC formation to initiate the IgG2c CSR process and thereafter appears to be redundant for the IgG2c associated GC B cell response.

B Cell Intrinsic Type I IFN Signaling Acts in Synergy With Type I IFN Dependent IFN-γ to Select the IgG2c Subclass

The finding that B cell intrinsic IFN-γ signaling involved in IgG2c CSR precedes GC formation predicts that 1) type I IFN dependent priming of IFN-γ producing Th1 cells also occurs early in the response and 2) cognate IFN-γ producing CD4 T cells appear earlier than detectable GCs. To test the first prediction, we neutralized type I IFN signaling by injecting an anti-IFNAR1 mAb either 16 hours before or 24 hours after immunization. Neutralization of type I IFN signaling before, but not after, immunization inhibited OT-II cell expansion, Tfh cell differentiation and IFN-γ production as assessed eight days after immunization (**Figures 4A–C**). Consistent with the reduced number of Tfh cells, the overall magnitude of the GC B cell response was reduced when anti-IFNAR1 treatment preceded immunization (**Figure 4D**). Additionally, the numbers of IgG2c$^+$ GC B cells were reduced after early but not late IFNAR1 blockade (**Figure 4E**). The type I IFN dependent signaling events that underlies Th1 development and IFN-γ dependent IgG2c CSR are therefore initiated during the first 24 hours of the poly I:C driven response.

To confirm that IFN-γ producing Th cells appear within the first 72 hours post-immunization, and to verify their dependence on upstream type I IFN signaling, we analyzed early Th cell differentiation in wt and *Ifnar1*$^{-/-}$ mice, respectively. IFN-γ producing OT-II cells were indeed detectable in wt mice 3 days after administration of OVA and poly I:C and the IFN-γ response was reduced in the *Ifnar1*$^{-/-}$ mice also at this earlier time point (**Figure 4F**). This correlated with significantly less T-bet protein in OT-II cells recovered from the *Ifnar1*$^{-/-}$ recipients (**Figures 4G, H**). Likewise, and as reported earlier (16), a reduction in OT-II cell Bcl6 expression was also evident already at this early stage in the *Ifnar1*$^{-/-}$ mice (**Figures 4G, H**). OT-II cells recovered from wt animals did however not express T-bet and Bcl6 in a mutually exclusive manner (**Figure 4G**), indicating the absence of clear Th1 versus Tfh cell dichotomy three days after immunization. Based on these results we conclude that type I IFNs drive development of the IFN-γ producing CD4 T cells that underpin IgG2c CSR within the first few days after immunization, prior to evident GC formation and appearance of fully committed Th1 and Tfh cells.

To determine how and to what extent direct type I IFN signaling in B cells influences the GC B cell response and IgG subclass selection after immunization with OVA/poly I:C, we again generated mixed BM chimeras, now by reconstituting irradiated wt mice with a 1:1 mix of wt with *Ifnar1*$^{-/-}$ or wt (control) BM. Analysis of immunized chimeric mice revealed that *Ifnar1*$^{-/-}$ B cells contributed to the GC B cell response to a lesser extent than IFNAR sufficient B cells present in the same animal. In this competitive setting, there was an approximately 2-fold lower number of *Ifnar1*$^{-/-}$ than wt GC B cells in the spleen (**Figure 5**). Strikingly, this reduction was mostly caused by a loss in IgG2c$^+$ and IgG2b$^+$ GC B cells; the frequency of GC B cells expressing either of these IgG subclasses was approximately 2-fold lower in the *Ifnar1*$^{-/-}$ than wt compartment of the same

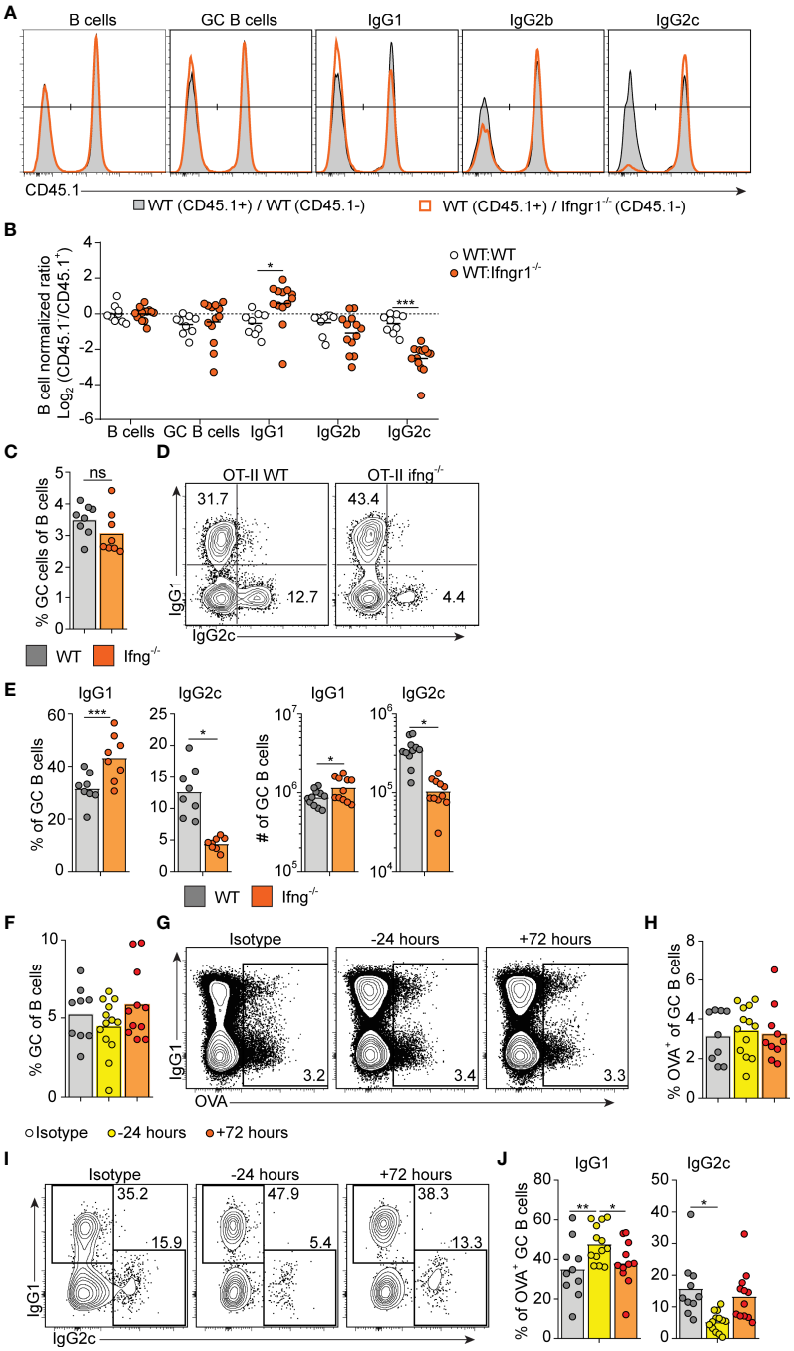

FIGURE 3 | Early IFN-γ derived from cognate CD4 T cells acts on B cells to drive IgG2c CSR. **(A, B)** Mixed BM chimeras were generated by reconstituting WT recipients with a 1:1 mix of CD45.1$^+$ CD45.2$^+$ WT and CD45.1$^-$ CD45.2$^+$ WT or *Ifngr1*$^{-/-}$ BM cells. Eight - 10 weeks after reconstitution, chimeras were immunized with OVA/poly I:C and the proportion of CD45.1$^+$ versus CD45.1$^-$ cells among total splenic B cells and within indicated GC B cell population determined by flow cytometry 8 dpi. **(A)** Representative results for control (WT : WT) and experimental (WT : *Ifngr1*$^{-/-}$) BM chimeras. **(B)** Pooled results of $\log_2$ normalized CD45.1$^-$ to CD45.1$^+$ cell ratio in individual control and experimental chimeric animals. **(C–E)** *Ifng*$^{-/-}$ mice were transferred with 50 000 WT or *Ifng*$^{-/-}$ OT-II cells and immunized with OVA/poly I:C. Splenocytes were analyzed by flow cytometry 8 days later. **(C)** Percentage of GC B cells of total B cells. **(D, E)** IgG subclass expression by GC B cells. Representative contour plots **(D)** and pooled results of percentages and numbers of IgG1$^+$ and IgG2$^+$ GC B cells **(E)**. **(F–J)** WT mice were treated i.p. with 1 mg anti-IFN-γ mAb or isotype control 16 hrs before or 72 hrs after immunization with OVA/poly I:C. Mice were transferred with 50 000 OT-II cells 16 hrs before immunization and splenocytes were analyzed 8 dpi. **(F)** Percentage GC B cells of total B cells. **(G, H)** Analysis of OVA-binding by GC B cells. Representative flow cytometry results of OVA-Alexa647 fluorescence versus IgG1 expression **(G)** and pooled results of percentages of OVA$^+$ GC B cells **(H)**. **(I–J)** IgG subclass expression by OVA$^+$ GC B cells. Representative contour plots **(I)** and pooled results of percentages IgG1$^+$ and IgG2$^+$ GC B cells **(J)**. Pooled results from two **(C–E)** or three **(A, B, F–J)** experiments are shown. Each symbol represents one mouse. ns = not significant, *p≤0.05 and **p<0.01.

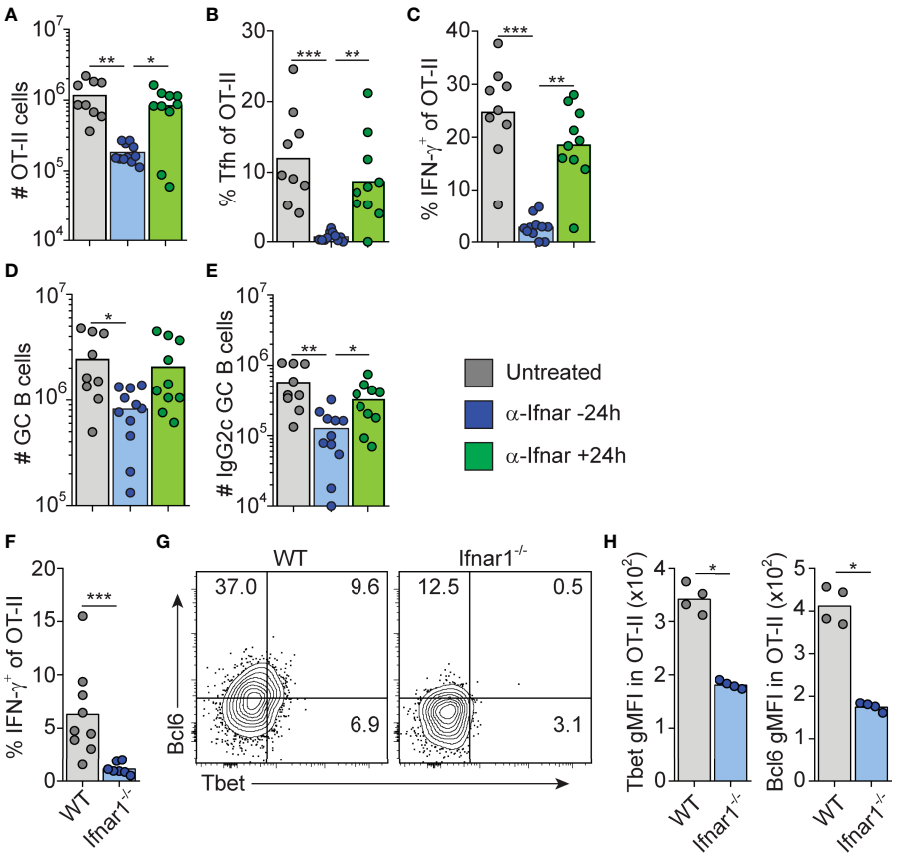

FIGURE 4 | Type I IFN signaling drives Tfh and Th1 cell differentiation within the first 24 hrs after immunization. **(A–E)** WT mice transferred with 50000 OT-II cells were treated i.p. with 1 mg anti-IFNAR1 or isotype control mAb 16 hrs before or 24 hrs after immunization with OVA/pI:C. Splenocytes were analyzed by flow cytometry 8 dpi. **(A)** Number of OT-II cells. **(B)** Percentage of Tfh cells of total OT-II cells. **(C)** Percentage of IFN-γ$^+$ cells of total OT-II cells. **(D)** Number of GC B cells. **(E)** Number of IgG2c$^+$ GC B cells. **(F–H)** WT and *Ifnar1*$^{-/-}$ mice were transferred with 500 000 OT-II cells and donor cells in spleen analyzed by flow cytometry 3 days after immunization with OVA/poly I:C. **(F)** Percentage of IFN-γ$^+$ cells of total OT-II cells. **(G–H)** Analysis of T-bet versus Bcl6 expression with representative contour plots **(G)** and geometric mean fluorescence intensity (GMFI) for T-bet and Bcl6, respectively. Individual mice and mean values **(A–F)** or representative results **(G–H)** of three independent experiments are shown. *p≤0.05, **p<0.01 and ***p<0.001.

chimeric animal. Altogether, these results show that type I IFN augments the IgG2c$^+$ and IgG2b$^+$ GC B cell response through direct signaling in B cells and that, in contrast to IFN-γ, this effect goes beyond CSR and enhances the overall magnitude of the GC B cell response.

Absence of B Cell Intrinsic Type I or Type II IFN Signaling Has Limited Effects on the Core GC B Cell Transcriptional Program but Results in Reduced T-Bet Expression and Altered Isotype Composition

Given the direct effect of both type I and type II IFN signaling, we next investigated how the respective IFN family influences the global transcriptional program of B cells within established GC. WT and IFN receptor deficient splenic GC B cells were thus sorted eight days after immunization from the same mixed BM chimeric mice described in **Figures 3**, **5**. Bulk mRNA sequencing analysis was preformed to generate datasets comparing gene expression in WT and *Ifnar1*$^{-/-}$ GC B cells or WT and *Ifngr1*$^{-/-}$ GC B cells, respectively.

To determine if IFN signaling had altered the core GC B cell program, we first compared these sequencing datasets to the transcriptional changes in GC B cell compared to naïve follicular B cells described in Shi et al. (48). We found that the GC B cell transcriptional signature was largely intact in the absence of either type I or type II IFN signaling (**Suppelementary Figures S3A, B**). Key GC B cell transcriptional changes, including mRNA encoding core transcription factors (*Bcl6* and *Bach2*), proteins involved in the somatic hypermutation program (*Aicda* and *Polh*), as well as proteins directing migration and localization of the B cells to the GC (*Sipr2*, *Gpr183*), were unaffected by the loss of B cell intrinsic IFN signaling. This suggests that type I IFN or IFN-γ signaling in B cells is not critical for the GC B cell program. We also compared our IFNAR dataset to the early type I IFN induced transcriptional changes in follicular B cells described by Mostavi et al. (49). Out of 71 genes that showed statistically significant differences in expression with at least a 2-

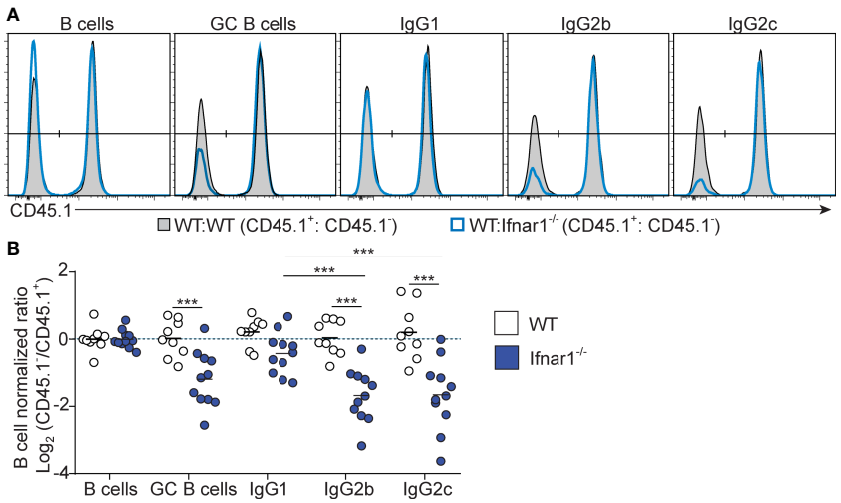

FIGURE 5 | B cell intrinsic type I IFN signaling selectively amplifies the magnitude of IgG2$^+$ GC B cell responses. Mixed BM chimeras were generated by reconstituting WT recipients with a 1:1 mix of CD45.1$^+$ CD45.2$^+$ WT and CD45.1$^-$ CD45.2$^+$ WT or *Ifnar1*$^{-/-}$ BM cells. Eight - 10 weeks after reconstitution, chimeras were immunized with OVA/poly I:C and the proportion of CD45.1$^+$ versus CD45.1$^-$ cells among total splenic B cells and within indicated GC B cell population determined by flow cytometry 8 dpi. **(A)** Representative results for control (WT : WT) and experimental (WT : *Ifnar1*$^{-/-}$) BM chimeras. **(B)** Pooled results of $\log_2$ normalized CD45.1$^-$ to CD45.1$^+$ cell ratio in individual control and experimental chimeric animals. Results are from three individual experiments. Each symbol represents one mouse. *p≤0.05, **p<0.01 and ***p<0.001.

fold change after IFN injection, only six were dysregulated in GC B cells at day eight after immunization with OVA and poly I:C (**Suppelementary Figure S3C**). This suggests that while a part of the IFN signature may be robustly conserved after IFN signaling has stopped, a majority of the IFN dependent transcriptional changes are transient.

For both the IFNAR and IFNGR dataset, we filtered genes that displayed at least a 2-fold and statistically significant difference in expression between the WT and IFN receptor deficient cells (**Figures 6A, B**). By this approach, both cytokine families were found to influence a relatively limited number of genes, with only 87 and 72 genes being affected by type I IFN and IFN-γ signaling, respectively (**Figure 6C**). While the type I and type II IFN gene expression signatures have been difficult to separate when assaying peripheral blood during infections or in autoimmunity (50, 51), only seven genes were found to be dysregulated in both the IFNAR and IFNGR datasets. Of these, upregulation of three genes, (*Ctse, Tbx21, and Igh2c*) were dependent on both IFNAR and IFNGR signaling. The downregulation of these genes in IFN receptor deficient B cells was confirmed by qrt-PCR analysis from the same sorted GC B cell populations (**Figures 6D, E**). This suggests that B cell intrinsic type I IFN and IFN-γ signaling predominately affect different aspects of the GC B cell response but that the two pathways synergize to control class switching to IgG2c, likely through the induction of *Tbx21* (22). In addition to IgG2c, the differential gene expression identified in the two data sets indicated that both type I IFN and IFN-γ signaling in B cells affect the expression of other Ig isotypes. While both may have a small impact on IgG2b expression, we found type I IFN signaling to be associated with increased *Ighg3* mRNA expression. IFN-γ signaling was instead required for optimal *Igha* expression. Thus, while type I IFN and IFN-γ signaling collaboratively support switching to IgG2c, and possibly IgG2b, they may have unique roles in controlling switching to other isotypes.

IFNAR on Non-Hematopoietic Cells and Cognate CD4 T Cells Is Dispensable for Th1 and Tfh Cell Differentiation After Poly I:C Adjuvanted Immunization

Given that type I IFNs are required for optimal generation of both Tfh and Th1 cells in poly I:C/OVA immunized mice, we next set out to determine the cellular targets for type I IFN signaling in the respective differentiation pathways. To this end we co-transferred CTV-labeled wt and *Ifnar1*$^{-/-}$ OT-II cells into BM chimeras, lacking IFNAR in either the hematopoietic, the non-hematopoietic (radio resistant) or both cell compartments. Cell cycle dependent dilution of CTV was examined three days after immunization (**Figures 7A–C**). The ability of type I IFNs to enhance CD4 T cell proliferation tracked with IFNAR expression by the BM donor cells (i.e. hematopoietic non T cell-intrinsic), likely reflecting the ability of type I IFNs to improve the antigen-presenting function and co-stimulatory capacity of APCs (16, 31, 52, 53). No change in CTV dilution was observed when comparing wt and *Ifnar1*$^{-/-}$ OT-II cells or wt and *Ifnar1*$^{-/-}$ irradiated recipient mice, demonstrating that T cell-intrinsic type I IFN signaling or signaling in radio resistant cells has no impact on early T cell proliferation under these conditions. The ability of type I IFNs to enhance Th1-associated T-bet and IFN-γ (**Figures 7D, E**) as well as Tfh cell associated Bcl6 and CXCR5 (**Figures 7F, G**) expression was also mostly a result of IFNAR

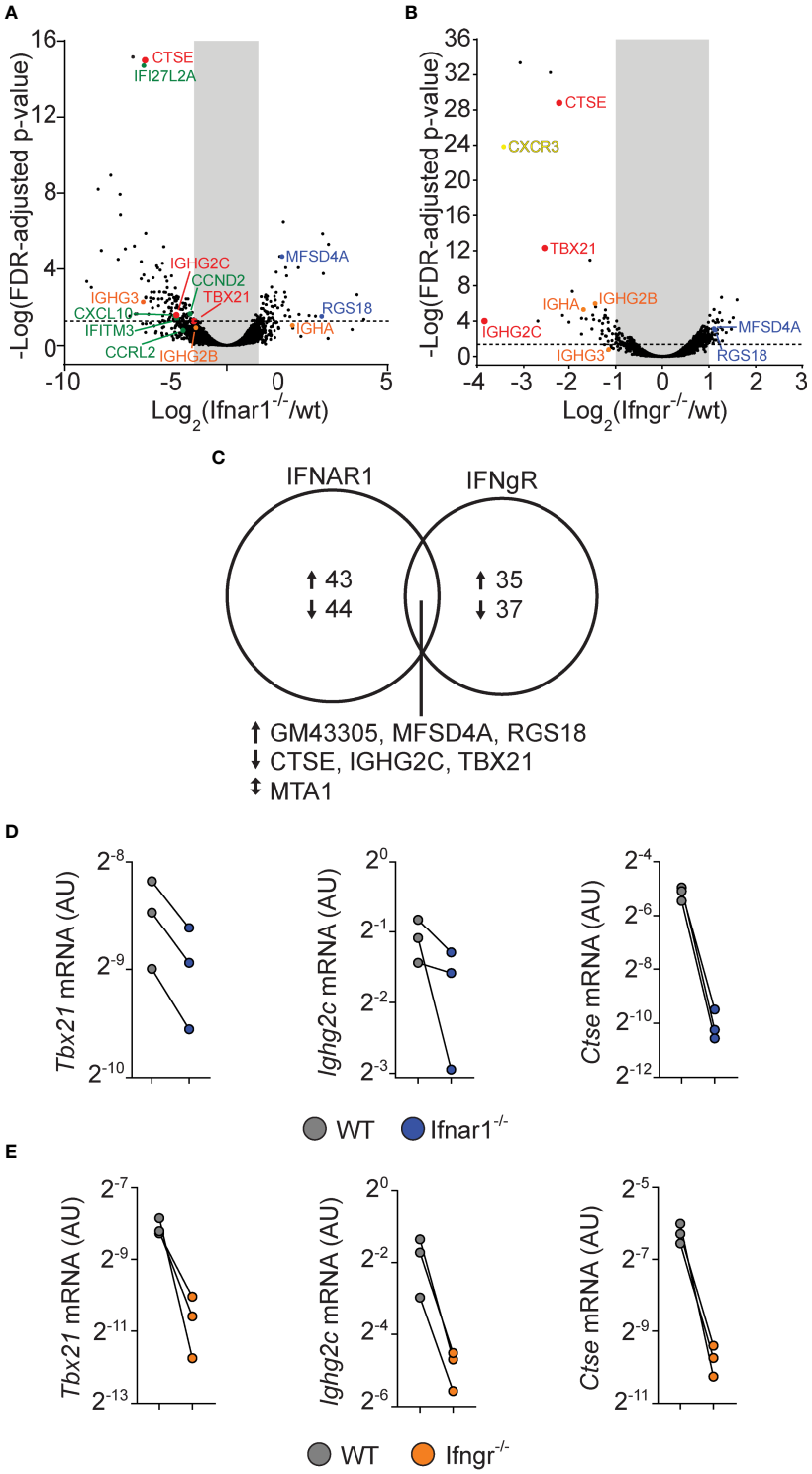

FIGURE 6 | B cell intrinsic type I and type II signaling confers largely non-overlapping gene expression programs in GC B cells but co-regulate enhanced *Tbx21* and *Ighg2c* expression. WT and gene-targeted GC B cells were separately sorted from the WT : *Ifngr1*$^{-/-}$ and WT: *Ifnar1*$^{-/-}$ mixed BM chimeras described in figures 3 and 5, respectively, and processed gene expression analysis. **(A–C)** mRNA sequencing results. **(A, B)** Volcano plots of changes in gene expression between WT and *Ifnar1*$^{-/-}$ **(A)** or *Ifngr1*$^{-/-}$ **(B)** GC B cells. **(C)** Venn diagram showing all genes with >2-fold change and FDR < 0.05 when comparing WT and *Ifnar1*$^{-/-}$ or *Ifngr1*$^{-/-}$ GC B cells. The genes regulated by both type I and type II IFN signaling in GC B cells are listed below the diagram. **(D, E)** Quantitative rt-PCR analysis of gene expression in *Ifnar1*$^{-/-}$ **(D)** and *Ifngr1*$^{-/-}$ **(E)** GC B cells of genes identified by mRNA sequencing to rely on both type I and type II IFN B cell intrinsic signaling. Results are from three individual mice.

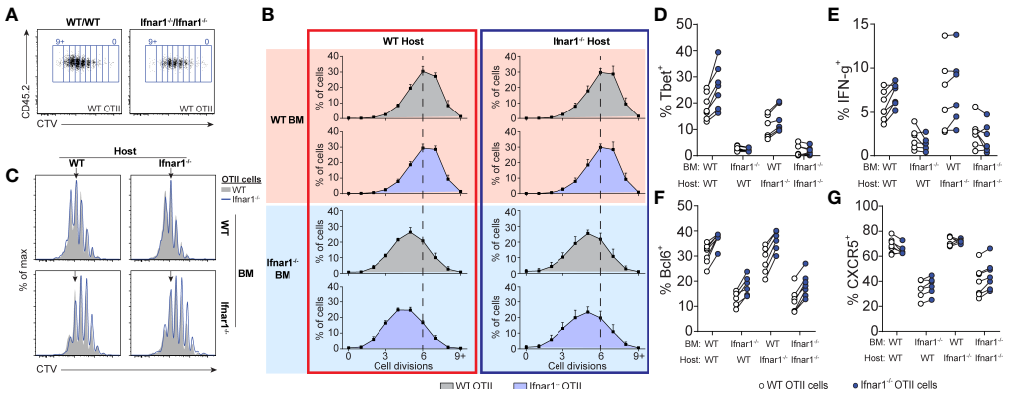

FIGURE 7 | Tfh- and Th1-cell development is supported by IFNAR-signaling in hematopoietic cells distinct from cognate CD4 T cells. Equal numbers (250 000) of CTV-labelled WT and *Ifnar1*$^{-/-}$ OT-II cells were co-transferred into *Ifnar1*$^{-/-}$ BM chimeric recipient mice and spleens were analyzed 3 days after immunization with OVA/poly I:C. **(A)** Representative CTV dot plots showing gating strategy of OT-II cells from mice receiving either WT or *Ifnar1*$^{-/-}$ BM. **(B)** Representative CTV profiles of OT-II cells from all experimental groups. Arrows indicate median division in the full WT group. **(C)** Percentages (mean ± SD) of OT-II cells in indicated cell cycle number as determined by CTV-dilution. Verticle lines indicate median division in the full WT group. **(D–G)** Percentage of T-bet^{+} **(D)**, IFN-γ^{+} **(E)**, Bcl6^{+} **(F)**, and CXCR5^{+} **(G)** WT and *Ifnar1*$^{-/-}$ OT-II cells, respectively. Results are pooled from two individual experiments consisting of a total of 6-7 mice per group. Each pair of symbols represents one mouse **(D–G)**.

expression on the BM donor cells. However, both T-bet and Bcl6 expression was slightly higher in *Ifnar1*$^{-/-}$ than wt OT-II cells, indicating that type I IFNs to some extent can counteract both Th1 and Tfh cell development through direct effects on T cells (**Figures 7D, F**). These effects were however subdominant to the enhanced T-bet and Bcl6 expression driven by T cell extrinsic type I IFN signaling in hematopoietic cells. In conclusion, these results indicate that IFNAR on cognate CD4 T cells or in the non-hematopoietic cell compartment is redundant for both Th1 and Tfh cell fate commitment and hence unlikely to have a major impact on the GC B cell response through these pathways.

Type I IFN Signaling in cDCs Orchestrates IgG Subclass Specific GC B Cell Differentiation Through IL-4-Secreting Tfh and IFN-γ υ> Producing Th1 Cells

We have previously demonstrated a reduction in early Tfh cell differentiation in CD11c-cre.*Ifnar1*$^{fl/fl}$ mice with deletion of *Ifnar1* in cDCs (16). Although CD11c expression can be induced also in GC B cells approximately two days after immunization (54, 55), we found no alteration in early Tfh cell development in CD19-cre.*Ifnar1*$^{fl/fl}$ mice with specific deletion in B cells in our previous study (16). Combined with the results in the current study, showing that the poly I:C driven GC B cell response is influenced by type I IFN signaling only during the first 24 hours after immunization, this lead us to revisit the CD11c-cre.*Ifnar1*$^{fl/fl}$ model to determine how deletion of *Ifnar1* in cDCs impacts on the IgG subclass composition within GCs. In particular, while the results presented so far reveal how B cell intrinsic type I IFN signaling acts in synergy with the switch factor IFN-γ, produced from cognate CD4 T cells, to enhance IgG2c associated GC B cell responses, it was still unclear why IgG1^{+} GC B cells also are strongly reduced in the complete IFNAR knockout (see **Figure 1**). Selection of the IgG1 subclass is promoted by IL-4 (43) and within secondary lymphoid organs IL-4 secreting T cells are largely confined to the Tfh cell subset (47, 56). To visualize active secretion of IL-4 from cognate CD4 T cells, we intercrossed the OT-II strain with KN2 mice, reporting IL-4 secretion through expression of membrane anchored human CD2 (34). Similar to OT-II cells activated in wild type C57Bl/6 recipients (see **Figure 2D**), donor KN2-OT-II cells developed into mutually exclusive Th1 (T-bet^{+}) and Tfh (Bcl6^{+}) cell subsets eight days after immunization of *Ifnar1*$^{fl/fl}$ control mice (hereafter referred to as Cre^{-} control mice) while in *CD11c-Cre.Ifnar1*$^{fl/fl}$ mice both subsets were significantly reduced in frequency and number (**Figures 8A–C**). In the Cre^{-} control group, active IL-4 secretion was largely confined to the Bcl6^{+} Tfh cells and although their capacity to produce IL-4 appeared to be at least partially maintained in *CD11c-Cre.Ifnar1*$^{fl/fl}$ recipients (**Figures 8D, E**), the number of IL-4 secreting Tfh cell was dramatically reduced due to the overall weakened Tfh cell response in these mice (**Figure 8F**). Consistent with the impaired generation of T-bet^{+} Th1 cells, IFN-γ producing OT-II cells were also strongly diminished in *CD11c-Cre.Ifnar1*$^{fl/fl}$ mice (**Figure 8G**). Collectively, these results demonstrate a bifunctional effect of type I IFN signaling in cDCs to promote the appearance of separable IFN-γ producing Th1 and IL-4 producing Tfh cell subsets.

Similar to the complete *Ifnar1* knockout, the expansion of GC B cells was strongly reduced after immunization of *CD11c-Cre.Ifnar1*$^{fl/fl}$ mice compared with their Cre^{-} controls (**Figure 8H**). The requirement for IFNAR-expressing cDC was equally evident when analyzing the number of OVA-binding GC B cells in the two groups of mice, confirming that the reduction in GC B cells was related to the immunization rather than differences in pre-existing GC B cell numbers (**Figures 8I, J**). In marked contrast to when B cells specifically lack IFNAR, the

reduced GC B cell response in the absence of IFNAR expressing cDCs was not caused by a selective loss of IgG2c expressing GC B cells; $IgG1^+$ GC B cells were now at least equally affected, again confirmed by analysis of OVA-binding GC B cells (**Figures 8K, L**).

To determine if IFNAR signaling in cDC1 was required for any of the effects that type I IFNs have on Th1, Tfh and GC B cell differentiation, we immunized *XCR1-cre.Ifnar1*$^{fl/fl}$ mice (35) as above and examined the OT-II cell response (**Suppelementary Figures S4A, B**). No difference in OT-II cell expansion or differentiation to Th1 and Tfh cells was observed at day 8 post-immunization. Similarly, no effects on GC B cell expansion or generation of OVA-specific $IgG1^+$ or $IgG2c^+$ GC B cells were observed (**Suppelementary Figures S4C, D**).

Finally, we examined PC generation in immunized *CD11c-Cre.Ifnar1*$^{fl/fl}$ mice. Similar to the GC B cell response in these mice we found reduced numbers of OVA-specific PCs at day eight post-immunization (**Figure 8M**). While the total number of OVA-binding PC thus was more than 10-fold lower in *CD11c-Cre.Ifnar1*$^{fl/fl}$ mice as compared with Cre^- controls, the reduction was most pronounced for the IgG1 producing subset, as evident from a significant reduction in the percentage of $IgG1^+$ but not $IgG2c^+$ events when comparing the OVA-specific PC that had developed in the two mouse strains (**Figures 8N, O**). Of note, the reduced affinity of PCs developing in the complete IFNAR knockout was not apparent in the absence of IFNAR on cDCs, indicating that type I IFN signaling in B cells may underlie this effect (**Figure 8P**). Altogether these results show that expansion of IL-4 secreting Tfh cells, through type I IFN signaling in cDCs, represents a third pathway whereby type I IFNs regulate the GC response, providing an explanation to how type I IFN in addition to its pronounced effect on IgG2 also amplifies the IgG1 response.

DISCUSSION

Type I IFNs possess a wide range of immune stimulatory properties with relevance for antiviral immunity, vaccination, and systemic autoimmune disease. Here, we have dissected how a succinct type I IFN response induced by dsRNA drives GC formation and IgG subclass specification. By selectively blocking receptor signaling in defined target populations or permitting signaling to occur only during defined time windows, we demonstrate that type I IFNs primarily act on B cells and cDCs to rapidly program the B and T cell responses underlying formation of GCs and class switching to a broad IgG subclass distribution. In addition to enhancing generation of Tfh cells and long-lived IgG1 responses, type I IFNs induce T-bet expression and support $IgG2c^+$ GC B cell development by mechanisms involving both direct effects on B cells and induction of IFN-γ production by cognate CD4 T cells.

Our results indicate that type I IFNs act on cDCs within the first 24 hours after immunization to initiate concurrent Tfh and Th1 cell differentiation. To assess the role of cDCs in this polarization process, we opted to delete *Ifnar1* in cDCs by using mice expressing the Cre recombinase under the control of the CD11c promoter. While CD11c also can be induced in GC B cells (54), which may have caused *Ifnar1* deletion also in GC B cells in the *CD11c-Cre.Ifnar1*$^{fl/fl}$ mice, this upregulation does not occur until two days after immunization (55). As we in the current study have isolated the effects of type I IFN to the first 24 hours after immunization, which is in line with the rapid and short-lived type I IFN response following poly I:C injections (31, 32), it is however unlikely that deletion of *Ifnar1* in GC B cells contributes to the observed phenotypes in this model. This conclusion is also in agreement with our previous study, showing a significant reduction in early Tfh cell development in *CD11c-Cre.Ifnar1*$^{fl/fl}$ mice but not in *CD19-Cre.Ifnar1*$^{fl/fl}$ mice with specific deletion in B cells (16).

Signaling in the cDC1 subset was redundant for both processes. It therefore seems likely that type I IFN signaling in cDC2 plays an important role for both Th cell fates, although we have not addressed this directly through cDC2 specific deletion of IFNAR. The demonstration that type I IFNs enhance both GC B cell responses and Th1 immunity stands in marked contrast to their immune suppressive role in chronic viral infections (4). The LCMV clone 13 strain establishes a persistent infection where long-lasting expression of IFN-β and IFN-α in cDCs leads to exhaustion of the protective Th1 cell response by a mechanism involving up-regulation of PD-L1 and IL-10 expression by the cDCs (57, 58). Likewise, the Th1-promoting property of cDC2 is suppressed by an excessive type I IFN response during severe blood-stage *Plasmodium* infection (59). The stimulatory effects of type I IFNs described in the current study are hence likely related to the short duration of the type I IFN response induced by poly I:C, a notion further supported by the beneficial effects these cytokines have in acute viral infections, including vesicular stomatitis virus (VSV) (19, 60), influenza (18), RSV (61) and adenovirus (13). Still, the ability of type I IFNs to concomitantly drive Th1 and Tfh cell development is not necessarily recapitulated in the acute viral infection models. While VSV similar to poly I:C gives rise to a rapid and transient peak of type I IFNs that stimulates generation of Tfh cells, this occurs at the expense of Th1 cell polarization (17). One explanation for this apparent discrepancy could be the mixed pro-inflammatory response induced by viral sensing through multiple innate receptors (62). The adjuvant effect of poly I:C is on the other hand completely lost in IFNAR deficient mice, as shown herein, and injection of purified IFN-β replicates the immune stimulatory effects of poly I:C when co-injected with a protein antigen (25).

The induction of T-bet associated GCs and long-lived IgG responses through the isolated effect of type I IFNs should be of considerable interest for the development of adjuvants to enhance antiviral vaccine efficacy. IgG2a/c represents the dominant anti-viral IgG subclass in mice (63) and B cell-specific T-bet deletion leads to impaired antiviral IgG2a/c production and viral clearance (64), as well as an inability to contain chronic viral infection (65). In addition, protective

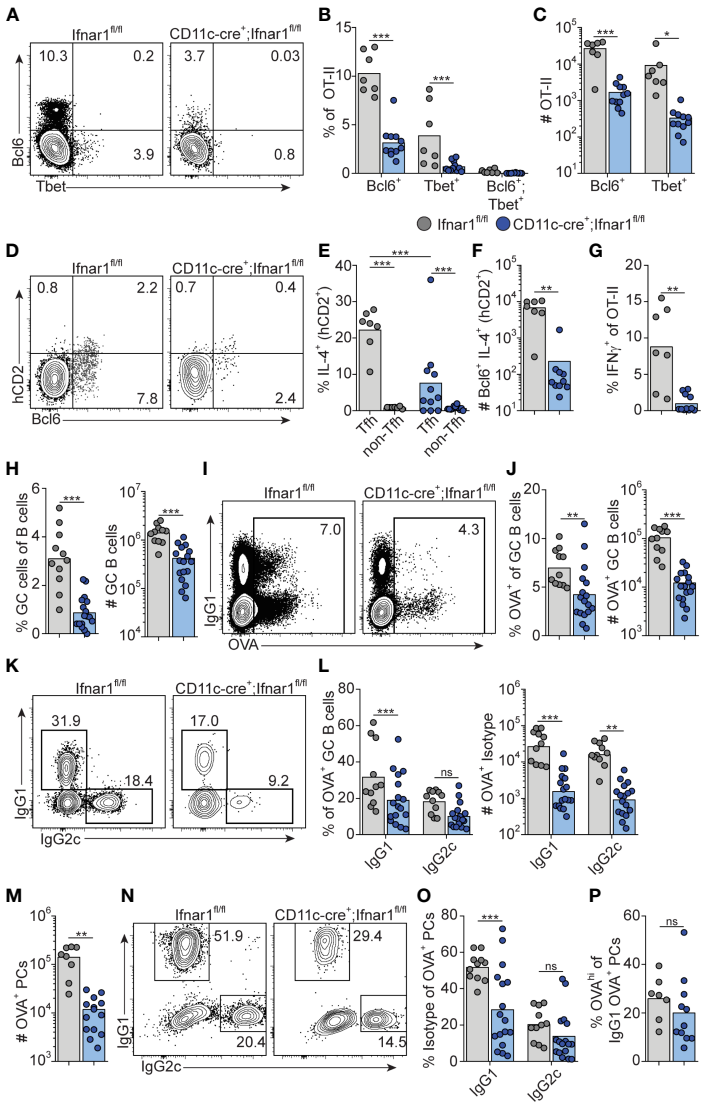

FIGURE 8 | Type I IFN signaling in cDC regulates Th1, Tfh and GC B cell development. *Ifnar1$^{fl/fl}$* and *CD11c-cre;Ifnar1$^{fl/fl}$* mice were transferred with 50 000 KN2-OT-II cells, immunized with OVA/poly I:C and splenocytes were analyzed by flow cytometry 8 dpi. **(A–G)** Analysis of donor KN2-OT-II cells gated as B220^{-} CD4^{+} TCRVβ5.1^{+} TCRVα2^{+} CD44^{+} cells. **(A–C)** T-bet versus Bcl6 expression with representative contour plots **(A)** and pooled results of frequency **(B)** and number **(C)** of Bcl6^{+} and T-bet^{+} KN2-OT-II cells. **(D–F)** IL-4 secretion reported by hCD2 expression by Tfh (Bcl6^{+}) donor cells. **(D)** Representative contour plots of Bcl6 versus hCD2 expression. **(E)** Percentage of IL-4 secreting Tfh and non-Tfh cells. **(F)** Number of IL-4 secreting Tfh cells. **(G)** Frequency of IFN-γ^{+} cells of total KN2-OT-II cells. **(H)** Percentages and number of GC B cells (B220^{+} CD95^{+} CD38^{-}). **(I–L)** Analysis of OVA-Alexa647 binding GC B cells. **(I, J)** Representative contour plots of OVA-binding versus IgG1 expression **(I)** and pooled results of percentages and number of OVA^{+} GC B cells **(J)**. **(K, L)** Analysis of IgG subclass distribution by OVA^{+} GC B cells with representative contour plots of IgG2c versus IgG1 expression **(K)** and pooled results of percentages and numbers of IgG1^{+} and IgG2c^{+} OVA^{+} GC B cells **(L)**. **(M–P)** Analysis of OVA-Alexa647 binding PCs (B220^{low} CD138^{+}). **(M)** Number of OVA^{+} PCs. **(N, O)** Analysis of IgG subclass distribution by OVA^{+} PCs with representative contour plots of IgG2c versus IgG1 expression (N) and pooled results of percentages of IgG1^{+} and IgG2c^{+} OVA^{+} PCs **(O)**. **(P)** Frequency of OVA^{hi} cells among OVA^{+} IgG1^{+} PCs. Results are pooled from three independent experiments. Each symbol represents one mouse. *p≤0.05, **p<0.01 and **p<0.001.

antibody responses against influenza were recently demonstrated to rely on T-bet associated GCs (24). The current study may also contribute towards understanding the immunogenicity of emerging mRNA vaccine approaches (66). Similar to poly I:C, mRNA vaccines induce a short-lived type I IFN response (33), and currently approved SARS-CoV-2 mRNA vaccines induce specific IgG serum concentrations higher or equivalent to the levels detected in convalescent sera (67, 68).

While antiviral immunity frequently has been associated with both type I IFN and IgG2a/c antibody production, it has not been clear how type I IFNs promote IgG2a/c dominated GCs. B cell-intrinsic type I IFN signaling was recently shown to be crucial for

spontaneous development of IgG2c$^+$ GCs in lupus prone *B6.Sle1b* mice (15). GC formation was however not affected by lack of type I IFN signaling when the same lupus-prone strain or wt mice were immunized with NP-conjugated chicken γ-globulin (15), probably reflecting an insufficient type I IFN response to this particular immunization regimen. In the current study, we show that IFN-γ production from cognate CD4 T cells, which requires type I IFN signaling in cDCs, is a critical component of the type I IFN-dependent IgG2c$^+$ GC B cell response. This pathway was however not sufficient but acted in concert with direct sensing of type I IFNs by the B cells and both pathways contributed to the induction of T-bet expression in GC B cells. Yet, the effects of type I IFNs and IFN-γ differed. While IFN-γ acted as a non-redundant IgG2c switch factor, only signaling through IFNAR amplified GC B cell expansion with specific effects on IgG2c$^+$ and IgG2b$^+$ GC B cells. How this occurs and why the effect was confined to GC B cells expressing the IgG2 subclasses remains to be determined. However only early, and not late, IFNAR neutralization resulted in reduced IgG2c$^+$ GC B cell numbers. Likewise, only few of the roughly 70 genes previously shown to be induced in B cells following type I IFN treatment (49) were affected in IFNAR deficient GC B cells eight days after immunization, further supporting that type I IFNs acted on the B cells early in the response, possibly during initial B cell activation. Indeed, type I IFNs have been shown to confer increased sensitivity to BCR stimulation and to promote B cell expansion by both enhancing proliferation and reducing sensitivity to apoptosis (15, 69).

Whereas targeted deletion of IFNγR in B cells, IFN-γ in cognate CD4 T cells or IFNAR in cDCs resulted in similar reduction in IgG2c$^+$ GC B cells, IFNAR deletion in cDCs additionally impaired development of IgG1$^+$ GC B cells and resulted in an overall reduced magnitude of the GC response. This coincided with reduced Tfh cell development, with a particularly pronounced effect on IL-4 producing Tfh cells. In the wt setting, Tfh cells thus became IL-4 producers also under the strong Th1 polarizing conditions otherwise conferred by poly I:C and downstream type I IFN production. In addition, T-bet was absent from the Tfh cells around the peak of the GC reaction, indicating limited Th1 cell characteristics of the Tfh cell subset. Consistent with this, we demonstrate that both IFN-γ and type I IFNs acted on B cells very early after immunization and induced IgG2c CSR prior to evident GC formation. These results are in agreement with previous studies, demonstrating that CSR mostly precedes GC formation (70–72). Nonetheless, similar to viral infection models (73–75), Bcl6 and T-bet were co-expressed by the T cells at this early stage. We could hence not identify divergent Th1 versus Tfh cell commitment at the time when B cells were receiving the IgG2c switch signals, in line with previous studies demonstrating incomplete commitment of the Bcl6-expressing Th cell subset at early stages of the GC response (76–78) Tfh cells with a history of T-bet expression have been shown to produce IFN-γ within established GCs (79). While it remains possible that equivalent IFN-γ producing T-bet$^-$ Tfh cells were present within the GCs studied herein, late IFN-γ neutralization had no detectable effect on the magnitude or IgG subclass composition of the GC response. This indicates that the IgG2c$^+$ GC B cells did not rely on continuous IFN-γ signaling within the GCs.

In summary, the current study describes how type I IFNs through at least three separate pathways can enhance and modulate the GC B cell response. Our results provide a detailed roadmap of how this family of cytokines confers long-lived humoral immunity. Exploiting the type I IFN dependent pathways identified herein could provide a means to enhance efficacy of e.g. mRNA vaccine regimens and to prolong the duration of vaccine-induced protection. On the other hand, the relative contribution of these pathways to onset of systemic autoimmune disease warrants further investigations.

DATA AVAILABILITY STATEMENT

The datasets presented in this study can be found in online repositories. The names of the repository/repositories and accession number(s) can be found below: https://www.ncbi.nlm.nih.gov/geo/, GSE201551.

ETHICS STATEMENT

The animal study was reviewed and approved by Lund/Malmo animal ethical committee (Sweden).

AUTHOR CONTRIBUTIONS

BJ-L, MD and AP conceived of the study and designed experiments. MD and AP performed experiments and analyzed results. KN and SB analyzed RNA-seq data. BJ-L secured funding for the study. SB and KL provided essential resources. BJL supervised the project. MD, AP and BJ-L synthesized results and wrote the manuscript with input from co-authors. All authors contributed to the article and approved the submitted version.

FUNDING

This work was supported by the Swedish Cancer foundation (Cancerfonden; 18 0324) and the Lundbeck foundation (R155-2014-4184). KL was supported by a Lundbeck Foundation Research Fellowship (R215-2015-4100). KN and SB were supported by the Novo Nordisk Foundation (NNF14CC0001).

ACKNOWLEDGMENTS

We thank Dr. Ulrich Kalinke and Dr. Bernard Malissen for providing *Ifnar1$^{fl/fl}$* and *XCR1-cre* mice, respectively. We also thank Drs. Jose Maria Gonzalez-Izarzugaza and Kristine Belling for help with analysis of mRNA sequencing results.

SUPPLEMENTARY MATERIAL

The Supplementary Material for this article can be found online at: https://www.frontiersin.org/articles/10.3389/fimmu.2022.932388/full#supplementary-material

Supplementary Figure 1 | B cell responses in *Ifnar1*$^{-/-}$ mice. OTII cells were transferred into *Ifnar1*$^{-/-}$ and WT mice before immunization with OVA/poly I:C. Splenocytes were analyzed by flow cytometry three or 14 days later. **(A)** Number of GC B cells. **(B)** Number of IgG1$^+$ GC B cells. **(C)** Number of IgG2c$^+$ GC B cells. **(D-E)** Analysis of relative affinities of OVA-specific IgG1$^+$ PCs. Representative contour plots **(D)** and pooled results showing frequency of OVA^{hi} PCs among total OVA$^+$ IgG1$^+$ PC eight days post infection **(E)**. Results are pooled from three **(A-C)** or two **(D-E)** independent experiments.

Supplementary Figure 2 | IL-27R signaling in B cells is redundant for GC B cell responses. **(A, B)** Mixed chimeras were generated by reconstituting lethally irradiated WT (CD45.1$^+$, CD45.2$^+$) recipients with a 1:1 mix of WT (CD45.1$^+$, CD45.2$^+$) and WT or *Il27r*$^{-/-}$ (CD45.1$^-$, CD45.2$^+$) BM cells. 8-10 weeks after reconstitution, chimeras were immunized with OVA plus poly I:C, and splenic GC B cell responses were analyzed 8 days later. **(A)** Representative histograms of WT : WT (shaded) and WT : *Il27r*$^{-/-}$ chimeras (blue) showing the distribution of B cells, GC B cells and GC B cells expressing indicated IgG isotypes (IgG1$^+$, IgG2b$^+$ and IgG2c$^+$). **(B)** Log_2 normalized ratio of B cells, GC B cells and GC B cells expressing indicated IgG isotype (IgG1, IgG2b and IgG2c) in WT : WT and WT : *Il27r*$^{-/-}$ chimeras. Results are pooled from two **(A, B)** individual experiments, each symbol represents one mouse.

Supplementary Figure 3 | The core GC B cell program is largely intact in absence of B cell intrinsic type I IFN and IFN-γ signaling. **(A, B)** RNA sequencing data from GC B cells with either IFNAR **(A)** or IFNγR **(B)** disruption was compared to sequencing data from Shi et al. (reference # 48), by plotting fold-change in GC B to naïve B cells vs *Ifnar1*$^{-/-}$ **(A)** or Ifngr$^{-/-}$ **(B)** to WT cells. **(C)** RNA sequencing data from GC B cells with IFNAR disruption was compared to gene expression changes induced in B cells following administration of type I IFN to mice as described in Mostavi et al. (reference # 49). Genes induced by injection of type I IFN with >2-fold change induction and statistical significance were plotted against the fold change in *Ifnar1*$^{-/-}$ vs WT cells. Results are from three individual mice.

Supplementary Figure 4 | Type 1 IFN signaling in cDC1 does not regulate Th1, Tfh or GC B cell responses. *Ifnar1*$^{fl/fl}$ and *XCR1-cre;Ifnar1*$^{fl/fl}$ mice were transferred with 50 000 OT-II cells and immunized with OVA/poly I:C. Lymphocyte responses in the spleen were analyzed 8 days later. **(A)** Number of OT-II cells from *Ifnar1*$^{fl/fl}$ and *XCR1-cre;Ifnar1*$^{fl/fl}$ mice. **(B)** Frequency of Bcl6$^+$ and T-bet$^+$ cells among transferred OT-II. **(C)** Number of total GC B cell. **(D)** Number of OVA$^+$ GC B cell. Results are pooled from two independent experiments. Each symbol represents one mouse.

REFERENCES

1. Vinuesa CG, Sanz I, Cook MC. Dysregulation of Germinal Centres in Autoimmune Disease. *Nat Rev Immunol* (2009) 9:845–57. doi: 10.1038/nri2637
2. Crotty S. Follicular Helper CD4 T Cells (TFH). *Annu Rev Immunol* (2011) 29:621–63. doi: 10.1146/annurev-immunol-031210-101400
3. Ivashkiv LB, Donlin LT. Regulation of Type I Interferon Responses. *Nat Rev Immunol* (2014) 14:36–49. doi: 10.1038/nri3581
4. Teijaro JR. Type I Interferons in Viral Control and Immune Regulation. *Curr Opin Virol* (2016) 16:31–40. doi: 10.1016/j.coviro.2016.01.001
5. Bastard P, Rosen LB, Zhang Q, Michailidis E, Hoffmann H-H, Zhang Y, et al. Auto-Antibodies Against Type I IFNs in Patients With Life-Threatening COVID-19. *Science* (2020) 129:eabd4585–19. doi: 10.1126/science.abd4585
6. Zhang Q, Bastard P, Liu Z, Le Pen J, Moncada-Velez M, Chen J, et al. Inborn Errors of Type I IFN Immunity in Patients With Life-Threatening COVID-19. *Science* (2020) 370(6515)eabd4570–23. doi: 10.1126/science.abd4570
7. Bastard P, Gervais A, Le Voyer T, Rosain J, Philippot Q, Manry J, et al. Autoantibodies Neutralizing Type I IFNs are Present in ~4% of Uninfected Individuals Over 70 Years Old and Account for ~20% of COVID-19 Deaths. *Sci Immunol* (2021) 6:1–26. doi: 10.1126/sciimmunol.abl4340
8. Theofilopoulos AN, Baccala R, Beutler B, Kono DH. Type I Interferons (Alpha/Beta) in Immunity and Autoimmunity. *Annu Rev Immunol* (2005) 23:307–36. doi: 10.1146/annurev.immunol.23.021704.115843
9. Baechler EC, Batliwalla FM, Karypis G, Gaffney PM, Ortmann WA, Espe KJ, et al. Interferon-Inducible Gene Expression Signature in Peripheral Blood Cells of Patients With Severe Lupus. *PNAS* (2003) 100:2610–5. doi: 10.1073/pnas.0337679100
10. Bennett L, Palucka AK, Arce E, Cantrell V, Borvak J, Banchereau J, et al. Interferon and Granulopoiesis Signatures in Systemic Lupus Erythematosus Blood. *J Exp Med* (2003) 197:711–23. doi: 10.1084/jem.20021553
11. Banchereau R, Hong S, Cantarel B, Baldwin N, Baisch J, Edens M, et al. Personalized Immunomonitoring Uncovers Molecular Networks That Stratify Lupus Patients. *Cell* (2016) 165:551–65. doi: 10.1016/j.cell.2016.03.008
12. Le Bon A, Thompson C, Kamphuis E, Durand V, Rossmann C, Kalinke U, et al. Cutting Edge: Enhancement of Antibody Responses Through Direct Stimulation of B and T Cells by Type I IFN. *J Immunol* (2006) 176:2074–8. doi: 10.4049/jimmunol.176.4.2074
13. Zhu J, Huang X, Yang Y. Type I IFN Signaling on Both B and CD4 T Cells is Required for Protective Antibody Response to Adenovirus. *J Immunol* (2007) 178:3505–10. doi: 10.4049/jimmunol.178.6.3505
14. Das A, Heesters BA, Bialas A, O'Flynn J, Rifkin IR, Ochando J, et al. Follicular Dendritic Cell Activation by TLR Ligands Promotes Autoreactive B Cell Responses. *Immunity* (2017) 46:106–19. doi: 10.1016/j.immuni.2016.12.014
15. Domeier PP, Chodisetti SB, Schell SL, Kawasawa YI, Fasnacht MJ, Soni C, et al. B-Cell-Intrinsic Type 1 Interferon Signaling Is Crucial for Loss of Tolerance and the Development of Autoreactive B Cells. *Cell Rep* (2018) 24:406–18. doi: 10.1016/j.celrep.2018.06.046
16. Cucak H, Yrlid U, Reizis B, Kalinke U, Johansson-Lindbom B. Type I Interferon Signaling in Dendritic Cells Stimulates the Development of Lymph-Node-Resident T Follicular Helper Cells. *Immunity* (2009) 31:491–501. doi: 10.1016/j.immuni.2009.07.005
17. De Giovanni M, Cutillo V, Giladi A, Sala E, Maganuco CG, Medaglia C, et al. Spatiotemporal Regulation of Type I Interferon Expression Determines the Antiviral Polarization of CD4+ T Cells. *Nat Immunol* (2020) 21:321–30. doi: 10.1038/s41590-020-0596-6
18. Coro ES, Chang WLW, Baumgarth N. Type I IFN Receptor Signals Directly Stimulate Local B Cells Early Following Influenza Virus Infection. *J Immunol* (2006) 176:4343–51. doi: 10.4049/jimmunol.176.7.4343
19. Fink K, Lang KS, Manjarrez-Orduno N, Junt T, Senn BM, Holdener M, et al. Early Type I Interferon-Mediated Signals on B Cells Specifically Enhance Antiviral Humoral Responses. *Eur J Immunol* (2006) 36:2094–105. doi: 10.1002/eji.200635993
20. Markine-Goriaynoff D, Coutelier J-P. Increased Efficacy of the Immunoglobulin G2a Subclass in Antibody-Mediated Protection Against Lactate Dehydrogenase-Elevating Virus-Induced Polioencephalomyelitis Revealed With Switch Mutants. *J Virol* (2002) 76:432–5. doi: 10.1128/JVI.76.1.432-435.2002
21. Haas C, Ryffel B, Le Hir M. IFN-Gamma is Essential for the Development of Autoimmune Glomerulonephritis in MRL/Ipr Mice. *J Immunol* (1997) 158:5484–91.
22. Peng SL, Szabo SJ, Glimcher LH. T-Bet Regulates IgG Class Switching and Pathogenic Autoantibody Production. *PNAS* (2002) 99:5545–50. doi: 10.1073/pnas.082114899
23. Wang NS, McHeyzer-Williams LJ, Okitsu SL, Burris TP, Reiner SL, McHeyzer-Williams MG. Divergent Transcriptional Programming of Class-Specific B Cell Memory by T-Bet and Rorα. *Nat Immunol* (2012) 13:604–11. doi: 10.1038/ni.2294
24. Johnson JL, Rosenthal RL, Knox JJ, Myles A, Naradikian MS, Madej J, et al. The Transcription Factor T-Bet Resolves Memory B Cell Subsets With Distinct Tissue Distributions and Antibody Specificities in Mice and Humans. *Immunity* (2020) 52:842–55.e6. doi: 10.1016/j.immuni.2020.03.020

25. Le Bon A, Schiavoni G, D'Agostino G, Gresser I, Belardelli F, Tough DF. Type I Interferons Potently Enhance Humoral Immunity and can Promote Isotype Switching by Stimulating Dendritic Cells In Vivo. *Immunity* (2001) 14:461–70. doi: 10.1016/s1074-7613(01)00126-1
26. Finkelman FD, Svetic A, Gresser I, Snapper C, Holmes J, Trotta PP, et al. Regulation by Interferon Alpha of Immunoglobulin Isotype Selection and Lymphokine Production in Mice. *J Exp Med* (1991) 174:1179–88. doi: 10.1084/jem.174.5.1179
27. Proietti E, Bracci L, Puzelli S, Di Pucchio T, Sestili P, De Vincenzi E, et al. Type I IFN as a Natural Adjuvant for a Protective Immune Response: Lessons From the Influenza Vaccine Model. *J Immunol* (2002) 169:375–83. doi: 10.4049/jimmunol.169.1.375
28. Swanson CL, Wilson TJ, Strauch P, Colonna M, Pelanda R, Torres RM. Type I IFN Enhances Follicular B Cell Contribution to the T Cell-Independent Antibody Response. *J Exp Med* (2010) 207:1485–500. doi: 10.1084/jem.20092695
29. Finkelman FD, Katona IM, Mosmann TR, Coffman RL. IFN-Gamma Regulates the Isotypes of Ig Secreted During *In Vivo* Humoral Immune Responses. *J Immunol* (1988) 140:1022–7.
30. Schijns VE, Haagmans BL, Rijke EO, Huang S, Aguet M, Horzinek MC. IFN-Gamma Receptor-Deficient Mice Generate Antiviral Th1-Characteristic Cytokine Profiles But Altered Antibody Responses. *J Immunol* (1994) 153:2029–37.
31. Longhi MP, Trumpfheller C, Idoyaga J, Caskey M, Matos I, Kluger C, et al. Dendritic Cells Require a Systemic Type I Interferon Response to Mature and Induce CD4+ Th1 Immunity With Poly IC as Adjuvant. *J Exp Med* (2009) 206:1589–602. doi: 10.1084/jem.20090247
32. Kumar H, Kumar H, Koyama S, Koyama S, Ishii KJ, Ishii KJ, et al. Cutting Edge: Cooperation of IPS-1- and TRIF-Dependent Pathways in Poly IC-Enhanced Antibody Production and Cytotoxic T Cell Responses. *J Immunol* (2008) 180:683–7. doi: 10.4049/jimmunol.180.2.683
33. Sahin U, Oehm P, Derhovanessian E, Jabulowsky RA, Vormehr M, Gold M, et al. An RNA Vaccine Drives Immunity in Checkpoint-Inhibitor-Treated Melanoma. *Nature* (2020) 9(10):1–24. doi: 10.1038/s41586-020-2537-9
34. Mohrs K, Wakil AE, Killeen N, Locksley RM, Mohrs M. A Two-Step Process for Cytokine Production Revealed by IL-4 Dual-Reporter Mice. *Immunity* (2005) 23:419–29. doi: 10.1016/j.immuni.2005.09.006
35. Wohn C, Le Guen V, Voluzan O, Fiore F, Henri S, Malissen B. Absence of MHC Class II on Cdc1 Dendritic Cells Triggers Fatal Autoimmunity to a Cross-Presented Self-Antigen. *Sci Immunol* (2020) 5:eaba1896. doi: 10.1126/sciimmunol.aba1896
36. Kamphuis E, Junt T, Waibler Z, Förster R, Kalinke U. Type I Interferons Directly Regulate Lymphocyte Recirculation and Cause Transient Blood Lymphopenia. *Blood* (2006) 108:3253–61. doi: 10.1182/blood-2006-06-027599
37. Jackson SW, Jacobs HM, Arkatkar T, Dam EM, Scharping NE, Kolhatkar NS, et al. B Cell IFN-γ Receptor Signaling Promotes Autoimmune Germinal Centers *via* Cell-Intrinsic Induction of BCL-6. *J Exp Med* (2016) 158: jem.20151724. doi: 10.1084/jem.20151724
38. Domeier PP, Chodisetti SB, Soni C, Schell SL, Elias MJ, Wong EB, et al. IFN-γ Receptor and STAT1 Signaling in B Cells are Central to Spontaneous Germinal Center Formation and Autoimmunity. *J Exp Med* (2016) 160: jem.20151722. doi: 10.1084/jem.20151722
39. Zhang Y, Tech L, George LA, Acs A, Durrett RE, Hess H, et al. Plasma Cell Output From Germinal Centers is Regulated by Signals From Tfh and Stromal Cells. *J Exp Med* (2018) 215:1227–43. doi: 10.1084/jem.20160832
40. Marrack P, Kappler J, Mitchell T. Type I Interferons Keep Activated T Cells Alive. *J Exp Med* (1999) 189:521–30. doi: 10.1084/jem.189.3.521
41. Havenar-Daughton C, Kolumam GA, Murali-Krishna K. Cutting Edge: The Direct Action of Type I IFN on CD4 T Cells is Critical for Sustaining Clonal Expansion in Response to a Viral But Not a Bacterial Infection. *J Immunol* (2006) 176:3315–9. doi: 10.4049/jimmunol.176.6.3315
42. Szabo SJ, Kim ST, Costa GL, Zhang X, Fathman CG, Glimcher LH. A Novel Transcription Factor, T-Bet, Directs Th1 Lineage Commitment. *Cell* (2000) 100:655–69. doi: 10.1016/s0092-8674(00)80702-3
43. Snapper CM, Paul WE. Interferon-Gamma and B Cell Stimulatory Factor-1 Reciprocally Regulate Ig Isotype Production. *Science* (1987) 236:944–7. doi: 10.1126/science.3107127
44. Yoshimoto T, Okada K, Morishima N, Kamiya S, Owaki T, Asakawa M, et al. Induction of IgG2a Class Switching in B Cells by IL-27. *J Immunol* (2004) 173:2479–85. doi: 10.4049/jimmunol.173.4.2479
45. Guo B, Chang EY, Cheng G. The Type I IFN Induction Pathway Constrains Th17-Mediated Autoimmune Inflammation in Mice. *J Clin Invest* (2008) 118:1680–90. doi: 10.1172/JCI33342
46. Pirhonen J, Sirén J, Julkunen I, Matikainen S. IFN-Alpha Regulates Toll-Like Receptor-Mediated IL-27 Gene Expression in Human Macrophages. *J Leukoc Biol* (2007) 82:1185–92. doi: 10.1189/jlb.0307157
47. Reinhardt RL, Liang H-E, Locksley RM. Cytokine-Secreting Follicular T Cells Shape the Antibody Repertoire. *Nat Immunol* (2009) 10:385–93. doi: 10.1038/ni.1715
48. Shi W, Liao Y, Willis SN, Taubenheim N, Inouye M, Tarlinton DM, et al. Transcriptional Profiling of Mouse B Cell Terminal Differentiation Defines a Signature for Antibody-Secreting Plasma Cells. *Nat Immunol* (2015) 16:663–73. doi: 10.1038/ni.3154
49. Mostafavi S, Yoshida H, Moodley D, LeBoité H, Rothamel K, Raj T, et al. Parsing the Interferon Transcriptional Network and Its Disease Associations. *Cell* (2016) 164:564–78. doi: 10.1016/j.cell.2015.12.032
50. Barrat FJ, Crow MK, Ivashkiv LB. Interferon Target-Gene Expression and Epigenomic Signatures in Health and Disease. *Nat Immunol* (2019) 20:1574–83. doi: 10.1038/s41590-019-0466-2
51. Banchereau R, Cepika A-M, Banchereau J, Pascual V. Understanding Human Autoimmunity and Autoinflammation Through Transcriptomics. *Annu Rev Immunol* (2017) 35:337–70. doi: 10.1146/annurev-immunol-051116-052225
52. Montoya M, Schiavoni G, Mattei F, Gresser I, Belardelli F, Borrow P, et al. Type I Interferons Produced by Dendritic Cells Promote Their Phenotypic and Functional Activation. *Blood* (2002) 99:3263–71. doi: 10.1182/blood.v99.9.3263
53. Kurche JS, Haluszczak C, McWilliams JA, Sanchez PJ, Kedl RM. Type I IFN-Dependent T Cell Activation is Mediated by IFN-Dependent Dendritic Cell OX40 Ligand Expression and is Independent of T Cell IFNR Expression. *J Immunol* (2012) 188:585–93. doi: 10.4049/jimmunol.1102550
54. Baumjohann D, Preite S, Reboldi A, Ronchi F, Ansel KM, Lanzavecchia A, et al. Persistent Antigen and Germinal Center B Cells Sustain T Follicular Helper Cell Responses and Phenotype. *Immunity* (2013) 38:596–605. doi: 10.1016/j.immuni.2012.11.020
55. Hong S, Zhang Z, Liu H, Tian M, Zhu X, Zhang Z, et al. B Cells Are the Dominant Antigen-Presenting Cells That Activate Naive CD4+ T Cells Upon Immunization With a Virus-Derived Nanoparticle Antigen. *Immunity* (2018) 49(4):1–19. doi: 10.1016/j.immuni.2018.08.012
56. King IL, Mohrs M. IL-4-Producing CD4+ T Cells in Reactive Lymph Nodes During Helminth Infection are T Follicular Helper Cells. *J Exp Med* (2009) 206:1001–7. doi: 10.1084/jem.20090313
57. Teijaro JR, Ng C, Lee AM, Sullivan BM, Sheehan KCF, Welch M, et al. Persistent LCMV Infection Is Controlled by Blockade of Type I Interferon Signaling. *Science* (2013) 340:207–11. doi: 10.1126/science.1235214
58. Wilson EB, Yamada DH, Elsaesser H, Herskovitz J, Deng J, Cheng G, et al. Blockade of Chronic Type I Interferon Signaling to Control Persistent LCMV Infection. *Science* (2013) 340:202–7. doi: 10.1126/science.1235208
59. Haque A, Best SE, Montes de Oca M, James KR, Ammerdorffer A, Edwards CL, et al. Type I IFN Signaling in CD8- DCs Impairs Th1-Dependent Malaria Immunity. *J Clin Invest* (2014) 124(6):2483–96. doi: 10.1172/JCI70698
60. Muller U, Steinhoff U, Reis LF, Hemmi S, Pavlovic J, Zinkernagel RM, et al. Functional Role of Type I and Type II Interferons in Antiviral Defense. *Science* (1994) 264:1918–21. doi: 10.1126/science.8009221
61. Remot A, Descamps D, Jouneau L, Laubreton D, Dubuquoy C, Bouet S, et al. Flt3 Ligand Improves the Innate Response to Respiratory Syncytial Virus and Limits Lung Disease Upon RSV Reexposure in Neonate Mice. *Eur J Immunol* (2016) 46:874–84. doi: 10.1002/eji.201545929
62. Akira S, Uematsu S, Takeuchi O. Pathogen Recognition and Innate Immunity. *Cell* (2006) 124:783–801. doi: 10.1016/j.cell.2006.02.015
63. Coutelier JP, van der Logt JT, Heessen FW, Warnier G, Van Snick J. IgG2a Restriction of Murine Antibodies Elicited by Viral Infections. *J Exp Med* (1987) 165:64–9. doi: 10.1084/jem.165.1.64
64. Rubtsova K, Rubtsov AV, van Dyk LF, Kappler JW, Marrack P. T-Box Transcription Factor T-Bet, a Key Player in a Unique Type of B-Cell

Activation Essential for Effective Viral Clearance. *Proc Natl Acad Sci USA* (2013) 110:E3216–24. doi: 10.1073/pnas.1312348110
65. Barnett BE, Staupe RP, Odorizzi PM, Palko O, Tomov VT, Mahan AE, et al. Cutting Edge: B Cell-Intrinsic T-Bet Expression Is Required To Control Chronic Viral Infection. *J Immunol* (2016) 197:1017–22. doi: 10.4049/jimmunol.1500368
66. Pardi N, Hogan MJ, Porter FW, Weissman D. mRNA Vaccines — a New Era in Vaccinology. *Nat Rev Drug Discov* (2018) 17:261–79. doi: 10.1038/nrd.2017.243. Nature Publishing Group.
67. Jackson LA, Anderson EJ, Rouphael NG, Roberts PC, Makhene M, Coler RN, et al. An mRNA Vaccine Against SARS-CoV-2 - Preliminary Report. *N Engl J Med* (2020) 383:NEJMoa2022483–1931. doi: 10.1056/NEJMoa2022483
68. Mulligan MJ, Lyke KE, Kitchin N, Absalon J, Gurtman A, Lockhart S, et al. Phase I/II Study of COVID-19 RNA Vaccine BNT162b1 in Adults. *Nature* (2020) 586:589–93. doi: 10.1038/s41586-020-2639-4
69. Braun D, Caramalho I, Demengeot J. IFN-Alpha/Beta Enhances BCR-Dependent B Cell Responses. *Int Immunol* (2002) 14:411–9. doi: 10.1093/intimm/14.4.411
70. Toellner KM, Gulbranson-Judge A, Taylor DR, Sze DM, MacLennan IC. Immunoglobulin Switch Transcript Production *In Vivo* Related to the Site and Time of Antigen-Specific B Cell Activation. *J Exp Med* (1996) 183:2303–12. doi: 10.1084/jem.183.5.2303
71. Toellner KM, Luther SA, Sze DM, Choy RK, Taylor DR, MacLennan IC, et al. T Helper 1 (Th1) and Th2 Characteristics Start to Develop During T Cell Priming and are Associated With an Immediate Ability to Induce Immunoglobulin Class Switching. *J Exp Med* (1998) 187:1193–204. doi: 10.1084/jem.187.8.1193
72. Roco JA, Mesin L, Binder SC, Nefzger C, Gonzalez-Figueroa P, Canete PF, et al. Class-Switch Recombination Occurs Infrequently in Germinal Centers. *Immunity* (2019) 51:337–50.e7. doi: 10.1016/j.immuni.2019.07.001
73. Fahey LM, Wilson EB, Elsaesser H, Fistonich CD, McGavern DB, Brooks DG. Viral Persistence Redirects CD4 T Cell Differentiation Toward T Follicular Helper Cells. *J Exp Med* (2011) 208:987–99. doi: 10.1084/jem.20101773
74. Nakayamada S, Kanno Y, Takahashi H, Jankovic D, Lu KT, Johnson TA, et al. Early Th1 Cell Differentiation Is Marked by a Tfh Cell-Like Transition. *Immunity* (2011) 35:919–31. doi: 10.1016/j.immuni.2011.11.012
75. Weinstein JS, Laidlaw BJ, Lu Y, Wang JK, Schulz VP, Li N, et al. STAT4 and T-Bet Control Follicular Helper T Cell Development in Viral Infections. *J Exp Med* (2018) 215:337–55. doi: 10.1084/jem.20170457
76. Poholek AC, Hansen K, Hernandez SG, Eto D, Chandele A, Weinstein JS, et al. *In Vivo* Regulation of Bcl6 and T Follicular Helper Cell Development. *J Immunol* (2010) 185:313–26. doi: 10.4049/jimmunol.0904023
77. Kerfoot SM, Yaari G, Patel JR, Johnson KL, Gonzalez DG, Kleinstein SH, et al. Germinal Center B Cell and T Follicular Helper Cell Development Initiates in the Interfollicular Zone. *Immunity* (2011) 34:947–60. doi: 10.1016/j.immuni.2011.03.024
78. Kitano M, Moriyama S, Ando Y, Hikida M, Mori Y, Kurosaki T, et al. Bcl6 Protein Expression Shapes Pre-Germinal Center B Cell Dynamics and Follicular Helper T Cell Heterogeneity. *Immunity* (2011) 34:961–72. doi: 10.1016/j.immuni.2011.03.025
79. Fang D, Cui K, Mao K, Hu G, Li R, Zheng M, et al. Transient T-Bet Expression Functionally Specifies a Distinct T Follicular Helper Subset. *J Exp Med* (2018) 215:2705–14. doi: 10.1084/jem.20180927

Conflict of Interest: The authors declare that the research was conducted in the absence of any commercial or financial relationships that could be construed as a potential conflict of interest.

Publisher's Note: All claims expressed in this article are solely those of the authors and do not necessarily represent those of their affiliated organizations, or those of the publisher, the editors and the reviewers. Any product that may be evaluated in this article, or claim that may be made by its manufacturer, is not guaranteed or endorsed by the publisher.

frontiers | Frontiers in Immunology

ORIGINAL RESEARCH
published: 13 July 2022
doi: 10.3389/fimmu.2022.897500

A Novel Type I Interferon Primed Dendritic Cell Subpopulation in TREX1 Mutant Chilblain Lupus Patients

*Anne Eugster[1], Denise Müller[1], Anne Gompf[1], Susanne Reinhardt[2], Annett Lindner[1], Michelle Ashton[1], Nick Zimmermann[3], Stefan Beissert[3], Ezio Bonifacio[1,4] and Claudia Günther[3]**

[1] Center for Regenerative Therapies Dresden, Faculty of Medicine Technische Universität (TU), Dresden, Germany, [2] Center for Molecular and Cellular Bioengineering (CMCB), DRESDEN-Concept Genome Center Technische Universität, Dresden, Germany, [3] Department of Dermatology, Faculty of Medicine, University Hospital Carl Gustav Carus, Technische Universität Dresden, Dresden, Germany, [4] Faculty of Medicine, Paul Langerhans Institute Dresden of Helmholtz Centre Munich at University Clinic Carl Gustav Carus, Technische Universität Dresden, Dresden, Germany

OPEN ACCESS

Edited by:
Clio Mavragani,
National and Kapodistrian University of Athens, Greece

Reviewed by:
Vanja Sisirak,
UMR5164 Immunologie Conceptuelle, Expérimentale et Translationnelle (Immuno ConcEpT), France
Sibel Balci,
Republic of Turkey Ministry of Health Sciences, Turkey

***Correspondence:**
Claudia Günther
Claudia.Guenther@ukdd.de

Specialty section:
This article was submitted to Antigen Presenting Cell Biology, a section of the journal Frontiers in Immunology

Received: 21 March 2022
Accepted: 07 June 2022
Published: 13 July 2022

Citation:
Eugster A, Müller D, Gompf A, Reinhardt S, Lindner A, Ashton M, Zimmermann N, Beissert S, Bonifacio E and Günther C (2022) A Novel Type I Interferon Primed Dendritic Cell Subpopulation in TREX1 Mutant Chilblain Lupus Patients. Front. Immunol. 13:897500. doi: 10.3389/fimmu.2022.897500

Heterozygous TREX1 mutations are associated with monogenic familial chilblain lupus and represent a risk factor for developing systemic lupus erythematosus. These interferonopathies originate from chronic type I interferon stimulation due to sensing of inadequately accumulating nucleic acids. We here analysed the composition of dendritic cell (DC) subsets, central stimulators of immune responses, in patients with TREX1 deficiency. We performed single-cell RNA-sequencing of peripheral blood DCs and monocytes from two patients with familial chilblain lupus and heterozygous mutations in TREX1 and from controls. Type I interferon pathway genes were strongly upregulated in patients. Cell frequencies of the myeloid and plasmacytoid DC and of monocyte populations in patients and controls were similar, but we describe a novel DC subpopulation highly enriched in patients: a myeloid DC CD1C$^+$ subpopulation characterized by the expression of LMNA, EMP1 and a type I interferon- stimulated gene profile. The presence of this defined subpopulation was confirmed in a second cohort of patients and controls by flow cytometry, also revealing that an increased percentage of patient's cells in the subcluster express costimulatory molecules. We identified a novel type I interferon responsive myeloid DC subpopulation, that might be important for the perpetuation of TREX1-induced chilblain lupus and other type I interferonopathies.

Keywords: monogenic familial chilblain lupus, SLE, Type I interferons, dendritic Cells (DC), LMNA, Lamin A/C, Trex1

INTRODUCTION

Chronic uncontrolled immune stimulation by alarming cytokines can break tolerance or hamper silencing of immune responses, leading to autoimmunity. Type I interferons (IFN) induce an antiviral state in immune cells and stimulate dendritic cell differentiation in an immunogenic rather than tolerogenic manner are potential mediators in various autoimmune diseases and especially in systemic lupus erythematosus (SLE) (1) as well as in type I interferonopathies (2). Type I interferonopathies are monogenic diseases characterized by chronic type I interferon activation (3). The first mutations were found in the three prime repair DNA exonuclease 1 (TREX1) and cause monogenic familial chilblain lupus (FCL) (4), Aicardi Goutières syndrome (3), a type I interferonopathy with features of autoimmunity, and represent a risk factor for the development of SLE (5). Defects in TREX1 cause an accumulation of DNA in the cell that can be sensed by the cyclic GMP-AMP synthase (cGAS)-stimulator of IFN genes (STING) pathway leading to chronic type I IFN activation (6, 7). TREX1 deficient mice succumb from autoimmune myocarditis, type I IFN upregulation and cutaneous lesions reminiscent of lupus. This phenotype can be induced by TREX1 deficiency in dendritic cells (DCs), suggesting an important role for DCs as a disease-initiator for this type I interferon driven autoimmune disease (8).

DCs are a heterogeneous population of antigen-presenting cells that orchestrate adaptive immune responses. Various DC subtypes with unique functions reside in all parts of the human body. Blood DC subtypes have classically been defined as $CD11c^+$ conventional DCs (cDCs), consisting of either $CD141^+$ (cDC1) or $CD1c^+$ (cDC2) cells, and $CD123^+$ plasmacytoid DCs (pDCs) (9). cDC1s are specialized in fighting intracellular pathogens, while cDC2s are involved in the adaptive immune response towards extracellular pathogens *via* Th1 cell activation by presenting antigens to $CD4^+$ T cells (10). Single-cell RNA-sequencing (scRNA-seq) combined with cytometry has further revealed new compartments of human blood DCs, monocytes and progenitors (10–12). The role of these DC populations in disease has not yet been well elucidated and led us to analyse in detail the composition and properties of DCs from patients with familial chilblain lupus and TREX1 deficiency.

MATERIALS AND METHODS

Subjects and PBMC Isolation

Human samples from 3 patients with familial chilblain lupus and a heterozygous mutation in TREX1 (H195Q or D18N) (**Supplemental Table 1** for details on patients) and from 5 age and sex matched Caucasian healthy donors were obtained for the isolation of peripheral blood mononuclear cells (PBMC). PBMC were isolated by density centrifugation. Use of the buffy coats was approved by the ethics committee and informed consent of the donors was obtained (EK 169052010). The study was approved by the ethics committee and informed consent of the donors was obtained (EK 169052010). Patients were involved in the dissemination plans of our research.

Isolation of Monocytes and Dendritic Cells

For isolation of cells for scRNAseq, freshly isolated PBMC were FC block- treated (2 ul FC blocking reagent human (Miltenyi Biotech) and 48 ul staining buffer (1% BSA in PBS, filtered through a 40 um filter)/$1x10^6$ cells) and incubated 10' on ice. Cells were washed and stained in 50 ul final/$1x10^6$ cells of antibody cocktail (CD3-APC (HIT3α, BD), CD19-APC (SJ25C1, BD), CD14-PE-Cy7 (M5E2, BD), CD56-PE-Cy7 (B159, BD), HLA-DR-APC-H7 (B159, BD), CD11c-AF700 (3.9, eBioscience), CD123-BV650 (6H6, Biolegends), CD16-BV605 (3G8, Biolegends)). Life- dead staining with 7AAD (BD) was done shortly before sorting on a FACS (ARIAII, BD) with the 100 uM nozzle using gating strategy shown in **Supplemental Figure 1**. For isolation of cells for qPCR, the same panel was used including also EMP1-FITC (Biozol) (**Supplemental Figure 4A**).

Intracellular Staining for Analytical Flow Cytometry

For flow cytometric analysis, cells were FC-block treated as described above and then first stained with extracellular antibodies described above in addition to EMP1-FITC (Biozol) and then with viability dye efluor 506 (eBioscience) followed by permeabilization using the eBioscience™ Foxp3/Transcription Factor Staining Buffer Set and staining with LAMIN-FITC (636, Santa Cruz). For staining of activation surface markers, the same panel was used, adding CD40-eFluor 405 (5C3, Thermo Fisher), CD80-PE/Dazzle (2D10, Biolegend) and CD86-BV650 (IT2.2, Biolegend) but omitting CD123-BV650. Measurements were done on FACS (ARIA Fusion, BD) using gating strategy shown in **Supplemental Figure 4A, B**. FMO controls were used in all Flow Cytometry experiments.

scRNAseq by 10x Genomics

For scRNAseq, 1000 cells from each cell type ($CD14^+$ Monocytes, $CD11c^+$ DC and pDC) were FACS sorted into 1 ul PBS in the same coated 1.5 ml tube (coated by filling with 1% BSA, by incubating overnight and complete removal of BSA and pre-lying 1 µl PBS). Sorted cells were immediately processed for reverse transcription and library preparation according to the 10x Genomics Protocol using the 10x Genomics Single Cell v2 kit. Libraries were sequenced on a complete Illumina NextSeq 500 high-output flowcell in PE mode (R1: 26 cycles; I1: 8 cycles; R2: 57 cycles. Raw sequencing data was processed with the Cell Ranger software (v2.1.0) provided by 10X Genomics. The human genome (hg38) as well as gene annotations (v87) were downloaded from Ensembl and the annotation was filtered with the 'mkgtf' command of Cell Ranger (–attribute=gene_biotype:protein_coding –attribute=gene_biotype:lincRNA –attribute=gene_biotype:antisense). Genome sequence and filtered gene annotation were used as input to build the appropriate Cellranger reference. Cells were removed if expressing fewer than 400 unique genes, more than 4,500 unique genes, or greater than 15% mitochondrial reads. Genes not detected in any cell were removed from subsequent analysis. Downstream analysis was conducted with Seurat V2.4 package in R (3.5.0) (13).

Multiplex qPCR by Biomark

1000 CD11c$^+$, 1000 CD14$^+$ cells or 500 CD11c$^+$EMP1$^+$ cells from 2 patients and 2 controls were FACS sorted in triplicates into PCR tubes containing 5 µl EB buffer (Qiagen), immediately snap-frozen and stored at -80°C until further usage. Gene expression by multiplex qPCR was performed as described (14), but using the primer pairs for 27 target genes and 3 house-keeping genes (POLR2F, SDHA, GNAS) (see **Supplemental Table 4**). Pre-processing and data analysis were conducted using KNIME 4.3.1, R (V4) and RStudio version 1.2.1335. Technical qPCR replicates were averaged. For normalisation to the 3 house-keeping genes the Delta CT method was used (15).

Statistical Analysis

Differences in proportions of patients or controls cells after scRNAseq and after FACS analysis were evaluated with multiple unpaired T tests in Prism 9. Differences in gene expression analysed by qPCR were calculated by the Wilcoxon test using R (3.5.0). A p-value < 0.05 was considered significant. Cluster Markers and differentially expressed genes were calculated in Seurat using the FindAllMarkers or FindMarkers command, applying a log fold threshold of 0.3 and requiring 30% of the cells to express the marker (13–15).

RESULTS

Type I Interferon and Viral Response Genes Are Upregulated in Patients With Mutations in TREX1

Monocytes (CD14$^+$), cDCs (CD11c$^+$CD123$^-$), and pDCs (CD11c$^-$CD123$^+$) were isolated from two patients with mutations in TREX1 and two control individuals and, after pooling the three cell types, subjected to scRNA-seq (**Supplemental Figure 1**). The expression of type I interferon-stimulated genes was increased in patients throughout all cell types (**Figure 1A**, **Supplemental Table 2**). Reactome pathway analysis revealed that upregulated genes in patients were predominantly enriched in pathways related to interferon-, interleukin- and antiviral-signalling (**Figure 1B**).

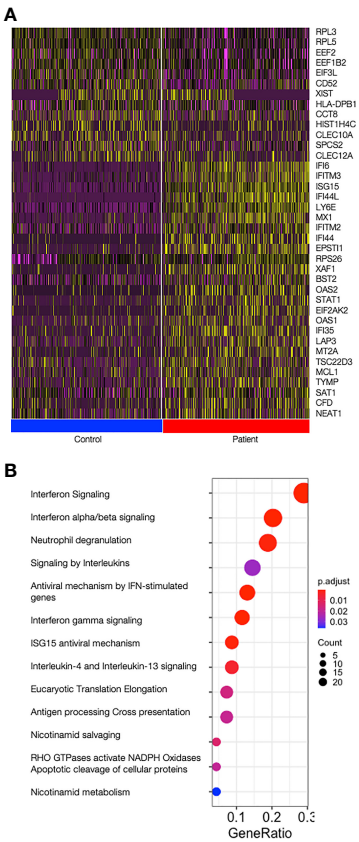

FIGURE 1 | Type I Interferon stimulated genes are upregulated in patients. **(A)** Heat map showing the top 25 most differentially expressed genes between patients and control cells over all cells analysed (all cell types joined); on top, all 13 genes upregulated in controls and on the bottom the top 25 genes upregulated in patients are shown. Control cells are shown on the left (blue bar) and patient's cells are shown on the right (red bar). Graduation of expression ranges from purple (absent) to yellow (high). **(B)** Dotplot showing significance of the pathways enriched in patients (ReactomePA). Count is the number of genes involved in the pathway. Gene Ratio is the ratio of the genes involved in each pathway to the total number of cluster genes. P adjust is the adjusted p-value.

A DC Population With Prominent Type I Interferon and Viral Response Gene Profile in Patients With Mutations in TREX1

Unsupervised clustering revealed the presence of previously described cell populations DC1, DC2, Mono2, DC5, Mono1, Mono3 and pDCs, characterised by the expression of, amongst others, CLEC9A and IDO1 (for DC1), CD1c and CLEC10A (for DC2), FCGR3A and APOBEC3A (for Mono2), AXL and LILRA4 (for DC5), CD14 and VCAN (for Mono1), GNLY and CD32 (for Mono3) and GZMB and JCHAIN genes (for pDCs) (12) (**Figures 2A, B**, **Supplemental Table 2**). The frequency of cells in the cell subsets were similar in patients and controls, but with some variation between individuals (**Figure 2C**). The largest DC cluster, DC2, representing around 40% of all cells was further sub-clustered. The two DC2 types previously described as CD1c$^+$_A and CD1c$^+$_B were found among the 5 identified sub-clusters (12) (**Figures 2D, E**, **Supplemental Table 2**). CD1c$^+$_A had high CD1C and HLA gene expression and CD1c$^+$_B expressed a number of chronic inflammatory genes such as S100A8 and S100A9. Three other sub-clusters (C, D, E) expressed marker genes that did not allow assignment to any cell types described so far in the literature. Sub-cluster E showed a statistically significant two-fold increase in patient's (17.3 and 21.0%) as compared to control cells (11.0 and 9.5%) (p=0.04 by unpaired t-test) whereas sub-cluster D, on the contrary, showed enrichment of control cells (20.0 and 19.9%) as compared to patient's cells (12.3 and 9.3%) (p=0.02 by unpaired t-test) (**Figure 2F**). LMNA, TPPP3 and EMP1 best defined sub-cluster E among all DC2 cells and were almost exclusively expressed in this novel DC2-E population (**Figure 2G**). Of the top 30 genes that identified sub-cluster E, 26 had entries as human Type I Interferon response genes in Interferome (http://www.interferome.org/interferome/home.jspx, v2.0). In addition,

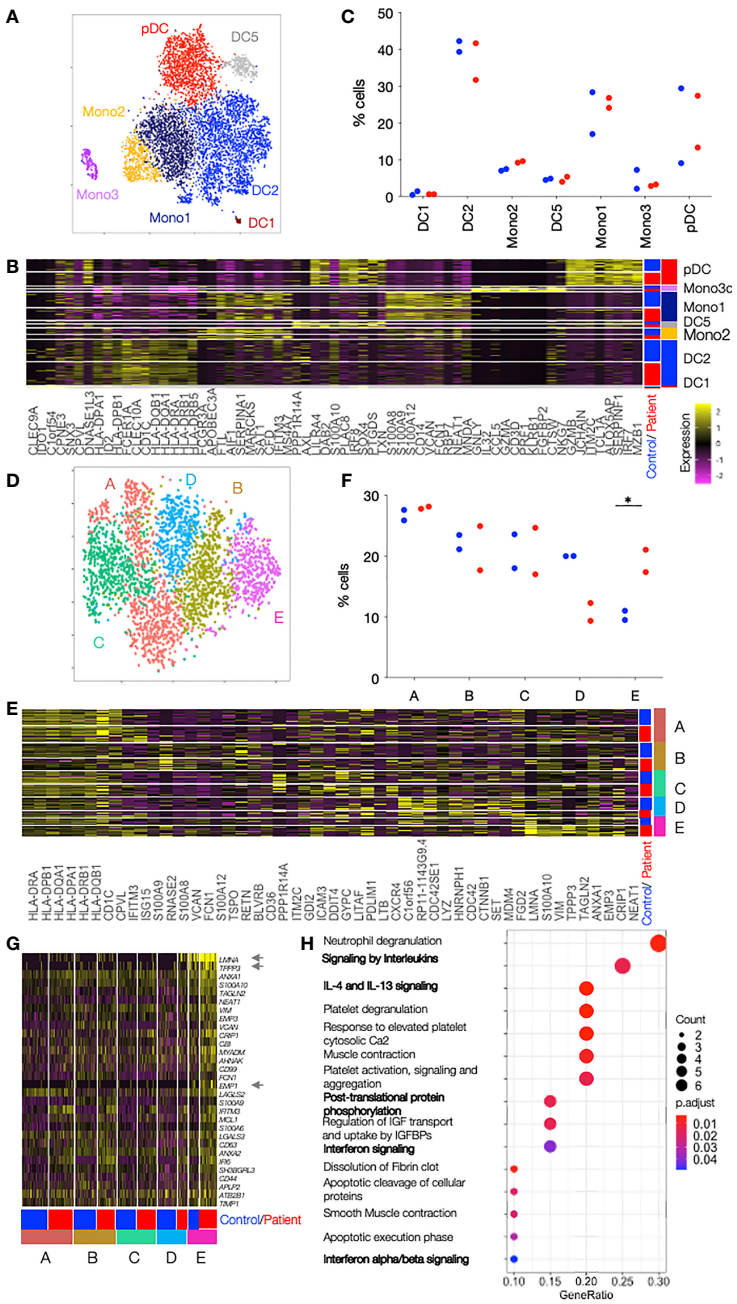

FIGURE 2 | Single cell RNAseq reveals clusters enriched in patient cells. **(A)** DCs and Monocytes isolated from blood of 2 patients with TREX1 mutation and 2 controls were analyzed by single cell RNaseq. tSNE of all sequenced cells after clustering into 7 clusters separates the cells into the 7 cell types annotated and color coded. **(B)** Heat map showing the top 10 cluster markers for each of the cell types. The row color bar on the right shows the color codes (as in A) for the cell types, and the bar on the left shows in blue cells from controls and in red cells from patients. Graduation of expression ranges from purple (absent) to yellow (high). **(C)** Dot plot showing the proportion of patients or control cells found in each cluster. Patients are shown in red and controls in blue. **(D)** tSNE of DC2 cells from 2 patients and controls after clustering into 5 subclusters. **(E)** Heat map showing the top 10 cluster markers for each DC2 subcluster. The row color bar on the right shows the color codes for the subclusters **(A–E)** (as in D), and the bar on the left shows in blue cells from controls and in red cells from patients. **(F)** Dot plot showing the proportion of patients or control cells found in each DC2 subcluster. Patients are shown in red and controls in blue. **(G)** Heat map showing all DC2-E marker genes in cells from all DC2 subclusters (A-E) in controls and patients. All genes belong to the Type I Interferon response according to Interferome. Asterisks point to genes whose expression is almost unique in DC2-E. The row color bar on the right shows the color codes for the subclusters **(A–E)** and the bar on the left shows in blue the cells from controls and in red the cells from patients. **(H)** Dotplot showing the significance of the pathways enriched in cluster DC2-E (ReactomePA). Pathways with relevance for the DCs are in bold. Count is the number of genes involved in the pathway. Gene Ratio is the ratio of the genes involved in each pathway to the total number of cluster genes. P adjust is the adjusted p-value. Comparisons with significance are marked with an *(p-value< 0.05, two-sided t- Comparisons with significance are marked with an *(p-value< 0.05, Mann-Whitney Test).

"Interferon signaling" and "Interferon alpha and beta signaling" were among the pathways found by the Reactome Pathway analysis (**Figure 2H**). The upregulation of the neutrophil degranulation pathway is most likely driven by the strong upregulation of laminA that has an important role in nuclear evolution in neutrophils (16). Enrichment in genes involved in interferon signaling was also found in sub-cluster A, but not in the other sub-clusters, B, C or D (**Supplemental Figure 2** and **Supplemental Table 3**). Sub-cluster D was characterized by genes important for the HO GTPase signaling (**Supplemental Figure 2C**), a complex pathway regulating activation, pathogen internalization and migration of innate immune cells (17)

The Novel DC2-E Population Can Be Isolated by FACS Analysis

To verify the existence of the novel DC2 cell type, DC2-E, PBMCs from the initial 2 patients and 2 controls, from 1 additional patient and from 3 additional controls were stained with a panel containing antibodies against the most exclusive cluster DC2-E markers with available antibodies, LMNA and EMP1 (**Supplemental Figure 4**). A $CD11c^+$ $CD123^-$ population co-expressing the surface marker EMP1 and the intracellular marker LaminA/C was enriched in patients (mean, 15.2% of $CD11c^+$ $CD123^-$) as compared to controls (mean, 7.9%; p=0.02) (**Figure 3A** and **Supplemental Figure 4C**). Cells positive for LaminA/C only were present in comparatively higher factions of $CD11c^+$ $CD123^-$ than the cells double positive for LaminA/C and EMP1 in patients and controls (mean=95.2% and 95.3% of $CD11c^+$ $CD123^-$, respectively, p=0.97). Cells positive for EMP1 only were as low as the double positive cells but were also higher in patients (mean=15.6% and 8.0% of $CD11c^+$ $CD123^-$, respectively, p=0.02) (**Figure 3A**). EMP1 and LaminA/C single- and double-positive cells were also found in $CD14^+$ Monocytes and pDCs (**Supplemental Figure 3B**). **Figure 3A** indicates that differences between patient and controls were seen when protein expression of EMP1 only was assessed whereas lamin A/C expression was similar between patients and controls (**Figure 3A**). Therefore, we used the surface marker EMP1 to isolate a surrogate DC2-E population by FACS from PBMC of patients and controls (**Supplemental Figure 4**) and used qPCR to show that the isolated $CD11c^+$ $CD123^-EMP1^+$ population was enriched for the mRNA of LMNA and EMP1 (**Supplemental Figure 5**) suggesting that a population at least closely resembling DC2-E can be isolated by FACS. The specificity of the population was further validated by qPCR analysis of additional cluster markers (**Figure 2G**). 19 out of 20 tested markers were expressed at a higher level in the DC2-E population than in DC2 cells or monocytes (**Supplemental Figure 5** and **Supplemental Table 4**).

To further analyse the DC2-E population we analysed the genes upregulated in patients and controls in this subpopulation in more detail (**Figure 3B**). 64 genes were found to be upregulated in patients as compared to controls by scRNAseq (**Figure 3B**, **Supplemental Table 2**) in DC2-E and 32 thereof had entries as human type I interferon response genes in Interferome (**Figure 3B**). Importantly, we quantified 17 of these genes by qPCR and confirmed 9 to be significantly elevated in patients in the FACS sorted surrogate DC2-E population (**Figure 3C** and **Supplemental Table 4**).

Further analysis revealed significantly more $CD11c^+CD123^-$ $EMP1^+$ $laminA/C^+$ (DC2-E) cells expressing the activation markers CD80 and CD86 in patients as compared to controls (**Supplemental Figure 6**) (CD80, mean=4.6% versus 2.1%, p= 0.047 and CD86, 92.9% versus and 87.4% p=0.045), but the median expression intensity of the activation markers CD40, CD80 and CD86 was similar in these cells in patients and controls.

DISCUSSION

Here, we describe a novel myeloid DC population enriched in lupus patients with TREX1 mutations. This DC population is characterized by strong expression of in interferon stimulated genes potential diagnostic. The general role of DCs as antigen presenting cells is well established but a specific function of myeloid DC and subpopulations in autoimmunity is less described. We were able to identify a specific DC subpopulation in patients with familial chilblain lupus using scRNAseq. This population was found by sub- clustering the $CD11c^+$ $CD1c^+$ myeloid DC population designated as DC2 (or $CD1C^+$_A + $CD1C^+$_B) by Villani et al (12) and therefore represents a subpopulation of cDC2 in the classical nomenclature (10) (see **Supplemental Figure 1**). We confirmed the presence of this new population in a second cohort by flow cytometry and we were able to sort this subpopulation using defined surface markers.

The identified DC2-E subpopulation was enriched among myeloid DC2 cells of TREX1 deficient patients and defined by the expression of LMNA (lamin A/C) and EMP1. Lamin A/C is an essential component of the nuclear envelope and upregulation of LMNA is a feature of mature DCs (18). LMNA might be induced by type I IFNs as protective cellular antiviral response to prevent egress of viral particles or chromatin from the nucleus (19). Lamin A/C- chromatin interaction has been described to prevent HIV-1 transcription and sustain viral latency (20). Our data suggest LMNA mRNA expression to be a specific antiviral response to chronic type I IFN activation in DC2-E. LMNA upregulation might also be a response mechanism to stress and DNA damage in TREX1 deficient cells aiming in decreasing the extent of nuclear membrane rupture (6, 21).

The function of EMP1 in DCs has not yet been defined. It has been described in cancer cells involved in migration and adhesion (22). Here, it was especially important because staining for EMP1 protein expression on the cell surface facilitated isolation of the DC2-E population from PBMC. The functional role of the DC2-E subpopulation needs further exploration. However, cells expressing the costimulatory molecules CD80 and CD86 were slightly enriched in the DC2-E population in patients versus controls, suggesting a possible role for these cells in T cell priming and activation. This feature is shared with the population of monocytes and CD11c+ DCs from patients with TREX1 mutation and might indicate the activated phenotype of antigen presenting cells in patients.

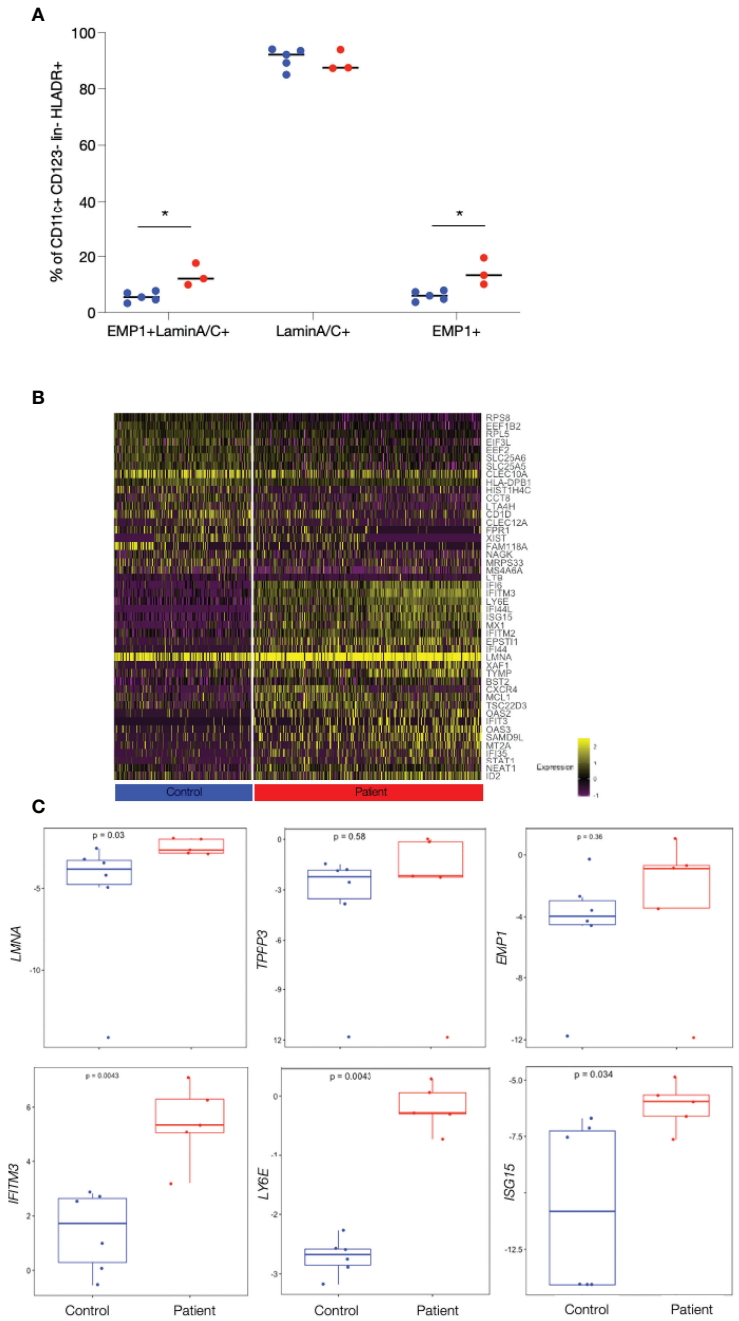

FIGURE 3 | Enrichment of patient's cells and confirming patient specific gene expression in a CD11c^{+} EMP1^{+} cell subset isolated by FACS. **(A)** Frequency of Lamin A/C $^{+}$, EMP1^{+} and of Lamin A/C $^{+}$EMP1^{+} (DC2-E) cells from patients and controls in CD11c+CD123^{-} cells determined by FACS analysis. Controls are shown as blue and patients as red dots. Comparisons with significance are marked with an *(p-value< 0.05, Mann-Whitney Test). **(B)** Heat map showing the top 25 genes differentially expressed between patients and controls in DC2-E cells found by scRNAseq (note that only 21 genes were found upregulated in controls). Genes upregulated and with entries in Interferome are shown in red. The bar below the heat map shows patient's cell in red (right) and control cells in blue (left). Graduation of expression ranges from purple (absent) to yellow (high). **(C)** Boxplots showing qPCR quantification of exemplary, patient specific genes (found by scRNAseq to be differentially expressed in patients and controls) in sorted CD11c^{+}CD123^{-} EMP1^{+} cells batches from patients and controls. The gene analysed is shown on the y-axis and p-values are shown within the plots. Measurements considered to be with significance show a p-value< 0.05, Wilcoxon Rank Sum Test.

Disease specificity in gene expression was detected in myeloid DCs but not in pDCs. This might correlate with the proposed functional role for myeloid but not plasmacytoid DCs in TREX1 deficient mice (8). The downregulation of TREX1 in $CD11c^+$ myeloid DCs was sufficient to induce autoimmunity in mice highlighting the importance of myeloid DCs for the induction of autoimmunity (8).

The limitations of this study include the small number of patients analysed. Follow up studies enrolling larger cohorts and cohorts with other interferonopathies will enable to overcome this.

Further analyzing type I IFN-responding cell subtypes in monogenic types of lupus will help understanding the development of autoimmunity due to TREX1 mutations and will shed light on other types of SLE induced by similar disturbance in intracellular nucleic acid metabolism. These mechanisms are potentially important also in complex cases of SLE and their pathogenic exploration will help to define more targeted therapies.

DATA AVAILABILITY STATEMENT

The datasets generated for this study has been deposited at the European Genome-Phenome Archive (EGA) and can be accessed through accession number EGAS00001006215.

ETHICS STATEMENT

The studies involving human participants were reviewed and approved by Ethikkommission an der Technischen Universität Dresden. The patients/participants provided their written informed consent to participate in this study.

AUTHOR CONTRIBUTIONS

AE was involved designing the studies, conducting experiments, acquiring data, analyzing data and writing the manuscript; DM, SR, AL and NZ conducted experiments; AG acquired and analyzed data; MA designed the studies; EB, SB and CG were involved in study design and manuscript writing. All authors contributed to the article and approved the submitted version.

FUNDING

This work was supported by the Deutsche Forschungsgemeinschaft (German Research Foundation), grant TRR237 369799452/404458960, KFO 249/GU1212/1-1 and 1-2 to CG and a CRTD grant to CG and AE and funding to DFG Research Center and Cluster of Excellence–Center for Regenerative Therapies Dresden (FZ 111 to AE, DM, MA and EB).

ACKNOWLEDGMENTS

We thank Andreas Petzold for processing of bioinformatical data Virag Sharma for uploading data to EGA and all members from the Günther and Bonifacio laboratory for technical assistance.

SUPPLEMENTARY MATERIAL

The Supplementary Material for this article can be found online at: https://www.frontiersin.org/articles/10.3389/fimmu.2022.897500/full#supplementary-material

REFERENCES

1. Banchereau J, Pascual V. Type I Interferon in Systemic Lupus Erythematosus and Other Autoimmune Diseases. *Immunity* (2006) 25(3):383–92. doi: 10.1016/j.immuni.2006.08.010
2. de Jesus AA, Hou Y, Brooks S, Malle L, Biancotto A, Huang Y, et al. Distinct Interferon Signatures and Cytokine Patterns Define Additional Systemic Autoinflammatory Diseases. *J Clin Invest* (2020) 130(4):1669–82. doi: 10.1172/JCI129301
3. Rodero MP, Crow YJ. Type I Interferon-Mediated Monogenic Autoinflammation: The Type I Interferonopathies, a Conceptual Overview. *J Exp Med* (2016) 213(12):2527–38. doi: 10.1084/jem.20161596
4. Lee-Kirsch MA, Chowdhury D, Harvey S, Gong M, Senenko L, Engel K, et al. A Mutation in TREX1 That Impairs Susceptibility to Granzyme A-Mediated Cell Death Underlies Familial Chilblain Lupus. *J Mol Med* (2007) 85(5):531–7. doi: 10.1007/s00109-007-0199-9
5. Lee-Kirsch MA, Gong M, Chowdhury D, Senenko L, Engel K, Lee YA, et al. Mutations in the Gene Encoding the 3'-5' DNA Exonuclease TREX1 are Associated With Systemic Lupus Erythematosus. *Nat Genet* (2007) 39 (9):1065–7. doi: 10.1038/ng2091
6. Wolf C, Rapp A, Berndt N, Staroske W, Schuster M, Dobrick-Mattheuer M, et al. RPA and Rad51 Constitute a Cell Intrinsic Mechanism to Protect the Cytosol From Self DNA. *Nat Commun* (2016) 7:11752. doi: 10.1038/ncomms11752
7. Berndt N, Wolf C, Fischer K, Cura Costa E, Knuschke P, Zimmermann N, et al. Photosensitivity and cGAS-Dependent IFN-1 Activation in Patients With Lupus and TREX1 Deficiency. *J Invest Dermatol* (2022) 142(3 Pt A):633–40.e6. doi: 10.1016/j.jid.2021.04.037
8. Peschke K, Achleitner M, Frenzel K, Gerbaulet A, Ada SR, Zeller N, et al. Loss of Trex1 in Dendritic Cells Is Sufficient To Trigger Systemic Autoimmunity. *J Immunol* (2016) 197(6):2157–66. doi: 10.4049/jimmunol.1600722
9. Guilliams M, Ginhoux F, Jakubzick C, Naik SH, Onai N, Schraml BU, et al. Dendritic Cells, Monocytes and Macrophages: A Unified Nomenclature Based on Ontogeny. *Nat Rev Immunol* (2014) 14(8):571–8. doi: 10.1038/nri3712
10. Bassler K, Schulte-Schrepping J, Warnat-Herresthal S, Aschenbrenner AC, Schultze JL. The Myeloid Cell Compartment—Cell by Cell. *Annu Rev Immunol* (2019) 37(1):269–93. doi: 10.1146/annurev-immunol-042718-041728
11. See P, Dutertre C-A, Chen J, Günther P, McGovern N, Irac SE, et al. Mapping the Human DC Lineage Through the Integration of High-Dimensional Techniques. *Science* (2017) 356(6342):eaag3009. doi: 10.1126/science.aag3009
12. Villani AC, Satija R, Reynolds G, Sarkizova S, Shekhar K, Fletcher J, et al. Single-Cell RNA-Seq Reveals New Types of Human Blood Dendritic Cells, Monocytes, and Progenitors. *Science* (2017) 356(6335). doi: 10.1126/science.aah4573
13. Butler A, Hoffman P, Smibert P, Papalexi E, Satija R. Integrating Single-Cell Transcriptomic Data Across Different Conditions, Technologies, and Species. *Nat Biotechnol* (2018) 36(5):411–20. doi: 10.1038/nbt.4096
14. Eugster A, Lindner A, Catani M, Heninger AK, Dahl A, Klemroth S, et al. High Diversity in the TCR Repertoire of GAD65 Autoantigen-Specific

Human CD4+ T Cells. *J Immunol* (2015) 194(6):2531–8. doi: 10.4049/jimmunol.1403031
15. Pfaffl MW, Horgan GW, Dempfle L. Relative Expression Software Tool (REST) for Group-Wise Comparison and Statistical Analysis of Relative Expression Results in Real-Time PCR. *Nucleic Acids Res* (2002) 30(9):e36. doi: 10.1093/nar/30.9.e36
16. Pelletier MGH, Malu K, Szymczak K, Barbeau AM, Prata GN, O'Fallon KS, et al. Critical Roles of α-Type Lamins in Neutrophil Differentiation Revealed By Analyses of Lmna Trancriptional Regulation and Myeloid Models With Aberrant Lamin α Expression. *Blood* (2016) 128(22):407–. doi: 10.1182/blood.V128.22.407.407
17. Bros M, Haas K, Moll L, Grabbe S. RhoA as a Key Regulator of Innate and Adaptive Immunity. *Cells* (2019) 8(7):733. doi: 10.3390/cells8070733
18. Saez A, Herrero-Fernandez B, Gomez-Bris R, Somovilla-Crespo B, Rius C, Gonzalez-Granado JM. Lamin a/C and the Immune System: One Intermediate Filament, Many Faces. *Int J Mol Sci* (2020) 21(17). doi: 10.3390/ijms21176109
19. Turan A, Grosche L, Krawczyk A, Mühl-Zürbes P, Drassner C, Düthorn A, et al. Autophagic Degradation of Lamins Facilitates the Nuclear Egress of Herpes Simplex Virus Type 1. *J Cell Biol* (2019) 218(2):508–23. doi: 10.1083/jcb.201801151
20. Sun WW, Jiao S, Sun L, Zhou Z, Jin X, Wang JH. SUN2 Modulates HIV-1 Infection and Latency Through Association With Lamin a/C To Maintain the Repressive Chromatin. *mBio* (2018) 9(3). doi: 10.1128/mBio.02408-17
21. Maciejowski J, Hatch EM. Nuclear Membrane Rupture and Its Consequences. *Annu Rev Cell Dev Biol* (2020) 36:85–114. doi: 10.1146/annurev-cellbio-020520-120627
22. Lin B, Zhang T, Ye X, Yang H. High Expression of EMP1 Predicts a Poor Prognosis and Correlates With Immune Infiltrates in Bladder Urothelial Carcinoma. *Oncol Lett* (2020) 20(3):2840–54. doi: 10.3892/ol.2020.11841

Conflict of Interest: The authors declare that the research was conducted in the absence of any commercial or financial relationships that could be construed as a potential conflict of interest.

Publisher's Note: All claims expressed in this article are solely those of the authors and do not necessarily represent those of their affiliated organizations, or those of the publisher, the editors and the reviewers. Any product that may be evaluated in this article, or claim that may be made by its manufacturer, is not guaranteed or endorsed by the publisher.

frontiers | Frontiers in Immunology

TYPE Original Research
PUBLISHED 05 August 2022
DOI 10.3389/fimmu.2022.876654

OPEN ACCESS

EDITED BY
Peter S. Linsley,
Benaroya Research Institute,
United States

REVIEWED BY
Nico Marr,
Sidra Medicine, Qatar
Amy H. Lee,
Simon Fraser University, Canada

*CORRESPONDENCE
James F. Read
James.Read@telethonkids.org.au
Anthony Bosco
abosco@arizona.edu

SPECIALTY SECTION
This article was submitted to Systems Immunology, a section of the journal Frontiers in Immunology

RECEIVED 15 February 2022
ACCEPTED 12 July 2022
PUBLISHED 05 August 2022

CITATION
Read JF, Serralha M, Mok D, Holt BJ, Cruickshank M, Karpievitch YV, Broadhurst DI, Sly PD, Strickland DH, Reinke SN, Holt PG and Bosco A (2022) Lipopolysaccharide-induced interferon response networks at birth are predictive of severe viral lower respiratory infections in the first year of life.
Front. Immunol. 13:876654.
doi: 10.3389/fimmu.2022.876654

Lipopolysaccharide-induced interferon response networks at birth are predictive of severe viral lower respiratory infections in the first year of life

James F. Read[1,2]*, Michael Serralha[1], Danny Mok[1], Barbara J. Holt[1], Mark Cruickshank[3], Yuliya V. Karpievitch[1,3], David I. Broadhurst[4], Peter D. Sly[5], Deborah H. Strickland[1,6], Stacey N. Reinke[4], Patrick G. Holt[1,6] and Anthony Bosco[1,6,7,8]*

[1]Telethon Kids Institute, The University of Western Australia, Perth, WA, Australia, [2]School of Medicine, The University of Western Australia, Nedlands, WA, Australia, [3]School of Biomedical Sciences, The University of Western Australia, Nedlands, WA, Australia, [4]Centre for Integrative Metabolomics & Computational Biology, School of Science, Edith Cowan University, Joondalup, WA, Australia, [5]Child Health Research Centre, The University of Queensland, Brisbane, QLD, Australia, [6]The University of Western Australia Centre for Child Health Research, The University of Western Australia, Nedlands, WA, Australia, [7]Asthma and Airway Disease Research Center, University of Arizona, Tucson, AZ, United States, [8]Department of Immunobiology, The University of Arizona College of Medicine, Tucson, AZ, United States

Appropriate innate immune function is essential to limit pathogenesis and severity of severe lower respiratory infections (sLRI) during infancy, a leading cause of hospitalization and risk factor for subsequent asthma in this age group. Employing a systems biology approach to analysis of multi-omic profiles generated from a high-risk cohort (n=50), we found that the intensity of activation of an LPS-induced interferon gene network at birth was predictive of sLRI risk in infancy (AUC=0.724). Connectivity patterns within this network were stronger among susceptible individuals, and a systems biology approach identified IRF1 as a putative master regulator of this response. These findings were specific to the LPS-induced interferon response and were not observed following activation of viral nucleic acid sensing pathways. Comparison of responses at birth versus age 5 demonstrated that LPS-induced interferon responses but not responses triggered by viral nucleic acid sensing pathways may be subject to strong developmental regulation. These data suggest that the risk of sLRI in early life is in part already determined at birth, and additionally that the developmental status of LPS-induced interferon responses may be a key determinant of susceptibility. Our findings provide a rationale for the identification of at-risk infants for early intervention aimed at sLRI prevention and identifies targets which may be relevant for drug development.

KEYWORDS

innate immunity, respiratory infection, interferon, lipopolysaccharide (LPS), multi-omics, systems biology, pathogen recognition receptor (PRR)

Introduction

Severe lower respiratory tract infections (sLRIs) are a leading cause of emergency room presentations by infants and children (1, 2), and are a major risk factor for the development of asthma and wheeze (3–6). Rhinovirus (RV) and Respiratory Syncytial Virus (RSV) are the most important triggers of early life respiratory infections and asthma development (7–9). Several studies have found that associations between sLRI and asthma are strongest in children with RV-related wheezing and early aeroallergen sensitization (5, 6, 10, 11), although a causal relationship remains to be established (7). However, RV can routinely be detected in asthmatic children in the absence of asthmatic symptoms, suggesting that RV may be necessary but not sufficient to drive the pathogenesis of asthma (12). In this regard it has been demonstrated that bacterial pathogens, including *Moraxell*a, *Streptococcus*, and *Haemophilus* species, are important triggers of wheezy episodes in young children (13, 14), and may also contribute towards asthma inception (15, 16). Furthermore, the presence of pathogenic bacteria in the nasopharynx during acute respiratory viral infections may increase the likelihood of infection spread to the lower airways, amplifying ensuing inflammatory symptoms and increasing risk of subsequent asthma development (17, 18), although much remains unknown regarding virus-bacteria interactions in the airways and asthma development (19, 20). Conversely, exposure to microbes and their products during early childhood has also been shown to protect against asthma, perhaps most elegantly illustrated through the "farm effect" (21, 22). The underlying immunological mechanisms that determine why some individuals are more susceptible to sLRIs in early life, and subsequent asthma, are not well understood. Innate immune function in the immediate postnatal period, which experiences drastic developmental changes (8, 23–25), provides a logical link between early life microbial exposure and infection susceptibility. This has prompted investigation of molecular events downstream of pathogen recognition receptor (PRR) activation, such as Toll-like receptors (TLRs), in blood collected at birth and in early life (26–31). For example, reduced type 1/3 interferon response capacity following stimulation with Polyinosinic-polycytidylic acid (Poly(I:C)) – a potent activator of TLR3 – in cord blood cells is associated with increased risk for febrile LRIs and early childhood wheeze (31). Moreover, enhanced production of the proinflammatory cytokine IL-1β following bacterial lipopolysaccharide (LPS) activation of cord blood was observed in individuals at risk of childhood-onset asthma, in association with increased *SMAD3* methylation and maternal asthma status (30). These examples reveal that aspects of innate immunity which may confer risk for sLRIs and subsequent asthma are already detectable at birth. The aim of the present study was to determine if innate immune response profiles induced by bacterial LPS or viral nucleic acid sensing pathways (Poly(I:C) and Imiquimod) at birth could predict sLRI in the first year of life. The rationale for selecting these pathways is that previous studies have highlighted the role of bacteria, respiratory viral infections, and innate immune responses to the selected TLR agonists in asthma risk (7, 9, 15, 30–33).

Materials and methods

Study population

Subjects were a subset of 50 individuals from the Childhood Asthma Study, a 10 year prospective birth cohort enrolled prenatally for high risk of asthma development, as described previously (5, 31, 34–36). Of the 60 subjects with at least one CBMC aliquot remaining from the cohort, nine were excluded due to insufficient information (withdrawn before the 1 year follow-up) and a further subject was excluded for insufficient sample volume. Acute respiratory infections were considered sLRIs if wheeze and/or fever was present in addition to chest rattle, as this definition has previously been linked to persistent wheeze and asthma in this cohort (5, 35) (Supplementary Methods). Respiratory viral infection histories were determined from detailed assessment and nasopharyngeal aspirates (RT-PCR) collected during home visits within 48 hours of symptom development (5, 34). Ethics was approved by The University of Western Australia (reference RA/4/1/7560), and fully informed parental consent was obtained for all subjects.

Immunophenotyping

Approximately $1x10^6$ CBMCs from each sample were immunophenotyped with a panel of 11 monoclonal antibodies to measure CD3, CD4, CD11c, CD14, CD19, CD25, CD123, CD127, FcεRIα, FoxP3, and HLA-DR. Individual cells were acquired using the LSRFortessa platform with FACSDiva software (BD Biosciences) following quality control measures. FlowJo (v10.5) software and R were used for pre-processing and analysis (Supplementary Methods).

In vitro cell culture

Samples were assigned randomized blocks and cultured sequentially by the same personnel using consistent reagent/stimuli stocks. Cord blood erythrocytes were immunomagnetically depleted (EasySep kit, StemCell, Cat no. 18170) and each sample was cultured in RPMI 1640 (Gibco, Cat No. 11875119) supplemented with 5% AB serum (Sigma-Aldrich, Cat. No. H3667) for 18 hours (37°C, 5% CO_2) with 1ng/ml LPS (Enzo Biochem, Cat No. ALX-581-007-L001;

derived from E. *coli*, serotype R515), 5µl/ml Imiquimod (*In vivo* Gen, Cat. Code: tlrl-imq) or 50µl/ml Poly(I:C) (*In vivo* Gen, Cat. Code: tlrl-pic), alongside matched unstimulated controls. Poly(I:C), bacterial LPS, and Imiquimod were selected as they are activators of TLRs 3, 4, and 7, respectively, thereby triggering innate immune responses to LPS and viral nucleic acid sensing pathways. However, it is noteworthy that Poly(I:C), a synthetic analogue of double-stranded RNA, can also activate the viral-related PRRs RIG-I and MDA5 (37). Aliquots of culture supernatant were immediately snap frozen in liquid nitrogen for metabolomic profiling or stored at -20°C for cytokine quantification. Cell pellets were stored in TRIzol reagent (Invitrogen, Cat No. 15596026) at -20°C for RNA extraction.

Data generation

Detailed information on sample and data processing and quality control are available in the Supplementary Methods.

RNA-Seq: RNA was purified with RNeasy MinElute Kits (Qiagen, Cat No. 74204) and libraries were prepared with NEBNext Ultra II Kits (NE BioLabs) for sequencing on the NovaSeq 6000 (Illumina) platform. Standard methods were applied for pre-processing, alignment (GRCh38), and transcript quantification. RNA-Seq data is available from the NCBI Gene Expression Omnibus repository (38) (accession number GSE184383).

Cytokines: The concentrations of 48 cytokines (Bio-plex Pro, BioRad, Cat. No: 12007283) were simultaneously quantified with the Luminex 200 system (Luminex). Nine cytokines were outside the limit of detection in >20% of stimulated samples and were removed. Raw and processed data are provided in Data S1.

Metabolites: Untargeted metabolomic data was generated with liquid chromatography (HILIC and C18 modes) separation coupled to a Q Exactive Orbitrap mass spectrometer (Thermo Fisher Scientific) in electrospray positive ionisation mode (LC-MS/MS). QC samples were interspersed throughout the run order to assess and correct variability. Metabolites were filtered according to stringent statistical and annotation thresholds (39). Raw and processed data are provided in Data S2.

Transcriptomic analysis

Differentially expressed genes (DEG) were identified [EdgeR (40)] using an absolute $\log_2$ fold change >1.5 and an adjusted P value < 0.01 (Benjamini-Hochberg adjusted False Discovery Rate). Moderated t-statistics were calculated with limma/voom (41). Pathways analysis of upregulated/downregulated genes was performed with InnateDB (42). Cellular composition was estimated from post-culture gene expression with CIBERSORTx (43) with single cell RNA-seq cord blood reference profiles curated from the Human Cell Atlas (44). Gene expression data was partitioned into response context-specific modules with WGCNA (45). Modules were annotated by employing a consensus approach derived from Gene Ontology (GOenrichmentAnalysis), ReactomePA (46), and clusterProfiler (47) R packages, and InnateDB (42). Additionally, we employed the blood transcriptional module repertoire from BloodGen3Module to confirm that the principal modules of interest related to innate immune function we identified following WGCNA analysis (interferon and proinflammatory modules) were captured with an independent method (48). Separate response networks were created for each condition and included matched unstimulated controls, as detailed in the Supplementary Methods.

Master regulator analysis

To identify transcription factors that act as master regulators of gene expression profiles, a gene regulator network was reverse engineered with ARACNe (49) and transcription factor activity was inferred with VIPER (50) (detailed in Supplementary Methods). Significant TFs ($p<0.05$) were considered drivers of the responses if they had known binding motifs in the region of regulon target genes (500bp upstream and 100bp downstream) determined by RcisTarget (51). Normalised expression scores (NES) outputted from VIPER were retained for downstream analysis.

Machine learning

Gene expression data was randomly assigned into training and validation sets and filtered to only the respective module genes for each analysis. The random assignment was 50% training/50% validation. The RandomForest R package was used for random forest model construction, and the number of decision trees (ntree) and candidate variables (mtry) were optimized according to the out-of-bag error rate (Supplementary Methods). Model construction and classification was repeated thousands of times after randomly re-assigning samples into train/validation groups (retaining the original optimized parameters) and this was repeated with 60/40 and 70/30 splits (Supplementary Methods). This step was included to ensure the results were robust with respect to the randomized train/test group assignment. The same random assignment with respect to individual subjects was applied for LPS/CTRL, Poly(I:C)/CTRL, and Imiquimod/CTRL models. For random forest models used to predict infection status in independent cohorts of infant/childhood infection, CAS cohort data was filtered to respective module genes and used as the training set, and the external gene expression data was used for validation (filtered to identical input genes).

TABLE 1 Characteristics and representativeness of the study subset.

	CAS subset (n=50)	Total CAS cohort (n=263)	OR (95% CI)	P value
Sex (female)	24/50 (48%)	115/251 (45.82%)	0.92 (0.48-1.77)	0.88
Gestation (weeks; mean [range])	39.14 [36-41]	39.03 [34-41]	NA	0.89
Birth weight (grams; mean [range])	3496.52 [2755-4415]	3406.17 [2085-5110]	NA	0.27
SPT$^+$ at 0.5, 2, or 5 years	24/50 (48%)	118/198 (59.6%)	1.59 (0.82-3.13)	0.15
URI in first year	47/50 (94%)	215/235 (91.49%)	0.69 (0.13-2.46)	0.78
LRI in first year	39/50 (78%)	160/235 (68.08%)	0.6 (0.26-1.28)	0.18
sLRI in first year	23/50 (46%)	101/235 (42.98%)	0.88 (0.46-1.72)	0.75
Current wheeze at 5 years	14/43 (32.56%)	56/198 (28.28%)	0.82 (0.38-1.8)	0.58
Asthma at 5 years	9/34 (26.47%)	37/198 (18.69%)	0.64 (0.26-1.69)	0.35

CAS, Childhood Asthma Study; OR, Odds Ratio; CI, Confidence Interval; URI, Upper respiratory Infection (viral); (s)LRI, (severe) Lower respiratory Infection (viral); SPT, Skin Prick Test. SPT positivity was determined from a panel of seven common allergens (house dust mite, cat dander, ryegrass, Alternaria, Aspergillus, cow's milk, and egg white), along with positive (Histamine) and negative (saline) controls at 6 months, 2 years, and 5 years (Supplementary Methods). sLRIy1 represents the primary outcome (sLRI incidence in the first year of life). For categorical variables, odds ratios, 95% CIs and accompanying P values were determined by Fishers Exact test. For continuous variables, P values were determined by Mann-Whitney U test. Variation in participant number relates to data availability (see *Methods*).

Multi-omic data integration

A DIABLO (52) model was constructed for supervised multi-omic data integration, which generalizes Partial Least Squares analysis to maximize co-expression between matched datasets. All datasets (except immunophenotyping) for LPS-stimulated CBMC samples were baseline adjusted prior to analysis, and gene expression data was filtered to significantly variable genes (n=6344) to reduce noise. The number of components and feature selection parameters were tuned with 5x cross-validation (Supplementary Methods).

Results

Study population

The study population consisted of a subset of 50 children within the Childhood Asthma Study (CAS) cohort (5, 34–36, 53). 23 subjects (46%) experienced at least one wheezy and/or febrile sLRI in their first year (infancy) and this was the primary outcome of interest (Table 1). These individuals typically experienced 1 or 2 sLRIs in the first year of life, and a similar number recorded both wheezy and febrile (8/23, 34.8%), wheezy only (7/23, 30.4%), and febrile only (8/23, 34.8%) sLRIs (Table S1 and Figure S1A). No difference was observed with respect to sex, gestational weeks, birth weight, skin prick test positivity to common aeroallergens, and URIs in infancy for the primary outcome (Table S1). Overall, this subset was found to be representative of the total CAS cohort (n=263) with respect to key clinical characteristics (Table 1). RV was the most frequent viral agent identified from the first year of life in this subset (present in 56.9% of infectious nasopharyngeal samples) followed by RSV (13.125%), and this was representative of the total cohort (Figures 1, S1).

Baseline flow cytometry

We applied an 11-colour flow cytometry panel to baseline cord blood mononuclear cell (CBMC) samples to assess cellular composition. Lymphocytes (T and B cells) composed the majority of cell types identified among CBMC (Figures 1B and S1B). CD14$^+$ monocytes and conventional dendritic cells (cDC) were identified among the myeloid compartment, and smaller proportions of plasmacytoid DCs (pDC) and basophils were also identified. The was no difference in baseline cellular composition with respect to sLRI in the first year of life (Figure S1C).

Multi-omic profiling of innate immune responses in CBMC

CBMC from all 50 subjects were cultured for 18 hours with LPS, or Imiquimod, or Poly(I:C) to trigger innate immune responses, along with unstimulated controls. This timepoint was selected to capture signalling cascades downstream of the immediate and secondary response programs (54–56). Gene expression was profiled from cell pellets (RNA-Seq) and supernatants were used to profile cytokines (multiplex assay) and metabolites (LC-MS/MS). Matching PBMC samples collected at age 5 were available for a subset of the subjects (n = 27), and these were cultured in parallel under the same conditions. Following data pre-processing and filtering, 17,363 transcripts, 39 cytokines, and 47 metabolites were available for analysis (see Methods). We applied unsupervised Principal Component Analysis (PCA; transcripts, cytokines) and supervised Canonical Variate Analysis (CVA; metabolites) dimensionality reduction for exploratory data analysis. The samples from each biological layer clustered by stimuli as expected (Figure 1C). For transcripts and cytokines, the first two principal components captured interferon (IFN) and

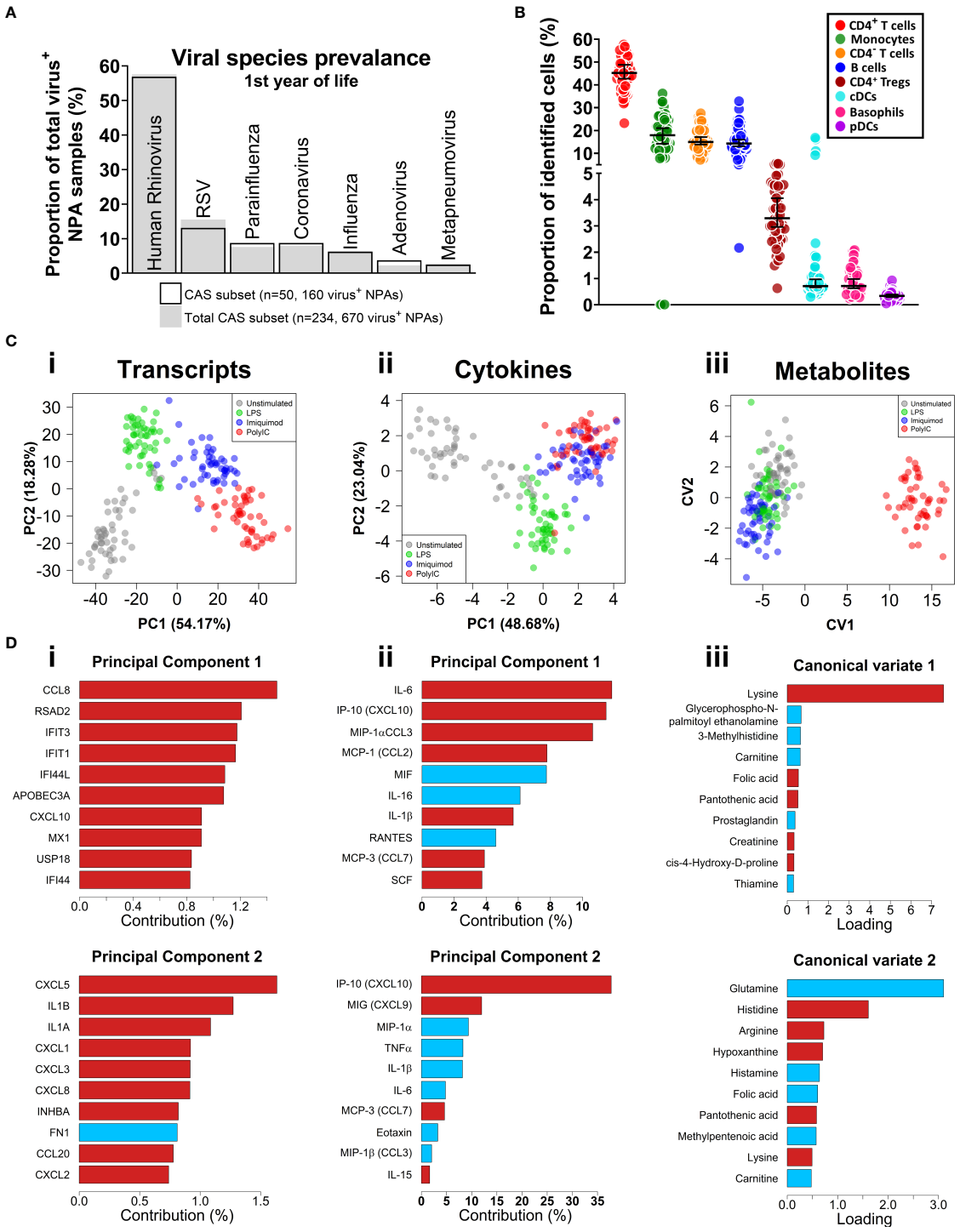

FIGURE 1
Respiratory virus prevalence, baseline CBMC cell proportions, multi-omic data set overview. **(A)** Bar plot of viral agents detected from infectious NPAs taken during year one (proportion of total virus+ NPAs). Bars denote study subset (n=50), grey fill represents individuals who recorded an sLRI in year 1 from the total cohort (n=234). **(B)** Immunophenotyping of baseline CBMC samples. Y-axis shows cell type as a proportion of identified cells. Scatterplots shows median and 95% CI. **(C)** Multi-level dimensionality reduction for gene expression (PCA), cytokine (PCA), and metabolite (cross validated CVA) datasets. Axes show coordinates of the first (x-axis) and second (y-axis) components/variates. **(D)** Horizontal bar plots showing top contributing features for the first **(i-iii)** and second **(iv-vi)** principal components or canonical variates for the corresponding plots in **(C)**, above. X-axis shows absolute contribution (%)/loading; red/blue indicates positive/negative relative contribution.

10.3389/fimmu.2022.876654

proinflammatory features (e.g., *CXCL10*/IP-10, IL-1β, IL-6) (Figure 1D). Poly(I:C)-stimulated cord blood sample clustering by metabolites was driven by lysine on the first canonical variate, and other amino acids (e.g., glutamine, histidine) were identified for the second and third canonical variates (Figures 1C, D, S1D,E).

IFN and proinflammatory gene expression programs are upregulated in CBMC responses

We focused on the transcriptomics data to further investigate cord blood responses to LPS, Poly(I:C), and Imiquimod treatment as these data provide genome-wide coverage. Employing differential expression analysis, we identified 641 differently expressed genes (DEGs) for the cord blood LPS response (Log_2-fold change > 1, FDR adjusted-P value < 0.01), and greater than 1000 DEGs for the imiquimod and Poly(I:C) responses (Figure 2A). Pathways analysis [InnateDB (42)] identified an enrichment of cytokine and chemokine signalling pathways from upregulated genes in all responses, and IFN signalling pathways were prominent for imiquimod and Poly(I:C) CBMC responses (Figures 2B, S1F). Notably, the viral-related stimuli triggered a common set of 429 upregulated genes and this constituted a core antiviral response shared between Poly(I:C) and Imiquimod responses (Figure S1G). In addition, we identified 462 and 243 genes that were specifically upregulated in response to Poly(I:C) and Imiquimod respectively, demonstrating unique signalling pathways downstream of their receptors (Figure S1G). We next employed CIBERSORTx to estimate the post-culture cellular composition from the RNA-Seq data (43). Prominent cell types included monocytes, B cells, and $CD4^+$ T cells (Figures S2A, B). The erythrocyte proportion was negligible as a result of immunomagnetic depletion (see Methods). Cell composition changes were identified between stimuli and age, but not sequence order or sex (Figures S2C,D). There was also no difference in the estimated cellular composition between individuals who were resistant or susceptible to sLRI in infancy, aligning with the baseline flow cytometry findings (Figures S1C, S2D). We also investigated variations in innate immune gene expression in the matching samples collected at birth versus age 5 (n=27 per age/stimuli) (Figures S2E, F). Interestingly, the LPS response at 5 years was characterised by upregulation of IFN-related genes, including *IRF1*, *STAT1*, and *IFIT1-3*, compared to birth. In contrast, IFN-related pathways were not prominent from differentially expressed genes between birth and age 5 following imiquimod or Poly(I:C) stimulation (Figures S2E, F). Finally, no genes were significantly different between individuals resistant and susceptible to sLRIs in infancy for any condition from this analysis (data not shown), suggesting that sLRI risk is not conferred by individual gene expression magnitude alone.

Identification of co-expression networks underlying the innate immune responses at birth

Genes do not function in isolation, they work together in networks (57), and for this reason gene expression data is not only informative for differences in expression magnitude (e.g. fold changes) but also in network structure (e.g. connectivity). We employed weighted gene co-expression network analysis (WGCNA) to elucidate the global connectivity structure and functional organisation of gene expression patterns observed from our CBMC samples. This analysis identified 11, 11, and 8 co-expression modules for the LPS, Imiquimod and Poly(I:C) responses, respectively (Figures 2C–E, S3A,B). All responses exhibited upregulation of IFN and proinflammatory modules, and as we had already identified these as integral components of the cord blood innate responses with dimensionality reduction and differential expression analysis, they were therefore carried forward for downstream analysis (Figures 2C–E, S3C–E). The LPS response had the smallest IFN module (180 genes) compared to Imiquimod (1114 genes) and Poly(I:C) (2201 genes) and the inverse was true of the proinflammatory modules (LPS, 2297 genes; Imiquimod, 924 genes; Poly(I:C), 646 genes) (Figure 2F). Notably, there was substantial overlap between IFN and proinflammatory module genes of different stimuli, particularly between the Poly(I:C) IFN and LPS proinflammatory modules (n=385 genes) (Figure S3F). We next compared gene network patterns between the respective responses. First, we calculated module preservation statistics, and the results showed that the LPS-induced IFN module was highly preserved within the IFN modules of the imiquimod and Poly(I:C) responses but not vice versa (Figure S3G). The IFN modules associated with the imiquimod and Poly(I:C) responses were preserved within one another and the proinflammatory modules were preserved between all responses (Figure S3G). Second, we calculated ranked gene expression and ranked connectivity to compare modules. A prominent disparity was observed between expression magnitude (r = 0.88 & 0.82) and intra-module connectivity (r = 0.57 & 0.59) between the cord blood LPS-induced IFN module genes and the same genes following Imiquimod and Poly(I:C) stimulation, respectively (Figure 2G). To examine connectivity within modules, we plotted the connectivity density across all genes in each module and also identified the top 20 most connected genes (Figures 3A, B). The connectivity of the LPS-induced IFN module was characterised by a normal distribution, whereas the viral stimuli produced left-skewed distributions (Figure 3A). Key IFN signalling genes (e.g. *IRF1*, *STAT1*) were present among the most connected genes within the LPS-induced IFN module, however the strength of the most connected genes was reduced compared to the IFN modules of the viral stimuli (Figure 3B). The LPS-induced proinflammatory module displayed greater connectivity compared to the imiquimod- or Poly(I:C)-induced proinflammatory modules

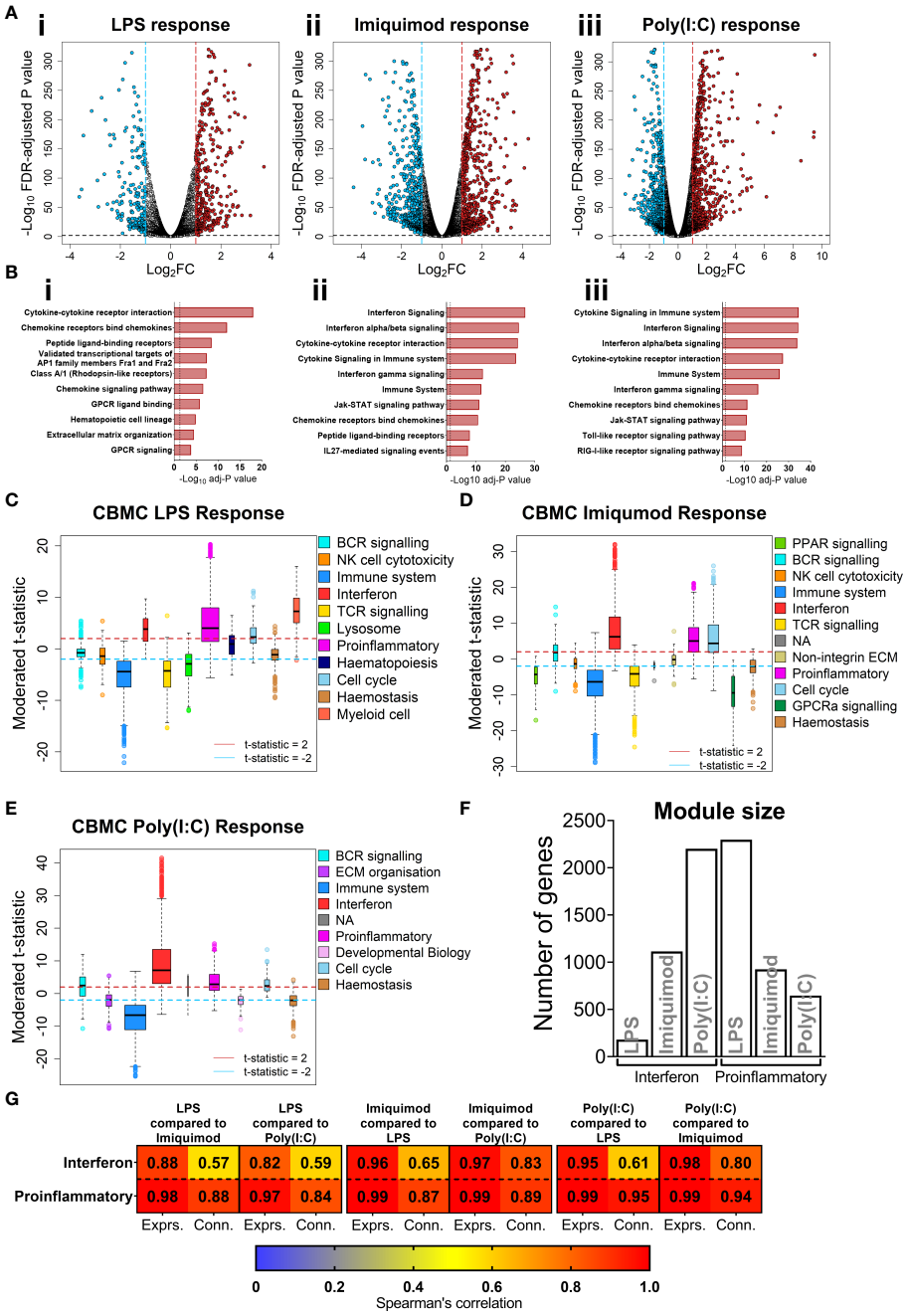

FIGURE 2
IFN and proinflammatory gene expression following TLRs 3/4/7 activation in CBMC. **(A)** Volcano plot showing significantly upregulated (red) and downregulated (blue) genes compared to matched unstimulated samples for the LPS (i), Imiquimod (ii), and Poly(I:C) (iii) responses, respectively. Plots show the Log_2 fold-change (x-axis) and FDR-adjusted p value ($-Log_{10}$ transformed). Blue and red dashed lines indicate a Log_2FC of -1 and 1, respectively; black dashed line denotes a $-Log_{10}$ FDR-adjusted p value of 2. **(B)** Top 10 overrepresented pathways from significantly upregulated genes of the CBMC LPS (i), Imiquimod (ii), and Poly(I:C) (iii) responses. X-axis shows the FDR corrected p value ($-Log_{10}$ transformed); black dashed line indicated corrected p ≈ 0.05. **(C–E)** Modules identified from network analysis (WGCNA) of the LPS, Imiquimod, and Poly(I:C) responses, respectively. Modules are plotted by moderated t-statistics (y-axis) and show the median, 25th and 75th quartiles ±1.5xIQR and outliers. Modules with medians above the red line (moderated t-statistic = 2) are considered significantly upregulated and those below the blue line (-2) are considered significantly downregulated. **(F)** Bar plot of the number of genes in the interferon and proinflammatory modules for the respective responses. **(G)** Heatmap showing Spearman's correlation values of ranked expression and ranked connectivity between CBMC response module genes. Expression of member genes from the IFN and proinflammatory modules of each response were correlated against the expression of the same genes from the other responses. The p value associated with all correlations was < 0.01.

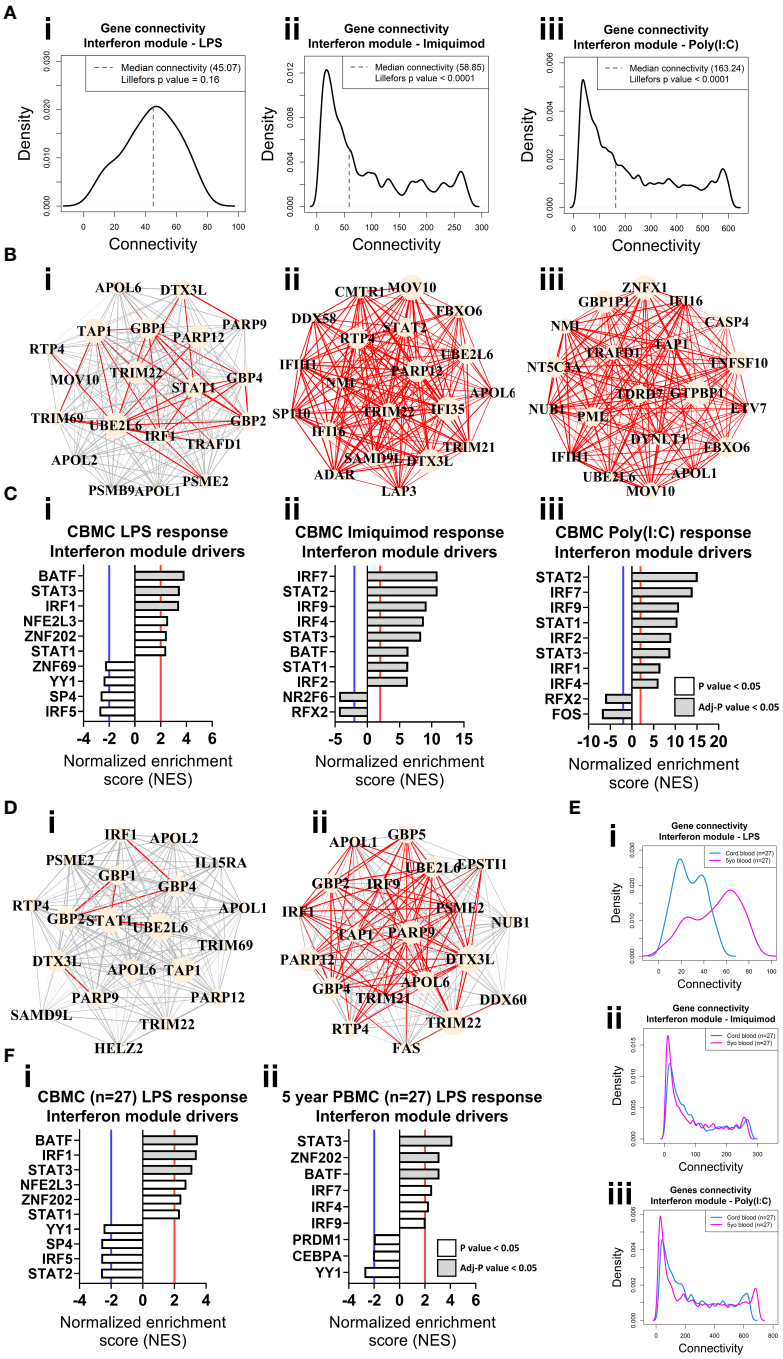

FIGURE 3
Network connectivity and master regulator analysis of IFN responses at birth and age 5 years identify IRF1 as a key driver. **(A)** Density plot of the LPS **(i)**, Imiquimod **(ii)**, and Poly(I:C) **(iii)** CBMC response IFN module connectivity, respectively. Dashed line denotes median. Lilliefors p value > 0.05 indicates normal distribution. **(B)** Network wiring diagrams of the top 20 most connected genes for the LPS **(i)**, Imiquimod **(ii)**, and Poly(I:C) **(iii)** CBMC IFN modules, respectively. Node size represents number of connections (degree) among the total network and edge width indicates strength of correlation (red edges > 0.8). **(C)** Top 10 master regulators for the respective CBMC IFN modules. Bar plots show normalized enrichment score (NES) for transcription factors which are significantly activated (NES>2, red line) or inactive/inhibited (NES<-2, blue line). Grey shading indicates an adjusted P value < 0.05. **(D)** Network wiring diagrams of the most connected CBMC LPS-induced IFN module genes from matched CBMC **(i)** and 5 year PBMC **(ii)** samples. Network characteristics are the same as above **(B). (E)** Network connectivity density plot for the interferon module gene connectivity of the matched CBMC (blue) and 5 year PBMC (magenta) responses to LPS **(i)**, Imiquimod **(ii)**, and Poly (I:C) **(iii)** stimulation. **(F)** Top drivers of the LPS-induced interferon module genes identified for matched CBMC **(i)** and 5 year PBMC (**ii**, 9 drivers were significant at P <0.05 samples. Bar plot characteristics are the same as above **(C)**.

(Figure S4A). Genes encoding innate immune/proinflammatory cytokines (e.g. *IL1A/B*, *CXCL2/3/8*) were among to most connected genes in the proinflammatory modules of all responses at birth (Figure S4A). In summary, although viral nucleic acid and bacterial related stimuli activated overlapping sets of proinflammatory and IFN response genes, the underlying network structure was markedly different.

Identification of master regulators of the innate immune responses at birth and age 5

We employed VIPER (50) analysis to identify master regulators which are predicted to drive module connectivity patterns. This approach revealed that the LPS-induced IFN module was putatively driven by BATF, STAT3 and IRF1 transcription factors (TFs) at birth, whereas the Imiquimod- and Poly(I:C)-induced IFN module top drivers included multiple STAT (e.g. STAT2) and IRF (e.g. IRF7) TFs (Figure 3C). The proinflammatory modules for all three responses were enriched for CEBPB, AP-1 (e.g. JUN, FOSL1/2) and NF-κB (e.g. NF-κB, RELB) (Figure S4A). Importantly, we repeated our analyses with input genes restricted to only those preserved from the LPS responses IFN (169/180, 93.89%) and proinflammatory (443/2297, 19.29%) modules and the result was unchanged (Figures S4B, C). Finally, we compared gene network patterns between CMBC and matched PBMCs samples (n=27) collected at 5 years. The connectivity of the genes of the LPS-induced IFN module was markedly higher at 5 years compared to birth among matched samples, suggesting that the wiring of this module is subject to developmental regulation (Figures 3D, E). Additionally, IRF1 enrichment was only identified from cord blood (Figure 3F). In contrast, the IFN responses provoked by imiquimod and Poly(I:C) stimulation displayed comparatively similar connectivity patterns between birth and age 5 years and, supporting this, the putative drivers were also comparable between birth and 5 years (e.g. STAT2, IRF7) (Figures 3E, S5A). Imiquimod and poly(I:C) proinflammatory modules were characterised by reduced intra-module connectivity in blood collected at 5 years compared to birth (Figures S5B, C).

Innate immune responses at birth are predictive of sLRI in the first year of life

To determine whether innate immune responses at birth could predict the development of sLRIs in the first year of life, we randomly assigned the data set into training (50%, n=25) and validation sets (50%, n=25) and trained a random forest classifier on the CBMC IFN modules. The classifier trained on the LPS-induced IFN module genes could predict sLRIs in the first year of life with an accuracy of 72% in the validation data set (Area under the ROC curve = 0.724) (Figure 4A). Whilst the accuracy of this model may appear modest, it is known that risk biomarkers in general possess poor accuracy to predict subsequent disease over a specific time interval because the at-risk population will almost always be heterogeneous with respect to the disease outcome (58). In contrast, classifiers built from the Imiquimod- or Poly(I:C)-induced IFN module genes were not predictive of sLRIs in the first year of life (Figure 4A). To test whether this finding was reproducible given the relatively small sample numbers available as input, we repeated the analysis by randomly re-sampling subject membership in the training/validation sets (retaining the initial optimization parameters), and again found that only the LPS-induced IFN module genes could predict sLRIs in infancy better than chance on average (Figures 4B, S6A–C). Furthermore, we observed markedly different connectivity patterns for the LPS-induced IFN modules when stratified by individuals who did and did not experience and sLRI in the first year of life (Figures 4C, D, S6D), and this was not evident from the imiquimod- or Poly(I:C)-induced IFN modules (Figures 4C, S6E, F). Specifically, susceptible individuals had stronger gene network patterns for the LPS-induced IFN module, although the putative drivers of the response were comparable (IRF1, STAT3, BATF) (Figures 4D, E). Restricting the Imiquimod and Poly(I:C) IFN responses to only those genes of the LPS-induced IFN module did not exhibit noticeable differences in connectivity density patterns in relation to sLRI susceptibility in infancy (Figures S6E(iii),F(iii)). Whist the connectivity density plot of the LPS-induced IFN module of CBMCs of susceptible individuals (Figure 4C) resembled the overall connectivity density of the 5 year PBMC connectivity (n=27) (Figure 3E), the intra-module connectivity was significantly different (Figures S6G, H), suggesting the similarity may emerge from different processes. However, it should be noted that among the subjects which had a PBMC sample available at 5 years (n=27), the proportion of individuals who experienced an sLRI in infancy (29.63%) differed to that of the total subset (n=50, 46% sLRI positive in infancy). We also calculated module eigengenes to summarise overall module expression and compared this with clinical traits. The CBMC LPS-induced IFN module eigengene stratified individuals susceptible to sLRIs in the first year of life (p=0.016), as well as those with asthma (p=0.015) and current wheeze (p=0.02) at 5 years of age (Figures 4F, S7A,B). This result was only significant for the LPS response, was specific for the IFN module, and was only observed for comparisons of severe LRIs (Figures 4G, S7C–E).

IFN responses induced in CBMCs by TLR ligands *in vitro* are representative of IFN responses during natural infections

We questioned whether the IFN module gene expression profiles exhibited by CBMCs following *in vitro* culture with model antigens in our study are reflective of naturally occurring

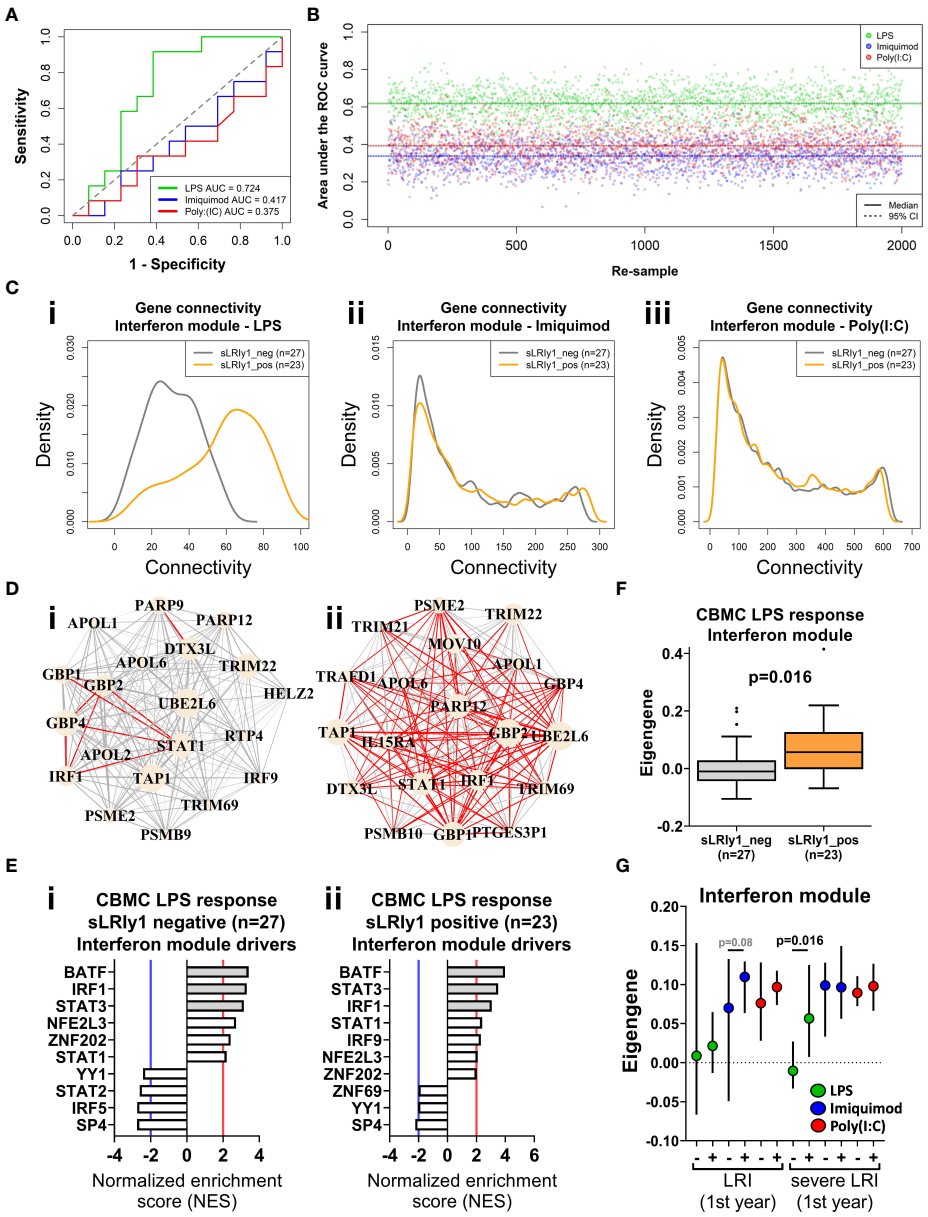

FIGURE 4
IFN genes activated following LPS stimulation at birth predict sLRI susceptibility in the first year of life. **(A)** Random forest (RF) classifiers were trained on the respective IFN module genes from half the study subjects and validated on the remaining subjects (50/50). RF models were optimised with respect to number of genes sampled at each split and number of trees grown. Plot depicts the area under the Receiver Operator Characteristic curve (AUC-ROC) defined by the rate of false (x-axis, 1-specificity) and true (y-axis, sensitivity) positives. **(B)** RF model predictions were repeated by re-sampling the training/validation set (50/50 random assignment) 2,000 times. Plot show the AUC-ROC for each re-sample, with median (solid lines) and 95% CIs (dashed lines). **(C)** Network connectivity density plot of IFN module gene networks stratified by individuals who did (orange) and did not (grey) record an sLRI in the first year of life. **(D)** Network wiring diagram of the most connected genes of the CBMC LPS-induced IFN module gene from individuals resistant (I, n=27) and susceptible (II n=23) to sLRIs in infancy. Node and edge characteristics are the same as Figure 3B. **(E)** Top 10 master regulators identified for the CBMC LPS-induced IFN response module for resistant (i) and susceptible (ii) subjects. Bar plot characteristics are the same Figure 3C. **(F)** Box-and-whisker plot of the CBMC LPS-induced IFN module eigengene, grouped by susceptible (orange) and resistant (grey) individuals. Boxes show median, 25th and 75th quartiles and whiskers are determined by the Tukey method; P value determined by Mann-Whitney U test. **(G)** Plot of IFN module eigengenes for CBMC responses grouped by individuals who were resistant (-) and susceptible (+) to LRIs and sLRIs in infancy. P values determined by Mann-Whitney U test and significant result reflects **(F)**. Plot shows median (symbol) and 95% CI (bars).

IFN responses to childhood infections *in vivo*. To address this issue, we trained RF classifiers on our CBMC-derived IFN module genes and used them to classify samples from publicly available data sets from the Gene Expression Omnibus. Gene expression data from external cohorts was filtered to only those genes present in the corresponding IFN modules for each analysis. The first data set comprised whole blood gene expression profiles from children (<17yrs) with febrile illnesses requiring hospitalization with confirmed bacterial (n = 52) or viral (n = 92) infections versus healthy controls (n = 52) [GSE72809 (59)]. We found that RF classifiers trained on LPS- and Imiquimod/Poly(I:C)-induced IFN module genes accurately predicted children with bacterial (AUC = 0.889) and viral (AUC = 0.874/0.838) infections, respectively (Figures 5A, S7F). The second data set consisted of PBMC samples from infants (<18mo, n=30) and young children (18mo-5yrs, n = 32) who were hospitalized with acute viral bronchiolitis [GSE113211 (60)]. Classifiers built on unstimulated and either Imiquimod- (AUC=0.8) or Poly(I:C)- (AUC=0.877) induced IFN genes could accurately stratify samples collected during acute illness compared to matched post-convalescent samples (symptom-free, 8.8 ± 2.5 weeks post-infection), independent of age (Figures 5B, S7G). The models performed well for infants (AUC = 0.922, Poly(I:C); AUC = 0.827, Imiquimod) and children (AUC = 0.789, Poly(I:C); AUC = 0.842, Imiquimod) separately (Figure S7G). The third data set consisted of nasal-derived gene expression profiles from study visits of asthmatic children (6-17yrs) with viral-related or non-viral "cold"-like illness (1-6 days post-onset), some of which later experienced exacerbations (n=83, 58 were viral-positive) [GSE115770 (61)]. Symptomatic children with respiratory viral infections were accurately predicted from symptomatic, yet virus-negative, children from Imiquimod (AUC=0.8) and Poly(I:C) (AUC=0.832) defined RF classifiers (Figures 5C, S7H). Additionally, there was comparable accuracy classifying virus-positive and virus-negative asthmatic children who subsequently experienced an exacerbation (within 10 days of symptom onset) (Figure S7H). In the same study, prediction performance was less accurate from peripheral blood-derived gene expression profiles (Figure S7H). Taken together, these analyses demonstrate that CBMC-derived IFN gene expression patterns induced with LPS, Imiquimod, or poly(I:C) in this study are representative of childhood IFN responses to microbial pathogens.

Multi-omic integration of LPS-stimulated CBMC data

Lastly, we employed multi-omic data integration (DIABLO (52)) to identify correlated molecular features across biological layers which may confer sLRI risk. Input data consisted of CBMC baseline immune cell type proportions (n = 8), significantly variable mRNA transcripts (n=6344), VIPER-derived regulon activity scores (n = 1224), metabolites (n = 49), and cytokine/chemokine proteins (n = 39). Importantly for this analysis, input genes were selected as those which were significantly variable between LPS-stimulated and unstimulated CBMC samples and were not selectively enriched for IFN-related transcripts. The data reinforced that LPS-induced IFN-signalling transcripts (*IRF9*, *STAT1*, *GBP2/4*) and IRF1 activity were key determinants of risk for sLRI in the first year of life, in combination with lymphocyte and monocyte proportions, immune regulators (e.g. RFX5, NFIX), amino acids, and proinflammatory cytokines/chemokines (IL-1β, MIP-1α, MIF) (Figure 5D). As we separately identified LPS-induced IRF1 activity from network, master regulator, and integrative analyses, we further investigated IRF1 gene expression correlations. *IRF1* gene expression at birth positively correlated with selective STAT and IRF family transcription factor genes (e.g. *STAT1*, *IRF7/9*), proinflammatory mediators (e.g. IL-1β, IL-6, CCL3/MIP-1α), and viral-related receptor genes (e.g. *ICAM1*, *IFIH1*) (Figure 6A). Additionally, CBMC *STAT1* and *IFIH1* gene expression was higher in response to LPS among individuals who were susceptible to sLRIs in infancy, and *IFIH1* expression correlated with *IRF1* and *STAT1* expression (Figures 6B, C).

Discussion

Severe viral lower respiratory tract infections (sLRIs) are a leading cause of hospitalization for infants and children and constitute a major risk factor for subsequent asthma development (2–6). Whilst it is increasingly recognised that bacterial and viral pathogens may interact to drive the pathogenesis of sLRIs, the underlying innate immune mechanisms are not well understood. We employed a multi-omic approach to systematically profile innate immune responses to bacterial (LPS) and viral nucleic acid (Poly(I:C)/Imiquimod) related stimuli at birth to first characterize these responses and then investigate whether any response patterns are associated with susceptibility to sLRI in the first year of life. The data showed that whilst innate immune responses to the panel of stimuli comprised overlapping proinflammatory and IFN-mediated gene expression programs, the LPS but not Poly(I:C)/Imiquimod response profiles at birth were predictive of sLRI incidence in the first year of life. Moreover, sLRI susceptibility was associated with the activation of a network of IFN genes, and the connectivity patterns of this network in cord blood LPS responses were strikingly exaggerated among infants susceptible to sLRI. Furthermore, the connectivity pattern of these genes was highly variable between the cord and 5 year LPS responses. These findings were specific for the LPS-induced IFN responses and were not observed following activation of viral nucleic acid sensing pathways, nor from proinflammatory module genes of any response tested, suggesting that the wiring of the LPS response is specifically altered in children who are at heightened risk for sLRI in infancy. It is noteworthy that expression of the LPS-induced IFN module was not associated

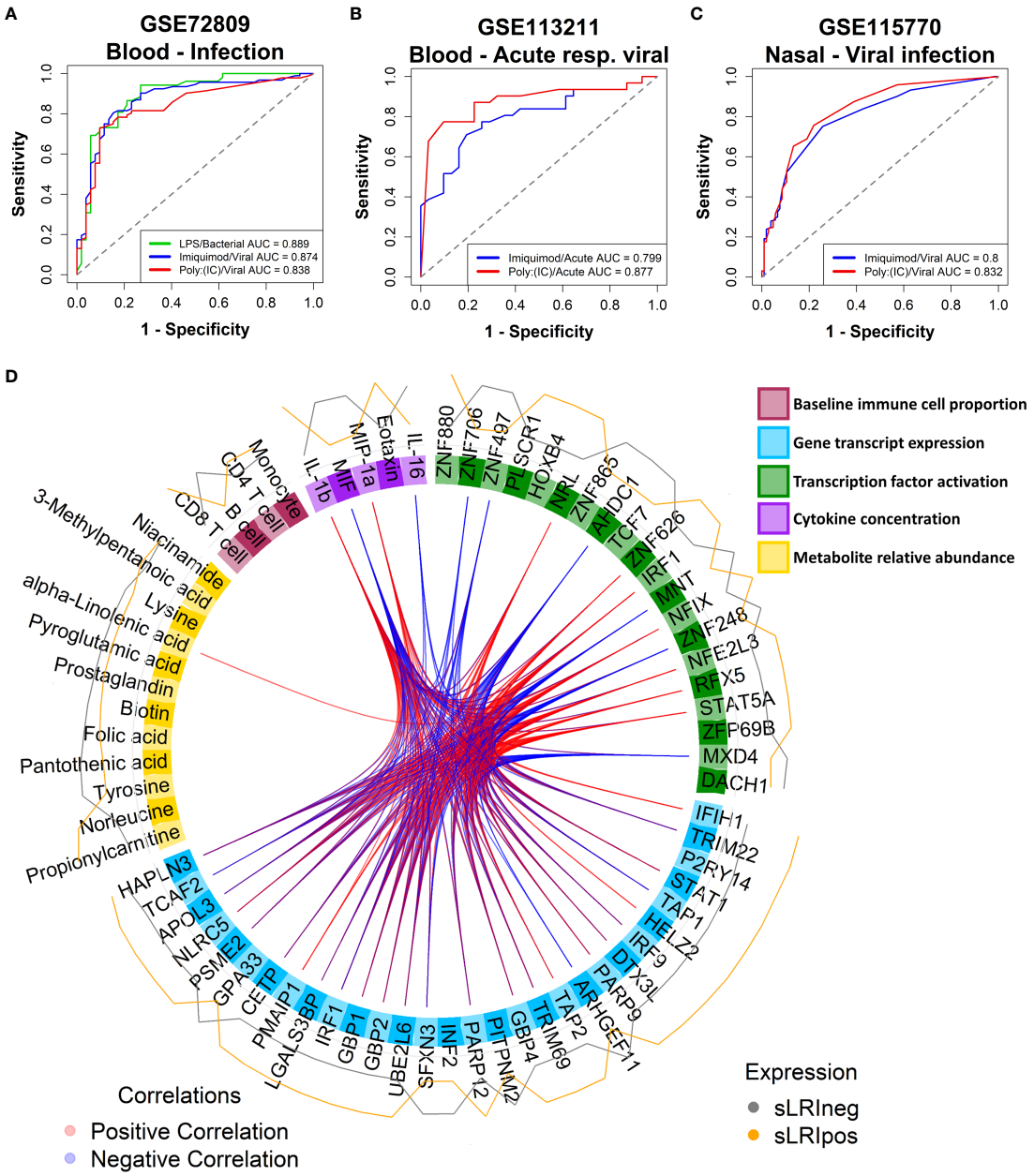

FIGURE 5
CBMC IFN responses reflect natural childhood response to infection; Multi-omic integration reinforces that LPS-induced IFN signalling at birth is a determinant of sLRI risk in infancy. **(A)** A random forest classifier was trained on Unstimulated and LPS or Imiquimod/Poly(I:C) CBMC IFN module gene expression data (n = 100) and used to predict children (<17yrs) hospitalized with bacterial (n = 52) and viral infections (n = 92), respectively, from healthy controls (n = 52) from blood-derived gene expression profiles. Gene expression data sets were restricted to available IFN module genes and RF models were optimised with respect to the number of genes and trees. Plot depicts the AUC-ROC defined by the rate of false (x-axis, 1-specificity) and true (y-axis, sensitivity) positives. **(B)** RF classifiers trained on Unstimulated and Imiquimod or Poly(I:C) CBMC IFN module gene expression data (n=100) and used to predict PBMC gene expression profiles from infants (<18mo; n=15) and children (18mo-5yrs; n=16) presenting to hospital with acute viral respiratory infections from profiles collected during convalescence. Plot depicts the AUC-ROC. **(C)** RF classifiers trained on Unstimulated and Imiquimod or Poly(I:C) CBMC IFN module gene expression data (n=100) and used to predict asthmatic children (6-17yrs) with cold-like symptoms who do (n=193) and do not (n=105) have detectable airway viral infection from nasal-derived gene expression profiles. Plot depicts the AUC-ROC. **(D)** Circos plot displaying the multi-layer risk profile for sLRI susceptibility in infancy determined from multi-omic data integration, showing between block correlation from the 1st latent component; correlations stronger that $\pm$0.8 are shown. Peripheral lines represent the relative expression of features from individuals who were resistant (grey) or susceptible (orange) to sLRIs in the first year of life. Input data was adjusted with respect to matched unstimulated samples (except baseline immunophenotype data).

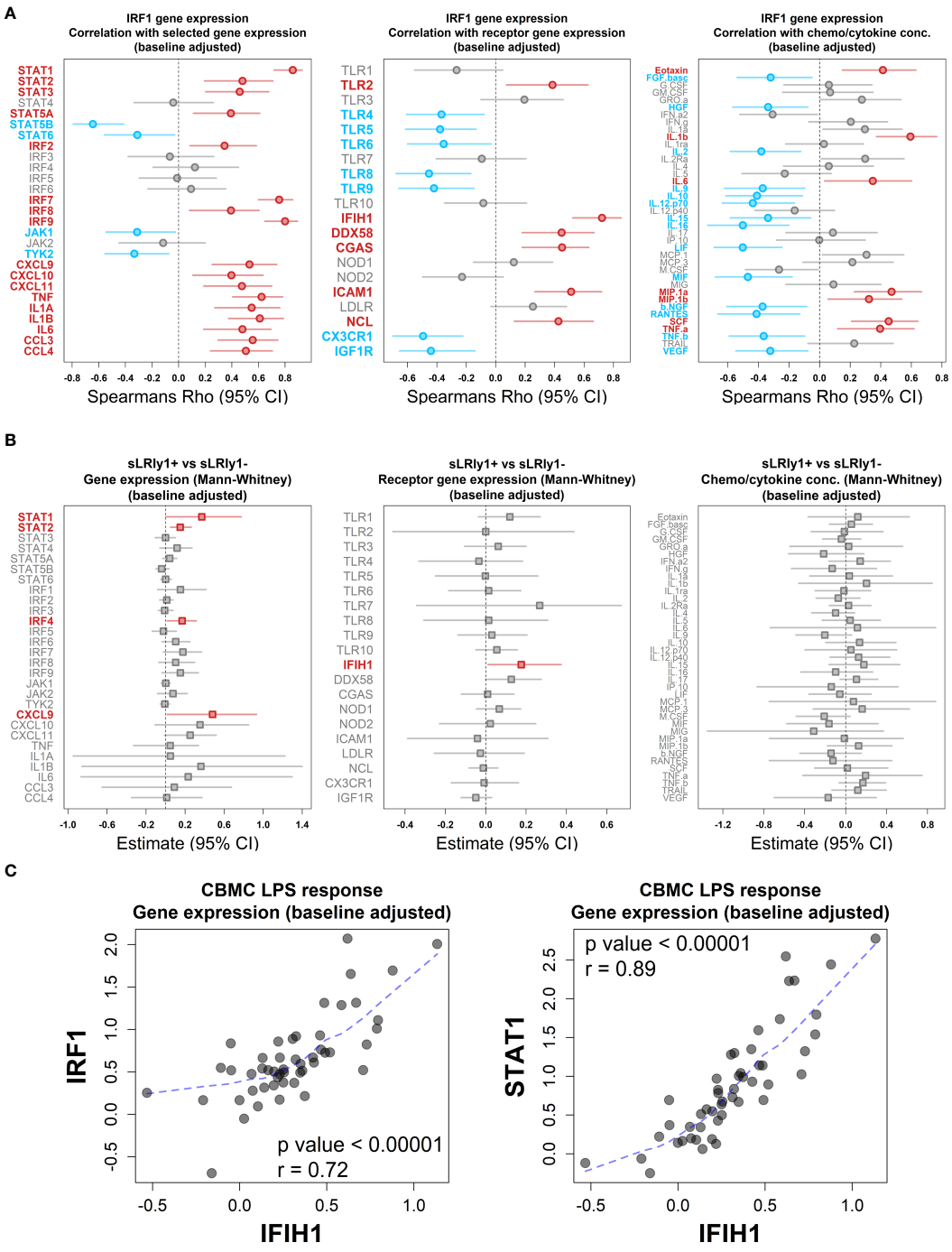

FIGURE 6
LPS-induced IRF1 correlates with key interferon/proinflammatory mediators. **(A)** Plot of the association between LPS-induced IRF1 gene expression with selected IFN and proinflammatory gene expression (left), viral-related receptor gene expression (center) and chemo/cytokine protein concentration (right). Data was adjusted with respect to matched unstimulated samples and plots shows Spearman's Rho value (symbol) and 95% CI (bars, 1000 bootstraps); Red and blue data points/labels denote positive and negative correlations, respectively, with a BH-adjusted p value <0.05. **(B)** Analysis of selected IFN and proinflammatory gene expression (left), viral-related receptor gene expression (center) and chemo/cytokine protein concentration (right) with respect to sLRI susceptibility in the first year of life. Data was adjusted with respect to matched unstimulated samples and plots show the Mann-Whitney U test estimates and 95% CIs for CBMC data of individuals who are susceptible compared to resistant to sLRIs in infancy. Red data points/labels indicate increased expression with a p value < 0.05. **(C)** Spearman's correlation and associated p value between IFIH1 (x-axis) and IRF1/STAT1 (y-axis) gene expression from CBMC samples stimulated with LPS (n=50). Data was adjusted with respect to matched unstimulated samples. Dashed blue line represents a loess fit of the data.

with mild (non-wheezy/non-febrile) lower respiratory tract infections, highlighting a specific link to infection severity. Master regulator analysis identified IRF1 as a key driver of LPS-induced IFN responses at birth. By age 5, the data showed that the activity of IRF1 may be replaced by other members of the IRF transcription factor family, including IRF7, suggesting that this response is subject to developmental regulation. In contrast, IRF7 was the dominant driver of Poly(I:C)-/Imiquimod-induced IFN response at birth and 5 years. IRF1 was also identified as a highly connected node of the LPS-induced IFN network and correlated with distinct IFN-signalling (e.g. *STAT1* but not *JAK1/TYK2*) and proinflammatory (e.g. *CXCL9/10/11*, IL-1β) mediators, several of which exhibited significantly higher expression in infants at risk of sLRI. These data suggest that an LPS-induced and IRF1-regulated IFN gene network, detectable at birth, is associated with sLRI susceptibility in infancy. Consequently, we conclude that susceptibility to sLRI in infancy may be in part already determined at birth and this may be exploited to identify at-risk infants for early intervention and identify potential targets for drug development.

The contribution of bacteria and their products to the severity of viral-related respiratory infections has been suggested by numerous studies. For example, environmental LPS exposure modulates the severity of RSV infections depending on the levels of LPS exposure and TLR4 genotype (62). Moreover, studies from our group in the same cohort have demonstrated that sLRIs are often preceded by the transient incursion of pathogenic bacteria in the airway microbiome (17, 18). Multiple other studies have reported that the presence of pathogenic bacteria in the airways is associated with more severe viral respiratory tract infections for both RSV and RV (63–66). Additionally, bacterial colonization of the airway in neonates with *Streptococcus pneumoniae*, *Haemophilus influenzae*, or *Moraxella catarrhalis* was associated with persistent wheeze and severe exacerbations of wheeze (15), which are generally initiated by viral respiratory infections. Finally, Illi et al. demonstrated that LPS responses at 12 months of age in individuals who carry asthma-risk alleles on 17q21 are associated with risk of wheeze (32).

The proposition that heightened LPS-induced IFN responses/gene network connectivity patterns at birth may confer risk of viral-related sLRI during infancy at first sight may appear counterintuitive given the acknowledged protective role of IFNs in antiviral immunity (67, 68). However, hyper-production of IFNs in the airways during viral-associated infections, especially during infancy, are also known to contribute to accompanying inflammatory symptom severity (60, 69). Furthermore, IFN responses during bacterial infections have pleiotropic effects which may be beneficial or detrimental, depending on the site of infection and the specific pathogen involved (70, 71). For example, type I IFN mediated suppression of IL-1β responses (72) on the one hand attenuates lethal hyperinflammation associated with S. *pyogenes* (73) and on the other hand diminishes the antimicrobial function of IL-1β, resulting in increased airway and systemic M. *tuberculosis* colonisation (74). This suggests a balance exists between IFN and proinflammatory responses which impacts the clinical outcome of bacterial infection, although it is not clear how anti-bacterial responses may protect against or exacerbate viral infections. IRF1 promotes the constitutive expression of interferon-mediated antiviral programs at baseline and the inducible expression of these programs triggered by respiratory viral infections (75–78), and acts as a branch point between IFN responses and induction of specific pro-inflammatory genes (79). The function of IRF1 following bacterial infections is incompletely understood, although it appears essential for IFN-related inflammasome activation during *Francisella novicida* infection (75, 80) indicating a role in IFN and proinflammatory responses following pathogenic bacterial exposure. It is also notable in this context that IRF1 gene variants have been linked to childhood asthma risk and dysregulated proinflammatory responses (81). We did not observe a direct difference in IRF1 expression between individuals who did or did not record an sLRI in the first year of life at the time point investigated in our study. This suggests that the sLRI risk putatively associated with IRF1 may be conferred by its regulatory actions rather than its gene expression magnitude, or that IRF1 expression dysregulation occurs earlier than was measured in this study (18hrs). It is our interpretation of the data that IRF1 is a key driver of the LPS-induced IFN response networks associated with sLRI susceptibility in the first year of life.

The immune system of newborns is subject to drastic developmental changes in the first weeks (82) and months (83) of life. Since our study focused on CBMC-derived innate immune responses, we explored the extent to which CBMC responses reflect immune responses to infections occurring at later ages during childhood by applying classifiers trained on gene expression data generate in this study to infection-associated host response data derived from published cohorts. This approach was not intended as validation of the principal findings linking LPS-induced IFN response at birth with subsequent sLRI risk, but rather to establish whether the IFN response networks characterized from our *in vitro* experiments in CBMCs are representative of those operating in nature. LPS-induced IFN responses from CBMCs were used to accurately stratify children presenting to hospital with current bacterial infections, compared to controls, from whole blood samples (59). Likewise, Imiquimod/Poly(I:C)-induced CBMC IFN responses accurately classified children with febrile viral infections. Moreover, the CBMC-derived IFN responses induced by imiquimod or Poly(I:C) could classify infants and children with viral bronchiolitis and asthma exacerbations from blood and airway samples compared to controls, suggesting that these signatures are robust to some extent to variations in cellular composition between circulating blood and airway

tissue. We also found that the accuracy of the random forest models was higher when predicting infants (<18mo) compared to younger (18mo-5yrs) (GSE113211 (60)) or older (6-17yrs) children (GSE115770 (61)). These data support that the IFN gene networks identified from our *in vitro* investigation of cord blood are *bona fide* response mediators of infection in real world contexts.

We acknowledge that our study has limitations that should be addressed. Firstly, gene expression profiles were generated from mixed cord blood cell populations and as such cannot distinguish cell-specific information. Further investigation with single-cell RNA sequencing may localize gene expression programs potentially responsible for sLRI risk in individual cells. Secondly, the study population consisted of 50 subjects from a high-risk cohort, limiting the power to detect disease-associated mechanisms. Follow-up studies with samples from large, unselected cohorts may identify more subtle mechanisms that confer risk for sLRI. Additionally, we utilised CBMC samples for this work, because they are readily available and abundant at birth. However, recent advances in sample processing methods now enable the generation of multi-omic data from small sample volumes, enabling longitudinal profiling of infants/children with natural infections (82). We profiled innate immune responses at a single timepoint (18hrs), and therefore our analyses cannot capture response dynamics. Finally, we employed three TLR ligands to mimic PRR activation events experienced during bacterial or viral infections. However, we acknowledge using TLR ligands is not equivalent to using live bacteria or virus. Notwithstanding these limitations, the major strengths of this study lie in the systems biology approach that provided genome-wide investigation of the CBMC responses, and the well characterized prospective cohort design, which allowed us to investigate sLRI risk with the totality of viral infections and relevant clinical outcomes recorded. In summary, our findings demonstrate that the risk of sLRI in early life is in part already determined at birth, and that the developmental status of LPS-induced interferon responses may represent a key factor which confers susceptibility. Our findings provide a rationale for the early identification of infants at risk for sLRI and identifies potential targets which may be relevant for drug development.

Data availability statement

The datasets presented in this study are available. RNA-Seq data is available from the NCBI Gene Expression Omnibus repository with accession number GSE184383. Raw and processed cytokine/chemokine data are provided as a Supplement (Data S1). Raw and processed metabolite data are provided as a Supplement (Data S2).

Ethics statement

Ethics was approved by The University of Western Australia (reference RA/4/1/7560). Written informed consent to participate in this study was provided by the participants' legal guardian/next of kin.

Author contributions

PGH, AB, and PDS conceived the study and designed the experiments. JFR analysed the data. JFR and MS assisted with the experimental design and optimized and performed the experiments. JFR, MS, AB, SNR, DM, BJH, DIB, and DHS were involved in data acquisition. JFR, AB, PGH, DHS, SNR, DIB, MC, and YVK were involved in determining the analysis approach and optimization. JFR, AB, and PGH interpreted the data and drafted the manuscript. All authors contributed to the article and approved the submitted version.

Funding

This work was funded by National Health and Medical Research Council (NHMRC) project grant #1129996. PDS is a Leadership Fellow (L3) of the NHMRC.

Acknowledgments

The authors would like to thank the study participants and their families for their involvement.

Conflict of interest

JFR and AB are co-inventors on a provisional patent filed subsequent to this work. JFR and AB are co-founders, equity holders, and directors of a startup company Respiradigm Pty Ltd related to this provisional patent.

The remaining authors declare that the research was conducted in the absence of any commercial or financial relationships that could be construed as a potential conflict of interest.

Publisher's note

Supplementary material

The Supplementary Material for this article can be found online at: https://www.frontiersin.org/articles/10.3389/fimmu.2022.876654/full#supplementary-material

DATA S1
Raw and normalized cytokines multiplex assay data.

DATA S2
Raw and corrected metabolite relative abundances.

References

1. Nair H, Nokes DJ, Gessner BD, Dherani M, Madhi SA, Singleton RJ, et al. Global burden of acute lower respiratory infections due to respiratory syncytial virus in young children: a systematic review and meta-analysis. *Lancet.* (2010) 375 (9725):1545–55. doi: 10.1016/S0140-6736(10)60206-1

2. Kieninger E, Fuchs O, Latzin P, Frey U, Regamey N. Rhinovirus infections in infancy and early childhood. *Eur Respir J* (2013) 41(2):443–52. doi: 10.1183/09031936.00203511

3. Sigurs N, Bjarnason R, Sigurbergsson F, Kjellman B. Respiratory syncytial virus bronchiolitis in infancy is an important risk factor for asthma and allergy at age 7. *Am J Respir Crit Care Med* (2000) 161(5):1501–7. doi: 10.1164/ajrccm.161.5.9906076

4. Jackson DJ. The role of rhinovirus infections in the development of early childhood asthma. *Curr Opin Allergy Clin Immunol* (2010) 10(2):133–8. doi: 10.1097/ACI.0b013e3283352f7c

5. Kusel MM, de Klerk NH, Kebadze T, Vohma V, Holt PG, Johnston SL, et al. Early-life respiratory viral infections, atopic sensitization, and risk of subsequent development of persistent asthma. *J Allergy Clin Immunol* (2007) 119(5):1105–10. doi: 10.1016/j.jaci.2006.12.669

6. Jackson DJ, Gangnon RE, Evans MD, Roberg KA, Anderson EL, Pappas TE, et al. Wheezing rhinovirus illnesses in early life predict asthma development in high-risk children. *Am J Respir Crit Care Med* (2008) 178(7):667–72. doi: 10.1164/rccm.200802-309OC

7. Jartti T, Gern JE. Role of viral infections in the development and exacerbation of asthma in children. *J Allergy Clin Immunol* (2017) 140(4):895–906. doi: 10.1016/j.jaci.2017.08.003

8. Heinonen S, Rodriguez-Fernandez R, Diaz A, Oliva Rodriguez-Pastor S, Ramilo O, Mejias A. Infant immune response to respiratory viral infections. *Immunol Allergy Clin North Am* (2019) 39(3):361–76. doi: 10.1016/j.iac.2019.03.005

9. Jartti T, Bonnelykke K, Elenius V, Feleszko W. Role of viruses in asthma. *Semin Immunopathol* (2020) 42(1):61–74. doi: 10.1007/s00281-020-00781-5

10. Rubner FJ, Jackson DJ, Evans MD, Gangnon RE, Tisler CJ, Pappas TE, et al. Early life rhinovirus wheezing, allergic sensitization, and asthma risk at adolescence. *J Allergy Clin Immunol* (2017) 139(2):501–7. doi: 10.1016/j.jaci.2016.03.049

11. Lukkarinen M, Koistinen A, Turunen R, Lehtinen P, Vuorinen T, Jartti T. Rhinovirus-induced first wheezing episode predicts atopic but not nonatopic asthma at school age. *J Allergy Clin Immunol* (2017) 140(4):988–95. doi: 10.1016/j.jaci.2016.12.991

12. Olenec JP, Kim WK, Lee WM, Vang F, Pappas TE, Salazar LE, et al. Weekly monitoring of children with asthma for infections and illness during common cold seasons. *J Allergy Clin Immunol* (2010) 125(5):1001–6.e1. doi: 10.1016/j.jaci.2010.01.059

13. Bisgaard H, Hermansen MN, Bonnelykke K, Stokholm J, Baty F, Skytt NL, et al. Association of bacteria and viruses with wheezy episodes in young children: prospective birth cohort study. *BMJ* (2010) 341:c4978. doi: 10.1136/bmj.c4978

14. Carlsson CJ, Vissing NH, Sevelsted A, Johnston SL, Bonnelykke K, Bisgaard H. Duration of wheezy episodes in early childhood is independent of the microbial trigger. *J Allergy Clin Immunol* (2015) 136(5):1208–14.e1-5. doi: 10.1016/j.jaci.2015.05.003

15. Bisgaard H, Hermansen MN, Buchvald F, Loland L, Halkjaer LB, Bonnelykke K, et al. Childhood asthma after bacterial colonization of the airway in neonates. *N Engl J Med* (2007) 357(15):1487–95. doi: 10.1056/NEJMoa052632

16. Larsen JM, Brix S, Thysen AH, Birch S, Rasmussen MA, Bisgaard H. Children with asthma by school age display aberrant immune responses to pathogenic airway bacteria as infants. *J Allergy Clin Immunol* (2014) 133 (4):1008–13. doi: 10.1016/j.jaci.2014.01.010

17. Teo SM, Mok D, Pham K, Kusel M, Serralha M, Troy N, et al. The infant nasopharyngeal microbiome impacts severity of lower respiratory infection and risk of asthma development. *Cell Host Microbe* (2015) 17(5):704–15. doi: 10.1016/j.chom.2015.03.008

18. Teo SM, Tang HHF, Mok D, Judd LM, Watts SC, Pham K, et al. Airway microbiota dynamics uncover a critical window for interplay of pathogenic bacteria and allergy in childhood respiratory disease. *Cell Host Microbe* (2018) 24(3):341–52.e5. doi: 10.1016/j.chom.2018.08.005

19. Bellinghausen C, Rohde GGU, Savelkoul PHM, Wouters EFM, Stassen FRM. Viral-bacterial interactions in the respiratory tract. *J Gen Virol* (2016) 97 (12):3089–102. doi: 10.1099/jgv.0.000627

20. Beigelman A, Bacharier LB. Early-life respiratory infections and asthma development: role in disease pathogenesis and potential targets for disease prevention. *Curr Opin Allergy Clin Immunol* (2016) 16(2):172–8. doi: 10.1097/ACI.0000000000000244

21. von Mutius E, Vercelli D. Farm living: effects on childhood asthma and allergy. *Nat Rev Immunol* (2010) 10(12):861–8. doi: 10.1038/nri2871

22. Stein MM, Hrusch CL, Gozdz J, Igartua C, Pivniouk V, Murray SE, et al. Innate immunity and asthma risk in Amish and Hutterite farm children. *N Engl J Med* (2016) 375(5):411–21. doi: 10.1056/NEJMoa1508749

23. Kollmann TR, Kampmann B, Mazmanian SK, Marchant A, Levy O. Protecting the newborn and young infant from infectious diseases: Lessons from immune ontogeny. *Immunity.* (2017) 46(3):350–63. doi: 10.1016/j.immuni.2017.03.009

24. Georgountzou A, Papadopoulos NG. Postnatal innate immune development: From birth to adulthood. *Front Immunol* (2017) 8:957. doi: 10.3389/fimmu.2017.00957

25. Yu JC, Khodadadi H, Malik A, Davidson B, Salles E, Bhatia J, et al. Innate immunity of neonates and infants. *Front Immunol* (2018) 9:1759. doi: 10.3389/fimmu.2018.01759

26. Belderbos ME, van Bleek GM, Levy O, Blanken MO, Houben ML, Schuijff L, et al. Skewed pattern of toll-like receptor 4-mediated cytokine production in human neonatal blood: low LPS-induced IL-12p70 and high IL-10 persist throughout the first month of life. *Clin Immunol* (2009) 133(2):228–37. doi: 10.1016/j.clim.2009.07.003

27. Kollmann TR, Crabtree J, Rein-Weston A, Blimkie D, Thommai F, Wang XY, et al. Neonatal innate TLR-mediated responses are distinct from those of adults. *J Immunol* (2009) 183(11):7150–60. doi: 10.4049/jimmunol.0901481

28. Nguyen M, Leuridan E, Zhang T, De Wit D, Willems F, Van Damme P, et al. Acquisition of adult-like TLR4 and TLR9 responses during the first year of life. *PLoS One* (2010) 5(4):e10407. doi: 10.1371/journal.pone.0010407

29. Marr N, Wang TI, Kam SH, Hu YS, Sharma AA, Lam A, et al. Attenuation of respiratory syncytial virus-induced and RIG-i-dependent type I IFN responses in human neonates and very young children. *J Immunol* (2014) 192(3):948–57. doi: 10.4049/jimmunol.1302007

30. DeVries A, Wlasiuk G, Miller SJ, Bosco A, Stern DA, Lohman IC, et al. Epigenome-wide analysis links SMAD3 methylation at birth to asthma in children of asthmatic mothers. *J Allergy Clin Immunol* (2017) 140(2):534–42. doi: 10.1016/j.jaci.2016.10.041

31. Holt PG, Mok D, Panda D, Renn L, Fabozzi G, deKlerk NH, et al. Developmental regulation of type 1 and type 3 interferon production and risk for infant infections and asthma development. *J Allergy Clin Immunol* (2019) 143 (3):1176–82.e5. doi: 10.1016/j.jaci.2018.08.035

32. Illi S, Depner M, Pfefferle PI, Renz H, Roduit C, Taft DH, et al. Immune responsiveness to LPS determines risk of childhood wheeze and asthma in 17q21 risk allele carriers. *Am J Respir Crit Care Med* (2022) 205(6):641–50. doi: 10.1164/rccm.202106-1458OC

33. Roponen M, Yerkovich ST, Hollams E, Sly PD, Holt PG, Upham JW. Toll-like receptor 7 function is reduced in adolescents with asthma. *Eur Respir J* (2010) 35(1):64–71. doi: 10.1183/09031936.00172008

34. Kusel MM, de Klerk NH, Holt PG, Kebadze T, Johnston SL, Sly PD. Role of respiratory viruses in acute upper and lower respiratory tract illness in the first year

of life: a birth cohort study. *Pediatr Infect Dis J* (2006) 25(8):680–6. doi: 10.1097/01.inf.0000226912.88900.a3

35. Kusel MM, Kebadze T, Johnston SL, Holt PG, Sly PD. Febrile respiratory illnesses in infancy and atopy are risk factors for persistent asthma and wheeze. *Eur Respir J* (2012) 39(4):876–82. doi: 10.1183/09031936.00193310

36. Holt PG, Rowe J, Kusel M, Parsons F, Hollams EM, Bosco A, et al. Toward improved prediction of risk for atopy and asthma among preschoolers: a prospective cohort study. *J Allergy Clin Immunol* (2010) 125(3):653–9.9.e1-9 e7. doi: 10.1016/j.jaci.2009.12.018

37. Yu M, Levine SJ. Toll-like receptor, RIG-i-like receptors and the NLRP3 inflammasome: key modulators of innate immune responses to double-stranded RNA viruses. *Cytokine Growth Factor Rev* (2011) 22(2):63–72. doi: 10.1016/j.cytogfr.2011.02.001

38. Barrett T, Wilhite SE, Ledoux P, Evangelista C, Kim IF, Tomashevsky M, et al. NCBI GEO: archive for functional genomics data sets–update. *Nucleic Acids Res* (2013) 41(Database issue):D991–5. doi: 10.1093/nar/gks1193

39. Broadhurst D, Goodacre R, Reinke SN, Kuligowski J, Wilson ID, Lewis MR, et al. Guidelines and considerations for the use of system suitability and quality control samples in mass spectrometry assays applied in untargeted clinical metabolomic studies. *Metabolomics.* (2018) 14(6):72. doi: 10.1007/s11306-018-1367-3

40. Robinson MD, McCarthy DJ, Smyth GK. edgeR: a bioconductor package for differential expression analysis of digital gene expression data. *Bioinformatics.* (2010) 26(1):139–40. doi: 10.1093/bioinformatics/btp616

41. Ritchie ME, Phipson B, Wu D, Hu Y, Law CW, Shi W, et al. Limma powers differential expression analyses for RNA-sequencing and microarray studies. *Nucleic Acids Res* (2015) 43(7):e47. doi: 10.1093/nar/gkv007

42. Breuer K, Foroushani AK, Laird MR, Chen C, Sribnaia A, Lo R, et al. InnateDB: systems biology of innate immunity and beyond–recent updates and continuing curation. *Nucleic Acids Res* (2013) 41(Database issue):D1228–33. doi: 10.1093/nar/gks1147

43. Newman AM, Steen CB, Liu CL, Gentles AJ, Chaudhuri AA, Scherer F, et al. Determining cell type abundance and expression from bulk tissues with digital cytometry. *Nat Biotechnol* (2019) 37(7):773–82. doi: 10.1038/s41587-019-0114-2

44. Regev A, Teichmann SA, Lander ES, Amit I, Benoist C, Birney E, et al. The human cell atlas. *Elife* (2017) 6:e27041. doi: 10.7554/eLife.27041

45. Langfelder P, Horvath S. WGCNA: an r package for weighted correlation network analysis. *BMC Bioinf* (2008) 9:559. doi: 10.1186/1471-2105-9-559

46. Yu G, He QY. ReactomePA: an R/Bioconductor package for reactome pathway analysis and visualization. *Mol Biosyst* (2016) 12(2):477–9. doi: 10.1039/C5MB00663E

47. Yu G, Wang LG, Han Y, He QY. clusterProfiler: an r package for comparing biological themes among gene clusters. *OMICS.* (2012) 16(5):284–7. doi: 10.1089/omi.2011.0118

48. Rinchai D, Roelands J, Toufiq M, Hendrickx W, Altman MC, Bedognetti D, et al. BloodGen3Module: Blood transcriptional module repertoire analysis and visualization using r. *Bioinformatics* (2021) 37(16):2382–9. doi: 10.1101/2020.07.16.205963

49. Margolin AA, Nemenman I, Basso K, Wiggins C, Stolovitzky G, Dalla Favera R, et al. ARACNE: an algorithm for the reconstruction of gene regulatory networks in a mammalian cellular context. *BMC Bioinf* (2006) 7 Suppl 1:S7. doi: 10.1186/1471-2105-7-S1-S7

50. Alvarez MJ, Shen Y, Giorgi FM, Lachmann A, Ding BB, Ye BH, et al. Functional characterization of somatic mutations in cancer using network-based inference of protein activity. *Nat Genet* (2016) 48(8):838–47. doi: 10.1038/ng.3593

51. Aibar S, Gonzalez-Blas CB, Moerman T, Huynh-Thu VA, Imrichova H, Hulselmans G, et al. SCENIC: single-cell regulatory network inference and clustering. *Nat Methods* (2017) 14(11):1083–6. doi: 10.1038/nmeth.4463

52. Singh A, Shannon CP, Gautier B, Rohart F, Vacher M, Tebbutt SJ, et al. DIABLO: an integrative approach for identifying key molecular drivers from multi-omics assays. *Bioinformatics.* (2019) 35(17):3055–62. doi: 10.1093/bioinformatics/bty1054

53. Kusel MM, Holt PG, de Klerk N, Sly PD. Support for 2 variants of eczema. *J Allergy Clin Immunol* (2005) 116(5):1067–72. doi: 10.1016/j.jaci.2005.06.038

54. Shalek AK, Satija R, Shuga J, Trombetta JJ, Gennert D, Lu D, et al. Single-cell RNA-seq reveals dynamic paracrine control of cellular variation. *Nature.* (2014) 510(7505):363–9. doi: 10.1038/nature13437

55. Jovanovic M, Rooney MS, Mertins P, Przybylski D, Chevrier N, Satija R, et al. Immunogenetics. dynamic profiling of the protein life cycle in response to pathogens. *Science.* (2015) 347(6226):1259038. doi: 10.1126/science.1259038

56. Lawlor N, Nehar-Belaid D, Grassmann JDS, Stoeckius M, Smibert P, Stitzel ML, et al. Single cell analysis of blood mononuclear cells stimulated through either LPS or anti-CD3 and anti-CD28. *Front Immunol* (2021) 12:636720. doi: 10.3389/fimmu.2021.636720

57. de Jong E, Bosco A. Unlocking immune-mediated disease mechanisms with transcriptomics. *Biochem Soc Trans* (2021) 49(2):705–14. doi: 10.1042/BST20200652

58. Burke HB. Predicting clinical outcomes using molecular biomarkers. *biomark Cancer* (2016) 8:89–99. doi: 10.4137/BIC.S33380

59. Herberg JA, Kaforou M, Wright VJ, Shailes H, Eleftherohorinou H, Hoggart CJ, et al. Diagnostic test accuracy of a 2-transcript host RNA signature for discriminating bacterial vs viral infection in febrile children. *JAMA.* (2016) 316 (8):835–45. doi: 10.1001/jama.2016.11236

60. Jones AC, Anderson D, Galbraith S, Fantino E, Gutierrez Cardenas D, Read JF, et al. Personalized transcriptomics reveals heterogeneous immunophenotypes in children with viral bronchiolitis. *Am J Respir Crit Care Med* (2019) 199 (12):1537–49. doi: 10.1164/rccm.201804-0715OC

61. Altman MC, Gill MA, Whalen E, Babineau DC, Shao B, Liu AH, et al. Transcriptome networks identify mechanisms of viral and nonviral asthma exacerbations in children. *Nat Immunol* (2019) 20(5):637–51. doi: 10.1038/s41590-019-0347-8

62. Caballero MT, Serra ME, Acosta PL, Marzec J, Gibbons L, Salim M, et al. TLR4 genotype and environmental LPS mediate RSV bronchiolitis through Th2 polarization. *J Clin Invest* (2015) 125(2):571–82. doi: 10.1172/JCI75183

63. de Steenhuijsen Piters WA, Heinonen S, Hasrat R, Bunsow E, Smith B, Suarez-Arrabal MC, et al. Nasopharyngeal microbiota, host transcriptome, and disease severity in children with respiratory syncytial virus infection. *Am J Respir Crit Care Med* (2016) 194(9):1104–15. doi: 10.1164/rccm.201602-0220OC

64. Diaz-Diaz A, Bunsow E, Garcia-Maurino C, Moore-Clingenpeel M, Naples J, Juergensen A, et al. Nasopharyngeal codetection of haemophilus influenzae and streptococcus pneumoniae shapes respiratory syncytial virus disease outcomes in children. *J Infect Dis* (2022) 225(5):912–23. doi: 10.1093/infdis/jiab481

65. McCauley K, Durack J, Valladares R, Fadrosh DW, Lin DL, Calatroni A, et al. Distinct nasal airway bacterial microbiotas differentially relate to exacerbation in pediatric patients with asthma. *J Allergy Clin Immunol* (2019) 144(5):1187–97. doi: 10.1016/j.jaci.2019.05.035

66. McCauley KE, Flynn K, Calatroni A, DiMassa V, LaMere B, Fadrosh DW, et al. Seasonal airway microbiome and transcriptome interactions promote childhood asthma exacerbations. *J Allergy Clin Immunol* (2022) 150(1):204–13. doi: 10.1016/j.jaci.2022.01.020

67. Fensterl V, Sen GC. Interferons and viral infections. *Biofactors.* (2009) 35 (1):14–20. doi: 10.1002/biof.6

68. McNab F, Mayer-Barber K, Sher A, Wack A, O'Garra A. Type I interferons in infectious disease. *Nat Rev Immunol* (2015) 15(2):87–103. doi: 10.1038/nri3787

69. Jones AC, Anderson D, Galbraith S, Fantino E, Cardenas DG, Read JF, et al. Immunoinflammatory responses to febrile lower respiratory infections in infants display uniquely complex/intense transcriptomic profiles. *J Allergy Clin Immunol* (2019) 144(5):1411–3. doi: 10.1016/j.jaci.2019.07.043

70. Boxx GM, Cheng G. The roles of type I interferon in bacterial infection. *Cell Host Microbe* (2016) 19(6):760–9. doi: 10.1016/j.chom.2016.05.016

71. Kovarik P, Castiglia V, Ivin M, Ebner F. Type I interferons in bacterial infections: A balancing act. *Front Immunol* (2016) 7:652. doi: 10.3389/fimmu.2016.00652

72. Guarda G, Braun M, Staehli F, Tardivel A, Mattmann C, Forster I, et al. Type I interferon inhibits interleukin-1 production and inflammasome activation. *Immunity.* (2011) 34(2):213–23. doi: 10.1016/j.immuni.2011.02.006

73. Castiglia V, Piersigilli A, Ebner F, Janos M, Goldmann O, Dambock U, et al. Type I interferon signaling prevents IL-1beta-Driven lethal systemic hyperinflammation during invasive bacterial infection of soft tissue. *Cell Host Microbe* (2016) 19(3):375–87. doi: 10.1016/j.chom.2016.02.003

74. Mayer-Barber KD, Andrade BB, Barber DL, Hieny S, Feng CG, Caspar P, et al. Innate and adaptive interferons suppress IL-1alpha and IL-1beta production by distinct pulmonary myeloid subsets during mycobacterium tuberculosis infection. *Immunity.* (2011) 35(6):1023–34. doi: 10.1016/j.immuni.2011.12.002

75. Feng H, Zhang YB, Gui JF, Lemon SM, Yamane D. Interferon regulatory factor 1 (IRF1) and anti-pathogen innate immune responses. *PLoS Pathog* (2021) 17(1):e1009220. doi: 10.1371/journal.ppat.1009220

76. Zaheer RS, Proud D. Human rhinovirus-induced epithelial production of CXCL10 is dependent upon IFN regulatory factor-1. *Am J Respir Cell Mol Biol* (2010) 43(4):413–21. doi: 10.1165/rcmb.2009-0203OC

77. Yang J, Tian B, Sun H, Garofalo RP, Brasier AR. Epigenetic silencing of IRF1 dysregulates type III interferon responses to respiratory virus infection in epithelial to mesenchymal transition. *Nat Microbiol* (2017) 2:17086. doi: 10.1038/nmicrobiol.2017.86

78. Panda D, Gjinaj E, Bachu M, Squire E, Novatt H, Ozato K, et al. IRF1 maintains optimal constitutive expression of antiviral genes and regulates the early antiviral response. *Front Immunol* (2019) 10:1019. doi: 10.3389/fimmu.2019.01019

79. Forero A, Ozarkar S, Li H, Lee CH, Hemann EA, Nadjsombati MS, et al. Differential activation of the transcription factor IRF1 underlies the distinct immune responses elicited by type I and type III interferons. *Immunity.* (2019) 51(3):451–64.e6. doi: 10.1016/j.immuni.2019.07.007

80. Man SM, Karki R, Malireddi RK, Neale G, Vogel P, Yamamoto M, et al. The transcription factor IRF1 and guanylate-binding proteins target activation of the AIM2 inflammasome by francisella infection. *Nat Immunol* (2015) 16(5):467–75. doi: 10.1038/ni.3118

81. Landgraf-Rauf K, Boeck A, Siemens D, Klucker E, Vogelsang V, Schmidt S, et al. IRF-1 SNPs influence the risk for childhood allergic asthma: A critical role for pro-inflammatory immune regulation. *Pediatr Allergy Immunol* (2018) 29(1):34–41. doi: 10.1111/pai.12821

82. Lee AH, Shannon CP, Amenyogbe N, Bennike TB, Diray-Arce J, Idoko OT, et al. Dynamic molecular changes during the first week of human life follow a robust developmental trajectory. *Nat Commun* (2019) 10(1):1092. doi: 10.1038/s41467-019-08794-x

83. Olin A, Henckel E, Chen Y, Lakshmikanth T, Pou C, Mikes J, et al. Stereotypic immune system development in newborn children. *Cell.* (2018) 174 (5):1277–92.e14. doi: 10.1016/j.cell.2018.06.045

frontiers | Frontiers in Immunology

TYPE Original Research
PUBLISHED 19 August 2022
DOI 10.3389/fimmu.2022.977327

OPEN ACCESS

EDITED BY
Ying Zhang,
Tsinghua University, China

REVIEWED BY
Xiaojun Zhang,
Yangzhou University, China
Mingchong Yang,
The Ohio State University,
United States

*CORRESPONDENCE
Jianguo He
lsshjg@mail.sysu.edu.cn
Chaozheng Li
lichaozh@mail2.sysu.edu.cn

SPECIALTY SECTION
This article was submitted to Molecular Innate Immunity, a section of the journal Frontiers in Immunology

RECEIVED 24 June 2022
ACCEPTED 01 August 2022
PUBLISHED 19 August 2022

CITATION
Li H, Li Q, Wang S, He J and Li C (2022) Stimulator of interferon genes defends against bacterial infection *via* IKKβ-mediated Relish activation in shrimp.
Front. Immunol. 13:977327.
doi: 10.3389/fimmu.2022.977327

Stimulator of interferon genes defends against bacterial infection *via* IKKβ-mediated Relish activation in shrimp

Haoyang Li[1,2,3,4,5], Qinyao Li[1,2,3,4,5], Sheng Wang[1,2,3,4,5], Jianguo He[1,2,3,4,5]* and Chaozheng Li[1,2,3,4,5]*

[1]State Key Laboratory of Biocontrol, School of Marine Sciences, Sun Yat-sen University, Guangzhou, China, [2]Southern Marine Science and Engineering Guangdong Laboratory (Zhuhai), Zhuhai, China, [3]Guangdong Provincial Key Laboratory of Marine Resources and Coastal Engineering/Guangdong Provincial Key Laboratory for Aquatic Economic Animals, Sun Yat-sen University, Guangzhou, China, [4]Guangdong Laboratory for Lingnan Modern Agriculture, Maoming, China, [5]China-ASEAN Belt and Road Joint Laboratory on Marine Aquaculture Technology, Zhuhai, China

Stimulator of interferon genes (STING) is crucial for the innate immune to defend against pathogenic infections. Our previous study showed that a STING homolog from Litopenaeus vannamei (LvSTING) was involved in antibacterial response *via* regulating antimicrobial peptides (AMPs). Nevertheless, how LvSTING induces AMPs expression to inhibit bacterial infection remains unknown. Herein, we revealed that the existence of a STING–IKKβ–Relish–AMPs axis in shrimp that was essential for opposing to Vibrio parahaemolyticus invasion. We observed that LvRelish was essential for host defense against V. parahaemolyticus infection *via* inducing several AMPs, such as LvALF1, LvCRU1, LvLYZ1 and LvPEN4. Knockdown of LvSTING or LvIKKβ *in vivo* led to the attenuated phosphorylation and diminished nuclear translocation of LvRelish, as well as the impaired expression levels of LvRelish-regulated AMPs. Accordingly, shrimps with knockdown of LvSTING or LvIKKβ or both were vulnerable to V. parahaemolyticus infection. Finally, LvSTING could recruit LvRelish and LvIKKβ to form a complex, which synergistically induced the promoter activity of several AMPs *in vitro*. Taken together, our results demonstrated that the shrimp STING–IKKβ–Relish–AMPs axis played a critical role in the defense against bacterial infection, and provided some insights into the development of disease prevention strategies in shrimp culture.

KEYWORDS

Litopenaeus vannamei, STING, IKKβ, relish, vibrio parahaemolyticus

Introduction

Shrimp farming is the important part of fishing industry, and the economic value of shrimp aquaculture has increased at an annual growth rate of 7.6% from ~26.1 billion dollars in 2013 to ~40.5 billion dollars in 2019 (1). Nevertheless, recent frequent outbreaks of bacterial diseases have resulted in tremendous economic losses (2). Vibrio species, the main pathogens causing bacterial diseases, have been frequently detected in penaeid shrimp culture ponds with at least 14 species implicated (e.g. *Vibrio parahaemolyticus*, *Vibrio harveyi* and *Vibrio alginolyticus*) (3). The white feces syndrome (WFS), a worldwide severe non-infectious shrimp disease, has been related to the Vibrio overrepresented in host intestine (4). Besides, *V. parahaemolyticus* that containing a virulence plasmid to encode a binary toxin PirA and PirB, is considered to cause acute hepatopancreatic necrosis disease (AHPND) (2). Shrimp innate immunity has become the focus of increased research in an effort to create disease prevention techniques due to the threat of bacterial infections.

Stimulator of interferon genes (STING) is the vital protein implicated in a wide range of innate immune responses to viral, bacterial, and parasite infections (5). The cyclic GMP-AMP synthase (cGAS) senses the DNA segments from pathogens and generates the second messenger cGAMP binding to STING. The activated STING promotes the activation of interferon (IFN) regulatory factor 3 (IRF3) and NF-κB transcription factors, leading to the production of type I interferons and inflammatory cytokines. Due to the loss of the zinc-ribbon domain, most invertebrate cGAS homologs have been considered to have no function as a DNA sensor (6). Therefore, invertebrate STING mediated signal pathways appear to have different activation mechanisms. In *Nematostella vectensis*, the cGAS (NvcGAS) activity of CDN synthesis can be activated by some unknown ligands instead of DNA, and NvSTING can recognize the 2'3'-cGAMP produced by NvcGAS (7). In *Crassostrea gigas*, there is a conservative STING-dependent signaling performed with STING binding to 2'3'-cGAMP (8). *Drosophila melanogaster* cGAS-like protein DmcGLR1 can sense viral dsRNA and produce 2'3'-cGAMP, while DmGLR2 can respond to virus infection and produce both 2'3'-cGAMP and 3'2'-cGAMP (9). DmSTING binds to 2'3'-cGAMP and 3'2'-cGAMP, then triggers the STING–IKKβ–Relish signaling axis to oppose virus infection in flies (10–12). A shrimp study shows that *Litopenaeus vannamei* cGAS homolog (LvMab21cp) is unable to increase dsDNA-activated LvSTING-dependent I IFN-β and IFN-ω production in HEK293T cells, because it lacks the typical structures for DNA sensing and cGAMP production (13). And *L. vannamei* STING (LvSTING) can react to *V. parahaemolyticus* infection by inducing LvPEN4, one kind of antimicrobial peptides, to protect shrimp from vibriosis (14). Regardless, how LvSTING regulates antimicrobial peptides (AMPs) remains unrevealed.

Herein, we established the shrimp STING–IKKβ–Relish–AMPs axis that conferred host defense against *V. parahaemolyticus* infection. These data provided several new insights into shrimp bacterial disease control.

Materials and methods

Shrimp and *V. parahaemolyticus*

Shrimp weighing an average of roughly 5 g were obtained from Guangzhou, Guangdong Province, China. The shrimp were cultured for 3 days in aerated seawater (30‰ salinity, 25°C) and fed a commercial food (HAID Group) three times daily prior to the experiment. *V. parahaemolyticus* (isolated from a diseased shrimp by our lab) were cultured in Luria broth (LB) medium overnight at a temperature of 37°C (4). The cultured *V. parahaemolyticus* were quantified through counting the microbial colony-forming units (CFUs) per milliliter on LB agar plates. The final injection concentration of *V. parahaemolyticus* was controlled to approximately 1 × 105 CFU/50 μl (15).

Plasmid construction

The open reading frame (ORF) of LvSTING (Genbank accession KY490589.1) was cloned into pAc5.1-HA vectors (16) to generate pAc-LvSTING-HA. The ORF of LvIKKβ (Genbank accession JN180642) was constructed into pAc5.1-FLAG vector (17) for expressing FLAG-tagged LvIKKβ protein. The ORF of LvRelish (Genbank accession EF432734) was constructed into pAc5.1-V5 vector (Invitrogen, Cat No. V4110-20, USA) for expressing V5-tagged LvRelish protein. GFP sequence was constructed into pAc5.1-HA vector to express HA-tagged GFP. The promoter sequences of *L. vannamei* anti-LPS-factor 1 (LvALF1, Genbank accession EW713395), Crustin 1 (LvCRU1, Genbank accession AF430071.1), Lysozyme 1 (LvLYZ1, Genbank accession JN039375.1) and (LvPEN4, Genbank accession DQ206402) were cloned into pGL3-basic vector (Promega, Cat No. E1751, USA). Primer sequences were listed in Table 1.

Co-immunoprecipitation and western blot

Co-immunoprecipitation (Co-IP) assays were performed to investigate the interaction of endogenous proteins ectopic expressed proteins in cells or in shrimp hemocytes. In *Drosophila* S2 cells, the plasmids pAc-LvRelish-V5 or pAc-

TABLE 1 Primers used in this study.

Protein expression	
LvRelish-F	AGGGGTACCATGGTGAGAGGTGACAGAGGTGG
LvRelish-R	ACCGGGCCCCGCCTGGTCCAGTACAGCTACACATTCC
LvIKKβ-F	CCGCTCGAGATGGCAGCAGCAGAAGACCGTC
LvIKKβ-R	GCTCTAGACAAGGAAGTTTCAACTGCCTTCTTAT
LvSTING-F	AGGGGTACCATGAAGGGAGACGAGCTGGTC
LvSTING-R	AACGGGCCCTCAGCAAAACAAAAGAGATTCTGCCGCT
GFP-F	AGGGGTACCATGGTGAGCAAGGGCGAGGAGCTGT
GFP-R	AACGGGCCCTCACTTGTACAGCTCGTCCATGCCGAGA
Dual luciferase assay	
LvALF1-F	GGGGTACCCTTGATTAGCCGATCCCAGAC
LvALF1-R	GGAGATCTACTACAGAGCTGACCAGCACCC
LvLYZ1-F	GGGGTACCCTATGGTGAATGCCACCGGGCAG
LvLYZ1-R	GGAGATCTGGTTCCGAAGTGTAAGTTGCTTG
LvCRU1-F	GGGGTACCCTGGAAAATACCAGGTGTTGATG
LvCRU1-R	GGAGATCTGTTGCCTCCAGTACAAGCTAGTG
LvPEN4-F	GGGGTACCACATGCAGATACAGATACATATATTCATATT
LvPEN4-R	GGAAGATCTGCGGACGCAGGAGGCAAC
Quantitative PCR (qPCR)	
LvEF-1α-F	TATGCTCCTTTTGGACGTTTTGC
LvEF-1α-R	CCTTTTCTGCGGCCTTGGTAG
LvRelish-F	AACACCTCCTCCTTCACCC
LvRelish-R	GGTCTCAGTGCCAGAGTAGGT
LvIKKβ-F	ACCACACTTTCCACCTTTGG
LvIKKβ-R	TCCCGATGAAGGAAGAACAC
LvSTING-F	CTCAGACACTCGTGGGAGGC
LvSTING-R	CCTGTGCTGCTGTTCGAAGG
LvLYZ1-F	TACGCGACCGATTACTGGCTAC
LvLYZ1-R	AGTCTTTGCTGCGACCACATTC
LvALF1-F	TTACTTCAATGGCAGGATGTGG
LvALF1-R	GTCCTCCGTGATGAGATTACTCTG
LvCRU1-F	GTAGGTGTTGGTGGTGGTTTC
LvCRU1-R	CTCGCAGCAGTAGGCTTGAC
LvPEN4-F	GTTACCCAAACCATCCCGAC
LvPEN4-R	CAGACTATCCTCTGTGACAACAATC
Vpa-16s-F	GGTGTAGCGGTGAAATGCGTAG
Vpa-16s-R	CCACAACCTCCAAGTAGACATCG
dsRNA templates amplification	
GFP-F	CGACGTAAACGGCCACAAGTT
GFP-R	ATGGGGGTGTTCTGCTGGTAG
GFP-T7-F	GGATCCTAATACGACTCACTATAGGCGACGTAAACGGCCACAAGTT
GFP-T7-R	GGATCCTAATACGACTCACTATAGGATGGGGGTGTTCTGCTGGTAG
LvRelish-F	TTGAGTTGGATGAGAATGATCGGGAAGT
LvRelish -R	CCTGAAGAAGGCTGTTATTGATGGTGGT
LvRelish -T7-F	GGATCCTAATACGACTCACTATAGGTTGAGTTGGATGAGAATGATCGGGAAGT
LvRelish -T7-R	GGATCCTAATACGACTCACTATAGGCCTGAAGAAGGCTGTTATTGATGGTGGT
LvIKKβ-F	GCTGCTGTCCGTTCCTGC
LvIKKβ-R	TTTCTCCATTGCGACCTTCA
LvIKKβ-T7-F	GGATCCTAATACGACTCACTATAGGGCTGCTGTCCGTTCCTGC

(Continued)

TABLE 1 Continued

Protein expression	
LvIKKβ-T7-R	GGATCCTAATACGACTCACTATAGGTTTCTCCATTGCGACCTTCA
LvSTING-F	GGCCATCGGCTACTACGTC
LvSTING -R	ATCCCGTACCATCGATTTCCAT
LvSTING -T7-F	GGATCCTAATACGACTCACTATAGGGGCCATCGGCTACTACGTC
LvSTING -T7-R	GGATCCTAATACGACTCACTATAGGATCCCGTACCATCGATTTCCAT

LvIKKβ-FLAG were co-transfected with pAc-LvSTING-HA. The pAc-LvRelish-V5 or pAc-IKKβ-FLAG was also co-transfected with pAc-GFP-HA as controls. Forty-eight hours after transfection, cells were harvested and lysed with IP lysis buffer (Pierce, Cat No. 87788, USA) with a Halt Protease Inhibitor Cocktail (Merck, Cat No. 524628, Germany). The 90% of the cell lysis were incubated with agarose affinity gel of anti-HA (Merck, Cat No. A2095, Germany) or anti-V5 Agarose Affinity Gel antibody produced in mouse (Merck, A7345-1ML, Germany). The remaining 10% of cell lysis were used as input controls. All samples were subjected to SDS-PAGE assays. The primary antibodies used in western blotting included rabbit anti-FLAG antibody (Merck, Cat No. F7425, Germany), rabbit anti-V5 antibody (Merck, Cat No. AB3792, Germany) and rabbit anti-HA antibody (Merck, Cat No. H6908, Germany). Anti-rabbit IgG HRP-conjugate (Promega, Cat No. W4011, USA) was used as the secondary antibody.

In order to detect endogenous LvSTING–LvRelish interaction *in vivo*, hemocytes were lysed in IP lysis buffer (Pierce, Cat No. 87788, USA) with Halt Protease Inhibitor Cocktail (Thermo, Cat No. 87786, USA), and then incubated with protein G agarose beads (CST, Cat No. 37478S, USA) coated with anti-LvRelish antibody (Prepared by Genecreate, China) or a normal rabbit IgG antibody (CST, Cat No. 7074S, USA) for 3 hours at 4 °C, and finally were detected by western blotting with anti-LvSTING antibody (Prepared by Genecreate, China). Five percent of the cell lysis was loaded as the input control.

Dual-luciferase reporter assays

Drosophila S2 cells were transfected with reporter gene plasmids, pRL-TK renilla luciferase plasmid (as an internal control), and expression plasmid (pAc-LvRelish-V5, pAc-IKKβ-FLAG and pAc-LvSTING-HA) or empty pAc5.1/V5-His A plasmid (as a control) using the FuGENE Transfection Reagent (Promega, Cat. No. e2311, USA) following the manufacturer's protocol. At 48 h after transfection, the firefly and renilla luciferase activity was measured following the manufacturer's protocol. Three replicates were performed for each experiment.

Double-stranded RNAs synthesis

DsRNAs specifically targeted to the LvSTING, LvIKKβ or LvRelish, were synthesized through *in vitro* transcription *via* T7 RiboMAX Express RNAi System kit (Promega, Cat. no. P1700, USA). DsRNA-GFP (dsGFP) targeting GFP (Genbank accession DQ389577) was used as a control. Primer sequences were listed in Table 1.

Quantitative PCR analysis

Sample gaining, total RNA extraction and quantitative PCR (qPCR) assays were conducted as previously described (18). The expression levels of target genes were determined using the Livak (2-ΔΔCT) method following normalization to *L. vannamei EF-1a* (GU136229). Primer sequences were listed in Table 1. Three replicates were performed for each experiment.

V. parahaemolyticus challenge experiments in LvRelish-knockdown shrimp

To investigate whether LvRelish played a protective role against *V. parahaemolyticus*, healthy shrimp were separated into two groups and injected with dsGFP or dsRNA-LvRelish (dsLvRelish). Each shrimp was injected with dsRNA (2 μg/g shrimp). Shrimp were then injected with *V. parahaemolyticus* or PBS after 48 h and maintained in culture flasks for approximately a week following infection. Surviving shrimp numbers were recorded every 4 h.

Another experiment was conducted to monitor the abundance of *V. parahaemolyticus* in LvRelish-knockdown shrimp. Quantitative PCR (qPCR) assays were conducted as previously described [10]. At 12 h after *V. parahaemolyticus* infection, gill tissue samples were collected from each group to extract DNA. The Marine Animals DNA Kit (TIANGEN, Cat. No. DP324, China) was used to extract gill DNA. The number of bacteria in gill tissue samples was quantified through qPCR using the *V. parahaemolyticus* 16S rRNA gene (rDNA, GenBank No. EU660325) with specific primers (Table 1) (19). In brief,

serial dilutions (108, 107, 106, 105, 104, and 103 copies) of plasmids containing *V. parahaemolyticus* 16S rRNA gene fragments were used to construct the standard curve. The genome copies of *V. parahaemolyticus* in 1 g gill tissue samples were then calculated. Hemocyte RNA was extracted to determine the expression of LvRelish for RNAi efficiency, and to detect the expression of shrimp NF-κB-mediated effector genes (LvALF1, LvLYZ1, LvCRU1, and LvPEN4). Three replicates were performed for each experiment.

Expression of LvSTING in hemocyte from *V. parahaemolyticus*-challenged shrimp

The expression patterns of LvSTING in the hemocytes from *V. parahaemolyticus*-challenged shrimp were investigated. For immune stimulations assay, the treated groups were injected with *V. parahaemolyticus* solution (1 × 105 CFU), and the control group was injected with PBS solution. Hemocytes of challenged shrimp were sampled at 0, 3, 6, 12, 24, 36, 48 h post injection (hpi), and each sample was collected and pooled from 5 shrimp. Primer sequences were listed in Table 1.

Immunofluorescence assay

Forty-eight hours post dsGFP, dsRNA-LvSTING (dsLvSTING) or dsRNA-LvIKKβ (dsLvIKKβ) injection, shrimp were injected with 50 μl PBS or a suspension of approximately 1 × 105 CFU of *V. parahaemolyticus*. At six hours after *V. parahaemolyticus* infection, shrimp hemocytes were obtained through centrifugation (1000 g for 5 *min*) at 25 °C and seeded onto the slides. The hemocytes were fixed with 4% paraformaldehyde, and then were permeabilized with methanol at -20 °C. The slides were blocked using 3% BSA for 1 h at 25 °C and then incubated overnight (at 4°C for approximately 8 h) in a mixture of rabbit anti-LvRelish antibody (Genecreate, China) and mouse anti-β-actin antibody (Merck, Cat. No. A2228, Germany). The hemocytes were then washed with PBS and incubated with the fluorescent antibody (CST, Cat. No. 4412S/8890S, USA) for 1 h at 25 °C in the dark. The hemocytes were washed with PBS and stained with Hoechst 33258 (Yeasen, Cat. No. 40729ES10, China) for 10 min at 25 °C before being washed another six times. The fluorescence was visualized using a confocal laser scanning microscope (Leica, TCS-SP8, Germany). WCIF ImageJ software was used to analyze the colocalization of LvRelish and Hochest-stained nuclei in hemocytes.

Relish phosphorylation detection

Shrimp hemocytes were harvested at 6 hours post *V. parahaemolyticus* infection and lysed with IP lysis buffer (Pierce, Cat No. 87788, USA) with a Halt Protease Inhibitor Cocktail (Merck, Cat No. 524628, Germany). All samples were subjected to SDS-PAGE assays. The primary antibodies used in western blotting included rabbit anti-pLvRelish antibody (Genecreate, China) and mouse anti-β-actin antibody (Merck, Cat. No. A2228, Germany). Anti-rabbit IgG (H+L) HRP-conjugate (Promega, Cat No. W4011, USA) and Anti-mouse IgG (H+L) HRP-conjugate (Promega, Cat No. W4021, USA) were used as the secondary antibody.

V. parahaemolyticus challenge experiments in shrimp treated with dsIKKβ or dsSTING

To investigate whether LvSTING can activate LvRelish, healthy shrimp were separated into two groups and injected with dsGFP or dsLvSTING. Each shrimp was injected with dsRNA (2 μg/g shrimp). 48 hours post dsRNA injection, shrimp were infected with *V. parahaemolyticus* or PBS. And 12 hours post *V. parahaemolyticus* infection, hemocytes were harvested for qPCR, western blotting and immunofluorescence assay, and gill tissue samples were collected for *V. parahaemolyticus* numbers. Three replicates were performed for each experiment.

To explore whether LvIKKβ participates in LvRelish activation, healthy shrimp were separated into two groups and injected with dsGFP or dsLvRelish. Each shrimp was injected with dsRNA (2 μg/g shrimp). 48 hours post dsRNA injection, shrimp were infected with *V. parahaemolyticus* or PBS. And 12 hours post *V. parahaemolyticus* infection, hemocytes were harvested for qPCR, western blotting and immunofluorescence assay. Gill tissue samples were collected for counting *V. parahaemolyticus* numbers. Three replicates were performed for each experiment.

To prove that the LvSTING–LvIKKβ–LvRelish–AMPs axis plays a protective role against *V. parahaemolyticus*, healthy shrimp were separated into four groups and injected with dsGFP (4 μg/g shrimp), dsLvSTING (2 μg/g shrimp) plus dsGFP (2 μg/g shrimp), dsLvIKKβ (2 μg/g shrimp) plus dsGFP (2 μg/g shrimp), and dsLvSTING (2 μg/g shrimp) plus dsLvIKKβ (2 μg/g shrimp). Shrimp were then injected with *V. parahaemolyticus* or PBS after 48 hours and maintained in culture flasks for approximately a week following infection. Surviving shrimp numbers were recorded every 4 h. And 12 hours post *V. parahaemolyticus* infection, hemocytes were harvested for qPCR, and gill tissue samples were collected for counting *V. parahaemolyticus* numbers. Three replicates were performed for each experiment.

Statistical analysis

All the data are presented as mean ± SD. Student's *t* test is used to calculate the comparisons between groups of numerical

data. For survival rates, data are subjected to statistical analysis using GraphPad Prism software to generate the Kaplan ± Meier plot (log-rank $\chi 2$ test). The following p values are considered to be statistically significant: $^{*}p < 0.05$, $^{**}p < 0.01$ and $^{***}p < 0.001$.

Results

LvRelish could defend against *V. parahaemolyticus* infection *via* inducing AMPs

Shrimp NF-κB pathway is crucial for AMPs expression, and LvRelish is a key transcription factor of NF-κB pathway. In this study, RNAi was performed to investigate the relationship between LvRelish and AMPs. We designed and synthesized dsRNA-LvRelish (dsLvRelish) targeting LvRelish expression, and checked the silencing efficiency of LvRelish at 48 h post dsRNA injection. The injection of dsLvRelish resulted in a significant decrease in LvRelish expression levels down-regulating to ~0.11-fold of the control group (Figure 1A), which was sufficient for the following experiments. Accordingly, the expression levels of LvALF1, LvCRU1, LvLYZ1 and LvPEN4 were remarkably down-regulated to ~0.47-fold, ~0.45-fold, ~0.36-fold and ~0.57-fold compared to those of dsGFP group at 48 h post dsRNA injection (Figure 1A).

Considering the relationship between LvRelish and AMPs, we were curious about the role played by LvRelish in the host defense against bacterial infection. As shown in Figure 1B, the expression of LvRelish in dsLvRelish treated group was down-regulated to ~0.30-fold comparing with the dsGFP group, which meant dsLvRelish was competent for LvRelish knockdown during *V. parahaemolyticus* infection. And the detection of AMPs during *V. parahaemolyticus* infection showed that the expression of AMPs in dsLvRelish injected shrimp were lower than those of the control group (Figure 1B). These results

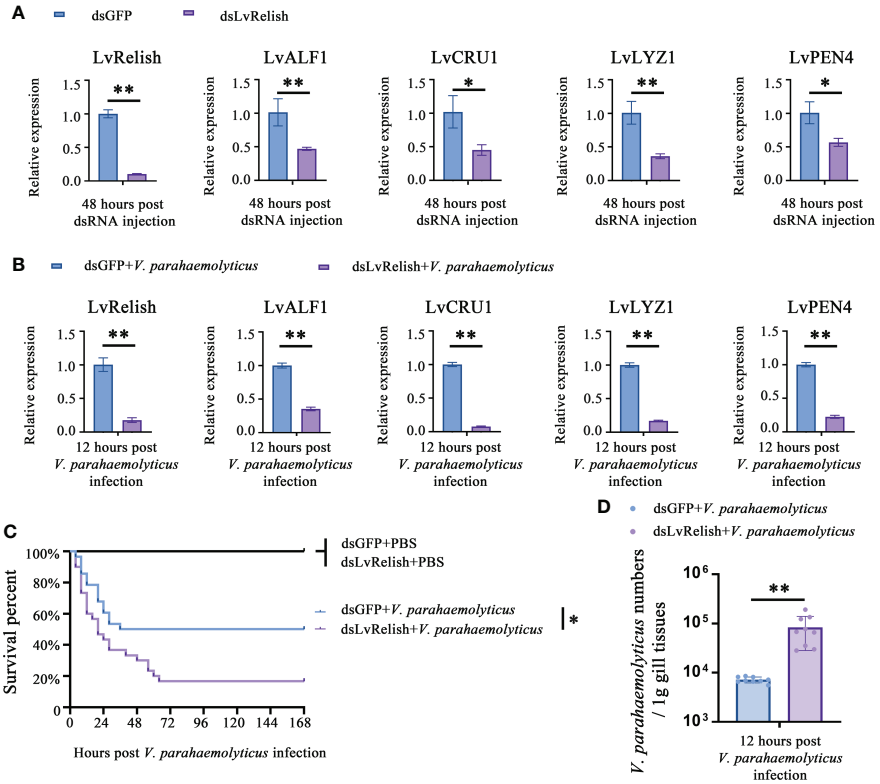

FIGURE 1
LvRelish defended against *V. parahaemolyticus* infection *via* inducing AMPs. **(A)** Relative expression of LvRelish and AMPs in LvRelish silenced shrimp at 48 hours post dsRNA injection. **(B)** Relative expression of LvRelish and AMPs in LvRelish silenced shrimp at 12 hours post *V. parahaemolyticus* infection. **(C)** Percent survival of LvRelish silenced shrimp after *V. parahaemolyticus* infection. The experiments were performed three times with identical results. Differences between groups were analyzed with Log-rank test using the software of GraphPad Prism 5.0 ($^{*}p < 0.05$). **(D)** *V. parahaemolyticus* numbers in gill tissues of LvRelish silenced shrimp at 12 hours post *V. parahaemolyticus* infection. One dot represents one sample and the column represents the median of the results. The data **(A, B, D)** was analyzed statistically by student's T test ($^{*}p < 0.05$, $^{**}p < 0.01$).

suggested that LvRelish could regulate AMPs expressions in both uninfected shrimp (Figure 1A) and *V. parahaemolyticus*-infected shrimp (Figure 1B).

During *V. parahaemolyticus* infection, the survival rate of dsLvRelish group was much lower than that of dsGFP group ($\chi 2$: 8.674, $p = 0.0340$), which indicated that LvRelish silenced shrimp were more sensitive to *V. parahaemolyticus* infection (Figure 1C). Besides, the higher numbers of *V. parahaemolyticus* were observed in dsLvRelish group at 12 h post *V. parahaemolyticus* infection (Figure 1D) that correlated well with the survival percent recorded in Figure 1C, and further confirmed that LvRelish played an antibacterial role in the innate immune response.

LvSTING triggered AMPs expression *via* interacting with LvRelish *in vitro*

Relish is the vital transcription factor of STING-mediated pathways in silkworm and fruit fly (12, 20), but whether LvSTING participates in Relish regulation is still unclear. In this study, we found that V5 tagged LvRelish was co-immunoprecipitated with HA tagged LvSTING, but no appreciable binding was observed for HA tagged GFP protein (Figure 2A), which suggested that LvSTING could interact with LvRelish.

Given the vital role acted by LvRelish in inducing AMPs, the discovery of the association between LvSTING and LvRelish implied that LvSTING might induce AMPs by LvRelish. As Figure 2B shown, LvRelish-triggered promoter activities of LvALF1, LvCRU1, LvLYZ1 and LvPEN4, were promoted by the co-expression of LvSTING in S2 cells, which demonstrated that LvSTING could enhance LvRelish-mediated AMPs expression *in vitro*.

LvSTING prompted LvRelish activation *in vivo*

To prove the interaction between LvSTING and LvRelish existed in shrimp hemocyte, IP experiments were performed with LvRelish antibody *in vivo*. IP assays demonstrated that LvRelish could interact with LvSTING in hemocyte (Figure 3A). In hemocyte of *V. parahaemolyticus* infected shrimp, LvSTING expressions were up-regulated at 3, 6, 12, 24 hours post *V. parahaemolyticus* infection, indicated that LvSTING also responded to *V. parahaemolyticus* infection in hemocyte (Figure 3B). Then, we confirmed the effects of LvSTING on LvRelish activation *in vivo*. As Figure 3C shown, dsLvSTING could efficiently suppress LvSTING expression to ~0.19-fold of control. LvRelish has been proved to transfer from cytoplasm into nuclear after *V. parahaemolyticus* infection (21), and LvRelish nuclear location was inhibited by LvSTING knockdown during *V. parahaemolyticus* infection (Figures 3D, E). And the phosphorylation of LvRelish was weakened in hemocytes from LvSTING knocked down shrimp (Figure 3F), suggesting that LvSTING was involved in activating LvRelish. LvSTING knockdown led to down-regulated the expression of LvALF1, LvCRU1, LvLYZ1 and LvPEN4 during *V. parahaemolyticus* infection (Figure 3G), which indicated that LvSTING was involved in AMPs expression in shrimp. To sum up, LvSTING prompted LvRelish phosphorylation and nuclear location to induce AMPs expression.

LvIKKß was required for AMPs expression and LvRelish activation

IKKβ is the phosphokinase targeting Relish in *Drosophila* IMD pathway (22), but no direct evidence supporting that shrimp IKKβ activates Relish. In this study, dsLvIKKβ was used to inhibit the expression of LvIKKβ (Figure 4A), and the effect of LvIKKβ on LvRelish activation was examined. LvRelish subcellular location was observed by immunofluorescence assay. The results showed that LvRelish moved into the nuclear in response to *V. parahaemolyticus* infection, and dsLvIKKβ injection could suppress nuclear import of LvRelish (Figures 4B, C). LvRelish phosphorylation levels in hemocytes were significantly reduced by silencing LvIKKβ expression (Figure 4D). QPCR performed that dsLvIKKβ inhibited AMPs

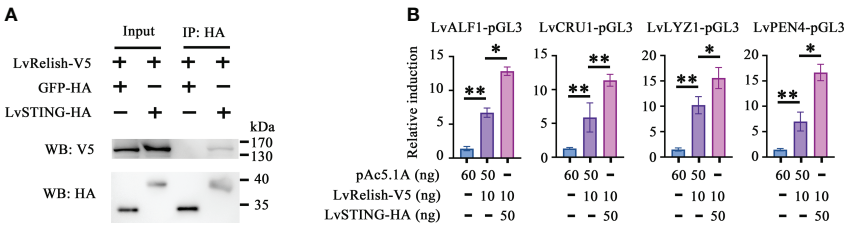

FIGURE 2
LvSTING triggered AMPs expression *via* interacting with LvRelish *in vitro*. **(A)** The Co-IP assays detecting the interaction between LvSTING and LvRelish. **(B)** The promoter activities of shrimp AMPs were induced by LvRelish with or without LvSTING in S2 cells. The data was analyzed statistically by student's T test (*$p < 0.05$, **$p < 0.01$).

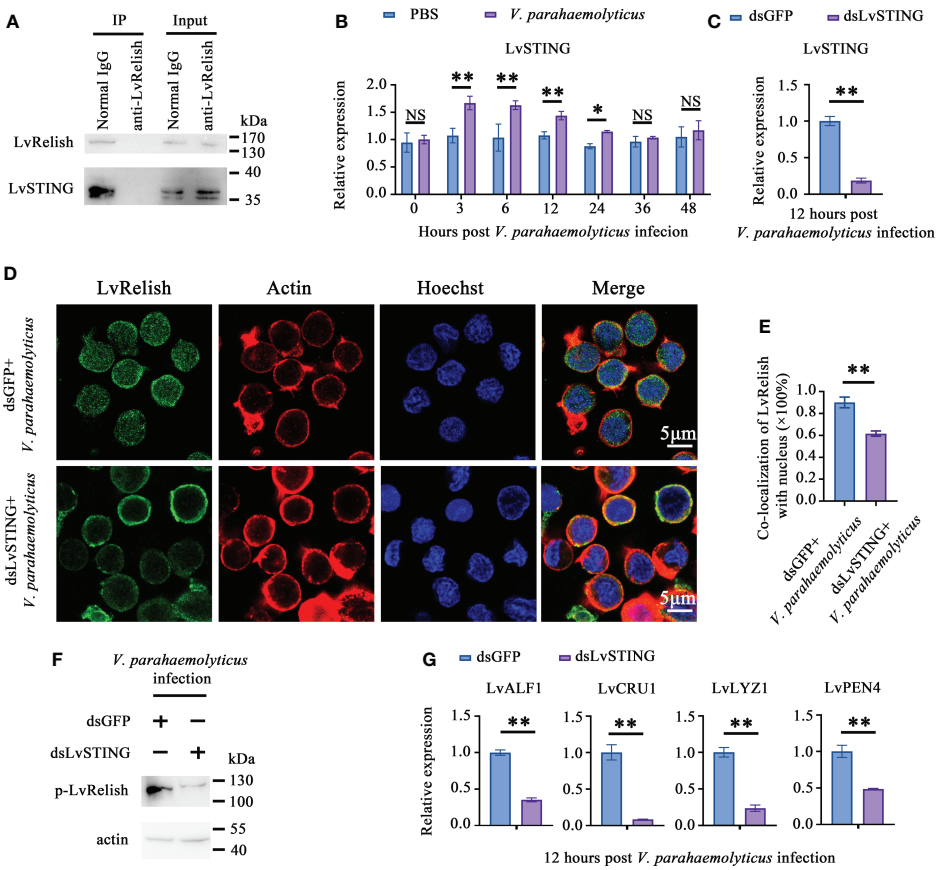

FIGURE 3
LvSTING prompted LvRelish activation *in vivo*. **(A)** IP assay detecting the interaction between LvSTING and LvRelish *in vivo*. **(B)** Expression profiles of LvSTING in hemocytes from PBS or *V. parahaemolyticus* challenged shrimp. The expression level at each time points were normalized to 0 h post PBS-injected group. **(C)** RNAi efficiency of dsLvSTING in shrimp hemocytes. **(D)** LvRelish nuclear translocation in LvSTING silenced hemocytes infected by *V. parahaemolyticus*. **(E)** Co-localization of LvRelish and Hochest-stained nucleus in hemocytes corresponding to Figure 3D calculated by WCIF ImageJ software. **(F)** The phosphorylation levels of LvRelish in the hemocytes from dsLvSTING or dsGFP treated shrimp during *V. parahaemolyticus* infection. **(G)** The expression of AMPs in the hemocytes of dsLvSTING or dsGFP treated shrimp. The data was analyzed statistically by student's T test (*$p < 0.05$, **$p < 0.01$).

expression (Figure 4E), which is consistent with the AMPs expression changes caused by dsLvRelish or dsLvSTING. The data above indicated that LvIKKβ induced AMPs expression *via* activating LvRelish.

LvSTING recruited LvIKKβ and LvRelish to synergistically induce AMPs *in vitro*

To explore the effects of LvSTING on LvIKKβ–LvRelish signaling transduction, the interaction between LvSTING and LvIKKβ was examined. The Co-IP demonstrated that FLAG-tagged LvIKKβ interacted with HA-tagged LvSTING but not HA-tagged GFP, which indicated that LvSTING could recruit LvIKKβ (Figure 5A). To prove the recruitment functions of LvSTING, FLAG-tagged LvIKKβ and V5-tagged LvRelish were co-expressed with or without HA-tagged LvSTING in S2 cells. As shown in Figure 5B, FLAG-tagged LvIKKβ was co-immunoprecipitated with V5-tagged LvRelish with the help of HA-tagged LvSTING, and the absence of LvSTING resulted in less LvIKKβ was co-immunoprecipitated with LvRelish. To confirm the effect of LvSTING on LvIKKβ–LvRelish–AMPs pathway, the dual luciferase assays was performed in S2 cells. The result showed that the promoter activities of shrimp AMPs (LvALF1, LvCRU1, LvLYZ1 and LvPEN4) could be positively regulated by the co-expression of LvIKKβ and LvRelish, which could be further upregulated by ectopic expression of LvSTING in a dose-dependent manner (Figure 5C).

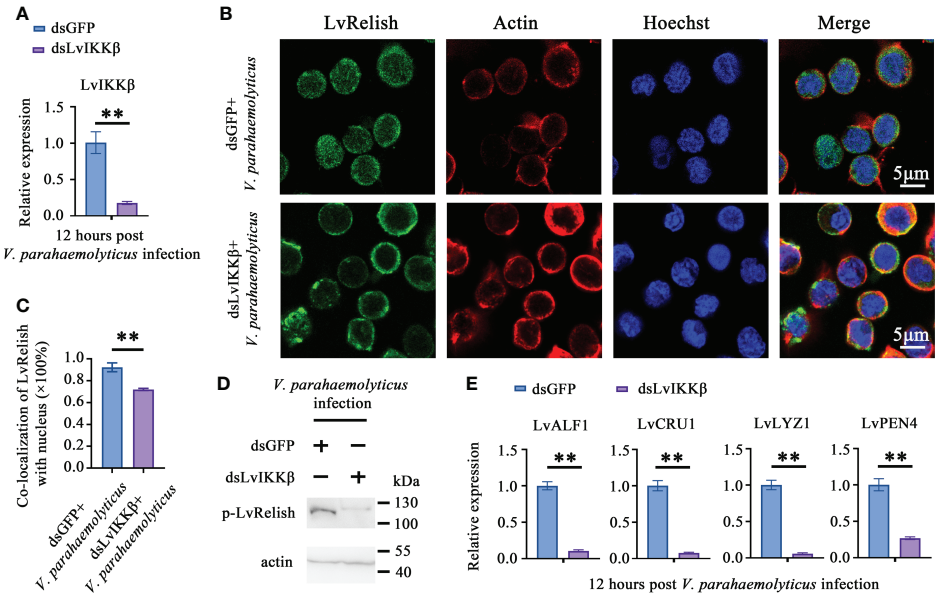

FIGURE 4
LvIKKß is required for AMPs expression and LvRelish activation. **(A)** RNAi efficiency of dsLvIKKβ in shrimp hemocytes. **(B)** LvRelish nuclear translocation in LvIKKβ silenced hemocytes infected by *V. parahaemolyticus*. **(C)** Co-localization of LvRelish and Hochest-stained nucleus in hemocytes corresponding to Figure 4B calculated by WCIF ImageJ software. **(D)** The phosphorylation levels of LvRelish in the hemocytes of dsLvIKKβ and dsGFP treated shrimp during *V. parahaemolyticus* infection. **(E)** The expression of AMPs in the hemocytes of dsIKKβ or dsGFP treated shrimp. The data was analyzed statistically by student's T test (**$p < 0.01$).

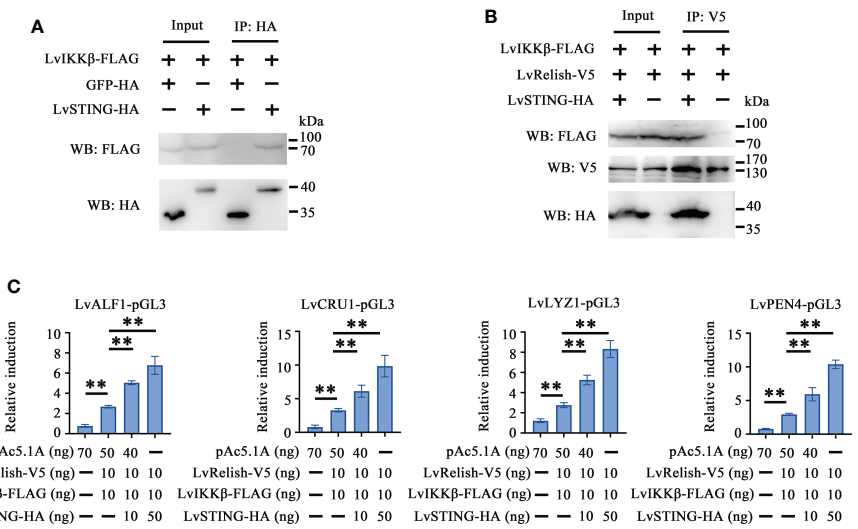

FIGURE 5
LvSTING recruited LvIKKβ and LvRelish to induce the promoter activities of AMPs *in vitro*. **(A)** The Co-IP assays confirmed the interaction between LvSTING and LvIKKβ. **(B)** The Co-IP assays proved that LvSTING recruited LvRelish and LvIKKβ. **(C)** The promoter activities of shrimp AMPs induced by LvIKKβ and LvRelish could be upregulated by ectopic expression of LvSTING in a dose-dependent manner. The data was analyzed statistically by student's T test (**$p < 0.01$).

The LvSTING–LvIKKβ–LvRelish–AMPs axis played a protective role against *V. parahaemolyticus*

As mentioned above, there was a LvSTING–LvIKKβ–LvRelish–AMPs signaling pathway in shrimp. We were curious about the roles played by the above signaling pathway in the host defense against *V. parahaemolyticus* infection. Double knockdown experiments were done to investigate whether LvSTING regulated the expression of AMPs through LvIKKβ. We observed that LvSTING- or LvIKKβ-knockdown reduced the expression of AMPs during *V. parahaemolyticus* infection. When compared to dsLvIKKβ-injected shrimp, LvSTING and LvIKKβ knockdown combined suppressed the expression of LvALF1 (~0.34-fold), LvCRU1 (~0.43-fold), LvLYZ1 (~0.53-fold) and LvPEN4 (~0.67-fold) (Figure 6A). Furthermore, Figure 6B showed that knockdown of LvSTING or LvIKKβ increased shrimp susceptibility to *V. parahaemolyticus* infection compared to the dsGFP group ($\chi2 = 10.32$, $p = 0.0013$; $\chi2 = 5.662$, $p = 0.0173$). In addition, when compared to LvIKKβ-silenced shrimp, LvSTING and LvIKKβ knockdown resulted in higher cumulative mortality ($\chi2 = 9.974$, $p = 0.0016$), suggesting that LvSTING improved shrimp resistance to *V. parahaemolyticus* infection *via* LvIKKβ (Figure 6B). In agreement with the survival curves, LvSTING- or LvIKKβ-knockdown boosted *V. parahaemolyticus* levels in shrimp gill tissues, and *V. parahaemolyticus* numbers in the dsLvSTING + dsLvIKKβ group were substantially greater than those in the LvIKKβ-silenced alone group (Figure 6C). Taken together, these results suggested that LvSTING could trigger an antibacterial response *via* the LvIKKβ–LvRelish–AMPs pathway during *V. parahaemolyticus* infection.

Discussion

In the last decade, studies on cytosolic surveillance systems have advanced significantly, highlighting the key role of the cGAS-STING signaling pathway in bacterial infection. In vertebrates, STING has been reported to be triggered by bacterial DNA-activated cGAS or another DNA sensor, IFI16, leading to the production of IFN-I during *Listeria monocytogenes* infection (23). STING is also able to recognize bacteria derived CDNs, including 3'3'-cGAMP, c-di-GMP and

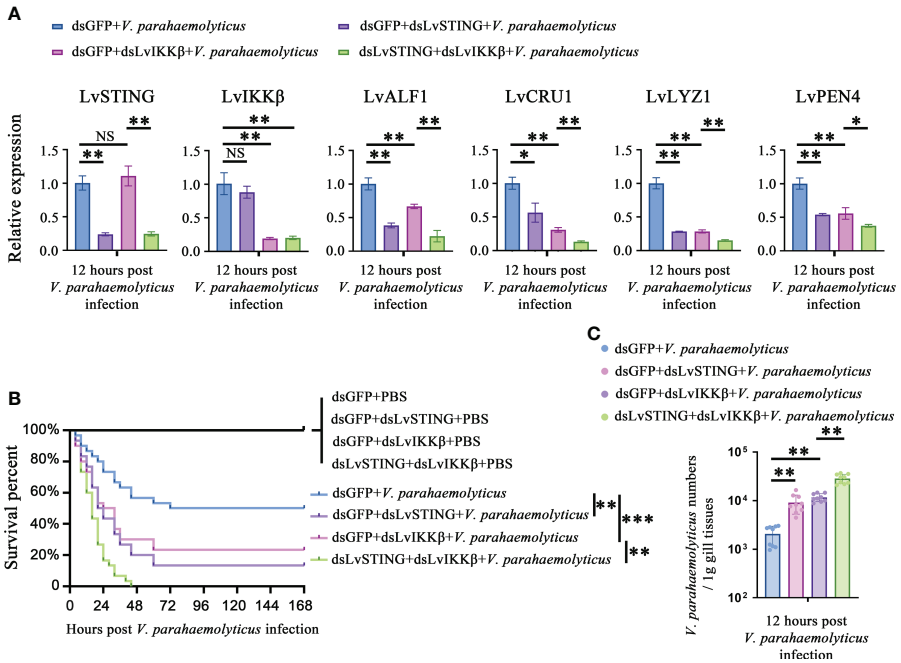

FIGURE 6
The LvSTING–LvIKKβ–LvRelish–AMPs axis played a protective role against *V. parahaemolyticus*. **(A)** Relative expression of LvSTING, LvIKKβ and AMPs in the hemocytes from dsLvIKKβ or dsGFP treated shrimp with or without dsLvSTING injection at 12 hours post *V. parahaemolyticus* infection. **(B)** Percent survival of dsLvIKKβ or dsGFP treated shrimp with or without dsLvSTING injection after *V. parahaemolyticus* infection. The experiments were performed three times with identical results. Differences between groups were analyzed with Log-rank test using the software of GraphPad Prism 5.0 (**$p < 0.01$, ***$p < 0.001$). **(C)** *V. parahaemolyticus* numbers in gill tissues of dsLvIKKβ or dsGFP treated shrimp with or without dsLvSTING injection at 12 hours post *V. parahaemolyticus* infection. One dot represents one sample and the column represents the median of the results. The data **(A, C)** was analyzed statistically by student's T test (*$p < 0.05$, **$p < 0.01$). ns, no significant difference.

c-di-AMP (24–26). Hence, vertebrates STINGs detect a wide range of ligands from bacterial infection, which leads to rapid antibacterial immune responses.

STING can also respond to bacterial infection in invertebrates. *D. melanogaster* STING (DmSTING) senses c-di-GMP and induces a set of AMPs production to control *L. monocytogenes* infection through transcription factor Relish (27). Likewise, *V. parahaemolyticus* infection substantially increased LvSTING expression in intestine and hepatopancreas, demonstrating that LvSTING played a role in innate immunity against bacterial infection (14). In this study, LvSTING expression in hemocytes was shown to be dramatically increased at 3, 6, 12, and 24 hours after *V. parahaemolyticus* infection, indicating that LvSTING was responding to *V. parahaemolyticus* invasion in hemocytes. Because hemocytes are considered as the most essential immune cells in shrimp for pathogen recognition and phagocytic function (28), the rapid increase of LvSTING in hemocytes indicated that it could play a role comparable to DmSTING in innate immune response to bacterial invasion.

Since IFN pathways are not widespread in invertebrates, STING-dependent Relish activation is a critical method for defending against pathogen invasion *via* inducing AMPs expression. A nucleopolyheedrovirus (NPV)-infected *Bombyx mori* cell produces the 2'3'-cGAMP, which binds to *B. mori* STING (BmSTING). Ligand-binding of BmSTING dissociates from the suppressor caspase-8-like protein (BmCasp8L), and triggers BmRelish cleavage by death-related ced-3/Nedd2-like caspase (BmDredd) to induce the expression of AMPs such as BmCecropinA and BmCecropinB (20). In Shrimp, Relish activation causes a rise in the expression of a variety of AMPs, which is one of the most important ways to eliminate germs from the host (29). The four kinds of AMPs from shrimp, such as anti-LPS-factor (ALF), Crustin (CRU), Lysozyme (LYZ) and Penaeidin (PEN), have been identified as Relish-mediated effectors and have broad anti-microbial properties to Gram-positive and Gram-negative bacteria (29–32). Our results showed that LvSTING activated LvRelish *via* LvIKKβ, and induced AMPs including LvALF1, LvCRU1, LvLYZ1 and LvPEN4, playing a protective role against *V. parahaemolyticus* infection. Accumulating evidence suggested that AMPs' synthesis *via* the STING–Relish cascade could be a powerful antibacterial mechanism of invertebrates.

Despite the fact that transcription of type I IFN genes is the primary antiviral output of STING signaling in mammals, these genes have only been discovered in vertebrates (33). IRF3, the transcription factor that drives to type I IFN transcription after STING activation, is only found in vertebrates and several kinds of invertebrates (6, 34). Therefore, IFN pathways regulated by STING are not widely distributed among invertebrates. NF-κB activation is another downstream consequence of STING-mediated signaling (35). Key components of NF-κB pathways are conserved in vertebrates and invertebrates, and NF-κB and IκB homologs have been identified in most animal lineages (36). Although STING-mediated NF-κB activation has been discovered in the insects including *B. mori* (20) and *D. melanogaster* (12), but not clear in other species of invertebrates. This study demonstrated that STING-mediated Relish activation happens in shrimp and protects them from bacterial invasion. The present work could contribute to the understanding of how STING-mediated NF-κB activation occurs in vertebrates.

In summary, we described an innate immune pathway against *V. parahaemolyticus*. LvSTING responded to *V. parahaemolyticus* invasion, then recruited LvIKKβ and LvRelish, leading to LvRelish phosphorylation and nuclear translocation. The activated LvRelish translocated into nuclear and induced AMPs expression, which were the crucial antibacterial effectors to kill *V. parahaemolyticus*. We identified the LvSTING–LvIKKβ–LvRelish–AMPs signaling pathway against *V. parahaemolyticus*, which helped us learn more about LvSTING's role in shrimp and gave us some insight into disease resistance breeding.

Data availability statement

The original contributions presented in the study are included in the article/Supplementary Material. Further inquiries can be directed to the corresponding authors.

Author contributions

HL: conceived, designed and performed the experiments, and analyzed data, as well as wrote the draft manuscript. QL and SW: performed the experiments and analyzed data. JH: conceived and designed the experiments, and acquired finding. CL: conceived and designed the experiments, acquired finding, and was responsible for forming the hypothesis, project development, data coordination, and writing, finalizing, and submitting the manuscript. All authors discussed the results and approved the final version.

Funding

This research was supported by National Natural Science Foundation of China (31930113/32173000/32022085), Natural Science Foundation of Guangdong Province (2021A1515010747), Science and Technology Planning Project of Guangzhou City (202102020354), Independent Research and Development Projects of Maoming Laboratory (2021ZZ007/2021TDQD004), Southern Marine Science and Engineering Guangdong Laboratory (Zhuhai) (SML2021SP301), and the Fundamental Research Funds for the Central Universities, Sun Yat-sen University (22lglj05). The

funders had no role in study design, data collection and analysis, decision to publish, or preparation of the manuscript.

Conflict of interest

The authors declare that the research was conducted in the absence of any commercial or financial relationships that could be construed as a potential conflict of interest.

Publisher's note

References

1. Food and Agriculture Organization of the United Nations, Rome, Italy. *Fishery and aquaculture statistics 2019*. (2021).

2. De Schryver, P, Defoirdt, T, and Sorgeloos, P. Early mortality syndrome outbreaks: a microbial management issue in shrimp farming? *PLoS Pathog* (2014) 10(4):e1003919. doi: 10.1371/journal.ppat.1003919

3. Chandrakala, N, and Priya, S. Vibriosis in shrimp aquaculture a review. *Int J Sci Res Sci Eng Tech* (2017) 3(2):27-33

4. Huang, Z, Zeng, S, Xiong, J, Hou, D, Zhou, R, Xing, C, et al. Microecological koch's postulates reveal that intestinal microbiota dysbiosis contributes to shrimp white feces syndrome. *Microbiome* (2020) 8(1):32. doi: 10.1186/s40168-020-00802-3

5. Barber, GN. Cytoplasmic DNA innate immune pathways. *Immunol Rev* (2011) 243(1):99–108. doi: 10.1111/j.1600-065X.2011.01051.x

6. Wu, X, Wu, FH, Wang, X, Wang, L, Siedow, JN, Zhang, W, et al. Molecular evolutionary and structural analysis of the cytosolic DNA sensor cGAS and STING. *Nucleic Acids Res* (2014) 42(13):8243–57. doi: 10.1093/nar/gku569

7. Gui, X, Yang, H, Li, T, Tan, X, Shi, P, Li, M, et al. Autophagy induction *via* STING trafficking is a primordial function of the cGAS pathway. *Nature* (2019) 567 (7747):262–6. doi: 10.1038/s41586-019-1006-9

8. Morehouse, BR, Govande, AA, Millman, A, Keszei, AFA, Lowey, B, Ofir, G, et al. STING cyclic dinucleotide sensing originated in bacteria. *Nature* (2020) 586 (7829):429–33. doi: 10.1038/s41586-020-2719-5

9. Slavik, KM, Morehouse, BR, Ragucci, AE, Zhou, W, Ai, X, Chen, Y, et al. cGAS-like receptors sense RNA and control 3'2'-cGAMP signalling in drosophila. *Nature* (2021) 597(7874):109–13. doi: 10.1038/s41586-021-03743-5

10. Holleufer, A, Winther, KG, Gad, HH, Ai, X, Chen, Y, Li, L, et al. Two cGAS-like receptors induce antiviral immunity in drosophila. *Nature* (2021) 597 (7874):114–8. doi: 10.1038/s41586-021-03800-z

11. Cai, H, Holleufer, A, Simonsen, B, Schneider, J, Lemoine, A, Gad, HH, et al. 2'3'-cGAMP triggers a STING- and NF-κB-dependent broad antiviral response in drosophila. *Sci Signal* (2020) 13(660):eabc4537. doi: 10.1126/scisignal.abc4537

12. Goto, A, Okado, K, Martins, N, Cai, H, Barbier, V, Lamiable, O, et al. The kinase IKKβ regulates a STING- and NF-κB-Dependent antiviral response pathway in drosophila. *Immunity* (2018) 49(2):225–34.e4. doi: 10.1016/j.immuni.2018.07.013

13. Li, S, Yang, F, Wang, F, Lv, X, and Li, F. An invertebrate gene encoding a Mab21-containing protein involves in antiviral response through regulating the STING pathway. *Dev Comp Immunol* (2021) 121:104101. doi: 10.1016/j.dci.2021.104101

14. Li, H, Wang, S, Lu, K, Yin, B, Xiao, B, Li, S, et al. An invertebrate STING from shrimp activates an innate immune defense against bacterial infection. *FEBS Lett* (2017) 591(7):1010–7. doi: 10.1002/1873-3468.12607

15. Li, H, Yin, B, Wang, S, Fu, Q, Xiao, B, Lǚ, K, et al. RNAi screening identifies a new toll from shrimp litopenaeus vannamei that restricts WSSV infection through activating dorsal to induce antimicrobial peptides. *PLoS Pathog* (2018) 14(9):e1007109. doi: 10.1371/journal.ppat.1007109

16. Wang, S, Li, H, Zhu, P, Fu, Q, Yin, B, Li, Q, et al. MAPKKK15 gene from shrimp litopenaeus vannamei is transcribed in larva development stages and contributes to WSSV pathogenesis. *Aquaculture* (2021) 534:736324. doi: 10.1016/j.aquaculture.2020.736324

17. Wang, S, Li, H, Weng, S, Li, C, and He, J. White spot syndrome virus establishes a novel IE1/JNK/c-jun positive feedback loop to drive replication. *iScience* (2020) 23(1):100752. doi: 10.1016/j.isci.2019.100752

18. Li, H, Wang, S, Chen, Y, Lǚ, K, Yin, B, Li, S, et al. Identification of two p53 isoforms from litopenaeus vannamei and their interaction with NF-κB to induce distinct immune response. *Sci Rep* (2017) 7(1):1–13. doi: 10.1038/srep45821

19. Huang, Z, Chen, Y, Weng, S, Lu, X, Zhong, L, Fan, W, et al. Multiple bacteria species were involved in hepatopancreas necrosis syndrome (HPNS) of litopenaeus vannamei. *Acta Scientiarum Naturalium Universitatis SunYatseni* (2016) 55(1):1–11.

20. Hua, X, Li, B, Song, L, Hu, C, Li, X, Wang, D, et al. Stimulator of interferon genes (STING) provides insect antiviral immunity by promoting dredd caspase-mediated NF-kappaB activation. *J Biol Chem* (2018) 293(30):11878–90. doi: 10.1074/jbc.RA117.000194

21. Wang, S, Li, H, Chen, R, Jiang, X, He, J, and Li, C. TAK1 confers antibacterial protection through mediating the activation of MAPK and NF-κB pathways in shrimp. *Fish Shellfish Immunol* (2022) 123:248–56. doi: 10.1016/j.fsi.2022.03.008

22. Stöven, S, Silverman, N, Junell, A, Hedengren-Olcott, M, Erturk, D, Engström, Y, et al. Caspase-mediated processing of the drosophila NF-κB factor relish. *Proc Natl Acad Sci* (2003) 100(10):5991–6. doi: 10.1073/pnas.1035902100

23. Hansen, K, Prabakaran, T, Laustsen, A, Jørgensen, SE, Rahbæk, SH, Jensen, SB, et al. Listeria monocytogenes induces IFNβ expression through an IFI16-, cGAS- and STING-dependent pathway. *EMBO J* (2014) 33(15):1654–66. doi: 10.15252/embj.201488029

24. Romling, U, Galperin, MY, and Gomelsky, M. Cyclic di-GMP: the first 25 years of a universal bacterial second messenger. *Microbiol Mol Biol Rev MMBR* (2013) 77(1):1–52. doi: 10.1128/MMBR.00043-12

25. Witte, CE, Whiteley, AT, Burke, TP, Sauer, JD, Portnoy, DA, and Woodward, JJ. Cyclic di-AMP is critical for listeria monocytogenes growth, cell wall homeostasis, and establishment of infection. *mBio* (2013) 4(3):e00282–13. doi: 10.1128/mBio.00282-13

26. Davies, BW, Bogard, RW, Young, TS, and Mekalanos, JJ. Coordinated regulation of accessory genetic elements produces cyclic di-nucleotides for v. cholerae virulence. *Cell* (2012) 149(2):358–70. doi: 10.1016/j.cell.2012.01.053

27. Martin, M, Hiroyasu, A, Guzman, RM, Roberts, SA, and Goodman, AG. Analysis of drosophila STING reveals an evolutionarily conserved antimicrobial function. *Cell Rep* (2018) 23(12):3537–50.e6. doi: 10.1016/j.celrep.2018.05.029

28. Tassanakajon, A, Piti, A, Kunlaya, S, and Premruethai, S. Cationic antimicrobial peptides in penaeid shrimp. *Mar Biotechnol* (2011) 13(4):639–57. doi: 10.1007/s10126-011-9381-8

29. Li, C, Wang, S, and He, J. The two NF-κB pathways regulating bacterial and WSSV infection of shrimp. *Front Immunol* (2019) 10:1785. doi: 10.3389/fimmu.2019.01785

30. Huang, X, Yin, Z, Liao, J, Wang, P, Yang, L, Ai, H, et al. Identification and functional study of a shrimp relish homologue. *Fish Shellfish Immunol* (2009) 27 (2):230–8. doi: 10.1016/j.fsi.2009.05.003

31. Aweya, J, Zheng, Z, Zheng, X, Yao, D, and Zhang, Y. The expanding repertoire of immune-related molecules with antimicrobial activity in penaeid shrimps: a review. *Rev Aquacult* (2021) 13(4):1907–37. doi: 10.1111/raq.12551

32. Lin, M, Hui, C, Chen, J, and Wu, J. The antimicrobial peptide, shrimp anti-lipopolysaccharide factor (SALF), inhibits proinflammatory cytokine expressions through the MAPK and NF-κB pathways in trichomonas vaginalis adherent to HeLa cells. *Peptides* (2012) 38(2):197–207. doi: 10.1016/j.peptides.2012.10.003

33. Gan, Z, Chen, SN, Huang, B, Hou, J, and Nie, P. Intronless and intron-containing type I IFN genes coexist in amphibian xenopus tropicalis: Insights into the origin and evolution of type I IFNs in vertebrates. *Dev Comp Immunol* (2017) 67:166–76. doi: 10.1016/j.dci.2016.10.007

34. Lu, M, Yang, C, Li, M, Yi, Q, Lu, G, Wu, Y, et al. A conserved interferon regulation factor 1 (IRF-1) from pacific oyster crassostrea gigas functioned as an activator of IFN pathway. *Fish Shellfish Immunol* (2018) 76:68–77. doi: 10.1016/j.fsi.2018.02.024

35. Ishikawa, H, and Barber, GN. STING is an endoplasmic reticulum adaptor that facilitates innate immune signalling. *Nature* (2008) 455(7213):674–8. doi: 10.1038/nature07317

36. Margolis, SR, Wilson, SC, and Vance, RE. Evolutionary origins of cGAS-STING signaling. *Trends Immunol* (2017) 38(10):733–43. doi: 10.1016/j.it.2017.03.004

frontiers | Frontiers in Immunology

TYPE Original Research
PUBLISHED 09 September 2022
DOI 10.3389/fimmu.2022.888427

OPEN ACCESS

EDITED BY
Horst von Bernuth,
Charité Universitätsmedizin Berlin,
Germany

REVIEWED BY
Steven M. Holland,
National Institutes of Health (NIH),
United States
Satoshi Okada,
Hiroshima University, Japan

*CORRESPONDENCE
Siobhan O. Burns
siobhan.burns@ucl.ac.uk

†These authors have contributed equally to this work

SPECIALTY SECTION
This article was submitted to Primary Immunodeficiencies, a section of the journal Frontiers in Immunology

RECEIVED 02 March 2022
ACCEPTED 17 August 2022
PUBLISHED 09 September 2022

CITATION
Daza-Cajigal V, Albuquerque AS, Young DF, Ciancanelli MJ, Moulding D, Angulo I, Jeanne-Julien V, Rosain J, Minskaia E, Casanova J-L, Boisson-Dupuis S, Bustamante J, Randall RE, McHugh TD, Thrasher AJ and Burns SO (2022) Partial human Janus kinase1 deficiency predominantly impairs responses to interferon gamma and intracellular control of mycobacteria.
Front. Immunol. 13:888427.
doi: 10.3389/fimmu.2022.888427

Partial human Janus kinase 1 deficiency predominantly impairs responses to interferon gamma and intracellular control of mycobacteria

Vanessa Daza-Cajigal[1,2,3,4,5†], Adriana S. Albuquerque[1†], Dan F. Young[6], Michael J. Ciancanelli[7], Dale Moulding[8], Ivan Angulo[9], Valentine Jeanne-Julien[10,11], Jérémie Rosain[10,11], Ekaterina Minskaia[1], Jean-Laurent Casanova[7,10,11,12], Stéphanie Boisson-Dupuis[7,10,11], Jacinta Bustamante[7,10,11,13], Richard E. Randall[6], Timothy D. McHugh[14], Adrian J. Thrasher[8,15] and Siobhan O. Burns[1,2*†]

[1]Institute of Immunity and Transplantation, University College London, London, United Kingdom, [2]Department of Immunology, Royal Free London National Health Service (NHS) Foundation Trust, London, United Kingdom, [3]School of Medicine, Universidad Complutense, Madrid, Spain, [4]Department of Immunology, Hospital Universitario Son Espases, Palma, Spain, [5]Research Unit, Institut d'Investigació Sanitària de les Illes Balears (IdISBa), Palma, Spain, [6]School of Biology, University of St. Andrews, St. Andrews, United Kingdom, [7]St. Giles Laboratory of Human Genetics of Infectious Diseases, Rockefeller Branch, Rockefeller University, New York, NY, United States, [8]Molecular and Cellular Immunology Section, University College London Institute of Child Health, London, United Kingdom, [9]Department of Medicine, University of Cambridge, Cambridge, United Kingdom, [10]Laboratory of Human Genetics of Infectious Diseases, Necker Branch, National Institute of Health and Medical Research (INSERM) U1163, Paris, France, [11]Paris Cité University, Imagine Institute, Paris, France, [12]Howard Hughes Medical Institute, New York, NY, United States, [13]Study Center of Immunodeficiencies, Necker Hospital for Sick Children, Paris, France, [14]Research Department of Infection, University College London Centre for Clinical Microbiology, London, United Kingdom, [15]Immunology Department, Great Ormond Street Hospital for Children NHS Foundation Trust, London, United Kingdom

Purpose: Janus kinase-1 (JAK1) tyrosine kinase mediates signaling from multiple cytokine receptors, including interferon alpha/beta and gamma (IFN-α/β and IFN-γ), which are important for viral and mycobacterial protection respectively. We previously reported autosomal recessive (AR) hypomorphic *JAK1* mutations in a patient with recurrent atypical mycobacterial infections and relatively minor viral infections. This study tests the impact of partial JAK1 deficiency on cellular responses to IFNs and pathogen control.

Methods: We investigated the role of partial JAK1 deficiency using patient cells and cell models generated with lentiviral vectors expressing shRNA.

Results: Partial JAK1 deficiency impairs IFN-γ-dependent responses in multiple cell types including THP-1 macrophages, Epstein-Barr Virus (EBV)-transformed B cells and primary dermal fibroblasts. In THP-1 myeloid cells, partial JAK1

deficiency reduced phagosome acidification and apoptosis and resulted in defective control of mycobacterial infection with enhanced intracellular survival. Although both EBV-B cells and primary dermal fibroblasts with partial JAK1 deficiency demonstrate reduced IFN-α responses, control of viral infection was impaired only in patient EBV-B cells and surprisingly intact in patient primary dermal fibroblasts.

Conclusion: Our data suggests that partial JAK1 deficiency predominantly affects susceptibility to mycobacterial infection through impact on the IFN-γ responsive pathway in myeloid cells. Susceptibility to viral infections as a result of reduced IFN-α responses is variable depending on cell type. Description of additional patients with inherited JAK1 deficiency will further clarify the spectrum of bacterial and viral susceptibility in this condition. Our results have broader relevance for anticipating infectious complications from the increasing use of selective JAK1 inhibitors.

KEYWORDS

JAK1, IFN immunity, immunodeficiency, mycobacterial disease, viral susceptibility

Introduction

The widely expressed Janus kinase (JAK) family of tyrosine kinases are essential for signal transduction through interleukin (IL) and interferon (IFN) cytokine receptors. JAK family members (JAK1, JAK2, JAK3 and TYK2) associate with receptors individually or in pairs resulting in recruitment and phosphorylation of signal transducers and activators of transcription (STAT) proteins and transcription of STAT-responsive genes (1–3). In total the JAK/STAT pathway regulates multiple cellular functions including growth, differentiation and homeostasis although individual JAK/STAT molecules play specific roles in different cell types (4).

The roles of several members of the JAK family for immune cell function have been clarified through investigation of human and murine deficiency states (5, 6). For example, autosomal recessive (AR) complete JAK3 deficiency typically cause severe combined immunodeficiency (SCID) characterized by absence of autologous T and NK cells, highlighting the importance of JAK3 signaling from interleukin (IL)-2 receptor subunit gamma (IL-2RG)-containing IL receptors for development of these lineages (7–10). On the other hand, AR complete TYK2 deficiency result in susceptibility to mycobacterial and viral disease as a result of impaired signaling from the IL-12/IL-23/IL-10 and IFN-α/β receptors respectively (5, 11–13). AR partial P1104A-TYK2 deficiency has limited predisposition to mycobacterial disease due to selectively impaired responses to IL-23 but not other cytokines (13, 14), highlighting that complete and partial deficiencies can have different cellular and clinical phenotypes. Autosomal dominant (AD) JAK1 gain of function (GOF) mutation was reported in patients with severe multisystem autoinflammatory disease (15). However, defining the specific effect of JAK1 deficiency on the immune system has been hampered by perinatal lethality in murine models of complete JAK1-deficiency as a result of neurological defects (1).

We have reported the first, and to date only, case of human inherited AR partial JAK1 deficiency associated with two germline homozygous missense mutations in the pseudokinase domain of JAK1 (16). Together these mutations had a hypomorphic effect on JAK/STAT signaling associated with reduced kinase function and a slight reduction in JAK1 protein expression (16, 17). Although JAK1 cooperates with JAK3 for common gamma chain (γc) receptor signaling, lymphocyte development and function were relatively well preserved. Instead, recurrent atypical mycobacterial disease was the dominant clinical phenotype, grouping JAK1 deficiency with other diverse genetic defects of the IFN-γ immunity as a cause of syndromic mendelian susceptibility to mycobacterial disease (MSMD, Supplementary Table 1), (18). Somewhat surprisingly given the partnership of JAK1 with TYK2 for IFN-α/βR signaling (12, 19–26), serious viral infections were not seen. Flat forehead warts, which are unusual in immunocompetent individuals, were present but not sampled for virus identification. These features suggest a non-redundant role for JAK1 in IFN-γR signaling but its relative importance for IFN-α/βR signaling remains unclear.

In our previous analysis of AR partial JAK1 deficiency, responses to IFN-α and IFN-γ were defective in primary

dermal fibroblasts and in whole blood analysis (16). As partial deficiency of another JAK family protein, TYK2, has different impact depending on the specific cell type examined (13), we set out to expand our previous findings and test the impact of partial JAK1 deficiency on pathogen control. Here, using a combination of patient cells and knock down cell lines, including fibroblasts, B- and myeloid cells, we specifically investigate the impact of partial JAK1-deficiency on IFN signaling in hematopoietic and non-hematopoietic cell lineages.

Materials and methods

Patients cells and human cell lines

THP-1 cells were obtained from the American Type Culture Collection (ATCC #TIB-202). EBV-B cells from patients and healthy controls were derived from peripheral blood mononuclear cells (PBMCs) (27). Informed written consent was obtained in accordance with the Declaration of Helsinki and ethical approval from the Great Ormond Street Hospital for Children NHS Foundation Trust and the Institute of Child Health Research Ethics Committee (Reference Number: 06/Q0508/16). For cell culture details, see Supplemental Methods.

Lentivirus preparation and transductions

JAK1 knock down (KD) and scrambled control (Sc) cell lines were generated using lentiviral vectors expressing short hairpin RNA (shRNA) sequences as previously described (17). For further information, see Supplemental Methods.

Determination of mRNA levels by real time-quantitative polymerase chain reaction and reverse transcription polymerase chain reaction

THP-1 cells were stimulated or left unstimulated with 50 ng/ml IFN-γ (Invitrogen) for 24h. Total RNA from cells was extracted using RNAeasy kit (Qiagen) and converted to cDNA by reverse-transcription using Quantitect reverse transcription kit (Qiagen). Determination of mRNA level was performed by RT-PCR using specific primers (Supplementary Table 2) and QuantiTect SYBR® Green PCR Kit (Qiagen) according to manufacturer's instructions. Fold changes were calculated using the DDCT2 (-Delta Delta C(T)) method and results normalized with respect to the values obtained for the endogenous *ACTIN* and *GAPDH* cDNA. See supplemental methods for assessment of *MX1* and *OAS1* following IFN-α stimulation.

Flow cytometry analysis of STAT phosphorylation

THP-1 cells were stimulated with 10^3 IU/ml IFN-α2b or 50 ng/ml IFN-γ. EBV- B cells were stimulated with 10^5 IU/ml IFN-α2b or 500 ng/ml IFN-γ for 10 min. Cells were fixed using fix buffer I and permeabilized using Perm Buffer III (BD Biosciences) for 30 min at 4°C, and labelled with anti-pSTAT1 (clone 4a, BD Biosciences) or anti-STAT1 (clone 1/Stat1, BD Biosciences) antibodies for 60 min at room temperature. At least 10000 gated events were acquired on a BD LSRFortessa cytometer and data were analyzed using FlowJo software (Tree Star Inc., USA). Data on graphs is shown as relative increase (mean fluorescence intensity (MFI) of stimulated cells – MFI of unstimulated cells/MFI unstimulated cells).

Infection models with bacteria *in vitro*

For details of *Mycobacterium bovis Calmette–Guérin* (BCG) and *Salmonella typhimurium*, including culture, see Supplemental Methods. THP-1 cells were differentiated into macrophages using 10 ng/ml of phorbol myristate acetate (PMA) for 48 h and then were left unstimulated or stimulated with IFN-γ 50 ng/ml for 18 h before infection. Cells were infected using stocks (BCG) or bacteria in mid-log grow phase (*Salmonella*), using a multiplicity of infection (MOI) of 20:1 for BCG expressing-mCherry and 10:1 for BCG and *Salmonella*. Monolayers were incubated for 4 h with BCG and 30 min with Salmonella at 37°C in 0.5% CO_2. Infected cells were washed to remove extracellular bacteria. To kill extracellular bacteria after *Salmonella* infection, cells were incubated in complete medium with Gentamicin (100 µg/ml) for two hours. Subsequently, macrophages were incubated in fresh complete medium, in the presence or absence of IFN-γ (50 ng/ml) for different time points (detailed in the legends).

Harvest of infected macrophage lysate for CFU plating

Cells were lysed at 3 days for BCG infection or 24 h for *Salmonella* infection with 0.05% SDS w/v in H_2O and serial dilutions plated out on Middlebrook 7H11 or LB agar plates followed by incubation at 37°C for 14 days for BCG infection or 12 h at 37°C after *Salmonella* infection. Bacterial survival,

measured as CFU for each condition, was expressed as a percentage of the CFU counted in the untreated Sc control.

Quantification of the infected cells by flow cytometry

Macrophages differentiated from Sc and KD THP-1 cell lines using PMA, were left unstimulated or stimulated with IFN-γ (50ng/ml) before infection with BCG expressing-mCherry strains (MOI 20:1). After phagocytosis, cells were washed and incubated in complete medium in the presence or absence of IFN-γ (50 ng/ml) for the given time points. Cells were removed from the plate using Accutase® solution (A6964, Sigma Aldrich), washed with PBS, fixed in 4% paraformaldehyde (PFA) for 10 min and analyzed by flow cytometry (BD LSRFortessa) using FlowJo.

Microscopy

200,000 THP-1 cells were differentiated on 35mm glass bottom dishes (Fluorodish) for microscopy experiments. For further details see Supplemental Methods.

pH sensitivity of pHrodo-labelled BCG

BCG-lux were labelled with pHrodo™ (Invitrogen) at a concentration of 25mM according to the manufacturer's instructions, except for omission of the 100% methanol step. Approximately 100,000 CFU were resuspended in 500 µl buffer at pH 7. Samples were then acquired on a BD Fortessa flow cytometer (BD LSRFortessa), and pHrodo fluorescence was measured in the PE-Texas Red channel, and analyzed using FlowJo.

Apoptosis assays

Macrophages were left unstimulated or stimulated with IFN-γ (50ng/ml) before BCG infection (MOI 10:1). Percentage of apoptosis was determined using APC Annexin V apoptosis detection kit with PI (BioLegend 640932) according to manufacturer's instructions by flow cytometry (BD LSRFortessa), and analyzed using FlowJo.

Viral assays

Primary dermal fibroblast and EBV-B cells viral assays were performed as previously described (24, 28–31). For further details see Supplemental Methods.

Statistical analysis

Statistical analysis was performed with Graph Prism Version 5.01. The following tests were used: One-way ANOVA; Wilcoxon-Signed Rank for pairwise comparisons; Mann-Whitney for unpaired comparisons. Results were expressed as mean ± SEM. *P*-values < 0.05 were considered significant.

Results

Partial JAK1 deficiency impairs STAT1 phosphorylation and expression of IFN-γ-inducible genes in THP-1 cells

As the patient with AR partial JAK1 deficiency presented predominantly with MSMD (Table S1), we sought to establish a model to examine the role of JAK1 in myeloid cells during mycobacterial infection. As patient blood was not accessible, for this study we generated a THP-1 monocytic cell line with sub-total JAK1 knock-down (KD) to model partial JAK1 deficiency using lentiviral vectors expressing short hairpin RNA (shRNA) sequences. The JAK1 KD model does not fully recapitulate the impact of the patient's variants which preserved expression of mutant JAK protein that had reduced signaling function (16) but allows assessment of reduced JAK1 function by reducing protein expression. Compared to control shRNA, *JAK1* shRNA substantially reduced *JAK1* messenger RNA expression for three out of four hairpins tested (Figure S1A). THP-1 cells transduced with *JAK1* shRNA #3 were utilized for further studies. Compared with shRNA control cells, 25-30% JAK1 protein expression was detected in *JAK1* shRNA #3 cell lines using western blotting, in keeping with partial knock down (Figure S1B). To test whether the level of JAK1 reduction was sufficient to impair JAK1 protein function, we studied JAK1-mediated phosphorylation of STAT1 in response to IFN-γ stimulation, using flow cytometry. We observed a significant decrease in STAT1 phosphorylation following IFN-γ stimulation in the THP-1 JAK1-KD cells compared to scrambled control shRNA cell lines (Sc) ($p<0.05$) (Figures 1A, B). Surprisingly, STAT1 phosphorylation in response to IFN-α stimulation was not significantly reduced (Figures 1C, D), suggesting that partial impairment of JAK1 function affects predominantly the IFN-γ response in THP-1 cells. Following stimulation with IFN-γ, upregulation of interferon regulatory factor 1 (*IRF1*) and Class II Transactivator (*CIITA*) mRNA was significantly lower in the KD than Sc lines, indicating impaired downstream gene transcription in JAK1 deficiency (Figures 1E, F). In contrast, upregulation of 2'-5'-oligoadenylate synthetase 1 (*OAS1*) and *MX1* in response to IFN-α stimulation was preserved (Figures 1G, H). Our findings were unlikely to be due to

alterations in the surface expression of IFN-γ or IFN-α receptors as surface levels of IFNGR1 and IFNAR2 were comparable between JAK1 KD and Sc cell lines at baseline and after stimulation with their ligand (Figures S2A–D). As seen in THP-1 cells, partial JAK1 deficiency had a clear impact on IFN-γ signaling in primary dermal fibroblasts and EBV B-cells from the patient with AR JAK-1 deficiency, resulting in significantly reduced STAT1 phosphorylation following IFN-γ stimulation (Figures 1I, J) and (Figures S3A, B), albeit to a lesser degree that seen in fibroblasts from a patient with complete IFN-γR deficiency (16) (Figure S3B).

Partial loss of JAK1 function enhances mycobacterial and salmonella survival in myeloid cells

To test the impact of reduced JAK1 function on IFN-γ-mediated host defense to intracellular pathogens we utilized BCG as a well-established model for mycobacterial infection (32). Macrophages differentiated from the THP-1-JAK1 KD and Sc cell lines were infected with BCG, with or without prior IFN-γ stimulation. JAK1 KD and Sc THP-1 cells were capable of internalizing BCG, as seen by confocal microscopy

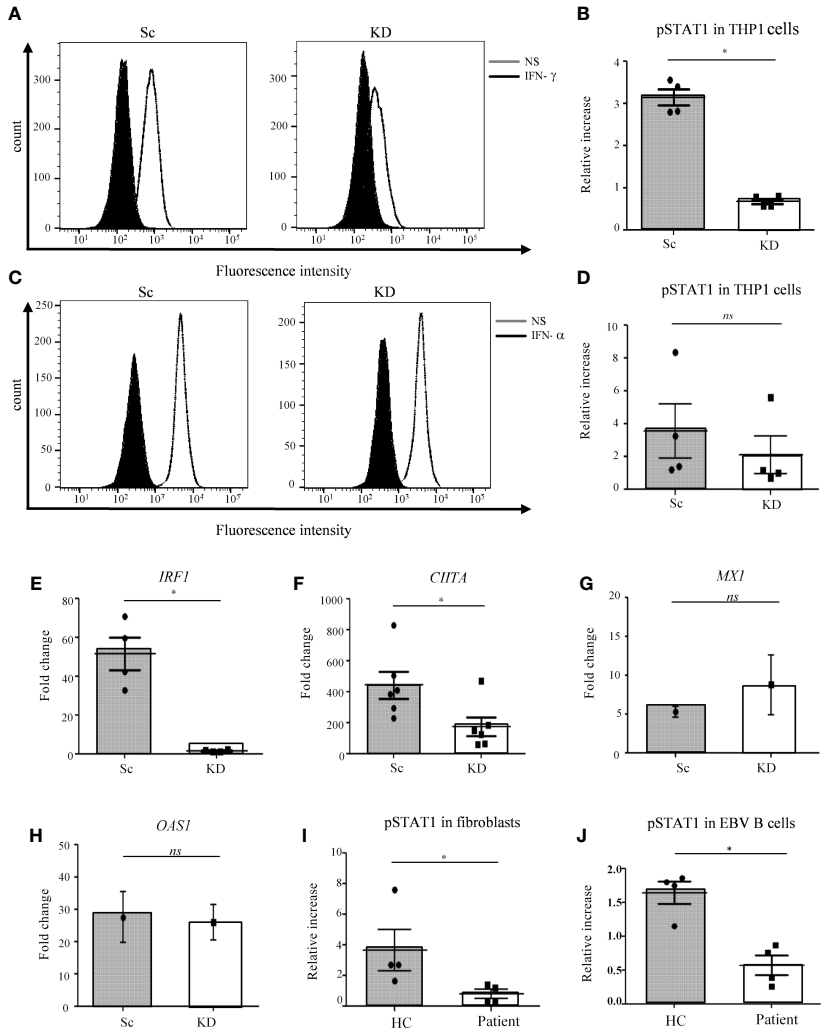

FIGURE 1
STAT1 responses are impaired in JAK1-deficient THP-1 cells, fibroblasts and EBV-B cells. **(A–D)** Analysis of JAK/STAT signaling by flow cytometry (FC) in THP-1 cells after IFN-γ/IFN-α stimulation. **(A)** and **(C)** display a representative experiment, **(B)** and **(D)** are from four independent experiments. Two-tailed Mann Whitney test. **(E, F)** RTqPCR analysis of *IRF1* and *CIITA* expression from THP-1 cells after IFN-γ stimulation. Data is from five independent experiments. Two-tailed Mann Whitney test. **(G, H)** RT-qPCR analysis of *MX1* and *OAS1* expression in THP-1 cells after stimulation with 1000 IU/ml IFN-α. Graphs represent the mean of three experiments. Data was compared using unpaired t-test. **(I, J)** Analysis of JAK/STAT signaling by FC in control and patient fibroblasts and EBV-B cells after stimulation with IFN-**γ**. Data are from four independent experiments. Two-tailed Mann Whitney test. *P <0.05; NS, not significant.

(Figure 2A). Using confocal analysis and a lysotracker dye which increases fluorescent intensity in low pH (33), both Sc and JAK1 KD cell lines were observed to traffic a proportion of internalized BCG into acidified compartments (Figure S4A).

To better quantitate BCG infection, THP-1 macrophages were co-cultured with mCherry-expressing BCG and analyzed by flow cytometry. Similar levels of bacteria were internalized by KD and Sc lines at 4 hours, and this was largely unaffected by IFN-γ stimulation (Figures 2B, C), indicating that loss of JAK1 does not significantly impact phagocytosis. As expected, at both 24 and 72 hours, IFN-γ stimulation significantly reduced mCherry fluorescence in Sc lines consistent with lower bacterial survival. In contrast, IFN-γ had no significant impact on mCherry levels in KD lines (Figures 2B, C). To confirm that JAK1 deficiency promotes intracellular BCG survival, KD and Sc lines were lysed on culture plates 3 days after infection and BCG titers were quantitated by counting colony forming units (CFU/ml). As seen in flow cytometry assays, BCG survival was higher in KD lines indicating an important role for JAK1 in controlling mycobacterial infection (Figure 2D). Similar findings were obtained with *Salmonella typhimurium* (Figure 2E), another intracellular pathogen known to require IFN-γ for control of the bacterial infection, with significantly higher bacterial survival seen in KD than Sc cells. Together these results demonstrate that JAK1-deficient myeloid cells permit enhanced intracellular mycobacterial and salmonella survival *in vitro*.

Partial JAK1 deficiency impairs IFN-γ-induced phagosome acidification and apoptosis in myeloid cells

To further explore the mechanisms promoting enhanced bacterial intracellular survival in myeloid cells with reduced JAK1 function, phagosome acidification and apoptosis were tested as these are key IFN-γ-dependent steps in the control of mycobacterial infection (34–39). Following infection of THP-1-derived macrophages with pHrodo-labelled BCG, phagosomal acidification was measured by measuring fluorescence, which is released in the context of low pH. Even in the absence of IFN-γ stimulation, both Sc and KD THP-1 cells had relatively high levels of pHrodo fluorescence, which relates to the high baseline lysosomal content in PMA differentiated THP-1 macrophages (40) (Figure 3A and Figure S4B). Fluorescence intensity was increased after IFN-γ-stimulation in Sc cells lines consistent with additional IFN-γ-mediated induction of acidification (Figures 3A, B). In contrast there was no increase in acidification in the KD cell line following IFN-γ stimulation.

To test whether partial JAK1 deficiency is sufficient to impair IFN-γ-induced apoptosis, Annexin V/PI staining was measured by flow cytometry. Sc control and KD THP-1 cells had similar baseline levels of apoptosis which was not significantly increased 5 days after BCG infection alone (Figures 3C, D). In contrast, IFN-γ pre-treatment induced significant apoptosis at both 3 and 5 days after BCG infection in Sc control cells compared with untreated Sc control cells, an effect that was abrogated in KD cells (Figures 3C, E and Figure S5). Together our data suggest that defective intracellular bacterial killing in myeloid cells with reduced JAK1 function is at least in part due to impaired IFN-γ-induced phagosome maturation and apoptosis.

Partial JAK1 deficiency impairs anti-viral response in EBV-B cells but not in fibroblasts

To test viral susceptibility in JAK1 deficient cells, we utilized established viral infection models in both fibroblast and EBV-B cells (24, 41, 42). We have previously demonstrated reduced STAT1 phosphorylation following IFN-α stimulation in primary dermal fibroblasts from the patient with AR partial JAK1 deficiency (16). We also observed reduced STAT1 phosphorylation following IFN-α in EBV-B cells from the same patient with AR partial JAK1 deficiency, albeit to a lesser degree than that seen in IFNAR-deficiency (Figures S6A, B). For fibroblast infections, we used Parinfluenza virus 5 (PIV5) and highly attenuated recombinant strains of PIV5 (PIV5VΔC) that lack defined functional IFN antagonists (33, 34). This virus is weakly virulent forming only pinpoint plaques in cells that produce and respond to IFN but with ability to form large plaques if the IFN system is impaired. As previously shown (41), fibroblast monolayers from patients with complete STAT2 deficiency supported the formation of large plaques (infected cells) of PIV5 and PIV5VΔC, demonstrating uncontrolled viral infection resulting from failure of the IFN-α response (Figure 4A). Fibroblast monolayers from heathy control and the patient with partial JAK1 deficiency prevented large viral plaque formation indicating successful viral control (Figure 4A). This assay relies on production of endogenous IFN-α by infected fibroblasts and therefore reflects cellular response to physiological concentrations of IFN.

We also tested whether partial JAK1 deficiency altered the capacity of fibroblasts to respond to exogenous addition of IFN-α to control PIV5 infection. Using immunostaining to visualize intracellular virus, loss of viral fluorescence was seen during successful suppression of viral infection in healthy control fibroblasts treated with IFN-α (Figure 4B). Comparable viral suppression was mediated by patient fibroblasts after IFN-α stimulation suggesting partly preserved IFN-α responses in fibroblasts with reduced JAK1-function (Figure 4B). Using a separate model, fibroblasts from healthy controls and patient were infected with herpes simplex virus-1 (HSV-1), showing control of viral infection 24h after treatment with exogenous IFN-α (Figure S7).

To further test the impact of partial JAK1 deficiency on host viral protection we used a separate model in which EBV-

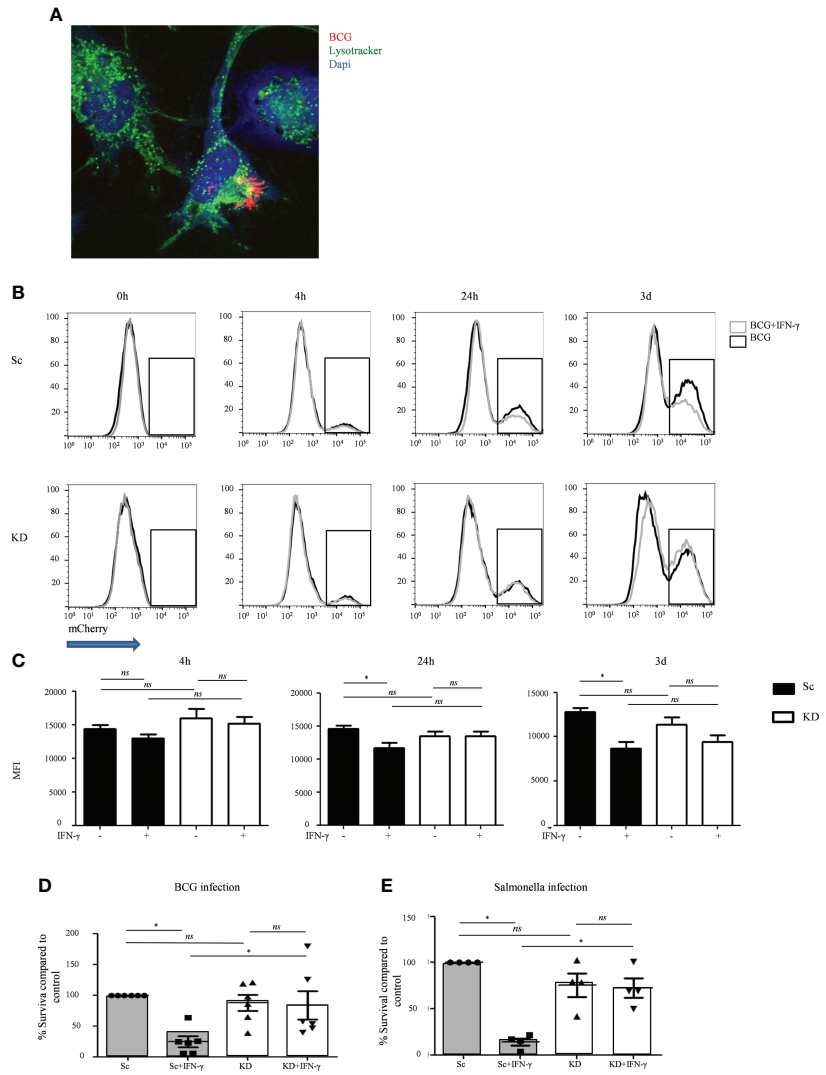

FIGURE 2
JAK1-deficient THP-1 cells show increased mycobacterial and *Salmonella* survival after IFNγ stimulation. **(A)** Internalization of mCherry-BCG by THP-1 cells, unstimulated or stimulated with IFN-γ. A is from a representative experiment. **(B, C)** FC quantitation of mCherry-BCG in THP-1 cells; mCherry fluorescence was measured in the PE-Texas Red channel. Black line – BCG infected cells, gray line – BCG infected cells + IFN-γ stimulation. B displays a representative experiment; C is from five independent experiments. **(D, E)** Bacterial survival in THP-1 cells infected with BCG or *Salmonella* strains, with or without IFNγ stimulation. Data is from six and four independent experiments respectively. Two-tailed Mann Whitney test. *P <0.05; NS, not significant.

B cells are infected with VSV. As expected, healthy control EBV-B cells controlled viral infection when treated with exogenous IFN-α, evidenced by lower viral titers compared with untreated cells at 24h and 48h after infection (Figure 4C). In contrast, EBV-B cells from the patient with AR partial JAK1-deficiency exhibited no reduction in viral titers in the presence of IFN-α indicating a significantly reduced response to IFN-α. In this assay, VSV titers in infected patient EBV-B cells were comparable to STAT1-deficient EBV B-cells after 24h and 48h of infection (Figure 4C). Together these results suggest that partial JAK1 deficiency results in impaired viral protection with variable impact according to the cell type involved.

Discussion

An increasing number of disease-causing mutations have been described in type I and type II IFN pathways (5, 18, 21, 25, 26, 41, 43–46) (Table S1). Defects of IFN-γ-mediated immunity give rise to mycobacterial susceptibility (MSMD) while loss of IFN-α/β function results in viral infection of varying severity,

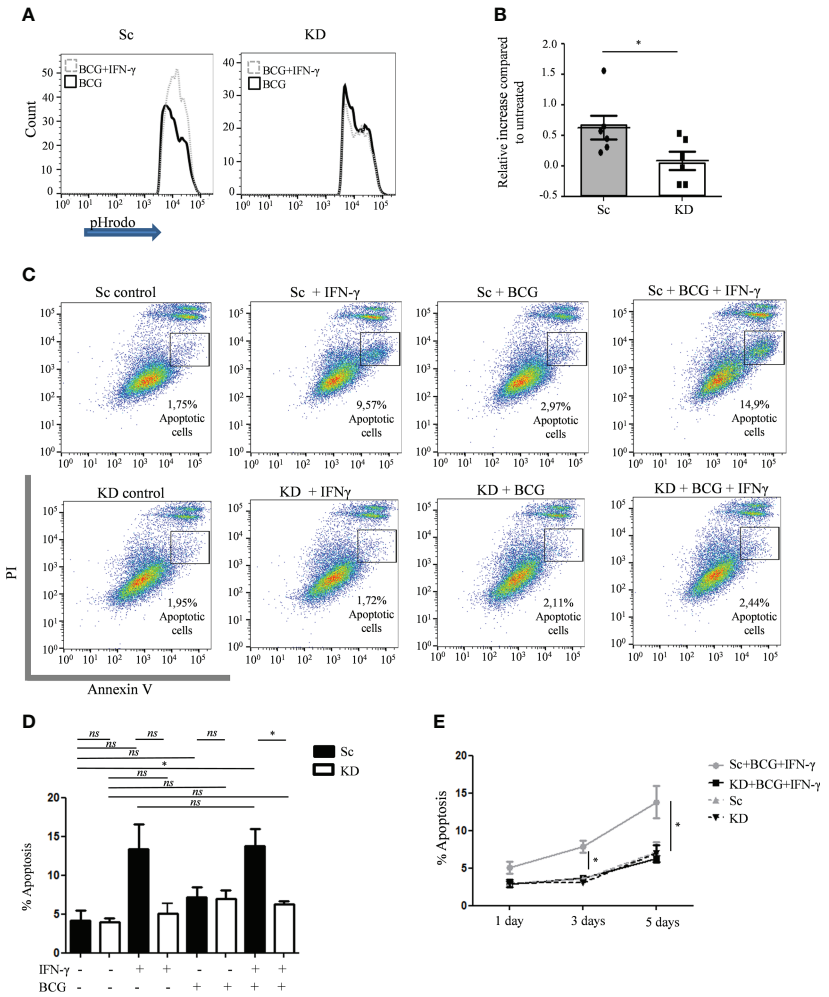

FIGURE 3
Phagosome acidification and apoptosis is reduced in JAK1-deficient THP-1 cells. **(A, B)** FC measurement of phagosome acidification using detection of pHrodo-labelled BCG post infection of THP-1 cells, with or without prior IFN-γ stimulation. Data is from six independent experiments. **(C–E)** Percentage of apoptosis quantified by FC using annexin V/PI staining in THP-1 cells at different time points following BCG infection, with or without IFN-γ stimulation. C displays a representative experiment 5 days post infection. D and E are from four independent experiments, showing 5 day **(D)** and 1, 3 and 5 day **(E)** timepoints. Statistical comparisons in E are for Sc+BCG+IFN *vs.* KD+BCG+IFN. Two-tailed Mann Whitney test. *P <0.05; NS, not significant.

ranging from relatively mild to fatal disease (18, 21, 24, 25, 41, 42, 45–49). Typically, overlap of mycobacterial and viral phenotypes occurs where the defective signaling molecule is shared by both pathways, for example in TYK2 or STAT1 deficiency (24), although the degree of infection susceptibility depends on how and to what extent signaling is impaired (50). We previously identified homozygous mutations in *JAK1* causing AR partial JAK1 deficiency in a patient with mycobacterial susceptibility (16). Although JAK1 is shared by both IFN-γ and IFN-α/β/λ signaling pathways, severe viral infections were absent into adulthood. In contrast with other inherited defects of IFN-α/β/λ signaling (43), vaccine strain measles, mumps and rubella as well as wildtype CMV, EBV and VZV were tolerated normally in this patient without serious clinical disease.

Here we investigated the specific impact of partial JAK1-deficiency on IFN-γ and IFN-α/β signaling using several different cell line models generated either from our patient, where mutations in the pseudokinase domain resulted in a slightly reduced level of JAK1 protein which lacked full kinase function (16), or using shRNA to reduce wild type JAK1 protein expression. While the shRNA JAK1 KD model does not fully recapitulate the patient's variants, it remains a useful model to assess the effects of partial JAK1 function on cell function. Using *in vitro* infection models with BCG and *Salmonella*, myeloid lineage THP-1 cells generated using shRNA to achieve partial

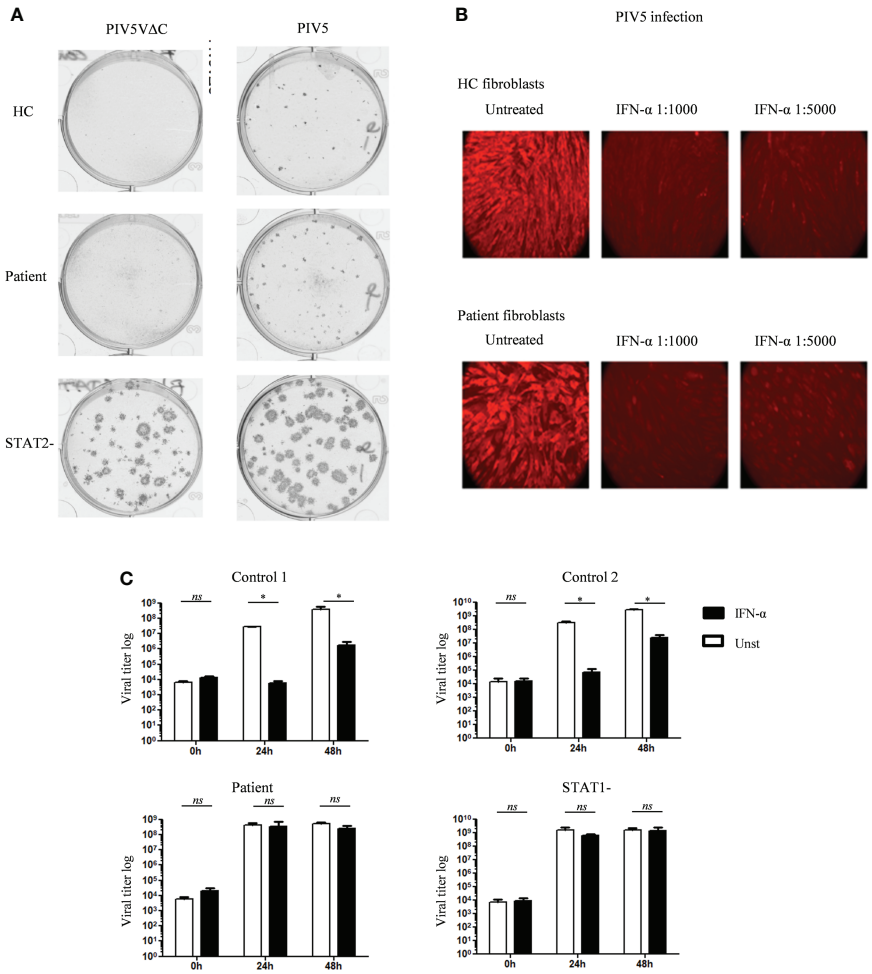

FIGURE 4
Variable *in vitro* antiviral response in fibroblasts and EBV B cells of the patient with JAK1 deficiency **(A)** Relative plaque sizes of the PIV5/PIV5VΔC virus visualized by immunostaining in fibroblasts from patients with partial JAK1, complete STAT2 deficiency and healthy control. **(B)** Visualization of PIV5 virus-infected cells by immunofluorescence in control and JAK1 deficient patient fibroblast, with or without IFN-α pre-treatment. Data display a representative experiment from three independent experiments. **(C)** Determination of VZV viral load in EBV-B cells from the patient with partial JAK1, complete STAT1 deficiency, and two healthy controls (C1 and C2), with or without pre-treatment with IFN-α. Data is from three independent experiments. One-tailed Mann Whitney test. *P <0.05; NS, not significant.

JAK1-deficiency (25-30% residual JAK1 protein expression) supported enhanced bacterial survival after IFN-γ stimulation, reminiscent of uncontrolled mycobacterial replication previously reported in IFN-γR1-deficient human iPSC-derived macrophages (51). IFN-γ-activated healthy macrophages are more resistant to mycobacterial infection by the induction of several discreet mechanisms that promote mycobacterial killing (52–55), such as expression of IFN-γ-inducible genes (*IRF1* and *CIITA*), phagosome maturation and apoptosis (35–37, 56, 57), all of which were found to be reduced in the JAK1 knock down cell line after IFN-γ stimulation. Therefore, we concluded that, in myeloid cells, JAK1 is non-redundant for multiple aspects of the IFN-γ-response required to control intracellular bacterial infection. Our data shows that partial disruption of JAK1 signaling is sufficient to impair anti-mycobacterial protection, which has implications for the expected phenotype of hypomorphic JAK1 mutations and for the increasing use of JAK1 inhibitors in other areas of medicine. In our THP-1 macrophage model, expression of JAK1 protein was reduced by 70-75% which significantly reduced STAT1 phosphorylation and gene expression following IFN-γ stimulation but supported relatively normal pSTAT1 and gene expression after IFN-α stimulation. Further work is required to determine what levels of residual JAK1 expression and signaling function are required to preserve immune competence against mycobacteria *in vitro* and, more importantly, *in vivo*.

Given the known role of JAK1 in signaling from the IFN-α/β receptor, we studied the ability of dermal fibroblasts and EBV-B

cells from the JAK1-deficient patient to develop antiviral responses *in vitro*. Surprisingly, despite a documented reduction in STAT1 signaling in patient primary dermal fibroblasts (16), we found no detectable susceptibility to viral infection using three different viruses, suggesting that residual JAK1 activity was sufficient to preserve sufficient IFN-α response for the control of viral proliferation in that cell type. In contrast, the patient's EBV-B cells showed lack of viral protection following VSV infection, which may indicate a more pronounced impact of partial JAK1 deficiency on the type I IFN response in hematologic cells. Although in our patient we observed only flat warts (which were presumed to be due to HPV) without life-threatening viral infections, the description of additional patients may broaden the phenotype of JAK1 deficiency in humans and provide opportunities to further assess the relative importance of JAK1 for viral protection in hematopoietic and non-hematopoietic cell types. Future studies should also address the impact of JAK1 deficiency on IFN-λ signaling which is important for viral protection in epithelial cells, natural killer and dendritic cells (58). It remains possible that patients with JAK1 deficiency retain relatively normal viral susceptibility in specific cell types *in vivo* as result of other antiviral mechanism, as has been suggested for patients with complete STAT2 deficiency who also have surprisingly mild viral infections (41).

Here we provide the first evidence that partial loss of JAK1 function results in mycobacterial susceptibility by reducing multiple aspects of the IFN-γ response in myeloid lineage cells. Our data suggest that the predominant effect of partial JAK1 deficiency is on the IFN-γ pathway, as IFN-α but not IFN-γ responses were preserved in our shRNA model despite 70-75% loss of JAK1 expression. Although viral susceptibility was also observed *in vitro*, this varied according to cell type. Our findings contrast with the adverse effect profile published with early trails of the selective JAK1 inhibitors, filgotinib and upadacitinib, where herpes zoster viral infections and not mycobacterial disease predominate (59–62). However, even though filgotinib is considered a JAK1 selective inhibitor, it still has a role in inhibiting other JAKs with IC50 of 10 nM, 28 nM, 810 nM, and 116 nM for JAK1, JAK2, JAK3, TYK2, respectively. This possible inhibitory effect to the other JAKs may influence viral susceptibility (63). More extensive use of the JAK1/JAK2 inhibitor ruxolitinib is associated with a greater risk of mycobacterial infections (*Mycobacterium tuberculosis* and atypical mycobacterial infections) in the treatment of patients with myelofibrosis and polycythemia vera (64, 65).

We support a recommendation that previous mycobacterial infection should be investigated when considering the use of JAK inhibitors (66) and suggest tuberculin skin testing and an IFN-γ release assay (IGRA) prior to the prescription of JAK1 inhibitors. Longer experience with pharmacological JAK1 inhibition and identification of additional patients with germline JAK1 deficiency, including perhaps patients with more common and milder forms of JAK1 deficiency as recently shown for TYK2 (13), will allow us to better understand the relative importance of JAK1 for specific cytokine pathways governing host protection *in vivo*.

Data availability statement

The original contributions presented in the study are included in the article/Supplementary Material. Further inquiries can be directed to the corresponding author.

Ethics statement

Ethical approval was obtained from the Great Ormond Street Hospital for Children NHS Foundation Trust and the Institute of Child Health Research Ethics Committee (Reference Number: 06/Q0508/16). The patients/participants provided their written informed consent to participate in this study. Written informed consent was obtained from the individual(s) for the publication of any potentially identifiable images or data included in this article.

Author contributions

VD-C, AA, DY, MC, DM, IA, VJ-J, JR, and EM performed experiments and analyzed data; J-LC, SB-D, JB, RR, TM, AT, and SB designed the project and supervised the work. VD-C, AA, MC, JB, and SB wrote and edited the manuscript. All authors contributed to the article and approved the submitted version.

Funding

This work was supported by the Alfonso Martin Escudero Foundation (VD-C), Rosetrees Trust Foundation (VD-C, SB), and the Wellcome Trust (104807/Z/14/Z and 101788/Z/13/Z) (AT, RR, and DY). The project was sponsored by University College London (UCL) and the National Institute for Health Research Biomedical Research Centre at Great Ormond Street Hospital for Children NHS Foundation Trust. AA and EM were supported by the National Institute for Health Research UCLH Biomedical Research Centre. The Laboratory of Human Genetics of Infectious Diseases is supported in part by institutional grants from INSERM, Paris Cité University, Foundation for Medical Research (FRM) (EQU201903007798), St. Giles Foundation, The Rockefeller University Center for Clinical and Translational Science (8UL1TR001866), the National Center for Research Resources, the National Center for Advancing Sciences (NCATS), National Institutes of Health,

the National Institute of Allergy and Infectious Diseases (5R01AI089970, 5R37AI095983 and U19AI111143) and grants from the French National Research Agency (ANR) under the "Investments for the future" program (ANR-10-IAHU-01) and GENMSMD (ANR-16-CE17-0005-01 for JB) grants. VJ-J was supported by LABEX IBEID. JR is supported by INSERM ("poste d'accueil") and the MD-PhD program of the Imagine Institute with the support of the Bettancourt-Schueller Foundation.

Acknowledgments

We thank the Alfonso Martin Escudero Foundation, Rosetrees Trust Foundation and the Wellcome Trust for their support. The content of the manuscript has previously appeared in the thesis: VD-C (2019) Investigating of the pathogenesis of JAK1 immunodeficiency. (dissertation/thesis). Madrid, Spain. Universidad Complutense (67).

Conflict of interest

SB has received grant support from the European Union, National Institute of Health Research, UCLH and GOSH/ICH Biomedical Research Centers and CSL Behring and personal fees or travel expenses from Immunodeficiency Canada/IAACI, CSL Behring, Baxalta US Inc and Biotest. VD-C has received travel expenses from CSL Behring and Takeda. IH is employed by Healx. J-LC serves on the board for ADMA and Elixiron Immunotherapeutics and serves as a consultant for Celgene, Kymera TX, Pfizer, Nimbus, Sanofi, Vitae Pharmaceuticals Inc. and Asahi Kasei.

The remaining authors declare that the research was conducted in the absence of any commercial or financial relationships that could be construed as a potential conflict of interest.

Publisher's note

Supplementary material

The Supplementary Material for this can be found online at: https://www.frontiersin.org/articles/10.3389/fimmu.2022.888427/full#supplementary-material

References

1. Rodig SJ, Meraz MA, White JM, Lampe PA, Riley JK, Arthur CD, et al. Disruption of the Jak1 gene demonstrates obligatory and nonredundant roles of the jaks in cytokine-induced biologic responses. *Cell* (1998) 93(3):373–83. doi: 10.1016/S0092-8674(00)81166-6

2. Kisseleva T, Bhattacharya S, Braunstein J, Schindler CW. Signaling through the JAK/STAT pathway, recent advances and future challenges. *Gene* (2002) 285 (1–2):1–24. doi: 10.1016/S0378-1119(02)00398-0

3. Ivashkiv LB, Donlin LT. Regulation of type I interferon responses. *Nat Rev Immunol* (2014) 14(1):36–49. doi: 10.1038/nri3581

4. Gadina M, Johnson C, Schwartz D, Bonelli M, Hasni S, Kanno Y, et al. Translational and clinical advances in JAK-STAT biology: The present and future of jakinibs. *J Leukoc Biol* (2018) 104(3):499–514. doi: 10.1002/JLB.5RI0218-084R

5. Casanova J-L, Holland SM, Notarangelo LD. Inborn errors of human JAKs and STATs. *Immunity* (2012) 36(4):515–28. doi: 10.1016/j.immuni.2012.03.016

6. Meyts I, Casanova J. Viral infections in humans and mice with genetic deficiencies of the type I IFN response pathway. *Eur J Immunol* (2021) 51(5):1039–61. doi: 10.1002/eji.202048793

7. Rochman Y, Spolski R, Leonard WJ. New insights into the regulation of T cells by γc family cytokines. *Nat Rev Immunol* (2009) 9(7):480–90. doi: 10.1038/nri2580

8. Macchi P, Villa A, Giliani S, Sacco MG, Frattini A, Porta F, et al. Mutations of jak-3 gene in patients with autosomal severe combined immune deficiency (SCID). *Nature* (1995) 377(6544):65–8. doi: 10.1038/377065a0

9. Russell SM, Tayebi N, Nakajima H, Riedy MC, Roberts JL, Aman MJ, et al. Mutation of Jak3 in a patient with SCID: Essential role of Jak3 in lymphoid development. *Science* (1995) 270(5237):797–800. doi: 10.1126/science.270.5237.797

10. Haan C, Rolvering C, Raulf F, Kapp M, Drückes P, Thoma G, et al. Jak1 has a dominant role over Jak3 in signal transduction through γc-containing cytokine receptors. *Chem Biol* (2011) 18(3):314–23. doi: 10.1016/j.chembiol.2011.01.012

11. Minegishi Y, Saito M, Morio T, Watanabe K, Agematsu K, Tsuchiya S, et al. Human tyrosine kinase 2 deficiency reveals its requisite roles in multiple cytokine signals involved in innate and acquired immunity. *Immunity* (2006) 25(5):745–55. doi: 10.1016/j.immuni.2006.09.009

12. Kreins AY, Ciancanelli MJ, Okada S, Kong X-F, Ramírez-Alejo N, Kilic SS, et al. Human TYK2 deficiency: Mycobacterial and viral infections without hyper-IgE syndrome. *J Exp Med* (2015) 212(10):1641–62. doi: 10.1084/jem.20140280

13. Boisson-Dupuis S, Ramirez-Alejo N, Li Z, Patin E, Rao G, Kerner G, et al. Tuberculosis and impaired IL-23–dependent IFN-γ immunity in humans homozygous for a common TYK2 missense variant. *Sci Immunol* (2018) 3(30): eaau8714. doi: 10.1126/sciimmunol.aau8714

14. Kerner G, Ramirez-Alejo N, Seeleuthner Y, Yang R, Ogishi M, Cobat A, et al. Homozygosity for TYK2 P1104A underlies tuberculosis in about 1% of patients in a cohort of European ancestry. *Proc Natl Acad Sci* (2019) 116 (21):10430–4. doi: 10.1073/pnas.1903561116

15. Gruber CN, Calis JJA, Buta S, Evrony G, Martin JC, Uhl SA, et al. Complex autoinflammatory syndrome unveils fundamental principles of JAK1 kinase transcriptional and biochemical function. *Immunity* (2020) 53(3):672–84.e11. doi: 10.1016/j.immuni.2020.07.006

16. Eletto D, Burns SO, Angulo I, Plagnol V, Gilmour KC, Henriquez F, et al. Biallelic JAK1 mutations in immunodeficient patient with mycobacterial infection. *Nat Commun* (2016) 7:13992. doi: 10.1038/ncomms13992

17. Daza-Cajigal V, Albuquerque AS, Pearson J, Hinley J, Mason AS, Stahlschmidt J, et al. Loss of janus associated kinase 1 alters urothelial cell function and facilitates the development of bladder cancer. *Front Immunol* (2019) 10:2065. doi: 10.3389/fimmu.2019.02065

18. Rosain J, Kong X-F, Martinez-Barricarte R, Oleaga-Quintas C, Ramirez-Alejo N, Markle J, et al. Mendelian susceptibility to mycobacterial disease: 2014-2018 update. *Immunol Cell Biol* (2018) 97(4):360–7. doi: 10.1111/imcb.12210

19. Randall RE, Goodbourn S. Interferons and viruses: An interplay between induction, signalling, antiviral responses and virus countermeasures. *J Gen Virol* (2008) 89(1):1–47. doi: 10.1099/vir.0.83391-0

20. Müller U, Steinhoff U, Reis LF, Hemmi S, Pavlovic J, Zinkernagel RM, et al. Functional role of type I and type II interferons in antiviral defense. *Science* (1994) 264(5167):1918–21. doi: 10.1126/science.8009221

21. Duncan CJA, Mohamad SMB, Young DF, Skelton AJ, Leahy TR, Munday DC, et al. Human IFNAR2 deficiency: Lessons for antiviral immunity. *Sci Transl Med* (2015) 7(307):307ra154–307ra154. doi: 10.1126/scitranslmed.aac4227

22. Pestka S. The interferons: 50 years after their discovery, there is much more to learn. *J Biol Chem* (2007) 282(28):20047–51. doi: 10.1074/jbc.R700004200

23. Pestka S, Krause CD, Walter MR. Interferons, interferon-like cytokines, and their receptors. *Immunol Rev* (2004) 202(1):8–32. doi: 10.1111/j.0105-2896.2004.00204.x

24. Dupuis S, Jouanguy E, Al-Hajjar S, Fieschi C, Al-Mohsen IZ, Al-Jumaah S, et al. Impaired response to interferon-α/β and lethal viral disease in human STAT1 deficiency. *Nat Genet* (2003) 33(3):388–91. doi: 10.1038/ng1097

25. Hernandez N, Bucciol G, Moens L, Le Pen J, Shahrooei M, Goudouris E, et al. Inherited IFNAR1 deficiency in otherwise healthy patients with adverse reaction to measles and yellow fever live vaccines. *J Exp Med* (2019) 216(9):2057–70. doi: 10.1084/jem.20182295

26. Sancho-Shimizu V, Perez de Diego R, Jouanguy E, Zhang S-Y, Casanova J-L. Inborn errors of anti-viral interferon immunity in humans. *Curr Opin Virol* (2011) 1(6):487–96. doi: 10.1016/j.coviro.2011.10.016

27. Tosato G, Cohen JI. Generation of Epstein-Barr virus (EBV)-immortalized b cell lines. In: *Current protocols in immunology*. (Hoboken, NJ, USA: John Wiley & Sons, Inc) (2007).

28. Chen S, Short JAL, Young DF, Killip MJ, Schneider M, Goodbourn S, et al. Heterocellular induction of interferon by negative-sense RNA viruses. *Virology* (2010) 407(2):247–55. doi: 10.1016/j.virol.2010.08.008

29. Carlos TS, Young DF, Schneider M, Simas JP, Randall RE. Parainfluenza virus 5 genomes are located in viral cytoplasmic bodies whilst the virus dismantles the interferon-induced antiviral state of cells. *J Gen Virol* (2009) 90(9):2147–56. doi: 10.1099/vir.0.012047-0

30. Randall RE, Young DF, Goswami KKA, Russell WC. Isolation and characterization of monoclonal antibodies to simian virus 5 and their use in revealing antigenic differences between human, canine and simian isolates. *J Gen Virol* (1987) 68(11):2769–80. doi: 10.1099/0022-1317-68-11-2769

31. Ljrh .M. A simple method of estimating fifty per cent endpoints. *Am J Epidemiol* (1938) 27(3):493–7.

32. Bange FC, Brown AM, Jacobs WR. Leucine auxotrophy restricts growth of mycobacterium bovis BCG in macrophages. *Infect Immun* (1996) 64(5):1794–9. doi: 10.1128/iai.64.5.1794-1799.1996

33. Erwig L-P, McPhilips KA, Wynes MW, Ivetic A, Ridley AJ, Henson PM. Differential regulation of phagosome maturation in macrophages and dendritic cells mediated by rho GTPases and ezrin-radixin-moesin (ERM) proteins. *Proc Natl Acad Sci* (2006) 103(34):12825–30. doi: 10.1073/pnas.0605331103

34. Chawla-Sarkar M, Lindner DJ, Liu Y-F, Williams BR, Sen GC, Silverman RH, et al. Apoptosis and interferons: role of interferon-stimulated genes as mediators of apoptosis. *Apoptosis* (2003) 8(3):237–49. doi: 10.1023/A:1023668705040

35. Ismail N, Olano JP, Feng H-M, Walker DH. Current status of immune mechanisms of killing of intracellular microorganims. *FEMS Microbiol Lett* (2002) 207(2):111–20. doi: 10.1111/j.1574-6968.2002.tb11038.x

36. Denis M, Wedlock DN, Buddle BM. IFN-γ enhances bovine macrophage responsiveness to mycobacterium bovis : Impact on bacterial replication, cytokine release and macrophage apoptosis. *Immunol Cell Biol* (2005) 83(6):643–50. doi: 10.1111/j.1440-1711.2005.01386.x

37. Zhang J, Sun B, Huang Y, Kouadir M, Zhou X, Wang Y, et al. IFN-γpromotes THP-1 cell apoptosis during early infection with mycobacterium bovis by activating different apoptotic signaling. *FEMS Immunol Med Microbiol* (2010) 60(3):191–8. doi: 10.1111/j.1574-695X.2010.00732.x

38. Awuh JA, Flo TH. Molecular basis of mycobacterial survival in macrophages. *Cell Mol Life Sci* (2017) 74(9):1625–48. doi: 10.1007/s00018-016-2422-8

39. Hostetter JM, Steadham EM, Haynes JS, Bailey TB, Cheville NF. Cytokine effects on maturation of the phagosomes containing mycobacteria avium subspecies paratuberculosis in J774 cells. *FEMS Immunol Med Microbiol* (2002) 34(2):127–34. doi: 10.1111/j.1574-695X.2002.tb00613.x

40. Daigneault M, Preston JA, Marriott HM, Whyte MKB, Dockrell DH. The identification of markers of macrophage differentiation in PMA-stimulated THP-1 cells and monocyte-derived macrophages. *Doherty TM editor PloS One* (2010) 5(1): e8668. doi: 10.1371/journal.pone.0008668

41. Hambleton S, Goodbourn S, Young DF, Dickinson P, Mohamad SMB, Valappil M, et al. STAT2 deficiency and susceptibility to viral illness in humans. *Proc Natl Acad Sci* (2013) 110(8):3053–8. doi: 10.1073/pnas.1220098110

42. Hernandez N, Melki I, Jing H, Habib T, Huang SSY, Danielson J, et al. Life-threatening influenza pneumonitis in a child with inherited IRF9 deficiency. *J Exp Med* (2018) 215(10):2567–85. doi: 10.1084/jem.20180628

43. Bucciol G, Moens L, Bosch B, Bossuyt X, Casanova J-L, Puel A, et al. Lessons learned from the study of human inborn errors of innate immunity. *J Allergy Clin Immunol* (2019) 143(2):507–27. doi: 10.1016/j.jaci.2018.07.013

44. Kerner G, Rosain J, Guérin A, Al-Khabaz A, Oleaga-Quintas C, Rapaport F, et al. Inherited human IFN-γ deficiency underlies mycobacterial disease. *J Clin Invest* (2020) 130(6):3158–71. doi: 10.1172/JCI135460

45. Zhang S-Y, Boisson-Dupuis S, Chapgier A, Yang K, Bustamante J, Puel A, et al. Inborn errors of interferon (IFN)-mediated immunity in humans: Insights into the respective roles of IFN-α/β, IFN-γ, and IFN-λ in host defense. *Immunol Rev* (2008) 226(1):29–40. doi: 10.1111/j.1600-065X.2008.00698.x

46. Bousfiha A, Jeddane L, Picard C, Al-Herz W, Ailal F, Chatila T, et al. Human inborn errors of immunity: 2019 update of the IUIS phenotypical classification. *J Clin Immunol* (2020) 40(1):66–81. doi: 10.1007/s10875-020-00758-x

47. Bastard P, Manry J, Chen J, Rosain J, Seeleuthner Y, AbuZaitun O, et al. Herpes simplex encephalitis in a patient with a distinctive form of inherited IFNAR1 deficiency. *J Clin Invest* (2021) 131(1):e139980. doi: 10.1172/JCI139980

48. Bustamante J, Boisson-Dupuis S, Abel L, Casanova J-L. Mendelian susceptibility to mycobacterial disease: Genetic, immunological, and clinical features of inborn errors of IFN-γ immunity. *Semin Immunol* (2014) 26(6):454–70. doi: 10.1016/j.smim.2014.09.008

49. Zhang Q, Bastard P, Liu Z, Le Pen J, Moncada-Velez M, Chen J, et al. Inborn errors of type I IFN immunity in patients with life-threatening COVID-19. *Science (80-)* (2020) 370(6515):eabd4570. doi: 10.1126/science.abd4570

50. Boisson-Dupuis S, Kong X-F, Okada S, Cypowyj S, Puel A, Abel L, et al. Inborn errors of human STAT1: Allelic heterogeneity governs the diversity of immunological and infectious phenotypes. *Curr Opin Immunol* (2012) 24(4):364–78. doi: 10.1016/j.coi.2012.04.011

51. Neehus A-L, Lam J, Haake K, Merkert S, Schmidt N, Mucci A, et al. Impaired IFN γ -signaling and mycobacterial clearance in IFN γ R1-deficient human iPSC-derived macrophages. *Stem Cell Rep* (2018) 10(1):7–16. doi: 10.1016/j.stemcr.2017.11.011

52. Repique CJ, Li A, Brickey WJ, Ting JPY, Collins FM, Morris SL. Susceptibility of mice deficient in the MHC class II transactivator to infection with mycobacterium tuberculosis. *Scand J Immunol* (2003) 58(1):15–22. doi: 10.1046/j.1365-3083.2003.01266.x

53. Pine R. Review: IRF and tuberculosis. *J Interf Cytokine Res* (2002) 22(1):15–25. doi: 10.1089/107999002753452629

54. Yamada H, Mizuno S, Sugawara I. Interferon regulatory factor 1 in mycobacterial infection. *Microbiol Immunol* (2002) 46(11):751–60. doi: 10.1111/j.1348-0421.2002.tb02760.x

55. Kamijo R, Harada H, Matsuyama T, Bosland M, Gerecitano J, Shapiro D, et al. Requirement for transcription factor IRF-1 in NO synthase induction in macrophages. *Science* (1994) 263(5153):1612–5. doi: 10.1126/science.7510419

56. Gutierrez MG, Master SS, Singh SB, Taylor GA, Colombo MI, Deretic V. Autophagy is a defense mechanism inhibiting BCG and mycobacterium tuberculosis survival in infected macrophages. *Cell* (2004) 119(6):753–66. doi: 10.1016/j.cell.2004.11.038

57. Kim B-H, Shenoy AR, Kumar P, Das R, Tiwari S, MacMicking JD. A family of IFN- -inducible 65-kD GTPases protects against bacterial infection. *Sci (80-)* (2011) 332(6030):717–21. doi: 10.1126/science.1201711

58. Stanifer ML, Pervolaraki K, Boulant S. Differential regulation of type I and type III interferon signaling. *Int J Mol Sci* (2019) 20(6):1445. doi: 10.3390/ijms20061445

59. Westhovens R, Taylor PC, Alten R, Pavlova D, Enríquez-Sosa F, Mazur M, et al. Filgotinib (GLPG0634/GS-6034), an oral JAK1 selective inhibitor, is effective in combination with methotrexate (MTX) in patients with active rheumatoid arthritis and insufficient response to MTX: Results from a randomised, dose-finding study (DARWIN 1). *Ann Rheum Dis* (2017) 76(6):998–1008. doi: 10.1136/annrheumdis-2016-210104

60. Kavanaugh A, Kremer J, Ponce L, Cseuz R, Reshetko OV, Stanislavchuk M, et al. Filgotinib (GLPG0634/GS-6034), an oral selective JAK1 inhibitor, is effective as monotherapy in patients with active rheumatoid arthritis: Results from a randomised, dose-finding study (DARWIN 2). *Ann Rheum Dis* (2017) 76 (6):1009–19. doi: 10.1136/annrheumdis-2016-210105

61. Genovese MC, Fleischmann R, Combe B, Hall S, Rubbert-Roth A, Zhang Y, et al. Safety and efficacy of upadacitinib in patients with active rheumatoid arthritis refractory to biologic disease-modifying anti-rheumatic drugs (SELECT-BEYOND): A double-blind, randomised controlled phase 3 trial. *Lancet* (2018) 391(10139):2513–24. doi: 10.1016/S0140-6736(18)31116-4

62. Burmester GR, Kremer JM, Van den Bosch F, Kivitz A, Bessette L, Li Y, et al. Safety and efficacy of upadacitinib in patients with rheumatoid arthritis and inadequate response to conventional synthetic disease-modifying anti-rheumatic drugs (SELECT-NEXT): A randomised, double-blind, placebo-controlled phase 3 trial. *Lancet* (2018) 391(10139):2503–12. doi: 10.1016/S0140-6736(18)31115-2

63. Van Rompaey L, Galien R, van der Aar EM, Clement-Lacroix P, Nelles L, Smets B, et al. Preclinical characterization of GLPG0634, a selective inhibitor of JAK1, for the treatment of inflammatory diseases. *J Immunol* (2013) 191(7):3568–77. doi: 10.4049/jimmunol.1201348

64. Anand K, Burns EA, Ensor J, Rice L, Pingali SR. Mycobacterial infections with ruxolitinib: A retrospective pharmacovigilance review. *Clin Lymphoma Myeloma Leuk* (2020) 20(1):18–23. doi: 10.1016/j.clml.2019.08.008

65. Lescuyer S, Ledoux M-P, Gravier S, Natarajan-Amé S, Duval C, Maloisel F, et al. Tuberculosis and atypical mycobacterial infections in ruxolitinib-treated patients with primary or secondary myelofibrosis or polycythemia vera. *Int J Infect Dis* (2019) 80:134–6. doi: 10.1016/j.ijid.2019.01.002

66. Krauth M-T, Burgstaller S, Buxhofer-Ausch V, Gastl G, Geissler K, Keil F, et al. Ruxolitinib therapy for myelofibrosis in Austria. *Wien Klin Wochenschr* (2018), 130(17–18)495–504. doi: 10.1007/s00508-018-1365-5

67. Daza Cajigal V. *Investigating the pathogenesis of JAK1 immunodeficiency*. (Madrid, Spain: Univ Complut) (2019).

Glossary

BCG	Bacillus Calmette-Guérin
CFU	Colony forming units
CIITA	Class II Transactivator
CMV	Cytomegalovirus
DMEM	Dulbecco's Modified Eagle's Medium
DMSO	Dimethyl sulfoxide
DNA	Deoxyribonucleic acid
EBV	Epstein-Barr virus
EBV-B cells	Epstein-Barr Virus-Transformed B cells
FC	Flow cytometry
FCS	Fetal calf serum
GAPDH	Glyceraldehyde-3-phosphate dehydrogenase
GFP	*Green fluorescent protein*
GOF	Gain of function
HPV	Human papilloma virus
HSV	Herpes simplex virus
IFN-α	Interferon alpha
IFN-λ	Interferon lambda
IFN-γ	Interferon gamma
IFNAR	Interferon alpha receptor
IFNGR	Interferon gamma receptor
IL	Interleukin
IRF	Interferon regulatory factor
IU	International unit
JAK	Janus Associated Kinase
KD	Knock down
LOF	Loss-of-function
MFI	Mean fluorescence intensity
MHC	Major histocompatibility complex
MOI	Multiplicity of infection
MSMD	Mendelian susceptibility to mycobacterial disease
OD	Optical density
PBMCs	Peripheral blood mononuclear cells
PBS	Phosphate-buffered saline
PCR	Polymerase chain reaction
PFA	Paraformaldehyde
PFU	Plaque-forming unit
PI	Propidium Iodide
PID	Primary immunodeficiency
PIV5	Parainfluenza virus 5
PIV5VΔC	Attenuated recombinant strain of PIV5
PMA	Phorbol myristate acetate
P/S	Penicillin-streptomycin
qPCR	Quantitative real-time PCR
RNA	Ribonucleic acid
RT-PCR	Reverse transcription polymerase chain reaction
RT-qPCR	Real time-quantitative polymerase chain reaction
SC	scrambled control
SCID	Severe combined immunodeficiency
SDS-PAGE	Sodium dodecyl sulphate–polyacrylamide gel electrophoresis
SE	Standard deviation
SEM	Standard error of the mean
shRNA	Short hairpin RNA
STAT	Signal transducer and activator of transcription
TYK2	Tyrosine kinase 2
VSV	Vesicular stomatitis virus
VZV	Varicella zoster virus
WT	Wild type
γc	Common gamma chain

frontiers | Frontiers in Immunology

TYPE Original Research
PUBLISHED 30 September 2022
DOI 10.3389/fimmu.2022.1016108

OPEN ACCESS

EDITED BY
Marcelo A. Soares,
National Cancer Institute (INCA), Brazil

REVIEWED BY
Sweety Samal,
Translational Health Science and Technology Institute (THSTI), India
Julie Boucau,
Ragon Institute, United States

*CORRESPONDENCE
Larissa Laine
larissa.laine@thl.fi

SPECIALTY SECTION
This article was submitted to Viral Immunology, a section of the journal Frontiers in Immunology

RECEIVED 10 August 2022
ACCEPTED 15 September 2022
PUBLISHED 30 September 2022

CITATION
Laine L, Skön M, Väisänen E, Julkunen I and Österlund P (2022) SARS-CoV-2 variants Alpha, Beta, Delta and Omicron show a slower host cell interferon response compared to an early pandemic variant.
Front. Immunol. 13:1016108.
doi: 10.3389/fimmu.2022.1016108

SARS-CoV-2 variants Alpha, Beta, Delta and Omicron show a slower host cell interferon response compared to an early pandemic variant

Larissa Laine[1]*, Marika Skön[1], Elina Väisänen[1,2], Ilkka Julkunen[2] and Pamela Österlund[1]

[1]Expert Microbiology Unit, Department of Health Security, Finnish Institute for Health and Welfare, Helsinki, Finland, [2]Infection and Immunity, Institute of Biomedicine, University of Turku, Turku, Finland

Since the start of the pandemic at the end of 2019, arising mutations in SARS-CoV-2 have improved its transmission and ability to circumvent the immunity induced by vaccination and previous COVID-19 infection. Studies on the effects of SARS-CoV-2 genomic mutations on replication and innate immunity will give us valuable insight into the evolution of the virus which can aid in further development of vaccines and new treatment modalities. Here we systematically analyzed the kinetics of virus replication, innate immune activation, and host cell antiviral response patterns in Alpha, Beta, Delta, Kappa, Omicron and two early pandemic SARS-CoV-2 variant-infected human lung epithelial Calu-3 cells. We observed overall comparable replication patterns for these variants with modest variations. Particularly, the sublineages of Omicron BA.1, BA.2 and a recombinant sublineage, XJ, all showed attenuated replication in Calu-3 cells compared to Alpha and Delta. Furthermore, there was relatively weak activation of primary innate immune signaling pathways, however, all variants produced enough interferons to induce the activation of STAT2 and production of interferon stimulated genes (ISGs). While interferon mRNA expression and STAT2 activation correlated with cellular viral RNA levels, ISG production did not. Although clear cut effects of specific SARS-CoV-2 genomic mutations could not be concluded, the variants of concern, including Omicron, showed a lower replication efficiency and a slower interferon response compared to an early pandemic variant in the study.

KEYWORDS

SARS-CoV-2, Omicron, variants, mutations, replication, innate immunity, interferon

10.3389/fimmu.2022.1016108

Introduction

Severe acute respiratory syndrome coronavirus 2 (SARS-CoV-2) is the causative agent of COVID-19 of which there has been over 570 million cases and 6.4 million deaths as of August 2022 (1). During these past two years, the virus has evolved into hundreds of variants which have affected the outcome of the pandemic. In Spring 2020, a D614G mutation in spike (S) protein and a concurrent P232L mutation in the RNA-dependent RNA polymerase (RdRp) made the virus more infectious and transmissible and variants with these mutations overran the original Wuhan SARS-CoV-2 strain (2–5). Mutations continued to accumulate and by the end of 2020, the variants of concern (VOCs), Alpha and Beta, had emerged and started to spread throughout the world (6). The Alpha variant became the globally dominant virus in May 2021 until it was substituted by the Delta variant in the end of summer 2021 (7). Thereafter, at the end of 2021 a genetically new variant, Omicron, swept across the world at an unprecedented speed (8). As herd immunity to SARS-CoV-2 induced by vaccination and infection rises, we have to be on alert for virus evolution. To further understand how the virus mutations contribute to pathogenicity or transmissibility of the variants, we need to study their ability to replicate and induce host cell responses in human cells.

SARS-CoV-2 belongs to the *Sarbecovirus* sub-genus of *Betacoronaviruses* and it has a large, single-stranded, positive-sense genome with approximately 30 000 bases (9). Starting from the 5' end, two thirds of the genome comprise the open reading frames ORF1a and ORF1b, which are translated into polyproteins that are post-translationally cleaved into 16 non-structural proteins (NSPs). These form the viral replication and transcription complex (RTC) that drives viral genomic and sub-genomic RNA (gRNA, sgRNA) replication (10). The viral structural (spike (S), envelope (E), membrane (M), nucleocapsid (N) proteins) and accessory proteins (11) reside in the 3' end of the genome. The SARS-CoV-2 entry into the host cells is initiated by the attachment of the S protein receptor-binding domain (RBD) to the angiotensin-converting enzyme 2 (ACE2) receptor (12). Fusion of the viral and host membranes occurs *via* cleavage of the S protein multi-basic cleavage site (MBCS) at the boundary of its two domains, S1 and S2, by furin which is followed by further priming at a S2' site by a transmembrane serine protease 2 (TMPRSS2) (13–15). Entry of SARS-CoV-2 may also occur *via* the endosomal entry route where cleavage of S by Cathepsin L facilitates fusion of viral and endosomal membranes (16, 17). The genomic RNA is released into the host cell, the RTC is formed and the virus creates a replication organelle where gRNA and sgRNA replication occurs (18). SgRNAs are translated by host cell ribosomes to synthesize the structural and accessory proteins (10), the new viral membrane is formed, genomic RNA is packaged with N protein and new virions are assembled (19, 20).

Airway epithelial cells function as the first defense mechanisms against respiratory pathogens as they form a complex protective environment that includes physical barriers, mucociliary clearance and production of surfactants which bind pathogen-associated molecular patterns (PAMPs) (21). Lung epithelial cells also express several pattern recognition receptors (PRRs) on the outer membrane, endosomes and in the cytoplasm, which activate innate immune responses that limit infection and enhance clearance of the pathogen. SARS-CoV-2 RNA replication products have been shown to be recognized mainly *via* the cytoplasmic sensors MDA5 and RIG-I, while of the Toll-like receptors (TLRs), only TLR2 on the outer cell membrane has been clearly shown to be involved in SARS-CoV-2 mediated immune signaling (22). SARS-CoV-2 infection activates the signaling cascades that induce the expression of type I and III interferons (IFNs) and further the IFN signaling pathway (22, 23). Several coronavirus proteins antagonize the signaling events inhibiting the activation of the immune response (23).

Comparative analyses how different SARS-CoV-2 variants replicate and activate innate immunity are lacking. Thorne et al. have compared innate immune activation of Alpha and wild type variants (24) and immune activation of early pandemic variants have been studied (25, 26). Here we analysed the ability of six genetically different pre-Omicron SARS-CoV-2 isolates to replicate and induce innate antiviral immunity in a human lung epithelial cell model system. Our study included two early pandemic variants (Fin3 and Fin22), the VOCs Alpha (Fin34-α), Beta (Fin32-β) and Delta (Fin37-δ) as well as a Kappa (Fin40-κ) variant. Furthermore, the replication characteristics and host cell interferon induction of three Omicron sublineages (Fin55-BA.1, Fin58-BA.2 and recombinant Fin60-XJ) were compared to Alpha and Delta. We showed that the replication profiles of the pre-Omicron variants in the human lung epithelial cell line, Calu-3, follow a similar trend, with only modest differences. However, the replication of all Omicron sublineages was attenuated, especially that of BA.2. We detected low levels of primary innate immune signaling but sufficient interferon induction for a robust activation of the JAK-STAT pathway. Interferon mRNA expression correlated with the intracellular levels of viral RNAs, but all the variants induced similar production levels of ISGs. Interferon and cytokine production was induced at a slow pace in all but one early variant (Fin22), which interferon response peaked 24 h earlier. These results suggest that the effects of the SARS-CoV-2 mutations are very complex as various mutational profiles resulted in similar replication and host cell activation patterns. However, looking at the overall picture from early pandemic SARS-CoV-2 variants and VOCs to Omicron, the shift to lower replication efficiency and slower interferon induction suggests that accumulated mutations likely contribute to viral adaptation.

10.3389/fimmu.2022.1016108

Materials and methods

Cell culture

VeroE6-TMPRSS2-H10 cell line (27) and a human airway epithelial cell line, Calu-3 (ATCC, HTB-55) were maintained in Eagle's minimum essential medium (E-MEM) supplemented with 0.6 µg/mL penicillin, 60 µg/mL streptomycin, 2 mM L-glutamine, 20 mM HEPES. The cell growth medium contained 10% and 15% fetal bovine serum (FCS, Sigma Aldrich) for VeroE6-TMPRSS2-H10 and Calu-3, respectively. Cells were incubated at 37°C in 5% CO_2.

Generation of virus stocks

SARS-CoV-2 variants used in the present study include Fin3 (B.1.1.29, hCoV-19/Finland/FIN-3/2020, EPI_ISL_2365908, ON531991), Fin22 (B.1.258, hCoV-19/Finland/THL-202039825/2020, EPI_ISL_3471857, ON532015), Fin32-β (B.1.351, Beta variant, hCoV-19/Finland/THL-202101018/2021, EPI_ISL_3471851, ON532063), Fin34-α (B.1.1.7, Alpha variant, hCoV-19/Finland/THL-202102301/2021, EPI_ISL_2590786, ON532062), Fin37-δ (B.1.617.2, Delta variant, hCoV-19/Finland/THL-202117309/2021, EPI_ISL_2557176, ON532078), Fin40-κ (B.1.617.1, Kappa variant, hCoV-19/Finland/THL-202109869/2021, EPI_ISL_2506747, ON532082), Fin55-BA.1 (Omicron sublineage BA.1, hCoV-19/Finland/THL-202126660/2021, EPI_ISL_8768822, ON532087), Fin58-BA.2 (Omicron sublineage BA.2, hCoV-19/Finland/THL-202203911/2022, EPI_ISL_9695067, ON532088), Fin60-XJ (Omicron sublineage XJ, hCoV-19/Finland/THL-202205928/2022, EPI_ISL_10148532, ON532089). The viruses were isolated from COVID-19 patient nasopharyngeal swab samples and the sequences had been confirmed to be the above SARS-CoV-2 variants by next generation sequencing. Virus isolation was carried out in VeroE6-TMPRSS2-H10 cells followed by a second passage in a fresh culture of the same cells to generate virus stocks. Virus stocks were collected two to five days after seeding the second passage. Fin58-BA.2 and Fin60-XJ required a third passage in VeroE6-TMPRSS2 cells for sufficient replication to generate usable viral stocks. Virus titers ($TCID_{50}$/mL) were obtained by endpoint dilution in VeroE6-TMPRSS2-H10 cells and they were as follows: Fin3 ($1x10^8$), Fin22 ($1x10^7$), Fin32-β ($1x10^8$), Fin34-α ($1x10^7$), Fin37-δ ($1x10^7$), Fin40-κ ($1x10^8$), Fin55-BA.1 ($1x10^7$), Fin58-BA.2 ($1x10^7$) and Fin60-XJ ($1x10^7$). All virus stocks were also whole genome sequenced. All work with infectious SARS-CoV-2 virus was carried out in the biosafety level 3 facility at the Finnish Institute for Health and Welfare, Finland.

Infectivity assay

A total of 1 x 10^6 Calu-3 cells were cultured in 12-well plates and after three days confluent cells were infected with SARS-CoV-2 variants. Briefly, viruses were added to the cells at MOI 1 based on the titers determined by the endpoint dilution assay. The dilution of the stock viruses for the infection were done in E-MEM media supplemented as above but without FCS. Cells were incubated with the inoculum viruses for 1h at 37°C in 5% CO_2 after which the medium containing virus was removed, the cells were washed once with PBS and supplemented with E-MEM containing 2% FCS. The 1h sample of the supernatant, cellular RNA and cell lysate for protein analysis were collected at this point. Cells were then placed in the incubator at 37°C in 5% CO_2 and subsequent samples were collected at 6, 24, 48 and 72 hours post-infection (p.i.).

Endpoint dilution assay

VeroE6-TMPRSS2-H10 cells were seeded into 96-well plates 24 hours prior to infection. Serial dilutions of the stock viruses or the supernatants collected from the infectivity assay at different time points were made and eight replicate wells were inoculated with each sample dilution. Cytopathic effect (CPE) was observed at three or six days p.i. to determine whether a well was positive or negative for viral growth and the virus titers represented as $TCID_{50}$/mL were calculated using the Spearman-Kärber method.

Sendai infection of Calu-3

Sendai virus (SV) (strain Cantell) was propagated in 11-day-old embryonated chicken eggs at 36°C for 3 days and stock virus titer was determined as infectious units/ml in human primary dendritic cells (DCs), and it was $1x10^9$ pfu/ml. A total of 1 x 10^6 Calu-3 cells were infected with SV at MOI of 5 based on the titers determined in DCs. Calu-3 cells were collected at 8 h p.i. for immunoblotting.

Isolation of RNA and RT-qPCR

Total cellular RNA and cell culture supernatant viral RNA (vRNA) were isolated using the RNeasy mini kit (Qiagen). For cellular RNA, DNase digestion (RNase-free DNase kit, Qiagen) was included, and the total RNA concentration was measured using Nanodrop.

A total of 500 ng of total cellular RNA or 5 µl of cell culture supernatant isolated vRNA was reverse transcribed (RT) to cDNA. The RT-PCR reaction mix contained 1x RT buffer (Applied Biosystems), 5.5 mM MgCl (Applied Biosystems), 2

mM of dNTP (0.5 mM each) (Applied Biosystems), 2.5 µM random hexamers (Invitrogen), 1 U/µl RNAse inhibitor (Applied Biosystems) and 1.25 U/µl RT enzyme (Thermo Fisher Scientific). A standard cDNA synthesis program was used for the reaction.

To determine relative cellular vRNA expression and mRNA expression levels of target genes, qPCR on cDNA was carried out using TaqMan Gene Expression Master Mix (Applied Biosystems) with primer and probe mixes for SARS-CoV-2 E gene (28), IFN-α1 (Hs00256882_s1), IFN-β1 (Hs01077958_s1), IFN-λ1 (Hs00601677_g1), IFN-λ2 (Hs00820125_g1), CXCL10 (Hs00171042_m1), CCL5 (Hs00174575_m1), IL-6 (Hs00174131_m1), IL-8 (Hs00174097_m1), TNF-α (Hs00174128_m1) and TGF-β (Hs99999918_m1) (all from Applied Biosystems). Target mRNA expression levels were normalized against human 18S (Ribosomal RNA Control Reagents VIC™ Probe, Applied Biosystems) and the 2-ΔΔCt method was used to calculate mRNA expression levels as a relative increase in mRNA compared to the uninfected mock samples.

For the quantification of SARS-CoV-2 vRNA in cell culture supernatant samples, 5 µl of cDNA was amplified with PCR using the TaqMan Gene Expression Master Mix (Applied Biosystems) and the above SARS-CoV-2 E gene primer and probe mix. To quantify viral RNA, the assay included a standard curve of known concentrations (10^1 - 10^7) of hCoV-Fin-E-pEBB-HA-N plasmid. The plasmid contains a GeneArt (Thermo Fisher Scientific) synthesized SARS-CoV-2 E gene, based on the hCoV-19/Finland/1/2020 sequence (GenBank MT020781), cloned into pEBB-N-HA mammalian expression vector. The Ct-value of the sample was compared to the ct-value of the known concentrations of the standard curve and the absolute quantity of SARS-CoV-2 in the PCR mix was extrapolated. From this the vRNA quantity in the initial sample was calculated.

Antibodies

In-house produced polyclonal antibodies were used for immunoblotting and they included rabbit antibodies against SARS-CoV N (cross-reactive against SARS-CoV-2 N) and SARS-CoV-2 S1 proteins (25), MxA protein (29) and IRF3 protein (30). Antibodies from Cell Signaling Technology included Phospho-IRF3 (Ser396) (4D4G) Rabbit mAb (P-IRF3; 4947), p38 MAPK Antibody (9212), Phospho-p38 MAPK (Thr180/Tyr182) Antibody (P-p38; 9211), IκB-α (44D4), Stat2 (D9J7L) Rabbit mAb (72604), Phospho-Stat2 (Tyr690) (D3P2P) Rabbit mAb (88410) and Glyceraldehyde-3-phosphate dehydrogenase (GAPDH; 2118). IFITM3 antibody was from Abgent (#AP1153a). The secondary antibody used was Horseradish peroxidase (HRP)-conjugated goat anti-rabbit antibody (Dako).

Immunoblotting

Cells were lysed in Passive Lysis Buffer (Promega) supplemented with 1 mM Na_3VO_4. Total protein concentrations were determined using the Bio-Rad protein assay. SDS-PAGE was used to separate equal amounts of protein (10 µg -20 µg) which was followed by transfer of the proteins onto Hybond-P polyvinylidene difluoride (PVDF) membranes (Amersham Biosciences). For in-house antibodies, membranes were blocked for 30 min at room temperature (RT) in blocking buffer (5% fat-free milk in PBS with 0.05% Tween-20). Primary and secondary antibodies were diluted in blocking buffer and membranes were incubated for 1h at RT. All washes were carried out for 3 x 10 min in PBS with 0.05% Tween-20. For commercial antibodies blocking and staining were performed according to manufacturer's instructions. Protein bands were visualised using Pierce™ ECL Western Blotting Substrate (Thermo Fisher) and BIOMAX XAR films (CareStream). Quantification of immunoblots was carried out using ImageJ software (31).

Sequencing

Sequencing was carried out with Illumina Novaseq 6000 and the data was collated using the HAVoC pipeline (32). The pangolin tool (33) was used to assign the SARS-CoV-2 lineages. Sequence alignments were done with Clustal Omega (34) and sequence analyses were done with BioEdit 7.0.5.3 (35).

Phylogenetic analysis

For phylogenetic analysis, reference sequences for the variants in this study were obtained from GISAID (https://www.gisaid.org). The reference sequences and sequences of variants in this study were aligned using Clustal Omega (36). A phylogenetic tree was constructed using Molecular Evolutionary Genetics Analysis software (MEGA (37), Version 10.0.5). The best fit model was first determined and the phylogenetic tree was constructed using the Maximum Likelihood method and Tamura-Nei model (38).

Statistics

GraphPad Prism 9.0 (GraphPad Software, San Diego, CA, USA.) was used for statistical analyses. One-way ANOVA with Tukey's multiple comparisons test was used.

10.3389/fimmu.2022.1016108

Results

Description of the mutations in pre-Omicron SARS-CoV-2 variants used in this study

All the SARS-CoV-2 variants in this study were isolated from patient samples. The original sample and the virus stocks were whole genome sequenced to confirm the identity of the variants and compare the mutations to the original Wuhan SARS-CoV-2 reference genome (Figure 1). Fin3 (Pangolin lineage B.1.1.29) is an early pandemic variant from March 2020 with only five mutations. The P323L and D614G mutations in Nsp12 (RdRp) and S protein, respectively, are present in the other variants as well. In addition to these, the Fin3 N protein contains R203K and G204R mutations, which are also seen in Alpha variants such as in Fin34-α. Fin22 (B.1.258) is from November 2020 and has accumulated a total of 12 mutations. Fin22 is the only variant in this study that does not harbor mutations in the N protein gene. Fin34-α (B.1.1.7) and Fin32-β (B.1.351) were the first VOCs and these viruses were isolated from patient samples collected in January 2021. Fin32-β has 23 mutations while Fin34-α contains a total of 25 mutations. Both have nine amino acid substitutions in the S protein. In the RBD, both Fin32-β and Fin34-α contain the N501Y mutation, while Fin32-β has an additional E484K mutation. Fin34-α harbors a P681H mutation in the MBCS. In the N protein, there is a T205I mutation in Fin32-β at a similar position to the R203K-G204R seen in Fin3 and Fin34-α. The N protein of Fin34-α also contains two additional mutations, D3L and S235F. Fin37-δ (B.1.617.2) and Fin40-κ (B.1.617.1) were isolated from patient samples collected in May 2021 and March 2021, respectively. Although the two strains are genetically close to each other, Fin40-κ has only 21 mutations, while Fin37-δ has 30. Both viruses contain eight mutations in the S protein of which some are the same. Both variants contain a L452R mutation in the RBD and a P681R mutation in the MBCS. There is also a R682W mutation in Fin40-κ, which can occur following viral passage in Vero-E6 cells. In the N protein, the first mutation in Fin37-δ is G215C and both Fin37-δ and Fin40-κ variants contain R203M and D377Y substitutions. Phylogenetic analysis showed Fin22 to cluster near the original Wuhan sequence, while Fin3 clustered nearer the Alpha variant (Supplementary Figure 1). The VOCs clustered with their reference counterparts as expected.

SARS-CoV-2 variants show different replication profiles in human lung epithelial Calu-3 cells

Calu-3 cells were infected with different variants at MOI 1 and cellular vRNA levels were determined by RT-qPCR for up to 72 hours (Figure 2). Overall, Fin3 and Fin34-α replication patterns were similar as cellular vRNA levels increased with a slow kinetics and maximal vRNA levels were reached within 48 h p.i. Fin22, Fin32-β and Fin37-δ, showed faster replication kinetics and submaximal/maximal vRNA levels were seen already at 24 h p.i., after which Fin32-β and Fin37-δ replication reached a plateau while Fin22 cellular vRNA levels

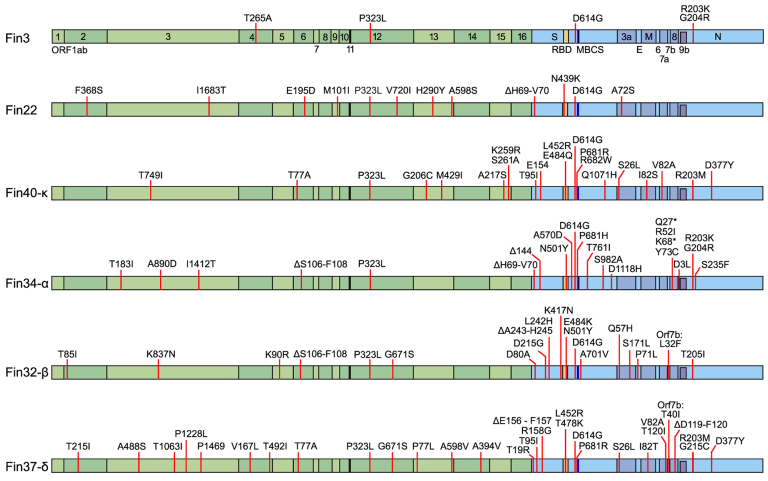

FIGURE 1
Mutations in the six pre-Omicron SARS-CoV-2 variants used to infect Calu-3 cells. The mutations are mapped against the hCoV-19/Wuhan/WIV04/2019 reference genome (EPI_ISL_402124). In green are the non-structural proteins located in Orf1ab and in blue are the structural proteins S, E, M, N, and accessory proteins. Receptor-binding domain (RBD, S protein amino acid residues 437-507, orange), multi-basic cleavage site (MBCS, S protein amino acid residues 681-685, (P-R-R-A-R), dark blue) are also marked.

10.3389/fimmu.2022.1016108

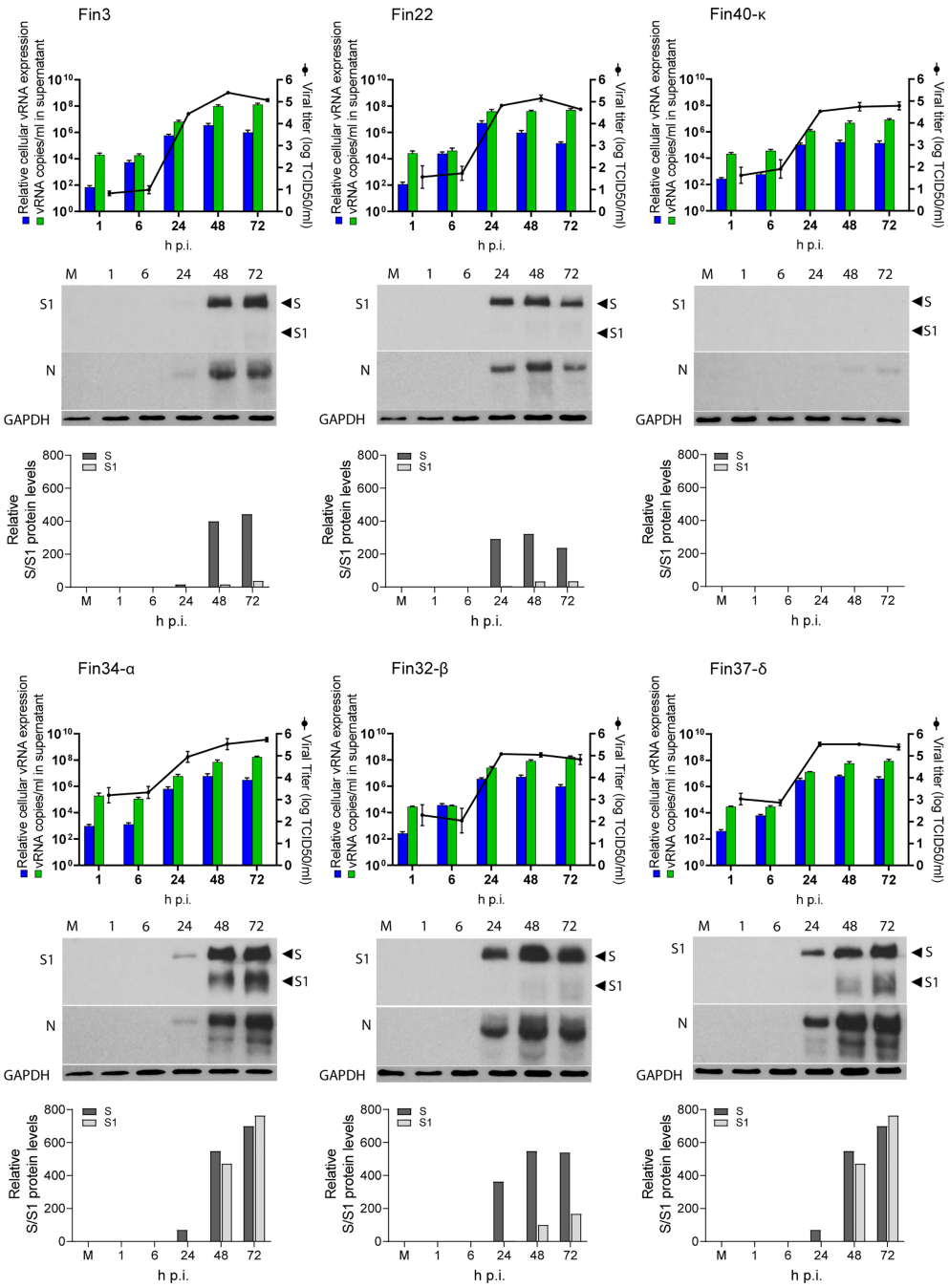

FIGURE 2
Replication of six SARS-CoV-2 variants in Calu-3 cells. Cells were infected with each variant at a MOI of 1 $TCID_{50}$/cell. Cell culture supernatant and total cellular RNA and protein samples were collected at 1, 6, 24, 48 and 72 hours post-infection (h p.i.). The figure shows the replication profiles for each variant. The relative cellular vRNA expression levels and the quantified vRNA copies/ml in cell culture supernatant (as determined by RT-qPCR) is shown in the graphs on the left Y-axis. The production of infectious virions (as determined by an end point dilution assay and shown as log $TCID_{50}$/ml) is shown on the right Y-axis. The results are the mean values ± SEM of three independent experiments. Cellular protein samples were analyzed by immunoblotting with anti-SARS-CoV-2 S1 (S1) specific and cross-reactive anti-SARS-CoV N protein (N) specific antibodies to show the replication kinetics of the viruses at a protein level. Immunoblotting was carried out once for S protein and three times for N protein. Representative immunoblots are shown. The anti-SARS-CoV-2 S1 antibody recognizes both the full-length S protein (S) and the cleaved S1 fragment. GAPDH was used as a loading control. The blots were exposed with an equal exposure time. S protein amounts quantified using ImageJ are shown below the immunoblots.

decreased. Fin40-κ replication was consistently an order of a magnitude lower compared to the other variants.

Viral RNA copies in the cell culture supernatant were also quantified (Figure 2). Cell culture supernatant vRNA patterns generally followed those of cellular vRNA levels. Importantly, the supernatant vRNA quantities were almost identical at 1h indicating roughly equal amounts of input stock viruses. For Fin34-α, the mean of three independent experiments was slightly higher than for the rest of the variants, nevertheless, the difference was not statistically significant when analyzed with the one-way ANOVA with Tukey's multiple comparisons test, which confirmed the input virus amounts were correctly normalized.

The endpoint dilution assay was done in VeroE6-TMPRSS2-H10 cells to assess the amount of infectious virus produced from Calu-3 cells at different time points after infection (Figure 2). The patterns of infectious virus release mainly correlated with the cellular and supernatant vRNA levels, and they were relatively similar in all variants. Although Fin34-α infected cells measured lower levels of cellular and supernatant vRNA at 24 h p.i., the viral titers were comparable to those of Fin22, Fin32-β and Fin37-δ. Mirroring the vRNA levels, the infectivity of Fin40-κ remained at a lower level.

An additional observation was made while carrying out endpoint dilution assays. CPE was easily identified at three days post infection for all variants except Fin37-δ, which consistently replicated with a slower kinetics in VeroE6-TMPRSS2-H10 cells. Fin37-δ required a longer incubation (six days) for reliable determination of its infectivity titer. The amount of CPE of the other variants did not significantly change after three days of incubation. Due to this the $TCID_{50}$/mL results for the infection assay supernatant samples were read at six days p.i. for all variants.

Western blot analyses (Figure 2) showed S and N protein expression in all variants apart from Fin40-κ, which agrees with the lower virus amounts in cells infected with this variant. The relatively slower replication kinetic of Fin3 and Fin34-α variants was also seen at protein level as lower expression of S and N proteins was detected at 24 h p.i. Likewise, Fin22, Fin32-β and Fin37-δ viral protein expression was clearly visible already at 24 h p.i although quantification of the S protein immunoblot showed a lower level of Fin37-δ S protein at this time point (Figure 2). Interestingly, S protein cleavage was very efficient for both Fin34-α and Fin37-δ compared to the other variants (Figure 2).

SARS-CoV-2 variants elicit a low level of IRF3, p38 and NF-κB pathway activation but induce strong STAT2 activation

Activation of various innate immune signaling pathways was assessed by immunoblotting. A very low level of IRF3 phosphorylation was elicited by Fin22 and Fin32-β at 48 h p.i. and by Fin34-α and Fin37-δ at 48 and 72 h p.i. (Figure 3A). Phosphorylated IRF3 was hardly detectable in Fin3 infected cells, while no p-IRF3 was seen in Fin40-κ infected cells. The phosphorylation of p38 was also weak and mainly seen at 48 h p.i. in cells infected by the VOCs Fin34-α, Fin32-β and Fin37-δ (Figure 3B). A decrease in the level of NF-κB inhibitor IκB-α was observed in Fin34-α, Fin32-β, Fin37-δ infected cells at 48 h p.i. and in the Fin40-κ infection already at 24 h p.i. A decrease in IκB-α was also seen in cells infected with Fin3 and Fin22 at 72 h p.i. (Figure 3B). Overall, these results show relatively weak activation of signaling pathways involved in interferon and cytokine gene expression.

On the other hand, a robust activation of the interferon stimulated STAT2 pathway was seen (Figure 3B). High levels of p-STAT2 were observed in Fin22, Fin32-β, Fin37-δ infected cells at 24 h p.i. after which the levels decreased. Cells infected with Fin3 and Fin34-α showed a slower phosphorylation kinetics with a peak in p-STAT2 level at 48 h p.i. Only weak STAT2 activation was detected for Fin40-κ. The phosphorylation of STAT2 seemed to occur simultaneously with virus replication (Figure 2) as the highest p-STAT2 levels were seen when the cellular vRNA levels reached high levels.

The expression of interferons and cytokine genes correlates with peak cellular viral RNA levels

The expression of interferon and cytokine genes was assessed at mRNA expression level with RT-qPCR. IFN-β1, IFN-λ1, IFN-λ2 and CXCL10 mRNA expression was detected (Figure 4A; Supplementary Figure 2 and Supplementary Table 1), while no increased expression of IFN-α, TNF-α, IL-6, IL-8, TFG-β and CCL5 mRNAs was observed (data not shown).

The expression levels of IFN-β1, IFN-λ1, IFN-λ2 and CXCL10 mRNAs were dependent on cellular vRNA levels although some differences in the cytokine mRNA expression patterns were seen in cells infected by different variants (Figure 4A). In Fin22 infected cells, IFN and CXCL10 mRNA expression levels peaked with cellular vRNA levels at 24 h p.i. In contrast, in Fin3, Fin34-α, Fin32-β and Fin37-δ infected cells IFN and CXCL10 mRNA levels did not peak until 48 h p.i. when cellular vRNA levels had reached a plateau. A weaker and slower IFN and CXCL10 mRNA expression pattern was seen in Fin40-κ infected cells, which was consistent with the lower viral replication levels.

The variation in viral replication levels at 24 h p.i. was not significant (Figure 4B), however, the level of IFN-β1 expression was significantly higher in cells infected with Fin22 compared to the other variants. IFN-λ1 mRNA levels were also significantly higher for Fin22 infected cells compared to those of Fin3, Fin34-α, Fin32-β and Fin40-κ infected cells. Although IFN-λ2 and CXCL10 mRNA expression patterns were similar, the differences were not statistically significant.

10.3389/fimmu.2022.1016108

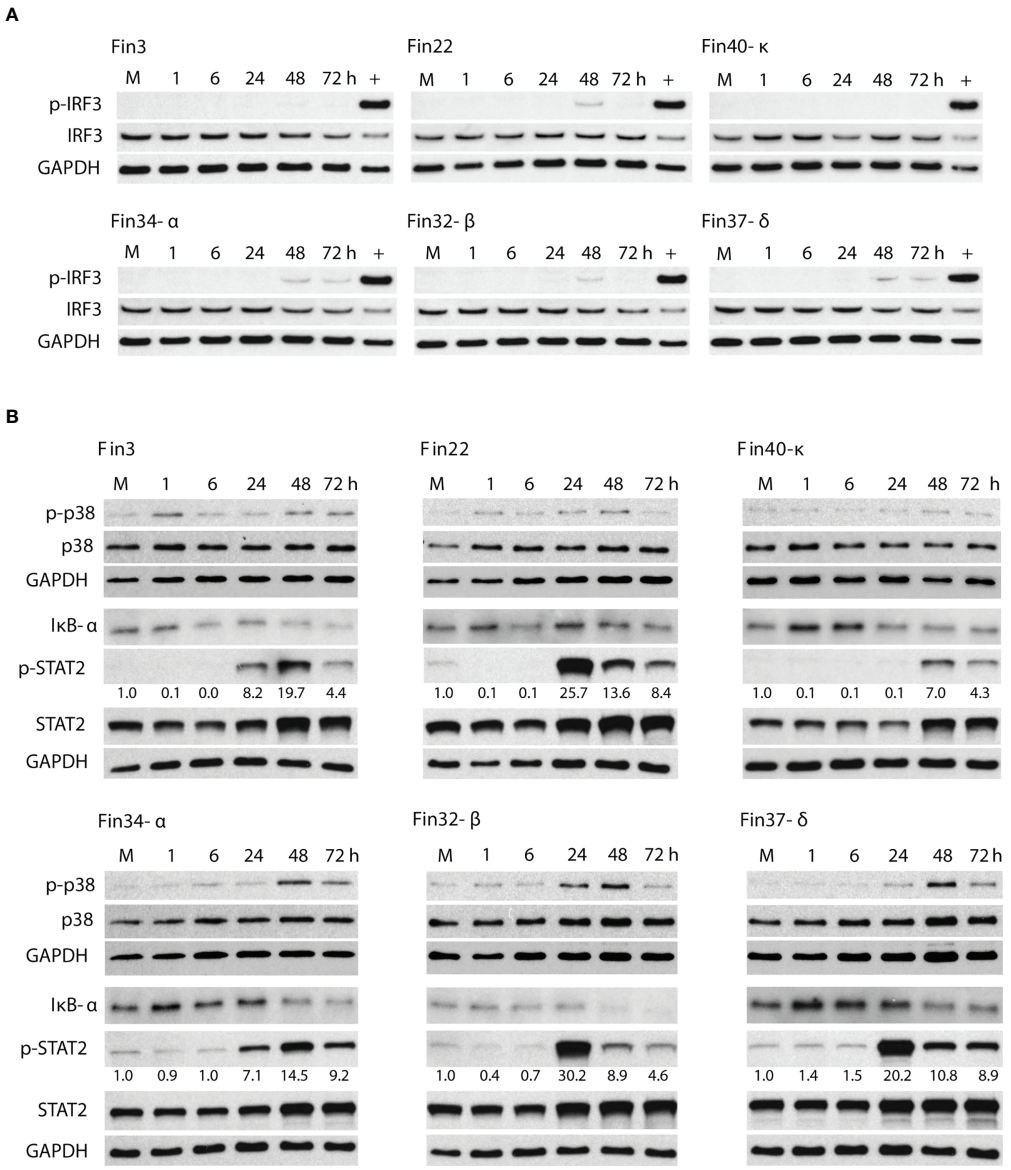

FIGURE 3
Activation of signaling molecules involved in the induction of interferon, cytokine and ISG gene expression. Total cellular protein samples were collected at various time points following infection of Calu-3 cells with different SARS-CoV-2 variants at a MOI of 1 $TCID_{50}$/cell. Representative immunoblots out of 3 repeated experiments are shown. **(A)** Immunoblots were probed with antibodies against phosphorylated interferon regulatory transcription factor 3 (p-IRF3) and total IRF3. Cellular protein samples collected at 8 h after Sendai virus infection in Calu-3 cells was used as a positive control (+). GAPDH was used as a loading control for p-IRF3. The immunoblot was carried out twice. **(B)** Immunoblots stained with antibodies against phosphorylated p38 (p-p38) and p38 (carried out once), nuclear factor of kappa light polypeptide gene enhancer in B-cells inhibitor alpha (IκB-α) and phosphorylated signal transducer (carried out twice) and activator of transcription 2 (p-STAT2) and STAT2 (carried out twice). p-STAT2 levels were quantified by ImageJ and the fold over mock values are seen below the p-STAT2 immunoblot. GAPDH was used as a loading control.

Induction of ISGs by SARS-CoV-2 infection is sensitive to IFNs

Secreted type I and type III IFNs induce the expression of ISGs such as IFITM3 and MxA proteins that mediate the antiviral actions against multiple viruses. The expression of IFITM3 and MxA proteins during SARS-CoV-2 infection in Calu-3 cells was analyzed by immunoblotting. All variants stimulated almost similar amounts of IFITM3 and MxA production in infected Calu-3 cells (Figure 5). A weak increase in ISGs was seen already at 24 h p.i. but the highest levels were observed at 48 and 72 h p.i. ISG expression levels were relatively

10.3389/fimmu.2022.1016108

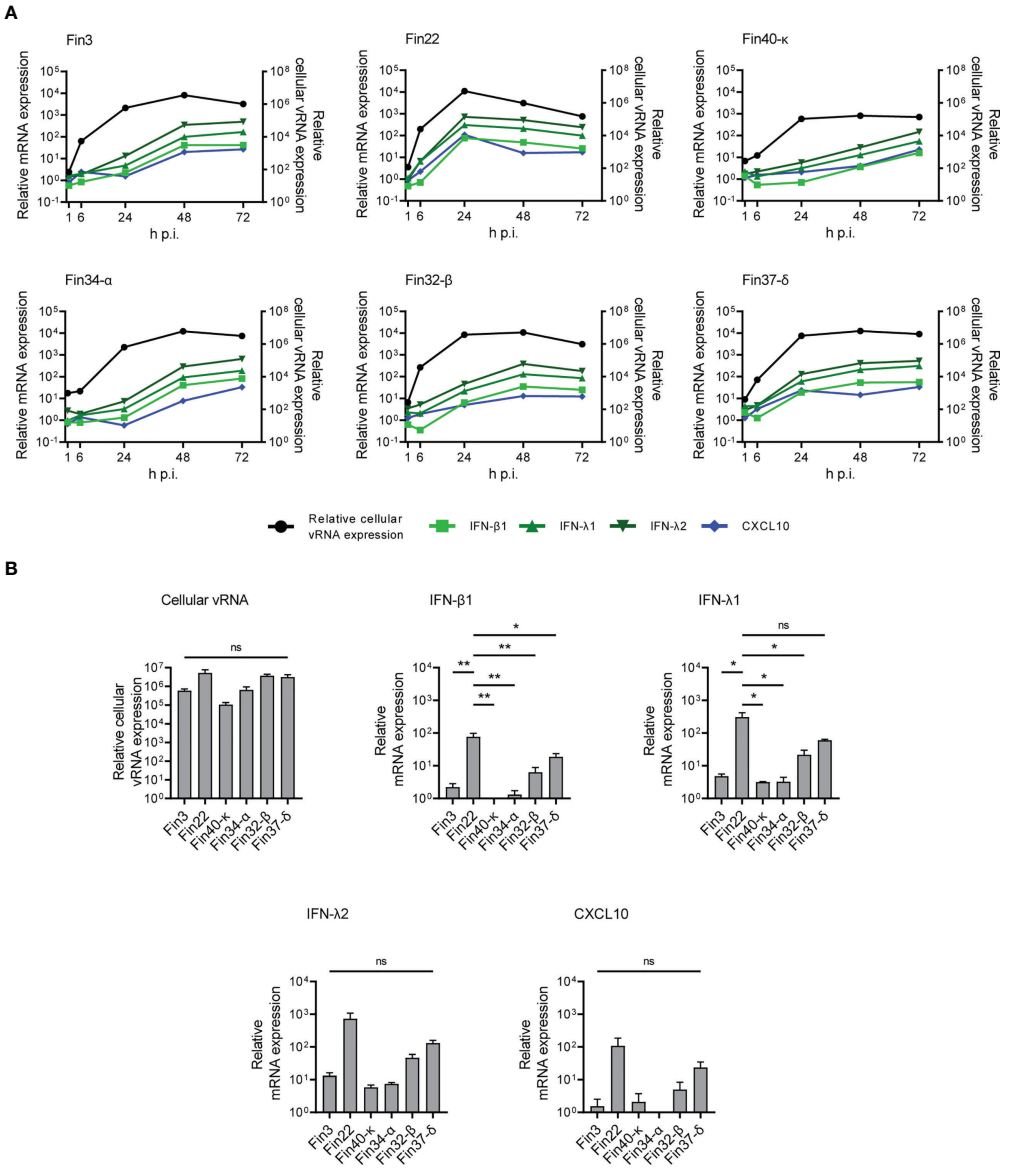

FIGURE 4
Interferon and CXCL10 mRNA expression levels in Calu-3 cells infected with SARS-CoV-2 variants. Cells were infected with each variant at a MOI of 1 $TCID_{50}$/cell and total cellular RNA samples were collected at different time points during infection. **(A)** The kinetics of vRNA and host cell IFN-β1, IFN-λ1, IFN-λ2 and CXCL10 mRNA expression profiles were determined by RT-qPCR. Relative cytokine mRNA expression profiles in different SARS-CoV-2 variant infected cells are shown on the left Y axes and the vRNA expression levels on the right Y axes. The means of three independent experiments are shown. **(B)** Comparative analysis of relative cellular vRNA and IFN-β1, IFN-λ1, IFN-λ2 and CXCL10 mRNA expression at 24 h p.i. The results are the mean values ± SEM of three independent experiments. One-way ANOVA with Tukey's multiple comparisons test was used for the statistics. $P < 0.05$ (*), $P < 0.01$ (**), not significant (ns).

similar regardless of the levels of cellular vRNAs, different kinetics and strength in the activation of cellular signaling pathways and interferon mRNA expression levels. In Fin40-κ infected cells almost similar amounts of IFITM3 and MxA protein expression was seen compared to the other variant infected cells even though the replication, interferon mRNA expression and STAT2 phosphorylation by Fin40-κ occurred at a lower level. On the other hand, Fin22, Fin32-β and Fin37-δ, which induced high levels of p-STAT2 activation, did not induce much higher levels of ISGs than Fin40-κ. Thus, the induction of IFITM3 and MxA is highly sensitive to even small amounts of IFNs produced.

10.3389/fimmu.2022.1016108

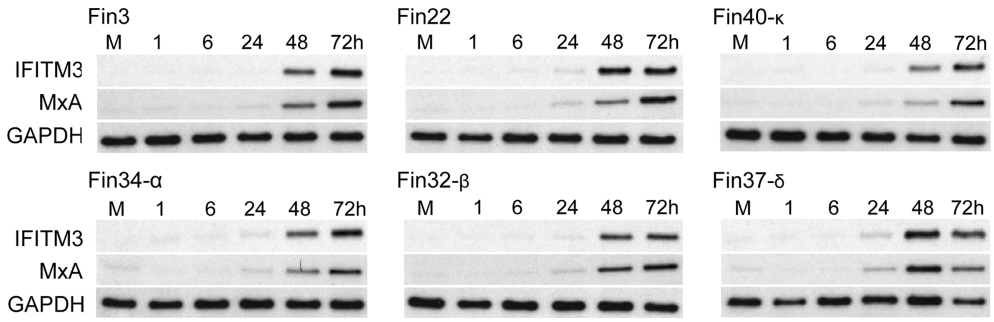

FIGURE 5
Kinetics of expression of antiviral ISGs in Calu-3 cells infected with different SARS-CoV-2 variants. Six different virus variants were used at MOI of 1 $TCID_{50}$/cell to infect Calu-3 cells and during the 3-day infection cellular protein samples were collected. Representative immunoblots were probed with antibodies against interferon induced transmembrane protein 3 (IFITM3) (carried out once) and human Myxovirus resistance protein A (MxA) (carried out twice). GAPDH was used as a loading control.

Omicron sublineage BA.2 does not replicate as well as BA.1 or the recombinant sublineage XJ in Calu-3 cells

Replication and interferon induction of three Omicron sublineages Fin55-BA.1, Fin58-BA.2 and recombinant Fin60-XJ was also studied. Fin55-BA.1 was isolated from a patient sample collected in December 2021 and whole genome sequencing confirmed all 62 defining mutations of the BA.1 sublineage (Figure 6). Fin58-BA.2 and Fin60-XJ patient samples were from January 2022. Fin58-BA.2 contained the 62 defining mutations in addition to a H78Y mutation in ORF3a, which has been seen in some BA.2 sublineages (39). Fin58-BA.2 also contained the R682W mutation in the S protein. Fin60-XJ is a recombinant sublineage in which the 5' end is from BA.1 and a cut off between nucleotides 13,296 and 15,240 in Nsp10 and Nsp12, respectively, switches the genome to BA.2 (40). Fin60-XJ did not have the R682W mutation seen in Fin58-BA.2. All the three Omicron sublineages harbored the P681H mutation in the S protein MBCS and the R203K/G204R mutations in N protein, which are seen in the Alpha variant as well. A phylogenetic analysis showed that Fin55-BA.1 and Fin58-BA.2 clustered with their reference counterparts and Fin60-XJ clustered between these two (Supplementary Figure 1).

Calu-3 cells were infected with Fin55-BA.1, Fin58-BA.2, Fin60-XJ, Fin34-α and Fin37-δ at a MOI of 1 and replication was observed for 72 hours. The intracellular vRNA levels of the Omicron sublineages, as determined by RT-qPCR, were lower than those for the Alpha and Delta variants (Figure 7A). Fin55-BA.1, Fin58-BA.2 and Fin60-XJ replication was similar up to 24 h p.i. after which Fin58-BA.2 reached a plateau. Interestingly, the recombinant variant Fin60-XJ had a replication profile more like Fin55-BA.1 as it replicated better than Fin58-BA.2 at later time points. The vRNA copies/ml in the cell culture supernatant (Figure 7B), however, were lower only for Fin58-BA.2. Consistent with this, an end point dilution assay carried out in VeroE6-TMPRSS2-H10 cells showed that Fin58-BA.2 also produced less infectious virus (Figure 7C).

S and N protein expression, as determined by immunoblotting, correlated with replication levels as less protein was detected with the Omicron sublineages (Figure 7D). Quantification of the S protein immunoblots (Figure 7D) showed that as with Fin34-α and Fin37-δ, efficient cleavage of Fin55-BA.1 and Fin60-XJ S protein was observed especially at 72 h p.i. S protein levels of Fin58-BA.2 were too low to detect the cleavage state.

Omicron sublineages show a similar slow interferon induction type as other VOCs

The mRNA expression levels of interferons and CXCL10 were determined with RT-qPCR. In concordance with lower vRNA expression, the mRNA expression levels of IFN-β1, IFN-λ1, IFN-λ2 and CXCL10 were lower for cells infected with Fin58-BA.2 than cells infected with Fin55-BA.1, Fin60-XJ, Fin34-α and Fin37-δ (Figure 8A; Supplementary Figure 3 and Supplementary Table 2). The greatest difference in interferon expression levels was observed at 24 h p.i., as IFN-β1, IFN-λ1, IFN-λ2 and CXCL10 mRNA expression levels were significantly lower in cells infected with Omicron subvariants and Fin34-α compared to Fin37-δ infected cells (Figure 8B). However, cellular vRNA levels were also significantly lower for these variants compared to Fin37-δ.

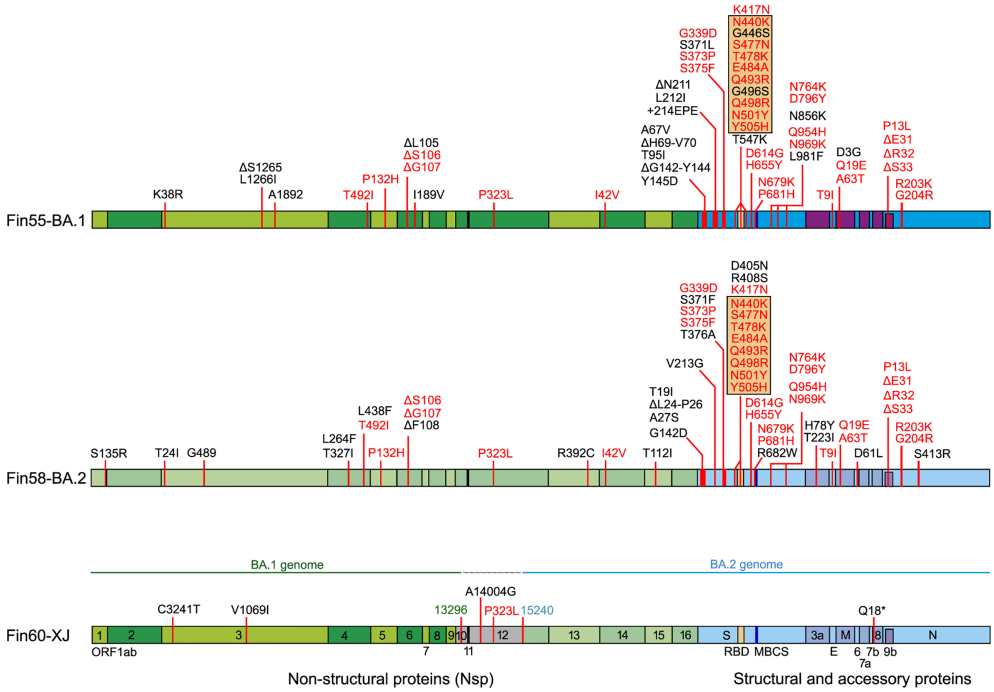

FIGURE 6
Mutations in three Omicron sublineages, Fin55-BA.1, Fin58-BA.2 and recombinant Fin60-XJ. The hCoV-19/Wuhan/WIV04/2019 reference genome (EPI_ISL_402124) was used to map the mutations. In black are unique mutations and in red are mutations that are found in all the above Omicron sublineages. Mutations in the orange box are found in the RBD. Fin60-XJ is a recombinant of BA.1 and BA.2 with a cut off between nucleotides 13 296 (green) in Nsp10 and 15 240 (blue) in Nsp12. Receptor-binding domain (RBD, S protein amino acid residues 437-507, orange), multi-basic cleavage site (MBCS, S protein amino acid residues 681-685, (P-R-R-A-R), dark blue).

Discussion

The aim of this study was to compare SARS-CoV-2 variants isolated from different epidemic peaks of the pandemic, to see whether there are differences in the replication and innate immune responses in genetically distinct SARS-CoV-2 viruses and whether we could relate the potential differences to some specific mutations in the genome. SARS-CoV-2 has been reported to mutate at a rate of 4 x 10^{-4} - 2 x 10^{-2} mutations per nucleotide per year (41). The majority of these mutations are neutral or even deleterious, nonetheless, some mutations do arise that increase viral fitness and immune evasion (42). Genotype to phenotype studies of viruses may provide us understanding of which changes in the genome are important for viral transmissibility and virulence. SARS-CoV-2 offers a unique opportunity to study this, since already 10 million SARS-CoV-2 genome sequences have been uploaded to the Global Initiative on Sharing All Influenza Data (GISAID) website (43) as of spring 2022.

Here we compared the ability of nine genetically different SARS-CoV-2 variants to replicate and induce innate immunity in a human lung epithelial cell model. Overall, the pre-Omicron variants replicated in a comparable fashion, however, Fin34-α replication took place at somewhat slower kinetics than Fin32-β and Fin37-δ, and the Kappa variant, Fin40-κ, replicated at ten-fold lower levels compared to the other variants. A slower replication pattern of the Alpha variant compared to Delta in Calu-3 cells was also shown by Mlcochova and co-workers (44). Elsewhere, the replication of Alpha, Beta and early pandemic variants in Calu-3 have shown almost identical growth characteristics (24, 45, 46). The Omicron BA.1 variant has been shown to replicate less efficiently in lower respiratory tract cells, including Calu-3 (46–49). We also observed that replication levels of BA.1 and a recombinant variant XJ in Calu-3 were an order of magnitude lower compared to Alpha and Delta, while replication of a BA.2 variant was two log lower at later time points. Hence, we can conclude that compared to Omicron, the earlier VOCs show only some minor variation in their replication kinetics in Calu-3 cells.

Studies on the effects of single mutations on viral replication have often been conducted computationally or with recombinant proteins, pseudoviruses and WT viruses with genetically engineered mutations. At the start of the pandemic, epidemiologic observations, studies on pseudoviruses and genetically engineered SARS-CoV-2 mutants with single mutations showed that the S protein D614G and RdRp P323L

10.3389/fimmu.2022.1016108

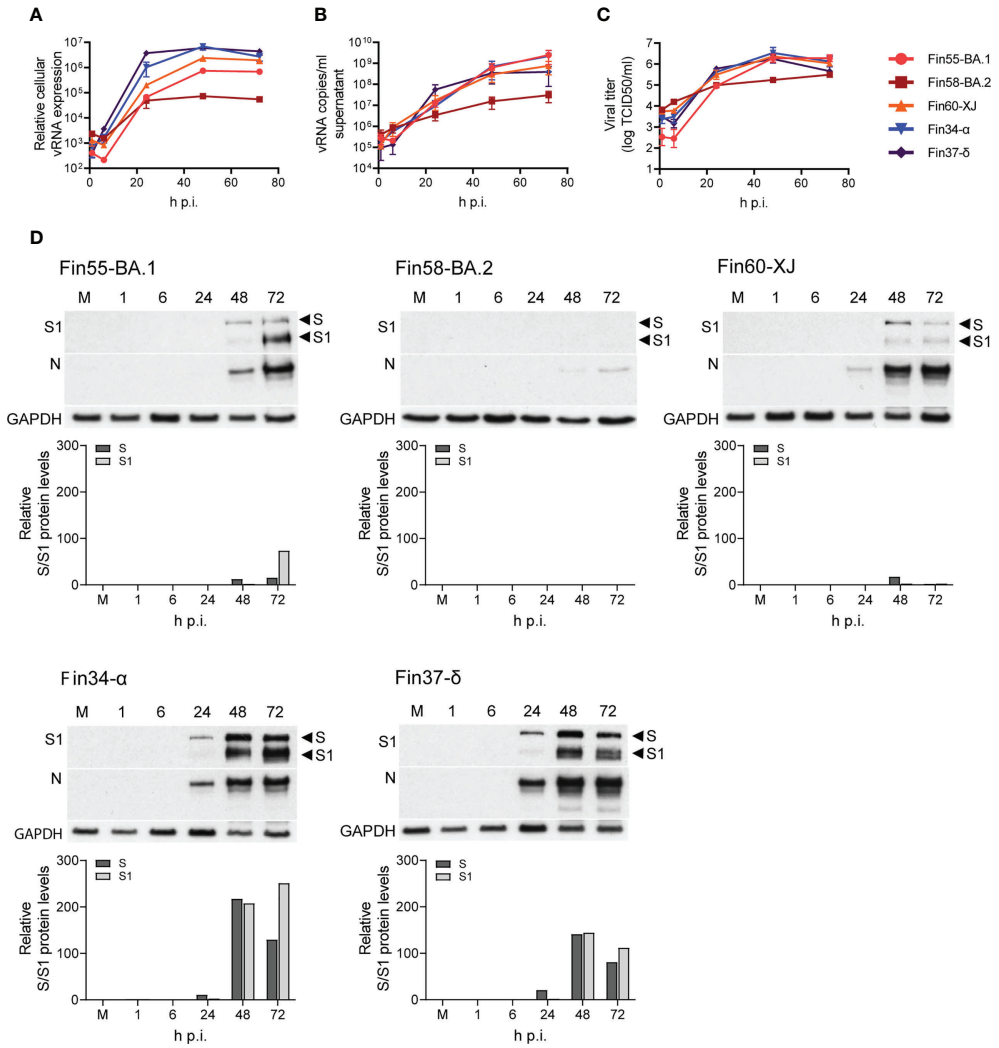

FIGURE 7
Replication of Omicron sublineages BA.1, BA.2 and XJ compared to Alpha and Delta. Calu-3 cells were challenged with three Omicron sublineages and Alpha and Delta variants at multiplicity of 1 for three days and different samples were collected for analysis of the viral molecules. **(A)** Relative cellular vRNA expression levels determined by RT-qPCR of Fin55-BA.1, Fin58-BA.2 and Fin60-XJ compared to Alpha (Fin34-α) and Delta (Fin37-δ). **(B)** Cell culture supernatant vRNA copies/ml were quantified by RT-qPCR. **(C)** An end point dilution assay was carried out to determine the production of infectious virions. Results shown as log $TCID_{50}$/ml. **(D)** Immunoblot analysis of SARS-CoV-2 S protein expression by anti-SARS-CoV-2 S1 fragment antibody (S1) and N protein expression using a cross-reactive anti-SARS-CoV-N protein antibody (N) were carried out once. Full length S protein (S) and the cleaved S1 fragment (S1) are marked with arrows. S protein amounts quantified using ImageJ are shown in graphs below the immunoblots. GAPDH was used as a loading control. The qPCR and end point dilution assay results are the mean values ± SEM of three independent experiments.

mutations rendered the original Wuhan SARS-CoV-2 variant more transmissible (2–5). These results are clearer as the genetic background did not yet contain various other mutations. As the virus evolved, subsequent mutations have been studied in the same way. For example, in the S protein the N501Y mutation in Alpha and Beta variants and E484K in Beta were shown computationally to increase the affinity of the RBD to ACE2 (50–52). Viral transmission and replication was shown to be enhanced in a genetically engineered N501Y mutant with a WT SARS-CoV-2 background (53). In our study with authentic viruses, however, we did not observe a great difference in replication of Fin34-α and Fin32-β, which contain these RBD mutations, compared to Fin3, Fin22 and Fin37-δ, which lack them. In the MBCS, the P681R mutation in Delta and Kappa and the P681H mutation in the Alpha variant have been shown to increase S protein cleavage (54–56) and cell entry compared to the WT virus (44). These studies were done using fluorogenic peptides (54, 56), pseudoviruses (44, 54, 56), and recombinantly generated mutant viruses (55). However, the enhanced cleavage of Alpha, Delta and Kappa S protein did not lead to increased

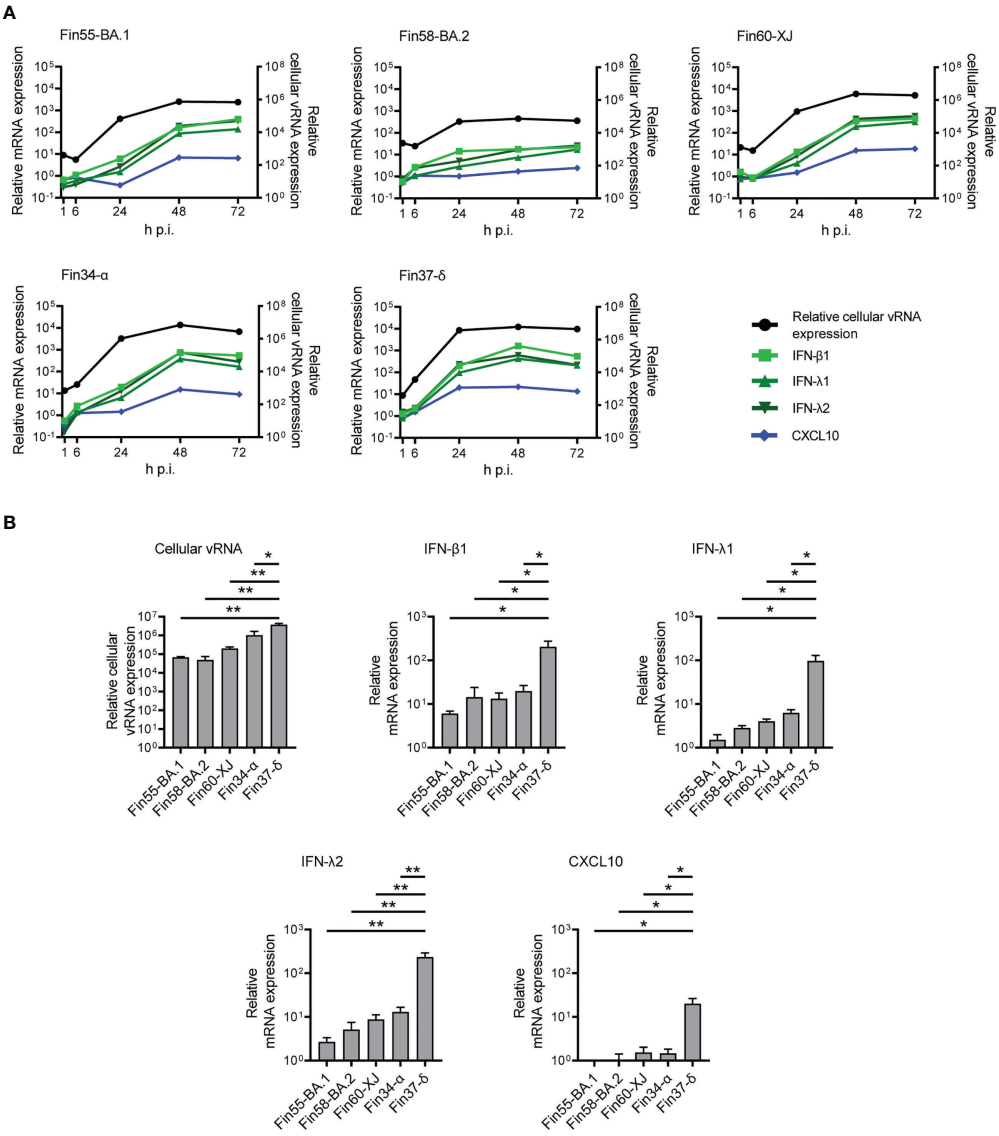

FIGURE 8
Interferon and CXCL10 mRNA expression levels in Calu-3 cells with Omicron infection. The Omicron sublineages BA.1, BA.2 and recombinant XJ as well as the Alpha and Delta variants were used for infecting Calu-3 cells at a MOI of 1 $TCID_{50}$/cell, and total RNA samples were collected at different time points for RT-qPCR analysis. **(A)** IFN-β1, IFN-λ1, IFN-λ2 and CXCL10 mRNA expression profiles determined by RT-qPCR (left Y axis) compared to the relative cellular vRNA expression profile (right Y axis) for cells infected with three Omicron variants (Fin55-BA.1, Fin58-BA.2 and Fin60-XJ), and with Alpha (Fin34-α) and Delta (Fin37-δ). The means of three independent experiments are shown. **(B)** Comparison of relative cellular vRNA and IFN-β1, IFN-λ1, IFN-λ2 and CXCL10 mRNA expression at 24 h p.i. The results are the mean values ± SEM of three independent experiments. One-way ANOVA with Tukey's multiple comparisons test was used for the statistics. $P < 0.05$ (*), $P < 0.01$ (**).

replication of natural viral isolates in Calu-3 cells (55, 56). In concordance with this, we observed similar levels of cleaved S protein in Fin34-α and Fin37-δ which were higher than that seen for Fin32-β and the early pandemic variants, but this did not affect the replication of the viruses in Calu-3 cells. Omicron also has the P681H mutation, and we could clearly see the cleavage of BA.1 and XJ sublineage S proteins in our study. Some studies have shown reduced cleavage of BA.1 S protein, thus hypothesizing that the Omicron S protein is less efficiently cleaved, which could cause the potential shift in the cell entry mechanism (46, 48, 57). However, the reduced cleavage was shown with S protein from pseudovirus (PV) studies (57) and live virus infection of VeroE6-TMPRSS2 cells (46, 48) but not with S protein from live virus infection of Calu-3 cells (47). The effects of the ever-increasing number of S protein mutations are complex and studies to pinpoint roles of certain mutations is challenging

as is evident, for example, with the Delta and Kappa variants. Both have many of the same beneficial mutations but the reason for the weaker replication of Fin40-κ or the decreased fitness of the Kappa variant epidemiologically is unclear as studies on the role of different mutations have remained elusive (7, 58, 59). Likewise, while the effects of S protein mutations in Omicron BA.1 and BA.2 on evasion of adaptive immunity are clear (60, 61), their role in the changed replication efficiency in the lower respiratory tract cells is still uncertain. Research on the BA.1 variant have suggested that the poorer replication could be due to the mutations resulting in less efficient use of TMPRSS2 (47, 48, 57). Whether this causes a shift in Omicron to use the endocytic pathway of entry (46, 48, 49, 57), or the S protein MBCS is merely cleaved by a serine protease other than TMPRSS2 and still uses the cell membrane fusion pathway (47) is still to be confirmed. Here we showed that especially the replication of the BA.2 sublineage was hampered compared to BA.1 and the recombinant XJ. The S protein of XJ is the same as in BA.2, hence mutations in BA.2 S protein might not be the cause of the lower replication efficiency of the sublineage.

The significance of mutations outside the S protein are also being increasingly studied. The N protein is an abundant structural protein (62) that has a crucial role in ribonucleocapsid formation and attachment to the viral membrane (20) and it is critical for vRNA replication and transcription (63, 64). The N protein also undergoes liquid-liquid phase separation (LLPS), which facilitates the compartmentalization of viral protein-protein or vRNA-protein interactions (65). Regulation of these functions is *via* phosphorylation of a serine and arginine rich (SR) motif (aa 175-206) in the central intrinsically disordered region (IDR) of the N protein (aa 175-246) (65–69). Within the SR motif is a R185-G204 site that has been shown to mutate more frequently than expected (11). The Delta and Kappa variants harbor a R203M mutation at this site, which was shown to increase virus replication in lung cells (70). In addition, the Alpha variant double mutation R203K/G204R, has been shown to enhance the replication and infectivity of SARS-CoV-2 *in vitro* and *in vivo* (71, 72). Increased phosphorylation of N protein in Alpha (R203K/G204R), Kappa (R203M) and Beta (contains a T205I mutation) variants was suggested to contribute to the replication efficiency of these variants in LLPS compartments (65, 72). The R203K/G204R mutant N protein also showed increased binding to vRNA, and there was differential expression of immune related genes in cells expressing the mutant N protein (73). These studies, however, have again been carried out using genetically modified WT SARS-CoV-2 viruses, pseudoviruses and recombinant proteins. In our study with natural viruses, the effects of the N protein mutations on replication were not clear as the variants' replication patterns did not seem to correlate with the presence of mutations in the protein. The Omicron sublineages, for example, also contain the R203K/G204R mutation and their replication is not enhanced.

In our cell model we observed a weak activation of IRF3, p38 and NF-κB by the pre-Omicron variants. This activation was, however, sufficient to induce interferon gene expression, JAK/STAT activation, and the production of ISGs. The levels of type I and type III interferons and phosphorylation of STAT2 correlated well with cellular vRNA levels but all the variants produced similar levels of ISGs, even the Fin40-κ variant, which showed a weaker ability to replicate compared to other variants. Previously we shown that Fin-25 (D614G/P323L variant) induced better interferon gene expression and MxA protein expression levels compared to a WT Fin-1 variant (25). However, Fin-1 replicated very poorly in Calu-3 cells, so there could be a minimum threshold required for the activation of ISG production. At RNA level, the Alpha variant has been shown to induce lower levels of ISG mRNA expression compared to WT SARS-CoV-2 (24). In a luciferase reporter assay, the N protein was shown to decrease Sendai virus-induced phosphorylation and nuclear translocation of STAT1/STAT2 dimers and thus inhibit the expression of ISGs (74). We, however, did not see an inhibition of STAT2 phosphorylation by any of the studied variants and IFN-induced MxA protein expression was also clearly detectable. This does not formally rule out that N or some other SARS-CoV-2 protein could at least to some extent inhibit the nuclear translocation of STAT1/STAT2 complexes downregulating ISG mRNA expression. This possibility has to be further considered and analyzed by using expression constructs for individual viral genes. Initial analyses have revealed that certain NSPs and accessory proteins may interfere with IFN signaling (75).

There have been reports of delayed immune activation in SARS-CoV-2 infected cells whereby the interferon and cytokine response seems to peak after the most productive replication stage of the virus (24, 76, 77). In our study we observed a similar type of pattern for cells infected with all the variants, including the Omicrons. The only exception was Fin22, in which cellular vRNA and interferon mRNA levels peaked earlier at 24h p.i. Among other SARS-CoV-2 proteins, the N protein has been shown to inhibit interferon gene expression (78), potentially by interacting with RIG-I (79). Mutations in the SARS-CoV-2 genome may have an effect on innate immune responses. For example, the expression of Orf9b, an alternate reading frame nested in the N protein gene sequence, was increased in the Alpha variant-infected cells possibly due to a D3L mutation and may be involved in delaying IFN gene expression by inhibiting TOMM70 interaction with MAVS (24). In accordance with these observations, we also observed weak activation of IRF3 phosphorylation in the pre-Omicron variant-infected cells. Also, a R203K/G204R mutation of SARS-CoV-2 N protein leads to expression of sgRNA N* in Alpha variant-infected cells but the role of N* in virus replication and regulating immune responses is yet to be elucidated (24, 80). It was of interest that Fin22, which lacks the R203K/G204R mutations in N protein, showed a faster kinetics of IFN gene expression compared to the other variants, especially Fin34-α and Omicrons which all harbor the

R203K/G204R mutation. However, regardless of the ability of the Fin22 variant to induce IFN gene expression faster and more efficiently, STAT2 phosphorylation and ISG expression occurred equally well in Fin22, Fin32-β and Fin37-δ virus-infected cells. Thus, the significance of potential variation in different variant-induced interferon response is presently unclear.

In conclusion, this comparative study showed that, in human lung epithelial Calu-3 cells, replication of the pre-Omicron VOCs and two early pandemic SARS-CoV-2 variants was similar while that of Kappa and three different Omicron sublineages was less efficient. Several studies analyzing the effects of the SARS-CoV-2 mutations have been done with pseudoviruses and artificial mutants created in a WT SARS-CoV-2 background. While these studies may provide interesting insights on the role of individual mutations, they do not provide a whole picture of the pathogenic characteristics of different variants. Thus, systematic analyses of virus-host cell interactions of different variant-infected cells are well justified. Our results with nine natural virus variants show that the mutations in SARS-CoV-2 variants have complex effects in combination. Highly beneficial mutations likely compensate for unfavorable ones and further research is required to decipher their roles. We also revealed that the activation of innate antiviral immunity occurs relatively late in the infection by all variants except Fin22, which was able to induce the interferon response faster. Fin22 is a variant without mutations in the N protein, which has many roles in replication and host immune responses, thus it could be an interesting research avenue to follow.

Data availability statement

The datasets presented in this study can be found in online repositories. The names of the repository/repositories and accession number(s) can be found below:

https://www.ncbi.nlm.nih.gov/genbank/, ON531991
https://www.ncbi.nlm.nih.gov/genbank/, ON532015
https://www.ncbi.nlm.nih.gov/genbank/, ON532063
https://www.ncbi.nlm.nih.gov/genbank/, ON532062
https://www.ncbi.nlm.nih.gov/genbank/, ON532078
https://www.ncbi.nlm.nih.gov/genbank/, ON532082
https://www.ncbi.nlm.nih.gov/genbank/, ON532087
https://www.ncbi.nlm.nih.gov/genbank/, ON532088
https://www.ncbi.nlm.nih.gov/genbank/, ON532089

Author contributions

LL contributed to the methodology, analysis, investigation, data curation, visualization, writing – original draft, writing – review & editing. MS contributed to the methodology, investigation, writing – review & editing. EV contributed to the methodology. IJ contributed to the conceptualization, investigation, resources, funding acquisition, writing – review & editing. PÖ contributed to the conceptualization, methodology, investigation, resources, supervision, funding acquisition, writing – original draft, writing – review & editing. All authors contributed to the article and approved the submitted version.

Funding

This research was funded by Academy of Finland, grant number 339511 CrossBar project (PÖ) and the Jane and Aatos Erkko Foundation (IJ). This study was supported by THL coordinated funding for Covid-19 research included in the Finnish Government's supplementary budget. The funders had no role in the conceptualization, investigation and analysis of the study or decision to publish the work.

Acknowledgments

We thank Tiina Sihvonen, Johanna Rintamäki, Hanna Valtonen, Miao Jiang, Soile Blomqvist, Erika Lindh, Kirsi Liitsola, Katri Keino, Mikko Määttä, Irmeli Iranto and Emilia Salejärvi. We gratefully acknowledge the authors and their respective laboratories, who analyzed and submitted the sequences to GISAID's EpiCoV and GenBank Database.

Conflict of interest

The authors declare that the research was conducted in the absence of any commercial or financial relationships that could be construed as a potential conflict of interest.

Publisher's note

Supplementary material

The Supplementary Material for this article can be found online at: https://www.frontiersin.org/articles/10.3389/fimmu.2022.1016108/full#supplementary-material

References

1. World Health Organization. *WHO coronavirus (COVID-19) dashboard*. Available at: https://covid19.who.int (Accessed August 8, 2022).

2. Ilmjärv S, Abdul F, Acosta-Gutiérrez S, Estarellas C, Galdadas I, Casimir M, et al. Concurrent mutations in RNA-dependent RNA polymerase and spike protein emerged as the epidemiologically most successful SARS-CoV-2 variant. *Sci Rep* (2021) 11:13705. doi: 10.1038/s41598-021-91662-w

3. Korber B, Fischer WM, Gnanakaran S, Yoon H, Theiler J, Abfalterer W, et al. Tracking changes in SARS-CoV-2 spike: Evidence that D614G increases infectivity of the COVID-19 virus. *Cell* (2020) 182:812–827.e19. doi: 10.1016/j.cell.2020.06.043

4. Yurkovetskiy L, Wang X, Pascal KE, Tomkins-Tinch C, Nyalile TP, Wang Y, et al. Structural and functional analysis of the D614G SARS-CoV-2 spike protein variant. *Cell* (2020) 183:739–751.e8. doi: 10.1016/j.cell.2020.09.032

5. Zhou B, Thao TTN, Hoffmann D, Taddeo A, Ebert N, Labroussaa F, et al. SARS-CoV-2 spike D614G change enhances replication and transmission. *Nature* (2021) 592:122–7. doi: 10.1038/s41586-021-03361-1

6. Thakur V, Bhola S, Thakur P, Patel SKS, Kulshrestha S, Ratho RK, et al. Waves and variants of SARS-CoV-2: Understanding the causes and effect of the COVID-19 catastrophe. *Infection* (2022) 50(2):309–25. doi: 10.1007/s15010-021-01734-2

7. Saville JW, Mannar D, Zhu X, Srivastava SS, Berezuk AM, Demers J-P, et al. Structural and biochemical rationale for enhanced spike protein fitness in delta and kappa SARS-CoV-2 variants. *Nat Commun* (2022) 13:742. doi: 10.1038/s41467-022-28324-6

8. WHO. *Statement on omicron sublineage BA.2* (2022). Available at: https://www.who.int/news/item/22-02-2022-statement-on-omicron-sublineage-ba.2 (Accessed February 28, 2022).

9. Lu R, Zhao X, Li J, Niu P, Yang B, Wu H, et al. Genomic characterisation and epidemiology of 2019 novel coronavirus: Implications for virus origins and receptor binding. *Lancet* (2020) 395:565–74. doi: 10.1016/S0140-6736(20)30251-8

10. Malone B, Urakova N, Snijder EJ, Campbell EA. Structures and functions of coronavirus replication–transcription complexes and their relevance for SARS-CoV-2 drug design. *Nat Rev Mol Cell Biol* (2022) 23:21–39. doi: 10.1038/s41580-021-00432-z

11. Jungreis I, Sealfon R, Kellis M. SARS-CoV-2 gene content and COVID-19 mutation impact by comparing 44 sarbecovirus genomes. *Nat Commun* (2021) 12:2642. doi: 10.1038/s41467-021-22905-7

12. Hartenian E, Nandakumar D, Lari A, Ly M, Tucker JM, Glaunsinger BA. The molecular virology of coronaviruses. *J Biol Chem* (2020) 295:12910–34. doi: 10.1074/jbc.REV120.013930

13. Hoffmann M, Kleine-Weber H, Schroeder S, Krüger N, Herrler T, Erichsen S, et al. SARS-CoV-2 cell entry depends on ACE2 and TMPRSS2 and is blocked by a clinically proven protease inhibitor. *Cell* (2020) 181:271–280.e8. doi: 10.1016/j.cell.2020.02.052

14. Hoffmann M, Kleine-Weber H, Pöhlmann S. A multibasic cleavage site in the spike protein of SARS-CoV-2 is essential for infection of human lung cells. *Mol Cell* (2020) 78:779–784.e5. doi: 10.1016/j.molcel.2020.04.022

15. Bestle D, Heindl MR, Limburg H, Van TVL, Pilgram O, Moulton H, et al. TMPRSS2 and furin are both essential for proteolytic activation of SARS-CoV-2 in human airway cells. *Life Sci Alliance* (2020) 3:e202000786. doi: 10.26508/lsa.202000786

16. Zhao M-M, Yang W-L, Yang F-Y, Zhang L, Huang W-J, Hou W, et al. Cathepsin l plays a key role in SARS-CoV-2 infection in humans and humanized mice and is a promising target for new drug development. *Signal Transduct Target Ther* (2021) 6:1–12. doi: 10.1038/s41392-021-00558-8

17. Rahbar Saadat Y, Hosseiniyan Khatibi SM, Zununi Vahed S, Ardalan M. Host serine proteases: A potential targeted therapy for COVID-19 and influenza (2021) (Accessed August 29, 2022).

18. Cortese M, Lee J-Y, Cerikan B, Neufeldt CJ, Oorschot VMJ, Köhrer S, et al. Integrative imaging reveals SARS-CoV-2-Induced reshaping of subcellular morphologies. *Cell Host Microbe* (2020) 28:853–866.e5. doi: 10.1016/j.chom.2020.11.003

19. V'kovski P, Kratzel A, Steiner S, Stalder H, Thiel V. Coronavirus biology and replication: implications for SARS-CoV-2. *Nat Rev Microbiol* (2021) 19:155–70. doi: 10.1038/s41579-020-00468-6

20. Dinesh DC, Chalupska D, Silhan J, Koutna E, Nencka R, Veverka V, et al. Structural basis of RNA recognition by the SARS-CoV-2 nucleocapsid phosphoprotein. *PloS Pathog* (2020) 16:e1009100. doi: 10.1371/journal.ppat.1009100

21. Whitsett JA, Alenghat T. Respiratory epithelial cells orchestrate pulmonary innate immunity. *Nat Immunol* (2015) 16:27–35. doi: 10.1038/ni.3045

22. Diamond MS, Kanneganti T-D. Innate immunity: The first line of defense against SARS-CoV-2. *Nat Immunol* (2022) 23:165–76. doi: 10.1038/s41590-021-01091-0

23. Park A, Iwasaki A. Type I and type III interferons – induction, signaling, evasion, and application to combat COVID-19. *Cell Host Microbe* (2020) 27:870–8. doi: 10.1016/j.chom.2020.05.008

24. Thorne LG, Bouhaddou M, Reuschl A-K, Zuliani-Alvarez L, Polacco B, Pelin A, et al. Evolution of enhanced innate immune evasion by SARS-CoV-2. *Nature* (2022) 602:487–95. doi: 10.1038/s41586-021-04352-y

25. Jiang M, Kolehmainen P, Kakkola L, Maljanen S, Melén K, Smura T, et al. SARS-CoV-2 isolates show impaired replication in human immune cells but differential ability to replicate and induce innate immunity in lung epithelial cells. *Microbiol Spectr* (2021) 9:e00774-21. doi: 10.1128/Spectrum.00774-21

26. Schroeder S, Pott F, Niemeyer D, Veith T, Richter A, Muth D, et al. Interferon antagonism by SARS-CoV-2: A functional study using reverse genetics. *Lancet Microbe* (2021) 2:e210–8. doi: 10.1016/S2666-5247(21)00027-6

27. Rusanen J, Kareinen L, Szirovicza L, Uğurlu H, Levanov L, Jääskeläinen A, et al. A generic, scalable, and rapid time-resolved förster resonance energy transfer-based assay for antigen detection–SARS-CoV-2 as a proof of concept. *mBio* (2021) 12:e00902–21. doi: 10.1128/mBio.00902-21

28. Corman VM, Landt O, Kaiser M, Molenkamp R, Meijer A, Chu DK, et al. Detection of 2019 novel coronavirus (2019-nCoV) by real-time RT-PCR. *Eurosurveillance* (2020) 25:2000045. doi: 10.2807/1560-7917.ES.2020.25.3.2000045

29. Ronni T, Melén K, Malygin A, Julkunen I. Control of IFN-inducible MxA gene expression in human cells. *J Immunol* (1993) 150:1715–26.

30. Österlund P, Veckman V, Sirén J, Klucher KM, Hiscott J, Matikainen S, et al. Gene expression and antiviral activity of Alpha/Beta interferons and interleukin-29 in virus-infected human myeloid dendritic cells. *J Virol* (2005) 79:9608–17. doi: 10.1128/JVI.79.15.9608-9617.2005

31. Schneider CA, Rasband WS, Eliceiri KW. NIH Image to ImageJ: 25 years of image analysis. *Nat Methods* (2012) 9:671–5. doi: 10.1038/nmeth.2089

32. Truong Nguyen PT, Plyusnin I, Sironen T, Vapalahti O, Kant R, Smura T. HAVoC, a bioinformatic pipeline for reference-based consensus assembly and lineage assignment for SARS-CoV-2 sequences. *BMC Bioinf* (2021) 22:373. doi: 10.1186/s12859-021-04294-2

33. O'Toole Á, Scher E, Underwood A, Jackson B, Hill V, McCrone JT, et al. Assignment of epidemiological lineages in an emerging pandemic using the pangolin tool. *Virus Evol* (2021) 7:veab064. doi: 10.1093/ve/veab064

34. Madeira F, Park YM, Lee J, Buso N, Gur T, Madhusoodanan N, et al. The EMBL-EBI search and sequence analysis tools APIs in 2019. *Nucleic Acids Res* (2019) 47:W636–41. doi: 10.1093/nar/gkz268

35. Hall TA. BioEdit: A user-friendly biological sequence alignment Editor and analysis program for windows 95/98/NT. *Nucleic Acids Symp Ser* (1999), 41:95–8.

36. Madeira F, Pearce M, Tivey ARN, Basutkar P, Lee J, Edbali O, et al. Search and sequence analysis tools services from EMBL-EBI in 2022. *Nucleic Acids Res* (2022) 47:gkac240. doi: 10.1093/nar/gkac240

37. Kumar S, Stecher G, Li M, Knyaz C, Tamura K. MEGA X: Molecular evolutionary genetics analysis across computing platforms. *Mol Biol Evol* (2018) 35:1547–9. doi: 10.1093/molbev/msy096

38. Tamura K, Nei M. Estimation of the number of nucleotide substitutions in the control region of mitochondrial DNA in humans and chimpanzees. *Mol Biol Evol* (1993) 10:512–26. doi: 10.1093/oxfordjournals.molbev.a040023

39. Desingu PA, Nagarajan K. Omicron BA.2 lineage spreads in clusters and is concentrated in Denmark. *J Med Virol* (2022) 94(6):2360–4. doi: 10.1002/jmv.27659

40. Lindh E, Smura T, Blomqvist S, Liitsola K, Vauhkonen H, Savolainen L, et al. Genomic and epidemiological report of the recombinant XJ lineage SARS-CoV-2 variant, detected in northern Finland, January 2022. *Eurosurveillance* (2022) 27:2200257. doi: 10.2807/1560-7917.ES.2022.27.16.2200257

41. Tao K, Tzou PL, Nouhin J, Gupta RK, de Oliveira T, Kosakovsky Pond SL, et al. The biological and clinical significance of emerging SARS-CoV-2 variants. *Nat Rev Genet* (2021) 22:757–73. doi: 10.1038/s41576-021-00408-x

42. Harvey WT, Carabelli AM, Jackson B, Gupta RK, Thomson EC, Harrison EM, et al. SARS-CoV-2 variants, spike mutations and immune escape. *Nat Rev Microbiol* (2021) 19:409–24. doi: 10.1038/s41579-021-00573-0

43. GISAID. *GISAID - initiative* (2022). Available at: https://www.gisaid.org/ (Accessed May 18, 2022).

44. Mlcochova P, Kemp SA, Dhar MS, Papa G, Meng B, Ferreira IATM, et al. SARS-CoV-2 B.1.617.2 delta variant replication and immune evasion. *Nature* (2021) 599:114–9. doi: 10.1038/s41586-021-03944-y

45. Rajah MM, Hubert M, Bishop E, Saunders N, Robinot R, Grzelak L, et al. SARS-CoV-2 alpha, beta, and delta variants display enhanced spike-mediated syncytia formation. *EMBO J* (2021) 40:e108944. doi: 10.15252/embj.2021108944

46. Shuai H, Chan JF-W, Hu B, Chai Y, Yuen TT-T, Yin F, et al. Attenuated replication and pathogenicity of SARS-CoV-2 B.1.1.529 omicron. *Nature* (2022) 603:693–9. doi: 10.1038/s41586-022-04442-5

47. Lamers MM, Mykytyn AZ, Breugem TI, Groen N, Knoops K, Schipper D, et al. SARS-CoV-2 omicron efficiently infects human airway, but not alveolar epithelium. *bioRxiv* (2022). doi: 10.1101/2022.01.19.476898

48. Meng B, Abdullahi A, Ferreira IATM, Goonawardane N, Saito A, Kimura I, et al. Altered TMPRSS2 usage by SARS-CoV-2 omicron impacts tropism and fusogenicity. *Nature* (2022) 603:706–4. doi: 10.1038/s41586-022-04474-x

49. Willett BJ, Grove J, MacLean OA, Wilkie C, De Lorenzo G, Furnon W, et al. SARS-CoV-2 Omicron is an immune escape variant with an altered cell entry pathway. *Nat Microbiol* (2022) 7:1161–1179. doi: 10.1038/s41564-022-01143-7

50. Luan B, Wang H, Huynh T. Enhanced binding of the N501Y-mutated SARS-CoV-2 spike protein to the human ACE2 receptor: Insights from molecular dynamics simulations. *FEBS Lett* (2021) 595:1454–61. doi: 10.1002/1873-3468.14076

51. Han Y, Wang Z, Wei Z, Schapiro I, Li J. Binding affinity and mechanisms of SARS-CoV-2 variants. *Comput Struct Biotechnol J* (2021) 19:4184–91. doi: 10.1016/j.csbj.2021.07.026

52. Wang WB, Liang Y, Jin YQ, Zhang J, Su JG, Li QM. E484K mutation in SARS-CoV-2 RBD enhances binding affinity with hACE2 but reduces interactions with neutralizing antibodies and nanobodies: Binding free energy calculation studies. *J Mol Graph Model* (2021) 109:108035. doi: 10.1016/j.jmgm.2021.108035

53. Liu Y, Liu J, Plante KS, Plante JA, Xie X, Zhang X, et al. The N501Y spike substitution enhances SARS-CoV-2 infection and transmission. *Nature* (2022) 602:294–9. doi: 10.1038/s41586-021-04245-0

54. Peacock TP, Sheppard CM, Brown JC, Goonawardane N, Zhou J, Whiteley M, et al. The SARS-CoV-2 variants associated with infections in India, B.1.617, show enhanced spike cleavage by furin. *bioRxiv* (2021). doi: 10.1101/2021.05.28.446163

55. Saito A, Irie T, Suzuki R, Maemura T, Nasser H, Uriu K, et al. Enhanced fusogenicity and pathogenicity of SARS-CoV-2 delta P681R mutation. *Nature* (2022) 602:300–6. doi: 10.1038/s41586-021-04266-9

56. Lubinski B, Fernandes MHV, Frazier L, Tang T, Daniel S, Diel DG, et al. Functional evaluation of the P681H mutation on the proteolytic activation of the SARS-CoV-2 variant B.1.1.7 (Alpha) spike. *iScience* (2022) 25:103589. doi: 10.1016/j.isci.2021.103589

57. Du X, Tang H, Gao L, Wu Z, Meng F, Yan R, et al. Omicron adopts a different strategy from delta and other variants to adapt to host. *Signal Transduct Target Ther* (2022) 7:1–3. doi: 10.1038/s41392-022-00903-5

58. McCallum M, Walls AC, Sprouse KR, Bowen JE, Rosen LE, Dang HV, et al. Molecular basis of immune evasion by the delta and kappa SARS-CoV-2 variants. *Science* (2021) 374:1621–6. doi: 10.1126/science.abl8506

59. Motozono C, Toyoda M, Zahradnik J, Saito A, Nasser H, Tan TS, et al. SARS-CoV-2 spike L452R variant evades cellular immunity and increases infectivity. *Cell Host Microbe* (2021) 29:1124–1136.e11. doi: 10.1016/j.chom.2021.06.006

60. Cao Y, Wang J, Jian F, Xiao T, Song W, Yisimayi A, et al. Omicron escapes the majority of existing SARS-CoV-2 neutralizing antibodies. *Nature* (2022) 602:657–63. doi: 10.1038/s41586-021-04385-3

61. Liu L, Iketani S, Guo Y, Chan JF-W, Wang M, Liu L, et al. Striking antibody evasion manifested by the omicron variant of SARS-CoV-2. *Nature* (2022) 602:676–81. doi: 10.1038/s41586-021-04388-0

62. Kim D, Lee J-Y, Yang J-S, Kim JW, Kim VN, Chang H. The architecture of SARS-CoV-2 transcriptome. *Cell* (2020) 181:914–921.e10. doi: 10.1016/j.cell.2020.04.011

63. Cong Y, Ulasli M, Schepers H, Mauthe M, V'kovski P, Kriegenburg F, et al. Nucleocapsid protein recruitment to replication-transcription complexes plays a crucial role in coronaviral life cycle. *J Virol* (2020) 94:e01925–19. doi: 10.1128/JVI.01925-19

64. Verheije MH, Hagemeijer MC, Ulasli M, Reggiori F, Rottier PJM, Masters PS, et al. The coronavirus nucleocapsid protein is dynamically associated with the replication-transcription complexes. *J Virol* (2010) 84:11575–9. doi: 10.1128/JVI.00569-10

65. Carlson CR, Asfaha JB, Ghent CM, Howard CJ, Hartooni N, Safari M, et al. Phosphoregulation of phase separation by the SARS-CoV-2 n protein suggests a biophysical basis for its dual functions. *Mol Cell* (2020) 80:1092–1103.e4. doi: 10.1016/j.molcel.2020.11.025

66. Bouhaddou M, Memon D, Meyer B, White KM, Rezelj VV, Correa Marrero M, et al. The global phosphorylation landscape of SARS-CoV-2 infection. *Cell* (2020) 182:685–712.e19. doi: 10.1016/j.cell.2020.06.034

67. Lu S, Ye Q, Singh D, Cao Y, Diedrich JK, Yates JR, et al. The SARS-CoV-2 nucleocapsid phosphoprotein forms mutually exclusive condensates with RNA and the membrane-associated m protein. *Nat Commun* (2021) 12:502. doi: 10.1038/s41467-020-20768-y

68. Peng Y, Du N, Lei Y, Dorje S, Qi J, Luo T, et al. Structures of the SARS-CoV-2 nucleocapsid and their perspectives for drug design. *EMBO J* (2020) 39:e105938. doi: 10.15252/embj.2020105938

69. Surjit M, Kumar R, Mishra RN, Reddy MK, Chow VTK, Lal SK. The severe acute respiratory syndrome coronavirus nucleocapsid protein is phosphorylated and localizes in the cytoplasm by 14-3-3-Mediated translocation. *J Virol* (2005) 79:11476–86. doi: 10.1128/JVI.79.17.11476-11486.2005

70. Syed AM, Taha TY, Tabata T, Chen IP, Ciling A, Khalid MM, et al. Rapid assessment of SARS-CoV-2–evolved variants using virus-like particles. *Science* (2021) 374:1626–32. doi: 10.1126/science.abl6184

71. Wu H, Xing N, Meng K, Fu B, Xue W, Dong P, et al. Nucleocapsid mutations R203K/G204R increase the infectivity, fitness, and virulence of SARS-CoV-2. *Cell Host Microbe* (2021) 29:1788–1801.e6. doi: 10.1016/j.chom.2021.11.005

72. Johnson BA, Zhou Y, Lokugamage KG, Vu MN, Bopp N, Crocquet-Valdes PA, et al. Nucleocapsid mutations in SARS-CoV-2 augment replication and pathogenesis. *PloS Pathog* (2022) 18:e1010627. doi: 10.1371/journal.ppat.1010627

73. Mourier T, Shuaib M, Hala S, Mfarrej S, Alofi F, Naeem R, et al. SARS-CoV-2 genomes from Saudi Arabia implicate nucleocapsid mutations in host response and increased viral load. *Nat Commun* (2022) 13:601. doi: 10.1038/s41467-022-28287-8

74. Mu J, Fang Y, Yang Q, Shu T, Wang A, Huang M, et al. SARS-CoV-2 n protein antagonizes type I interferon signaling by suppressing phosphorylation and nuclear translocation of STAT1 and STAT2. *Cell Discovery* (2020) 6:1–4. doi: 10.1038/s41421-020-00208-3

75. Lin J, Tang C, Wei H, Du B, Chen C, Wang M, et al. Genomic monitoring of SARS-CoV-2 uncovers an Nsp1 deletion variant that modulates type I interferon response. *Cell Host Microbe* (2021) 29:489–502.e8. doi: 10.1016/j.chom.2021.01.015

76. Hatton CF, Botting RA, Dueñas ME, Haq IJ, Verdon B, Thompson BJ, et al. Delayed induction of type I and III interferons mediates nasal epithelial cell permissiveness to SARS-CoV-2. *Nat Commun* (2021) 12:7092. doi: 10.1038/s41467-021-27318-0

77. Thorne LG, Reuschl A-K, Zuliani-Alvarez L, Whelan MVX, Turner J, Noursadeghi M, et al. SARS-CoV-2 sensing by RIG-I and MDA5 links epithelial infection to macrophage inflammation. *EMBO J* (2021) 40:e107826. doi: 10.15252/embj.2021107826

78. Li J-Y, Liao C-H, Wang Q, Tan Y-J, Luo R, Qiu Y, et al. The ORF6, ORF8 and nucleocapsid proteins of SARS-CoV-2 inhibit type I interferon signaling pathway. *Virus Res* (2020) 286:198074. doi: 10.1016/j.virusres.2020.198074

79. Chen K, Xiao F, Hu D, Ge W, Tian M, Wang W, et al. SARS-CoV-2 nucleocapsid protein interacts with RIG-I and represses RIG-mediated IFN-β production. *Viruses* (2021) 13:47. doi: 10.3390/v13010047

80. Parker MD, Stewart H, Shehata OM, Lindsey BB, Shah DR, Hsu S, et al. Altered subgenomic RNA abundance provides unique insight into SARS-CoV-2 B.1.1.7/Alpha variant infections. *Commun Biol* (2022) 5:1–10. doi: 10.1038/s42003-022-03565-9

frontiers | Frontiers in Immunology

TYPE Original Research
PUBLISHED 07 October 2022
DOI 10.3389/fimmu.2022.992819

OPEN ACCESS

EDITED BY
Attila Szabo,
University of Oslo, Norway

REVIEWED BY
Wenjing Li,
Army Medical University, China
Deng-Ho Yang,
Taichung Armed Forces General Hospital, Taiwan

*CORRESPONDENCE
Chi-Ching Chang
ccchang@tmu.edu.tw

†These authors have contributed equally to this work

SPECIALTY SECTION
This article was submitted to Autoimmune and Autoinflammatory Disorders: Autoinflammatory Disorders, a section of the journal Frontiers in Immunology

RECEIVED 13 July 2022
ACCEPTED 20 September 2022
PUBLISHED 07 October 2022

CITATION
Chou S-M, Yeh H-J, Lin T-M, Chang Y-S, Hsu H-C, Shen Y-C, Kuo T-T, Chen J-H, Chen S-C and Chang C-C (2022) Association of interferon-based therapy with risk of autoimmune diseases in patients with chronic hepatitis C virus infection: A population-based Taiwanese cohort study. *Front. Immunol.* 13:992819. doi: 10.3389/fimmu.2022.992819

Association of interferon-based therapy with risk of autoimmune diseases in patients with chronic hepatitis C virus infection: A population-based Taiwanese cohort study

Shu-Ming Chou[1†], Hsing-Jung Yeh[2,3†], Tzu-Min Lin[4,5], Yu-Sheng Chang[4,6], Hui-Ching Hsu[4,7], Yu-Chuan Shen[7], Tzu-Tung Kuo[8], Jin-Hua Chen[8,9†], Shu-Chuan Chen[10] and Chi-Ching Chang[4,5*]

[1]Department of Internal Medicine, Taipei Medical University Hospital, Taipei, Taiwan, [2]Division of Gastroenterology and Hepatology, Department of Internal Medicine, Taipei Medical University Hospital, Taipei, Taiwan, [3]Division of Gastroenterology and Hepatology, Department of Internal Medicine, School of Medicine, College of Medicine, Taipei Medical University, Taipei, Taiwan, [4]Division of allergy, immunology and Rheumatology, Department of Internal Medicine, School of Medicine, College of Medicine, Taipei Medical University, Taipei, Taiwan, [5]Division of Allergy, Immunology and Rheumatology, Department of Internal Medicine, Taipei Medical University Hospital, Taipei, Taiwan, [6]Division of Allergy, Immunology, and Rheumatology, Department of Internal Medicine, Shuang Ho Hospital, Taipei Medical University, New Taipei City, Taiwan, [7]Division of Allergy, Immunology and Rheumatology, Department of Internal Medicine, Wan Fang Hospital, Taipei Medical University, Taipei, Taiwan, [8]Biostatistics Center, College of Management, Taipei Medical University, Taipei, Taiwan, [9]Graduate Institute of Data Science, College of Management, Taipei Medical University, Taipei, Taiwan, [10]Department of Mathematics and Statistics, Idaho State University, Pocatello, ID, United States

Background: Interferon in combination with ribavirin has been the standard of care for chronic hepatitis C virus infection (HCV) for the past few decades. However, its effect on the risk of autoimmune diseases (ADs) among patients with HCV infection remains unclear. We assessed the potential association between interferon-based therapy (IBT) and AD risk in patients with HCV infection.

Methods: This retrospective cohort study identified patients diagnosed with HCV infection between January 1, 2006, and December 31, 2015, from Taiwan's National Health Insurance Research Database. In total, 16,029 patients with HCV infection who received IBT and 141,214 patients with HCV infection who did not receive IBT were included. Both cohorts were followed up to assess the development of ADs. Hazard ratios (HRs) were calculated using the Cox proportional hazards regression model, which was adjusted for potential confounders.

Results: The median follow-up period for IBT and non-IBT users was 4.53 and 3.34 years, respectively. No significant difference in the risk of overall ADs (adjusted HR [aHR]: 0.96, 95% confidence interval [CI]: 0.81–1.14) or systemic

ADs (aHR: 0.88, 95% CI: 0.71–1.10) was noted during the study period. However, a slight increase in the risk of organ-specific ADs was noted among IBT users (incidence rate ratio: 1.33, 95% CI: 1.02–1.72). Furthermore, analysis of AD subgroups revealed a significant increase in the risks of Graves' disease (aHR: 6.06, 95% CI: 1.27–28.8) and Hashimoto's thyroiditis (aHR 1.49, 95% CI 1.01–2.21) among IBT users.

Conclusions: IBT use increases the risk of autoimmune thyroid diseases (Hashimoto's thyroiditis and Graves' disease) in patients with HCV infection to a greater extent than non-IBT use.

KEYWORDS

hepatitis C virus, interferon-based therapy, autoimmune disease, Grave's disease, Hashimoto thyroiditis

Introduction

Hepatitis C virus (HCV) is the causative agent of a type of hepatitis, previously known as non-A, non-B hepatitis (1). More than 71 million people worldwide are chronically infected with HCV in 2015 (2). According to Taiwan's National Health Insurance Research Database (NHIRD), 400,000 hepatitis C carriers existed in Taiwan till 2015. HCV infection predisposes patients to hepatocellular carcinoma, liver failure, and liver cirrhosis (3).

Chronic HCV infection can trigger an immune response in the host. Thus, HCV infection is associated with numerous extrahepatic disorders (4), such as type 2 mixed cryoglobulinemia and B-cell lymphoma. Agnello et al. (5) found at least 36 extrahepatic disease manifestations, mainly autoimmune disorders such as Sjogren's syndrome, systemic lupus erythematosus, autoimmune hemolytic anemia, antiphospholipid syndrome, autoimmune hemolytic anemia, Behcet's syndrome, autoimmune thyroiditis and dermatomyositis have been reported to be associated with HCV infection. Sayiner et al. also reported 2%–38% of patients with HCV infection have manifestations of rheumatological features and associated with many autoimmune rheumatic disorders, such as rheumatoid arthritis (RA) (6).

Type I interferons (IFNs) are cytokines and they exhibit pleiotropic effects, such as the induction of inhibition of cell growth, regulation of apoptosis, and cell-autonomous antiviral resistance. Moreover, type I IFNs can regulate immune effector functions and act as signals linking innate and adaptive immune responses (7). IFN-α has become the cornerstone of antiviral therapy for HCV infection since the 1980s. After the completion of antiviral treatment, Pegylated IFNs can lead to a significant increase in a sustained virologic response (8). Although direct-acting antiviral agents are now becoming a popular and successful therapeutic option, the effect of IFN-based therapy (IBT) still needs to be investigated. The occurrence of IFN-α-associated autoimmunity has been reported to range from 4% to 19% (9, 10). Furthermore, autoimmune disorders, such as systemic lupus erythematosus (SLE), RA, polymyositis psoriatic arthropathy, sarcoidosis, autoimmune hemolysis, autoimmune thyroid disease, and immune thrombocytopenia, may occur during IFN-α therapy (8, 11).

Few studies have assessed the effect of IBT on the risk of autoimmune diseases (ADs) in patients with HCV infection and it is impossible to conduct a randomized clinical trial to know the effect of IBT. Hence, we used reimbursement claims data from NHIRD to examine the association between IBT for HCV infection and the risk of ADs.

Materials and methods

Data sources

NHI program which covers more than 99% of Taiwan's population was launched in 1995 by the Taiwanese government (12). The NHRI maintains and updates the NHIRD, which contains the registration files and claims data of the beneficiaries of the NHI program. After the NHRI approved this study, we were able to assess the data of patients using scrambled patient identification numbers. In this dataset, the diagnostic codes were based on the International Classification of Diseases, Ninth Revision, Clinical Modification (ICD-9-CM), and the diagnoses were performed in accordance with the approved guidelines. Our study was approved by the Taipei Medical University Institutional Review Board (Approval Number N201908055). Informed consent was not required due to the dataset contained deidentified secondary data only for research purposes.

Study design and participants

This retrospective cohort study was conducted using data from the NHIRD. To ensure the validity and reliability of diagnoses, only adult patients who received HCV infection diagnoses (ICD-9-CM codes 070.41, 070.44, 070.51, 070.54, and V02.62) that were confirmed by in an inpatient setting or three or more ambulatory care claims. Patients who (1) were diagnosed with HBV infection (2), were younger than 18 years and had unknown age or sex (3), were diagnosed with ADs before the index date (4), were diagnosed with ADs within 6 months after the index date (5), had a follow-up duration of less than 6 months (6), were diagnosed with any form of cancer within 1 year before the cohort entry date, and (7) received IBT for less than 16 weeks were excluded from the study. The index date was the first date of receiving IBT for the treated cohort. The patients who never received IBT were consisted of untreated cohort during the study period. Patients were followed up from the entry date to the development of loss to follow-up, death, ADs or the end of the study.

Interferon-based therapy exposure

Six months IBT for all HCV genotypes has been reimbursed by the NHI Administration since October 1, 2 003. A combination of IBT and ribavirin is most prescribed among patients with HCV infection (97.8%) (13). The IBT regimen in our study consisted of a combination of pegylated IFN-α-2b (including the non-pegylated form) and ribavirin according to Anatomical Therapeutic codes. The duration of antiviral therapy ranged from 24 to 48 weeks.

Outcome measurement and comorbidities

Enrolled patients were observed up until occurrence of the interest outcomes and the end of the study. They were followed up for AD outcomes included systemic ADs (many different organs and tissues is targeted by immune system)and organ-specific ADs(a particular organ or tissue is targeted by immune system): Patients with systemic ADs were identified by Registry for Catastrophic Illness Patient Database (RCIPD) for the following diseases: SLE (ICD-9-CM code 710.0); RA (ICD-9-CM code 714.0); SSc (ICD-9-CM code 710.1); primary SjS (ICD-9-CM code 710.2); PM/DM (ICD-9-CM code 710.4/710.3); and Takayasu arteritis (ICD-9-CM code 446.7), temporal arteritis (ICD-9-CM code 446.5), polyarteritis nodosa (ICD-9-CM code 446.0), myasthenia gravis (ICD-9-CM code 358.0), and IBD (ICD-9-CM code 555.9). Takayasu arteritis, temporal arteritis, and polyarteritis nodosa are types of systemic vasculitis. In addition, we excluded patients with comorbidities such as systemic lupus erythematous, rheumatoid arthritis, scleroderma, polymyositis, dermatomyositis and HCV infection to limit our study sample to pSS. The following organ-specific ADs without catastrophic illness certification were identified using ICD-9-CM codes that appeared once in the discharge diagnosis for hospitalized patients or thrice within a year in outpatient diagnoses: ankylosing spondylitis (ICD-9-CM code 720.0), and psoriasis (ICD-9-CM code 696), type 1 diabetes mellitus (ICD-9-CM code 250.01), autoimmune hemolytic anemia (ICD-9-CM code 283.0), Addison's disease (ICD-9-CM code 255), Graves' disease (ICD-9-CM code 242.0), Henoch-Schönlein purpura (ICD-9-CM code 287.0), Hashimoto's thyroiditis (ICD-9-CM code 245.2).

For each patient, comorbidities were assessed using the Charlson comorbidity index (CCI) score. The CCI categorizes comorbidities based on the ICD diagnosis codes found in administrative data, such as hospital abstract data.

Statistical analysis

The incidence rates of ADs were estimated during the follow-up period in patients who received pegylated IFN α-2b and in those who did not. In addition, the incidence rate ratio (IRR) was calculated to assess the unadjusted risk of AD occurrence in the two groups. The confidence intervals (CIs) of IRRs were calculated using Poisson distribution and test-based methods. We used Cox proportional hazards regression model to estimate the adjusted hazard ratios (aHRs) and 95% CIs. In the Cox regression model, the aHRs were adjusted for sex, age, and comorbidities. We used the Kaplan–Meier estimator to assess the cumulative incidence of overall ADs, organ-specific ADs, and systemic ADs, and $p < 0.05$ was considered statistically significant. We used Student's t test and Pearson's chi-squared test, respectively to analyze the baseline characteristics, differences in continuous and categorical variables between the groups. We considered the all results of statistical analyses are significant at $p < 0.05$. SAS 9.4 and R 3.6.3 were used for the analyses.

Results

Baseline characteristics of the IBT and non-IBT groups

As shown in Figure 1, in this study, 325,799 patients diagnosed with HCV infection between January 1, 2006, and December 31, 2015, were identified. Patients who (1) were diagnosed with HBV infection (n = 260,260) (2), were diagnosed with AD before the index date (n = 260,178) (3),

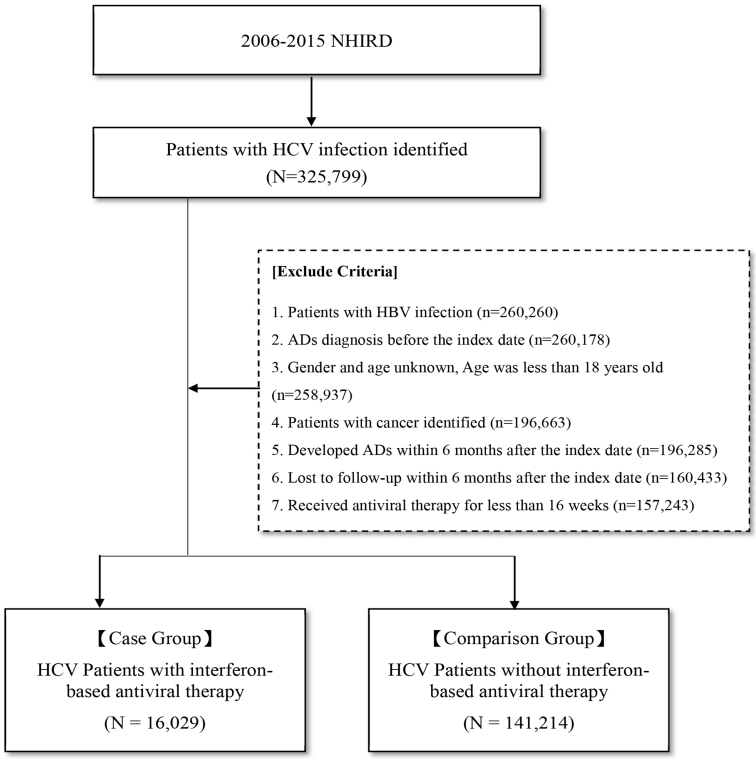

FIGURE 1
Flow Chart for Study Design. AD, autoimmune disease; HCV, hepatitis C virus; NHIRD, National Health Insurance Research Database.

had unknown sex or age or were aged less than 18 years (n = 258,937) (4), had cancer (n = 196,663) (5), were diagnosed with ADs within 6 months after the index date (n = 196,285) (6), were lost to follow-up within 6 months after the index date (n = 160,433), and (7) received antiviral therapy for less than 16 weeks (n = 157,243) were excluded from this study. After excluding these patients, a total of 16,029 patients with HCV infection who received IBT were included in the IBT group (case group), and 141,214 patients with HCV infection who did not receive IBT were included in the non-IBT group (comparison or control group). The non-IBT group had higher mean CCI scores and a higher number of male patients than the IBT group (Table 1).

IRR and HR of the risk of ADs between the IBT and non-IBT groups

Table 2 presents the incidence of ADs in the two groups. During the study period, no significant difference in the risk of overall ADs (IRR: 1.10, 95% CI: 0.93–1.29; aHR: 0.96, 95% CI: 0.81–1.14) or systemic ADs (IRR: 0.99, 95% CI: 0.80–1.21; aHR: 0.88, 95% CI: 0.71–1.10) was noted between the groups. By contrast, the IBT group had a higher risk of organ-specific ADs (IRR: 1.33, 0.99, 95% CI: 1.02–1.72).

IRR and HR of the risk of AD subtypes between the IBT and non-IBT groups

Regarding organ-specific ADs, the incidence rates of Graves' disease (IRR: 8.67, 95% CI: 1.94–38.7; aHR: 8.67, 95% CI: 1.94–38.7) and Hashimoto's thyroiditis (IRR: 1.71, 95% CI: 1.17–2.50; aHR: 1.49, 95% CI: 1.01–2.21) were significantly higher in the IBT group than in the non-IBT group (Table 3). No significant difference was noted in the incidence of systemic ADs between the two groups (Table 4).

Comparison of cumulative incidence of organ-specific ADs between the IBT and non-IBT groups

A comparison of the cumulative incidence of organ-specific ADs between the IBT and non-IBT groups is presented in Figure 2. The Kaplan–Meier estimates of organ-specific AD–free survival revealed a significantly higher incidence rate of organ-specific ADs in the IBT group than in the non-IBT group (Graves' disease, Figure 2A; Hashimoto's thyroiditis, Figure 2B).

10.3389/fimmu.2022.992819

TABLE 1 Baseline Characteristics of IBT and Non-IBT Group.

	IBT group (N = 16029)	Non-IBT group (N = 141214)	P-Value
Gender			<.0001
Female	7784 (48.56%)	71692 (50.77%)	
Male	8245 (51.44%)	69522 (49.23%)	
Age Group			<.0001
18-30	540 (3.37%)	5493 (3.25%)	
31-40	1782 (11.12%)	14338 (10.15%)	
41-50	3452 (21.54%)	23520 (16.66%)	
51-60	5708 (35.61%)	34864 (24.69%)	
61-70	3659 (22.83%)	30353 (21.49%)	
71-80	857 (5.35%)	23776 (16.84%)	
> 80	31 (0.19%)	9770 (6.92%)	
Mean (SD)	53.48 (11.51)	58.43 (15.02)	<.0001
Median (IQR)	55 (15)	59 (22)	<.0001
CCI Score			<.0001
0	3201 (19.97%)	61495 (43.55%)	
1	8273 (51.61%)	46756 (33.11%)	
2	3318 (20.70%)	20146 (14.27%)	
3	744 (4.64%)	6875 (4.87%)	
>=4	493 (3.08%)	5942 (4.21%)	
Mean (SD)	1.23 (1.08)	0.98 (1.24)	<.0001
Median (IQR)	1 (1)	1 (1)	<.0001
Follow up time			
Mean (SD)	4.53 (2.40)	3.34 (2.31)	<.0001
Median (IQR)	4.41 (3.39)	2.79 (3.48)	<.0001

CCI, Charlson comorbidity index; IBT, interferon-based therapy.

Discussion

To the best of our knowledge, this is the largest study to assess the association between IBT and the risk of ADs in patients with HCV infection. Our findings revealed that patients with HCV infection who received IBT did not have an increased risk of overall ADs or systemic ADs but had a slightly increased risk of organ-specific ADs. Furthermore, the IBT group had a significantly increased risk of autoimmune thyroid diseases (Graves' disease and Hashimoto's thyroiditis).

TABLE 2 Incidence Rate Ratio and Hazard Rate of the Risk of ADs between IBT and non-IBT group.

	Event	Person Year	IncidenceRate†	IRR	aHR
Overall ADs					
IBT Group	169	72538.54	232.98	1.10 (0.93-1.29)	0.96 (0.81-1.14)
Non-IBT Group	1000	472137.61	211.80	Ref.	Ref.
Organ-Specified ADs					
IBT Group	68	72799.57	93.41	1.33 (1.02-1.72)*	1.10 (0.84-1.43)
Non-IBT Group	333	473678.61	70.30	Ref.	Ref.
Systemic ADs					
IBT Group	102	72746.42	140.21	0.99 (0.80-1.21)	0.88 (0.71-1.10)
Non-IBT Group	673	472902.14	142.31	Ref.	Ref.

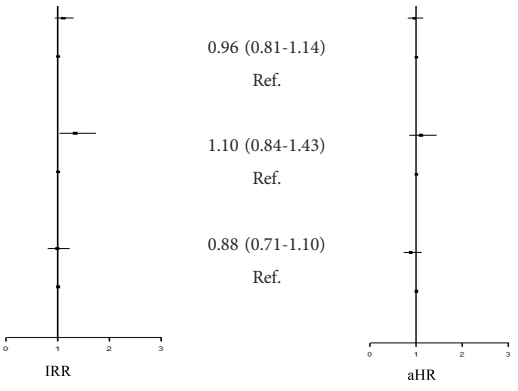

IR, incidence rate was incidences of per 100,000 person-years. HR, hazard ratio; aHR, adjusted hazard ratio; CI, confidence interval.
*P <0.05.

TABLE 3 Incidence Rate Ratio and Hazard Rate of the Risk of subgroup ADs between IBT and non-IBT group.

	Event	Person Year	IncidenceRate†	IRR	aHR
Addison's disease					
IBT Group	0	73009.17	0.00	N.A	N.A
Non-IBT Group	1	474449.96	0.21	Ref.	Ref.
Autoimmune hemolytic anemia					
IBT Group	6	72991.22	8.22	1.30 (0.54-3.12)	1.19 (0.47-2.96)
Non-IBT Group	30	474390.59	6.32	Ref.	Ref.
DM Type I					
IBT Group	19	72948.69	26.05	1.10 (0.68-1.79)	0.83 (0.50-1.37)
Non-IBT Group	112	474196.08	23.62	Ref.	Ref.
Graves' disease					
IBT Group	4	72999.83	5.48	8.67 (1.94-38.7)**	6.06 (1.27-28.8)*
Non-IBT Group	3	474441.99	0.63	Ref.	Ref.
Hashimoto's thyroiditis					
IBT Group	34	72900.38	46.64	1.71 (1.17-2.50)**	1.49 (1.01-2.21)*
Non-IBT Group	129	474111.38	27.21	Ref.	Ref.
Henoch-Schonlein purpura					
IBT Group	4	73001.99	5.48	0.70 (0.25-1.97)	0.59 (0.20-1.67)
Non-IBT Group	37	474381.40	7.80	Ref.	Ref.

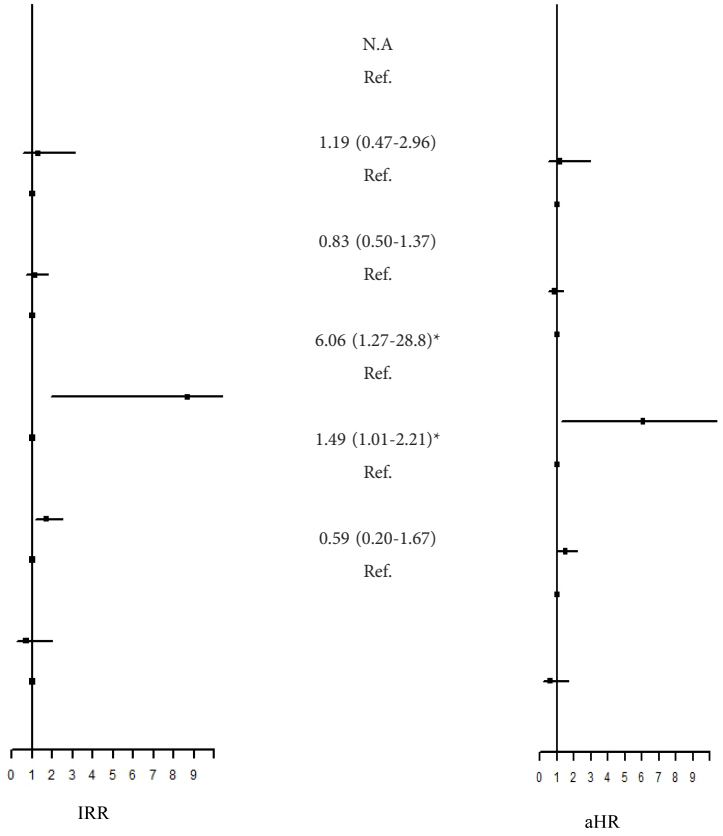

(Continued)

10.3389/fimmu.2022.992819

TABLE 3 Continued

	Event	Person Year	IncidenceRate†	IRR	aHR
Immune thrombocytopenic purpura					
IBT Group	0	73009.17	0.00	N.A	N.A
Non-IBT Group	0	474450.33	0.00	Ref.	Ref.
Lupoid hepatitis					
IBT Group	0	73009.17	0.00	N.A	N.A
Non-IBT Group	0	474450.33	0.00	Ref.	Ref.
Myasthenia gravis					
IBT Group	0	73009.17	0.00	N.A	N.A
Non-IBT Group	17	474413.93	3.58	Ref.	Ref.
Inflammatory bowel disease					
IBT Group	1	73003.04	1.37	1.08 (0.13-8.99)	1.53 (0.17-13.7)
Non-IBT Group	6	474439.44	1.26	Ref.	Ref.
Ankylosing Spondylitis					
IBT Group	54	72886.06	74.09	0.98 (0.74-1.31)	0.84 (0.63-1.13)
Non-IBT Group	357	473684.09	75.37	Ref.	Ref.
Psoriasis					
IBT Group	0	73009.17	0.00	N.A	N.A
Non-IBT Group	5	474435.43	1.05	Ref.	Ref.

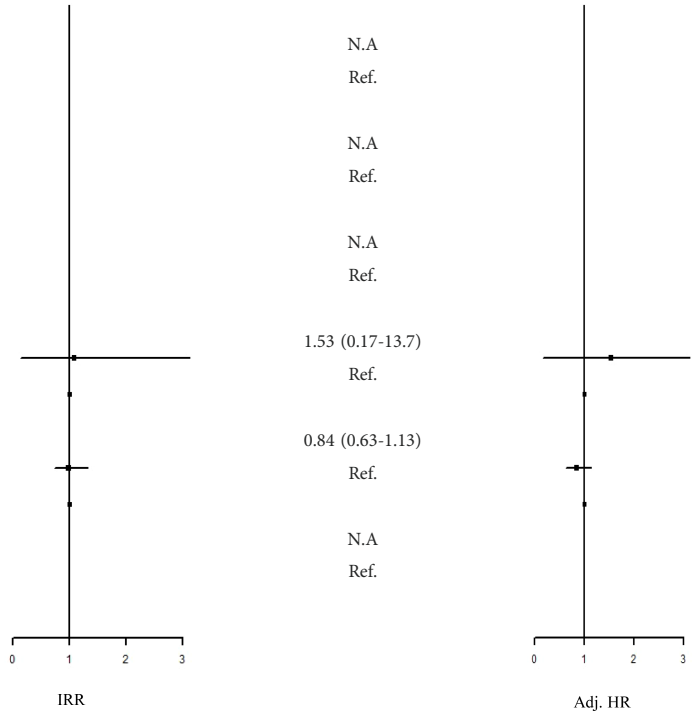

IR, incidence rate was incidences of per 100,000 person-years. HR, hazard ratio; aHR, adjusted hazard ratio; CI, confidence interval.
**P <0.01.
NA, not available.

10.3389/fimmu.2022.992819

TABLE 4 Incidence Rate Ratio and Hazard Ratio of the Risk of systemic ADs between IBT and non-IBT group.

	Event	Person Year	IncidenceRate†	IRR	aHR
Polymyositis/dermatomyositis					
IBT Group	0	73009.17	0.00	N.A	N.A
Non-IBT Group	7	474442.69	1.48	Ref.	Ref.
Rheumatoid arthritis					
IBT Group	18	72946.54	24.68	1.04 (0.63-1.70)	0.91 (0.55-1.52)
Non-IBT Group	113	474132.51	23.83	Ref.	Ref.
Primary Sjogren's syndrome					
IBT Group	28	72940.62	38.39	1.12 (0.75-1.68)	1.06 (0.70-1.60)
Non-IBT Group	162	474072.65	34.17	Ref.	Ref.
Systemic lupus erythematosus					
IBT Group	2	73000.58	2.74	0.39 (0.09-1.64)	0.38 (0.09-1.62)
Non-IBT Group	33	474384.46	6.96	Ref.	Ref.
Systemic sclerosis					
IBT Group	1	73006.74	1.37	0.81 (0.10-6.49)	0.94 (0.11-7.97)
Non-IBT Group	8	474436.63	1.69	Ref.	Ref.
Systemic vasculitis					
IBT Group	0	73009.17	0.00	N.A	N.A
Non-IBT Group	1	474444.39	0.21	Ref.	Ref.

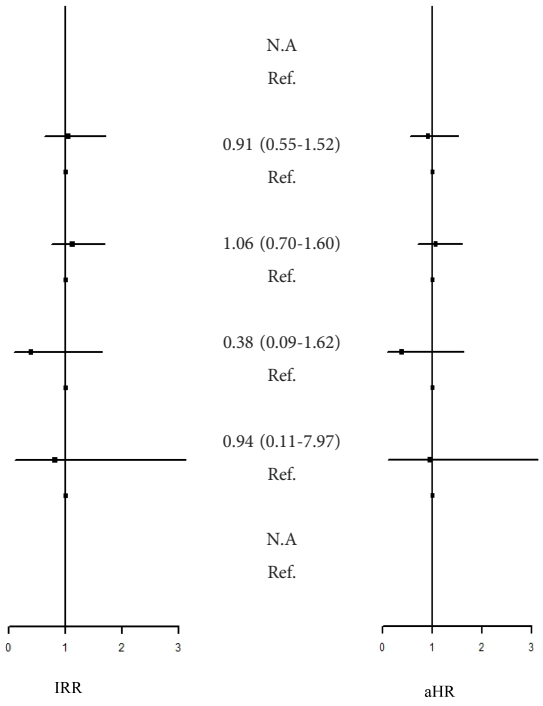

IR, incidence rate was incidences of per 100,000 person-years. HR, hazard ratio; aHR, adjusted hazard ratio; CI, confidence interval; NA, not available.

Chronic HCV infection can increase the risk of autoimmune thyroid diseases (14–16). However, our findings suggested that patients with HCV infection who were treated with IBT had a higher risk of autoimmune thyroid diseases than those who were not treated with IBT. A recent study using the NHIRD also reported a higher incidence rate of thyroid dysfunction among IFN-treated patients than among untreated patients with chronic HCV (17).

In a previous study, the incidence rate of thyroid disease was slightly higher than that of other ADs in patients receiving IBT (18). Among patients with HCV infection who were treated with IFNs, approximately 1.7% developed hypothyroidism and 0.6% developed hyperthyroidism (18). In another study, the incidence rate of thyroid disease after IBT was approximately 13.3% (19).

Tomer, Y. et al. reported that both immune-mediated and direct effects of IFN-α on thyroid function are involved in the mechanism of IFN-induced thyroiditis (20). Several pathways can underlie the immune-mediated effects of IFN-α. In particular, IFN-α receptor activation leads to the activation of the JAK–STAT pathway (21), resulting in the activation of

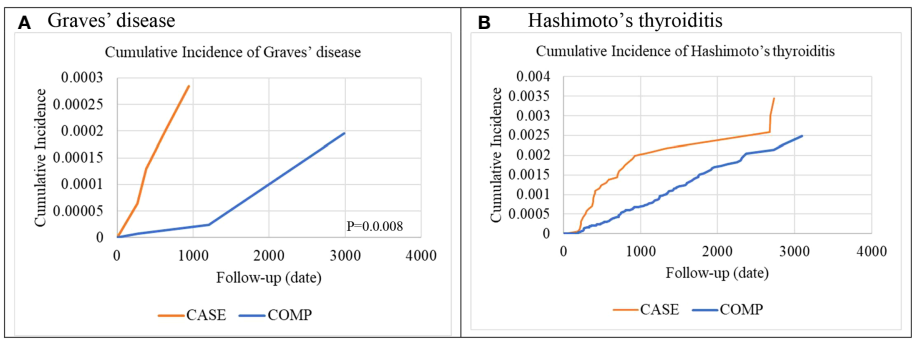

FIGURE 2
Cumulative incidence of organ-specific autoimmune diseases **(A)** Graves' disease **(B)** Hashimoto's thyroiditis.

numerous IFN-stimulated genes, including those encoding cytokines and adhesion molecules (19, 20). These effects can induce thyroid autoimmunity. IFN-α can increase the expression of major histocompatibility complex class I antigens on thyroid epithelial cells (22), which can lead to the activation of cytotoxic T cells and result in tissue damage and inflammatory response (23).

IFN-α can also shift the immune response to a T helper cell type 1 (Th1)-mediated pattern (24), leading to an increase in the production of IFN-γ and interleukin (IL)-2 (25). Ribavirin, an oral guanosine analog frequently used in combination with IFN to improve response and decrease relapse, may also alter the immune response (26). Moreover, IBT may result in autoimmune thyroiditis by enhancing the activity of lymphocytes, macrophages, and natural killer cells (23, 27–29); activating neutrophils and lymphocytes (20); inducing the release of IL-6 (23); and decreasing T-regulatory cell function by affecting the production of immunoglobulin (30, 31).

Hashimoto's thyroiditis is a hypothyroidism-related disease. Although it is a Th1-mediated disease, it is also associated with the Th2 response. Hypothyroidism has been reported in patients with HCV infection (32). In a recent study assessing the thyroid function of patients with HCV infection who received IBT for 24–48 weeks, hypothyroidism was found to be the most frequent thyroid disease (33). Genetic and environmental factors play an important role in the occurrence of thyroid disease (19, 34).

Graves' disease is a hyperthyroidism-related disease that is driven by the humoral immune response and Th2 cytokines. Although it is an antibody-mediated disease, it is predominantly a Th1-type cytokine disease (35). Therefore, Graves' disease and Hashimoto's thyroiditis have many common features. In both the diseases, the autoimmune response comprises both Th1 and Th2 types. Therefore, these diseases may be noted in patients with HCV infection who receive IBT.

Other ADs, such as RA, psoriasis, and polymyositis, have also been reported in patients with HCV infection who are treated with IFN-α (10, 36, 37). In addition, SLE is a frequently reported autoimmune rheumatic manifestation associated with IFN-α therapy. Despite many reports have been anecdotal (38–41), a few studies with large study groups have reported that the frequency of IFN-α-induced SLE ranges from 0.15% (10) to 0.7% (42). By contrast, none of the systemic ADs exhibited a higher risk in the IBT group than in the non-IBT group in our study.

With Regard to a mechanistic perspective, IFN-α is characterized by increased numbers of circulating autoreactive B and T cells (43). IFN-α therapy can tilt the usually tightly controlled balance toward the activation of these autoreactive cells through a vast array of mechanisms (7). Genetic susceptibility factors determine the type of autoimmunity to be developed. The expression of numerous target genes in antigen-presenting cells (APCs) is induced by IFN-α. As a consequence, stimulated APCs enhance promote isotype switching, potently activate autoreactive T cells (44) and humoral autoimmunity. In addition, T-cell autoreactivity by directly promoting T-cell activation and keeping activated T cells alive can be synergistically amplified by IFN-α (7). Type I IFN genes confer dominant disease resistance and trigger autoimmunity in genetically susceptible host (7).

Although our results demonstrated that the standard interferon-based treatment is associated with an increase of the immune-mediated thyroid damage. Autoimmune thyroid diseases are also common in HCV infected patients (45). The HCV is one of the most important viruses associated with autoimmune diseases. HCV may interfere with the mechanisms of self-recognition and functions both on thyroid cells and the immune system (45), where HCV may mimic the structure of some components of thyroid gland or directly destroy thyroid tissue, starting the autoimmune disease. In fact, the lymphoid tissue is a site for the persistence of the infection and chronic immune stimulus, HCV has a significant lymphotropism (46, 47, 48). The chronic stimulation results in: anti-apoptotic effects, autoantibody production, increased cytokine and chemokine secretion and drive for autoimmunity (45).

The strengths of our study include long-term assessment of concurrent ADs, large validation cohort and the large sample size. However, some limitations of our study should be addressed. First, the possibility of misclassification or miscoding cannot be completely ruled out, although the Bureau of NHI randomly and routinely checks patient charts to ensure the quality of claims from all medical institutions. Second, the relationship between the severity of ADs and disease activity in IBT-treated patients with HCV infection could not be analyzed. Third, there is still a possibility of unmeasurable bias given the observational nature of this study, although we used many methods to avoid potential confounders. Finally, some clinical and laboratory data were not available in the administrative database. Additional studies are needed to investigate this association.

In conclusion, our findings revealed that IBT in patients with HCV infection may increase the risk of autoimmune thyroid diseases (Graves' disease and Hashimoto's thyroiditis). Therefore, the development of ADs, particularly Graves' disease and Hashimoto's thyroiditis, must be monitored in patients receiving IBT. Further mechanistic research should also be conducted.

Data availability statement

The original contributions presented in the study are included in the article/supplementary material. Further inquiries can be directed to the corresponding author.

Ethics statement

This study was reviewed and approved by Taipei Medical University Institutional Review Board (Approval Number N201908055). Written informed consent for participation was not required for this study in accordance with the national legislation and the institutional requirements.

Author contributions

S-MC and H-JY designed research, wrote paper and final approval of the submitted version. T-ML, Y-SC, H-CH, Y-CS, T-TK and S-CC contributed to the data analysis, and final approval of the submitted version. J-HC and C-CC were responsible for the study conception and design, critical article revision for crucial intellectual content, and correspondence regarding the final approval of the submitted version. All authors contributed to the article and approved the submitted version.

Acknowledgments

This manuscript was edited by Wallace Academic Editing.

Conflict of interest

The authors declare that the research was conducted in the absence of any commercial or financial relationships that could be construed as a potential conflict of interest.

Publisher's note

References

1. Choo Q, Kuo G, Weiner AJ, Overby LR, Bradley DW, Houghton M, et al. Isolation of a cDNA clone derived from a blood-borne non-a, non-b viral hepatitis genome. *Science* (1989) 244(4902):359–62. doi: 10.1126/science.2523562

2. Blach S, Zeuzem S, Manna M, Altraif I, Duberg AS, Muljono DH, et al. Global prevalence and genotype distribution of hepatitis c virus infection in 2015: A modelling study. *Lancet Gastroenterol Hepatol* (2017) 2(3):161–76. doi: 10.1016/S2468-1253(16)30181-9

3. Messina JP, Humphreys I, Flaxman A, Brown A, Cooke GS, Pybus OG, et al. Global distribution and prevalence of hepatitis c virus genotypes. *Hepatology* (2015) 61(1):77–87. doi: 10.1002/hep.27259

4. Zignego AL, Ferri C, Pileri SA, Caini P, Bianchi FB. Extrahepatic manifestations of hepatitis c virus infection: A general overview and guidelines for a clinical approach. *Digestive Liver Dis* (2007) 39(1):2–17. doi: 10.1016/j.dld.2006.06.008

5. Agnello V, De Rosa FG. Extrahepatic disease manifestations of HCV infection: some current issues. *J Hepatol* (2004) 40(2):341–52. doi: 10.1016/j.jhep.2003.10.009

6. Sayiner ZA, Haque U, Malik MU, Gurakar A. Hepatitis c virus infection and its rheumatologic implications. *Gastroenterol Hepatol (N Y)* (2014) 10(5):287–93.

7. Conrad B. Potential mechanisms of interferon-alpha induced autoimmunity. *Autoimmunity* (2003) 36:519–23. doi: 10.1080/08916930310001602137

8. Pockros PJ, Jensen D, Tsai N, Taylor R, Ramji A, Cooper C, et al. JUMP-c: A randomized trial of mericitabine plus pegylated interferon alpha-2a/ribavirin for 24 weeks in treatment-naïve HCV genotype 1/4 patients. *Hepatology* (2013) 58 (2):514–23. doi: 10.1002/hep.26275

9. Gota C, Calabrese L. Induction of clinical autoimmune disease by therapeutic interferon-α. *Autoimmunity* (2003) 36(8):511–8. doi: 10.1080/08916930310001605873

10. Okanoue T, Sakamoto S, Itoh Y, Minami M, Yasui K, Sakamoto M, et al. Side effects of high-dose interferon therapy for chronic hepatitis c. *J Hepatol* (1996) 25(3):283–91. doi: 10.1016/S0168-8278(96)80113-9

11. Ioannou Y, Isenberg DA. Current evidence for the induction of autoimmune rheumatic manifestations by cytokine therapy. *Arthritis Rheum* (2000) 43:1431–42. doi: 10.1002/1529-0131(200007)43:7<1431::AID-ANR3>3.0.CO;2-E

12. NHRI. *National health insurance research database*. Available at: https://nhird.nhri.org.tw/.

13. Hsu CS, Kao JH, Chao YC, Lin HH, Fan YC, Huang CJ, et al. Interferon-based therapy reduces risk of stroke in chronic hepatitis c patients: A population-based cohort study in Taiwan. *Aliment Pharmacol Ther* (2013) 38:415–23. doi: 10.1111/apt.12391

14. Jadali Z, Alavian S-M. Autoimmune diseases co-existing with hepatitis c virus infection. *Iranian J allergy asthma Immunol* (2010) 9(4):191–206.

15. TESTA A. Prevalence of HCV antibodies in autoimmune thyroid disease. *Eur Rev Med Pharmacol Sci* (2006) 10:183–6.

16. Ganne-Carrie N, Medini A, Coderc E, Seror O, Christidis C, Grimbert S, et al. Latent autoimmune thyroiditis in untreated patients with HCV chronic hepatitis: a case-control study. *J Autoimmun* (2000) 14(2):189–93. doi: 10.1006/jaut.1999.0360

17. Chang Y-K, Tseng YT, Chen KH, Chen KT. Long-term outcomes and risk factors of thyroid dysfunction during pegylated interferon and ribavirin treatment in patients with chronic hepatitis c infection in Taiwan. *BMC Endocr Disord* (2019) 19(1):36. doi: 10.1186/s12902-019-0362-7

18. Ioannou Y, Isenberg DA. Current evidence for the induction of autoimmune rheumatic manifestations by cytokine therapy. *Arthritis Rheumatism* (2000) 43 (7):1431–42. doi: 10.1002/1529-0131(200007)43:7<1431::AID-ANR3>3.0.CO;2-E

19. Lenzi M, Johnson PJ, McFarlane IG, Ballardini G, Smith HM, McFarlane BM, et al. Antibodies to hepatitis c virus in autoimmune liver disease: Evidence for geographical heterogeneity. *Lancet* (1991) 338(8762):277–80. doi: 10.1016/0140-6736(91)90418-O

20. Tomer Y, Blackard JT, Akeno N. Interferon alpha treatment and thyroid dysfunction. *Endocrinol Metab Clin North Am* (2007) 36(4):1051–66; x-xi. doi: 10.1016/j.ecl.2007.07.001

21. Nguyen KB, Watford WT, Salomon R, Hofmann SR, Pien GC, Morinobu A, et al. Critical role for STAT4 activation by type 1 interferons in the interferon-gamma response to viral infection. *Science* (2002) 297(5589):2063–6. doi: 10.1126/science.1074900

22. You X, Teng W, Shan Z. Expression of ICAM-1, B7.1 and TPO on human thyrocytes induced by IFN-alpha. *Chin Med J (Engl)* (1999) 112(1):61–6.

23. Corssmit EP, de Metz J, Sauerwein HP, Romijn JA. Biologic responses to IFN-alpha administration in humans. *J Interferon Cytokine Res* (2000) 20 (12):1039–47. doi: 10.1089/107999000750053690

24. Farrar JD, Murphy KM. Type I interferons and T helper development. *Immunol Today* (2000) 21(10):484–9. doi: 10.1016/S0167-5699(00)01710-2

25. Tilg H. New insights into the mechanisms of interferon alfa: An immunoregulatory and anti-inflammatory cytokine. *Gastroenterology* (1997) 112 (3):1017–21. doi: 10.1053/gast.1997.v112.pm9041265

26. Thomas E, Ghany MG, Liang TJ. The application and mechanism of action of ribavirin in therapy of hepatitis c. *Antiviral Chem Chemother* (2012) 23(1):1–12. doi: 10.3851/IMP2125

27. Aulitzky WE, Tilg H, Vogel W, Aulitzky W, Berger M, Gastl G, et al. Acute hematologic effects of interferon alpha, interferon gamma, tumor necrosis factor alpha and interleukin 2. *Ann Hematol* (1991) 62(1):25–31. doi: 10.1007/BF01714980

28. Corssmit EP, Heijligenberg R, Hack CE, Endert E, Sauerwein HP, Romijn JA. Effects of interferon-alpha (IFN-alpha) administration on leucocytes in healthy humans. *Clin Exp Immunol* (1997) 107(2):359–63. doi: 10.1111/j.1365-2249.1997.269-ce1161.x.

29. Pfeffer LM, Dinarello CA, Herberman RB, Williams BR, Borden EC, Bordens R, et al. Biological properties of recombinant alpha-interferons: 40th anniversary of the discovery of interferons. *Cancer Res* (1998) 58(12):2489–99.

30. Lindahl P, Leary P, Gresser I. Enhancement by interferon of the expression of surface antigens on murine leukemia l 1210 cells. *Proc Natl Acad Sci U.S.A.* (1973) 70(10):2785–8. doi: 10.1073/pnas.70.10.2785

31. Krause I, Valesini G, Scrivo R, Shoenfeld Y. Autoimmune aspects of cytokine and anticytokine therapies. *Am J Med* (2003) 115(5):390–7. doi: 10.1016/S0002-9343(03)00390-5

32. Marazuela M, García-Buey L, González-Fernández B, García-Monzón C, Arranz A, Borque MJ, et al. Thyroid autoimmune disorders in patients with chronic hepatitis c before and during interferon-α therapy. *Clin Endocrinol* (1996) 44(6):635–42. doi: 10.1046/j.1365-2265.1996.751768.x

33. Pavan MH, Pavin EJ, Gonçales FL Jr, Zantut-Wittmann DE. Virus c genotype predisposes to primary hypothyroidism during interferon-α treatment for chronic hepatitis c. *Braz J Infect Dis* (2011) 15(5):449–56. doi: 10.1590/S1413-86702011000500006

34. Minelli R, et al. Effects of excess iodine administration on thyroid function in euthyroid patients with a previous episode of thyroid dysfunction induced by interferon-alpha treatment. *Clin Endocrinol* (1997) 47(3):357–61. doi: 10.1046/j.1365-2265.1997.2721081.x

35. Rapoport B, McLachlan SM. Graves' hyperthyroidism is antibody-mediated but is predominantly a Th1-type cytokine disease. *J Clin Endocrinol Metab* (2014) 99(11):4060–1. doi: 10.1210/jc.2014-3011

36. Fattovich G, Giustina G, Favarato S, Ruol A. A survey of adverse events in 11 241 patients with chronic viral hepatitis treated with alfa interferon. *J Hepatol* (1996) 24(1):38–47. doi: 10.1016/S0168-8278(96)80184-X

37. Kälkner KM, Rönnblom L, Karlsson Parra AK, Bengtsson M, Olsson Y, Oberg K. Antibodies against double-stranded DNA and development of polymyositis during treatment with interferon. *QJM: Int J Med* (1998) 91 (6):393–9. doi: 10.1093/qjmed/91.6.393

38. Tolaymat A, Leventhal B, Sakarcan A, Kashima H, Monteiro C. Systemic lupus erythematosus in a child receiving long-term interferon therapy. *J Pediatr* (1992) 120:429–32. doi: 10.1016/S0022-3476(05)80913-8

39. Schilling PJ, Kurzrock R, Kantarjian H, Gutterman JU, Talpaz M. Development of systemic lupus erythematosus after interferon therapy for chronic myelogenous leukemia. *Cancer* (1991) 68:1536–7. doi: 10.1002/1097-0142(19911001)68:7<1536::AID-CNCR2820680713>3.0.CO;2-B

40. Flores A, Olive´ A, Feliu E, Tena X. Systemic lupus erythematosus following interferon therapy [letter]. *Br J Rheumatol* (1994) 33:787. doi: 10.1093/rheumatology/33.8.787

41. Conlon KC, Urba WJ, Smith JWD, Steis RG, Longo DL, Clark JW. Exacerbation of symptoms of autoimmune disease in patient receiving alpha-interferon therapy. *Cancer* (1990) 65:2237– 42. doi: 10.1002/1097-0142(19900515)65:10<2237::AID-CNCR2820651013>3.0.CO;2-5

42. Ronnblom LE, Alm GV, Oberg KE. Autoimmunity after alpha interferon therapy for malignant carcinoid tumors. *Ann Intern Med* (1991) 115:178–83. doi: 10.7326/0003-4819-115-3-178

43. Le Bon A, Tough DF. Links between innate and adaptive immunity *via* type I interferon. *Curr Opin Immunol* (2002) 14(4):432–6. doi: 10.1016/S0952-7915(02)00354-0

44. Santini SM, Lapenta C, Logozzi M, Parlato S, Spada M, Di Pucchio T, et al. Type I interferon as a powerful adjuvant for monocyte-derived dendritic cell development and activity *in vitro* and in hu-PBL-SCID mice. *J Exp Med* (2000) 191 (10):1777–88. doi: 10.1084/jem.191.10.1777

45. Pastore F, Martocchia A, Stefanelli M, Prunas P, Giordano S, Toussan L, et al. Hepatitis c virus infection and thyroid autoimmune disorders: A model of interactions between the host and the environment. *World J Hepatol* (2016) 8 (2):83–91. doi: 10.4254/wjh.v8.i2.83

46. Ferri C, Antonelli A, Mascia MT, Sebastiani M, Fallahi P, Ferrari D, et al. HCV-related autoimmune and neoplastic disorders: The HCV syndrome. *Dig Liver Dis* (2007) 39(Suppl):S13–21. doi: 10.1016/S1590-8658(07)80005-3

47. Calvaruso V, Craxì A. Immunological alterations in hepatitis c virus infection. *World J Gastroenterol* (2013) 19:8916–23. doi: 10.3748/wjg.v19.i47.8916

48. Roti E, Minelli R, Giuberti T, Marchelli S, Schianchi C, Gardini E, et al. Multiple changes in thyroid function in patients with chronic active HCV hepatitis treated with recombinant interferon-alpha. *Am J Med* (1996) 101(5):482–7. doi: 10.1016/S0002-9343(96)00259-8

frontiers | Frontiers in Immunology

TYPE Original Research
PUBLISHED 14 October 2022
DOI 10.3389/fimmu.2022.983000

OPEN ACCESS

EDITED BY
José Mordoh,
IIBBA-CONICET Leloir Institute Foundation, Argentina

REVIEWED BY
Koji Yasutomo,
Tokushima University, Japan
Rupsa Basu,
Humane Genomics, United States

*CORRESPONDENCE
Tanapat Palaga
tanapat.p@chula.ac.th

SPECIALTY SECTION
This article was submitted to Vaccines and Molecular Therapeutics, a section of the journal Frontiers in Immunology

RECEIVED 30 June 2022
ACCEPTED 26 September 2022
PUBLISHED 14 October 2022

CITATION
Sittplangkoon C, Alameh M-G, Weissman D, Lin PJC, Tam YK, Prompetchara E and Palaga T (2022) mRNA vaccine with unmodified uridine induces robust type I interferon-dependent anti-tumor immunity in a melanoma model. *Front. Immunol.* 13:983000. doi: 10.3389/fimmu.2022.983000

mRNA vaccine with unmodified uridine induces robust type I interferon-dependent anti-tumor immunity in a melanoma model

Chutamath Sittplangkoon[1,2], Mohamad-Gabriel Alameh[3], Drew Weissman[3], Paulo J. C. Lin[4], Ying K. Tam[4], Eakachai Prompetchara[5,6] and Tanapat Palaga[2,7]*

[1]Graduate Program in Biotechnology, Faculty of Science, Chulalongkorn University, Bangkok, Thailand, [2]Center of Excellence in Immunology and Immune-Mediated Diseases, Chulalongkorn University, Bangkok, Thailand, [3]Division of Infectious Diseases, University of Pennsylvania Perelman School of Medicine, Philadelphia, PA, United States, [4]Acuitas Therapeutics, Vancouver, BC, Canada, [5]Center of Excellence in Vaccine Research and Development (Chula Vaccine Research Center-Chula VRC), Faculty of Medicine, Chulalongkorn University, Bangkok, Thailand, [6]Department of Laboratory Medicine, Faculty of Medicine, Chulalongkorn University, Bangkok, Thailand, [7]Department of Microbiology, Faculty of Science, Chulalongkorn University, Bangkok, Thailand

An mRNA with unmodified nucleosides induces type I interferons (IFN-I) through the stimulation of innate immune sensors. Whether IFN-I induced by mRNA vaccine is crucial for anti-tumor immune response remains to be elucidated. In this study, we investigated the immunogenicity and anti-tumor responses of mRNA encoding tumor antigens with different degrees of N1-methylpseudouridine (m1Ψ) modification in B16 melanoma model. Our results demonstrated that ovalbumin (OVA) encoding mRNA formulated in a lipid nanoparticle (OVA-LNP) induced substantial IFN-I production and the maturation of dendritic cells (DCs) with negative correlation with increasing percentages of m1Ψ modification. In B16-OVA murine melanoma model, unmodified OVA-LNP significantly reduced tumor growth and prolonged survival, compared to OVA-LNP with m1Ψ modification. This robust anti-tumor effect correlated with the increase in intratumoral $CD40^+$ DCs and the frequency of granzyme B^+/IFN-γ^+/TNF-α^+ polyfunctional OVA peptide-specific $CD8^+$ T cells. Blocking type I IFN receptor completely reversed the anti-tumor immunity of unmodified mRNA-OVA reflected in a significant decrease in OVA-specific IFN-γ secreting T cells and enrichment of PD-1^+ tumor-infiltrating T cells. The robust anti-tumor effect of unmodified OVA-LNP was also observed in the lung metastatic tumor model. Finally, this mRNA vaccine was tested using B16 melanoma neoantigens (*Pbk-Actn4*) which resulted in delayed tumor growth. Taken together, our findings

demonstrated that an unmodified mRNA vaccine induces IFN-I production or the downstream signaling cascades which plays a crucial role in inducing robust anti-tumor T cell response for controlling tumor growth and metastasis.

KEYWORDS

mRNA vaccine, type I interferon, cancer immunotherapy, melanomas, unmodified nucleosides

Introduction

Cancer immunotherapy educates immune cells to recognize tumor-derived antigens, which usually have a low immunogenicity to induce a potent antigen-specific immune response to eradicate tumor cells (1). Peptide-based cancer immunotherapy has been successfully demonstrated and several trials are ongoing (2, 3). Although tumor antigen-derived peptide immunogens for cancer therapeutic vaccines are traditionally used, there are various limitations, including the manufacturing cost and the need for strong adjuvants to induce anti-tumor immunity (4). Alternative types of cancer vaccines in clinical trials such as DNA vaccines (5), autologous patient-derived immune cell vaccines (6), tumor antigen-expressing recombinant virus vaccines (7), and heterologous whole cell vaccines derived from established human tumor cell lines (8) have been reported. Prior to the widely use of mRNA vaccine for COVID-19, the mRNA-based cancer vaccines have been tested in clinical trials (9) such as personalized RNA mutanome vaccine (10) that is highly effective in inducing anti-tumor immunity. With the current use of mRNA vaccines worldwide to control the COVID-19 pandemic, the efficacy and safety of this type of vaccine platform was demonstrated (11).

The benefits of mRNA-based vaccines have been demonstrated over conventional and DNA-based vaccines. These include the safety of mRNA that will not undergo genome integration and the relatively low production cost as *in vitro* transcribed (IVT) mRNA is relatively easy to produce with a scalable manufacturing process (11). mRNAs can be prepared for any protein antigen by using host cell's translational machinery avoiding MHC restriction in contrast to peptide vaccines (12, 13). The short half-life of mRNA and transient antigen expression enables repeated administration alleviating potential issues such as the low risk of immune suppression due to chronic persistence of antigens (14). Furthermore, mRNA can efficiently transfect nondividing cells (15) and may be engineered and manufactured to provide self-adjuvanticity (16).

Over the past decades, obstacles in applying mRNA as vaccines including the inherent instability and low level of protein expression as a result of high innate immunogenicity and inefficient delivery have been resolved (17). Purified unmodified IVT mRNA induces high level of type I interferon (IFN-I) through activation of toll-like receptors (TLRs). Activation of TLRs results in upregulation of proinflammatory cytokines such as IFN-I, IL-6, IL-12, TNF-α and chemokines (18). This can be circumvented by the incorporation of naturally occurring nucleosides and by applying stringent purification to remove double-stranded RNA contaminants (19–21). Karikó et al. reported that mRNA with nucleoside modifications were insensitive to ribonuclease L (RNase L) degradation, did not activate TLRs and protein kinase R, which subsequently resulted in improved translational efficiency and stability, compared to unmodified mRNA (20). On the other hand, Thess et al. reported that codon-optimized unmodified mRNA showed higher translational efficiency with low immunogenicity compared to the modified mRNA (22). This study, however, engineered the regulatory regions of the construct so that the internal ribosome entry site was modified, reducing ribosome binding leading to less efficient translation.

Due to the heterogeneity of tumor antigens as a result of high mutation rates, neo-antigens with tumor-specific mutations are ideal targets for cancer immunotherapy as they can potentially be recognized by the mature T-cell repertoire as non-self antigens (23). Recently, nonsynonymous somatic point mutations in B16F10 murine melanoma cells have been reported. Using this dataset, tumor-specific mutations were identified by algorithms and selected vaccine targets were based on their expression levels and major histocompatibility complex (MHC) binding capacity (24, 25). Surprisingly, when immunized with IVT mRNA, most of the mutation-specific immune response biased toward mutation-specific $CD4^+$ T cells. Repeated vaccination of mRNA encoding a lysine to asparagine (K739N) mutation in the *Kif18b* slowed tumor growth, prolonged survival, and inhibited lung metastasis in B16F10 tumor model (25). However, the impact of different degrees of nucleoside modifications on mRNA-LNP cancer vaccine-induced anti-tumor immunity has not been investigated.

In this study, we aimed to compare the anti-tumor efficacy of mRNA vaccines with various degrees of nucleoside modification

in a mouse melanoma model of localized and metastatic tumor. Furthermore, the roles of IFN-I from innate immune induction by mRNA vaccine on T cell responses and therapeutic efficacy to control tumor growth were investigated. Finally, we investigated the therapeutic efficacy mRNA vaccine encoding neoantigens of PDZ-binding kinase (PBK) and actinin alpha 4 (ACTN4), which were identified from the B16F10 murine melanoma mutanomes (26).

Materials and methods

Animals

Wild type C57BL/6 mice were purchased from Charles River Laboratories (Wilmington, MA, USA) or Nomura Siam International (Bangkok, Thailand). Age-matched (6–12 weeks) female mice were used in all experiments. Mice were maintained in a specific pathogen-free facility, and all protocols involving laboratory animals were approved by the institutional animal care and use committee (IACUC) at the University of Pennsylvania and Chulalongkorn University (Protocol Review No. 803941; 1723013; 1873005; 003/2565). The results are reported under the Animal Research: Reporting of *In Vivo* Experiments (ARRIVE) Guidelines.

RNA constructs, *in vitro* transcription, and lipid nanoparticle formulation

Plasmid templates for *in vitro* transcription of antigen-encoding RNAs were based on the previously published pUC-ccTEV-A101 vector (27). pUC-ccTEV-ovalbumin-A101 (OVA), pUC-ccTEV-neoantigens-A101 (Neo), pUC-ccTEV-luciferase-A101 (Luc2), pUC-ccTEV-mCherry-A101 (mCherry), and pUC-ccTEV-PR8HA-A101 (PR8HA) vectors were synthesized by GenScript (Piscataway, NJ, USA). The Neo construct contained the sequence encoding two point-mutated 27-meric peptides (Pbk and Actn4) linked by a sequence encoding a 10 amino-acid long glycine-serine linker. The mRNAs were produced from plasmids encoding codon-optimized antigens. Plasmids were linearized with restriction enzymes, mRNA was produced using the MEGAscript T7 Transcription Kit (Ambion, USA), and purified using cellulose-loaded column (28). Percent of 1-methylpseudouridine-5′-triphosphate (m1ψ) (TriLink, USA) and UTP nucleotides were varied by mole (0, 5, 10, 20, 30, 40, 50, 60, 70, 80, 90 and 100% m1ψ). RNAs were capped using CleanCap AG (3'OMe) (TriLink). All RNAs were analyzed for the integrity by native agarose gel electrophoresis and for double-stranded RNA using dot blot. mRNAs were stored frozen at −80°C until use.

Purified mRNAs were formulated into lipid nanoparticles using a self-assembly process wherein an ethanolic lipid mixture of an ionizable cationic lipid, phosphatidylcholine, cholesterol, and polyethylene glycol-lipid was rapidly combined with an aqueous solution containing mRNA at acidic pH as previously described (29). The ionizable cationic lipid (pKa in the range of 6.0-6.5, proprietary to Acuitas Therapeutics) and LNP composition are described in the patent application WO 2017/004143. The average hydrodynamic diameter was ~80 nm with a polydispersity index of 0.02-0.06 as measured by dynamic light scattering using a Zetasizer Nano ZS (Malvern Instruments Ltd, Malvern, UK) and an encapsulation efficiency of ~95% as determined using a Ribogreen assay.

Cell transfection

Bone marrow-derived macrophages (BMDMs) were harvested after 7-days of differentiation with cold phosphate-buffered saline (PBS) and seeded 5×10^4 cells/well in 200 µl of DMEM complete media in a 96-well plate. Bone marrow-derived dendritic cells (BMDCs) were used for transfection after 12 days of differentiation. BMDCs and BMDMs were incubated with mRNA encoding mCherry complexed with TransIT transfection reagent (0.1 µg mRNA in 17 µl TransIT transfection reagent) (Mirus Bio, USA). This complex was added to cells in 183 µl media. Reporter proteins in mRNA-transfected cultured cells were detected and quantified at 48 hr after transfection. mCherry positive cells were quantified by LSR II flow cytometer (BD Biosciences, USA).

Generation of BMDMs

Bone marrow cells (BMs) were flushed from humerus, femur and tibia of 6-8 weeks old C57BL/6 mice. To obtain BMDMs, BMs were cultured in tissue culture non-treated petri dish (Hycon, Thailand) with 8 ml of DMEM complete media (Cytiva, UK) supplemented with 10% (v/v) Fetal Bovine Serum (FBS) (Gibco, USA), 10 mM HEPES (Cytiva), 1 mM sodium pyruvate (Cytiva) and 1x Penicillin/Streptomycin G (Cytiva), supplemented with 5% (v/v) horse serum (Cytiva), and 20% (v/v) L929-conditioned media. On day 4, three ml of fresh media supplemented with 20% L929-conditioned media and 5% horse serum was added to the culture. Cells were harvested on day 7 using ice-cold PBS. Macrophage phenotype was confirmed by flow cytometry by staining using mouse anti-F4/80 and CD11b antibodies (BioLegend, USA). The derived BMDMs were seeded at 5×10^4 cells/well in 200 µl of DMEM complete media without horse serum and L929-conditioned media in 96-well plate before transfection.

Generation of BMDCs

BMs were cultured in 96-well tissue culture treated plate (Nunc, USA) at 1×10^4 cells/well in 100 µl of BMDC media containing RPMI-1640 (Cytiva) supplemented with 10% (v/v) FBS, 10 mM HEPES, 1 mM sodium pyruvate, 1x Penicillin/Streptomycin G, 1x GlutaMAX™ (Gibco), 1x MEM Non-Essential Amino Acid (Gibco), 55 µM β-mercaptoethanol (Gibco). On day 0, recombinant mouse GM-CSF (20 ng/ml) (Peprotech, USA) was added to the media. On day 3, 6, and 8, fresh BMDC media containing recombinant mouse GM-CSF (20 ng/ml) was added. On day 10, the culture supernatant was discarded and the same volume of fresh BMDC media containing recombinant mouse GM-CSF (20 ng/ml) and recombinant mouse IL-4 (10 ng/ml) (Peprotech) were added. On day 11, ¾ the volume of culture supernatant was discarded and the same volume of fresh BMDC media containing recombinant mouse GM-CSF (20 ng/ml) and recombinant mouse IL-4 (5 ng/ml) was added. The derived BMDCs were cultured in BMDC media without cytokines and used for transfection on day 12. Dendritic cell phenotype was confirmed by flow cytometry by staining with mouse anti-CD11c, MHC class II, CD40, CD86 antibodies (BioLegend).

Tumor cell lines

B16F10-Luc2 melanoma cells were obtained from the American Type Culture Collection (ATCC CRL-6475-LUC2™). Cells were maintained in DMEM media supplemented with 10% FBS and 10 µg/ml Blasticidin (*In vivo*Gen, USA). The OVA-secreting B16F0-OVA cell line was kindly provided by Dr. Edith Lord (Univiversity of Rochester, Rochester, NY, USA). Cells were maintained in RPMI-1640 supplemented with 10% FBS, 10 mM HEPES, 1 mM sodium pyruvate, 1x GlutaMAX™, 1x MEM Non-Essential Amino Acid, 55 µM β-mercaptoethanol, 1x Penicillin/Streptomycin G and G418 (400 µg/ml) (*In vivo*Gen).

Melanoma tumor model

For immunogenicity studies, age-matched female (8-12 weeks old) C57BL/6 mice were immunized with mRNA encoding ovalbumin or neoantigens on day 0 and boosted on day 4 with the same dose and formulation. Vaccination was performed by intramuscular (i.m.) injection of 10 µg mRNA-LNP. Mice were sacrificed 7 days after the booster vaccine for spleen collection.

For therapeutic study, anesthetized mice were injected subcutaneously (s.c.) into the flank with 2×10^5 B16F0-OVA or B16F10-Luc2 tumor cells in 200 µl of sterile Hanks' Balanced Salt Solution (Gibco). For B16F0-OVA model, two doses of 10 µg of mRNA encoding ovalbumin or irrelevant antigen were administered i.m. on day 4 and 8 after tumor inoculation. For the B16F10-Luc2 model, mice were immunized i.m. with two doses of 10 µg of mRNA encoding neoantigen or irrelevant antigen on day 4 and 8 after tumor inoculation. Tumor growth was monitored 2–3 times a week, and the survival was recorded for at least 31 days. Tumor volumes were monitored by using a vernier caliper and calculated using the equation: $V = (4\times3.14\times A \times B^2)/3$, where V = volume ($mm^3$), A = the largest diameter (mm), and B = the smallest diameter (mm) (30). Mice were sacrificed when tumor size reached 20 mm in diameter or 400 mm^2 (31).

For the cancer lung metastasis model, 2×10^6 B16F0-OVA tumor cells in 200 µl of sterile Hanks' Balanced Salt Solution were injected intravenously (i.v.) through lateral tail veins. On day 4 and 8 after tumor inoculation, mice were immunized *i.m.* with 10 µg of mRNA encoding ovalbumin or irrelevant antigen. On day 18, mice were euthanized with isoflurane. Lungs were fixed and bleached in Fekete's solution to count the tumor nodules on the lung surface.

ELISA

Culture supernatants from treated BMDMs and BMDCs were harvested at 48 hr after transfection as described above. Serum collected from immunized mice treated as indicated was prepared. Mouse IFN-α (Invitrogen, USA) and IFN-β ELISA (BioLegend) was carried out according to the manufacturer's instructions.

Synthetic peptides

For the *in vitro* re-stimulation of splenocytes, a pool of six synthetic peptides (Jerini Peptide Technologies, Germany) of 11-27 amino acids (a.a.) in length, with eight overlapping residues were used. The purity of the peptides was > 95% HPLC purified. Peptides corresponded to the mutated sequences of *Pbk* (PAAVILRDALH, VILRDALHMAR and DSGSPFPAA VILRDALHMARGLKYLHQ) and *Actn4* (FQAFIDVMSRE, FIDVMSRETTD and NHSGLVTFQAFIDVMSRET TDTDTADQ) were used as neoantigens. The peptides were used at a final concentration of 2.5 µg/ml. A synthetic peptide 8 a.a. in length from the sequence of ovalbumin (H2-K^b-restricted $OVA_{257-264}$ SIINFEKL) was used at a concentration of 2.5 µg/ml (*In vivo*gen, USA).

Serum and tissue preparation

Serum prepared from peripheral blood was collected with capillary tube and were stored at -80°C until use. Spleens and draining lymph nodes were collected, and single-cell

suspensions were prepared in RPMI-1640 containing 10% (v/v) FBS after filtering through 70-µm cell strainer (BD Falcon, USA). Erythrocytes were removed by ACK lysing buffer (Quality Biological, USA). Murine B16 tumors were harvested and minced into small pieces. Cells were washed once with FBS (10% (v/v)) in RPMI-1640. After centrifugation at 2,000 rpm for 10 minutes at 4°C, collagenase IV (1 mg/ml) and DNase I (100 mg/ml) (both were from Sigma-Aldrich, USA) in RPMI-1640 containing 10% (v/v) FBS, 1x Penicillin/Streptomycin G, 55 µM β-mercaptoethanol were added and incubated at 37°C for 20 minutes in 250 rpm shaking incubator to disperse aggregates. Cell suspensions were passed through 40-µm cell strainer and washed once with 2% (v/v) FBS in RPMI-1640 and centrifuged at 2,000 rpm for 10 minutes at 4°C. Erythrocytes in tumor suspension were removed by ACK lysing buffer. Cell numbers were counted with Vi-Cell XR cell counter (Beckman Coulter, USA).

In vitro re-stimulation and cell surface staining and intracellular cytokine staining (ICS) of splenocytes

After *in vitro* re-stimulation of 2 × 10^6 splenocytes with $OVA_{257-264}$ SIINFEKL (2.5 µg/ml) or a pool of six synthetic peptides of Pbk and Actn4 neoantigens (2.5 µg/ml each) in the presence of purified anti-mouse CD28 antibody (1 µg/ml) (BioLegend) for 6 hr with brefeldin A (20 µg/ml), and GolgiStop™ (40 µg/ml) (BD Pharmingen, USA) for the last 5 hr, cells were washed in PBS and stained with the LIVE/DEAD Fixable Aqua Dead Cell Stain Kit (Life Technologies, USA) for 10 minutes at room temperature. Cells were washed once in FACS buffer containing 2% (v/v) FBS in PBS and blocked with purified anti-mouse CD16/CD32 (0.5 µg) (BD Biosciences, USA) for 20 minutes at 4°C. Monoclonal antibodies used for surface staining and ICS are shown in Supplementary Table 1. ICS was performed using Cytofix/Cytoperm kit (BD Biosciences). Data were acquired on an LSR Fortessa flow cytometer (BD Biosciences, USA) and analyzed with FlowJo 10.6.0 software (Tree Star, USA).

ICS of tumor infiltrating immune cells

After single cell suspensions were prepared as stated above, cells were counted, and 2 × 10^6 cells were stained with the LIVE/DEAD Fixable Aqua Dead Cell Stain Kit or PI (BioLegend, USA) for 10 minutes at room temperature. Cells were washed once in FACS buffer containing 2% (v/v) FBS in PBS and blocked with purified anti-mouse CD16/CD32 (0.5 µg) for 20 minutes at 4°C. Monoclonal antibodies used for surface staining and ICS are shown in Supplementary Table 1. ICS was performed using Cytofix/Cytoperm kit.

Blocking IFN-I by IFNAR1-specific monoclonal antibody

B16F0-OVA cell lines were injected into mice to allow for tumor formation as described above. At day 4 and day 8, mice were intraperitoneally injected with 400 µg/dose of IFNAR1-specific MAR1-5A3 mAb (BioLegend) (32) or MOPC-21 isotype control mAb (BioLegend, USA) as described previously (33) 1 hr before mRNA-LNP vaccination (30). Tumor growth and immune infiltrated cells were analyzed at day 42.

ELISpot

Splenocytes from immunized mice (2×10^6 cells) were cultured for 48 hr in IFN-γ (BD Biosciences) pre-coated 96-well plates in the presence of OVA (20 µg/ml) (*In vivo*Gen) or concanavalin A (10 µg/ml) (Sigma-Aldrich). ELISpots were performed according to the manufacturer's instructions by ELISpot plate reader (ImmunoSpot, USA).

Statistical analysis

Statistical analyses were performed with Prism 8.0 (GraphPad Software). Data were compared with an unpaired two-tailed Student's t test, one-way or two-way ANOVA with Bonferroni multiple comparisons test. Statistical significance was defined by a value of $P < 0.05$. The log-rank test followed by the Mantel-Cox posttest was used for the survival analysis.

Results

Translation efficiency is inversely related to IFN-I secretion, APC maturation and levels of nucleoside modification

The effect of nucleoside modified mRNA on protein translation, IFN-I production and APC maturation, were initially evaluated *in vitro* using the commercial reagent TransIT to deliver mCherry encoding mRNA with different levels of m1ψ modification (0, 5, 10, 20, 30, 40, 50, 60, 70, 80, 90, and 100%) into BMDCs and BMDMs. *In vitro* transfection of 0.1 µg mRNA with levels of m1ψ substitution in the range of 70-100% showed significantly higher percentages of $mCherry^+$ cells, compared to the untreated control in both BMDCs and BMDMs at 48 hr post-transfection (Figures 1A, B; Figures S1A, B). Only mRNA with 0% of m1ψ subsitution (referred to as unmodified mRNA) showed a strong induction of IFN-I production in both cells (Figures 1C, D). Based on this initial result, mRNA with 0,

10.3389/fimmu.2022.983000

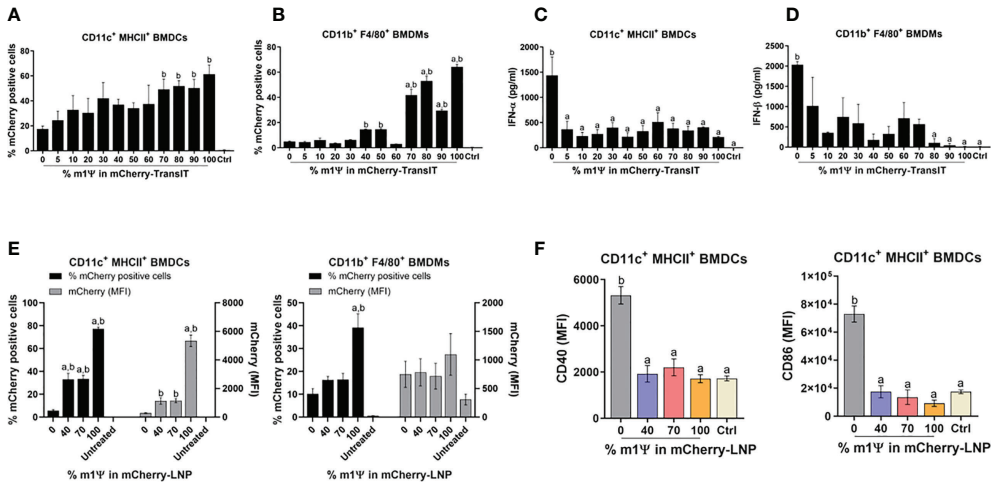

FIGURE 1
TransIT and LNP efficiently delivered mRNA to murine BMDCs and BMDMs *in vitro*. **(A–D)** mCherry-encoding mRNA modified with different % of m1Ψ (0.1 μg) were transfected into BMDCs and BMDMs using TransIT reagent. The frequencies of mCherry positive **(A)** BMDCs and **(B)** BMDMs were determined by flow cytometry at 48 hr after transfection. **(C)** The levels of IFN-α and **(D)** IFN-β released upon mRNA transfection from BMDCs and BMDMs, respectively were examined by ELISA. **(E)** mCherry-encoding mRNA modified with different % of m1Ψ (0.1 μg) were delivered into BMDCs and BMDMs using LNP. The frequencies of mCherry positive BMDCs (left) and BMDMs (right) and MFI of mCherry delivered by LNP were determined by flow cytometry. **(F)** MFI of CD40 (left) and CD86 (right) on BMDCs upon mRNA-LNP transfection was shown. The control were untranfected cells. The results are presented as the mean ± SEM of at least duplicate samples and experiments were performed at least two times. Statistical significance by one-way ANOVA with Bonferroni multiple comparisons test were indicated when $p < 0.05$ compared to the unmodified target antigen: a, or control (PBS): b.

40, 70, and 100% of m1ψ substituting conditions were selected for LNP encapsulation in subsequent experiments.

Similar to the results obtained by TransIT reagent, LNP formulated modified mRNA with 100% of m1ψ substitution resulted in a significantly higher percentages and median fluorescence intensity (MFI) of mCherry$^+$ cells than other conditions in both BMDCs and BMDMs with 77% and 39% of mCherry$^+$ cells, respectively (Figure 1E; Figures S1A, B). Although modified mRNA with 100% of m1ψ substitution showed efficient protein translation, this treatment did not significantly induce maturation of BMDCs. In contrast, cells transfected with unmodified mRNA significantly upregulated CD40 and CD86 expression, suggesting DC maturation (Figure 1F; Figure S1A).

For an *in vivo* delivery of mRNA, DCs and macrophages in draining lymph nodes (LN) (popliteal and inguinal LNs) and spleens were examined. Intramuscular administration (i.m.) of 10 μg mRNA-LNP with 100% of m1ψ substitution was efficiently taken up and translated into proteins by cDC1, cDC2 and macrophages in both LNs and spleens with the highest percentages of mCherry$^+$ cells observed after 48 hr (Figures 2A, B; Figure S1C). CD40 upregulation in LN cDC1 was equally observed in all types of mRNA, regardless of m1ψ modification that is higher than the untreated control (Figure 2C; Figure S1C). However, exposure to mRNA with 0 and 40% of m1ψ substitutions significantly enhanced CD40 expression in LN cDC2 and splenic cDC1 and cDC2, respectively (Figures 2C, D; Figure S1C). Taken together, these results indicated that modified mRNA with 100% m1ψ substitutions significantly improves translation efficiency and decreases innate immunogenicity. Although unmodified mRNA compromises the translation efficiency, it induces high levels of type I IFN and robust expression of costimulatory molecules in major APCs.

Immunization with OVA mRNA-LNP induces robust immune responses and activates OVA-specific cytotoxic effector T cells

To evaluate whether mRNA prepared with varying degrees of m1Ψ modification differentially induces antigen-specific CD8$^+$ T cell responses, mice were i.m. immunized with two doses of ovalbumin encoding mRNA (OVA-LNP) (10 μg/dose) or PBS with 4 days interval between the two doses (Figure 3A). Luciferase encoding mRNA (Luc-LNP) was used as unrelated antigen control. Immunization with OVA-LNP with unmodified mRNA or with 40% m1Ψ modification significantly increased serum IFN-α concentration at 6 hr post first and second

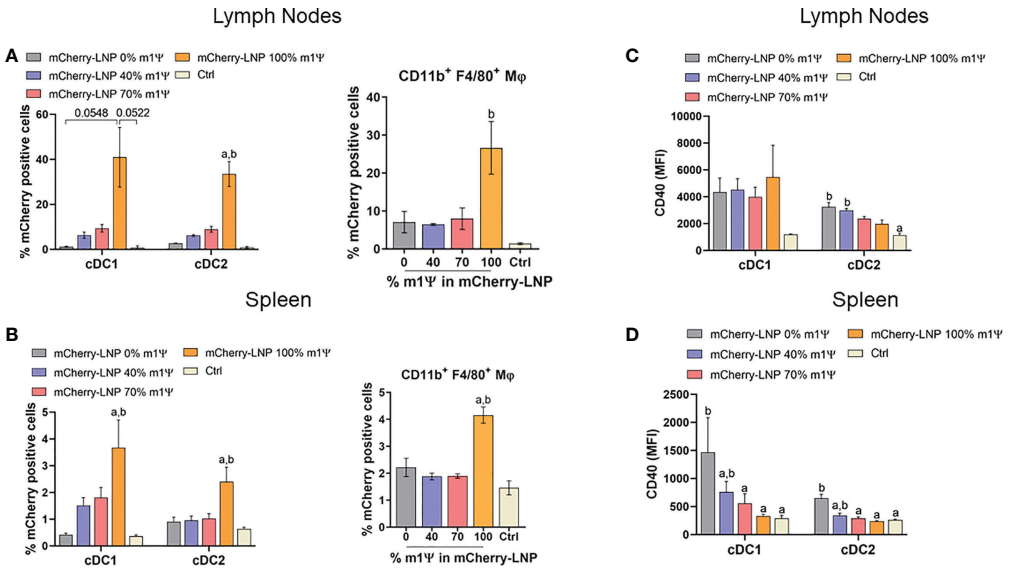

FIGURE 2
mRNA-LNP uptake by APCs in lymph nodes (LNs) and spleens *in vivo*. Mice were intramuscular injected with 10 μg of mCherry mRNA-LNP with 0, 40, 70, or 100% of m1Ψ modification and the control group received PBS. At 48 hr of mRNA administration, quantification of mCherry-positive cells in **(A)** LNs and **(B)** spleen of conventional type 1 (cDC1) and conventional type 2 (cDC2) dendritic cells (left), and MΦ (right) were determined. MFI of costimulatory molecule CD40 on cDC1 and cDC2 from **(C)** LNs and **(D)** spleen were shown. Statistical significance by one-way ANOVA with Bonferroni multiple comparisons test when $p < 0.05$ compared to the unmodified target antigen: a, or control (PBS): **(D)** cDC1 subset was defined as Dump$^-$ (B220$^-$ NK1.1$^-$ CD3$^-$ TER-119$^-$ CD19$^-$) CD11c$^+$ MHCII$^+$ XCR1$^+$. cDC2 subset was defined as Dump$^-$ (B220$^-$ NK1.1$^-$ CD3$^-$ TER-119$^-$ CD19$^-$) CD11c$^+$ MHCII$^+$ CD172a$^+$.

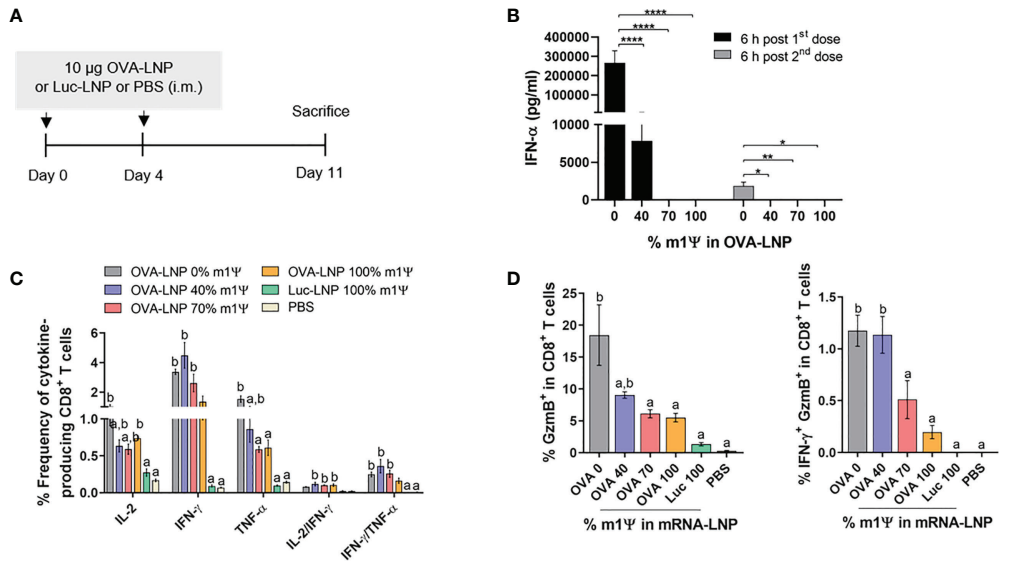

FIGURE 3
Immunization of mRNA-LNP elicits robust antigen-specific CD8$^+$ T cell responses. **(A)** Schematic representation of the immunization regimen (see methods for details). **(B)** IFN-α concentration in the serum 6 hr after the first (day0) and the second (day4) immunizations of OVA mRNA-LNP were detected by ELISA. **(C, D)** The frequencies of IL-2, IFNγ, TNFα and Granzyme B (GzmB) and IFN-γ/GzmB-producing CD8$^+$ T cells after 6 hr stimulation with $OVA_{257-264}$ (SIINFEKL) were measured by flow cytometry. The results are presented as the mean ± SEM, n = 4-5 biologically independent mice per group. Statistical significance: Statistical significance by one-way ANOVA with Bonferroni multiple comparisons test were indicated as (*)$p < 0.05$, (**)$p < 0.01$ and (****)$p < 0.0001$ or $p < 0.05$ compared to the unmodified target antigen: a, or control (PBS): b.

immunization, compared to the mRNA with m1Ψ modification of 70 and 100% (Figure 3B). After the second dose, the level of IFN-α induced by unmodified mRNA was much lower compared to that from the first dose but remained at detectable level.

Seven days after the second mRNA immunization, splenocytes were restimulated with CTL epitope SIINFEKL OVA peptide *in vitro*. The frequency of IL-2- and IFN-γ producing $CD8^+$ T cells increased in all groups of mice receiving OVA-LNP, regardless of the level of m1Ψ modification. On the other hand TNFα-producing $CD8^+$ T cells were higher in mice receiving OVA-LNP with m1Ψ modification of 0 and 40% than 70% or 100% modification (Figure 3C; Figure S1D). Significantly increased percentages of IL-2/IFN-γ-double producers were detected in the groups receiving OVA-LNP with m1Ψ substitution of 40, 70, and 100% (Figure 3C; Figure S1D). In addition, a significantly higher percentages of granzyme B and IFN-γ/granzyme B-producing $CD8^+$ T cells were observed in the group with OVA-LNP with m1Ψ modification of 0 and 40%, compared to those with 70 or 100% m1Ψ substitution (Figure 3D; Figure S1D). Taken together, these results demonstrated that administration of OVA-LNP robustly activates OVA-specific $CD8^+$ T cell responses, particularly unmodified mRNA effectively stimulates CTL responses.

Unmodified mRNA induces antitumor immunity and alters tumor-infiltrating immune cell profiles

To determine whether the immune responses induced by OVA-LNP is sufficient to control tumor growth, murine B16F0-OVA melanoma expressing OVA was used as a model. Mice were transplanted s.c. with B16F0-OVA at day 0 and i.m. immunized with two doses of OVA-LNP (10 μg/dose) with unmodified and m1Ψ modification of 100% mRNA or control Luc-LNP with m1Ψ modification of 100% or PBS on day 4 and 8 (Figure 4A). The vaccination schedule in our studies was based on previous reports on cancer vaccines by the Fotin-Mleczek et al. sponsored by CureVac (34) and Kranz et al. (30). The schedule was designed to prevent the typical post-expansion T-cell retraction phase and maintain high frequencies of antigen-specific T cells. All animals reached termination criteria without significant weight loss (Figure S2). Mice immunized with unmodified OVA-LNP survived until the end of the experimental period of 31 days while all mice in the PBS or Luc-LNP control group were dead (Figure 4B). For OVA-LNP with m1Ψ modification of 100%, half of the mice survived. The survival rates reflected the delay and significant decrease in tumor growth in unmodified OVA-LNP groups compared with the other groups (Figure 4C).

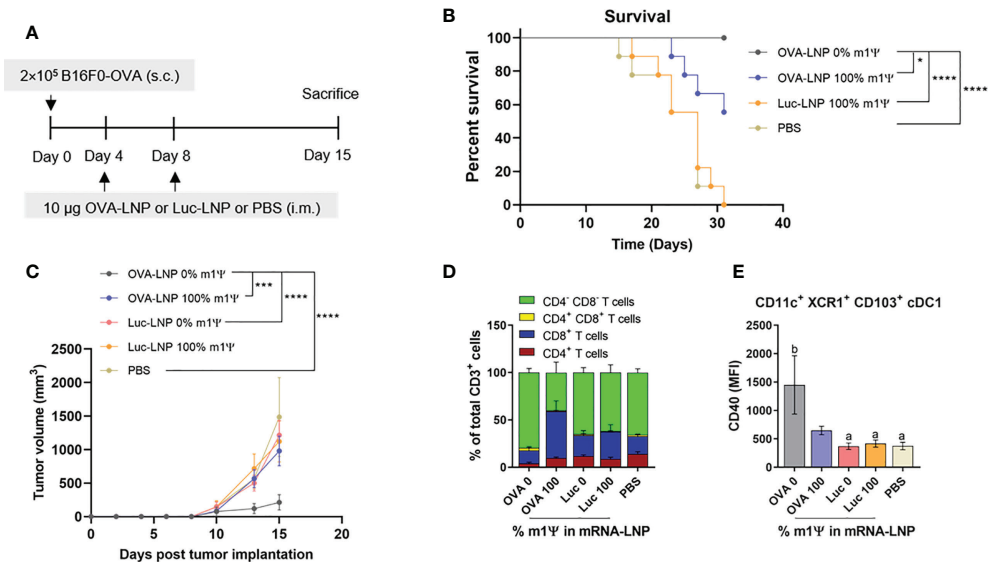

FIGURE 4
Intramuscular immunization of unmodified OVA-LNP inhibits tumor growth and prolongs survival. **(A)** Schematic representation of the immunization and tumor implantatioin schedule. **(B)** The percentages of survival mice was followed until day 31 after tumor implantation. Mice that reached the maximal allowed tumor size of 20 mm, or 400 mm^2 were euthanized and recorded as having tumor areas of 400 mm^2 (n = 9). **(C)** Tumor volume was shown during the 15 days after tumor implantation (n = 10). **(D)** Compositions of tumor-infiltrating T cells and **(E)** MFI of costimulatory molecule CD40 on cDC1 are shown (n = 6). The results are presented as the mean ± SEM. Statistical significance: (*)$p < 0.05$, (***)$p < 0.001$ and (****)$p < 0.0001$ by two-way ANOVA with Bonferroni multiple comparisons test. Survival curves were compared using log-rank (Mantel–Cox) test.

To monitor the impact of mRNA vaccine on tumor infiltrated immune cells, seven days after a boost, mice were sacrificed and the tumor infiltrated immune cells (T cells and DCs) were characterized. The majority of tumor-infiltrating $CD3^+$ T cell population in the unmodified OVA-LNP group were $CD4^-CD8^-$ T cells, while the group receiving OVA-LNP with m1Ψ modification of 100% had $CD8^+$ T cells as the major population (Figure 4D; Figure S3). We next characterized the intratumoral migratory cDC1 ($CD11c^+$ $XCR1^+$ $CD103^+$). In a group receiving unmodified OVA-LNP, a significant increase in CD40 level among cDC1 subset was observed (Figure 4E; Figure S3). This result strongly supports that unmodified mRNA induces more efficient DC activation that may augment the anti-tumor immunity and skews toward Th1 in the tumor microenvironment.

We next investigated the impact of OVA-LNP vaccination on phenotypes of immune cell population in the spleens on day 15 after tumor implantation and mRNA vaccine administration. Consistent with the strong anti-tumor phenotype, mice immunized with unmodified OVA-LNP or with m1Ψ modification of 100% showed significant expansion of effector $CD8^+$ T cells ($CD8^+$ $CD44^+$ $CD62L^-$). Within the memory $CD8^+$ T cell population ($CD8^+$ $CD44^+$ $CD62L^+$), mice receiving unmodified OVA-LNP showed relatively higher frequency of memory $CD8^+$ T cell population than mice receiving OVA-LNP with m1Ψ modification of 100% (Figure 5A; Figure S4). This relative increase in memory CD8 T cell expansion observed in unmodified OVA-LNP group may be due to the smaller percentage of effector subset. In addition, PD-1 exhaustion marker on T cells of immunized mice was investigated. There was a significant increase in PD-1^+ $CD8^+$ T cells in the group with OVA-LNP with m1Ψ modification of 100% whereas the PD-1^+ $CD4^+$ T cells increased in the unmodified OVA-LNP group (Figure 5B; Figure S4).

We also evaluated the induction of SIINFEKL-specific $CD8^+$ T cell responses. As shown in Figure 5C; Figure S4, both modified and unmodified OVA-LNP significantly induced higher frequencies of cytokine producing cells in SIINFEKL-specific $CD8^+$ T cells. More importantly, compared with the modified OVA-LNP group, unmodified OVA-LNP induced higher percentages of grazyme B^+ or IFN-γ/TNFα-double producers and granzyme B/IFN-γ-double producers in $CD8^+$ T cells (Figure 5D; Figure S4). This coordinated anti-tumor immunity induced by unmodified OVA-LNP reflects the delayed tumor growth and higher survival rate in tumor transplanted animals.

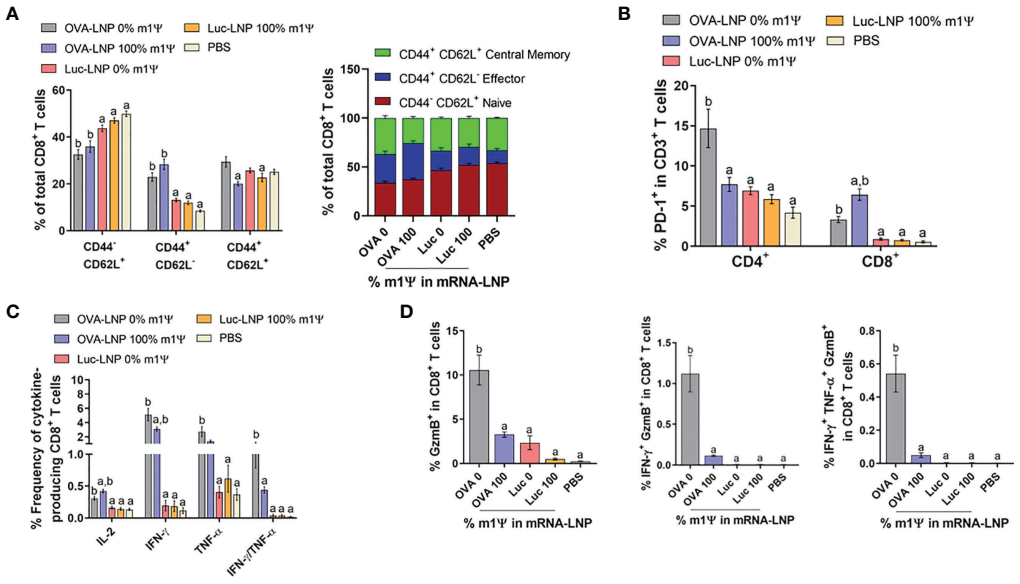

FIGURE 5
Immunization of unmodified OVA-LNP enhances the activation of antigen-specific CD8+ T cells. Mice were treated as described in Figure 4A and the splenocytes were re-stimulated for 6 h with $OVA_{257-264}$ (SIINFEKL) peptide. **(A)** The frequencies of naïve cells ($CD44^-CD62L^+$), effector cells ($CD44^+CD62L^-$), and memory cells ($CD44^+CD62L^+$) in $CD3^+$ $CD8^+$ T cell subsets **(B)** the frequencies of PD-1+ $CD4^+$ and $CD8^+$ T cells and **(C)** the frequencies of cytokines-producing $CD8^+$ T cells are shown. **(D)** The $OVA_{257-264}$-specifc responses were determined and the percentages of $CD8^+$ T cells producing GzmB, IFN-γ/GzmB, or IFN-γ/TNF-α/GzmB are shown. The results are presented as the mean ± SEM of biologically independent mice (n=7) per group. Statistical significance by one-way ANOVA with Bonferroni multiple comparisons test when $p < 0.05$ compared to the unmodified target antigen: a, control (PBS): b.

Type I interferon (IFN-I) is crucial for anti-tumor effect induced by unmodified mRNA vaccine

In order to gain an insight how unmodified mRNA induces robust anti-tumor immunity, we evaluated the role of IFN-I in the therapeutic efficacy of mRNA vaccine. Mice were implanted with B16F0-OVA on day 0, followed by intraperitoneally administration of anti-IFNAR1 antibody or isotype control (400 μg per mouse) on day 4 and day 8. One hour after the administration of anti-IFNAR1 antibody or isotype control, mice were i.m. immunized with unmodified OVA-LNP (Figure 6A). All animals showed no significant weight loss (Figure S5). When the tumor was allowed to grow until day 42, anti-IFNAR1 antibody treatment significantly abrogated the tumor growth control effect observed with the unmodified OVA-LNP in the isotype control group (Figure 6B). Mechanistically, anti-IFNAR1 antibody treatment reduced the expansion of splenic $CD8^+$ T cell (Figure 6C) and antigen (OVA) specific IFN-γ-producing T cells (Figure 6D; Figure S6), compared with the isotype control treated group. Finally, we determined the phenotypes of tumor-infiltrating immune cells on day 42. Mice receiving anti-IFNAR1 antibody showed a significant increase in PD-1 expressing tumor-infiltrated $CD4^+$ and $CD8^+$ T cells (Figure 6E) and a significant increase in tumor-infiltrating M2-like macrophages ($CD206^+$ $F4/80^+$), compared to the isotype control treated group (Figure 6F). Overall, these results strongly indicated the crucial role of IFN-I signaling in unmodified mRNA-LNP-mediated anti-tumor immunity.

Unmodified OVA-LNP suppresses metastasis to lung in a melanoma model

Next, we tested whether unmodified OVA-LNP induces an immune response against lung metastasis in a melanoma model. B16F0-OVA cells were injected intravenously to establish lung metastasis. On day 4 and 8 after tumor cell injection, mice were i.m. immunized with two doses of OVA-LNP (10 μg/dose) with unmodified or m1Ψ modification of 100% or with unrelated antigen encoding mRNA-LNP (PR8HA-LNP) or PBS (Figure 7A). All animals reached endpoint without significant weight loss (Figure S7). On day 18, lung metastasis were observed and the number of lung nodules were counted (Figures 7B, C). The results showed that only unmodified OVA-LNP clearly suppressed nodule formation. In contrast, nucleoside modified OVA-LNP (100% m1Ψ modification) failed to control lung metastasis with comparable numbers of lung

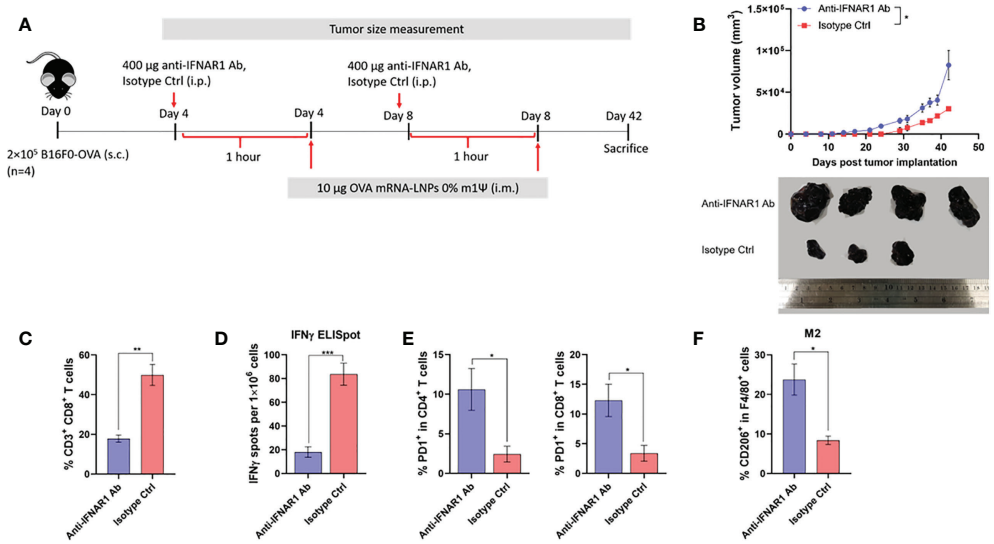

FIGURE 6
Type I IFN signaling promotes antitumor effect and modulated immune cell profile. **(A)** Scheme of immunization regimen and IFNAR1 antibody or isotype control treatment. See details in methods. **(B)** The tumor volume (top panel) and the representative tumor mass (lower panel) harvested 42 days after the tumor implantation from mice treated with anti-IFNAR1 antibody or isotype control followed by immunization with unmodified OVA-LNP. **(C)** The frequency of splenic $CD8^+$ T cells was examined by flow cytometry. **(D)** ELISpot of IFN-γ producing cells among splenocytes after 48 hr of *ex vivo* re-stimulation with OVA on day 42 after tumor implantation and mRNA vaccine treatments is shown. **(E)** The frequency of $PD\text{-}1^+$ cells among tumor infiltrated $CD4^+$ (left) and $CD8^+$ (right) T cells were examined by flow cytometry. **(F)** The frequency of tumor infiltrated $CD206^+$ macrophages was determined by flow cytometry. The results are presented as the mean ± SEM, $n = 4$ biologically independent mice per group. Statistical significance: (*)$p < 0.05$, (**)$p < 0.01$, (***)$p < 0.001$ by unpaired two-tailed Student's t test.

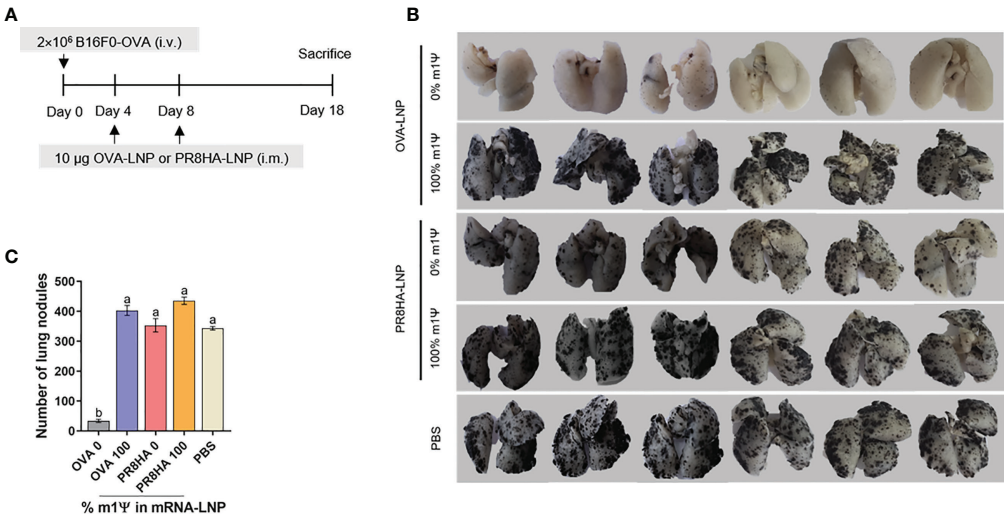

FIGURE 7
Immunization of unmodified mRNA-LNP inhibits lung metastasis of B16F0-OVA melanoma. **(A)** Schematic immunization schedule for melanoma metastatic model. See methods for details. **(B)** The lungs were observed and **(C)** the metastatic nodules on the surface of the lungs were counted. The results are presented as the mean ± SEM of biologically independent mice (n = 6) per group. Statistical significance by one-way ANOVA with Bonferroni multiple comparisons test when $p < 0.05$ compared to the unmodified target antigen: a, control: b.

nodules as the PBS control or unrelated antigen (PR8HA-LNP). This result highlights the positive effect of antigen speicific unmodified mRNA-LNP on robust anti-tumor immunity including metastasis.

Neoantigens (Pbk-Actn4) encoding mRNA-LNP is immunogenic

Based on the previous reports on mutanomes of B16F10 tumor (25, 26), we selected two of the somatic mutations of *Pbk* and *Actn4* as neoantigens to test in our study. These mutated epitopes of *Pbk* and *Actn4* were recognized and reacted to by $CD8^+$ or $CD4^+$ T cells, respectively, upon RNA monotope vaccinations and showed good MHC class I binding scores ('low score' 0.1 and 0.2, respectively) (25). These selected neoepitopes were linked with 10-mer non-immunogenic glycine/serine linkers and used as a neoantigen vaccine. To evaluate whether *Pbk-Actn4* encoding mRNA vaccines induce antigen-specific $CD4^+$ and $CD8^+$ T cell responses, mice were i.m. immunized with two doses of 10 μg/dose neoantigens (Neo-LNP) or control mCherry (mCherry-LNP) encoding mRNAs or PBS on day 0 and boosted with the same dose on day 4 (Figure S8A). Seven days after the boost, splenocytes were restimulated with overlapping peptide pools of *Pbk* and *Actn4*. Increased percentages of both $CD4^+$ and $CD8^+$ T cells producing IL-2, IFN-γ and TNF-α in the group receiving unmodified Neo-LNP were also observed (Figures S8B, C, S9). In addition, a significant increase in the frequencies of granzyme B and IFN-γ/granzyme B-producing $CD8^+$ T cell were observed only in unmodified Neo-LNP (Figures S8D, S10). Taken together, epitope-specific $CD4^+$ and $CD8^+$ T cell responses were significantly induced upon immunization with unmodified Neo-LNP at a higher level, compared to that from Neo-LNP with m1Ψ modification of 100%.

Neoepitope-specific immune responses induced by unmodified mRNA control B16F10 melanoma growth

To examine the anti-tumor efficacy of Neo-LNP in B16F10 melanoma model, mice were i.m. immunized with two doses of Neo-LNP (10 μg/dose) or control mCherry-LNP (10 μg/dose) with unmodified and m1Ψ modification of 100% or PBS on day 4 and 8 after tumor implantation (Figure 8A). Repeated vaccination with the unmodified Neo-LNP in B16F10 tumour-bearing mice increased splenic antigen-specific granzyme B^+ $CD8^+$ T cells (Figure 8B; Figure S8). Consistent with the robust anti-neoantigen response, tumour growth was profoundly delayed and size/burden significantly decreased in unmodified Neo-LNP vaccinated group (Figure 8C). Mice given unmodified Neo-LNP showed a significant increase in $CD69^+$ tumor-infiltrating T cells (Figure 8D; Figure S9) and the expression levels of CD40 in cDC1 ($CD11c^+$ $XCR1^+$) (Figure 8E; Figure S9). One third of the Neo-LNP treated mice survived until day 35, while all mice in the control group died by day 29 (Figure 8F). All animals reached endpoint termination without significant

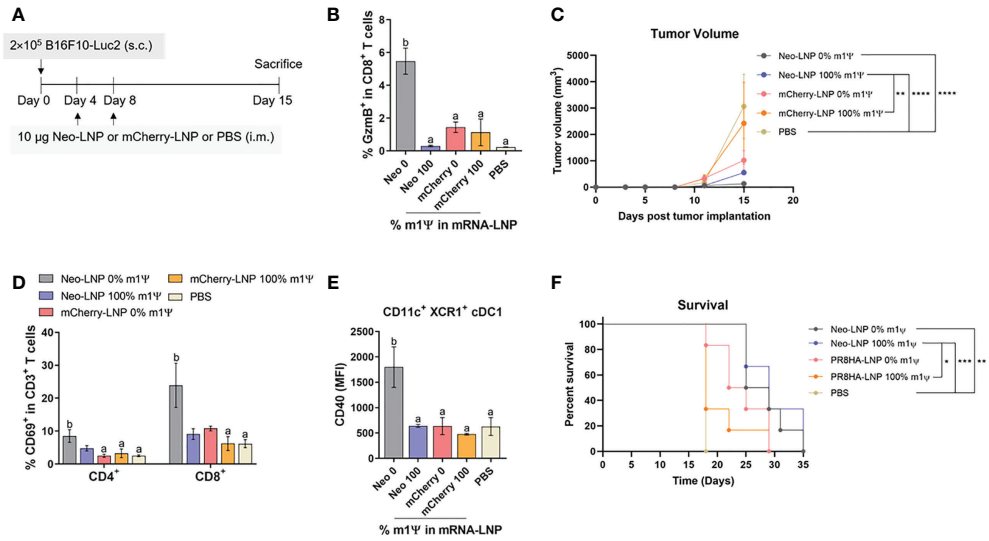

FIGURE 8
Neoantigens (Pbk-Actn4) encoding mRNA-LNP inhibits tumor growth *in vivo* and prolongs survival. **(A)** Schematic representation of the immunization regimen to test the anti-tumor efficacy of neoantigen encoding mRNA-LNP. See methods for details. **(B)** The frequency of GzmB-producing splenic $CD8^+$ T cells on $CD3^+$ $CD8^+$ T cell subsets was determined by flow cytometry. **(C)** Tumor volume was measured (n = 10) **(D)** The frequencies of $CD69^+$ T cells among tumor infiltrated $CD4^+$ and $CD8^+$ T cells are shown. **(E)** The MFI of costimulatory molecule CD40 on tumor-infiltrating cDC1 is shown (n = 4). **(F)** The percentage of survival was followed until day 35 (n = 6). GzmB, granzyme; cDC1, conventional type 1 dendritic cell. **(B)** The results are presented as the mean ± SEM. Statistical significance: (*)$p < 0.05$, (**)$p < 0.01$, (***)$p < 0.001$ and (****)$p < 0.0001$ by two-way ANOVA with Bonferroni multiple comparisons test. Survival curves were compared using log-rank (Mantel–Cox) test.

weight loss (Figure S10). Taken together, we confirmed that unmodified mRNA encoding tumor neoantigen formulated in LNP induced a strong anti-tumor immune response that retarded tumor growth and partially prolonged survival of tumor-bearing mice.

Discussion

Recognition of uridine bases by innate immune sensors subsequently triggers cascades of innate immune responses that dictate the adaptive immune phenotypes. Substitution of uridine with m1Ψ in mRNA significantly improves the translation efficiency and decreases innate immunogenicity (20). Antitumor innate immune signals, particularly type I IFNs, which are the main cytokines secreted from DCs upon mRNA transfection (35) play an important role in antigen presentation and T cell differentiation into cytolytic effector cells. Herein, we addressed the impact of different m1Ψ percentages incorporated in mRNA on the immunogenicity and anti-tumor effects of the mRNA-LNP platform in B16 melanoma models using model antigen OVA and neoantigens.

cDC1 are critical for antigen cross-presentation required to prime $CD8^+$ T cells for optimal anti-tumor immunity and priming of $CD4^+$ T cells at early stages, partly because cDC1 provides antigen transportation to lymph nodes for processing by cDC2 (36). CD40 signaling in cDC1 is required for tumor rejection by playing a key role in augmenting the proliferation of antigen-specific $CD8^+$ T cells (36). Engagement of CD40 with its ligand induces recruitment of TNF receptor-associated factor family of proteins (TRAFs) and initiates signaling cascades that activate genes involved in cytokine production, as well as upregulation of co-stimulatory molecules such as CD80 and CD86 (37). We demonstrated that the maturation of cDC1 and cDC2 upon delivery of unmodified and 40% modification with m1Ψ mRNA/LNP was evident compared with mRNA with 100% modification with m1Ψ. Intratumoral cDC1 also increased CD40 expression with the unmodified mRNA-LNP (Figure 4E). While unmodified mRNA/LNP compromises the translation efficiency of mRNA into protein antigen, its superior impact on DC maturation is beneficial for anti-tumor immunity.

Recent study identified the intrinsic adjuvant activity of the LNP itself. When used in mRNA and protein subunit vaccines, LNP exerts potent stimulatory activity against T follicular helper cell and the immune induction was superior to what induced by AddaVax formulated vaccine. Adjuvant activity of the LNP critically relies on IL-6 and its constituent ionizable lipid. Remarkably, potent immune responses from a single immunization of LNP loaded non-inflammatory nucleoside-modified mRNA was related to LNP adjuvanticity (38). Unmodified mRNA itself provides adjuvant activity through binding and activation of the innate immune sensors, mainly

TLRs 3, 7, and 8 (39). In our study, we did not distinguish adjuvant activity of mRNA from LNP and the impact on anti-tumor responses may derive from LNP and/or mRNA.

Unmodified mRNA-LNP administration is associated with large amounts of systemic IFN-I at 6 h after immunization. Surprisingly, the level of IFN-I dramatically drops after the second dose of immunization which is likely the effect of unmodified mRNA. It is possible that repeated exposure to unmodified mRNA epigenetically enforces innate immune tolerance where the cells are incapable of activating certain inflammatory gene transcription (40).

The prominent therapeutic efficacy of unmodified mRNA is possibly due to activation of endosomal toll-like receptor 7/8 (TLR7/8) and subsequently causes pro-inflammatory cytokine secretion *via* MyD88-dependent IRF-5 phosphorylation (41). IRF-5 is critically involved in M1- macrophage polarization (42), which possesses phagocytic capacity, and the ability to secrete reactive nitrogen and oxygen species and pro-inflammatory cytokines such as IL-6, IL-12, IL-23 and TNF-α, which in turn promote $CD8^+$ T cell and NK cell cytotoxicity. In addition, M1 macrophages secrete CXCL9, CXCL10 and CXCL15 chemokines upon STAT1 signaling, which recruit cytotoxic T lymphocytes (CTLs) to the tumor (43). Furthermore, the decrease of M2-like macrophages favors lung metastasis inhibition due to a lack of tumor-angiogenesis factors such as vascular endothelial growth factor (VEGF), epidermal growth factor (EGF) and fibroblast growth factor (FGF), and matrix metalloproteases (MMP-2 and MMP-9) which promote tumor angiogenesis, and metastasis (44).

Better tumor control with unmodified mRNA/LNP is associated with the presence of mature tumor-infiltrating migratory cDC1. The presence of mature cDC1 in tumor may lead to more efficient antigen presentation and cross-presentation of tumor antigens and subsequent augment antigen-specific T cell immunity (45) as shown in relevant results of antigen-specific effector CD8+ T cell ($CD44^+CD62L^-$) expansion and polyfunctional cytokine secretion after restimulated splenocytes with the $OVA_{257-264}$ (SIINFEKL) peptide. Interestingly, we found that a substantial tumor infiltrated T cell subset ($CD3^+$) in unmodified mRNA-LNP group is $CD4^-CD8^-$ double negative (DN) T cells (Figure 4D). Both TCRαβ T cells and TCRγδ T cells contain a small subset of DN T cells, suggesting both innate and adaptive functions. Althought the roles of these cells in tumors are still controversial, the use of DN T cells for cancer immunotherpy against blood and solid tumor were reported (46). Our results indicated that DN T cells may play a crucial role in anti-tumor immunity raised by mRNA vaccines. Therefore, characterization of the DN T cells may provide insight into the anti-tumor immunity induced by mRNA-LNP.

In the previous study by Kranz et al., a systemic immunization with three doses (40 μg/dose) of mRNA encoding OVA cleared B16-OVA lung metastasis with no tumor at 20 days after the last immunization. Their OVA mRNA construct encoded for the $H\text{-}2K^b$-restricted immunodominant epitope $OVA_{257-264}$ and the lipid formulation contained DOTAP and DOPE with the mean diameter of mRNA-LNP was 200 nm (30). In our study, using two doses (10 μg/dose) of mRNA encoding whole OVA protein, we observed a similar anti-metastatic effect. Although unmodified mRNA was used in the current work and that by Kranz et al., differences in the use of whole protein rather than peptide antigens, the LNP formulation and its size may result in the modest differences observed between the two reports. LNP used in our study is the proprietary to Acuitas Therapeutics, contains a proprietary ionizable cationic lipid, cholesterol, DSPC, and a PEG-lipid with a mean diameter of 80 nm (38).

In the tumor microenvironment, immunosuppression and tumor evasion strategies cause an inability of the immune cells to detect and eliminate with subsequent exhaustion (47). Generally, PD-1 expression on cell surface of activated T cells is induced after T cell receptor (TCR) activation (48). Ligation of PD-1 with its ligands programmed death-ligand 1 or 2 (PD-L1 or PD-L2) induces tyrosine phosphorylation of the PD-1 cytoplasmic domain by phosphorylating kinase Lck and subsequent recruitment of cytosolic tyrosine phosphatase SHP-2 and PD-1-associated SHP-2 preferentially dephosphorylates CD28 and suppresses CD28 costimulatory signaling leading to restrained effector T cell function (49–51). In our studies, we consistenly observed higher frequency of $PD\text{-}1^+$ cells in tumor infiltrating $CD4^+$ and $CD8^+$ T cells when IFNAR1 was blocked. This result may imply that unmodified mRNA may help alleviate T cell exhaustion *via* IFN-I that allows anti-tumor T cells to be fully functional. Consistent with this observation, more M2-like tumor-associated macrophages were observed when IFN-I is blocked in the mRNA-LNP vaccinated group.

Accumulating data suggest that IFN-I strengthens antitumor T cell immunity by acting either indirectly or directly on T cells. IFN-I indirectly influences on T cell priming by upregulation of co-stimulatory molecules on APCs and directly acts as activating stimuli to prevent the abortive T-cell responses. Furthermore, IFN-I also exhibits direct stimulatory effect on immune cells by promoting IFN-γ secretion. Previous study showed that DC-specific *Ifnar*$^{-/-}$ mice were unble to reject highly immunogenic tumor cells due to the defects in antigen cross-presentation to $CD8^+$ T cells. This evidence strongly shows that IFN-I can act through DCs to promote T cell immunity (52). Taken together, we provide strong evidence that IFN-I, directly or indirectly, through plays an indispensable role in inducing anti-tumor response by mRNA vaccine.

Although $CD8^+$ T cells are known to play a pivotal role in antitumor immunity, $CD4^+$ T cells also contribute to direct tumor killing besides their supporting role as cytokine producers. Previous study reported the observation of a cytotoxic subset of $CD4^+$ T cells (CD4 CTLs). $CD4^+$ CTLs are characterized by their cytotoxic functions to secrete granzyme B and perforin, two major tools to directly kill the target cells. CD4

CTL recognizes target cells *via* peptide-MHC II complex on APCs (53). Upon transferring of naive tumor reactive $CD4^+$ T cells into lymphopenic recipients, substantial T cell expansion and differentiation were observed. Tumor regression was dependent on class II-restricted recognition of tumors by tumor-reactive $CD4^+$ CTLs which developed cytotoxic activity and kill tumor (54).

For mRNA vaccine, modifying the structural elements of mRNA including the 5′ cap, 5′-and 3′-untranslated regions, the coding region, and polyadenylation tail help improved the intracellular stability of mRNA (55). Replacing of uridine by pseudouridine into mRNA gives superior nonimmunogenic mRNA with increased translational capacity and biological stability (20). Furthermore, lyophilization of modified mRNA-LNP provides long-term stability at room temperature (56). Whether unmodified mRNA-LNP shows similarly enhanced stability upon lyophilization is not known.

Finally, more relevant to real cancer settings with non-dominant antigens and tumor heterogeneity, Pbk-Actn4 somatic mutations of B16F10 tumor were selected and linked together as target neoantigens in mRNA-LNP vaccines. We observed less robust, but significant tumor growth retardation effect with the neoantigen vaccine compared to the OVA model. Additional neoatigens formulated in the mRNA vaccine may help improve the anti-tumor response of mRNA vaccines using neoantigens, such as demonstrated by Kreiter et al. (25). Taken together, we provide strong evidence for the anti-tumor immune response by unmodified mRNA vaccines encoding dominant and neoantigens.

Data availability statement

The original contributions presented in the study are included in the article/Supplementary Material. Further inquiries can be directed to the corresponding author.

Ethics statement

The animal study was reviewed and approved by The institutional animal care and use committee (IACUC) at the University of Pennsylvania and Chulalongkorn University.

Author contributions

CS, M-GA, DW and TP: study conception and design, CS, M-GA: data collection, CS, M-GA and TP: analysis and interpretation of results, PL and YT: reagent preparation and analysis, CS and TP: draft manuscript preparation. EP and TP: grant funding acquisition. All authors contributed to the article and approved the submitted version.

Funding

This study was supported in part by the Chulaongkorn Academic Advancement into its Second Century (CUAASC) Project, Ratchadaphiseksomphot Endowment Fund, by the National Research Council of Thailand and by the National Science, Research and Innovation Fund (NSRF) via Program Management Unit for Human Resources amp; Institutional Development, Research and Innovation (PMU-B) Grant No. B16F640117. CS received a scholarship from Science Achievement Scholarship of Thailand (SAST) and also The 90th Anniversary of Chulalongkorn University Fund (Ratchadaphiseksomphot Endowment Fund).

Conflict of interest

PL and YT are employees of Acuitas Therapeutics, a company involved in the development of mRNA-LNP therapeutics. YT, DW, and M-GA are named on patents that describe lipid nanoparticles for delivery of nucleic acid therapeutics, including mRNA and the use of modified mRNA in lipid nanoparticles as a vaccine platform.

The remaining authors declare that the research was conducted in the absence of any commercial or financial relationships that could be construed as a potential conflict of interest.

Publisher's note

Supplementary material

The Supplementary Material for this article can be found online at: https://www.frontiersin.org/articles/10.3389/fimmu.2022.983000/full#supplementary-material

SUPPLEMENTARY FIGURE 1
Flow gating strategies. **(A)** Representative flow gating strategy of translation efficiency of mRNA-LNP and BMDC maturation for and 1f is shown. **(B)** Representative flow gating strategy of translation efficiency of mRNA-LNP in BMDM for is shown. **(C)** Representative flow gating strategy of translation efficiency of mRNA-LNP and APC maturation in lymphoid organs for is shown. **(D)** Representative flow gating strategies of antigen-specific splenic $CD8^+$ T cell response induced by mRNA-LNP for are shown.

SUPPLEMENTARY FIGURE 2
Effect of immunization of OVA-LNP on body weight changes in tumor bearing mice. Percent of body weight changes of B16F0-OVA tumor-bearing mice which received OVA mRNA-LNP is shown.

SUPPLEMENTARY FIGURE 3
Flow gating strategies. Representative flow gating strategies of tumor-infiltrating immune cell profiles for are shown.

SUPPLEMENTARY FIGURE 4
Flow gating strategies. Representative flow gating strategies of antigen-specific CD8+ T cells for are shown.

SUPPLEMENTARY FIGURE 5
Effect of immunization of OVA-LNP in tumor-bearing mice in the presence of IFN-I blocking on body weight changes. Percent of body weight changes of B16F0-OVA tumor-bearing mice that were immunized with OVA mRNA-LNP in the absence or presence of type I IFN neutralizing antibody is shown.

SUPPLEMENTARY FIGURE 6
ELISpot for IFN-γ in splenic T cells receiving mRNA-LNP in the presence of IFN-I blocking. Representative IFN-γ ELISpot of OVA-specific splenic T cell response is shown.

SUPPLEMENTARY FIGURE 7
Effect of immunization of OVA-LNP on weight loss in a melanoma metastasis model. Percent of body weight changes of mice implanted with B16F0-OVA tumor for lung metastasis and OVA mRNA-LNP is shown.

SUPPLEMENTARY FIGURE 8
Immunization of neoantigens (Pbk-Actn4) encoding mRNA-LNP elicits robust antigen-specific T cell responses. **(A)** Schematic representation of the immunization regimen. On days 0 and 4, mice were intramuscularly immunized with 10 μg of Neo-LNP constituting 0, or 100% of m1Ψ. Mice were treated with mCherry-LNP or PBS as controls. Mice were sacrificed on day 11 (7 days after the boost) and spleens were collected. Frequencies of cytokines-producing **(B)** $CD4^+$ and **(C)** $CD8^+$ T cells on $CD3^+$ T cell subsets determined by flow cytometry after 6 h stimulation with pool of Pbk and Actn4 peptides at 7 days post-boost. **(D)** Frequencies of GzmB (left) and IFN-γ/GzmB (right)-producing $CD8^+$ T cells on $CD3^+$ $CD8^+$ T cell subsets were determined by flow cytometry. GzmB, granzyme B. Each column are represented as the mean ± SEM, n = 4 biologically independent mice per group. Statistical significance by one-way ANOVA with Bonferroni multiple comparisons test when $p < 0.05$ compared to the unmodified target antigen: a, control (PBS): b.

SUPPLEMENTARY FIGURE 9
Flow gating strategies. Representative flow gating strategies of tumor-infiltrating immune cell profiles for are shown.

SUPPLEMENTARY FIGURE 10
Flow gating strategies. Representative flow gating strategies of tumor-infiltrating immune cell profiles for are shown.

SUPPLEMENTARY FIGURE 11
Effect of immunization of Neo-LNP on body weight changes in tumor bearing mice. Percent of body weight changes of B16F10-Luc2 tumor-bearing mice which was immunized with Neo mRNA-LNP is shown. Each dot are represented as the mean ± SEM, n = 4-9 biologically independent mice per group.

SUPPLEMENTARY TABLE 1
List of antibodies.

References

1. Wang RF, Wang HY. Immune targets and neoantigens for cancer immunotherapy and precision medicine. *Cell Res* (2017) 27(1):11–37. doi: 10.1038/cr.2016.155

2. Li W, Joshi MD, Singhania S, Ramsey KH, Murthy AK. Peptide vaccine: Progress and challenges. *Vaccines (Basel)* (2014) 2(3):515–36. doi: 10.3390/vaccines2030515

3. Zhang L, Huang Y, Lindstrom AR, Lin TY, Lam KS, Li Y. Peptide-based materials for cancer immunotherapy. *Theranostics* (2019) 9(25):7807–25. doi: 10.7150/thno.37194

4. Nelde A, Rammensee HG, Walz JS. The peptide vaccine of the future. *Mol Cell Proteom* (2021) 20:100022. doi: 10.1074/mcp.R120.002309

5. Lopes A, Vandermeulen G, Preat V. Cancer DNA vaccines: current preclinical and clinical developments and future perspectives. *J Exp Clin Cancer Res* (2019) 38(1):146. doi: 10.1186/s13046-019-1154-7

6. Sobol I, Thompson RH, Dong H, Krco C, Kwon ED. Immunotherapy in prostate cancer. *Curr Urol Rep* (2015) 16(6):34. doi: 10.1007/s11934-015-0509-7

7. Kantoff PW, Schuetz TJ, Blumenstein BA, Glode LM, Bilhartz DL, Wyand M, et al. Overall survival analysis of a phase II randomized controlled trial of a poxviral-based PSA-targeted immunotherapy in metastatic castration-resistant prostate cancer. *J Clin Oncol* (2010) 28(7):1099–105. doi: 10.1200/JCO.2009.25.0597

8. Springett GM. Novel pancreatic cancer vaccines could unleash the army within. *Cancer Control* (2014) 21(3):242–6. doi: 10.1177/107327481402100311

9. Bidram M, Zhao Y, Shebardina NG, Baldin AV, Bazhin AV, Ganjalikhany MR, et al. mRNA-based cancer vaccines: A therapeutic strategy for the treatment of melanoma patients. *Vaccines (Basel)* (2021) 9(10):1060. doi: 10.3390/vaccines9101060

10. Sahin U, Derhovanessian E, Miller M, Kloke BP, Simon P, Lower M, et al. Personalized RNA mutanome vaccines mobilize poly-specific therapeutic immunity against cancer. *Nature* (2017) 547(7662):222–6. doi: 10.1038/nature23003

11. Verbeke R, Lentacker I, De Smedt SC, Dewitte H. The dawn of mRNA vaccines: The COVID-19 case. *J Control Release* (2021) 333:511–20. doi: 10.1016/j.jconrel.2021.03.043

12. Shyu AB, Wilkinson MF, van Hoof A. Messenger RNA regulation: To translate or to degrade. *EMBO J* (2008) 27(3):471–81. doi: 10.1038/sj.emboj.7601977

13. Slevin MK, Meaux S, Welch JD, Bigler R, Miliani de Marval PL, Su W, et al. Deep sequencing shows multiple oligouridylations are required for 3' to 5' degradation of histone mRNAs on polyribosomes. *Mol Cell* (2014) 53(6):1020–30. doi: 10.1016/j.molcel.2014.02.027

14. Snell LM, McGaha TL, Brooks DG. Type I interferon in chronic virus infection and cancer. *Trends Immunol* (2017) 38(8):542–57. doi: 10.1016/j.it.2017.05.005

15. Bettinger T, Carlisle RC, Read ML, Ogris M, Seymour LW. Peptide-mediated RNA delivery: A novel approach for enhanced transfection of primary and post-mitotic cells. *Nucleic Acids Res* (2001) 29(18):3882–91. doi: 10.1093/nar/29.18.3882

16. Edwards DK, Jasny E, Yoon H, Horscroft N, Schanen B, Geter T, et al. Adjuvant effects of a sequence-engineered mRNA vaccine: Translational profiling demonstrates similar human and murine innate response. *J Transl Med* (2017) 15(1):1. doi: 10.1186/s12967-016-1111-6

17. Pardi N, Hogan MJ, Porter FW, Weissman D. mRNA vaccines - a new era in vaccinology. *Nat Rev Drug Discovery* (2018) 17(4):261–79. doi: 10.1038/nrd.2017.243

18. Vlatkovic I. Non-immunotherapy application of LNP-mRNA: Maximizing efficacy and safety. *Biomedicines* (2021) 9(5):530. doi: 10.3390/biomedicines9050530

19. Andries O, Mc Cafferty S, De Smedt SC, Weiss R, Sanders NN, Kitada T. N (1)-methylpseudouridine-incorporated mRNA outperforms pseudouridine-incorporated mRNA by providing enhanced protein expression and reduced immunogenicity in mammalian cell lines and mice. *J Control Release* (2015) 217:337–44. doi: 10.1016/j.jconrel.2015.08.051

20. Kariko K, Muramatsu H, Welsh FA, Ludwig J, Kato H, Akira S, et al. Incorporation of pseudouridine into mRNA yields superior nonimmunogenic vector with increased translational capacity and biological stability. *Mol Ther* (2008) 16(11):1833–40. doi: 10.1038/mt.2008.200

21. Anderson BR, Muramatsu H, Nallagatla SR, Bevilacqua PC, Sansing LH, Weissman D, et al. Incorporation of pseudouridine into mRNA enhances translation by diminishing PKR activation. *Nucleic Acids Res* (2010) 38 (17):5884–92. doi: 10.1093/nar/gkq347

22. Thess A, Grund S, Mui BL, Hope MJ, Baumhof P, Fotin-Mleczek M, et al. Sequence-engineered mRNA without chemical nucleoside modifications enables an effective protein therapy in Large animals. *Mol Ther* (2015) 23(9):1456–64. doi: 10.1038/mt.2015.103

23. Yang F, Kim DK, Nakagawa H, Hayashi S, Imoto S, Stein L, et al. Quantifying immune-based counterselection of somatic mutations. *PloS Genet* (2019) 15(7):e1008227. doi: 10.1371/journal.pgen.1008227

24. Vormehr M, Schrors B, Boegel S, Lower M, Tureci O, Sahin U. Mutanome engineered RNA immunotherapy: Towards patient-centered tumor vaccination. *J Immunol Res* (2015) 2015:595363. doi: 10.1155/2015/595363

25. Kreiter S, Vormehr M, van de Roemer N, Diken M, Lower M, Diekmann J, et al. Mutant MHC class II epitopes drive therapeutic immune responses to cancer. *Nature* (2015) 520(7549):692–6. doi: 10.1038/nature14426

26. Castle JC, Kreiter S, Diekmann J, Lower M, van de Roemer N, de Graaf J, et al. Exploiting the mutanome for tumor vaccination. *Cancer Res* (2012) 72 (5):1081–91. doi: 10.1158/0008-5472.CAN-11-3722

27. Freyn AW, Ramos da Silva J, Rosado VC, Bliss CM, Pine M, Mui BL, et al. A multi-targeting, nucleoside-modified mRNA influenza virus vaccine provides broad protection in mice. *Mol Ther* (2020) 28(7):1569–84. doi: 10.1016/j.ymthe.2020.04.018

28. Baiersdorfer M, Boros G, Muramatsu H, Mahiny A, Vlatkovic I, Sahin U, et al. A facile method for the removal of dsRNA contaminant from *In vitro*-transcribed mRNA. *Mol Ther Nucleic Acids* (2019) 15:26–35. doi: 10.1016/j.omtn.2019.02.018

29. Pardi N, Tuyishime S, Muramatsu H, Kariko K, Mui BL, Tam YK, et al. Expression kinetics of nucleoside-modified mRNA delivered in lipid nanoparticles to mice by various routes. *J Control Release* (2015) 217:345–51. doi: 10.1016/j.jconrel.2015.08.007

30. Kranz LM, Diken M, Haas H, Kreiter S, Loquai C, Reuter KC, et al. Systemic RNA delivery to dendritic cells exploits antiviral defence for cancer immunotherapy. *Nature* (2016) 534(7607):396–401. doi: 10.1038/nature18300

31. Fujimura T, Nakagawa S, Ohtani T, Ito Y, Aiba S. Inhibitory effect of the polyinosinic-polycytidylic acid/cationic liposome on the progression of murine B16F10 melanoma. *Eur J Immunol* (2006) 36(12):3371–80. doi: 10.1002/eji.200636053

32. Sheehan KC, Lai KS, Dunn GP, Bruce AT, Diamond MS, Heutel JD, et al. Blocking monoclonal antibodies specific for mouse IFN-alpha/beta receptor subunit 1 (IFNAR-1) from mice immunized by *in vivo* hydrodynamic transfection. *J Interferon Cytokine Res* (2006) 26(11):804–19. doi: 10.1089/jir.2006.26.804

33. Ben-Yehuda H, Matcovitch-Natan O, Kertser A, Spinrad A, Prinz M, Amit I, et al. Maternal type-I interferon signaling adversely affects the microglia and the behavior of the offspring accompanied by increased sensitivity to stress. *Mol Psychiatry* (2020) 25(5):1050–67. doi: 10.1038/s41380-019-0604-0

34. Fotin-Mleczek M, Duchardt KM, Lorenz C, Pfeiffer R, Ojkic-Zrna S, Probst J, et al. Messenger RNA-based vaccines with dual activity induce balanced TLR-7 dependent adaptive immune responses and provide antitumor activity. *J Immunother* (2011) 34(1):1–15. doi: 10.1097/CJI.0b013e3181f7dbe8

35. Pollard C, Rejman J, De Haes W, Verrier B, Van Gulck E, Naessens T, et al. Type I IFN counteracts the induction of antigen-specific immune responses by lipid-based delivery of mRNA vaccines. *Mol Ther* (2013) 21(1):251–9. doi: 10.1038/mt.2012.202

36. Ferris ST, Durai V, Wu R, Theisen DJ, Ward JP, Bern MD, et al. cDC1 prime and are licensed by CD4(+) T cells to induce anti-tumour immunity. *Nature* (2020) 584(7822):624–9. doi: 10.1038/s41586-020-2611-3

37. Ma DY, Clark EA. The role of CD40 and CD154/CD40L in dendritic cells. *Semin Immunol* (2009) 21(5):265–72. doi: 10.1016/j.smim.2009.05.010

38. Alameh MG, Tombacz I, Bettini E, Lederer K, Sittplangkoon C, Wilmore JR, et al. Lipid nanoparticles enhance the efficacy of mRNA and protein subunit vaccines by inducing robust T follicular helper cell and humoral responses. *Immunity* (2021) 54(12):2877–92 e7. doi: 10.1016/j.immuni.2021.11.001

39. Dalpke A, Helm M. RNA Mediated toll-like receptor stimulation in health and disease. *RNA Biol* (2012) 9(6):828–42. doi: 10.4161/rna.20206

40. Divangahi M, Aaby P, Khader SA, Barreiro LB, Bekkering S, Chavakis T, et al. Trained immunity, tolerance, priming and differentiation: distinct immunological processes. *Nat Immunol* (2021) 22(1):2–6. doi: 10.1038/s41590-020-00845-6

41. Schoenemeyer A, Barnes BJ, Mancl ME, Latz E, Goutagny N, Pitha PM, et al. The interferon regulatory factor, IRF5, is a central mediator of toll-like receptor 7 signaling. *J Biol Chem* (2005) 280(17):17005–12. doi: 10.1074/jbc.M412584200

42. Chistiakov DA, Myasoedova VA, Revin VV, Orekhov AN, Bobryshev YV. The impact of interferon-regulatory factors to macrophage differentiation and polarization into M1 and M2. *Immunobiology* (2018) 223(1):101–11. doi: 10.1016/j.imbio.2017.10.005

43. Liu J, Geng X, Hou J, Wu G. New insights into M1/M2 macrophages: key modulators in cancer progression. *Cancer Cell Int* (2021) 21(1):389. doi: 10.1186/s12935-021-02089-2

44. Lakshmi Narendra B, Eshvendar Reddy K, Shantikumar S, Ramakrishna S. Immune system: a double-edged sword in cancer. *Inflammation Res* (2013) 62 (9):823–34. doi: 10.1007/s00011-013-0645-9

45. Liang Y, Hannan R, Fu YX. Type I IFN activating type I dendritic cells for antitumor immunity. *Clin Cancer Res* (2021) 27(14):3818–24. doi: 10.1158/1078-0432.CCR-20-2564

46. Wu Z, Zheng Y, Sheng J, Han Y, Yang Y, Pan H, et al. CD3(+)CD4(-)CD8(-) (Double-negative) T cells in inflammation, immune disorders and cancer. *Front Immunol* (2022) 13:816005. doi: 10.3389/fimmu.2022.816005

47. Yang L, Li A, Lei Q, Zhang Y. Tumor-intrinsic signaling pathways: key roles in the regulation of the immunosuppressive tumor microenvironment. *J Hematol Oncol* (2019) 12(1):125. doi: 10.1186/s13045-019-0804-8

48. Meng X, Liu X, Guo X, Jiang S, Chen T, Hu Z, et al. FBXO38 mediates PD-1 ubiquitination and regulates anti-tumour immunity of T cells. *Nature* (2018) 564 (7734):130–5. doi: 10.1038/s41586-018-0756-0

49. Hui E, Cheung J, Zhu J, Su X, Taylor MJ, Wallweber HA, et al. T Cell costimulatory receptor CD28 is a primary target for PD-1-mediated inhibition. *Science* (2017) 355(6332):1428–33. doi: 10.1126/science.aaf1292

50. Yokosuka T, Takamatsu M, Kobayashi-Imanishi W, Hashimoto-Tane A, Azuma M, Saito T. Programmed cell death 1 forms negative costimulatory microclusters that directly inhibit T cell receptor signaling by recruiting phosphatase SHP2. *J Exp Med* (2012) 209(6):1201–17. doi: 10.1084/jem.20112741

51. Sheppard KA, Fitz LJ, Lee JM, Benander C, George JA, Wooters J, et al. PD-1 inhibits T-cell receptor induced phosphorylation of the ZAP70/CD3zeta signalosome and downstream signaling to PKCtheta. *FEBS Lett* (2004) 574(1-3):37–41. doi: 10.1016/j.febslet.2004.07.083

52. Fuertes MB, Kacha AK, Kline J, Woo SR, Kranz DM, Murphy KM, et al. Host type I IFN signals are required for antitumor CD8+ T cell responses through CD8{alpha}+ dendritic cells. *J Exp Med* (2011) 208(10):2005–16. doi: 10.1084/jem.20101159

53. Takeuchi A, Saito T. CD4 CTL, a cytotoxic subset of CD4(+) T cells, their differentiation and function. *Front Immunol* (2017) 8:194. doi: 10.3389/fimmu.2017.00194

54. Quezada SA, Simpson TR, Peggs KS, Merghoub T, Vider J, Fan X, et al. Tumor-reactive CD4(+) T cells develop cytotoxic activity and eradicate large established melanoma after transfer into lymphopenic hosts. *J Exp Med* (2010) 207(3):637–50. doi: 10.1084/jem.20091918

55. Kim SC, Sekhon SS, Shin WR, Ahn G, Cho BK, Ahn JY, et al. Modifications of mRNA vaccine structural elements for improving mRNA stability and translation efficiency. *Mol Cell Toxicol* (2022) 18(1):1–8. doi: 10.1007/s13273-021-00171-4

56. Muramatsu H, Lam K, Bajusz C, Laczko D, Kariko K, Schreiner P, et al. Lyophilization provides long-term stability for a lipid nanoparticle-formulated, nucleoside-modified mRNA vaccine. *Mol Ther* (2022) 30(5):1941–51. doi: 10.1016/j.ymthe.2022.02.001

frontiers | Frontiers in Immunology

TYPE Original Research
PUBLISHED 02 November 2022
DOI 10.3389/fimmu.2022.1016982

OPEN ACCESS

EDITED BY
Ralph A. Tripp,
University System of Georgia,
United States

REVIEWED BY
Raymond P. Donnelly,
United States Food and Drug Administration, United States
Susetta Finotto,
University Hospital Erlangen, Germany
Jordan Metcalf,
University of Oklahoma, United States

*CORRESPONDENCE
Herman W. Favoreel
herman.favoreel@ugent.be

SPECIALTY SECTION
This article was submitted to Viral Immunology, a section of the journal Frontiers in Immunology

RECEIVED 11 August 2022
ACCEPTED 17 October 2022
PUBLISHED 02 November 2022

CITATION
Yin Y, Ma J, Van Waesberghe C, Devriendt B and Favoreel HW (2022) Pseudorabies virus-induced expression and antiviral activity of type I or type III interferon depend on the type of infected epithelial cell. *Front. Immunol.* 13:1016982. doi: 10.3389/fimmu.2022.1016982

Pseudorabies virus-induced expression and antiviral activity of type I or type III interferon depend on the type of infected epithelial cell

Yue Yin, Jinglin Ma, Cliff Van Waesberghe, Bert Devriendt and Herman W. Favoreel*

Department of Translational Physiology, Infectiology and Public Health, Faculty of Veterinary Medicine, Ghent University, Merelbeke, Belgium

Type I and III Interferons (IFNs) are the initial antiviral cytokines produced in response to virus infection. These IFNs in turn bind to their respective receptors, trigger JAK-STAT signaling and induce the expression of IFN-stimulated genes (ISGs) to engage antiviral functions. Unlike the receptor for type I IFNs, which is broadly expressed, the expression of the type III IFN receptor is mainly confined to epithelial cells that line mucosal surfaces. Accumulating evidence has shown that type III IFNs may play a unique role in protecting mucosal surfaces against viral challenges. The porcine alphaherpesvirus pseudorabies virus (PRV) causes huge economic losses to the pig industry worldwide. PRV first replicates in the respiratory tract, followed by spread *via* neurons and *via* lymph and blood vessels to the central nervous system and internal organs, e.g. the kidney, lungs and intestinal tract. In this study, we investigate whether PRV triggers the expression of type I and III IFNs and whether these IFNs exert antiviral activity against PRV in different porcine epithelial cells: porcine kidney epithelial cells (PK-15), primary respiratory epithelial cells (PoREC) and intestinal porcine epithelial cells (IPEC-J2). We show that PRV triggers a multiplicity of infection-dependent type I IFN response and a prominent III IFN response in PK-15 cells, a multiplicity of infection-dependent expression of both types of IFN in IPEC-J2 cells and virtually no expression of either IFN in PoREC. Pretreatment of the different cell types with equal amounts of porcine IFN-λ3 (type III IFN) or porcine IFN-α (type I IFN) showed that IFN-α, but not IFN-λ3, suppressed PRV replication and spread in PK-15 cells, whereas the opposite was observed in IPEC-J2 cells and both types of IFN showed anti-PRV activity in PoREC cells, although the antiviral activity of IFN-α was more potent than that of IFN-λ3 in the latter cell type. In conclusion, the current data show that PRV-induced type I and III

10.3389/fimmu.2022.1016982

IFN responses and their antiviral activity depend to a large extent on the epithelial cell type used, and for the first time show that type III IFN displays antiviral activity against PRV in epithelial cells from the respiratory and particularly the intestinal tract.

KEYWORDS

epithelial cell, pseudorabies virus, alphaherpesvirus, type I interferon, type III interferon, respiratory, gastrointestinal, kidney

Introduction

Mucosal surfaces, including the gastrointestinal tract, respiratory tract and reproductive tract are mainly composed of epithelial cells. They provide a crucial physical barrier between the body and the external environment and present the initial target cells for the establishment of viral infections (1, 2). Meanwhile they also have evolved unique defense mechanisms to protect against virus infection.

Type I and/or type III interferons (IFNs) are the initial antiviral cytokines that are produced as part of the innate immune response against virus infection, before activation of the adaptive immune system. Interferons are typically produced upon recognition of pathogen-associated molecular patterns (PAMPs) by cytosolic (e.g., RIG-I, MDA5, and cGAS) or endosomal (e.g., TLR3 and TLR9) pattern recognition receptors (PRRs). During virus infections, viral nucleic acids, i.e. viral DNA and/or RNA, are the major PAMPs. The activation of PRRs leads to the activation of several transcription factors, including interferon regulatory factor 3/7 (IRF3, IRF7) and nuclear factor-κB (NF-κB) to induce transcription, translation, and secretion of type I and/or type III IFNs and pro-inflammatory cytokines (3, 4). Type I and III IFNs bind to their respective receptors which, in both cases, results in activation of the JAK-STAT signaling pathway, which culminates in the expression of a plethora of IFN-stimulated genes (ISGs) that restrict viral replication and spread. Type I IFNs such as IFN-α and IFN-β bind the two chains of the type I IFN receptor (IFNAR1/2), whereas type III IFNs bind the two chains of the type III IFN receptor (IL-10R2, IFNLR1). Whereas the type I IFN receptor is expressed broadly, the expression of the IFNLR1 receptor is mainly restricted to mucosal epithelial cells. Accumulating evidence has shown that type III IFNs are of particular importance in protecting mucosal surfaces against viral challenges (5, 6).

Pseudorabies virus (PRV) (also referred to as suid herpesvirus 1 or Aujeszky's disease virus) belongs to the subfamily *Alphaherpesvirinae* of the herpesviruses and is an enveloped, double-stranded DNA virus. PRV has a very broad host range, including most mammals and some avian species (7). Pigs are the only natural host and reservoir of PRV. PRV first replicates in the respiratory tract, followed by spread *via* neurons and *via* lymph and blood vessels to the central nervous system and internal organs, e.g. the kidney, lungs, and intestinal tract (8). PRV causes Aujeszky's disease or pseudorabies (PR) in pigs, with high mortality in young piglets and reduced growth and reproductive failure in older pigs. Some of the major clinical symptoms include respiratory problems, diarrhea, vomiting, and nervous system disorders. The consequences of PRV infection result in huge economic losses to the pig industry worldwide (9).

Although type I IFNs have been shown to display antiviral activity against several alphaherpesviruses, the antiviral activity of type III IFNs has thus far been shown against the human alphaherpesvirus herpes simplex virus type 1 and 2 (HSV-1 and HSV-2) in human corneal explants and vaginal mucosa, respectively (10, 11). With regard to PRV, antiviral activity has been reported using recombinant porcine IFN-λ1 in PK-15 cells using the wild type Ea strain and using porcine IFN-λ3 in PK-15 cells using an attenuated gEnull/gInull PRV strain (12, 13). There is currently no information available about whether type III IFN suppress alphaherpesviruses infection in cells of the respiratory epithelium or intestinal epithelium or whether porcine IFN-λ3 displays antiviral activity against a wild type PRV strain. PRV is widely used as a model system to study general aspects of alphaherpesvirus biology. In the current study, we investigate the type I and III IFN response to PRV infection and the antiviral activity of both types of IFN in porcine kidney epithelial cells (PK-15), primary respiratory epithelial cells (PoREC) and intestinal porcine epithelial cells (IPEC-J2). We show that type I and III IFNs are produced in response to PRV infection in PK-15 cells and IPEC-J2 cells, with limited to no detection of either type of IFN in PoREC. Pretreatment of cells with the same amount of porcine IFN-λ3 (type III IFN) or porcine IFN-α (type I IFN) indicated that, depending on the cell type, both types of IFN may display antiviral activity (PoREC) or either one of the IFN types may display antiviral activity (IFN-λ3 in IPEC-J2 cells and IFN-α in PK-15 cells).

Material and methods

Cell cultures, virus and interferon

Porcine kidney-15 (PK-15) cells were cultured at 37°C with 5% CO2, in minimal essential medium (MEM; ThermoFisher), supplemented with 10% inactivated fetal bovine serum (FBS), 100-U/ml penicillin, 0.1-mg/ml streptomycin, 50-ug/ml gentamicin.

The intestinal porcine epithelial cell line J2 (IPEC-J2) was cultured at 37°C with 5% CO2 in Dulbecco's Modified Eagle's Medium Nutrient Mixture F-12 (DMEM/F12, Gibco) supplemented with 0.1 mM HEPES (Gibco, USA), 10% inactivated fetal bovine serum (FBS), 100 U/ml penicillin, 0.1 mg/ml streptomycin, 1% insulin-transferrin-selenium (ITS), 2% l-glutamine, and 5 ng/ml epidermal growth factor (EGF).

PRV strain Kaplan was described before and was kindly provided to us by T. C. Mettenleiter (Friedrich-Loeffler-Institute, Germany) (14).

Porcine recombinant IFN-α and IFN-λ3 were purchased from Kingfisher Biotech (USA).

Isolation of primary PoRECs

Isolation and culture of porcine primary respiratory epithelial cells (PoREC) was performed as previously described (15). In brief, tracheae were collected from healthy 7-weeks-old piglets and were immediately placed in ice-cold transport solution (phosphate buffered saline (PBS), supplemented with 100U/mL penicillin, 0.1mg/mL streptomycin, 0.1µg/mL gentamycin, 0.1mg/ml kanamycin [Sigma-Aldrich] and 250ng/mL fungizone (Gibco, Thermo Fisher Scientific)) for transportation to the laboratory. Connective tissue and fat were removed from the trachea, which were then washed with PBS to remove red blood cells and incubated in a Pronase/DNase I solutiuon for 72 h at 4°C. After incubation, cells were harvested and then added to uncoated plastic petri dish (Nunc; Thermo Fisher Scientific) for 2h to remove fibroblasts by plastic adherence. Epithelial cells were seeded at a concentration of 1.2 million cells/well in 12-well plate transwells with a 0.4-µm pore size (catalog number 3460; Costar; Corning) that were pre-coated with type IV collagen (catalog number C5533; Sigma-Aldrich). Cells were cultivated in Afi1 medium (DMEM plus Ham's F-12 medium, supplemented with 5% FBS, 1% MEM nonessential amino acids (Gibco, Thermo Fisher Scientific), 100U/ml penicillin, 0.1mg/ml streptomycin, 1.25 µg/ml amphotericin B). One day after seeding, cells were carefully washed with DMEM/F12 medium and Afi2 medium supplemented with 2% Ultroser G was added to the bottom of the transwell, resulting in an air-liquid interface to simulate conditions of the respiratory tract. PoREC were incubated at 37°C with 5% CO2 until they reached full confluence, upon which they were apically infected with PRV Kaplan at multiplicity of infection (MOI) of 10 for 24h.

Cell viability assay

Confluent PK-15, PoREC, IPEC-J2 cells were treated with 300ng/ml IFN-α or IFN-λ3 for 24h, incubated for 20 min at 37°C with accutase and collected in 96-well V-bottom plates. Cells were washed two times in PBS between each step. Cells were fixed with Fix buffer (BD Biosciences) for 20min at 4°C as positive control for propidium iodide (PI) staining, which was used to measure cell viability. Flow cytometry was performed using a NovoCyte Flow Cytometer (ACEA Biosciences, Agilent, Santa Carla, CA, USA), and samples were analyzed with NovoExpress software (ACEA Biosciences).

RNA isolation and RT-QPCR

RNA isolation and RT-QPCR were performed as described before (16).The primers used in this assay are listed in Table 1.

SDS-PAGE and Western blot analysis

SDS-PAGE and Western blot analysis were performed as described before (16). Rabbit anti-IFNAR2 polyclonal antibody (catalog no. GTX105770; GeneTex)(1:500 dilution), rabbit anti-

TABLE 1 Forward and reverse primer sequences used in real-time PCR assays.

Target, (GenBank Accession No.)	Forward primer 5'-3'	Reverse primer 5'-3'
28S (17)	GGGCCGAAACGATCTCAACC	GCCGGGCTTCTTACCCAT
pIFN-λ1 (18)	GGTGCTGGCGACTGTGATG	GATTGGAACTGGCCCATGTG
pIFN-λ3 (19)	ACTTGGCCCAGTTCAAGTCT	CATCCTTGGCCCTCTTGA
pIFN-α (20)	TCTCATGCACCAGAGCCA	CCTGGACCACAGAAGGGA
OAS1(NM_002534.4)	GAGCTGCAGCGAGACTTCCT	TGCTTGACAAGGCGGATGA
ISG15(NM_001128469.3)	AGCACAGTCCTGTTGATGGTG	CAGAACTGGTCAGCTTGCACG
ISG54(XM_005671264.3)	GCCCTAAGGACCCAGAAGTCA	CGAGGAGGTGGCCAGTTATC
IFIT3 (21)	GCACCAAATTCATGGTATCTCC	TTCCTTCCTGTCTCTGTCAGCC

IFNLR1 polyclonal antibody (catalog no. ARP48070_P050; Aviva Systems Biology)(1:500 dilution) and goat anti-rabbit IgG (catalog number P0448; Dako)(1:3,000 dilution) were used.

Titrations

PK-15, PoREC and IPEC-J2 were either left untreated or pre-treated with the indicated concentrations of IFN for 24 h. Cells were then inoculated with PRV strain Kaplan at an MOI of 0.1. At 2h post inoculation (hpi), cells were washed with PBS and incubated with sodium citrate buffer (pH 3.0; 40 mM sodium citrate, 10 mM KCl, and 135 mM NaCl) for 2 min at room temperature to inactivate residual virus, followed by several washing steps before adding fresh medium. At 24hpi, PRV-infected cell supernatants were harvested and immediately frozen at −80°C. Extracellular titers were determined on ST cells. To this end, ST cells were seeded in 96-well-plates and inoculated with serial 10-fold dilutions of PRV-infected cell supernatants and, after 7 days, extracellular virus titer was calculated in plaque forming units (PFU) per milliliter (PFU/ml).

Plaque assays

PK-15, PoREC and IPEC-J2 cells were either left untreated or pretreated with the indicated concentrations of IFN for 24 h, then infected with PRV at 1,000 PFU/well. At 2hpi, medium was replaced by 1mL of semisolid medium consisting of a 1:1 mixture of 2 × DMEM with 4% FBS and 2% methylcellulose solution. At 24hpi, cells were fixed with 3% paraformaldehyde at room temperature for 15 min followed by three washing steps with PBS and subsequent permeabilization using 0.1% Triton X-100 at room temperature for 2 min. Afterwards, cells were washed three times with PBS. For PoREC cells, cells were incubated with antibodies against the epithelial cell-specific marker cytokeratin (rabbit polyclonal anti-pan-cytokeratin antibody (1:200); Abcam) overnight at 4°C and fluorochrome-linked goat anti-rabbit IgG secondary antibodies (1:200; Invitrogen) for 1 h at 37°C. For PRV plaque detection, cells were incubated in fluorescein isothiocyanate (FITC)-labeled porcine polyclonal anti-PRV antibodies (1:200) at 37°C for 1h, diluted in incubation buffer (10% FBS diluted in PBS). After three washing steps with PBS, Hoechst 33342 (1:200; Invitrogen) diluted in PBS was added at room temperature for 10 min to counterstain the cell nuclei. After three washing steps, coverslips were mounted on microscope slides in glycerin-DABCO. Samples were imaged using a Leica SPE confocal microscope (Leica) and were analyze with Image J software.

Statistical analysis

Statistical analyses were performed using Prism 7 (GraphPad Software). Statistical differences among the experimental groups were determined by unpaired t tests.

Results

In PK-15 cells, PRV triggers a multiplicity of infection (MOI)-dependent type I and prominent type III IFN response and IFN-α displays anti-PRV activity

Most types of cells are able to produce type I interferons upon virus infection. However, type III interferons are typically only produced in epithelial cells and specialized interferon-producing innate immune cells, the plasmacytoid dendritic cells (pDC) (22). In combination with the fact that the expression of the type III IFN receptor is largely restricted to epithelial cells, type III IFNs particularly provide a local antiviral response in epithelial cells, whereas type I IFNs may evoke more systemic antiviral responses.

PK-15 cells are porcine kidney epithelial cells that are widely used in PRV research. To investigate whether PRV infection induces type I and/or III IFN production in PK-15 cells, mRNA levels of type I IFN (IFN-α) and type III IFN (IFNλ1 and IFN-λ3) were examined by RT-qPCR at 3, 6, 9, 12 and 24hpi at an MOI of 0.1PFU/cell. Substantial levels of IFN-λ1/3 and IFN-α were only detected from 6hpi-9hpi onwards (Figure 1A). Interestingly, IFN-α expression reached its peak at 12h and decreased afterwards, whereas expression of both IFNλ1 and IFN-λ3 continued to increase until the end of the experiment at 24hpi (Figure 1A). To assess whether expression of type I and/or type III IFN in response to PRV is MOI-dependent, additional assays were performed using an MOI of 10PFU/cell. Inoculation of PK-15 cells at an MOI of 10PFU/cell resulted in a rapid and temporal expression of IFNλ1 and IFN-λ3 (Figure 1B). Interestingly, this high MOI inoculation dose did not trigger detectable expression of IFN-α (Figure 1B).

Next, we evaluated the antiviral activity of type I and III IFN against PRV in PK-15 cells by assessing infectious virus production and plaque formation. To this end, PK-15 cells were pretreated with different concentrations of porcine recombinant IFN-α or IFN-λ3 for 24 h prior to infection. Treatment with either type I or type III IFN did not negatively affect PK-15 cell viability (Figure 1C). To determine infectious virus production, cell culture supernatants were collected at 24hpi and viral titers were determined. Plaque sizes were determined by immunofluorescence at 24hpi. As shown in Figure 1D, we observed that PRV titers were significantly reduced upon treatment with IFN-α, whereas IFN-λ3 only minimally and

10.3389/fimmu.2022.1016982

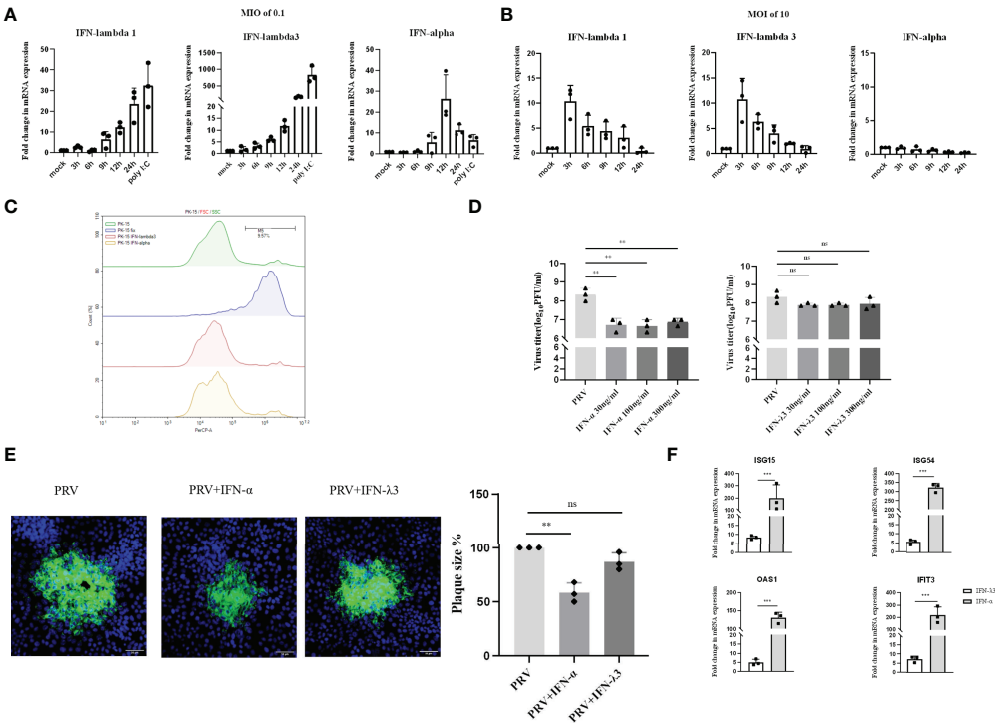

FIGURE 1
Expression and antiviral effect of type I and type III IFNs in response to PRV infection in PK-15 cells. PK-15 cells were inoculated with **(A)** low dose PRV (MOI of 0.1PFU/cell) or **(B)** high dose PRV (MOI of 10PFU/cell). At different time points post inoculation, cell lysates were prepared for RT-qPCR analysis of expression of porcine IFN-α, IFN-λ1 and IFN-λ3. **(C)** PK-15 cells were treated with IFN-α or IFN-λ3 (300ng/ml) for 24 h, followed by PI staining and flow cytometric analysis to assess cell viability. **(D)** PK-15 cells were pretreated with recombinant porcine IFN-α or IFN-λ3 (30, 100, 300ng/ml) for 24 h prior, followed by PRV inoculation (MOI of 0.1PFU/cell). At 24hpi, cell culture supernatants were collected and viral titers were determined. **(E)** PK-15 cells were pretreated with recombinant porcine IFN-α or IFN-λ3 (300ng/ml) for 24 h, followed by PRV inoculation. At 2hpi, medium was replaced with a semisolid medium to prevent cell-free spread of PRV particles. Plaque sizes were determined by immunofluorescence at 24hpi. **(F)** PK-15 cells were treated with recombinant porcine IFN-α (grey bars) or IFN-λ3 (black bars) (each at 300ng/ml) for 24 h followed by RT-qPCR analysis of the expression of different ISGs (ISG15, ISG54, OAS, IFIT3). Asterisks indicate statistically significant differences (ns: non-significant, **p < 0.01, ***p < 0.001).

non-significantly reduced PRV titers. No dose-dependent differences were observed, indicating that the lowest concentration (of IFN-α) used was likely sufficient to trigger maximal signaling and/or intracellular antiviral responses. In line with the results of virus titrations, plaque assays showed that IFN-α significantly inhibited PRV spread in PK-15 cells, whereas IFN-λ3 had only a minimal, non-statistically significant effect on PRV plaque sizes in this cell type (Figure 1E).

In line with these results, we found that IFN-α triggered much more robust ISG expression in PK-15 cells compared to IFN-λ3 (Figure 1F).

These data indicate that PRV triggers expression of both types of IFN in PK-15 cells infected at low MOI with PRV, but only expression of type III IFN in PK-15 cells infected at high MOI. In addition, only type I IFN triggered robust expression of ISGs and significantly suppressed PRV infectious virus production and plaque formation in this cell type.

In PoREC cells, PRV infection does not trigger a detectable type I or type III IFN response, but both types of interferon display antiviral activity against PRV

Primary respiratory epithelial cells (PoREC) cultured at air-liquid interface (ALI) mimic the natural environment found in respiratory epithelium. This is a particularly relevant model in the context of the early phase of PRV infection, as PRV causes a primary infection in porcine respiratory epithelial cells. We previously showed successful infection of PoREC cells (15). Interestingly, we found that PRV infection at an MOI of 0.1PFU/cell triggers minimal to no detectable mRNA levels of type I or III IFN (Figure 2A). Increasing the infectious dose to an MOI of 10PFU/cell still did not trigger detectable mRNA expression of either type of IFN (Figure 2B). Quite contrary, PRV infection of PoREC at high MOI appeared to result in

10.3389/fimmu.2022.1016982

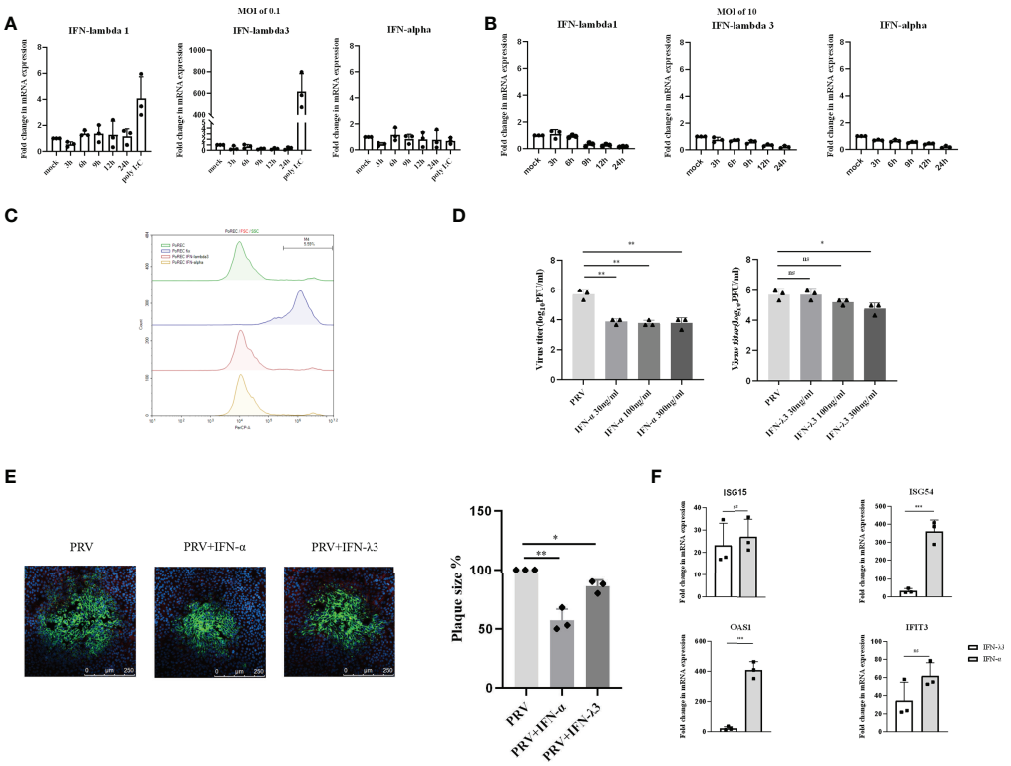

FIGURE 2
Expression and antiviral effect of type I and type III IFNs in response to PRV infection in porcine primary respiratory epithelial cells (PoREC). PoREC were inoculated with **(A)** low dose PRV (MOI of 0.1PFU/cell) or **(B)** high dose PRV (MOI of 10PFU/cell) on the apical side. At different time points post inoculation, cell lysates were prepared for RT-qPCR analysis of expression of porcine IFN-α, IFN-λ1 and IFN-λ3. **(C)** PoREC were treated with IFN-α or IFN-λ3 (300ng/ml) for 24 h, followed by PI staining and flow cytometric analysis to assess cell viability. **(D)**PoREC were pretreated with recombinant porcine IFN-λ3 or IFN-α (30, 100, 300ng/ml) for 24h on the basolateral side, followed by PRV inoculation on the apical side (MOI of 0.1PFU/cell). At 24hpi, cell culture supernatants were collected and viral titers were determined. **(E)** PoREC were pretreated with recombinant porcine IFN-α or IFN-λ3 (300ng/ml) for 24 h, followed by PRV inoculation. At 2hpi, medium was replaced with a semisolid medium to prevent cell-free spread of PRV particles. Plaque sizes were determined by immunofluorescence at 24hpi. **(F)** PoREC were treated with recombinant porcine IFN-α (grey bars) or IFN-λ3 (black bars)(each at 300ng/ml) for 24 h followed by RT-qPCR analysis of the expression of different ISGs (ISG15, ISG54, OAS, IFIT3). Asterisks indicate statistically significant differences (ns: non-significant, *p < 0.05, **p < 0.01, ***p < 0.001).

mRNA expression levels of type I and type III IFN that were lower than those observed in mock-infected cells (Figure 2B).

The expression of type I IFN receptors is largely restricted to the basolateral side of respiratory epithelial cells (23). In addition, other reports used basolateral pretreatment to assess the antiviral activity of type I and type III IFN in respiratory epithelial cells, e.g. against SARS-CoV-2 (24, 25). Hence, to determine whether PRV is sensitive to type I and III IFNs in PoREC, we pretreated the basolateral side of PoREC cultures with IFN-λ3 or IFN-α for 24h, followed by infection of PoREC cultures with PRV from the apical side. Treatment with either type I or type III IFN did not negatively affect PoREC cell viability (Figure 2C). Infectious virus production was assessed by collecting cell culture supernatants at 24hpi and determining viral titers. Compared to untreated cells, we observed that both types of IFN suppressed PRV infectious virus production in PoREC. However, IFN-α suppressed infectious virus production more effectively and was equally active over the range of different concentrations tested. IFN-λ3, on the other hand, showed a more limited and dose-dependent antiviral effect, with only the highest concentration resulting in a statistically significant reduction in virus titer (Figure 2D). In line with these results, plaque assays showed that IFN-α significantly inhibited PRV spread in PoREC cells, whereas IFN-λ3 had a less significant effect on PRV plaque sizes in this cell type (Figure 2E).

In line with these results, we found that IFN-α triggered much more robust ISG expression in PoREC compared to IFN-λ3, particularly ISG54 and OAS1(Figure 2F), whereas the expression of ISG15 and IFIT3 were equal or non-statistically different upon treatment with either type of IFN, respectively.

Altogether, these results indicate that PRV-infected PoREC cells do not trigger detectable expression of either type I or type III IFN and that both types of IFN, in particular type I IFN, display antiviral activity against PRV in this cell type.

In IPEC-J2 cells, PRV infection triggers a rapid and temporal expression of type I and type III IFNs, but only type III IFN displays antiviral activity against PRV

PRV infection causes diarrhea and necrotizing enteritis in weaning and starter piglets (26, 27). Hence, we next investigated the type I and III IFNs response to PRV infection in porcine intestinal IPEC-J2 cells. We found that, within 3hpi, PRV infection of IPEC-J2 cells at an MOI of 0.1PFU/ml triggers expression of both type I and type III IFN mRNA, followed by a rapid decrease in the corresponding transcript levels (Figure 3A). Interestingly, increasing the PRV infectious dose to an MOI of 10PFU/cell resulted in expression of IFN-λ1 but did not result in detectable expression of IFN-α or IFN-λ3 (Figure 3B). In fact, PRV infection of IPEC-J2 at high MOI appeared to result in mRNA expression levels of IFN-α or IFN-λ3 that were lower than those observed in mock-infected cells (Figure 3B).

To determine whether type I and/or III IFN suppresses PRV infection in IPEC-J2 cells, cells were pretreated with different concentrations of porcine IFN-α or IFN-λ3 for 24h before virus inoculation. Treatment with either type of IFN did not negatively affect IPEC-J2 cell viability (Figure 3C). Interestingly, although IFN-α did not suppress PRV infectious virus production in this cell type, IFN-λ3 treatment resulted in a dose-dependent decrease in infectious virus production, which reached statistical significance with the highest dose that was used (Figure 3D). In line with this, plaque assays showed that IFN-λ3 significantly inhibited PRV spread in IPEC-J2 cells, while IFN-α did not (Figure 3E).

Further in line with these results, we found that IFN-λ3 triggered a much more robust ISG expression in IPEC-J2 cells compared to IFN-α (Figure 3F).

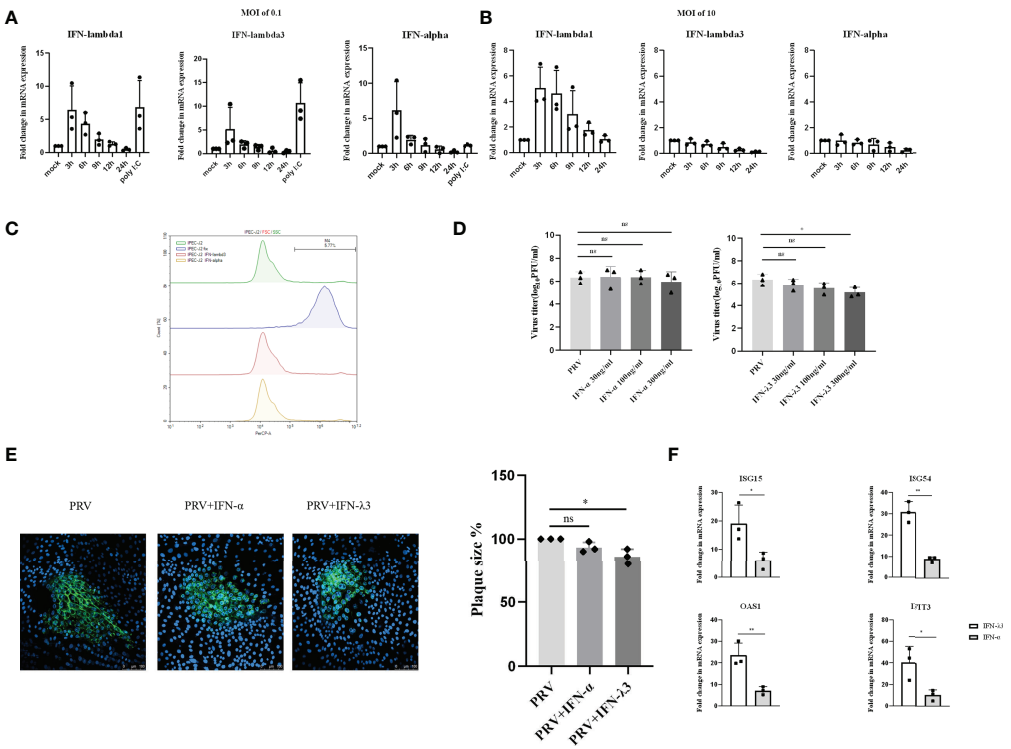

FIGURE 3
Expression and antiviral effect of type I and type III IFNs in response to PRV infection in IPEC-J2 cells. IPEC-J2 cells were inoculated **(A)** low dose PRV (MOI of 0.1PFU/cell) or **(B)** high dose PRV (MOI of 10PFU/cell). At different time points post inoculation, cell lysates were prepared for RT-qPCR analysis of expression of porcine IFN-α, IFN-λ1 and IFN-λ3. **(C)** IPEC-J2 cells were treated with IFN-α or IFN-λ3 (300ng/ml) for 24 h, followed by PI staining and flow cytometric analysis to assess cell viability. **(D)** IPEC-J2 were pretreated with recombinant porcine IFN-λ3 or IFN-α (30, 100, 300ng/ml) for 24h, followed by PRV inoculation (MOI of 0.1PFU/cell). At 24hpi, cell culture supernatants were collected and viral titers were determined. **(E)** IPEC-J2 cells were pretreated with recombinant porcine IFN-α or IFN-λ3 (300ng/ml) for 24 h, followed by PRV inoculation. At 2hpi, medium was replaced with a semisolid medium to prevent cell-free spread of PRV particles. Plaque sizes were determined by immunofluorescence at 24hpi. **(F)** IPEC-J2 cells were treated with recombinant porcine IFN-α (grey bars) or IFN-λ3 (black bars)(each at 300ng/ml) for 24 h followed by RT-qPCR analysis of the expression of different ISGs (ISG15, ISG54, OAS, IFIT3). Asterisks indicate statistically significant differences (ns: non-significant, *p < 0.05, **p < 0.01).

In conclusion, in IPEC-J2 cells, PRV infection triggers a MOI-dependent, rapid but temporal expression of both type I and III IFNs, but only type III IFN suppresses PRV infection in this cell type.

Expression of type I and III IFNs receptor chains

Type I and III IFN bind to different receptors, in both cases triggering JAK-STAT signaling pathway to induce ISG expression that mediate antiviral activity. Unlike type I IFN receptors, which are ubiquitously expressed on all nucleated cells, expression of the specific type III IFN receptor chain (IFNLR1) is limited and largely restricted to epithelial cells (6, 28). Since we found that ISG expression and the antiviral effect of IFN-α or IFN-λ3 against PRV depended on the type of epithelial cell, we determined whether this correlated with differences in IFN receptor expression. Expression of the type I IFN receptor chain IFNAR2 and the type III IFN receptor chain IFNLR1 was detected by Western blot in PK-15, PoREC and IPEC-J2 cells. As shown in Figure 4, IFNAR2 expression was abundant in PK-15 cells and PoREC but rather weakly expressed in IPEC-J2 cells. IFNLR1, on the other hand, was strongly expressed in IPEC-J2 cells and, to a lesser extent, in PoREC, whereas expression of this receptor chain was relatively weak in PK-15 cells, all in line with the ISG expression and anti-PRV activity of type I and type III IFNs in the different cell types.

Discussion

Type I and III IFNs are critical antiviral cytokines that are produced as part of the innate immune response to viral infection and are able to establish an antiviral state in host cells. Type III IFN are increasingly regarded to play a unique role in protecting local mucosal surfaces against viral infections, compared to type I IFN which triggers more systemic antiviral responses (29). In this study, we investigated both the expression of type I and III IFN in response to PRV infection and their antiviral effect against PRV infection in different porcine epithelial cells: kidney epithelial cells (PK-15), primary respiratory epithelial cells (PoREC) and intestinal epithelial cells (IPEC-J2). We observed that type I and III IFNs were produced in response to PRV infection in PK-15 cells and IPEC-J2 cells, but that PoREC did not express detectable levels of either type of IFN. A limitation of the current study is that type I and type III IFN mRNA expression levels, rather than protein levels, were analyzed. However, the lack of reliable porcine type III IFN ELISA precluded indisputable detection of porcine type III IFN protein levels. Pretreatment of the different cell types with recombinant porcine IFN-λ3 or IFN-α showed that IFN-α, but not IFN-λ3 inhibited PRV replication in PK-15 cells, whereas the opposite was true for IPEC-J2 cells and both IFN-λ3 and IFN-α suppressed PRV infection in PoREC (although the antiviral effect of IFN-α was more potent in this cell type). These data highlight that, even within the epithelial cell type compartment, substantial differences can be observed both in expression and antiviral activity of type I versus type III IFNs against a viral pathogen like PRV.

PK-15 cells arguably represent the most widely used cell system in PRV studies, as it is very commonly used for virus isolation, propagation and basic research. We found that both type I and type III IFN were induced in response to low MOI PRV infection in PK-15 cells. Interestingly, upon high MOI infection, PRV infection still triggered temporal type III IFN production in PK-15 cells, but did not trigger detectable IFN-α production. Like several alphaherpesviruses, PRV infection of host cells has been reported to rapidly interfere with production of type I IFN. This rapid shutdown of interferon

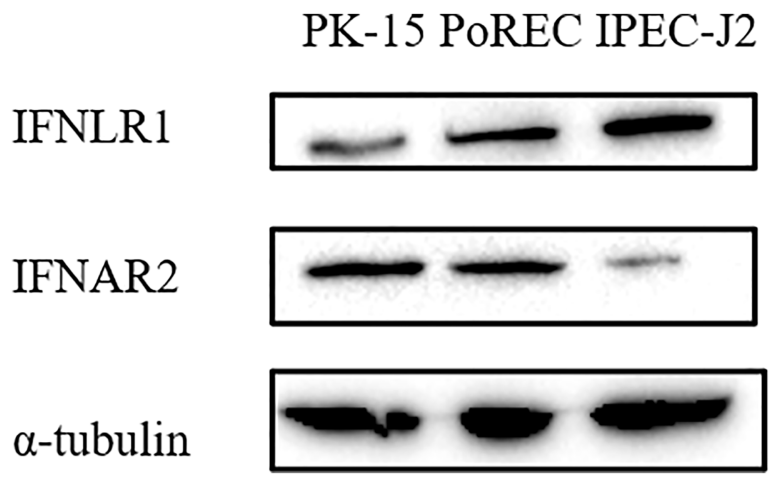

FIGURE 4
Different porcine epithelial cells show differences in protein expression levels of the type I IFN receptor chain IFNAR2 and type III IFN receptor chain IFNL1. PK-15, PoREC, IPEC-J2 cells were harvested and prepared for Western blot analysis using antibodies against IFNLR1, IFNAR2 and α-tubulin.

production is carried out by viral tegument proteins that are released during entry of the virus and by (immediate) early viral proteins. For example, the UL13 tegument protein kinase of PRV suppresses type I IFN production *via* degradation of PRDX1, IRF3 and STING (30–32), the US3 tegument protein kinase of PRV triggers degradation of IRF3 and Bclaf1 to suppress type I IFN production (33, 34), and the early EP0 protein of PRV antagonizes type I IFN production by inhibiting IRF9 (35). Hence, although speculative, we hypothesize that, in comparison with low MOI infection, high MOI PRV infection leads to increased intracellular concentration of incoming tegument viral proteins and increased production of (immediate) early viral proteins, which counteract the type I IFN response. Based on our results in PK-15 cells and IPEC-J2 cells, this high MOI-dependent inhibition of IFN production appears to mainly affect type I IFN rather than type III IFN.

We observed that PK-15 cells produce both IFN-λ1 and IFN-λ3 in response to PRV infection, which is in line with observations in PK-15 cells infected with other porcine viruses, including classical swine fever virus (CSFV) and Seneca virus A (SVA) (36, 37). Since porcine type III IFN has been reported to induce antiviral activity against porcine epidemic diarrhea virus (PEDV) infection in Vero E6 cells, which are monkey kidney epithelial cells, and in MARC-145, which are African green monkey kidney cells (19, 38), we assumed that porcine type III IFN may suppress PRV infection in porcine kidney epithelial cells like PK-15 cells. However, although IFN-α significantly inhibited PRV infection, IFN-λ3 did not significantly inhibit PRV infection in PK-15 cells, which corresponded with a very weak induction of ISG expression by IFN-λ3 compared to IFN-α in this cell type. Although the specific receptor chain for type III IFN, IFNLR1, is expressed in PK-15 cells (16), we found that protein expression levels of this receptor chain are less abundant in this cell type compared to PoREC and IPEC-J2 cells (Figure 4), in line with the apparent weak ISG induction and antiviral activity of type III IFN in PK-15 cells. Interestingly, very recently, another study reported that porcine IFN-λ3 does display antiviral activity against PRV in PK-15 cells (12). A very important difference of the latter study compared to the current study is that we made use of wild type, virulent PRV whereas the other study made use of an attenuated gEnullgInull PRV strain (12). Since the gE/gI virulence complex of PRV has been reported to interfere with the antiviral IFN system (39, 40), it is likely that the lack of gE and/or gI renders the virus more susceptible to the (relatively weak) antiviral response of IFN-λ3 in PK-15 cells, which may explain the differences between both studies. In addition, an earlier study reported that another type III IFN, IFN-λ1, displays antiviral activity against the wild type PRV strain Ea in PK-15 cells (13). This suggests that, in PK-15 cells, porcine IFN-λ1 may possibly trigger a more robust antiviral effect against PRV compared to IFN-λ3.

The (upper) respiratory tract is a common target for virus entry into the host, including for PRV. In the current study, we isolated porcine primary respiratory epithelial cells (PoREC) from the porcine trachea region. PoREC cultivated at an air-liquid interface have been shown earlier to be permissive to PRV infection (15). We observed a lack of detectable expression of either type I or type III IFN in PoREC following PRV infection, either at low or high MOI infection. Similarly, previous research showed that SARS-CoV-2 does not induce detectable type I and III IFN production or signaling in primary human bronchial/tracheal epithelial cells and human lung alveolar epithelial cells (24, 41, 42), although, using the same primary human bronchial/tracheal epithelial cells system, influenza virus induced a robust type I and III IFNs response (24). Also, human nasal epithelial cells can express both type I and IFNs in response to SARS-CoV-2 infection (43). Meanwhile, porcine primary tracheal epithelial cells did induce both type I and III IFN expression in response to swine IAV infection (44). Hence, the lack of IFN expression in primary porcine trachea epithelial cells following PRV infection appears to be specific for this virus and likely points to a powerful IFN production evasion strategy in this cell type, which warrants further investigation.

Although PoREC cultures did not detectably produce IFN in response to PRV infection, exogenous IFN-λ3 and IFN-α were able to restrict PRV replication in PoREC, and IFN-α provided a more potent antiviral protection against PRV than IFN-λ3 in this cell type. Although speculative, these results may possibly relate to different requirement for type I versus III IFNs in the upper and lower respiratory tract, respectively. Indeed, it has been shown before that type III IFNs appear to be more important than type I IFN to control viral infections at the level of the upper respiratory tract, whereas this may not be the case in the lower respiratory tract. Indeed, using an upper respiratory tract IAV infection model in mice, IFNLR1-/- mice were unable to control IAV spread from the upper airways to the lungs, whereas IFNAR1-/- mice were able to do so, whereas both type I and type III IFNs displayed redundant functions in the lower airway epithelium (45). In the current study, we pretreated PoREC with IFN *via* the basolateral side. Interestingly, aerosol inhalation (which leads to apical exposure) has been assessed as a route of IFN-α2b administration in the context of SARS-CoV-2 infection, and was found to significantly shorten the duration of SARS-CoV-2 shedding (46). Hence, in future assays, it may be of interest to investigate whether apical addition of type III IFN may or may not trigger an antiviral effect of type III IFN against PRV in PoREC.

Upon primary infection at the respiratory tract, PRV may spread to other organs, including the intestinal tract. PRV infection causes diarrhea and necrotizing enteritis in weaning and starter piglets, and PRV antigen can be detected in the intestinal tract (47). The IPEC-J2 cell line is derived from porcine intestinal columnar epithelial cells that were isolated from the mid-jejunum of a neonatal piglet. This cell line displays a high similarity to primary porcine intestinal epithelial cells and is therefore often used as a model to investigate the interaction between viruses and the intestinal tract (48). Our data show rapid and temporal expression of both type I and III IFNs in response to low MOI PRV infection in IPEC-J2 cells. Similarly, PEDV has also been reported to trigger a rapid and temporal expression of type III IFNs in porcine epithelial cells, with detectable expression at 3hpi that quickly declined by 9hpi and 12hpi (19). In human intestinal epithelial cells, type III IFNs were

strongly upregulated in response to enteric virus infection, while the expression of type I IFNs was less prominent (49, 50). In line with our observation in PK-15 cells, no IFN-α (or IFN-λ3) production was detected upon high MOI infection of IPEC-J2 cells with PRV, again possibly pointing to the increased activity of IFN production-inhibiting viral tegument and (immediate) early proteins upon high MOI infection.

Interestingly, whereas exogenously added IFN-λ3 significantly restricted PRV replication in IPEC-J2 cells, IFN-α did not, suggesting that type III IFN plays a key role in the antiviral response against PRV in the intestinal tract. In line with this, in IPEC-J2 cells, IFN-λ3 triggered a much more robust expression of ISGs compared to IFN-α and protein levels of the type III IFN receptor chain IFNLR1 were high in IPEC-J2 whereas those of the type I IFN receptor chain IFNAR2 were low. Further in line with these results, using the same IPEC-J2 cells, type III IFN triggered a stronger anti-PEDV effect than type I IFNs, which also correlated with similar differences in ISG expression (21, 38, 51). Exogenous addition of either type of IFN efficiently inhibited SARS-CoV-2 replication and reduced release of infectious virus particles in T84 and Caco-2 human intestinal cell lines. However, depletion of the type I IFN receptor from human intestinal cells resulted in only a slight increase in SARS-CoV-2 infection, whereas depletion of the type III IFN receptor resulted in significantly increased virus infection, replication, and *de novo* virus production (52), again in line with our current results that type III IFN appears to play a critical role in the intestinal antiviral response.

Overall, these data highlight that in specific types of epithelial cells, particularly intestinal epithelial cells, type III IFN provides effective antiviral activity against PRV infection and highlight that the expression as well as the antiviral activity of type I and type III IFNs is highly dependent of the cell type, even within the epithelial cell compartment, and that expression of type I/III IFNs upon PRV infection also depends on the infectious dose that is used.

Data availability statement

The raw data supporting the conclusions of this article will be made available by the authors, without undue reservation.

Author contributions

YY and HF conceived and designed the study, YY performed the experiments with support of JM, CVW and BD, YY and HF wrote the paper. All authors contributed to the article and approved the submitted version.

Funding

YY and JM are supported by PhD scholarship grants of the China Scholarship Council (CSC) (201806910083 and 201906350196). Research of YY and HF is supported by grants from the Special Research Fund of Ghent University (CSC-cofunding grant and Concerted Research Action GOA013-17).

Acknowledgments

We thank Sofie Denaeghel for help with flow cytometry and Thomas Mettenleiter (Friedrich-Loeffler-Institute, Germany) for providing us with the PRV Kaplan strain.

Conflict of interest

The authors declare that the research was conducted in the absence of any commercial or financial relationships that could be construed as a potential conflict of interest.

Publisher's note

References

1. Ye L, Schnepf D, Staeheli P. Interferon-λ orchestrates innate and adaptive mucosal immune responses. *Nat Rev Immunol* (2019) 19:614–25. doi: 10.1038/s41577-019-0182-z

2. Stanifer ML, Guo C, Doldan P, Boulant S. Importance of type I and III interferons at respiratory and intestinal barrier surfaces. *Front Immunol* (2020) 11:608645. doi: 10.3389/fimmu.2020.608645

3. Park A, Iwasaki A. Type I and type III interferons–induction, signaling, evasion, and application to combat COVID-19. *Cell Host Microbe* (2020) 27:870–8. doi: 10.1016/j.chom.2020.05.008

4. Kotenko SV, Rivera A, Parker D, Durbin JE. Type III IFNs: beyond antiviral protection. *Semin Immunol* (2019) 43:101303. doi: 10.1016/j.smim.2019.101303

5. Lazear HM, Schoggins JW, Diamond MS. Shared and distinct functions of type I and type III interferons. *Immunity* (2019) 50:907–23. doi: 10.1016/j.immuni.2019.03.025

6. Dowling JW, Forero A. Beyond good and evil: Molecular mechanisms of type I and III IFN functions. *J Immunol* (2022) 208:247–56. doi: 10.4049/jimmunol.2100707

7. Pomeranz LE, Reynolds AE, Hengartner CJ. Molecular biology of pseudorabies virus: impact on neurovirology and veterinary medicine. *Microbiol Mol Biol Rev* (2005) 69:462–500. doi: 10.1128/MMBR.69.3.462-500.2005

8. Nauwynck H, Glorieux S, Favoreel H, Pensaert M. Cell biological and molecular characteristics of pseudorabies virus infections in cell cultures and in

pigs with emphasis on the respiratory tract. *Vet Res* (2007) 38:229–41. doi: 10.1051/vetres:200661

9. Yin Y, Xu Z, Liu X, Li P, Yang F, Zhao J, et al. A live gI/gE-deleted pseudorabies virus (PRV) protects weaned piglets against lethal variant PRV challenge. *Virus Genes* (2017) 53:565–72. doi: 10.1007/s11262-017-1454-y

10. Miner JJ, Platt DJ, Ghaznavi CM, Chandra P, Santeford A, Menos AM, et al. HSV-1 and zika virus but not SARS-CoV-2 replicate in the human cornea and are restricted by corneal type III interferon. *Cell Rep* (2020) 33:108339. doi: 10.1016/j.celrep.2020.108339

11. Ank N, West H, Bartholdy C, Eriksson K, Thomsen AR. Paludan SRJJov. 2006. lambda interferon (IFN-λ), a type III IFN, is induced by viruses and IFNs and displays potent antiviral activity against select virus infections in vivo. *J Virol* (2006) 80:4501–9. doi: 10.1128/JVI.80.9.4501-4509.2006

12. Deng H, Jian Z, Zhu L, Li F, Zhao J, Deng J, et al. Investigation of the anti-pseudorabies virus activity of interferon lambda 3 in cultured porcine kidney epithelial cells. *Vet Med Sci* (2022). doi: 10.1002/vms3.933

13. Wang D, Fang L, Zhao F, Luo R, Chen H, Xiao S. Molecular cloning, expression and antiviral activity of porcine interleukin-29 (poIL-29). *Dev Comp Immunol* (2011) 35:378–84. doi: 10.1016/j.dci.2010.11.003

14. Kaplan AS, Vatter A. A comparison of herpes simplex and pseudorabies viruses. *Virology* (1959) 7:394–407. doi: 10.1016/0042-6822(59)90068-6

15. Romero N, Van Waesberghe C, Favoreel HW. Pseudorabies virus infection of epithelial cells leads to persistent but aberrant activation of the NF-κB pathway, inhibiting hallmark NF-κB-induced proinflammatory gene expression. *J Virol* (2020) 94:e00196–20. doi: 10.1128/JVI.00196-20

16. Yin Y, Romero N, Favoreel HW. Pseudorabies virus inhibits type I and type III interferon-induced signaling *via* proteasomal degradation of janus kinases. *J Virol* (2021) 95:e00793–21. doi: 10.1128/JVI.00793-21

17. Tombácz D, Tóth JS, Petrovszki P, Boldogkői Z. Whole-genome analysis of pseudorabies virus gene expression by real-time quantitative RT-PCR assay. *BMC Genomics* (2009) 10:1–22. doi: 10.1186/1471-2164-10-491

18. Wang D, Fang L, Liu L, Zhong H, Chen Q, Luo R, et al. Foot-and-mouth disease virus (FMDV) leader proteinase negatively regulates the porcine interferon-λ1 pathway. *Mol Immunol* (2011) 49:407–12. doi: 10.1016/j.molimm.2011.09.009

19. Zhang Q, Ke H, Blikslager A, Fujita T, Yoo D. Type III interferon restriction by porcine epidemic diarrhea virus and the role of viral protein nsp1 in IRF1 signaling. *J Virol* (2018) 92:e01677–17. doi: 10.1128/JVI.01677-17

20. Xu Z, Gong L, Peng P, Liu Y, Xue C, Cao Y. Porcine enteric alphacoronavirus inhibits IFN-α, IFN-β, OAS, Mx1, and PKR mRNA expression in infected peyer's patches *in vivo*. *Front Vet Sci* (2020) 7:449. doi: 10.3389/fvets.2020.00449

21. Li L, Xue M, Fu F, Yin L, Feng L, Liu P. IFN-lambda 3 mediates antiviral protection against porcine epidemic diarrhea virus by inducing a distinct antiviral transcript profile in porcine intestinal epithelia. *Front Immunol* (2019) 10:2394. doi: 10.3389/fimmu.2019.02394

22. Yin Z, Dai J, Deng J, Sheikh F, Natalia M, Shih T, et al. Kotenko and Patricia Fitzgerald-bocarsly. 2012. type III IFNs are produced by and stimulate human plasmacytoid dendritic cells. *J Immunol* (2012) 189:2735–45. doi: 10.4049/jimmunol.1102038

23. Ciencewicki JM, Brighton LE, Jaspers I. Localization of type I interferon receptor limits interferon-induced TLR3 in epithelial cells. *J Interferon Cytokine Res* (2009) 29:289–97. doi: 10.1089/jir.2008.0075

24. Vanderheiden A, Ralfs P, Chirkova T, Upadhyay AA, Zimmerman MG, Bedoya S, et al. Type I and type III interferons restrict SARS-CoV-2 infection of human airway epithelial cultures. *J Virol* (2020) 94:e00985–20. doi: 10.1128/JVI.00985-20

25. Vanderwall ER, Barrow KA, Rich LM, Read DF, Trapnell C, Okoloko O, et al. Airway epithelial interferon response to SARS-CoV-2 is inferior to rhinovirus and heterologous rhinovirus infection suppresses SARS-CoV-2 replication. *Sci Rep* (2022) 12:1–15. doi: 10.1038/s41598-022-10763-2

26. Narita M, Kubo M, Fukusho A, Haritani M, Moriwaki M. Necrotizing enteritis in piglets associated with aujeszky's disease virus infection. *Vet Pathol* (1984) 21:450–2. doi: 10.1177/030098588402100414

27. Zhang C, Liu Y, Chen S, Qiao Y, Zheng Y, Xu M, et al. Effects of intranasal pseudorabies virus AH02LA infection on microbial community and immune status in the ileum and colon of piglets. *Viruses* (2019) 11:518. doi: 10.3390/v11060518

28. Kotenko SV, Rivera A, Parker D, Durbin JE. Type III IFNs: beyond antiviral protection. *Semin Immunol* (2019) 43:101303. doi: 10.1016/j.smim.2019.101303

29. Stanifer ML, Guo C, Doldan P, Boulant S. Importance of type I and III interferons at respiratory and intestinal barrier surfaces. *Front Immunol* (2020) 30:608645. doi: 10.3389/fimmu.2020.608645

30. Lv L, Cao M, Bai J, Jin L, Wang X, Gao Y, et al. PRV-encoded UL13 protein kinase acts as an antagonist of innate immunity by targeting IRF3-signaling pathways. *Vet Microbiol* (2020) 250:108860. doi: 10.1016/j.vetmic.2020.108860

31. Bo Z, Miao Y, Xi R, Zhong Q, Bao C, Chen H, et al. PRV UL13 inhibits cGAS–STING-mediated IFN-β production by phosphorylating IRF3. *Vet Res* (2020) 51:1–16. doi: 10.1186/s13567-020-00843-4

32. Kong Z, Yin H, Wang F, Liu Z, Luan X, Sun L, et al. Pseudorabies virus tegument protein UL13 recruits RNF5 to inhibit STING-mediated antiviral immunity. *PloS Pathog* (2022) 18:e1010544. doi: 10.1371/journal.ppat.1010544

33. Xie J, Zhang X, Chen L, Bi Y, Idris A, Xu S, et al. Pseudorabies virus US3 protein inhibits IFN-β production by interacting with IRF3 to block its activation. *Front Microbiol* (2021) 12. doi: 10.3389/fmicb.2021.761282

34. Qin C, Zhang R, Lang Y, Shao A, Xu A, Feng W, et al. Bclaf1 critically regulates the type I interferon response and is degraded by alphaherpesvirus US3. *PloS Pathog* (2019) 15:e1007559. doi: 10.1371/journal.ppat.1007559

35. Wang M, Liu Y, Qin C, Lang Y, Xu A, Yu C, et al. Pseudorabies virus EP0 antagonizes the type I interferon response *via* inhibiting IRF9 transcription. *J Virol* (2022) 96:e02171–21. doi: 10.1128/jvi.02171-21

36. Peng K, Deng L, Wei J, Zhao J, Deng H, Tao Q, et al. Transcriptome analyses of senecavirus a-infected PK-15 cells: RIG-I and IRF7 are the important factors in inducing type III interferons. *Front Microbiol* (2022) 13. doi: 10.3389/fmicb.2022.846343

37. Cai B, Bai Q, Chi X, Goraya MU, Wang L, Wang S, et al. Infection with classical swine fever virus induces expression of type III interferons and activates innate immune signaling. *Front Microbiol* (2017) 8:2558. doi: 10.3389/fmicb.2017.02558

38. Li L, Fu F, Xue M, Chen W, Liu J, Shi H, et al. IFN-lambda preferably inhibits PEDV infection of porcine intestinal epithelial cells compared with IFN-alpha. *Antiviral Res* (2017) 140:76–82. doi: 10.1016/j.antiviral.2017.01.012

39. Lu M, Qiu S, Zhang L, Sun Y, Bao E, Lv Y. Pseudorabies virus glycoprotein gE suppresses interferon-β production *via* CREB-binding protein degradation. *Virus Res* (2021) 291:198220. doi: 10.1016/j.virusres.2020.198220

40. Lamote JA, Kestens M, Van Waesberghe C, Delva J, De Pelsmaeker S, Devriendt B, et al. The pseudorabies virus glycoprotein gE/gI complex suppresses type I interferon production by plasmacytoid dendritic cells. *J Virol* (2017) 91:e02276–16. doi: 10.1128/JVI.02276-16

41. Huang J, Hume AJ, Abo KM, Werder RB, Villacorta-Martin C, Alysandratos K-D, et al. SARS-CoV-2 infection of pluripotent stem cell-derived human lung alveolar type 2 cells elicits a rapid epithelial-intrinsic inflammatory response. *Cell Stem Cell* (2020) 27:962–973. e7. doi: 10.1016/j.stem.2020.09.013

42. Blanco-Melo D, Nilsson-Payant BE, Liu W-C, Uhl S, Hoagland D, Møller R, et al. Imbalanced host response to SARS-CoV-2 drives development of COVID-19. *Cell* (2020) 181:1036–1045. e9. doi: 10.1016/j.cell.2020.04.026

43. Felgenhauer U, Schoen A, Gad HH, Hartmann R, Schaubmar AR, Failing K, et al. Inhibition of SARS–CoV-2 by type I and type III interferons. *J Biol Chem* (2020) 295:13958–64. doi: 10.1074/jbc.AC120.013788

44. Krishna VD, Roach E, Zaidman NA, Panoskaltsis-Mortari A, Rotschafer JH, O'Grady SM, et al. Differential induction of type I and type III interferons by swine and human origin H1N1 influenza a viruses in porcine airway epithelial cells. *PloS One* (2015) 10:e0138704. doi: 10.1371/journal.pone.0138704

45. Klinkhammer J, Schnepf D, Ye L, Schwaderlapp M, Gad HH, Hartmann R, et al. IFN-λ prevents influenza virus spread from the upper airways to the lungs and limits virus transmission. *elife* (2018) 7:e33354. doi: 10.7554/eLife.33354

46. Zhou Q, Chen V, Shannon CP, Wei X-S, Xiang X, Wang X, et al. Interferon-α2b treatment for COVID-19. *Front Immunol* (2020) 11:1061. doi: 10.3389/fimmu.2020.01061

47. Narita M, Zhao Y, Kawashima K, Arai S, Hirose H, Yamada S, et al. Enteric lesions induced by different pseudorabies (Aujeszky's disease) virus strains inoculated into closed intestinal loops of pigs. *J Vet Diagn Invest* (1998) 10:36–42. doi: 10.1177/104063879801000107

48. Schierack P, Nordhoff M, Pollmann M, Weyrauch KD, Amasheh S, Lodemann U, et al. Characterization of a porcine intestinal epithelial cell line for *in vitro* studies of microbial pathogenesis in swine. *Histochem Cell Biol* (2006) 125:293–305. doi: 10.1007/s00418-005-0067-z

49. Saxena K, Simon LM, Zeng X-L, Blutt SE, Crawford SE, Sastri NP, et al. A paradox of transcriptional and functional innate interferon responses of human intestinal enteroids to enteric virus infection. *Proc Natl Acad Sci* (2017) 114:E570–9. doi: 10.1073/pnas.1615422114

50. Pervolaraki K, Stanifer ML, Münchau S, Renn LA, Albrecht D, Kurzhals S, et al. Type I and type III interferons display different dependency on mitogen-activated protein kinases to mount an antiviral state in the human gut. *Front Immunol* (2017) 8:459. doi: 10.3389/fimmu.2017.00459

51. Zhao M, Li L, Zhai L, Yue Q, Liu H, Ren S, et al. Comparative transcriptomic and proteomic analyses prove that IFN-λ1 is a more potent inducer of ISGs than IFN-α against porcine epidemic diarrhea virus in porcine intestinal epithelial cells. *J Proteome Res* (2020) 19:3697–707. doi: 10.1021/acs.jproteome.0c00164

52. Stanifer ML, Kee C, Cortese M, Zumaran CM, Triana S, Mukenhirn M, et al. Critical role of type III interferon in controlling SARS-CoV-2 infection in human intestinal epithelial cells. *Cell Rep* (2020) 32:107863. doi: 10.1016/j.celrep.2020.107863

frontiers | Frontiers in Immunology

TYPE Original Research
PUBLISHED 24 November 2022
DOI 10.3389/fimmu.2022.1050718

OPEN ACCESS

EDITED BY
Emilie Narni-Mancinelli,
INSERM U1104 Centre d'immunologie de Marseille-Luminy (CIML), France

REVIEWED BY
Norberto Walter Zwirner,
Consejo Nacional de Investigaciones Científicas y Técnicas (CONICET), Argentina
Stephen Noel Waggoner,
Cincinnati Children's Hospital Medical Center, United States

*CORRESPONDENCE
Bree Foley
bree.foley@telethonkids.org.au

†These authors have contributed equally to this work

SPECIALTY SECTION
This article was submitted to NK and Innate Lymphoid Cell Biology, a section of the journal Frontiers in Immunology

RECEIVED 22 September 2022
ACCEPTED 04 November 2022
PUBLISHED 24 November 2022

CITATION
Barnes SA, Audsley KM, Newnes HV, Fernandez S, de Jong E, Waithman J and Foley B (2022) Type I interferon subtypes differentially activate the anti-leukaemic function of natural killer cells.
Front. Immunol. 13:1050718.
doi: 10.3389/fimmu.2022.1050718

Type I interferon subtypes differentially activate the anti-leukaemic function of natural killer cells

Samantha A. Barnes[1,2], Katherine M. Audsley[1,2], Hannah V. Newnes[1,2], Sonia Fernandez[2], Emma de Jong[1], Jason Waithman[1,2†] and Bree Foley[1*†]

[1]Telethon Kids Institute, The University of Western Australia, Nedlands, WA, Australia, [2]School of Biomedical Sciences, The University of Western Australia, Crawley, WA, Australia

Natural killer (NK) cells have an intrinsic ability to detect and eliminate leukaemic cells. Cellular therapies using cytokine-activated NK cells have emerged as promising treatments for patients with advanced leukaemia. However, not all patients respond to current NK cell therapies, and thus improvements in efficacy are required. Type I interferons (IFN-I) are a family of potent immunomodulatory cytokines with a known ability to modulate NK cell responses against cancer. Although the human IFN-I family comprises 16 distinct subtypes, only IFNα2 has been widely explored as an anti-cancer agent. Here, we investigated the individual immunomodulatory effects each IFNα subtype and IFNβ had on NK cell functionality to determine whether a particular subtype confers enhanced effector activity against leukaemia. Importantly, IFNα14 and IFNβ were identified as superior activators of NK cell effector function *in vitro*. To test the ability of these subtypes to enhance NK cell activity *in vivo*, IFN-I stimulation was overlaid onto a standard *ex vivo* expansion protocol to generate NK cells for adoptive cell therapy. Interestingly, infusion of NK cells pre-activated with IFNα14, but not IFNβ, significantly prolonged survival in a preclinical model of leukaemia compared to NK cells expanded without IFN-I. Collectively, these results highlight the diverse immunomodulatory potencies of individual IFN-I subtypes and support further investigation into the use of IFNα14 to favourably modulate NK cells against leukaemia.

KEYWORDS

natural killer cells, leukemia, interferon subtypes, adoptive cell therapy, immunotherapy

10.3389/fimmu.2022.1050718

Introduction

Natural killer (NK) cells are a cytotoxic group of innate lymphoid cells that play an important role in the elimination of virally infected and malignant cells. Over the past two decades the therapeutic antitumour potential of NK cells has become well established across the settings of allogeneic haematopoietic stem cell transplantation and adoptive cell therapy (ACT) [reviewed (1)]. Following repeated success in clinical trials, donor-derived NK cell therapies have emerged as a safe and effective treatment option for patients with haematological malignancies such as leukaemia. While consistent progress has been made over the past 20 years, not all patients respond to current NK cell therapies. As such, the development and optimisation of strategies which can potently enhance NK cell anti-leukaemic function has become a major focus of the field.

Type I interferons (IFN-I) are well-known for their capacity to modulate NK cell immunity (2). IFN-I has been shown to be critical in controlling NK cell anti-tumour responses in several murine models [reviewed (2)] including limiting metastasis formation in a breast cancer model (3). Additionally, IFN-I has also been shown to play an important role in NK cell development (4), homeostasis (5), and the formation of memory responses (6). Despite their role in immunity often being regarded universal, 16 functional IFN-I subtypes exist. These include 12 distinct IFNα subtypes (IFNα1, -α2, -α4, -α5, -α6, -α7, -α8, -α10, -α14, -α16, -α17 and -α21), IFNβ, and the lesser-known IFNϵ, IFNκ, and IFNw (7). Although each subtype binds to the common IFNα/β receptor (IFNAR), their biological activities are not equivalent. In a viral setting individual IFN-I subtypes harbour differing capacities to suppress viral replication (8, 9) and to modulate $CD4^+$ and $CD8^+$ T cell responses (10, 11) and NK cell activity (11, 12). Additionally, we have recently demonstrated that individual IFN-I subtypes also harbor differing capacities for driving antitumor immunity in murine models of melanoma (13, 14); however, this has yet to be explored in a human setting. To date, IFNα2 (IFNα2B) remains the only IFNα subtype clinically approved for the treatment of cancer (15).

While earlier studies have explored the ability of a small subset of IFNα subtypes to augment NK cell cytotoxicity *in vitro* (16), there has been no systematic analysis to determine whether a particular IFN-I subtype confers enhanced NK cell responses against leukaemia. As such, it remains possible that several of the untested IFNα subtypes or IFNβ may drive a more potent NK cell response than the clinically approved IFNα2B subtype. Here, we aim to close this knowledge gap by investigating the individual immunomodulatory properties of the 12 IFNα subtypes and IFNβ on NK cells. We directly compared the effect each IFN-I subtype has on enhancing NK cell functionality, focussing on their ability to promote NK cell degranulation, cytokine production and polyfunctionality against target cells *in vitro*, upregulate expression of activation markers and cytotoxic molecules, activate STAT signalling pathways, and synergise with an established *ex vivo* pre-activation strategy to generate therapeutic NK cells for ACT.

In a cohort of 50 healthy adult donors, we report that nearly all IFN-I subtypes tested were more effective at enhancing NK cell degranulation and cytokine production in response to target cell stimulation than the clinical IFNα2B subtype. From this initial screen we identified three top candidate subtypes (IFNα6, IFNα14, IFNβ) with increased ability to upregulate activation markers and cytotoxic effector molecules, enhanced potential for JAK/STAT signalling, and improved capacities to prime NK cells to respond to respond to IL-15-mediated signalling. Furthermore, when incorporated into a standard *ex vivo* expansion protocol to generate NK cells for ACT, these subtypes were superior at increasing NK cell anti-leukaemic activity over IFNα2B. Importantly, adoptive transfer of IFNα14-activated NK cells significantly prolonged survival in a preclinical model of leukaemia compared to control NK cells expanded without IFN-I. These results demonstrate the need to take into consideration the different potential of IFN-I subtypes to enhance NK cell anti-leukaemic responses and support further clinical development of these subtypes for optimal cancer treatments.

Materials and methods

NK cell donors

Blood was obtained from 50 blood donors attending The Australian Red Cross Blood Service, Western Australia, with informed consent obtained in accordance with the Declaration of Helsinki. Written approval to use blood samples was obtained from the University of Western Australia (RA/4/1/7311). Peripheral blood mononuclear cells (PBMCs) were purified by density centrifugation using Lymphoprep (Stemcell Technologies) and cryopreserved. Before analysis, the thawed cells were incubated overnight at 37°C in complete media (R10) (RPMI (Life Technologies) supplemented with 10% foetal calf serum (CellSera), 100 U mL^{-1} penicillin, 100 mg mL^{-1} streptomycin, 2 mM GlutaMax, 50 mM 2-ME, 1% sodium pyruvate and 1% non-essential amino acids (all Life Technologies)). Where indicated, cells were immediately stimulated following thawing with either 100 IU mL^{-1} IFNα (PBL Assay Science) or IFNβ (Stemcell Technologies) for 16-18 hours prior to analysis.

K562 cell line

The MHC class I-negative cell line K562 was obtained from the American Type Culture Collection (ATCC). Cells were maintained in complete media (R10) and used within three weeks after thawing.

Functional flow assay

Expression of CD107a and production of TNFα and IFNγ were measured as described previously (17). Briefly, PBMCs were either left unstimulated or were stimulated overnight. The next day, cells were washed and then co-incubated with K562 target cells at an effector-to-target (E:T) ratio of 2:1 for 5 hours. Anti-CD107a (H4A3) was added at the start of culture. Brefeldin A and monensin (both BD Biosciences) were added after 1 hour. The following antibodies were used: anti-CD56 (clone B159), anti-CD3 (SK7), anti-IFNγ (B27), anti-TNFα (MAb11) and fixable viability stain FV575 (all BD Biosciences). Cells were analysed on an BD LSR Fortessa X-20 and using FlowJo Version 10 software (BD Biosciences).

Phenotyping of NK cells

NK cell expression of activation markers and cytotoxic effector molecules was assessed using the following antibodies: anti-CD56 (B159), anti-CD3 (SK7), anti-NKG2D (1D11), anti-NKp30 (p30-15), anti-NKp46 (9E2/NKp46), anti-CD2 (RPA-2.10), anti-CD108 (KS-2), anti-CD160 (BY55), anti-CD244 (C1.7), anti-granzyme B (GB11) and anti-perforin (δG9). Cells were analysed on an BD LSR Fortessa X-20 and using FlowJo Version 10 software.

Phosflow

PBMCs were either left unstimulated or were stimulated with 100 IU mL^{-1} IFNα or IFNβ overnight (pSTAT5) or for 30 min (pSTAT1 and pSTAT3). For pSTAT5 analysis, cells were washed and re-stimulated with 5 ng mL^{-1} IL-15 for 15 min. Cells were then immediately fixed in Lyse/Fix Buffer and permeabilised in Perm Buffer III (both BD Biosciences). The following antibodies were used: anti-CD56 (B159), anti-CD3 (SK7), anti-pSTAT1 (pY701), anti-pSTAT3 (pY705) and anti-pSTAT5 (pY694) (all BD Biosciences). Cells were analysed on a BD LSR Fortessa X-20 and using FlowJo version 10 software.

NK cell expansion

PBMCs were thawed on day -1 and cultured at $3x10^6$ cells mL^{-1} in R10. The following day, NK cells were expanded with irradiated K562 cells at a 6:1 ratio in R10 supplemented with 10 IU mL^{-1} (increasing to 100 IU mL^{-1} on day 7) recombinant human IL-2 (Life Technologies) and 5 ng mL^{-1} recombinant human IL-15 (Peprotech), replacing half the media every 2-3 days and splitting 1:2 ($<4x10^6$ cells mL^{-1}) or 1:4 ($\geq4x10^6$ cells mL^{-1}) on day 7. Where indicated, 100 IU mL^{-1} IFNα or IFNβ was added on day -1 and/or day 13. NK cells were collected on day 14, washed, and effector function was assessed. For *in vivo* experiments, NK cells were expanded as described above in CellGenix® GMP Stem Cell Growth Medium (Sartorius CellGenix), either with or without addition of 100 IU mL^{-1} IFNα14 or IFNβ on day -1 and day 13. Cells were collected on day 14 and washed three times in PBS in preparation for adoptive transfer.

Adoptive NK cell transfer

Eight- to ten-week-old NOD.Cg-Prkdc^{scid} Il2rg^{tm1Wjl}/SzJ (NSG) mice were purchased from the Animal Research Centre, Perth, Australia. Animals were housed under specific pathogen-free conditions and all studies were approved by the Animal Ethics Committee, Telethon Kids Institute, Perth, Australia. Mice received adoptive transfer of $1x10^6$ K562 cells on day 0. Following engraftment of leukaemic cells mice received adoptive transfer of $4.5x10^6$ NK cells on day 4. Mice received thrice weekly intraperitoneal injections of 0.5 mg recombinant human IL-15 (Miltenyi Biotech) starting on the day of adoptive NK cell transfer and continuing for the following two weeks. Mice were then monitored for disease progression and were euthanised once symptoms of leukaemia developed.

Statistics

Data were summarized with mean and standard error of the mean (mean ± SEM). Where appropriate, data were tested for normal distribution using the Shapiro-Wilk normality test. For comparisons between independent samples, the Student's t-test was used. For comparisons of matched samples, the paired t-test was used. For *in vivo* experiments, length of survival between groups was compared using the Log Rank (Mantel-Cox) test. Statistical significance was indicated as $^*p < 0.05$, $^{**}p < 0.01$, $^{***}p < 0.001$ and $^{****}p < 0.0001$. Statistical analyses were performed using Prism 8 (GraphPad Software).

Results

Individual IFN-I subtypes display different capacities to modulate NK cell effector function against leukaemia *in vitro*

To compare the potential of each individual IFN-I subtype to activate NK cells, we carried out a comprehensive *in vitro* screening assay of NK cell anti-leukaemic activity. PBMCs from 50 healthy donors were left unstimulated (baseline) or were stimulated with or 100 IU mL^{-1} of each IFNα subtype or IFNβ overnight (16-18 hours). Cells were then washed and co-cultured with the class-I negative leukaemic cell line K562 for 5

hours, after which NK cells were assessed for their capacity to degranulate (as evidenced by expression of CD107a on the cell surface) or produce cytokines (IFNγ and TNFα) (Supplementary Figure 1A). Stimulation with IFN-I enhanced NK cell degranulation and production of IFNγ and TNFα compared to baseline (24.83% ± 1.19%, 7.6% ± 0.64% and 13.68% ± 1.18%, respectively; data not shown), with individual IFN-I subtypes modulating NK cell effector functions to varying extents (Figure 1A). Despite variability between individual donors, the pattern of enhanced NK cell activity was largely maintained across the donor pool for each IFN-I subtype. Stimulation with IFNβ, IFNα6 or IFNα14 resulted in the most robust increase in NK cell degranulation, cytokine production and polyfunctionality on average across all donors (Figure 1B; Supplementary Figure 1B). IFNβ and IFNα14 stimulation resulted in the highest mean percentage of total NK cells expressing CD107a (61.04% ± 1.27% and 60.34% ± 1.35%, respectively), whereas IFNβ and IFNα6 stimulation resulted in the highest levels of IFNγ (26.74% ± 1.4% and 25.23% ± 1.26%, respectively) and TNFα production (39.86% ± 1.96% and 39.26% ± 1.92%, respectively). IFNβ stimulation also promoted the greatest levels of polyfunctionality, resulting in the highest mean percentage of NK cells co-expressing CD107a and IFNγ (24.27% ± 1.35%), CD107a and TNFα (37.54% ± 1.95%), IFNγ and TNFα (21.89% ± 1.37%), and CD107a and IFNγ and TNFα (20.66% ± 1.33%). Furthermore, stimulation with IFNβ, IFNα6 or IFNα14 resulted in a significantly greater fold-change increase in NK cell degranulation, cytokine production and polyfunctionality compared to baseline than the clinically approved subtype IFNα2B (Figure 1C). As such, we selected these top three candidate subtypes (IFNα6, IFNα14 and IFNβ) to carry forward in this study, alongside the representative clinical subtype IFNα2B.

IFN-I stimulation primes NK cells for cytotoxicity

The release of granules containing cytotoxic proteins, such as perforin and granzyme B, is the major mechanism through which NK cells lyse target cells (18). Since activation with IFNα6, IFNα14 and IFNβ significantly enhanced NK cell degranulation in response to leukaemic target cells, we next evaluated the effect of IFN-I stimulation on the expression of these cytotoxic proteins. Overnight stimulation with each of the selected IFN-I subtypes (IFNβ, IFNα2B, IFNα6 or IFNα14) was found to significantly increase expression of granzyme B and perforin compared to baseline (unstimulated) (Figure 2A). However, no significant differences in expression levels were identified between the IFN-I subtypes.

NK cell activation relies on the complex and hierarchical integration of signals through various activating receptors (19). To investigate how our top candidate IFN-I subtypes prime NK cells for enhanced effector activity, we next sought to investigate the effect of IFN-I stimulation on the expression of activating and costimulatory NK cell receptors. Following overnight stimulation with either media alone (unstimulated) or each of the selected IFN-I subtypes, NK cells were analysed for expression of several key markers involved in NK cell activation, adhesion and functional potential including NKG2D, NKp30, NKp46, CD244 (2B4), CD2, CD108 and CD160. No difference in the expression of 2B4 or NKp30 was observed following IFN-I stimulation (data not shown). Stimulation with each of the selected IFN-I subtypes resulted in an increase in the expression of CD2, NKp46, CD108 and NKG2D compared to baseline, whereas CD160 expression was selectively increased by stimulation with IFNα6 and IFNα14 but not IFNβ or IFNα2B (Figure 2B). Interestingly, IFNα14 stimulation also resulted in significantly greater expression of CD108, NKG2D and CD160 compared to IFNα2B.

Selected IFN-I subtypes differentially activate STAT1 and STAT3 signalling pathways

Despite all binding to the common IFNAR, it has been reported that individual IFN-I subtypes drive distinct downstream signalling cascades, and thus biological effects, through phosphorylation of various STAT molecules (20). In NK cells, IFN-I stimulation predominantly activates STAT1 and, to a lesser degree, STAT3 signalling (21). STAT1 and STAT3 are major regulators of NK cell cytotoxicity and IFNγ production (22–25). As such, we investigated the individual capacity for each of our top-performing IFN-I subtypes to activate STAT1 and STAT3 signalling in NK cells. We observed a significant increase in the expression of phosphorylated STAT1 (pSTAT1) and phosphorylated STAT3 (pSTAT3) following stimulation with each of the selected IFN-I subtypes compared to baseline (Figure 3). Strikingly, stimulation with IFNβ, IFNα6 and IFNα14 also resulted in significantly higher expression of both pSTAT1 and pSTAT3 compared to IFNα2B.

IFNα6 and IFNα14 stimulation primes NK cells to respond to IL-15

It has previously been reported that IFNα stimulation primes NK cells to respond to IL-15, increasing IL-15-mediated phosphorylation of STAT5 and subsequently enhancing cytotoxicity against K562 target cells (26). To study the capacity of individual IFN-I subtypes to mediate this effect, we analysed the expression of IL-15-mediated phosphorylated STAT5 (pSTAT5) in NK cells that had been pre-activated overnight with either media alone (unprimed) or with each of the selected IFN-I subtypes (Figure 4A). Pre-activation with IFNα6 and IFNα14 significantly

10.3389/fimmu.2022.1050718

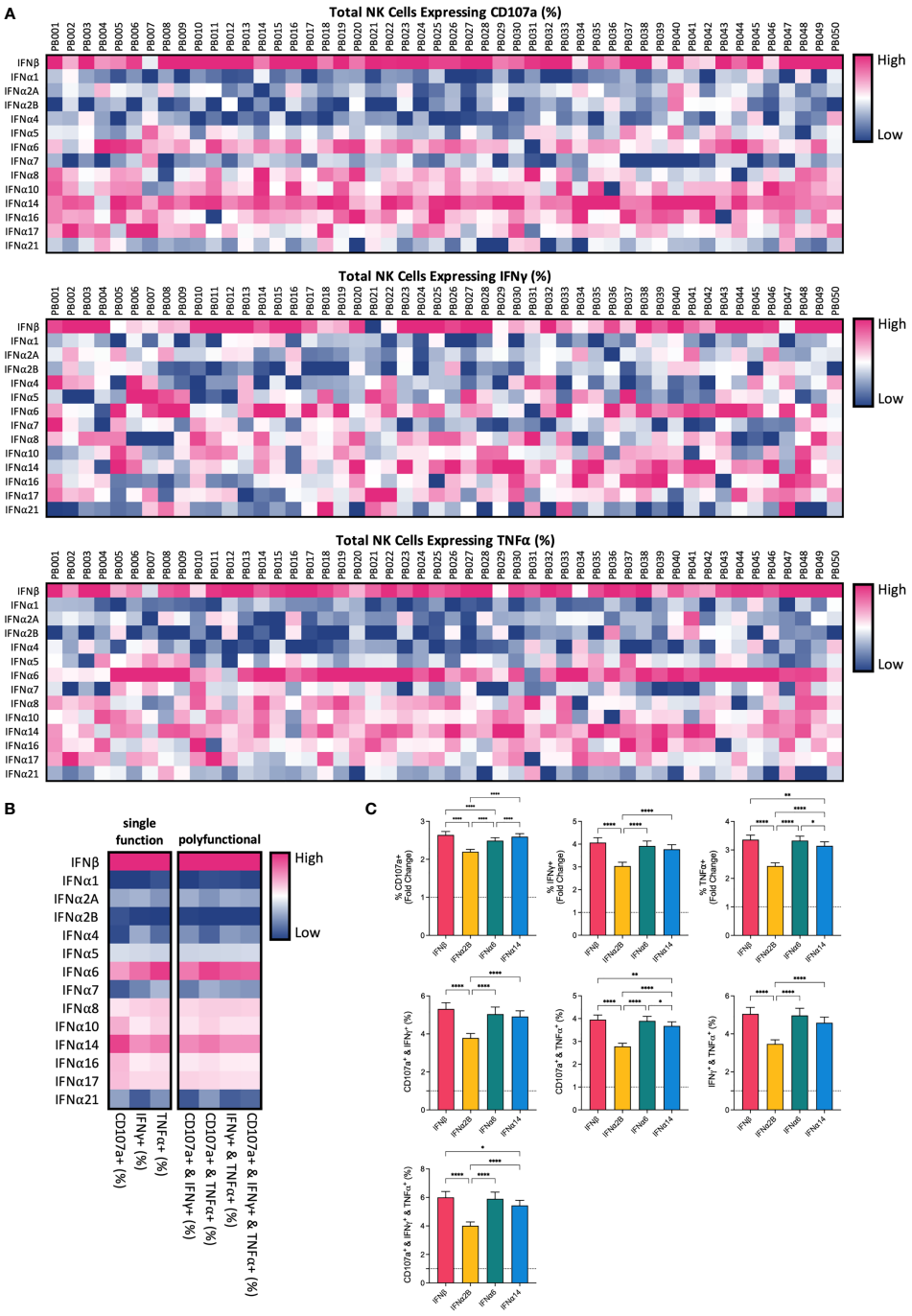

FIGURE 1
IFN-I subtypes differentially activate NK cell effector functions PBMCs from 50 healthy donors (PB001-PB050) were either left unstimulated (baseline; data not shown) or were stimulated with 100 IU mL^{-1} of each IFNα; subtype or IFNβ overnight. Following overnight activation, cells were washed and then co-incubated with K562 cells for 5 hours at a 2:1 E:T ratio and NK cell effector functions were assessed. **(A)** Heatmaps summarizing the percentage of $CD56^{+}CD3^{neg}$ NK cells expressing CD107a (range: 17.40-81.10%) or producing IFNγ (range: 4.19-50.20%) or TNFα (range: 2.24-74.4%) for each donor in response to individual IFN-I subtypes. **(B)** The mean percentage of NK cells expressing CD107a, IFNγ or TNFα, or a combination of two or more of these functional markers, was calculated for each IFN-I subtype across all donors. **(C)** Summary data show mean ± SEM fold change difference in the percentage of NK cells expressing CD107a, IFNγ or TNFα, or a combination of two or more of these functional markers, following stimulation with selected IFN-I subtypes compared to baseline (dotted line). Data were compared using paired Student's *t* tests. *$p < 0.05$, **$p < 0.01$, ****$p < 0.0001$.

10.3389/fimmu.2022.1050718

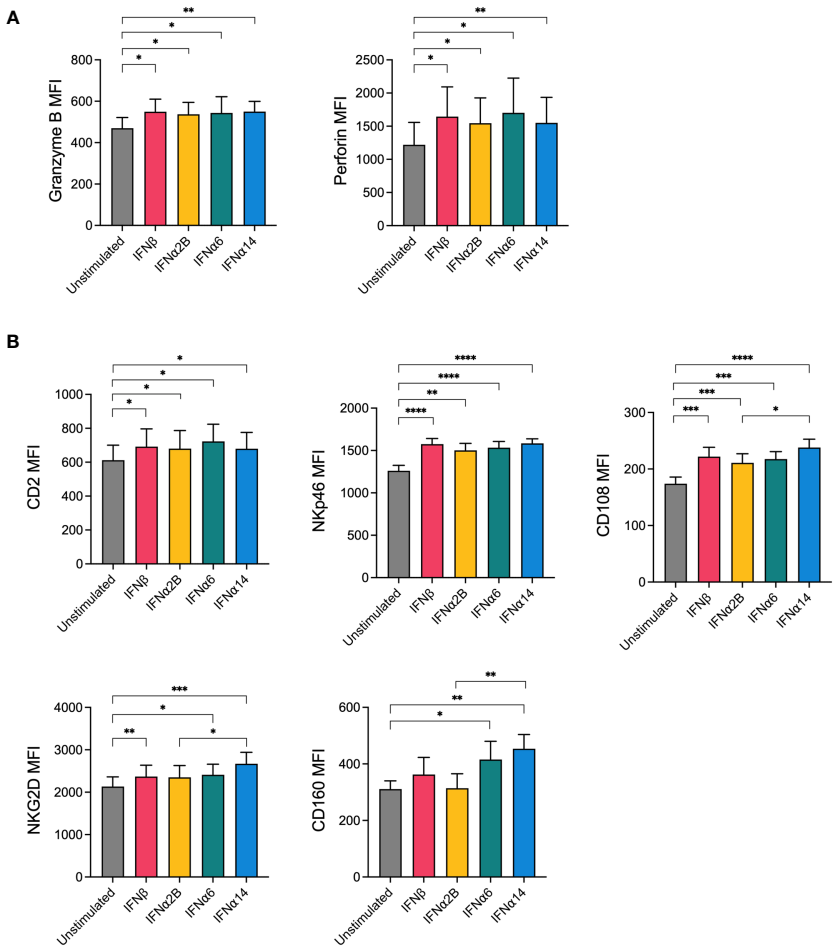

FIGURE 2
NK cells display increased expression of cytotoxic effector molecules and activation markers following IFN-I activation PBMCs were either left unstimulated or were stimulated with 100 IU mL^{-1} of IFNβ, IFNα2B, IFNα6 or IFNα14 overnight. Following overnight activation, $CD56^{+}CD3^{neg}$ NK cells were assessed for the expression of granzyme B and perforin or for the expression of five activation markers (CD2, NKp46, CD108, NKG2D, CD160). **(A)** Summary plots show the mean ± SEM granzyme B or perforin MFI in unstimulated and IFN-I stimulated NK cells. **(B)** Summary plots show the mean ± SEM MFI of the indicated activation markers in unstimulated and IFN-I stimulated NK cells. n = 8-13 healthy donors. Data were compared using paired Student's *t* tests. $*p < 0.05$, $**p < 0.01$, $***p < 0.001$, $****p < 0.0001$.

increased the level of IL-15-induced STAT5-phosphorylation compared to the unprimed controls (Figure 4B). In contrast, there was no difference in pSTAT5 expression following pre-activation with IFNα2B and IFNβ, suggesting that not all IFN-I subtypes mediate this priming effect.

IFNα14 and IFNβ stimulation enhances NK cell anti-leukaemic activity *in vitro* following *ex vivo* expansion

IL-2 and IL-15 form the backbone of many current *ex vivo* expansion protocols to generate therapeutic NK cells for ACT (27). To investigate the ability for IFN-I stimulation to boost the activity of an NK cell therapy product, we next incorporated the selected IFN-I subtypes into a 14-day *ex vivo* NK cell expansion strategy using IL-2, IL-15 and irradiated K562 feeder cells (Figure 5A). We first optimised the timing of IFN-I stimulation using IFNα14 and IFNβ and found that two doses of IFN-I (administered on day -1 and day 13) resulted in the greatest levels of NK cell degranulation and IFNγ production in response to K562 target cells on day 14 (Figure 5B). Interestingly, even a single dose of IFN-I given at the start of the culture resulted in significantly increased NK cell activity compared to cells that received no IFN-I. Nevertheless, as the greatest increase in NK cell activity resulted from the two-dose schedule we selected these timepoints to carry forward in this study.

Using this two-dose schedule we next screened each of the selected IFN-I subtypes to identify which subtype(s) generated an NK cell therapy product with heightened anti-leukaemic

10.3389/fimmu.2022.1050718

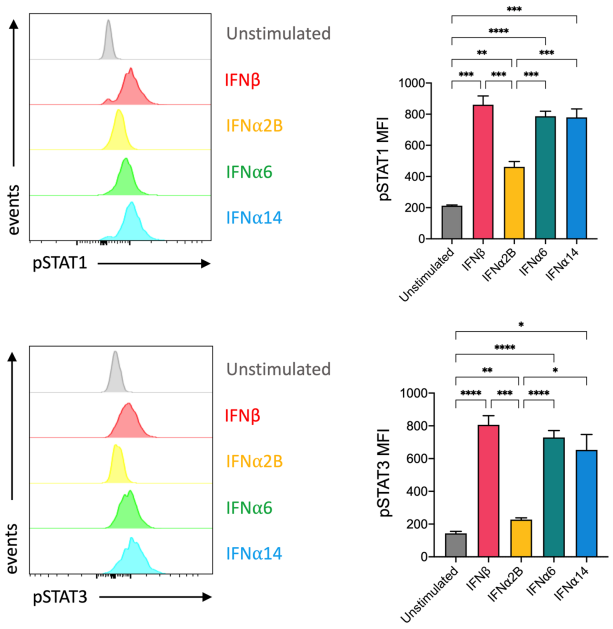

FIGURE 3
IFNβ, IFNα6 and IFNα14 activation induces stronger phosphorylation of STAT1 and STAT3 in NK cells than the clinical standard IFNα2B PBMCs were assessed for the expression of phosphorylated STAT1 (pY701) or STAT3 (pY705) at baseline (unstimulated) and following stimulation with 100 IU mL^{-1} of IFNβ, IFNα2B, IFNα6 or IFNα14 for 30 mins. Representative histogram plots show per-cell pSTAT1 or pSTAT3 expression in $CD56^{+}CD3^{-}$ NK cells. Summary data show mean ± SEM pSTAT1 or pSTAT3 MFI in unstimulated and IFN-I stimulated NK cells. n = 7 healthy donors, 2 independent experiments. Data were compared using a paired Student's *t* test. *$p < 0.05$, **$p < 0.01$, ***$p < 0.001$, ****$p < 0.0001$.

activity. Upon comparison of NK cell effector functions on day 14, we demonstrated that NK cells activated with each of the selected IFN-I subtypes exhibited varying levels of degranulation and production of IFNγ and TNFα in response to K562 target cells (Figure 5C). IFNα2B-activated and control NK cells harboured similar levels of activity, further demonstrating the importance of subtype selection in enhancing NK cell effector function. Notably, NK cells activated with IFNα14 and IFNβ harboured the greatest anti-leukaemic potential, demonstrating significantly greater levels of degranulation and cytokine production compared to both control NK cells and those activated with IFNα2B. It should be noted that activation with IFNα14, but not the other tested IFN-I subtypes, resulted in a small but significantly lower average yield of NK cells on day 14 compared to control (data not shown). Nevertheless, the two highest performing subtypes, IFNα14 and IFNβ, were selected to test the therapeutic efficacy of IFN-I activated NK cells *in vivo*.

Pre-activation with IFNα14, but not IFNβ, improves efficacy of NK cell ACT against leukaemia

Finally, we evaluated the ability of IFNα14- or IFNβ-activated NK cells to control leukaemia *in vivo*. Cohorts of NSG mice were inoculated with K562 leukaemic cells four days prior to receiving adoptive transfer of $4.5x10^{6}$ activated NK cells which had been expanded either without IFN-I (control NK) or with two doses of IFNα14 or IFNβ (Figure 6A). Strikingly, adoptive transfer of IFNα14-activated NK cells significantly prolonged survival compared to both no treatment and treatment with control NK cells (Figure 6B). In contrast, no difference in survival was observed following adoptive transfer of IFNβ-activated NK cells. These findings highlight the diverse immunomodulatory effects individual IFN-I subtypes induce and provide further evidence supporting IFNα14 as the optimal subtype for enhancing NK cell functional responses against leukaemia.

Discussion

NK cells are ideal candidates for cellular therapy due to their intrinsic ability to detect and eliminate leukaemic cells. Although NK cells are unique in their ability to lyse malignant cells without prior sensitisation, cytokines are commonly used to prime NK cells for enhanced antitumor activity. Here, we investigated the ability of each human IFNα subtype and IFNβ to boost NK cell effector functions against leukaemia. We report that individual IFN-I subtypes differ in their capacity to activate NK cell degranulation and cytokine production. Critically, we identified IFNα14 and

10.3389/fimmu.2022.1050718

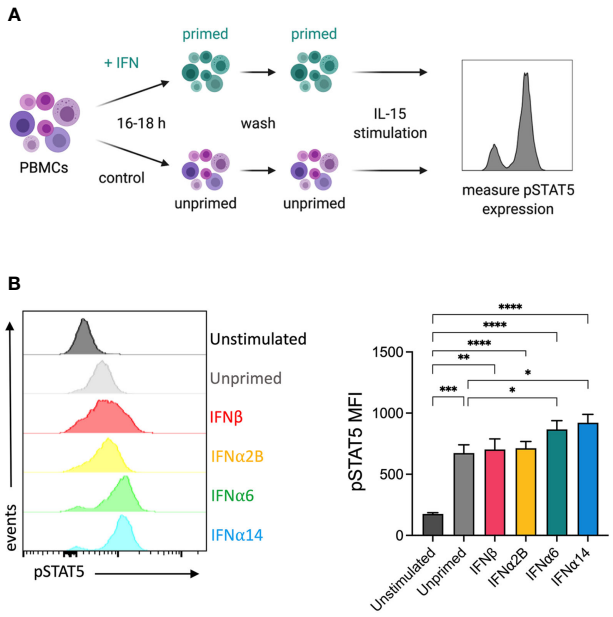

FIGURE 4
IFNα6 and IFNα14 activation primes NK cells to respond to IL-15 stimulation **(A)** Experimental design. PBMCs were either left unstimulated or were primed with 100 IU mL^{-1} of IFNβ, IFNα2B, IFNα6 or IFNα14 overnight. Following overnight activation, cells were washed and then assessed for the expression of phosphorylated STAT5 (Y694) at baseline (unstimulated) or following stimulation with 5 ng mL^{-1} IL-15 for 15 mins. **(B)** Representative histogram plot shows per-cell pSTAT5 expression in unstimulated, unprimed, and IFN-I primed $CD56^{+}CD3^{-}$ NK cells. Summary data show mean ± SEM pSTAT5 MFI in unstimulated, unprimed, and IFN-I primed NK cells. n = 10 healthy donors, 3 independent experiments. Data were compared using a paired Student's *t* test. *$p < 0.05$, **$p < 0.01$, ***$p < 0.001$, ****$p < 0.0001$.

IFNβ as the most potent subtypes for enhancing NK cell activity *in vitro* following both overnight activation and as part of a prolonged 14-day *ex vivo* activation strategy. When tested therapeutically, adoptive transfer of NK cells activated with IFNα14, but not IFNβ, significantly prolonged survival in an NSG xenograft model of K562 leukaemia. Collectively, these results highlight the differing potencies of IFN-I subtypes as modulators of NK cell immunity and provide support for the development of IFNα14-based NK cellular therapy strategies.

Whilst previous studies have primarily focussed on the antitumour activity of IFNα2, the human genome encodes 12 functional IFNα subtypes and one IFNβ subtype which have been shown to mediate distinct biological effects (7). The differing activities of individual IFN-I subtypes have been attributed to a variety of mechanisms, including binding affinities for IFNAR1 and IFNAR2 subunits (28, 29); stability of the ternary IFN-I/IFNAR complex (30); sensitivity to negative feedback (31); and stimulation of distinct interferon stimulated gene (ISG) expression patterns (29, 32). Interestingly, we report that both IFNα2 variants (IFNα2A and IFNα2B) were among the lowest performing subtypes in our overnight screening assay of NK cell activation. Compared to IFNα2, IFNβ binds to IFNAR with higher affinity (33), forms a longer-lived IFN-I/IFNAR complex (30), and drives a unique gene expression pattern (29), all of which may contribute towards its superior ability to enhance NK cell effector activity. Although IFNα14 has a lower binding affinity to both IFNAR1 (0.68 μM to 3.8 μM) and IFNAR2 (0.7 nM to 1.3 nM) subunits than IFNα2B (34), our findings suggest that both IFNα14 and IFNβ may induce more robust activation of downstream STAT signalling cascades. We observed that stimulation with IFNα14 and IFNβ resulted in greater activation of both STAT1 and STAT3 signalling than IFNα2B. These findings are supported in a recent study by Karakoese and colleagues, in which increased STAT1 and STAT3 signalling was demonstrated in both NK cells and $CD4^{+}$ and $CD8^{+}$ T cells following stimulation with IFNα14 and IFNβ in comparison to IFNα2 (11). Furthermore, both IFNα14 and IFNβ significantly increased the percentage of $CD107a^{+}$ NK and T cells from *in vitro* HIV-infected PBMCs, further demonstrating the enhanced functional potential conferred by these subtypes (11). STAT1 is known to be a critical regulator of NK cell cytotoxicity and IFNγ production (22–24), however there is conflicting evidence about the role STAT3 plays in NK cell function. Although STAT3 activation has been reported to suppress NK cell cytotoxicity in mice (35, 36), there is also evidence for a STAT3-dependent increase in NKG2D expression which may contribute towards enhanced NKG2D-mediated antitumor responses (37, 38). Whilst we observed an increase in NKG2D expression on both IFNα14- and IFNβ-activated NK cells, only IFNα14 stimulation yielded a significant increase in NKG2D expression compared to those activated with IFNα2B. In addition, IFNα14-activated NK cells also demonstrated

10.3389/fimmu.2022.1050718

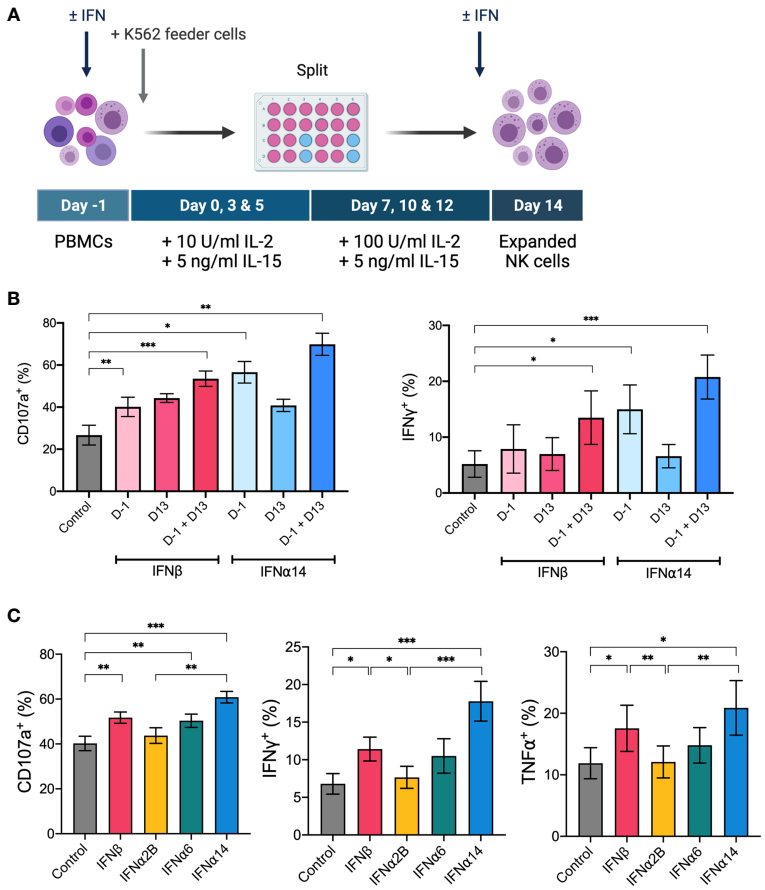

FIGURE 5
IFNα14 and IFNβ stimulation enhances NK cell activity *in vitro* following *ex vivo* expansion PBMCs were expanded *ex vivo* for 14 days either with or without IFN-I stimulation. **(A)** Schematic of NK cell expansion strategy. On day -1 PBMCs were left unstimulated or stimulated with 100 IU mL^{-1} IFN-I overnight. Following overnight activation, NK cells were expanded for 13 days with IL-15, IL-2, and irradiated K562 feeder cells. On day 13 NK cells were either left unstimulated or stimulated with 100 IU mL^{-1} IFN-I overnight. **(B)** Expanded NK cells that received either no IFN-I activation (control), one dose of IFN-I (D-1 or D13), or two doses of IFN-I (D-1 + D13) were collected on day 14, washed, and assessed for effector function following stimulation with K562 cells for 5 hours at a 2:1 E:T ratio. Summary plots show the mean + SEM percentage of $CD56^{+}CD3^{neg}$ NK cells expressing CD107a or producing IFNγ or TNFα. n = 5, 2 independent experiments. Data were compared to the control condition using a paired Student's *t* test. *$p < 0.05$, **$p < 0.01$, ***$p < 0.001$. **(C)** PBMCs from 16 healthy donors were expanded either without IFN-I stimulation (control) or with IFN-I stimulation on day -1 and day 13. Expanded NK cells were collected on day 14, washed, and assessed for effector function following stimulation with K562 cells at a 2:1 E:T for 5 hours. Summary data show mean ± SEM percentage of $CD56^{+}CD3^{neg}$ NK cells expressing CD107a or producing IFNγ or TNFα. Data were compared using a paired Student's *t* test. *$p < 0.05$, **$p < 0.01$, ***$p < 0.001$.

significantly greater expression of the activating receptor CD160, which has been shown to plan an essential role in IFNγ production (39), and CD108 (semaphorin 7A), a potent immunomodulator that is strongly upregulated on both highly activated and cytokine-induced memory-like NK cells (40), which may have further contributed towards their enhanced effector response. Taken together, these findings highlight the diverse immunomodulatory effects of individual IFN-I subtypes and future studies exploring the mechanisms that drive enhanced anti-leukaemic responses are certainly warranted.

IL-15 currently forms the backbone of many current clinical *ex vivo* expansion protocols to generate NK cells for ACT (27). IL-15 plays an essential role in NK cell development, promoting survival and enhancing NK cell mediated anti-tumour responses (41). In a previous study, IFNα stimulation was reported to prime NK and T cells for greater IL-15-mediated signalling and cytotoxicity (26). Here, we report that our top performing IFN-I subtypes differed in their capacity to prime NK cells for IL-15-mediated signalling, with only IFNα6- and IFNα14-priming resulting in increased pSTAT5 expression following subsequent IL-15 stimulation. As our *ex vivo* expansion protocol utilised IL-15 to generate NK cells for ACT, and mice received recombinant human IL-15 for two weeks following adoptive transfer, this increased priming capacity may contribute towards the superior *in vitro* and *in vivo* antitumour activity displayed by IFNα14-activated NK cells. Indeed, we report that even a single dose of IFNα14 given at the start of the expansion

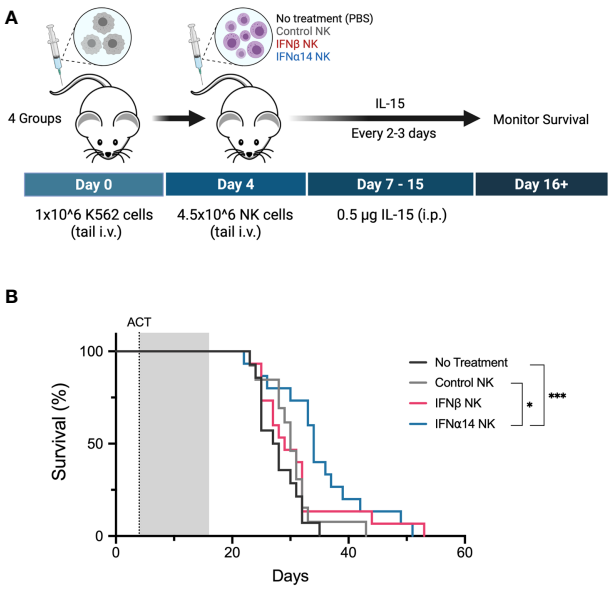

FIGURE 6
Activation with IFNα14, but not IFNβ, enhances NK cell antitumor responses against K562 leukaemia *in vivo* in NSG mice **(A)** Experimental design. Day 0: NSG mice received 1 x 10^6 K562 cells *via* tail vein injection. Day 4: NSG mice received 200 µL PBS (no treatment) or 4.5 x 10^6 14-day-expanded NK cells (control NK, IFNβ NK, IFNα14 NK) *via* tail vein injection. IL-15 (0.5 µg) was administered on day 0 and every 2-3 days thereafter until day 15. **(B)** Kaplan-Meier curves summarize the survival of mice treated. A total of 13-15 mice were used per group, and each experiment was performed independently three times. Groups were compared using the log-rank (Mantel-Cox) test. *$p < 0.05$, ***$p < 0.001$.

protocol was capable of boosting NK cell effector activity to similar levels obtained from two doses of IFNβ. Furthermore, adoptive transfer of IFNα14-activated, but not IFNβ-activated NK cells, resulted in significantly prolonged survival in our preclinical model of leukaemia. It should also be noted that whilst IL-2 was also present throughout the expansion strategy, IFNα stimulation is not known to prime NK cells for an enhanced response to IL-2 (42). Nevertheless, whilst the extent to which the synergy between IFNα14 and IL-15 contributes towards enhanced antitumour activity remains unclear, further investigation into the biological programs affected by IFNα14 stimulation is required to pinpoint the mechanisms conferring superior anti-leukaemic activity.

In summary, our data provides evidence for diverse IFN-I subtype-specific enhancement of NK cell activity against leukaemia. Although it is now apparent that individual IFN-I subtypes display distinct biological activities, only IFNα2 has been used in the clinic to treat cancer. This study highlights the need for further research into the distinct antitumor and immunomodulatory properties of the remaining IFNα subtypes and IFNβ. Additionally, we describe a strategy whereby NK cells activated with IFNα14 *ex vivo* demonstrate enhanced antitumour activity following adoptive transfer. Identifying the mechanisms underlying the superior activating potential of IFNα14 will provide translational pathways for novel strategies to enhance the efficacy of NK cell-based therapies.

Data availability statement

The original contributions presented in the study are included in the article/Supplementary Material. Further inquiries can be directed to the corresponding authors.

Ethics statement

The studies involving human participants were reviewed and approved by University of Western Australia Human Research Ethics Committee. The patients/participants provided their written informed consent to participate in this study. The animal study was reviewed and approved by Telethon Kids Institute Animal Ethics Committee.

Author contributions

SB, BF, and JW designed the experiments. SB, KA, HN, and BF performed the experiments and analysed the data. SB, EJ, BF, and JW wrote the manuscript. SB, KA, HN, SF, EJ, BF, and JW edited the manuscript. SF, EJ, BF, and JW provided supervision. All authors contributed to the article and approved the submitted version.

Funding

This work was supported by the Australian Government Research Training Program Scholarship at The University of Western Australia and the Lions Cancer Institute Karen & Joshua Chinnery PhD Top Up Scholarship administered by Cancer Council WA (scholarships to SB and HN), the Richard Walter Gibbon Medical Research Scholarship and Rachel Kierath Top-Up Scholarship in Paediatric Cancer Research (scholarships to KA), and funding from the Government of Western Australia Department of Health, Cancer Council WA, Brady Cancer Support Foundation, and the Children's Leukaemia and Cancer Research Foundation (research funding to BF).

Acknowledgments

We thank the Telethon Kids Institute Bioresources team for their excellent animal care and the Telethon Kids Institute Flow Facility for assistance.

Conflict of interest

The authors declare that the research was conducted in the absence of any commercial or financial relationships that could be construed as a potential conflict of interest.

Publisher's note

Supplementary material

The Supplementary Material for this article can be found online at: https://www.frontiersin.org/articles/10.3389/fimmu.2022.1050718/full#supplementary-material

SUPPLEMENTARY FIGURE 1
IFN-I Activation of NK Cell Function. PBMCs from 50 healthy donors were either left unstimulated or were stimulated with 100 IU mL^{-1} of each IFNα subtype or IFNβ overnight. Following overnight activation, cells were washed and then co-incubated with K562 cells for 5 hours at a 2:1 E:T ratio and NK cell effector functions were assessed. **(A)** Representative gating strategy. NK cell function was assessed as the percentage of $CD56^{+}CD3^{neg}$ NK cells expressing CD107a, IFNγ or TNFα, or a combination of two or more of these markers. The percentage of $CD107\alpha^{+}IFN\gamma^{+}TNF\alpha^{+}$ NK cells was determined using Boolean gating. **(B)** Percentage of NK cells expressing CD107a, IFNγ or TNFα, or a combination of two or more of these functional markers, following stimulation with selected IFN-I subtypes. Data were compared using paired Student's *t* tests. $*p < 0.05$, $**p < 0.01$, $***p < 0.001$, $****p < 0.0001$.

References

1. Myers JA, Miller JS. Exploring the NK cell platform for cancer immunotherapy. *Nat Rev Clin Oncol* (2021) 18(2):85–100. doi: 10.1038/s41571-020-0426-7

2. Muller L, Aigner P, Stoiber D. Type I interferons and natural killer cell regulation in cancer. *Front Immunol* (2017) 8:304. doi: 10.3389/fimmu.2017.00304

3. Bidwell BN, Slaney CY, Withana NP, Forster S, Cao Y, Loi S, et al. Silencing of Irf7 pathways in breast cancer cells promotes bone metastasis through immune escape. *Nat Med* (2012) 18(8):1224–31. doi: 10.1038/nm.2830

4. Mizutani T, Neugebauer N, Putz EM, Moritz N, Simma O, Zebedin-Brandl E, et al. Conditional IFNAR1 ablation reveals distinct requirements of type I IFN signaling for NK cell maturation and tumor surveillance. *Oncoimmunology* (2012) 1(7):1027–37. doi: 10.4161/onci.21284

5. Swann JB, Hayakawa Y, Zerafa N, Sheehan KC, Scott B, Schreiber RD, et al. Type I IFN contributes to NK cell homeostasis, activation, and antitumor function. *J Immunol* (2007) 178(12):7540–9. doi: 10.4049/jimmunol.178.12.7540

6. Madera S, Rapp M, Firth MA, Beilke JN, Lanier LL, Sun JC. Type I IFN promotes NK cell expansion during viral infection by protecting NK cells against fratricide. *J Exp Med* (2016) 213(2):225–33. doi: 10.1084/jem.20150712

7. Genin P, Vaccaro A, Civas A. The role of differential expression of human interferon–a genes in antiviral immunity. *Cytokine Growth Factor Rev* (2009) 20 (4):283–95. doi: 10.1016/j.cytogfr.2009.07.005

8. Gibbert K, Schlaak JF, Yang D, Dittmer U. IFN-alpha subtypes: distinct biological activities in anti-viral therapy. *Br J Pharmacol* (2013) 168(5):1048–58. doi: 10.1111/bph.12010

9. Schuhenn J, Meister TL, Todt D, Bracht T, Schork K, Billaud JN, et al. Differential interferon-alpha subtype induced immune signatures are associated with suppression of SARS-CoV-2 infection. *Proc Natl Acad Sci U.S.A.* (2022) 119 (8):e2111600119. doi: 10.1073/pnas.2111600119

10. Dickow J, Francois S, Kaiserling RL, Malyshkina A, Drexler I, Westendorf AM, et al. Diverse immunomodulatory effects of individual IFNalpha subtypes on virus-specific CD8(+) T cell responses. *Front Immunol* (2019) 10:2255. doi: 10.3389/fimmu.2019.02255

11. Karakoese Z, Schwerdtfeger M, Karsten CB, Esser S, Dittmer U, Sutter K. Distinct type I interferon subtypes differentially stimulate T cell responses in HIV-1-Infected individuals. *Front Immunol* (2022) 13:936918. doi: 10.3389/fimmu.2022.936918

12. Lavender KJ, Gibbert K, Peterson KE, Van Dis E, Francois S, Woods T, et al. Interferon alpha subtype-specific suppression of HIV-1 infection. *In Vivo J Virol* (2016) 90(13):6001–13. doi: 10.1128/JVI.00451-16

13. Buzzai AC, Wagner T, Audsley KM, Newnes HV, Barrett LW, Barnes S, et al. Diverse anti-tumor immune potential driven by individual IFNalpha subtypes. *Front Immunol* (2020) 11:542. doi: 10.3389/fimmu.2020.00542

14. Audsley KM, Wagner T, Ta C, Newnes HV, Buzzai AC, Barnes SA, et al. IFNbeta is a potent adjuvant for cancer vaccination strategies. *Front Immunol* (2021) 12:735133. doi: 10.3389/fimmu.2021.735133

15. Asmana Ningrum R. Human interferon alpha-2b: a therapeutic protein for cancer treatment. *Scientifica (Cairo)* (2014) 2014:970315. doi: 10.1155/2014/970315

16. Verhagen A, Mackay IR, Rowley M, Tymms M. Comparison of augmentation of human natural killer cell cytotoxicity by interferon-alpha subtypes. *Nat Immun Cell Growth Regul* (1990) 9(5):325–33.

17. Foley B, Cooley S, Verneris MR, Curtsinger J, Luo X, Waller EK, et al. NK cell education after allogeneic transplantation: dissociation between recovery of cytokine-producing and cytotoxic functions. *Blood* (2011) 118(10):2784–92. doi: 10.1182/blood-2011-04-347070

18. Krzewski K, Coligan JE. Human NK cell lytic granules and regulation of their exocytosis. *Front Immunol* (2012) 3:335. doi: 10.3389/fimmu.2012.00335

19. Lanier LL. Up on the tightrope: natural killer cell activation and inhibition. *Nat Immunol* (2008) 9(5):495–502. doi: 10.1038/ni1581

20. Cull VS, Tilbrook PA, Bartlett EJ, Brekalo NL, James CM. Type I interferon differential therapy for erythroleukemia: specificity of STAT activation. *Blood* (2003) 101(7):2727–35. doi: 10.1182/blood-2002-05-1521

21. Gotthardt D, Trifinopoulos J, Sexl V, Putz EM. JAK/STAT cytokine signaling at the crossroad of NK cell development and maturation. *Front Immunol* (2019) 10:2590. doi: 10.3389/fimmu.2019.02590

22. Au-Yeung N, Mandhana R, Horvath CM. Transcriptional regulation by STAT1 and STAT2 in the interferon JAK-STAT pathway. *JAKSTAT* (2013) 2(3): e23931. doi: 10.4161/jkst.23931

23. Miyagi T, Gil MP, Wang X, Louten J, Chu WM, Biron CA. High basal STAT4 balanced by STAT1 induction to control type 1 interferon effects in natural killer cells. *J Exp Med* (2007) 204(10):2383–96. doi: 10.1084/jem.20070401

24. Liang S, Wei H, Sun R, Tian Z. IFNα regulates NK cell cytotoxicity through STAT1 pathway. *Cytokine* (2003) 23(6):190–9. doi: 10.1016/S1043-4666(03)00226-6

25. Cacalano NA. Regulation of natural killer cell function by STAT3. *Front Immunol* (2016) 7:128. doi: 10.3389/fimmu.2016.00128

26. Hansen ML, Woetmann A, Krejsgaard T, Kopp KL, Sokilde R, Litman T, et al. IFN-alpha primes T- and NK-cells for IL-15-mediated signaling and cytotoxicity. *Mol Immunol* (2011) 48(15-16):2087–93. doi: 10.1016/j.molimm.2011.07.008

27. Granzin M, Wagner J, Kohl U, Cerwenka A, Huppert V, Ullrich E. Shaping of natural killer cell antitumor activity by ex vivo cultivation. *Front Immunol* (2017) 8:458. doi: 10.3389/fimmu.2017.00458

28. Jaks E, Gavutis M, Uze G, Martal J, Piehler J. Differential receptor subunit affinities of type I interferons govern differential signal activation. *J Mol Biol* (2007) 366(2):525–39. doi: 10.1016/j.jmb.2006.11.053

29. de Weerd NA, Vivian JP, Nguyen TK, Mangan NE, Gould JA, Braniff SJ, et al. Structural basis of a unique interferon-beta signaling axis mediated *via* the receptor IFNAR1. *Nat Immunol* (2013) 14(9):901–7. doi: 10.1038/ni.2667

30. Kalie E, Jaitin DA, Podoplelova Y, Piehler J, Schreiber G. The stability of the ternary interferon-receptor complex rather than the affinity to the individual subunits dictates differential biological activities. *J Biol Chem* (2008) 283 (47):32925–36. doi: 10.1074/jbc.M806019200

31. Francois-Newton V, Magno de Freitas Almeida G, Payelle-Brogard B, Monneron D, Pichard-Garcia L, Piehler J, et al. USP18-based negative feedback control is induced by type I and type III interferons and specifically inactivates interferon alpha response. *PLoS One* (2011) 6(7):e22200. doi: 10.1371/journal.pone.0022200

32. Guo K, Shen G, Kibbie J, Gonzalez T, Dillon SM, Smith HA, et al. Qualitative differences between the IFNalpha subtypes and IFNbeta influence chronic mucosal HIV-1 pathogenesis. *PLoS Pathog* (2020) 16(10):e1008986. doi: 10.1371/journal.ppat.1008986

33. Jaitin DA, Roisman LC, Jaks E, Gavutis M, Piehler J, van der Heyden J, et al. Inquiring into the differential action of interferons (IFNs): an IFN-alpha2 mutant with enhanced affinity to IFNAR1 is functionally similar to IFN-beta. *Mol Cell Biol* (2006) 26(5):1888–97. doi: 10.1128/MCB.26.5.1888-1897.2006

34. Lavoie TB, Kalie E, Crisafulli-Cabatu S, Abramovich R, DiGioia G, Moolchan K, et al. Binding and activity of all human alpha interferon subtypes. *Cytokine* (2011) 56(2):282–9. doi: 10.1016/j.cyto.2011.07.019

35. Gotthardt D, Putz EM, Straka E, Kudweis P, Biaggio M, Poli V, et al. Loss of STAT3 in murine NK cells enhances NK cell-dependent tumor surveillance. *Blood* (2014) 124(15):2370–9. doi: 10.1182/blood-2014-03-564450

36. Kortylewski M, Kujawski M, Wang T, Wei S, Zhang S, Pilon-Thomas S, et al. Inhibiting Stat3 signaling in the hematopoietic system elicits multicomponent antitumor immunity. *Nat Med* (2005) 11(12):1314–21. doi: 10.1038/nm1325

37. Zhu S, Phatarpekar PV, Denman CJ, Senyukov VV, Somanchi SS, Nguyen-Jackson HT, et al. Transcription of the activating receptor NKG2D in natural killer cells is regulated by STAT3 tyrosine phosphorylation. *Blood* (2014) 124(3):403–11. doi: 10.1182/blood-2013-05-499707

38. Takaki R, Hayakawa Y, Nelson A, Sivakumar PV, Hughes S, Smyth MJ, et al. IL-21 enhances tumor rejection through a NKG2D-dependent mechanism. *J Immunol* (2005) 175(4):2167–73. doi: 10.4049/jimmunol.175.4.2167

39. Tu TC, Brown NK, Kim TJ, Wroblewska J, Yang X, Guo X, et al. CD160 is essential for NK-mediated IFN-gamma production. *J Exp Med* (2015) 212(3):415–29. doi: 10.1084/jem.20131601

40. Ghofrani J, Lucar O, Dugan H, Reeves RK, Jost S. Semaphorin 7A modulates cytokine-induced memory-like responses by human natural killer cells. *Eur J Immunol* (2019) 49(8):1153–66. doi: 10.1002/eji.201847931

41. Rautela J, Huntington ND. IL-15 signaling in NK cell cancer immunotherapy. *Curr Opin Immunol* (2017) 44:1–6. doi: 10.1016/j.coi.2016.10.004

42. Nielsen CM, Wolf AS, Goodier MR, Riley EM. Synergy between common gamma chain family cytokines and IL-18 potentiates innate and adaptive pathways of NK cell activation. *Front Immunol* (2016) 7:101. doi: 10.3389/fimmu.2016.00101

frontiers | Frontiers in Immunology

TYPE Review
PUBLISHED 26 January 2023
DOI 10.3389/fimmu.2023.1125246

OPEN ACCESS

EDITED BY
Chang Li,
Chinese Academy of Agricultural Sciences (CAAS), China

REVIEWED BY
Xiaozhou Feng,
New Jersey Medical School, Rutgers, The State University of New Jersey, United States
Xiaoyang Ye,
Institute for Systems Biology (ISB), United States

*CORRESPONDENCE
Ruijuan Liu
rj182@163.com
Duomeng Yang
dyang@uchc.edu

†These authors have contributed equally to this work

SPECIALTY SECTION
This article was submitted to Molecular Innate Immunity, a section of the journal Frontiers in Immunology

RECEIVED 16 December 2022
ACCEPTED 03 January 2023
PUBLISHED 26 January 2023

CITATION
Yuan Y, Jiao B, Qu L, Yang D and Liu R (2023) The development of COVID-19 treatment. *Front. Immunol.* 14:1125246. doi: 10.3389/fimmu.2023.1125246

The development of COVID-19 treatment

Yongliang Yuan[1†], Baihai Jiao[2†], Lili Qu[3†], Duomeng Yang[3*] and Ruijuan Liu[1*]

[1]Department of Pharmacy, The First Affiliated Hospital of Zhengzhou University, Zhengzhou, Henan, China, [2]Division of Nephrology, Department of Medicine, School of Medicine, University of Connecticut Health Center, Farmington, CT, United States, [3]Department of Immunology, School of Medicine, University of Connecticut Health Center, Farmington, CT, United States

The emergence of severe acute respiratory syndrome coronavirus 2 (SARS-CoV-2) caused a pandemic named coronavirus disease 2019 (COVID-19) that has become the greatest worldwide public health threat of this century. Recent studies have unraveled numerous mysteries of SARS-CoV-2 pathogenesis and thus largely improved the studies of COVID-19 vaccines and therapeutic strategies. However, important questions remain regarding its therapy. In this review, the recent research advances on COVID-19 mechanism are quickly summarized. We mainly discuss current therapy strategies for COVID-19, with an emphasis on antiviral agents, neutralizing antibody therapies, Janus kinase inhibitors, and steroids. When necessary, specific mechanisms and the history of therapy are present, and representative strategies are described in detail. Finally, we discuss key outstanding questions regarding future directions of the development of COVID-19 treatment.

KEYWORDS

COVID-19, treatments, antiviral agents, neutralizing antibody therapy, Janus kinase inhibitors

Introduction

At the end of 2019, a new coronavirus that quickly causes severe respiratory syndrome and lethal pneumonia emerged in Wuhan, China, and, 3 months later, the World Health Organization characterized the outbreak as a severe acute respiratory syndrome coronavirus 2 (SARS-CoV-2)–induced pandemic that is coronavirus disease 2019 (COVID-19) (1). The pandemic has led to a profound strike on medical care systems, economic progress, and social cohesion around the world. The magnificent research work on developing an effective COVID-19 vaccine has resulted in several safe and effective options (2–4). However, there is still a need to focus on developing potential drug candidates for treating patients with severe clinical symptoms. During the COVID-19 public health emergency, the Food and Drug Administration (FDA) issued Emergency Use Authorization (EUA) for various new drugs and medical products without full FDA approval. Currently, the primary treatments for the disease are antiviral drugs, immunomodulators, neutralizing antibody, and cell and gene therapies (5, 6). Our understanding about the effect of different categories of potential treatments due to their diversity has significantly improved. This study summarized the

current therapeutic approaches (Figure 1) for COVID-19 with a simple review of SARS-CoV-2 infection pathogenesis, aiming to help researchers and doctors involved in the epidemic to improve their further work.

Mechanism of COVID-19

Coronaviruses have ignited big-scale pandemics for three times over the past 20 years: SARS from 2002 to 2003, Middle Eastern Respiratory Syndrome in 2012, and COVID-19 emerged at the end of 2019. The COVID-19, caused by SARS-CoV-2, led to an outbreak of unusual viral pneumonia that has spread worldwide and becomes the greatest global public health crisis of this century (7, 8). As of August 2022, there have been over 59 million confirmed COVID-19 cases, and more than 6 million COVID-19–related deaths worldwide. Although a total of 1.2 billion vaccine doses have been administered, COVID-19 is still a huge threat to life due to the lack of effective medical treatment (1).

SARS-CoV-2 characteristics

CoVs, including SARS-CoV-2, are enveloped viruses with positive-sense single-stranded RNA that possess the largest genomes (~30 kb) among the known RNA viruses, which belong to the Betacoronavirus genus of the family Coroaviridae (9). The genome of SARS-CoV-2 comprises 14 open reading frames encoding nine accessory proteins; four structural proteins of spike (S), envelope (E), membrane (M), and nucleocapsid (N); and 16 nonstructural proteins (nsp1–16). In all these viral proteins, protein S mediates host cell entry of SARS-CoV-2 by direct contact with its cellular receptor–angiotensin-converting enzyme 2 (ACE2). Moreover, the transmembrane protease serine 2 and cathepsin L can also facilitate SARS-CoV-2 cellular entry using a different manner at the plasma membrane surface and endosomal compartments (7, 10, 11). Once enter the host cell, cytosol release of RNA genome of SARS-CoV-2 is activated and starts to replicate. New virions are then assembled and secreted to the intercellular space for infection of neighbor cells (12). SARS-CoV-2 infections often lead to "flu-like" symptoms such as headache, fever, sore throat, backache, cough, and loss of taste or smell. Although plenty of infection cases are asymptomatic or mild, there are certain cases that show severe outcomes and are associated with systemic inflammation, acute respiratory distress syndrome, tissue damage, and cardiac injury. The severe COVID-19 disease with multiorgan damage can be fatal, and its risk largely depends on comorbidities including diabetes, obesity, hypertension, and others (8, 13, 14).

Host innate immune responses and cytokine storm

Once SARS-CoV-2 invasion happens, the host innate immune response will be rapidly activated followed by the involvement of adaptive immune system (15). As the frontline defense of host, innate immune system employs different strategies for virus detection and elimination to fight against SARS-CoV-2. During the virus infection, the innate immune cells, including natural killer cells, macrophages, monocytes, dendritic cells, and neutrophils, are rapidly recruited and activated first to produce inflammatory cytokines efficiently, such as type I interferons (IFNs) for antiviral activities. Later, B and T lymphocytes are activated for the engagement of immunological memory (16). Host innate immune system primarily relies on pattern recognition receptors (PRRs) to sense virus, bacteria, and other pathogen-associated molecular patterns and/or damage-associated molecular patterns to trigger inflammatory responses that limit viral lifecycle, promote viral clearance, and accelerate the establishment of adaptive immunity (17). The PRRs, expressed by epithelial cells and innate immune cells, are classified into several families: retinoic acid–inducible gene I (RIG-I)–like receptors (RLRs) [including RIG-I and melanoma differentiation-associated protein 5 (MDA5)], Toll-like receptors (TLRs), nucleotide-binding oligomerization domain (NOD)–like receptors (NLRs), the cyclic GMP-AMP synthase (cGAS), absent in melanoma 2–like receptors, and C-type lectin receptors (18). In all the PRRs, intracellular RLR pathways are essential for sensing RNA virus invasion to trigger innate antiviral immune response. Following activation by viral RNA, RIG-I and MDA5 translocate and bind to mitochondria to activate the adaptor protein mitochondrial antiviral signaling (MAVS) that subsequently induces TANK-binding kinase activation and IFN regulatory factor 3 (IRF3) phosphorylation, which, in turn, promotes production of IFNs to prevent virus infection (19, 20). SARS-CoV-2, belonging to single-stranded RNA viruses, can also be detected by MDA5 and RIG-I. However, their roles in regulating

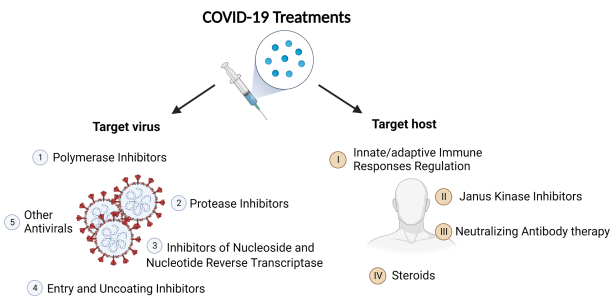

FIGURE 1
Category of COVID-19 treatments. On the basis of their targets, the treatments can be divided into two big categories: antiviral agents and therapies targeting host.

SARS-CoV-2 infection seem different (21–24). By screening RNA sensors for SARS-CoV-2 infection in a model of human lung epithelial cells (Calu-3), Yin and colleagues identified MDA5 and LGP2 as the dominant sensors to trigger IFN production in response to SARS-CoV-2 infection (21). Another two independent research groups found that knocking out genes encoding MDA5 or MAVS in human lung epithelial cells leads to impairment of SARS-CoV-2–induced type I IFN production (22, 23). These studies demonstrate the indispensable role of MDA5 in mediating type I IFN expression in response to SARS-CoV-2 infection. However, RIG-I seems to function in a MAVS-IFN–independent way. RIG-I deletion either by small interfering RNA or CRISPR-Cas9 in Calu-3 failed to reduce IFN-β production but still enhanced viral replication (21–23). RIG-I likely restrains full-length ACE2 expression or binds the 3′ untranslated region of the viral RNA genome *via* its helicase domains and consequently restricts cellular entry or replication of virus independently of IFNs (22, 25).TLRs and NLRs also are reported to play roles in anti–SARS-CoV-2 responses. As a classic innate immune signaling, TLRs express widely from tissue cells to innate immune cells, which generally trigger MyD88 or TRIF to transduce signals *via* nuclear factor–κB, mitogen-activated protein kinases, and IRFs to mediate transcriptional activation of pro-inflammatory cytokines (26). Upon SARS-CoV-2 infection, TLR2 senses E protein to enhance inflammatory responses and TLR4 can be activated by S protein to contribute to the release of cytokines (27, 28). In patients with COVID-19, NLRP3 inflammasome activation and its dependent caspase-1 and GSDMD cleavage as well as subsequently IL-1β secretion have been demonstrated, suggesting that NLRs and inflammasome sensors are involved in SARS-CoV-2 infection as well (29–31). In addition, the cGAS–STING signaling pathway, triggered by cytosolic DNA, is also involved in the campaign of fighting against SARS-CoV-2 invasion (32–34). In the case of severe COVID-19, PRRs and cGAS–STING signaling engaged by SARS-CoV-2 induce the expression of both IFNs and numerous pro-inflammatory cytokines, including TNF, IL-6, IL-1β, IL-12, and IL-17 (35, 36). These cytokines act as a two-edged sword, not only aiding in clearing virus infections but also contributing to life-threatening condition caused by cytokine storm. A recent study shows the combination of TNF-α and IFN-γ promotes inflammatory programmed cell death-PANoptosis by activating the Janus kinase (JAK)/signal transducer and activator of transcription (STAT1)/IRF1 axis and caspase-8/FADD signaling (36). The lethal shock phenotype observed in mice administrated with TNF-α and IFN-γ combination mirrors the cytokine storm syndrome in patients with severe COVID-19, emphasizing the link between the dysregulated release of cytokines and the multiorgan damage in patients with SARS-CoV-2 infection (37–39). In addition, the identification of elevated IL-6 levels in serum as a strong predictor of respiratory failure in patients with COVID-19 makes IL-6 one of the critical cytokines in the COVID-19–related hyperinflammatory syndrome (40, 41).

Adaptive immunity and vaccines

Adaptative immune response, established by activation of T and B cells, sent us a powerful weapon to fight against SARS-CoV-2 pandemic: the vaccine. The activation of innate immune cells during SARS-CoV-2 infection drives T and B cells to respond efficiently to secrete specific antibodies and to kill infected cells, which accelerates the development of acquired immunological memory. The adaptive immunity produced by B and T cells in response to SARS-CoV-2 infection and the vaccines have been discussed in other reviews (42, 43).

Treatments

All the treatments can be subcategorized into two big groups on the basis of their targets: antiviral agents and therapies targeting host.

Antiviral agents

Antiviral agents against COVID-19 reported mainly include polymerase inhibitors, protease inhibitors, inhibitors of nucleoside and nucleotide reverse transcriptase, entry and uncoating inhibitors, and other antivirals.

Polymerase inhibitors

Remdesivir is a nucleotide prodrug, and its active metabolite can inhibit the activity of RNA polymerases, which is a key enzyme for the replication of many viruses, including coronaviridae. Remdesivir showed antiviral effect on SARS-CoV-2 (44, 45), and it was approved by FDA for treating COVID-19. However, the clinical antiviral effect of remdesivir against SARS-CoV-2 remains controversial. One study reported a clinical trial of non-hospitalized patients with COVID-19. Among the enrolled patients, the safety was acceptable following 3 days of treatment with remdesivir, and the risk of hospitalization or death was reduced by 87% compared with the placebo (46). Another clinical trial demonstrated that remdesivir outperforms placebo. The recovery time of adults hospitalized with COVID-19 and lower respiratory tract infection is shortened after receiving remdesivir treatment (47). Whereas, other studies including a multicenter trial conducted in 10 hospitals in Hubei, China, showed that there was no statistically significant difference in the clinical status of patients with COVID-19 receiving remdesivir compared with standard care (48–52). In addition, the researchers also evaluated the effect of baricitinib combined with remdesivir in hospitalized adults with COVID-19. In terms of shortening the recovery time of patients with COVID-19 and speeding up the improvement of their clinical symptoms, remdesivir combined with baricitinib was more effective than remdesivir alone (53).

Favipiravir, an antiviral drug, selectively inhibits the RNA polymerase of viral and has antiviral effects on a variety of RNA viruses (54, 55). A clinical study demonstrated that standard supportive care plus early oral favipiravir monotherapy significantly decreased the recovery time of patients with mild-to-moderate COVID-19 compared with the standard supportive care alone (56).

Protease inhibitors

Protease is one of the key enzymes in the processing of coronavirus polyproteins. Many studies have been carried out on protease inhibitors for treating COVID-19 in recent years. Lopinavir

is a viral protease inhibitor and is primarily used to treat human immunodeficiency virus (HIV). Ritonavir can increase the serum concentration of lopinavir *in vivo* by inhibiting CYP3A-mediated metabolism of lopinavir (57). Therefore, lopinavir/ritonavir is marketed as a combination product. Cao et al. conducted a clinical trial involving 199 hospitalized adult patients with COVID-19. The results showed that lopinavir-ritonavir treatment had no effect on adult patients with severe COVID-19 (58). Moreover, another clinical trial with more participants enrolled at 176 hospitals in the UK was reported subsequently. In this study, 1,616 patients were assigned to lopinavir/ritonavir group and 3,424 patients to the usual care group. Similarly, no efficacy was observed in hospitalized patients with COVID-19 treated with lopinavir/ritonavir (59).

Lopinavir/ritonavir might be more effective if combined with other antiviral regimens. In one study, four patients with COVID-19 were given antiviral treatment, including lopinavir/ritonavir, arbidol, and Shufeng Jiedu Capsule (a traditional Chinese medicine). The pneumonia-related symptoms of three patients were significantly improved; however, the efficacy of the combinational treatment still needs further studies to confirm (60). Moreover, the results of a phase 2 trial showed that early triple antiviral therapy (combined IFN-β1b, lopinavir/ritonavir, and ribavirin) was safe and had a better effect in patients with mild-to-moderate COVID-19 for alleviating symptoms, shortening the time of viral shedding and hospital stay than lopinavir/ritonavir alone (61). Nirmatrelvir is an inhibitor of the SARS-CoV-2 main protease (Mpro) enzyme (62). A phase 2–3 clinical trial was performed in symptomatic, unvaccinated, nonhospitalized adults at high risk for progression to severe COVID-19. In this study, 1,120 patients received nirmatrelvir plus ritonavir therapy and 1,126 patients received placebo. Symptomatic patients with COVID-19 treated with nirmatrelvir plus ritonavir had an 89% lower risk of developing severe COVID-19 than placebo (63).

Inhibitors of nucleoside and nucleotide reverse transcriptase

Azvudine (FNC), a nucleoside reverse transcriptase inhibitor, has broad-spectrum antivirus activity including HIV-1. FNC had been approved by the national medical products administration (NMPA, China) for AIDS treatment on 21 July 2021. One clinical trial of FNC confirmed that oral FNC (5 mg, qd) could cure patients with COVID-19, and the viral RNA turned negative in about 3.29 ± 2.22 days. The results demonstrated that FNC could be used against SARS-CoV-2 (64). Another clinical trial was performed in China to investigate the anti–COVID-19 effect of FNC. The results of this study showed that FNC could shorten the time of nucleic acid turning negative compared with the standard antiviral drugs for patients with mild and common COVID-19. This work also suggests that FNC is effective for COVID-19, and larger–sample size clinical trials of FNC for treating COVID-19 are needed (65, 66). Recently, NMPA conditionally approved FNC to treat common COVID-19 in adults on 25 July 2022.

Molnupiravir is a small-molecule ribonucleoside prodrug of N-hydroxycytidine and has activity against coronaviruses including SARS-CoV-2 (67). Molnupiravir reduced the risk of hospital admission or death by approximately 50% in nonhospitalized adults with mild-to-moderate COVID-19 who were at risk for poor outcomes (68). To evaluate the efficacy and safety of treatment with molnupiravir in nonhospitalized, unvaccinated adults with mild-to-moderate COVID-19, a phase 3 clinical trial was conducted. Study results suggested that the risk of hospitalization or death of unvaccinated adults with COVID-19 could be reduced by early treatment with molnupiravir (69). Another study showed that molnupiravir was active against the three predominant circulating variants (delta, gamma, and mu) of SARS-CoV-2 and showed a modest antiviral effect (70, 71). Moreover, the UK's Medicines regulator and the US FDA have authorized the emergency use of molnupiravir for treating mild-to-moderate COVID-19 in adults.

Entry and uncoating inhibitors

Amantadine can block the early stage of viral replication, which has been used to treat influenza A (72). Amantadine, because of its lipophilic and alkaline physicochemical properties, could cross the lysosome membrane and prevents the release of viral RNA into the cells (73). One study has shown that adamantane may have protective effects against COVID-19. This study has limitations such as a small sample size, and further research is needed to confirm it (74). Enfuvirtide, an HIV-1 fusion inhibitor peptide, could be used as a potent SARS-CoV-2 fusion inhibitor (75). Clinical trials need to be performed to confirm the effect of enfuvirtide against COVID-19.

Other antivirals

Azithromycin is a synthetic macrolide antibiotic with a broad range of antibacterial, anti-inflammatory, and antiviral properties (76). A prospective, randomized superiority trial done at 19 hospitals in the UK reported that adding azithromycin to standard care treatment did not reduce the risk of subsequent hospital admission or death in patients with mild-to-moderate COVID-19 (77). Moreover, another study also showed that the routine use of azithromycin did not reduce the recovery time or risk of hospitalization for people who were suspected with COVID-19 (78).

Hydroxychloroquine and chloroquine, used to treat malaria and rheumatologic conditions, have been suggested as potential treatments for COVID-19. Currently, at least 80 trials of chloroquine, hydroxychloroquine, or both, sometimes in combination with other drugs, are registered worldwide (79). In one study of 1,561 patients with COVID-19 treated with hydroxychloroquine and 3,155 in usual care, hydroxychloroquine did not lower patient mortality compared with usual care (80). Moreover, hydroxychloroquine did not provide significant improvement in symptom severity for early, mild COVID-19 outpatients (81), and could not prevent symptomatic infection after SARS-CoV-2 exposure (82, 83). In addition, studies had shown that comparing standard care, hydroxychloroquine, alone or with azithromycin did not improve clinical outcomes for patients with COVID-19 (84, 85). Therefore, there is no need to combine azithromycin with hydroxychloroquine in patients with COVID-19.

IFNs, as one of many inflammatory mediators induced by SARS-CoV-2 infection, have been noticed since the beginning of the pandemic, but the effect of IFNs of type I (IFN-I) or type III (IFN-III) families remains controversial (86). Research reported that, unlike other infectious or noninfectious lung pathologies, the expression of INFs was increased in the lower respiratory tract of patients with severe COVID-19. The results indicated that IFNs played opposing roles at distinct anatomical sites of patients with SARS-CoV-2 (86). The hyperinflammation makes the patients succumb rapidly to COVID-19 without the help of IFN. Therefore, IFN improves the prognosis of patients with COVID-19 (87). Kalil et al. found that IFN-β1a plus remdesivir was not superior to remdesivir alone in hospitalized patients with COVID-19 pneumonia (88). Another study showed that IFN-α decreased the mean days of virus clearance and the average days of hospitalization. This study suggests that early administration of IFN-α could be a promising treatment for COVID-19 (89).

Targeting host

The treatments targeting host include neutralizing antibody therapy, Janus kinase inhibitors, and steroids.

Neutralizing antibody therapy

The history of antibody therapy can date back to the early 1890s, and, at that time, Dr. Behring and Dr. Kitasato found that the serum from an animal recovered from diphtheria infection could protect diphtheria- and tetanus-infected patients and developed the first serum therapy. Forty years later, serum therapy was widely applied in the treatment of various infectious diseases. However, it had been abandoned with the development of the first antibiotics by the late 1940s. In 1959, a big discovery about the molecular formula of antibodies was made by Gerald Edelman and Rodney Porter (90, 91). Thirty years later, the first antibody "muromonab" was approved in clinics around the world (92). However, the application of the therapeutic antibody was still limited because of the restricted resource at that time. In the 1990s, with the development of antibody engineering technologies (93), the restriction of the antibody resource was broken, which made it possible to check the effectiveness of antibody treatment on a large scale. Since then, antibody treatment has been quickly developed. So far, over 80 therapeutic monoclonal or polyclonal antibodies have been endorsed in the world, which have been mainly adopted in passive immunotherapy. However, with the outburst of COVID-19 and following severe and emergent world health situations, the interest in plasma therapy has been renewed.

Convalescent plasma

Convalescent plasma from patients who recovered from infection was adopted to treat severe patients. In 2019, the first peer-reviewed study about the effect of convalescent plasma was carried out in China (94). Compared with patients who received standard treatment, 103 patients with severe COVID-19 did not show a statistical difference after transfusion of convalescent plasma. Unfortunately, the trial was halted because of slow and limited enrollment. However, similar studies were carried out in other countries on a smaller scale in 2020. A phase 1 clinical trial study was carried out to inspect the potential of convalescent plasma in Switzerland. Thirty inpatients with COVID-19 were transfused 3 units of 200 ml plasma in 3 consecutive days, followed by comprehensive longitudinal monitoring for over 70 days. The safety of convalescent plasma therapy was confirmed with the absence of transfusion-related adverse events throughout the whole process as a consequence of smaller plasma volumes being adopted in the treatment. Furthermore, faster virus clearance and fewer comorbidities were confirmed in the following monitoring (95). However, this trial was less persuasive by virtue of the small sample size and shortage of control. In later 2020, Spanish scientists did another a higher-scale trial that is multicenter, double-blind, and randomized placebo-controlled. A total of 376 patients with mild-to-moderate COVID-19 with were recruited to receive 250–300 ml of convalescent plasma with high anti–SARS-CoV-2 IgG titers or 250-ml sterile 0.9% saline solution as the control group. The authors did not see a significant viral load decrease and the prevention of progression of the illness at the end of the trial. In addition, one patient showed a serious adverse event after infusion for 7 days (96). At the same time, another trial with 1,181 patients across 23 sites in the US was carried out with the opposite conclusion. This study found that 37 COVID-19–related hospitalization occurred in 589 patients who received control plasma, whereas only 17 of the 592 patients who were infused with convalescent plasma showed disease progression, leading to hospitalization, which means convalescent plasma greatly reduced the hospitalization risk. However, 149 participants among these 1,181 patients were fully vaccinated, and participants older than 65 years only account for 6.8%, all of which made the effectiveness of the treatment controversial (97). Another large convalescent plasma conducted in the UK involving 11,558 patients confirmed that high-titer convalescent plasma treatment failed to improve the survival of hospitalized patients with COVID-19 (98). Estcourt et al. discussed that the reason for the discrepancy between different trials was the standard of patients' enrollment (99). Moreover, they mentioned another two ongoing trials: the COVID-19 trial and the REMAP-CAP trial, which may bring additional clarity to the effectiveness of convalescent plasma.

Neutralizing monoclonal and polyclonal antibody therapies

Although convalescent plasma showed partial effectiveness in selected patients, its potential is still controversial. In addition, only part of plasma antibodies will be neutralizing, and those non-neutralizing antibodies will bind to non-spike protein viral antigens, which will sabotage antibody reactions to further cause tissue damage. Indeed, in some convalescent plasma trials, allergic responses and lung damage occurred. Furthermore, the antibody titer in convalescent plasma is low and the resource of the blood is constrained. All these disadvantages restricted the application of convalescent plasma therapy in clinics. In contrast, monoclonal/polyclonal antibodies therapy, as another type of passive

immunotherapy, can precisely target the neutralizing sites, and they can be massively produced and easily scalable, which conquers all the disadvantages of convalescent plasma. All these advantages attract medical scientists to put more effort into monoclonal or polyclonal antibodies to develop more potent therapies. As above mentioned, the S protein can bind to receptors for ACE2 to enter host cells. For the early stage, many monoclonal antibody trials targeting S protein were conducted since the routes of the virus entering host cells have been uncovered.

The first monoclonal antibody that was found effective for COVID-19 infection was LY-CoV555. The effect of LY-CoV555 in anti–SARS-CoV-2 infection in nonhuman primates was first reported by Jones et al. (100, 101). In this study, LY-CoV555 (Bamlanivimab) showed strong binding to ACE2 and neutralizing activity. It could reduce viral load in respiratory tract samples even at a low dose. Later, the effectiveness of LY-CoV555 was tested on outpatients and hospitalized patients (102, 103). For the outpatients' trials, 309 patients were injected with 700, 2,800, or 7,000 mg of LY-CoV555. The viral load of the patients was checked on day 11. Compared with placebo patients, viral RNA showed a significant decrease in the 2,800-mg group patients. In addition, LY-CoV555 decreased the ratio of hospitalization or visiting emergency (102, 104). Two months later, another trial was conducted for the efficacy of LY-CoV555 on hospitalized patients. A total of 163 hospitalized patients were infused with LY-CoV555 and Remdesivir. However, the status of patients was not improved by LY-CoV555 (103, 105). Monoclonal antibodies are restricted only to the same or single epitope due to their monovalent affinity, which may be ineffective against the virus variance. To solve this problem, researchers combined two monoclonal antibodies. Etesevimab, as another monoclonal antibody, was always used jointly with bamlanivimab. A randomized phase 2/3 trial with 613 participants enrolled was carried out at 49 US centers to compare the efficacy of Bamlanivimab as monotherapy or together with etesevimab (106, 107). Bamlanivimab/Etesevimab showed stronger efficacy than bamlanivimab monotherapy in decreasing viral amount in outpatients with mild-to-moderate symptoms. The same conclusion was drawn by another larger trial that bamlanivimab plus etesevimab could decrease the potential of COVID-19–related hospitalization and death (108, 109). Because of their strong efficacy in patients with mild-to-moderate COVID-19, they were issued together for emergency use on 9 February 2021. However, because of the high frequency of the Omicron variant, FDA already retracted this monoclonal antibody for the post-exposure prevention or treatment under the EUA. Later, the study published by VanBlargan et al. also confirmed the futility of LY-CoV555 to Omicron variance (109, 110). So far, the only neutralizing monoclonal antibody issued by FDA for emergency use is bebtelovimab. Iketani et al. confirmed three sublineages of Omicron showed resistance to 17 neutralizing antibodies except for bebtelovimab (111, 112). Westendorf et al. were able to isolate bebtelovimab through a high-throughput B cell screening pipeline. The authors uncovered the LY-CoV1404 epitope is highly conserved in contact residues, which is why they still show neutralizing activity against omicron variance (113, 114). The efficacy of bebtelovimab was also confirmed by another study conducted by Wang et al. and published 1 month ago (115, 116). In this study, they also identified that the Omicron variance showed more transmissible and more evasive to antibodies.

Janus kinase inhibitors

Serum concentrations of proinflammatory cytokines and chemokines—including IFN-γ, TNF-α, IP-10, G-CSF, IL-2, IL-6, IL-8, IL-9, IL-10, and IL-17—were increased in patients with severe COVID-19 and strongly correlated with disease outcome (117). The JAK/STAT pathway regulates a number of inflammatory cytokines and growth factors by transferring signals from receptors in the cell membrane to the nucleus, leading to hematopoiesis, lactation, and the immune system and mammary gland development (118, 119). JAKs are tyrosine kinases that bind to the cytoplasmic domains of type I and type II cytokine receptors. When ligands bind to their receptors, the intracellular portion of JAKs will be activated, which recruits and phosphorylates STATs. Activated STATs translocate into the nucleus and bind to the promoters of related genes, inducing the expression of specific genes (120–123). These cytokines are highly important in initiating and orchestrating innate and adaptive immune responses but may also be a source of excessive or uncontrolled inflammation and tissue damage in patients with COVID-19. The importance of JAK/STAT pathway in malignancies and autoimmune diseases has been reported (124–131); therefore, inhibition of the JAK/STAT pathway is a promising approach for the treatment of various diseases.

JAK inhibitors can competitively bind to the adenosine triphosphate-binding site of JAKs and interfere with the phosphorylation of STATs proteins, thereby inhibiting the expression of downstream inflammatory genes and growth factors (132, 133). Currently, JAK inhibitors have achieved efficacy in a wide range of immune-mediated inflammatory diseases, such as rheumatoid arthritis (RA) (134), myelofibrosis, and polycythemia vera (135–137). The severity of COVID-19 is strongly associated with SARS-CoV-2–induced hypercytokinemia and inflammation (138, 139). Up to now, some JAKi (such as Baricitinib, Ruxolitinib, Tofacitinib, and Nerizutinib) have had significant clinical impacts on improving clinical outcomes of hospitalized patients with COVID-19. These kinase inhibitors are used as treatments for COVID-19 because they inhibit virus-induced immune activation and signaling of inflammation (140).

Baricitinib

Baricitinib is a JAK1/JAK2 inhibitor that blocks cytokine and growth factor receptor stimulation, thereby reducing downstream immune cell function (117). Baricitinib is used for the treatment of RA and has shown success in clinical studies in RA. Baricitinib is reliably absorbed when administered orally and is therefore highly bioavailable and well tolerated in patients with RA (141, 142). COVID-19 infection–induced cytokine signaling pathways—including IL-6, IL-2, IL-10, IFN-γ, and GM-CSF—are elevated in hyperinflammatory conditions but are disrupted by baricitinib (53, 117). Furthermore, baricitinib may also have direct anti–SARS-CoV-2

activity by interfering with viral endocytosis, thus hindering SARS-CoV-2 entry and infection of susceptible cells (143).

Numerous studies have established the potency of baricitinib in hospitalized participants with COVID-19. Improved oxygenation and reduced levels of systemic inflammatory cytokines have been reported in patients with COVID-19 treated with baricitinib (144–146). A meta-analysis of randomized controlled trials shows that treatment with JAK inhibitors (including baricitinib) in hospitalized patients with COVID-19 can significantly reduce the risk for COVID-19 death by 43%, whereas it led to a significant decrease in the risk for mechanical ventilation or ECMO (extracorporeal membrane oxygenation) initiation by 36% (147). A study demonstrated that baricitinib plus standard of care including corticosteroids predominantly reduced mortality at 28 days and 60 days in patients who were receiving National Institute of Allergy and Infectious Disease (NIAID) ordinal scale score 7 population (NIAID-OS 7; hospitalized and on IMV or ECMO). Overall, 28-day all-cause mortality among patients on IMV or ECMO at baseline was 58% among those receiving placebo and 39% among participants receiving baricitinib. Sixty-day mortality was significantly lower in the baricitinib group compared with that in the placebo (45% *vs.* 62%, respectively) (148). In addition, another two studies showed that baricitinib absolutely reduced mortality in patients with moderate-to-severe or severe COVID-19 (149, 150). Another meta-analysis of randomized controlled trials evaluated the safety and efficacy of baricitinib in hospitalized patients with COVID-19 and showed that baricitinib could lead to better clinical outcomes for hospitalized patients with COVID-19 (151).

Since baricitinib's continued success in COVID-19 clinical studies, FDA issues the first EUA for baricitinib in combination with remdesivir for the treatment of hospitalized adults with COVID-19 and pediatric patients 2 years or older requiring assisted invasive mechanical ventilation or ECMO. The EUA, revised on 28 July 2021, to address safety concerns and protect public health, authorizes baricitinib as a stand-alone therapy. In May 2022, baricitinib was approved by the US FDA for the treating hospitalized adults with COVID-19 requiring supplemental oxygen, mechanical ventilation, or ECMO.

Tofacitinib

Tofacitinib, an orally available JAK inhibitor, can inhibit inflammatory cytokines such as IL-2, IL-4, IL-6, and IL-7 through inhibiting JAK3 and JAK1, which is approved for treating autoimmune diseases and RA (152–155). Many studies suggest that tofacitinib therapy can be continued in patients with COVID-19.

A double-blind, interventional phase 3 trial (NCT04469114) including 289 patients evaluated the safety and efficacy of tofacitinib in hospitalized patients with COVID-19 with pneumonia (156). The cumulative incidence of death or respiratory failure through day 28 was 18.1% in the tofacitinib group and 29.0% in the placebo group. Specifically, 28-day all-cause mortality was significantly lower in the tofacitinib group than in the placebo group (2.8% vs. 5.5%, respectively) (156). In another study by Roman and colleagues on 62 patients with severe COVID-19, it has shown that tofacitinib group showed lower mortality and the incidence of admission to intensive care than the control group (16.6% *vs.* 40.0% and 15.6% *vs.* 50.0%) (157). Furthermore, an ongoing randomized, double-blinded, placebo-controlled phase 2 study developed by Yale University evaluated the safety and efficacy of tofacitinib in 60 hospitalized patients with COVID-19 (18–99 years old) who require supplemental oxygen and have serologic markers of inflammation but do not need mechanical ventilation (NCT04415151). Analysis of these RCT studies demonstrated the promising efficacy of tofacitinib in mortality and the incidence of invasive mechanical ventilation.

Ruxolitinib

Ruxolitinib, a JAK1 and JAK2 protein kinase inhibitor, can suppress cytokine production associated with myelofibrosis, polycythemia vera, and acute graft-versus-host disease (158–163), which is similar to SARS-CO-V2 infection. The antiviral potency of ruxolitinib has also been shown to be effective against HIV and Epstein–Barr virus infection (164, 165). Since ruxolitinib has been successfully used to treat the diseases associated with hyperimmune syndrome, it has been employed in patients with COVID-19.

Several studies are being conducted with ruxolitinib in several clinical settings. In a global, double-blind, placebo-controlled, 29-day, multicenter phase 3 trial, 432 patients were randomly assigned to receive ruxolitinib (n = 287) or placebo (n = 145) plus the standard of care to assess the efficacy and safety of ruxolitinib in hospitalized patients with COVID-19. In this study, the primary objective was missing: the composite endpoint was 12% in both ruxolitinib-treated patients and placebo-treated patients; the mortality rate by day 29 was 3% in patients receiving ruxolitinib, compared with 2% in the placebo group. In addition, 8% ruxolitinib-treated patients had received invasive ventilation compared with 7% of 145 placebo-treated patients, and 11% ruxolitinib-treated patients had received ICU care compared with 12% placebo-treated patients (166). Another phase 3 study was conducted to assess the efficacy and safety of ruxolitinib with 5 mg bidaily or 15 mg bidaily in patients with COVID-19–associated ARDS who require mechanical ventilation. There was no statistically significant improvement in mortality in ruxolitinib group at day 29 compared with that in the placebo. However, it is significant when US study participants were analyzed separately, and when data from both treatment arms were pooled, it could also be detected for the overall population (167). In addition, a beneficial effect of ruxolitinib was reported in COVID-19 pneumonia in a multicenter study with 43 participants. In this study, 90% of ruxolitinib-treated patients showed computed tomography improvement at day 14 compared with 61.9% of placebo-treated patients. Three patients in the control group died of respiratory failure, with an overall mortality rate of 14.3% on day 28; no patients in the ruxolitinib group died. This study demonstrates that ruxolitinib tends to improve the clinical status of patients with COVID-19 in a shorter time (168).

Nezulcitinib

Nezulcitinib, an inhaled, lung-selective, pan-JAK inhibitor, has shown strong, broad inhibition of JAK/STAT signaling in the respiratory tract in experimental mouse models, which is a promising therapy for broad intervention in excessive immune

response in the airways. Therefore, nezutinib, administered by nebulization, may provide a new therapeutic modality to inhibit cytokine release and decrease morbidity and mortality in patients with COVID-19 with acute lung injury. A phase 2 clinical trial with inhaled nezulcitinib 3 doses (1, 3, and 10 mg once daily for 7 days) explored the safety and efficacy in 25 patients with severe COVID-19 and initially reported trends toward improving the clinical status and decreasing mortality in patients requiring supplemental oxygen (169). The lower mortality rate and earlier clinical recovery in patients receiving nezulcitinib compared with that in patients receiving a placebo suggest that it is a promising therapy for cytokine-driven lung inflammation.

Steroids

The latest research shows that SARS-CoV-2 infection can motivate the immune system and ignite inflammation, which occasionally causes lethal cytokine storm. Corticosteroids have been used to treat inflammation related diseases in the last decade, such as RA and asthma. However, the trials of corticosteroids in patients with COVID were not encouraged in the beginning considering their function in suppressing the immune system. After several randomized clinical trials, corticosteroids have been proved to be able to improve survival in severe COVID-19 (170), which will be discussed in the following part.

Dexamethasone

In 2020, a controlled and open-label trial, including around 6,425 hospitalized patients, that lasted for 28 days was started in the UK (171). A total of 4,321 patients receiving usual care were taken as control, whereas another 2,104 patients received dexamethasone treatment. After 28 days, dexamethasone decreased the death rate of patients rely on invasive mechanical ventilation or oxygen. Another clinical trial stated that intravenous dexamethasone was able to increase ventilator-free days in patients with COVID-19 with moderate or severe ARDS in comparison with standard care alone (172). However, long-term treatment with 12 or 6 mg of dexamethasone for 10 days in patients with COVID-19 with severe hypoxemia did not show improvement in mortality or health-related quality of life (173). Similarly, another clinical trial study that lasted for 10 days showed that dexamethasone at 12 mg/day compared with that at 6 mg/day did not decrease the death rate of patients with COVID-19 and severe hypoxemia in the absence of life support (174), whereas a 90-day follow-up of which revealed the benefits of the high dose compared with that of the low dose (175). Furthermore, an open-label and randomized clinical trial demonstrated that high-dose dexamethasone, compared with low-dose, improved clinical symptoms within 11 days in hospitalized patients with COVID-19 who rely on oxygen therapy (176).

Budesonide

The study carried out in Spain and Argentina stated that inhaled budesonide was safe and could reduce the incidence of severe syndrome in inpatients with COVID-19 (177). Another similar study was accomplished in the UK community, which showed that inhaled budesonide could promote the recovery rate and reduces hospitalization or death in patients with COVID-19 (178). In addition, a phase 2 randomized controlled trial indicated that administration of inhaled budesonide in early COVID-19 could reduce the chance of worsening, which may be due to its inflammatory modulating effect through improving T-cell response (179, 180).

Ciclesonide

CONTAIN phase 2 randomized controlled trial exhibited that patients with inhalation and intranasal ciclesonide showed less severe symptoms than the patients in placebo groups, which did not show in young patients. However, further research is required due to insufficient evidence (181). Another randomized clinical trial of the efficacy of inhaled ciclesonide in outpatients showed that ciclesonide did not reduce the recovery time in adolescents and adult patients (182). Nevertheless, it is still early to get a conclusion about the effect of ciclesonide.

Glucocorticoids

Hydrocortisone and methylprednisolone all showed positive effects in patients with COVID-19 with severe symptoms revealed by two clinical trials (183, 184). Prednisolone showed a protective effect in patients with post–COVID-19 diffuse parenchymal abnormalities, which did not show dose dependency (185).

Conclusions

COVID-19, as a worldwide spreading virus with high transfection and lethal, caused millions of people to die, exposing the weakness of the human healthcare system in coping with emergent and serious health risks. All the above-illustrated treatments with different advantages or disadvantages (Figure 2) have been developed, targeting the virus or the host, which indeed saved lots of lives before effective vaccines were produced. Although some trials failed, they still played positive roles in the human healthcare development. The effect of many treatments is compromised or controversial, such as the antiviral agents and neutral antibody therapies, which may be caused by viral variants, and combinational treatment can be considered based on the results of some clinical trials. Many studies reported combinational therapies showing better effects than single treatment, such as molnupiravir/fluvoxamine/Paxlovid, IFN-β1b/lopinavir/ritonavir/ribavirin, and lopinavir/ritonavir/arbidol/Shufeng Jiedu Capsule. In general, combinational therapy showed more advantages than single treatment. In addition, compared with antiviral agents and neutral antibody treatments, JAK inhibitors show more promising effects, which may be worthy to continue in future studies. For the effect of steroids, it is still early to get a conclusion. Although current vaccines restrain the development of the invisible "war" ignited by COVID-19, humans should be getting ready anytime for future pandemic threats that may jeopardize the whole world. It is impossible for humans to predict the next pandemic, which makes it impractical to prepare effective vaccines in advance. However,

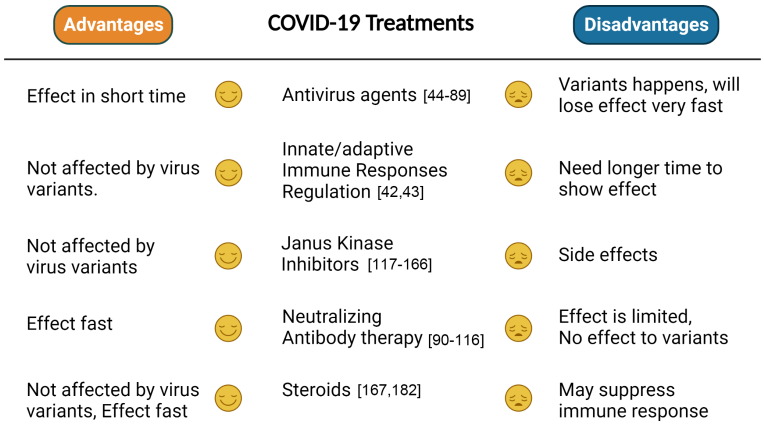

FIGURE 2
Comparison between different treatments. The advantages and disadvantages of each treatment are summarized on the basis of whether they will be efficient to variants, have side effects, or effect fast.

effective treatments targeting symptoms caused by infection are still significant, with respect to being prepared for another potential pandemic threat. Hence, more efforts are still needed to be put into developing effective treatments for COVID-19.

Author contributions

YY and DY arranged an overview of the content. All authors contributed to the article and approved the submitted version.

Funding

This study was supported by the program of the National natural science Foundation of China.(Grant number 81903874 and 81903720).

Conflict of interest

The authors declare that the research was conducted in the absence of any commercial or financial relationships that could be construed as a potential conflict of interest.

Publisher's note

References

1. Cucinotta D, Vanelli M. WHO declares COVID-19 a pandemic. *Acta BioMed* (2020) 91(1):157–60. doi: 10.23750/abm.v91i1.9397

2. Abbasi J. Fourth COVID-19 vaccine dose increases low antibodies. *JAMA* (2022) 327(6):517. doi: 10.1001/jama.2022.0727

3. Altmann DM, Boyton RJ. COVID-19 vaccination: The road ahead. *Science* (2022) 375(6585):1127–32. doi: 10.1126/science.abn1755

4. Dube E, MacDonald NE. COVID-19 vaccine hesitancy. *Nat Rev Nephrol* (2022) 18 (7):409–10. doi: 10.1038/s41581-022-00571-2

5. Niknam Z, Golchin A, Danesh Pouya F, Nemati M, Rezaei-Tavirani M. Potential therapeutic options for COVID-19: an update on current evidence. *Eur J Med Res* (2022) 27(1):6. doi: 10.1186/s40001-021-00626-3

6. Drozdzal S, Rosik J, Lechowicz K, Machaj F, Szostak B, Przybycinski J, et al. An update on drugs with therapeutic potential for SARS-CoV-2 (COVID-19) treatment. *Drug Resist Update* (2021) 59:100794. doi: 10.1016/j.drup.2021.100794

7. Zhou P, Yang XL, Wang XG, Hu B, Zhang L, Zhang W, et al. A pneumonia outbreak associated with a new coronavirus of probable bat origin. *Nature* (2020) 579(7798):270–3. doi: 10.1038/s41586-020-2012-7

8. Huang C, Wang Y, Li X, Ren L, Zhao J, Hu Y, et al. Clinical features of patients infected with 2019 novel coronavirus in wuhan, China. *Lancet* (2020) 395(10223):497–506. doi: 10.1016/S0140-6736(20)30183-5

9. Coronaviridae Study Group of the International Committee on Taxonomy of, V. The species severe acute respiratory syndrome-related coronavirus: classifying 2019-nCoV and naming it SARS-CoV-2. *Nat Microbiol* (2020) 5(4):536–44. doi: 10.1038/s41564-020-0695-z

10. Lu R, Zhao X, Li J, Niu P, Yang B, Wu H, et al. Genomic characterisation and epidemiology of 2019 novel coronavirus: implications for virus origins and receptor binding. *Lancet* (2020) 395(10224):565–74. doi: 10.1016/S0140-6736(20)30251-8

11. Hoffmann M, Kleine-Weber H, Schroeder S, Kruger N, Herrler T, Erichsen S, et al. SARS-CoV-2 cell entry depends on ACE2 and TMPRSS2 and is blocked by a clinically proven protease inhibitor. *Cell* (2020) 181(2):271–280 e8. doi: 10.1016/j.cell.2020.02.052

12. Harrison AG, Lin T, Wang P. Mechanisms of SARS-CoV-2 transmission and pathogenesis. *Trends Immunol* (2020) 41(12):1100–15. doi: 10.1016/j.it.2020.10.004

13. Mizrahi B, Shilo S, Rossman H, Kalkstein N, Marcus K, Barer Y, et al. Longitudinal symptom dynamics of COVID-19 infection. *Nat Commun* (2020) 11(1):6208. doi: 10.1038/s41467-020-20053-y

14. Subramanian A, Nirantharakumar K, Hughes S, Myles P, Williams T, Gokhale KM, et al. Symptoms and risk factors for long COVID in non-hospitalized adults. *Nat Med* (2022) 28(8):1706–14. doi: 10.1038/s41591-022-01909-w

15. Zhang W, Chua BY, Selva KJ, Kedzierski L, Ashhurst TM, Haycroft ER, et al. SARS-CoV-2 infection results in immune responses in the respiratory tract and peripheral blood that suggest mechanisms of disease severity. *Nat Commun* (2022) 13(1):2774. doi: 10.1038/s41467-022-30088-y

16. Brodin P. Immune determinants of COVID-19 disease presentation and severity. *Nat Med* (2021) 27(1):28–33. doi: 10.1038/s41591-020-01202-8

17. Li D, Wu M. Pattern recognition receptors in health and diseases. *Signal Transduct Target Ther* (2021) 6(1):291. doi: 10.1038/s41392-021-00687-0

18. Kanneganti TD. Intracellular innate immune receptors: Life inside the cell. *Immunol Rev* (2020) 297(1):5–12. doi: 10.1111/imr.12912

19. Loo YM, Gale M Jr. Immune signaling by RIG-i-like receptors. *Immunity* (2011) 34(5):680–92. doi: 10.1016/j.immuni.2011.05.003

20. Horner SM, Liu HM, Park HS, Briley J, Gale M Jr. Mitochondrial-associated endoplasmic reticulum membranes (MAM) form innate immune synapses and are targeted by hepatitis c virus. *Proc Natl Acad Sci U.S.A.* (2011) 108(35):14590–5. doi: 10.1073/pnas.1110133108

21. Yin X, Riva L, Pu Y, Martin-Sancho L, Kanamune J, Yamamoto Y, et al. MDA5 governs the innate immune response to SARS-CoV-2 in lung epithelial cells. *Cell Rep* (2021) 34(2):108628. doi: 10.1016/j.celrep.2020.108628

22. Yang DM, Geng TT, Harrison AG, Wang PH. Differential roles of RIG-I like receptors in SARS-CoV-2 infection. *Mil Med Res* (2021) 8(1):49. doi: 10.1186/s40779-021-00340-5

23. Rebendenne A, Valadao ALC, Tauziet M, Maarifi G, Bonaventure B, McKellar J, et al. SARS-CoV-2 triggers an MDA-5-dependent interferon response which is unable to control replication in lung epithelial cells. *J Virol* (2021) 95(8):e02415–20. doi: 10.1128/JVI.02415-20

24. Thorne LG, Reuschl AK, Zuliani-Alvarez L, Whelan MVX, Turner J, Noursadeghi M. SARS-CoV-2 sensing by RIG-I and MDA5 links epithelial infection to macrophage inflammation. *EMBO J* (2021) 40(15):e107826. doi: 10.15252/embj.2021107826

25. Yamada T, Sato S, Sotoyama Y, Orba Y, Sawa H, Yamauchi H, et al. RIG-I triggers a signaling-abortive anti-SARS-CoV-2 defense in human lung cells. *Nat Immunol* (2021) 22(7):820–8. doi: 10.1038/s41590-021-00942-0

26. Akira S, Takeda K. Toll-like receptor signalling. *Nat Rev Immunol* (2004) 4(7):499–511. doi: 10.1038/nri1391

27. Zheng M, Karki R, Williams EP, Yang D, Fitzpatrick E, Vogel P, et al. TLR2 senses the SARS-CoV-2 envelope protein to produce inflammatory cytokines. *Nat Immunol* (2021) 22(7):829–38. doi: 10.1038/s41590-021-00937-x

28. Zhao Y, Kuang M, Li J, Zhu L, Jia Z, Guo X, et al. SARS-CoV-2 spike protein interacts with and activates TLR41. *Cell Res* (2021) 31(7):818–20. doi: 10.1038/s41422-021-00495-9

29. Pan P, Shen M, Yu Z, Ge W, Chen K, Tian M, et al. SARS-CoV-2 n protein promotes NLRP3 inflammasome activation to induce hyperinflammation. *Nat Commun* (2021) 12(1):4664. doi: 10.1038/s41467-021-25015-6

30. Rodrigues TS, de Sa KSG, Ishimoto AY, Becerra A, Oliveira S, Almeida L, et al. Inflammasomes are activated in response to SARS-CoV-2 infection and are associated with COVID-19 severity in patients. *J Exp Med* (2021) 218(3):e20201707. doi: 10.1084/jem.20201707

31. Ferreira AC, Soares VC, de Azevedo-Quintanilha IG, Dias S, Fintelman-Rodrigues N, Sacramento CQ, et al. SARS-CoV-2 engages inflammasome and pyroptosis in human primary monocytes. *Cell Death Discovery* (2021) 7(1):43. doi: 10.1038/s41420-021-00428-w

32. Rui Y, Su J, Shen S, Hu Y, Huang D, Zheng W, et al. Unique and complementary suppression of cGAS-STING and RNA sensing- triggered innate immune responses by SARS-CoV-2 proteins. *Signal Transduct Target Ther* (2021) 6(1):123. doi: 10.1038/s41392-021-00515-5

33. Li M, Ferretti M, Ying B, Descamps H, Lee E, Dittmar M, et al. Pharmacological activation of STING blocks SARS-CoV-2 infection. *Sci Immunol* (2021) 6(59):eabi9007. doi: 10.1126/sciimmunol.abi9007

34. Humphries F, Shmuel-Galia L, Jiang Z, Wilson R, Landis P, Ng SL, et al. A diamidobenzimidazole STING agonist protects against SARS-CoV-2 infection. *Sci Immunol* (2021) 6(59):eabi9002. doi: 10.1126/sciimmunol.abi9002

35. Hadjadj J, et al. Impaired type I interferon activity and inflammatory responses in severe COVID-19 patients. *Science* (2020) 369(6504):718–24. doi: 10.1126/science.abc6027

36. Karki R, Sharma BR, Tuladhar S, Williams EP, Zalduondo L, Samir P, et al. Synergism of TNF-alpha and IFN-gamma triggers inflammatory cell death, tissue damage, and mortality in SARS-CoV-2 infection and cytokine shock syndromes. *Cell* (2021) 184(1):149–168 e17. doi: 10.1016/j.cell.2020.11.025.

37. Zhang F, Mears JR, Shakib L, Beynor JI, Shanaj S, Korsunsky I, et al. IFN-gamma and TNF-alpha drive a CXCL10+ CCL2+ macrophage phenotype expanded in severe COVID-19 lungs and inflammatory diseases with tissue inflammation. *Genome Med* (2021) 13(1):64. doi: 10.1186/s13073-021-00881-3

38. Belhadjer Z, Meot M, Bajolle F, Khraiche D, Legendre A, Abakka S, et al. Acute heart failure in multisystem inflammatory syndrome in children in the context of global SARS-CoV-2 pandemic. *Circulation* (2020) 142(5):429–36. doi: 10.1161/CIRCULATIONAHA.120.048360

39. Mehandru S, Merad M. Pathological sequelae of long-haul COVID. *Nat Immunol* (2022) 23(2):194–202. doi: 10.1038/s41590-021-01104-y

40. Herold T, Jurinovic V, Arnreich C, Lipworth BJ, Hellmuth JC, von Bergwelt-Baildon M, et al. Elevated levels of IL-6 and CRP predict the need for mechanical ventilation in COVID-19. *J Allergy Clin Immunol* (2020) 146(1):128–136 e4. doi: 10.1016/j.jaci.2020.05.008

41. Chen X, Zhao B, Qu Y, Chen Y, Xiong J, Feng Y, et al. Detectable serum severe acute respiratory syndrome coronavirus 2 viral load (RNAemia) is closely correlated with drastically elevated interleukin 6 level in critically ill patients with coronavirus disease 2019. *Clin Infect Dis* (2020) 71(8):1937–42. doi: 10.1093/cid/ciaa449

42. Roltgen K, Boyd SD. Antibody and b cell responses to SARS-CoV-2 infection and vaccination. *Cell Host Microbe* (2021) 29(7):1063–75. doi: 10.1016/j.chom.2021.06.009

43. Moss P. The T cell immune response against SARS-CoV-2. *Nat Immunol* (2022) 23(2):186–93. doi: 10.1038/s41590-021-01122-w

44. Wang M, Cao R, Zhang L, Yang X, Liu J, Xu M, et al. Remdesivir and chloroquine effectively inhibit the recently emerged novel coronavirus (2019-nCoV) in vitro. *Cell Res* (2020) 30(3):269–71. doi: 10.1038/s41422-020-0282-0

45. Williamson BN, Feldmann F, Schwarz B, Meade-White K, Porter DP, Schulz J, et al. Clinical benefit of remdesivir in rhesus macaques infected with SARS-CoV-2. *Nature* (2020) 585(7824):273–6. doi: 10.1038/s41586-020-2423-5

46. Gottlieb RL, Vaca CE, Paredes R, Mera J, Webb BJ, Perez G, et al. Early remdesivir to prevent progression to severe covid-19 in outpatients. *N Engl J Med* (2022) 386(4):305–15. doi: 10.1056/NEJMoa2116846

47. Beigel JH, Tomashek KM, Dodd LE, Mehta AK, Zingman BS, Kalil AC, et al. Remdesivir for the treatment of covid-19 - final report. *N Engl J Med* (2020) 383(19):1813–26. doi: 10.1056/NEJMoa2007764

48. Spinner CD, Gottlieb RL, Criner GJ, Arribas Lopez JR, Cattelan AM, Soriano Viladomiu A, et al. Effect of remdesivir vs standard care on clinical status at 11 days in patients with moderate COVID-19: A randomized clinical trial. *JAMA* (2020) 324(11):1048–57. doi: 10.1001/jama.2020.16349

49. Goldman JD, Lye DCB, Hui DS, Marks KM, Bruno R, Montejano R, et al. Remdesivir for 5 or 10 days in patients with severe covid-19. *N Engl J Med* (2020) 383(19):1827–37. doi: 10.1056/NEJMoa2015301

50. Singh KP, Tong SYC. In adults hospitalized with COVID-19, adding remdesivir to standard care did not reduce in-hospital mortality. *Ann Intern Med* (2022) 175(5):JC51. doi: 10.7326/J22-0025

51. Ader F, Bouscambert-Duchamp M, Hites M, Peiffer-Smadja N, Poissy J, Belhadi D, et al. Remdesivir plus standard of care versus standard of care alone for the treatment of patients admitted to hospital with COVID-19 (DisCoVeRy): a phase 3, randomised, controlled, open-label trial. *Lancet Infect Dis* (2022) 22(2):209–21. doi: 10.1016/S1473-3099(21)00485-0

52. Wang Y, Zhang D, Du G, Du R, Zhao J, Jin Y, et al. Remdesivir in adults with severe COVID-19: a randomised, double-blind, placebo-controlled, multicentre trial. *Lancet* (2020) 395(10236):1569–78. doi: 10.1016/S0140-6736(20)31022-9

53. Kalil AC, Patterson TF, Mehta AK, Tomashek KM, Wolfe CR, Ghazaryan V, et al. Baricitinib plus remdesivir for hospitalized adults with covid-19. *N Engl J Med* (2021) 384(9):795–807. doi: 10.1056/NEJMoa2031994

54. Delang L, Abdelnabi R, Neyts J. Favipiravir as a potential countermeasure against neglected and emerging RNA viruses. *Antiviral Res* (2018) 153:85–94. doi: 10.1016/j.antiviral.2018.03.003

55. Furuta Y, Gowen BB, Takahashi K, Shiraki K, Smee DF, Barnard DL. Favipiravir (T-705), a novel viral RNA polymerase inhibitor. *Antiviral Res* (2013) 100(2):446–54. doi: 10.1016/j.antiviral.2013.09.015

56. Udwadia ZF, Singh P, Barkate H, Patil S, Rangwala S, Pendse A, et al. Efficacy and safety of favipiravir, an oral RNA-dependent RNA polymerase inhibitor, in mild-to-moderate COVID-19: A randomized, comparative, open-label, multicenter, phase 3 clinical trial. *Int J Infect Dis* (2021) 103:62–71. doi: 10.1016/j.ijid.2020.11.142

57. Yao TT, Qian JD, Zhu WY, Wang Y, Wang GQ. A systematic review of lopinavir therapy for SARS coronavirus and MERS coronavirus-a possible reference for coronavirus disease-19 treatment option. *J Med Virol* (2020) 92(6):556–63. doi: 10.1002/jmv.25729

58. Cao B, Wang Y, Wen D, Liu W, Wang J, Fan G, et al. A trial of lopinavir-ritonavir in adults hospitalized with severe covid-19. *N Engl J Med* (2020) 382(19):1787–99. doi: 10.1056/NEJMoa2001282

59. Group RC. Lopinavir-ritonavir in patients admitted to hospital with COVID-19 (RECOVERY): a randomised, controlled, open-label, platform trial. *Lancet* (2020) 396(10259):1345–52. doi: 10.1016/S0140-6736(20)32013-4

60. Wang Z, Chen X, Lu Y, Chen F, Zhang W. Clinical characteristics and therapeutic procedure for four cases with 2019 novel coronavirus pneumonia receiving combined Chinese and Western medicine treatment. *Biosci Trends* (2020) 14(1):64–8. doi: 10.5582/bst.2020.01030

61. Hung IF, Lung KC, Tso EY, Liu R, Chung TW, Chu MY, et al. Triple combination of interferon beta-1b, lopinavir-ritonavir, and ribavirin in the treatment of patients admitted to hospital with COVID-19: an open-label, randomised, phase 2 trial. *Lancet* (2020) 395(10238):1695–704. doi: 10.1016/S0140-6736(20)31042-4

62. Owen DR, Allerton CMN, Anderson AS, Aschenbrenner L, Avery M, Berritt S, et al. An oral SARS-CoV-2 m(pro) inhibitor clinical candidate for the treatment of COVID-19. *Science* (2021) 374(6575):1586–93. doi: 10.1126/science.abl4784

63. Hammond J, Leister-Tebbe H, Gardner A, Abreu P, Bao W, Wisemandle W, et al. Oral nirmatrelvir for high-risk, nonhospitalized adults with covid-19. *N Engl J Med* (2022) 386(15):1397–408. doi: 10.1056/NEJMoa2118542

64. Zhang JL, Li YH, Wang LL, Liu HQ, Lu SY, Liu Y, et al. Azvudine is a thymus-homing anti-SARS-CoV-2 drug effective in treating COVID-19 patients. *Signal Transduct Target Ther* (2021) 6(1):414. doi: 10.1038/s41392-021-00835-6

65. Ren Z, Luo H, Yu Z, Song J, Liang L, Wang L, et al. A randomized, open-label, controlled clinical trial of azvudine tablets in the treatment of mild and common COVID-19, a pilot study. *Adv Sci (Weinh)* (2020) 7(19):e2001435. doi: 10.1002/advs.202001435

66. Yu B, Chang J. Azvudine (FNC): a promising clinical candidate for COVID-19 treatment. *Signal Transduct Target Ther* (2020) 5(1):236. doi: 10.1038/s41392-020-00351-z

67. Wahl A, Gralinski LE, Johnson CE, Yao W, Kovarova M, Dinnon KH 3rd, et al. SARS-CoV-2 infection is effectively treated and prevented by EIDD-2801. *Nature* (2021) 591(7850):451–7. doi: 10.1038/s41586-021-03312-w

68. Mahase E. Covid-19: Molnupiravir reduces risk of hospital admission or death by 50% in patients at risk, MSD reports. *BMJ* (2021) 375:n2422. doi: 10.1136/bmj.n2422

69. Jayk Bernal A, Gomes da Silva MM, Musungaie DB, Kovalchuk E, Gonzalez A, Delos Reyes V, et al. Molnupiravir for oral treatment of covid-19 in nonhospitalized patients. *N Engl J Med* (2022) 386(6):509–20. doi: 10.1056/NEJMoa2116044

70. Mahase E. Covid-19: UK becomes first country to authorise antiviral molnupiravir. *BMJ* (2021) 375:n2697. doi: 10.1136/bmj.n2697

71. Whitley R. Molnupiravir - a step toward orally bioavailable therapies for covid-19. *N Engl J Med* (2022) 386(6):592–3. doi: 10.1056/NEJMe2117814

72. Araujo R, Aranda-Martinez JD, Aranda-Abreu GE. Amantadine treatment for people with COVID-19. *Arch Med Res* (2020) 51(7):739–40. doi: 10.1016/j.arcmed.2020.06.009

73. Smieszek SP, Przychodzen BP, Polymeropoulos MH. Amantadine disrupts lysosomal gene expression: A hypothesis for COVID19 treatment. *Int J Antimicrob Agents* (2020) 55(6):106004. doi: 10.1016/j.ijantimicag.2020.106004

74. Rejdak K, Grieb P. Adamantanes might be protective from COVID-19 in patients with neurological diseases: multiple sclerosis, parkinsonism and cognitive impairment. *Mult Scler Relat Disord* (2020) 42:102163. doi: 10.1016/j.msard.2020.102163

75. Ahmadi K, Farasat A, Rostamian M, Johari B, Madanchi H. Enfuvirtide, an HIV-1 fusion inhibitor peptide, can act as a potent SARS-CoV-2 fusion inhibitor: an in silico drug repurposing study. *J Biomol Struct Dyn* (2022) 40(12):5566–76. doi: 10.1080/07391102.2021.1871958

76. Oliver ME, Hinks TSC. Azithromycin in viral infections. *Rev Med Virol* (2021) 31(2):e2163. doi: 10.1002/rmv.2163

77. Dontcheff L. [Discontinuous evolution of oxygen consumption in relation to weight, during fasting in rats]. *C R Seances Soc Biol Fil* (1970) 164(6):1370–1.

78. Group PTC. Azithromycin for community treatment of suspected COVID-19 in people at increased risk of an adverse clinical course in the UK (PRINCIPLE): a randomised, controlled, open-label, adaptive platform trial. *Lancet* (2021) 397(10279):1063–74. doi: 10.1016/S0140-6736(21)00461-X

79. Ferner RE, Aronson JK. Chloroquine and hydroxychloroquine in covid-19. *BMJ* (2020) 369:m1432. doi: 10.1136/bmj.m1432

80. Group RC, Horby P, Mafham M, Linsell L, Bell JL, Staplin N, et al. Effect of hydroxychloroquine in hospitalized patients with covid-19. *N Engl J Med* (2020) 383(21):2030–40. doi: 10.1056/NEJMoa2022926

81. Correction: Hydroxychloroquine in nonhospitalized adults with early COVID-19. *Ann Intern Med* (2021) 174(3):435. doi: 10.7326/L20-1220

82. Boulware DR, Pullen MF, Bangdiwala AS, Pastick KA, Lofgren SM, Okafor EC, et al. A randomized trial of hydroxychloroquine as postexposure prophylaxis for covid-19. *N Engl J Med* (2020) 383(6):517–25. doi: 10.1056/NEJMoa2016638

83. Mitja O, Pullen MF, Bangdiwala AS, Pastick KA, Lofgren SM, Okafor EC, et al. A cluster-randomized trial of hydroxychloroquine for prevention of covid-19. *N Engl J Med* (2021) 384(5):417–27. doi: 10.1056/NEJMoa2021801

84. Furtado RHM, Berwanger O, Fonseca HA, Correa TD, Ferraz LR, Lapa MG, et al. Azithromycin in addition to standard of care versus standard of care alone in the treatment of patients admitted to the hospital with severe COVID-19 in Brazil (COALITION II): a randomised clinical trial. *Lancet* (2020) 396(10256):959–67. doi: 10.1016/S0140-6736(20)31862-6

85. Cavalcanti AB, Zampieri FG, Rosa RG, Azevedo LCP, Veiga VC, Avezum A, et al. Hydroxychloroquine with or without azithromycin in mild-to-Moderate covid-19. *N Engl J Med* (2020) 383(21):2041–52. doi: 10.1056/NEJMoa2019014

86. Sposito B, Broggi A, Pandolfi L, Crotta S, Clementi N, Ferrarese R, et al. The interferon landscape along the respiratory tract impacts the severity of COVID-19. *Cell* (2021) 184(19):4953–4968 e16. doi: 10.1016/j.cell.2021.08.016

87. Ramasamy S, Subbian S. Erratum for ramasamy and subbian, "Critical determinants of cytokine storm and type I interferon response in COVID-19 pathogenesis". *Clin Microbiol Rev* (2021) 34(4):e0016321. doi: 10.1128/CMR.00163-21

88. Kalil AC, Mehta AK, Patterson TF, Erdmann N, Gomez CA, Jain MK, et al. Efficacy of interferon beta-1a plus remdesivir compared with remdesivir alone in hospitalised adults with COVID-19: a double-bind, randomised, placebo-controlled, phase 3 trial. *Lancet Respir Med* (2021) 9(12):1365–76. doi: 10.1016/S2213-2600(21)00384-2

89. Nakhlband A, Fakhari A, Azizi H. Interferon-alpha position in combating with COVID-19: A systematic review. *J Med Virol* (2021) 93(9):5277–84. doi: 10.1002/jmv.27072

90. Porter RR. The hydrolysis of rabbit y-globulin and antibodies with crystalline papain. *Biochem J* (1959) 73(1):119–26. doi: 10.1042/bj0730119

91. Edelman GM, Benacerraf B, Ovary Z, Poulik MD. Structural differences among antibodies of different specificities. *Proc Natl Acad Sci U.S.A.* (1961) 47(11):1751–8. doi: 10.1073/pnas.47.11.1751

92. Todd PA, Brogden RN. Muromonab CD3. a review of its pharmacology and therapeutic potential. *Drugs* (1989) 37(6):871–99. doi: 10.2165/00003495-198937060-00004

93. Rajewsky K. The advent and rise of monoclonal antibodies. *Nature* (2019) 575(7781):47–9. doi: 10.1038/d41586-019-02840-w

94. Li L, Zhang W, Hu Y, Tong X, Zheng S, Yang J, et al. Effect of convalescent plasma therapy on time to clinical improvement in patients with severe and life-threatening COVID-19: A randomized clinical trial. *JAMA* (2020) 324(5):460–70. doi: 10.1001/jama.2020.10044

95. Marconato M, Abela IA, Hauser A, Schwarzmüller M, Katzensteiner R, Braun DL, et al. Antibodies from convalescent plasma promote SARS-CoV-2 clearance in individuals with and without endogenous antibody response. *J Clin Invest* (2022) 132(12):e158190. doi: 10.1172/JCI158190

96. Alemany A, Millat-Martinez P, Corbacho-Monne M, Malchair P, Ouchi D, Ruiz-Comellas A, et al. High-titre methylene blue-treated convalescent plasma as an early treatment for outpatients with COVID-19: a randomised, placebo-controlled trial. *Lancet Respir Med* (2022) 10(3):278–88. doi: 10.1016/S2213-2600(21)00545-2

97. Sullivan DJ, Gebo KA, Shoham S, Bloch EM, Lau B, Shenoy AG, et al. Early outpatient treatment for covid-19 with convalescent plasma. *N Engl J Med* (2022) 386(18):1700–11. doi: 10.1056/NEJMoa2119657

98. RECOVERY Collaborative Group. Convalescent plasma in patients admitted to hospital with COVID-19 (RECOVERY): a randomised controlled, open-label, platform trial. *Lancet* (2021) 397(10289):2049–59. doi: 10.1016/S0140-6736(21)00897-7

99. Estcourt L, Callum J. Convalescent plasma for covid-19 - making sense of the inconsistencies. *N Engl J Med* (2022) 386(18):1753–4. doi: 10.1056/NEJMe2204332

100. Jones BE, Brown-Augsburger PL, Corbett KS, Westendorf K, Davies J, Cujec TP, et al. The neutralizing antibody, LY-CoV555, protects against SARS-CoV-2 infection in nonhuman primates. *Sci Transl Med* (2021) 13(593):eabf1906. doi: 10.1126/scitranslmed.abf1906

101. Matz AJ, Qu L, Karlinsey K, Zhou B. MicroRNA-regulated b cells in obesity. *Immunometabolism (Cobham)* (2022) 4(3):e00005. doi: 10.1097/IN9.0000000000000005

102. Chen P, Nirula A, Heller B, Gottlieb RL, Boscia J, Morris J, et al. SARS-CoV-2 neutralizing antibody LY-CoV555 in outpatients with covid-19. *N Engl J Med* (2021) 384(3):229–37. doi: 10.1056/NEJMoa2029849

103. ACTIV-3/TICO LY-CoV555 Study Group, Lundgren JD, Grund B, Barkauskas CE, Holland TL, Gottlieb RL, et al. A neutralizing monoclonal antibody for hospitalized patients with covid-19. *N Engl J Med* (2021) 384(10):905–14. doi: 10.1056/NEJMoa2033130

104. Matz A, Qu L, Karlinsey K, Zhou B. Impact of microRNA regulated macrophage actions on adipose tissue function in obesity. *Cells* (2022) 11(8):1336. doi: 10.3390/cells11081336

105. Qu L, Matz AJ, Karlinsey K, Cao Z, Vella AT, Zhou B, et al. Macrophages at the crossroad of meta-inflammation and inflammaging. *Genes (Basel)* (2022) 13(11):2074. doi: 10.3390/genes13112074

106. Gottlieb RL, Nirula A, Chen P, Boscia J, Heller B, Morris J, et al. Effect of bamlanivimab as monotherapy or in combination with etesevimab on viral load in patients with mild to moderate COVID-19: A randomized clinical trial. *JAMA* (2021) 325(7):632–44. doi: 10.1001/jama.2021.0202

107. Karlinsey K, Qu L, Matz AJ, Zhou B. A novel strategy to dissect multifaceted macrophage function in human diseases. *J Leukoc Biol* (2022) 112(6):1535–42. doi: 10.1002/JLB.6MR0522-685R

108. Dougan M, Nirula A, Azizad M, Mocherla B, Gottlieb RL, Chen P, et al. Bamlanivimab plus etesevimab in mild or moderate covid-19. *N Engl J Med* (2021) 385(15):1382–92. doi: 10.1056/NEJMoa2102685

109. Li C, Phoon YP, Karlinsey K, Tian YF, Thapaliya S, Thongkum A, et al. A high OXPHOS CD8 T cell subset is predictive of immunotherapy resistance in melanoma patients. *J Exp Med* (2022) 219(1):e20202084. doi: 10.1084/jem.20202084

110. VanBlargan LA, Errico JM, Halfmann PJ, Zost SJ, Crowe JE Jr, Purcell LA, et al. An infectious SARS-CoV-2 B.1.1.529 omicron virus escapes neutralization by therapeutic monoclonal antibodies. *Nat Med* (2022) 28(3):490–5. doi: 10.1038/s41591-021-01678-y

111. Iketani S, Liu L, Guo Y, Liu L, Chan JF, Huang Y, et al. Antibody evasion properties of SARS-CoV-2 omicron sublineages. *Nature* (2022) 604(7906):553–6. doi: 10.1038/s41586-022-04594-4

112. Li C, Qu L, Matz AJ, Murphy PA, Liu Y, Manichaikul AW, et al. AtheroSpectrum reveals novel macrophage foam cell gene signatures associated with atherosclerotic cardiovascular disease risk. *Circulation* (2022) 145(3):206–18. doi: 10.1161/CIRCULATIONAHA.121.054285

113. Westendorf K, Zentelis S, Wang L, Foster D, Vaillancourt P, Wiggin M, et al. LY-CoV1404 (bebtelovimab) potently neutralizes SARS-CoV-2 variants. *Cell Rep* (2022) 39(7):110812. doi: 10.1016/j.celrep.2022.110812

114. Li C, Qu L, Farragher C, Vella A, Zhou B. MicroRNA regulated macrophage activation in obesity. *J Transl Int Med* (2019) 7(2):46–52. doi: 10.2478/jtim-2019-0011

115. Wang Q, Guo Y, Iketani S, Nair MS, Li Z, Mohri H, et al. Antibody evasion by SARS-CoV-2 omicron subvariants BA.2.12.1, BA.4 and BA.5. *Nature* (2022) 608(7923):603–8. doi: 10.1038/s41586-022-05053-w

116. Qu LL, Yu B, Li Z, Jiang WX, Jiang JD, Kong WJ. Gastrodin ameliorates oxidative stress and proinflammatory response in nonalcoholic fatty liver disease through the AMPK/Nrf2 pathway. *Phytother Res* (2016) 30(3):402–11. doi: 10.1002/ptr.5541

117. Hoang TN, Pino M, Boddapati AK, Viox EG, Starke CE, Upadhyay AA, et al. Baricitinib treatment resolves lower-airway macrophage inflammation and neutrophil recruitment in SARS-CoV-2-infected rhesus macaques. *Cell* (2021) 184(2):460–475 e21. doi: 10.1016/j.cell.2020.11.007

118. Duan X, Li S, Holmes JA, Tu Z, Li Y, Cai D, et al. MicroRNA 130a regulates both hepatitis c virus and hepatitis b virus replication through a central metabolic pathway. *J Virol* (2018) 92(7):e02009-17. doi: 10.1128/JVI.02009-17

119. Chen X, Ye H, Li S, Jiao B, Wu J, Zeng P, et al. Severe fever with thrombocytopenia syndrome virus inhibits exogenous type I IFN signaling pathway through its NSs invitro. *PloS One* (2017) 12(2):e0172744. doi: 10.1371/journal.pone.0172744

120. Hu X, Li J, Fu M, Zhao X, Wang W. The JAK/STAT signaling pathway: from bench to clinic. *Signal Transduct Target Ther* (2021) 6(1):402. doi: 10.1038/s41392-021-00791-1

121. Jiao B, Shi X, Chen Y, Ye H, Yao M, Hong W, et al. Insulin receptor substrate-4 interacts with ubiquitin-specific protease 18 to activate the Jak/STAT signaling pathway. *Oncotarget* (2017) 8(62):105923–35. doi: 10.18632/oncotarget.22510

122. Shi X, Jiao B, Chen Y, Li S, Chen L. MxA is a positive regulator of type I IFN signaling in HCV infection. *J Med Virol* (2017) 89(12):2173–80. doi: 10.1002/jmv.24867

123. Villarino AV, Gadina M, O'Shea JJ, Kanno Y. SnapShot: Jak-STAT signaling II. *Cell* (2020) 181(7):1696–1696 e1. doi: 10.1016/j.cell.2020.04.052

124. O'Shea JJ, Schwartz DM, Villarino AV, Gadina M, McInnes IB, Laurence A. The JAK-STAT pathway: impact on human disease and therapeutic intervention. *Annu Rev Med* (2015) 66:311–28. doi: 10.1146/annurev-med-051113-024537

125. Li Y, Li S, Duan X, Chen Y, Jiao B, Ye H, et al. Interferon-stimulated gene 15 conjugation stimulates hepatitis b virus production independent of type I interferon signaling pathway in vitro. *Mediators Inflammation* (2016) 2016:7417648. doi: 10.1155/2016/7417648

126. Chen Y, Jiao B, Yao M, Shi X, Zheng Z, Li S, et al. ISG12a inhibits HCV replication and potentiates the anti-HCV activity of IFN-alpha through activation of the Jak/STAT signaling pathway independent of autophagy and apoptosis. *Virus Res* (2017) 227:231–9. doi: 10.1016/j.virusres.2016.10.013

127. Jiao B, An C, Du H, Tran M, Wang P, Zhou D, et al. STAT6 deficiency attenuates myeloid fibroblast activation and macrophage polarization in experimental folic acid nephropathy. *Cells* (2021) 10(11):3057. doi: 10.3390/cells10113057

128. Banerjee S, Biehl A, Gadina M, Hasni S, Schwartz DM. JAK-STAT signaling as a target for inflammatory and autoimmune diseases: Current and future prospects. *Drugs* (2017) 77(5):521–46. doi: 10.1007/s40265-017-0701-9

129. Villarino AV, Kanno Y, O'Shea JJ. Mechanisms and consequences of jak-STAT signaling in the immune system. *Nat Immunol* (2017) 18(4):374–84. doi: 10.1038/ni.3691

130. O'Shea JJ, Plenge R. JAK and STAT signaling molecules in immunoregulation and immune-mediated disease. *Immunity* (2012) 36(4):542–50. doi: 10.1016/j.immuni.2012.03.014

131. Jiao B, An C, Tran M, Du H, Wang P, Zhou D, et al. Pharmacological inhibition of STAT6 ameliorates myeloid fibroblast activation and alternative macrophage polarization in renal fibrosis. *Front Immunol* (2021) 12:735014. doi: 10.3389/fimmu.2021.735014

132. Lin CM, Cooles FA, Isaacs JD. Basic mechanisms of JAK inhibition. *Mediterr J Rheumatol* (2020) 31(Suppl 1):100–4. doi: 10.31138/mjr.31.1.100

133. Zarrin AA, Bao K, Lupardus P, Vucic D. Kinase inhibition in autoimmunity and inflammation. *Nat Rev Drug Discovery* (2021) 20(1):39–63. doi: 10.1038/s41573-020-0082-8

134. Baldini C, Moriconi FR, Galimberti S, Libby P, De Caterina R. The JAK-STAT pathway: an emerging target for cardiovascular disease in rheumatoid arthritis and myeloproliferative neoplasms. *Eur Heart J* (2021) 42(42):4389–400. doi: 10.1093/eurheartj/ehab447

135. Wolfe L. Ruxolitinib in myelofibrosis and polycythemia Vera. *J Adv Pract Oncol* (2016) 7(4):436–44.

136. Sorensen AL, Mikkelsen SU, Knudsen TA, Bjorn ME, Andersen CL, Bjerrum OW, et al. Ruxolitinib and interferon-alpha2 combination therapy for patients with polycythemia vera or myelofibrosis: a phase II study. *Haematologica* (2020) 105(9):2262–72. doi: 10.3324/haematol.2019.235648

137. Alvarez-Larran A, Garrote M, Ferrer-Marin F, Perez-Encinas M, Mata-Vazquez MI, Bellosillo B, et al. Real-world analysis of main clinical outcomes in patients with polycythemia vera treated with ruxolitinib or best available therapy after developing resistance/intolerance to hydroxyurea. *Cancer* (2022) 128(13):2441–8. doi: 10.1002/cncr.34195

138. Shrock E, Fujimura E, Kula T, Timms RT, Lee IH, Leng Y, et al. Viral epitope profiling of COVID-19 patients reveals cross-reactivity and correlates of severity. *Science* (2020) 370(6520):eabd4250. doi: 10.1126/science.abd4250

139. Carvalho T, Krammer F, Iwasaki A. The first 12 months of COVID-19: a timeline of immunological insights. *Nat Rev Immunol* (2021) 21(4):245–56. doi: 10.1038/s41577-021-00522-1

140. Zhang W, Zhao Y, Zhang F, Wang Q, Li T, Liu Z, et al. The use of anti-inflammatory drugs in the treatment of people with severe coronavirus disease 2019 (COVID-19): The perspectives of clinical immunologists from China. *Clin Immunol* (2020) 214:108393. doi: 10.1016/j.clim.2020.108393

141. Smolen JS, Landewe RBM, Bijlsma JWJ, Burmester GR, Dougados M, Kerschbaumer A, et al. EULAR recommendations for the management of rheumatoid arthritis with synthetic and biological disease-modifying antirheumatic drugs: 2019 update. *Ann Rheum Dis* (2020) 79(6):685–99. doi: 10.1136/annrheumdis-2019-216655

142. Kerschbaumer A, Sepriano A, Smolen JS, van der Heijde D, Dougados M, van Vollenhoven R, et al. Efficacy of pharmacological treatment in rheumatoid arthritis: a systematic literature research informing the 2019 update of the EULAR recommendations for management of rheumatoid arthritis. *Ann Rheum Dis* (2020) 79(6):744–59. doi: 10.1136/annrheumdis-2019-216656

143. Stebbing J, Phelan A, Griffin I, Tucker C, Oechsle O, Smith D, et al. COVID-19: combining antiviral and anti-inflammatory treatments. *Lancet Infect Dis* (2020) 20(4):400–2. doi: 10.1016/S1473-3099(20)30132-8

144. Kulkarni S, Fisk M, Kostapanos M, Banham-Hall E, Bond S, Hernan-Sancho E, et al. Repurposed immunomodulatory drugs for covid-19 in pre-ICu patients - mulTi-arm therapeutic study in pre-ICu patients admitted with covid-19 - repurposed drugs (TACTIC-r): A structured summary of a study protocol for a randomised controlled trial. *Trials* (2020) 21(1):626. doi: 10.1186/s13063-020-04535-4

145. Moreno-Gonzalez G, Mussetti A, Albasanz-Puig A, Salvador I, Sureda A, Gudiol C, et al. A phase I/II clinical trial to evaluate the efficacy of baricitinib to prevent respiratory insufficiency progression in onco-hematological patients affected with COVID19: A structured summary of a study protocol for a randomised controlled trial. *Trials* (2021) 22(1):116. doi: 10.1186/s13063-021-05072-4

146. Bronte V, Ugel S, Tinazzi E, Vella A, De Sanctis F, Cane S, et al. Baricitinib restrains the immune dysregulation in patients with severe COVID-19. *J Clin Invest* (2020) 130(12):6409–16. doi: 10.1172/JCI141772

147. Patoulias D, Doumas M, Papadopoulos C, Karagiannis A. Janus kinase inhibitors and major COVID-19 outcomes: time to forget the two faces of janus! a meta-analysis of randomized controlled trials. *Clin Rheumatol* (2021) 40(11):4671–4. doi: 10.1007/s10067-021-05884-4

148. Ely EW, Ramanan AV, Kartman CE, de Bono S, Liao R, Piruzeli MLB, et al. Efficacy and safety of baricitinib plus standard of care for the treatment of critically ill hospitalised adults with COVID-19 on invasive mechanical ventilation or extracorporeal membrane oxygenation: an exploratory, randomised, placebo-controlled trial. *Lancet Respir Med* (2022) 10(4):327–36. doi: 10.1016/S2213-2600(22)00006-6

149. Stebbing J, Sánchez Nievas G, Falcone M, Youhanna S, Richardson P, Ottaviani S, et al. JAK inhibition reduces SARS-CoV-2 liver infectivity and modulates inflammatory responses to reduce morbidity and mortality. *Sci Adv* (2021) 7(1):eabe4724. doi: 10.1126/sciadv.abe4724

150. Abizanda P, Calbo Mayo JM, Mas Romero M, Cortes Zamora EB, Tabernero Sahuquillo MT, Romero Rizos L, et al. Baricitinib reduces 30-day mortality in older adults with moderate-to-severe COVID-19 pneumonia. *J Am Geriatr Soc* (2021) 69(10):2752–8. doi: 10.1111/jgs.17357

151. Chen CY, Chen WC, Hsu CK, Chao CM, Lai CC. Clinical efficacy and safety of janus kinase inhibitors for COVID-19: A systematic review and meta-analysis of randomized controlled trials. *Int Immunopharmacol* (2021) 99:108027. doi: 10.1016/j.intimp.2021.108027

152. Pillaiyar T, Laufer S. Kinases as potential therapeutic targets for anti-coronaviral therapy. *J Med Chem* (2022) 65(2):955–82. doi: 10.1021/acs.jmedchem.1c00335

153. Mease P, Hall S, FitzGerald O, van der Heijde D, Merola JF, Avila-Zapata F, et al. Tofacitinib or adalimumab versus placebo for psoriatic arthritis. *N Engl J Med* (2017) 377(16):1537–50. doi: 10.1056/NEJMoa1615975

154. Dhillon S. Tofacitinib: A review in rheumatoid arthritis. *Drugs* (2017) 77(18):1987–2001. doi: 10.1007/s40265-017-0835-9

155. Wollenhaupt J, Lee EB, Curtis JR, Silverfield J, Terry K, Soma K, et al. Safety and efficacy of tofacitinib for up to 9.5 years in the treatment of rheumatoid arthritis: final results of a global, open-label, long-term extension study. *Arthritis Res Ther* (2019) 21(1):89. doi: 10.1186/s13075-019-1866-2

156. Guimaraes PO, Quirk D, Furtado RH, Maia LN, Saraiva JF, Antunes MO, et al. Tofacitinib in patients hospitalized with covid-19 pneumonia. *N Engl J Med* (2021) 385(5):406–15. doi: 10.1056/NEJMoa2101643

157. Maslennikov R, Ivashkin V, Vasilieva E, Chipurik M, Semikova P, Semenets V, et al. Tofacitinib reduces mortality in coronavirus disease 2019 tofacitinib in COVID-19. *Pulm Pharmacol Ther* (2021) 69:102039. doi: 10.1016/j.pupt.2021.102039

158. Yan B, Freiwald T, Chauss D, Wang L, West E, Mirabelli C, et al. SARS-CoV-2 drives JAK1/2-dependent local complement hyperactivation. *Sci Immunol* (2021) 6(58):eabg0833. doi: 10.1126/sciimmunol.abg0833

159. Verstovsek S, Mesa RA, Gotlib J, Levy RS, Gupta V, DiPersio JF, et al. A double-blind, placebo-controlled trial of ruxolitinib for myelofibrosis. *N Engl J Med* (2012) 366(9):799–807. doi: 10.1056/NEJMoa1110557

160. Mascarenhas J, Hoffman R, Talpaz M, Gerds AT, Stein B, Gupta V, et al. Pacritinib vs best available therapy, including ruxolitinib, in patients with myelofibrosis: A randomized clinical trial. *JAMA Oncol* (2018) 4(5):652–9. doi: 10.1001/jamaoncol.2017.5818

161. Vannucchi AM, Kiladjian JJ, Griesshammer M, Masszi T, Durrant S, Passamonti F, et al. Ruxolitinib versus standard therapy for the treatment of polycythemia vera. *N Engl J Med* (2015) 372(5):426–35. doi: 10.1056/NEJMoa1409002

162. Zeiser R, von Bubnoff N, Butler J, Mohty M, Niederwieser D, Or R, et al. Ruxolitinib for glucocorticoid-refractory acute graft-versus-Host disease. *N Engl J Med* (2020) 382(19):1800–10. doi: 10.1056/NEJMoa1917635

163. Gratwohl A. Ruxolitinib for acute graft-versus-Host disease. *N Engl J Med* (2020) 383(5):501–2. doi: 10.1056/NEJMc2020763

164. Zhang Q, Zhao YZ, Ma HH, Wang D, Cui L, Li WJ, et al. A study of ruxolitinib response-based stratified treatment for pediatric hemophagocytic lymphohistiocytosis. *Blood* (2022) 139(24):3493–504. doi: 10.1182/blood.2021014860

165. Marconi VC, Moser C, Gavegnano C, Deeks SG, Lederman MM, Overton ET, et al. Randomized trial of ruxolitinib in antiretroviral-treated adults with human immunodeficiency virus. *Clin Infect Dis* (2022) 74(1):95–104. doi: 10.1093/cid/ciab212

166. Han MK, Antila M, Ficker JH, Gordeev I, Guerreros A, Bernus AL, et al. Ruxolitinib in addition to standard of care for the treatment of patients admitted to hospital with COVID-19 (RUXCOVID): a randomised, double-blind, placebo-controlled, phase 3 trial. *Lancet Rheumatol* (2022) 4(5):e351–61. doi: 10.1016/S2665-9913(22)00044-3

167. Levy G, Guglielmelli P, Langmuir P, Constantinescu SN. JAK inhibitors and COVID-19. *J Immunother Cancer* (2022) 10(4):e002838. doi: 10.1136/jitc-2021-002838

168. Cao Y, Wei J, Zou L, Jiang T, Wang G, Chen L, et al. Ruxolitinib in treatment of severe coronavirus disease 2019 (COVID-19): A multicenter, single-blind, randomized controlled trial. *J Allergy Clin Immunol* (2020) 146(1):137–146 e3. doi: 10.1016/j.jaci.2020.05.019

169. Singh D, Bogus M, Moskalenko V, Lord R, Moran EJ, Crater GD, et al. A phase 2 multiple ascending dose study of the inhaled pan-JAK inhibitor nezulcitinib (TD-0903) in severe COVID-19. *Eur Respir J* (2021) 58(4):2100673. doi: 10.1183/13993003.00673-2021

170. WHO Rapid Evidence Appraisal for COVID-19 Therapies (REACT) Working Group, Sterne JAC, Murthy S, Diaz JV, Slutsky AS, Villar J, et al. Association between administration of systemic corticosteroids and mortality among critically ill patients with COVID-19: A meta-analysis. *JAMA* (2020) 324(13):1330–41. doi: 10.1001/jama.2020.17023

171. RECOVERY Collaborative Group, Horby P, Lim WS, Emberson JR, Mafham M, Bell JL, et al. Dexamethasone in hospitalized patients with covid-19. *N Engl J Med* (2021) 384(8):693–704. doi: 10.1056/NEJMoa2021436

172. Tomazini BM, Maia IS, Cavalcanti AB, Berwanger O, Rosa RG, Veiga VC, et al. Effect of dexamethasone on days alive and ventilator-free in patients with moderate or severe acute respiratory distress syndrome and COVID-19: The CoDEX randomized clinical trial. *JAMA* (2020) 324(13):1307–16. doi: 10.1001/jama.2020.17021

173. Granholm A, Kjaer MN, Munch MW, Myatra SN, Vijayaraghavan BKT, Cronhjort M, et al. Long-term outcomes of dexamethasone 12 mg versus 6 mg in patients with COVID-19 and severe hypoxaemia. *Intensive Care Med* (2022) 48(5):580–9. doi: 10.1007/s00134-022-06677-2

174. Incorrect equivalent dose and p values in figure 3. *JAMA* (2022) 327(3):286. doi: 10.1001/jama.2021.24153

175. Granholm A, Munch MW, Myatra SN, Vijayaraghavan BKT, Cronhjort M, Wahlin RR, et al. Dexamethasone 12 mg versus 6 mg for patients with COVID-19 and severe hypoxaemia: a pre-planned, secondary Bayesian analysis of the COVID STEROID 2 trial. *Intensive Care Med* (2022) 48(1):45–55. doi: 10.1007/s00134-021-06573-1

176. Taboada M, Rodríguez N, Varela PM, Rodríguez MT, Abelleira R, González A, et al. Effect of high versus low dose of dexamethasone on clinical worsening in patients hospitalised with moderate or severe COVID-19 pneumonia: an open-label, randomised clinical trial. *Eur Respir J* (2022) 60(2):2102518. doi: 10.1183/13993003.02518-2021

177. Agusti A, De Stefano G, Levi A, Muñoz X, Romero-Mesones C, Sibila O, et al. Add-on inhaled budesonide in the treatment of hospitalised patients with COVID-19: a randomised clinical trial. *Eur Respir J* (2022) 59(3):2103036. doi: 10.1183/13993003.03036-2021

178. Yu LM, Bafadhel M, Dorward J, Hayward G, Saville BR, Gbinigie O, et al. Inhaled budesonide for COVID-19 in people at high risk of complications in the community in the UK (PRINCIPLE): a randomised, controlled, open-label, adaptive platform trial. *Lancet* (2021) 398(10303):843–55. doi: 10.1016/S0140-6736(21)01744-X

179. Ramakrishnan S, Nicolau DV, Jr , Langford B, Mahdi M, Jeffers H, Mwasuku C, et al, et al. Inhaled budesonide in the treatment of early COVID-19 (STOIC): a phase 2, open-label, randomised controlled trial. *Lancet Respir Med* (2021) 9(7):763–72. doi: 10.1016/S2213-2600(21)00160-0

180. Baker JR, Mahdi M, Nicolau DV Jr, Ramakrishnan S, Barnes PJ, Simpson JL, et al. Early Th2 inflammation in the upper respiratory mucosa as a predictor of severe COVID-19 and modulation by early treatment with inhaled corticosteroids: a mechanistic analysis. *Lancet Respir Med* (2022) 10(6):545–56. doi: 10.1016/S2213-2600(22)00002-9

181. Ezer N, Belga S, Daneman N, Chan A, Smith BM, Daniels SA, et al. Inhaled and intranasal ciclesonide for the treatment of covid-19 in adult outpatients: CONTAIN phase II randomised controlled trial. *BMJ* (2021) 375:e068060. doi: 10.1136/bmj-2021-068060

182. Clemency BM, Varughese R, Gonzalez-Rojas Y, Morse CG, Phipatanakul W, Koster DJ, et al. Efficacy of inhaled ciclesonide for outpatient treatment of adolescents and adults with symptomatic COVID-19: A randomized clinical trial. *JAMA Intern Med* (2022) 182(1):42–9. doi: 10.1001/jamainternmed.2021.6759

183. Angus DC, Derde L, Al-Beidh F, Annane D, Arabi Y, Beane A, et al. Effect of hydrocortisone on mortality and organ support in patients with severe COVID-19: The REMAP-CAP COVID-19 corticosteroid domain randomized clinical trial. *JAMA* (2020) 324(13):1317–29. doi: 10.1001/jama.2020.17022

184. Edalatifard M, Akhtari M, Salehi M, Naderi Z, Jamshidi A, Mostafaei S, et al. Intravenous methylprednisolone pulse as a treatment for hospitalised severe COVID-19 patients: results from a randomised controlled clinical trial. *Eur Respir J* (2020) 56(6):2002808. doi: 10.1183/13993003.02808-2020

185. Dhooria S, Chaudhary S, Sehgal IS, Agarwal R, Arora S, Garg M, et al. High-dose versus low-dose prednisolone in symptomatic patients with post-COVID-19 diffuse parenchymal lung abnormalities: an open-label, randomised trial (the COLDSTER trial). *Eur Respir J* (2022) 59(2):2102930. doi: 10.1183/13993003.02930-2021

Frontiers in Immunology

Explores novel approaches and diagnoses to treat immune disorders.

The official journal of the International Union of Immunological Societies (IUIS) and the most cited in its field, leading the way for research across basic, translational and clinical immunology.

Discover the latest Research Topics

See more →

Frontiers

Avenue du Tribunal-Fédéral 34
1005 Lausanne, Switzerland
frontiersin.org

Contact us

+41 (0)21 510 17 00
frontiersin.org/about/contact